frontiers | Research Topics

Integrative multi-omics and artificial intelligence (AI)-driven approaches for superior nutritional quality and stress resilience in crops

Edited by
Simardeep Kaur, Naseeb Singh, Gurjeet Singh and Rakesh Bhardwaj

Published in
Frontiers in Nutrition
Frontiers in Sustainable Food Systems

ISSN 1664-8714
ISBN 978-2-8325-6861-3
DOI 10.3389/978-2-8325-6861-3

Generative AI statement
Any alternative text (Alt text) provided alongside figures in the articles in this ebook has been generated by Frontiers with the support of artificial intelligence and reasonable efforts have been made to ensure accuracy, including review by the authors wherever possible. If you identify any issues, please contact us.

About Frontiers

Frontiers is more than just an open access publisher of scholarly articles: it is a pioneering approach to the world of academia, radically improving the way scholarly research is managed. The grand vision of Frontiers is a world where all people have an equal opportunity to seek, share and generate knowledge. Frontiers provides immediate and permanent online open access to all its publications, but this alone is not enough to realize our grand goals.

Frontiers journal series

The Frontiers journal series is a multi-tier and interdisciplinary set of open-access, online journals, promising a paradigm shift from the current review, selection and dissemination processes in academic publishing. All Frontiers journals are driven by researchers for researchers; therefore, they constitute a service to the scholarly community. At the same time, the *Frontiers journal series* operates on a revolutionary invention, the tiered publishing system, initially addressing specific communities of scholars, and gradually climbing up to broader public understanding, thus serving the interests of the lay society, too.

Dedication to quality

Each Frontiers article is a landmark of the highest quality, thanks to genuinely collaborative interactions between authors and review editors, who include some of the world's best academicians. Research must be certified by peers before entering a stream of knowledge that may eventually reach the public - and shape society; therefore, Frontiers only applies the most rigorous and unbiased reviews. Frontiers revolutionizes research publishing by freely delivering the most outstanding research, evaluated with no bias from both the academic and social point of view. By applying the most advanced information technologies, Frontiers is catapulting scholarly publishing into a new generation.

What are Frontiers Research Topics?

Frontiers Research Topics are very popular trademarks of the *Frontiers journals series*: they are collections of at least ten articles, all centered on a particular subject. With their unique mix of varied contributions from Original Research to Review Articles, Frontiers Research Topics unify the most influential researchers, the latest key findings and historical advances in a hot research area.

Find out more on how to host your own Frontiers Research Topic or contribute to one as an author by contacting the Frontiers editorial office: frontiersin.org/about/contact

Integrative multi-omics and artificial intelligence (AI)-driven approaches for superior nutritional quality and stress resilience in crops

Topic editors

Simardeep Kaur — The ICAR Research Complex for North Eastern Hill Region (ICAR RC NEH), India

Naseeb Singh — The ICAR Research Complex for North Eastern Hill Region (ICAR RC NEH), India

Gurjeet Singh — Texas A and M University, United States

Rakesh Bhardwaj — National Bureau of Plant Genetic Resources, Indian Council of Agricultural Research (ICAR), India

Citation

Kaur, S., Singh, N., Singh, G., Bhardwaj, R., eds. (2025). *Integrative multi-omics and artificial intelligence (AI)-driven approaches for superior nutritional quality and stress resilience in crops*. Lausanne: Frontiers Media SA.

doi: 10.3389/978-2-8325-6861-3

Table of contents

frontiers | Frontiers in Nutrition

TYPE Editorial
PUBLISHED 29 August 2025
DOI 10.3389/fnut.2025.1678669

OPEN ACCESS

EDITED AND REVIEWED BY
Kathleen L. Hefferon,
Cornell University, United States

*CORRESPONDENCE
Naseeb Singh
✉ naseeb501@gmail.com

RECEIVED 03 August 2025
ACCEPTED 15 August 2025
PUBLISHED 29 August 2025

CITATION
Kaur S, Singh N, Singh G and Bhardwaj R (2025) Editorial: Integrative multi-omics and artificial intelligence (AI)-driven approaches for superior nutritional quality and stress resilience in crops. *Front. Nutr.* 12:1678669. doi: 10.3389/fnut.2025.1678669

Editorial: Integrative multi-omics and artificial intelligence (AI)-driven approaches for superior nutritional quality and stress resilience in crops

Simardeep Kaur[1], Naseeb Singh[1,2]*, Gurjeet Singh[3] and Rakesh Bhardwaj[4]

[1]Indian Council of Agricultural Research (ICAR)-Research Complex for North Eastern Hill Region, Umiam, Meghalaya, India, [2]Department of Biosystems and Agricultural Engineering, Michigan State University, East Lansing, MI, United States, [3]Texas A&M University, AgriLife Research Center, Beaumont, TX, United States, [4]Indian Council of Agricultural Research (ICAR)-National Bureau of Plant Genetic Resources, New Delhi, India

KEYWORDS

nutritional quality, genetic diversity, multivariate techniques, artificial intelligence, multi-omics, stress resilience, sustainable agriculture

Editorial on the Research Topic
Integrative multi-omics and artificial intelligence (AI)-driven approaches for superior nutritional quality and stress resilience in crops

Overview

The increasing demand for sustainable agriculture and nutrient-rich crops has driven the need for innovative strategies that go beyond the conventional breeding approaches. The Research Topic titled "*Integrative multi-omics and artificial intelligence (AI)-driven approaches for superior nutritional quality and stress resilience in crops*," published in *Frontiers in Nutrition*, sought to address the growing demand for nutritious and climate-resilient crops by leveraging cutting-edge tools such as multi-omics and AI. The multi-omics approach integrating genomics, transcriptomics, proteomics, metabolomics, and phenomics offers a comprehensive view of plant systems and allows for the identification of key genes, regulatory pathways, and metabolites involved in nutrition and stress adaptation. AI further enhances these efforts by enabling predictive modeling, big data analysis, and real-time decision-making. Together, these technologies offer a powerful platform for understanding the complex interactions that govern desirable traits and for accelerating crop improvement. Despite considerable progress, translating omics insights into field-ready innovations remains challenging. This Research Topic provides an interdisciplinary platform to address this gap, focusing on crops like wheat, chickpea, taro, fenugreek, cassava, and pigeon pea, as well as technological solutions such as drones and remote sensing. The Research Topic comprises nine articles (seven original research articles and two reviews), each offering novel insights and innovative applications of multi-omics and AI. Collectively, these studies advance the understanding and practical implementation of integrative technologies in plant science, contributing to a more sustainable and food-secure future.

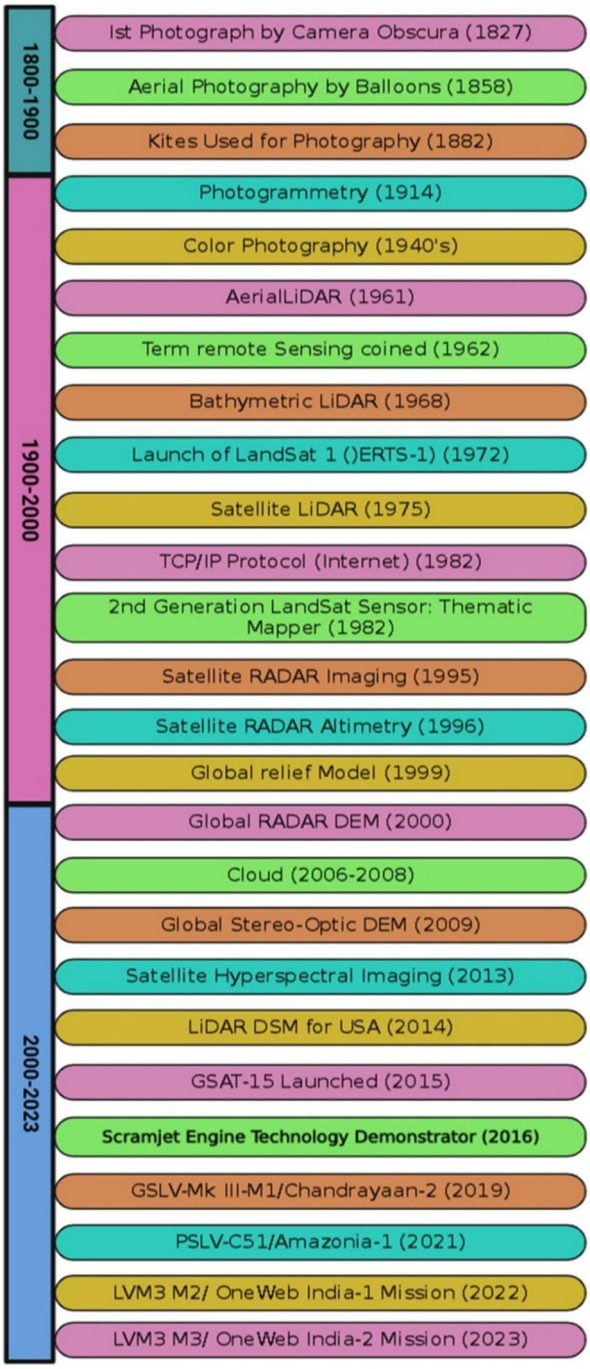

FIGURE 1
Timeline showing the history of remote sensing (Aziz et al.).

Published articles and summaries

1. *Enhancing micronutrient bioavailability in wheat grain through organic fertilizer substitution* (Wang et al.)

This study reported that 15% organic fertilizer substitution (OFS) in wheat significantly enhanced grain micronutrient bioavailability without reducing yield. While average yield was 9.06 Mg/ha, the highest (9.58 Mg/ha) occurred under 15% OFS. Grain iron and zinc increased by 24.7% and 19.2%, respectively, with no major change in soil micronutrient levels, indicating improved plant uptake and reduced phytate interference. OFS also lowered PA:Fe and PA:Zn ratios, enhancing bioavailability. Health impact modeling suggested reductions in Fe and Zn deficiency by up to 3.94% and 7.15%, respectively. Random forest analysis identified phytate content, soil organic carbon, and yield as key predictors.

2. *Assessment of nutritional quality of Taro (Colocasia esculenta L. Schott.) genotypes of the Eastern Himalaya, India* (Talang et al.)

This study evaluated taro genotypes from the Eastern Himalaya, revealing significant variation in agronomic, nutritional, and mineral traits. "Tamachongkham" and "Tamitin" excelled in total and cormel yield, respectively, while "Megha Taro 1" and "Megha Taro 2" showed high cormel number and yield. Crude protein ranged from 3.25% to 7.10%, with notable differences in fiber, ash, starch, and sugar contents across genotypes. Antioxidant traits correlated positively with phenolic and anthocyanin levels. "Tamitin" was rich in N, K, Zn, Cu, and Mn; "Tagitung White" in P; and "BCC 2" in Fe and Ca+Mg. PCA identified sugar, starch, fiber, anthocyanin, and FRAP as key contributors to diversity, highlighting several genotypes for nutritional breeding.

3. *Remote sensing and artificial intelligence: revolutionizing pest management in agriculture* (Aziz et al.)

This study highlighted the transformative potential of integrating remote sensing and AI in agricultural pest management. By analyzing multispectral data through AI algorithms, pest damage could be detected at early stages, well before visible symptoms emerge, allowing for timely and localized intervention. The fusion of remote sensing with weather and phenology datasets enabled dynamic modeling of pest spread, thereby improving the resilience of pest forecasting under changing climatic conditions. AI-driven precision pest control strategies were shown to optimize resource use by significantly reducing pesticide application and labor costs while enhancing treatment efficacy. Despite these advancements, the study also identified key challenges to adoption, including data heterogeneity, lack of algorithm transparency, high implementation costs, and the need for adequate farmer training and capacity building (Figure 1).

4. *Identification of methyltransferase and demethylase genes and their expression profiling under biotic and abiotic stress in pigeon pea (Cajanus cajan [L.] Millspaugh)* (Kumari et al.)

This study identified and characterized methyltransferase and demethylase gene families in pigeon pea, with a focus on their expression profiles under various biotic and abiotic stress conditions. Notably, the demethylase gene CcALKBH10B exhibited strong upregulation in response to drought, salinity, and pest stress, while CcALKBH8 showed peak expression under heat stress, indicating their stress-responsive roles. Tissue-specific expression patterns suggested that these genes may also be involved in developmental and organ-level regulation. Phylogenetic analysis revealed that m6A-related proteins in pigeon pea cluster closely with those of other legumes, pointing to conserved evolutionary functions and potential cross-species functional relevance.

5. *Prospects of cold plasma in enhancing food phenolics: analyzing nutritional potential and process optimization through RSM and AI techniques* (Shanker and Rana)

This study highlighted cold plasma (CP) as a promising non-thermal technology to enhance food nutritional quality, particularly phenolic content and antioxidant capacity. Using dielectric barrier discharge, CP's effects depend on factors like gas type, voltage, and exposure time. Optimization via RSM, ANN, and genetic algorithms effectively modeled non-linear influences on phenolic retention. Evidence showed a 10–15% increase in total phenolics and antioxidant activity with minimal sensory changes, emphasizing CP's potential for improving food quality through precise process control.

6. *Improving agricultural spraying with multi-rotor drones: a technical study on operational parameter optimization* (Yallappa et al.)

This study optimized multi-rotor drone parameters for agricultural spraying, finding that a 2.0 m hovering height minimized drift and improved deposition. A hexa nozzle setup with 0.6 m spacing ensured maximum spray uniformity, while spray pressure mainly affected width, not uniformity. Boom design significantly influenced spray patterns. Drone sprayers covered ~3 ha/h, vastly outperforming knapsack sprayers (~1 ha/11 h), offering greater efficiency and reduced labor demands for precision agriculture.

7. *Metabolomics profiles of the liquid co-culture of Sanghuangporus vaninii and Pleurotus sapidus* (Lu and Liu)

This study investigated the metabolomic profiles of a liquid co-culture system involving *Sanghuangporus vaninii* and *Pleurotus sapidus*, revealing significant enhancements in fungal biomass and intracellular polysaccharide (IPS) yield. Although *P. sapidus* exhibited inhibitory effects on the growth of *S. vaninii*, the overall co-cultivation process led to a synergistic increase in bioactive compound production. Metabolomic analysis showed substantial shifts in amino acid, nucleotide, and glycerophospholipid metabolism, suggesting the activation of previously silent biosynthetic pathways. Importantly, several novel secondary metabolites were identified exclusively in the co-culture, absent in individual monocultures. These changes not only reflect a dynamic metabolic interplay between the two fungi but also point toward enhanced nutraceutical and pharmaceutical potential due to the enriched IPS and diverse bioactive compound profiles.

8. *Demystifying the nutritional and anti-nutritional genetic divergence of Pakistani chickpea (Cicer arietinum L.) genetic resource via multivariate approaches* (Jameel et al.)

This study analyzed genetic variation in nutritional and anti-nutritional traits among Pakistani chickpea genotypes using multivariate tools. Punjab 2000 (desi) showed the highest total soluble proteins (34.9%) and crude protein (30.1%), while wild hybrid 15 had the highest free amino acids (~3.34 g/100 g DW). Several genotypes exhibited low phytate and tannin levels, indicating better nutrient bioavailability. PCA and clustering identified nutritionally elite genotypes for targeted breeding and crop improvement.

9. *Deciphering agronomic traits, biochemical components, and color in unique green-seeded fenugreek (Trigonella foenum-graecum L.) genotypes* (Singh et al.)

This study evaluated unique green-seeded fenugreek genotypes for agronomic, biochemical, and visual traits, highlighting their superior nutritional potential over yellow-seeded types. Genotype GSF8 recorded the highest yield (~2473.7 kg/ha), while GSF6 and GSF1 showed elevated 4-hydroxyisoleucine (~0.90%) and chlorophyll (~0.45 mg/100 g), respectively. Most green-seeded genotypes had higher oil, phenolic, and protein content, with GSF9 showing low soluble sugars (~3.50%). Darker seed color correlated with higher chlorophyll and 4 OHIle but lower sugars. PCA identified chlorophyll, 4 OHIle, oil, phenolics, and harvest index as key traits contributing to their nutritional and medicinal value.

In conclusion, this Research Topic has successfully laid a robust foundation, highlighting the transformative potential of integrative multi-omics and AI in agricultural sciences. Future advancements will require sustained, collaborative efforts across disciplines and stakeholders. Continued investment and innovation in these integrative approaches will undeniably play a pivotal role in developing nutritionally enhanced, climate-resilient crops, contributing significantly toward achieving global food security and agricultural sustainability in the face of accelerating climate change and increasing population pressures.

Author contributions

SK: Writing – original draft, Writing – review & editing. NS: Writing – original draft, Writing – review & editing. GS: Writing – original draft, Writing – review & editing. RB: Writing – original draft, Writing – review & editing.

Conflict of interest

The authors declare that the research was conducted without any commercial or financial relationships that could be interpreted as a potential conflict of interest.

The author(s) declared that they were an editorial board member of Frontiers, at the time of submission. This had no impact on the peer review process and the final decision.

Generative AI statement

The author(s) declare that no Gen AI was used in the creation of this manuscript.

Any alternative text (alt text) provided alongside figures in this article has been generated by Frontiers with the support of artificial intelligence and reasonable efforts have been made to ensure accuracy, including review by the authors wherever possible. If you identify any issues, please contact us.

Publisher's note

frontiers | Frontiers in Nutrition

TYPE Original Research
PUBLISHED 04 October 2024
DOI 10.3389/fnut.2024.1407096

OPEN ACCESS

EDITED BY
Uday Chand Jha,
Indian Institute of Pulses Research (ICAR), India

REVIEWED BY
Sankar Devarajan,
University of Arkansas at Pine Bluff, United States
Muthukumar Serva Peddha,
Central Food Technological Research Institute (CSIR), India

*CORRESPONDENCE
Amjad Hameed
amjad46pk@yahoo.com

RECEIVED 28 March 2024
ACCEPTED 06 September 2024
PUBLISHED 04 October 2024

CITATION
Jameel S, Hameed A, Shah TM and Coyne CJ (2024) Demystifying the nutritional and anti-nutritional genetic divergence of Pakistani chickpea (*Cicer arietinum* L.) genetic resource via multivariate approaches. *Front. Nutr.* 11:1407096. doi: 10.3389/fnut.2024.1407096

Demystifying the nutritional and anti-nutritional genetic divergence of Pakistani chickpea (*Cicer arietinum* L.) genetic resource via multivariate approaches

Saima Jameel[1], Amjad Hameed[1]*, Tariq Mahmud Shah[1] and Clarice J. Coyne[2]

[1]Nuclear Institute for Agriculture and Biology College, Pakistan Institute of Engineering and Applied Sciences, Faisalabad, Pakistan, [2]USDA–ARS Plant Germplasm Introduction and Testing, Washington State University, Pullman, WA, United States

Chickpeas are a highly versatile functional food legume that possesses the capacity to boost human health and has the potential to alleviate malnutrition-related deficiencies. To investigate whole seed-based nutritional and anti-nutritional composition, a set of 90 chickpea genotypes (66 desi and 24 kabuli) was collected from different research organizations in Pakistan. Significant variation (Tukey HSD test, $p < 0.05$) was perceived among genotypes for traits under investigation. The genotypes, with maximum total soluble proteins (TSPs) (34.92%), crude proteins (CPs) (30.13%), and reducing sugars (17.33 mg/g s. wt.), i.e., Punjab-2000 (desi); total free amino acids (TFAs) (3.34 g/100 g DW), i.e., Wild Hybrid-15 (desi), albumins (227.67 mg/g s. wt.), i.e., Sheenghar-2000 (desi); globulins (720 g s. wt.), i.e., ICCV-96030 (desi); salt-soluble proteins (200 mg/g s. wt.), i.e., ILWC-247 (desi); total soluble sugars (TSSs) (102.63 mg/g s. wt.), i.e., CM1051/11 (desi); non-reducing sugars (95.28 mg/g s. wt.), i.e., NIAB-CH2016 (desi); starch content (83.69%), i.e., CH55/09 (kabuli); and the genotypes with least value of anti-nutritional factors glutelin (3.33 mg/g s. wt.), i.e., Wild Hybrid-9 (desi); hordein (1.38 mg/g s. wt.), i.e., Noor-2013 (kabuli); tannins (5,425 uM/g s. wt.), i.e., Wild Hybrid-1 (desi); and phytic acid (PA) (0.18 mg/g s. wt.), i.e., Bhakhar-2011 (desi), could be the promising genotypes to formulate health-promoting plant-based food products. Data were also analyzed for principal component analysis (PCA), correlation, and agglomerative hierarchical clustering. PC-1 revealed the highest contribution (20.83%) toward cumulative variability, and maximum positive factor loading was delivered by TSSs (0.85) followed by starch content (0.729). Genotypes were grouped into three distinct clusters based on high average values of traits under investigation. Cluster I encompassed genotypes with a high mean value of CP content, albumins, hordein, and glutelin; Cluster II encompassed genotypes with a high mean value of TSPs, TSSs, non-reducing sugars, globulins, salt-soluble sugars, starch, and TFAs; Cluster III encompassed genotypes with high tannins, reducing sugars, and PA. Identified desi and kabuli genotypes exhibiting superior seed quality traits and minimal anti-nutritional factors can be used in chickpea breeding programs aimed at improving seed nutritional quality in future breeding lines.

KEYWORDS

chickpeas, differential proteins, phytic acid, PCA, correlation

Introduction

The world's current population stands at approximately 6.5 billion individuals; projections indicate that this number will surge to approximately 9 billion by 2050. This impending population growth presents a mounting dilemma: how to meet the escalating demand for food with limited resources (1, 2). The relentless increase in the global population is surpassing the capacity of worldwide food production, leading to extensive food insecurity and malnutrition in numerous regions, notably across Asia, Africa, and South America (3, 4). Simultaneously, in developing countries, the dearth of high nutritional quality and nutrient-dense agricultural food commodities increases disease prevalence, particularly among the poor (5). Food insecurity arises when people are commonly anxious about their capacity to acquire a sufficient amount of nutritious, safe, affordable food (6). It is a worldwide issue and can occur because of the non-availability of healthier food choices or lack of income to afford a healthier diet by common people (7). Food insecurity and malnutrition in all their forms are more responsible for poor health than any other cause in low-income countries (8). Malnutrition is exacerbated by low consumption, a lack of diet diversity, and nutrient-deficient food. Malnutrition has been reported to reduce global gross domestic product (GDP) by 10% annually (9). It is expected that more than two billion people globally are affected by hidden hunger, and more than double the 805 million individuals do not get sufficient calories to consume (10, 11). According to research, the consumption of plant-based nutritional-rich foods is a low-risk, cost-effective intervention that May lower blood pressure, cholesterol level, and body mass index. They May also minimize the mortality rate from myocardial infarction and the number of medications required to cure chronic illnesses. Low consumption of fruits and vegetables is also one of the top 10 risk factors for mortality. Both urban and rural populations eat primarily cereal-based diets, deficient in essential minerals, which leads to poor diets and a higher frequency of nutritional deficiency illnesses (12). Serious complications, such as muscle deterioration and deformity, hindered growth and development in infants and young children, and compromised the immune system, resulting from protein deficiency. Moreover, individuals with a protein C deficiency face an elevated risk of encountering anomalous blood agglutination (13). Because of these complications, people are now more interested in "eating well" rather than simply aiming to be satiated (14). Legumes are recognized internationally as an economical and environmentally friendly alternative to meat, positioning them as the second most crucial dietary resource following cereal grains (15). The increased availability of nutritionally dense legumes, particularly for individuals in low-income areas, would play a pivotal role in addressing hidden hunger and malnutrition, ultimately contributing to the augmentation of cereal-based diets (16, 17). Legumes are referred to as "nutritional seeds for a sustainable future," while the United Nations and Food and Agriculture Organization (FAO) have declared 2016 "The International Year of Pulses" (18).

Chickpeas (*Cicer arietinum* L.) are one of the most economically important food legumes grown worldwide because they play an important role in human nutrition (19). Enhancing the nutritional value of chickpeas and other food legumes has the ability not only to improve human health but also to fight micronutrient malnutrition deficiency (20). Cultivated chickpeas are grouped into two distinct types: desi and kabuli. The presence of anthocyanin-pigmented stem and pink flowers distinguishes features of the desi type, while the kabuli type lacks anthocyanin pigmentation and has white-colored flowers (21). It was grown to 14.84 million ha in 2021–2022, generating 18.09 million tons on an average of 1,016 kg/ha all over the world. Asia is the main chickpea-growing region in the world with an 84% production share, and Pakistan is the seventh largest chickpea-producing country in the world after India, Australia, Turkey, Ethiopia, Myanmar, and Russia (22). In Pakistan, it is mainly grown in arid/semi-arid parts of the Thal region of Punjab. These areas are completely reliant on rainfall to meet their water needs (23). In Pakistan, chickpeas are consumed in multiple forms, such as fresh green seeds, dried whole seeds, dhal, and flour, for different purposes (24). To make a variety of traditional chickpea-based products, several processing methods are being used, including roasting, frying, boiling, and puffing (18). Chickpeas are a nutrient-dense legume that encompasses a wide range of valuable nutritious components, including proteins, carbohydrates, minerals, unsaturated fatty acids, dietary fibers, vitamins, and a wide range of isoflavones (25); however, it also contains some anti-nutritional factors such as tannins and phytates that bind with proteins and minerals such as Zn and Fe (26). In comparison to other pulses, chickpeas are unique because they are a vital source of high-quality protein and carbohydrates, accounting for approximately 80% of the total dry seed mass (27, 28). Chickpeas are an imperative functional food crop as they provide not only essential nutrients but also have numerous potential health benefits against type 2 diabetes, cardiovascular disease, some cancers, and digestive diseases (29). Genetic variation and environmental conditions significantly affect the chemical composition of all crops, including cereal grains and legumes (30). Nevertheless, the advancement of quality-related research and breeding practices for chickpeas lags far behind the progress made in amplifying chickpea yield (31). To address this gap, it is crucial to prioritize the selection and breeding of cultivars that are rich in specific nutrients while also possessing the least anti-nutritional factors. Due to its expanding usage in agricultural development and the selection of appropriate genotypes for breeding crops, advances in germplasm characterization using biochemical fingerprinting have unusual advantages (32). In this perspective, the present study aimed to investigate the whole seed-based nutritional and anti-nutritional composition of chickpea genetic resources through biochemical study.

Materials and methods

Genetic resource

A diverse set of 90 chickpea genotypes, comprising 66 desi and 24 kabuli types, with diverse genetic backgrounds were collected from different research stations in Pakistan during 2017, and seeds were multiplied for two consecutive years (2017–2018 and 2018–2019) at the Nuclear Institute for Agriculture and Biology (NIAB), Faisalabad. Among these 66 desi genotypes, there were 25 approved Pakistani varieties, 14 advanced lines, 7 mutants, 16 wild crosses, 1 wild parent, and 3 exotic lines utilized. Overall, approximately 95 diverse parents contributed to the development of these desi lines. Regarding the Kabuli type, among the 24 Kabuli genotypes used in the present study, there were 7 approved varieties, 14 advanced lines, 2 mutants, and 1 exotic line. In total, approximately 15 diverse parents contributed to

the development of these lines. The genotypes used in this study were cataloged for the year of release, institution, pedigree information, average yield, type, and other important traits, which are already cited in Table 1 of our previously published paper (33). The mature dry seeds of the germplasm, harvested during the season 2018–2019, were used for the determination of their seed-based nutritional and anti-nutritional profiling. Seed nitrogen analysis was performed at USDA-ARS Plant Germplasm Introduction and Testing, Washington State University, Pullman, WA 99164, United States.

Nutritional parameters

Sample preparation

A laboratory mini mill grinder was used to grind 20 healthy (4 to 6 g) disease-free whole seeds of each genotype into a fine powder, and to get fine flour, the material was passed through an 80 µm sieve. The fine flour was stored at room temperature in air-tight zipper bags for further analysis. Approximately 0.2 g flour sample was extracted in 2 mL of potassium phosphate buffer (50 mM) with pH 7.4. To homogenize the mixture, all the samples were vortexed and then centrifuged at 14,462 × g at 4°C for 10 min. For the determination of different biochemical analyses, the supernatant was separated and used according to different methods (34). Data were recorded in triplicate for all biochemical parameters.

Total soluble protein

The previously reported approach was used to estimate quantitative protein (35). Absorbance was computed at 595 nm through a spectrophotometer.

Seed nitrogen/crude protein

Seed sample preparation

Twenty healthy seeds of all genotypes were ground to a fine powder using a coffee grinder before nitrogen/protein analyses.

Seed nitrogen analyses and protein calculations

Seed nitrogen (N)/CP concentrations were determined using a LECO FP-528 nitrogen/CP determinator (Leco Corp., St. Joseph, MI, United States), according to the manufacturer's instruction manual. Weighed aliquots of ethylene diamine tetra acetic acid (EDTA) were used as nitrogen standards to calibrate the instrument. Two sub-samples (0.15 g each) of each accession were analyzed for nitrogen concentration; each sample was measured two times internally in the instrument with the average reported to the operator. The two sub-sample averages were then averaged to get a nitrogen concentration value for each accession. Protein concentrations were calculated using a conversion factor of 6.25 (seed nitrogen concentration) x 6.25 (36).

Differential proteins

Albumins

To obtain the protein extract, 0.02 g of ground seed flour was dissolved in 1 mL of buffer A. After 2 h of continuous stirring, the mixture was centrifuged at 4000 g for 10 min, and the supernatant corresponding to the albumin fraction was collected. The pellet was then treated with 1 mL of buffer A, centrifuged, and the supernatant was collected; repeat the same procedure and pool the collected supernatant. After mixing 5 µL of supernatant and 1 mL of Bradford dye in a cuvette, the absorbance was measured at 595 nm using a spectrophotometer (37).

Globulins

The albumin pellet was mixed with 1 mL of buffer B (0.01 M Tris–HCl pH 7.5 and 1 M NaCl) and stirred for 2 h before being centrifuged at 4,000 g for 10 min, twice. This fraction represents the globulin extraction. Absorbance was measured at 595 nm using a spectrophotometer with 5 µL of supernatant and 1 mL of Bradford dye (37).

Salt-soluble proteins

Fine ground seed samples (0.02 g) of each genotype were mixed in 2.5 mL of 0.15 M potassium phosphate buffer (pH 7.5) and 2.5 mL of 5 mM dithiothreitol (DDT), stirred for 30 min at room temperature, centrifuged at 2,000 g for 5 min, and extracted three times as before. The recovered supernatant contained salt-soluble protein. Absorbance was measured at 595 nm by adding 5 µL of salt-soluble fraction and 1 mL of Bradford dye (37).

Hordein

The salt-soluble protein pellet was extracted in 1% acetic acid and 2% β-mercaptoethanol, stirred for 0.5 h at 60°C, centrifuged at 2000 g for 5 min, and repeated three times to extract the hordein fraction. The absorbance was measured by taking 5 µL of supernatant and 1 mL of Bradford dye at 595 nm using a spectrophotometer (37).

Glutelin

The hordein pellet was used to extract glutelin protein fraction by adding 0.05 M sodium borate, 2% β-mercaptoethanol, and 1% sodium dodecyl sulphate (SDS). The mixture was stirred for 30 min and then centrifuged at 2000 g. The supernatant was recovered in fresh tubes three times. The absorbance was measured at 595 nm using a spectrophotometer with 5 µL of supernatant and 1 mL of Bradford dye (37).

Sugar content

Total soluble sugar

TSSs were estimated by the method of Dubois et al. (38). For the determination of TSSs, extraction was performed in 80% ethanol (V/V) and the supernatant was transferred to fresh tubes. A reaction mixture was performed using 100 µL of sample and 3 mL of freshly prepared anthrone reagent in H_2SO_4. The mixture was heated at 97°C for 10 min and then cooled the test tubes in an ice bath. The absorbance was measured at 625 nm using a spectrophotometer.

Reducing and non-reducing sugars

Reducing and non-reducing sugars were determined by the method Miller (39). For the estimation of reducing sugars, 1 g of 3,5-dinitrosalicylic acid (DNS) was mixed in distilled water, followed by 30 g of sodium potassium tartrate tetrahydrate and 20 mL of 2 N NaOH, and the volume was increased to 100 mL. A reaction mixture

TABLE 1 Scale for grouping chickpea genotypes in high, medium, and low categories for seed nutritional and anti-nutritional traits under investigation.

	Parameters	Low	Genotypes	Medium	Genotypes	High	Genotypes
1	**Total soluble proteins (mg/g s .wt)**	14.72–17.88	CM-88 (Desi)	18.88–32.98	CH64/11 (Kabuli)	33.17–34.92	Sheenghar-2000 (Desi)
			CH98/99 (kabuli)		Aug-242 (Desi)		CH61/09 (kabuli)
			ICCV96029 (Desi)		CH74/08 (kabuli)		Noor 2009 (kabuli)
			BKK-2174 (kabuli)		CM877/10 (kabuli)		ILWC-247 (Desi)
			CH54/07 (kabuli)		NIAB-CH2016 (Desi)		CH39/08 (Desi)
			CM3457/91 (Desi)		CH63/11 (kabuli)		CM1235/08 (kabuli)
					Paidar-91 (Desi)		CH28/07 (Desi)
					NIFA-88 (Desi)		Gocke (kabuli)
					NIFA-95 (Desi)		Punjab-2000 (Desi)
					CM2008 (kabuli)		
2	**Crude proteins (%)**	20.97–21.94	CM-2000 (kabuli)	22.50–26.97	Wild Hybrid-3 (Desi)	27.13–30.13	ICCV-96030 (Desi)
			BKK-2174 (kabuli)		Wild Hybrid-16 (Desi)		Wild Hybrid-10 (Desi)
			CH74/10 (kabuli)		Noor 2009 (kabuli)		Wild Hybrid-1 (Desi)
			CM2984/91 (Desi)		Wild Hybrid-11 (Desi)		NIAB-CH104 (Desi)
					Bittle-98 (Desi)		NIAB-CH2016 (Desi)
					CH63/11 (kabuli)		ILWC-247 (Desi)
					CM68/08 (kabuli)		CM3384/00 (Desi)
					CM2008 (kabuli)		Bittle-2016 (Desi)
					CH72/08 (kabuli)		NIFA-95 (Desi)
					Wild Hybrid-8 (Desi)		CM-72 (Desi)
3	**Total free amino acid (%)**	1.62–1.87	Tamaman-13 (kabuli)	2.00–2.97	CM98 (Desi)	3.00–3.34	CM3384/00 (Desi)
			Noor 2013 (kabuli)		CH16/06 (Desi)		CM1681/8 (Desi)
			Wanhar-2000 (Desi)		Wild Hybrid-5 (Desi)		CH61/09 (kabuli)
			Noor 2009 (kabuli)		NIFA-88 (Desi)		CH64/11 (kabuli)
					Punab2008 (Desi)		CH98/99 (kabuli)
					Wild Hybrid-6 (Desi)		Wild Hybrid-15 (Desi)
					CH60/10 (kabuli)		
					Wild Hybrid-9 (Desi)		
					NIAB-CH104 (Desi)		
					Wild Hybrid-4 (Desi)		

(Continued)

10.3389/fnut.2024.1407096

TABLE 1 (Continued)

	Parameters	Low	Genotypes	Medium	Genotypes	High	Genotypes
4	**Albumin (mg/g s .wt)**	11.50–22.67	CM-72 (Desi)	83.33–198.17	CH24/11 (Desi)	201.67–227.67	Thall-2006 (Desi)
			NIFA-88 (Desi)		CH2/11 (Desi)		Punjab-2000 (Desi)
			Paidar-91 (Desi)		CH77/08 (kabuli)		CM2008 (kabuli)
			C-44 (Desi)		CH98/99 (kabuli)		Sheenghar-2000 (Desi)
			ILWC-247 (Desi)		CH28/07 (Desi)		
			CM-2000 (kabuli)		CM68/08 (kabuli)		
					CH49/09 (Desi)		
					ICCV96029 (Desi)		
					CH54/07 (kabuli)		
					CH13/11 (Desi)		
5	**Globulin (mg/g s. wt)**	243.33–399.00	Wild Hybrid-15 (Desi)	400.33–596.00	Punjab-91 (Desi)	674.00–720.00	Wild Hybrid-13 (Desi)
			CH39/08 (Desi)		Parbat 98 (Desi)		ICCV-96030 (Desi)
			CH24/07 (Desi)		CM-72 (Desi)		
			CH74/10 (kabuli)		Wild Hybrid-3 (Desi)		
			CM2008 (kabuli)		Wild Hybrid-1 (Desi)		
			Dashat 98 (Desi)		CH74/08 (kabuli)		
			CH54/07 (kabuli)		Karak-1 (Desi)		
			Punab2008 (Desi)		Noor 2009 (kabuli)		
			CH72/08 (kabuli)		Wild Hybrid-4 (Desi)		
					Balkasar2000 (Desi)		
6	**Salt-soluble protein (mg/g s .wt)**	99.50–120.00	Wild Hybrid-1 (Desi)	120.17–187.67	CM2984/91 (Desi)	191.33–200.00	Wild Hybrid-10 (Desi)
			Noor-91 (kabuli)		CM3384/00 (Desi)		CH35/10 (Desi)
			Sheenghar-2000 (Desi)		CH49/09 (Desi)		Karak-1 (Desi)
			CM1681/8 (Desi)		NIAB-CH2016 (Desi)		CH72/08 (kabuli)
			Wild Hybrid-14 (Desi)		CH28/07 (Desi)		CH98/99 (kabuli)
			CH54/07 (kabuli)		Wild Hybrid-8 (Desi)		ICCV-96030 (Desi)
			CM98 (Desi)		CH55/09 (kabuli)		CH61/09 (kabuli)
			Wild Hybrid-15 (Desi)		Thall-2006 (Desi)		Wild Hybrid-3 (Desi)
			Wild Hybrid-11 (Desi)		CH10/11 (Desi)		Paidar-91 (Desi)
			Punjab-2000 (Desi)		Tamaman-13 (kabuli)		NIFA-88 (Desi)

(Continued)

10.3389/fnut.2024.1407096

TABLE 1 (Continued)

	Parameters	Low	Genotypes	Medium	Genotypes	High	Genotypes
7	**Hordein (mg/g s .wt)**	1.38–6.83	Noor-2013 (kabuli)	10.00–91.33	Sheenghar-2000 (Desi)	99.33–112.36	Noor 2009 (kabuli)
			Wild Hybrid-16 (Desi)		CH54/07 (kabuli)		CH56/09 (kabuli)
			CH28/07 (Desi)		Wanhar-2000 (Desi)		NIAB-CH104 (Desi)
			CM1235/08 (kabuli)		Wild Hybrid-13 (Desi)		
			CH49/09 (Desi)		Balkasar2000 (Desi)		
			CM3444/92 (Desi)		Bhakhar-2011 (Desi)		
			ILWC-247 (Desi)		ICC-4951 (Desi)		
					CH74/08 (kabuli)		
					CH13/11 (Desi)		
					Wild Hybrid-6 (Desi)		
8	**Glutelin (mg/g s .wt)**	3.33–29.33	Wild Hybrid-9 (Desi)	30.00–148.67	ILWC-247 (Desi)	154.00–203.33	CH55/09 (kabuli)
			CH49/09 (Desi)		Wild Hybrid-2 (Desi)		Wild Hybrid-1 (Desi)
			CM1051/11 (Desi)		CH56/09 (kabuli)		CH60/10 (kabuli)
			CH28/07 (Desi)		C-44 (Desi)		Noor 2009 (kabuli)
			CH35/10 (Desi)		CH74/08 (kabuli)		Wanhar-2000 (Desi)
			Noor-91 (kabuli)		CH32/10 (Desi)		CH16/06 (Desi)
			CH72/08 (kabuli)		CH40/09 (Desi)		
			Wild Hybrid-16 (Desi)		CH74/10 (kabuli)		
			NIAB-CH2016 (Desi)		CH24/11 (Desi)		
			Wild Hybrid-14 (Desi)		CM68/08 (kabuli)		
9	**Total soluble sugars (mg/g. s .wt)**	77.98–86.80	Paidar-91 (Desi)	87.23–100.84	CM2984/91 (Desi)	101.24–102.63	CH13/11 (Desi)
			Wild Hybrid-11 (Desi)		Wild Hybrid-4 (Desi)		Wild Hybrid-16 (Desi)
			CM-72 (Desi)		CH28/07 (Desi)		CH35/10 (Desi)
			CH16/06 (Desi)		Punab2008 (Desi)		ICCV-96030 (Desi)
			Noor 2009 (kabuli)		Bhakhar-2011 (Desi)		Wild Hybrid-14 (Desi)
			Wild Hybrid-5 (Desi)		Punjab-91 (Desi)		CH39/08 (Desi)
			Wild Hybrid-6 (Desi)		Wild Hybrid-1 (Desi)		CH61/09 (kabuli)
			Noor 2013 (kabuli)		Karak-2 (Desi)		CM1051/11 (Desi)
					Wild Hybrid-8 (Desi)		
					CM3457/91 (Desi)		

(Continued)

10.3389/fnut.2024.1407096

TABLE 1 (Continued)

	Parameters	Low	Genotypes	Medium	Genotypes	High	Genotypes
10	**Non-reducing sugars (mg/g. s .wt)**	64.62–76.73	Paidar-91 (Desi)	77.11–91.95	Punab2008 (Desi)	92.17–95.28	CM1235/08 (kabuli)
			CH28/07 (Desi)		Wild Hybrid-9 (Desi)		CH35/10 (Desi)
			Wild Hybrid-4 (Desi)		Noor 2009 (kabuli)		CH32/10 (Desi)
			Punjab-2000 (Desi)		Tamaman-13 (kabuli)		Parbat 98 (Desi)
					CH54/07 (kabuli)		CM1051/11 (Desi)
					Noor 2013 (kabuli)		Bittle-98 (Desi)
					CM-72 (Desi)		NIAB-CH2016 (Desi)
					Wild Hybrid-11 (Desi)		
					Wild Hybrid-6 (Desi)		
					CH16/06 (Desi)		
11	**Reducing sugars (mg/g.s .wt)**	3.59–4.59	Wild Hybrid-1 (Desi)	5.10–11.93	Wild Hybrid-10 (Desi)	12.39–17.33	CH2/11 (Desi)
			Wild Hybrid-12 (Desi)		Dashat 98 (Desi)		CH61/09 (kabuli)
			Wild Hybrid-2 (Desi)		C-44 (Desi)		CH39/08 (Desi)
			Punjab-91 (Desi)		CM2984/91 (Desi)		Paidar-91 (Desi)
			Wild Hybrid-5 (Desi)		NIFA-95 (Desi)		CH39/11 (Desi)
			Bhakhar-2011 (Desi)		Wild Hybrid-6 (Desi)		CH28/07 (Desi)
			Thall-2006 (Desi)		Wanhar-2000 (Desi)		Wild Hybrid-15 (Desi)
			Balkasar2000 (Desi)		CM3444/92 (Desi)		Punjab-2000 (Desi)
			CH64/11 (kabuli)		NIAB-CH2016 (Desi)		
			CH16/06 (Desi)		Parbat 98 (Desi)		
12	**Starch (%)**	14.13–18.15	Wild Hybrid-6 (Desi)	19.25–69.40	Wild Hybrid-4 (Desi)	70.54–83.69	Tamaman-13 (kabuli)
			Wild Hybrid-11 (Desi)		CM98 (Desi)		CH54/07 (kabuli)
			Thall-2006 (Desi)		CH77/08 (kabuli)		Wild Hybrid-15 (Desi)
			C-44 (Desi)		CM2008 (kabuli)		CH39/08 (Desi)
			Wild Hybrid-10 (Desi)		Wild Hybrid-8 (Desi)		CM407/13 (Desi)
					CM2984/91 (Desi)		BKK-2174 (kabuli)
					Wild Hybrid-5 (Desi)		ICC-4951 (Desi)
					Wild Hybrid-14 (Desi)		CH40/09 (Desi)
					CM-72 (Desi)		CH32/10 (Desi)

(Continued)

10.3389/fnut.2024.1407096

TABLE 1 (Continued)

	Parameters	Low	Genotypes	Medium	Genotypes	High	Genotypes
					Karak-2 (Desi)		CH63/11 (kabuli)
13	**Tannins (uM/g. s .wt)**	5,425–5,925	CM2008 (kabuli)	6,250–8,900	CH54/07 (kabuli)	9,050–13,775	CH74/08 (kabuli)
			NIAB-CH2016 (Desi)		Karak-2 (Desi)		CM877/10 (kabuli)
			CH98/99 (kabuli)		CH56/09 (kabuli)		CH28/07 (Desi)
			CM1235/08 (kabuli)		C-44 (Desi)		NIFA-95 (Desi)
			Dashat 98 (Desi)		CH24/11 (Desi)		Wild Hybrid-5 (Desi)
			CM3457/91 (Desi)		CH13/11 (Desi)		CH35/10 (Desi)
			Karak-1 (Desi)		Punjab-91 (Desi)		Wild Hybrid-4 (Desi)
			Thall-2006 (Desi)		CM68/08 (kabuli)		Wild Hybrid-9 (Desi)
			CH16/06 (Desi)		CH2/11 (Desi)		Wild Hybrid-7 (Desi)
			CM-88 (Desi)		ICC-4951 (Desi)		Wild Hybrid-3 (Desi)
14	**Phytic acid (mg/g s. wt)**	0.18–1.92	Bhakhar-2011 (Desi)	2.02–3.96	Wild Hybrid-11 (Desi)	4.06–6.42	CH32/10 (Desi)
			ICCV-96030 (Desi)		Wild Hybrid-4 (Desi)		CM3384/00 (Desi)
			CM1681/8 (Desi)		Wanhar-2000 (Desi)		Wild Hybrid-8 (Desi)
			NIAB-CH104 (Desi)		Bittle-2016 (Desi)		CH60/10 (kabuli)
			Wild Hybrid-7 (Desi)		Karak-2 (Desi)		CH72/08 (kabuli)
					Noor 2009 (kabuli)		CH64/11 (kabuli)
					Wild Hybrid-2 (Desi)		CH74/08 (kabuli)
					BKK-2174 (kabuli)		CM877/10 (kabuli)
					CH77/08 (kabuli)		CM3457/91 (Desi)
					Wild Hybrid-5 (Desi)		Noor 2013 (kabuli)

10.3389/fnut.2024.1407096

was prepared with 200 µL of the extracted sample, 1 mL of DNS, and 1.8 mL of distilled water. Then, set it in a water bath for 15 min, cool to room temperature, and dilute with 9 mL of distilled water. The absorbance was measured at 540 nm using a spectrophotometer. Non-reducing sugars were calculated by the difference between total sugar and reducing sugars.

Starch content

The starch content of chickpea seed flour was determined according to the method of Malik and Srivastava (40). The fine ground seed sample (0.1 g) was extracted with 80% ethanol and centrifuged at 2900 rpm. In this method, 52% perchloric acid and anthrone solution were used, with absorbance measured at 625 nm.

Total free amino acid (TFA)

Sample preparation

For the determination of TFAs, a 0.5 g of sample was weighed for all genotypes and dissolved in 10 mL of phosphate buffer (pH 7.0, 0.02 M) in 90 different tubes. The phosphate buffer (0.02 M) with pH 7.0 was prepared by adding K_2HPO_4 and KH_2PO_4 and increasing the volume to 800 mL. The pH was adjusted to 7 using di-sodium hydrogen phosphate dihydrate.

Assay

TFAs were determined as per Hamilton and Van Slyke (41) method. The reaction mixture was prepared by adding 1 mL of sample extract, 1 mL of 2% ninhydrin, and 1 mL of 10% pyridine solution in test tubes. This mixture was heated at 97°C for 30 min in a water bath. The samples were cooled and diluted by adding 5 mL of distilled water to each test tube. The absorbance of the colored solution was measured at 570 nm using a spectrophotometer (Hitachi, 220, Japan). The TFAs were calculated by using the following formula:

$$\text{Total amino acids}\left(\mu g\ \text{g}-1\ \text{fresh wt}\right) = \frac{\text{Sample reading} \times \text{sample volume} \times \text{diluton factor}}{\text{Sample weight} \times 1000} \times 100$$

Anti-nutritional parameters

Tannins

A microcolorimetric method (42) was used to measure tannins by using the Folin–Ciocalteu (F–C) reagent. A measure of 0.05 g of seed samples was treated in 500 µL of 95% methanol. The samples were then incubated for 48 h at room temperature in the darkness. Following incubation, samples were centrifuged at 14,462 g for 5 min at room temperature. The supernatant was collected after centrifugation and mixed with 100 µL of supernatant with 100 µL of 10% (v/v) F–C reagent, then vortexed thoroughly, and then 800 µL of 700 mM Na_2CO_3 was added. The mixture was then placed in an incubator for 1 h. To measure tannin (0.1 g), PVPP was added to the above-prepared mixture, vortexed vigorously, and centrifuged again at 14000 g and then the absorbance was measured at 765 nm.

Phytic acid

Phytic acid phosphorus is determined by the modified colorimetric method described in Dhole and Reddy (43). For the estimation of phytin phosphorus, seed flour (0.05 g) was extracted in a 2.4% HCl solution, placed overnight on the shaker, centrifuged at 10,000 rpm, and the supernatant was transferred to tubes having NaCl. Salt was dissolved and incubated at-20°C for 20 min to precipitate the remaining matrix, which could interfere with the colorimetric reaction. The reaction mixture was prepared by combining 750 µL of diluted supernatant and 250 µL of modified Wade's reagent (prepared by mixing 0.03% of $FeCl_3$ and 0.3% of sulfosalicylic acid). Record the absorbance of a color reaction in a spectrophotometer at a 500 nm wavelength. The standard for sodium phytate was prepared in the range of 3–30 µg/mL.

Statistical analysis

Statistical analysis was performed using XL-STAT software version 2014.1.02 (Copyright Addinsoft 1995–2012). To analyze and organize the resulting data, descriptive statistics were applied. Data were subjected to analysis of variance (ANOVA) with three replications. Tukey HSD test at a p-value of <0.05, and ANOVA was used to test the significance of the data. In the graphs, the values presented are mean ± SE. Mean data for all the traits under study was subjected to PCA. Genotype by trait biplots was created by using the first two principle components, i.e., PC-I and PC-II. Cluster analysis through agglomerative hierarchical clustering and correlation (Pearson's test) was also used for nutritional and anti-nutritional constituents by using the same software.

Results

Total soluble protein (TSP)

Based on the observed differences in TSPs, desi and kabuli genotypes were assembled into three distinct groups, i.e., low, medium, and high (Table 1). In the low category, six genotypes (three kabuli and three desi types) were placed with TSP ranging from 14.72 to 17.88 g/100 g s. wt. The low category comprised 13% of kabuli and 5% of desi type of the total genotypes under investigation. The lowest value of TSP (14.72 ± 1.033 g/100 g s. wt.) was found in desi-type CM-88. Out of all tested genotypes, 75 (17 kabuli and 58 desi) genotypes were grouped in the intermediate category, with values ranging from 18.08 to 32.98 g/100 g s. wt. In this class, 70% of the genotypes were of the kabuli type, and 89% were of the desi type. In the high category, nine genotypes (4 kabuli and 5 desi) were grouped with TSP values ranging from 33.17 to 34.92 g/100 g s. wt., containing 17% kabuli and 8% desi type (Supplementary Figure S1). However, among all the tested genotypes, Punjab-2000 (desi type) depicted the highest value (34.92 ± 0.45 g/100 g s. wt.), followed by Gocke (kabuli) and the average value was 27.26 g/100 g s. wt. (Table 2).

TABLE 2 Average and range values for different studied parameters in respective desi and kabuli chickpea genotypes.

Sr#	Parameters	Range	Average	Genotype (Min value)	Genotype (Max value)
(I) Nutritional components					
1	Total soluble proteins (g/100 s. wt.)	14.72–34.92	27.26	CM-88 (D)	Punjab-2000 (D)
2	Crude proteins (g/100 g s. wt.)	20.97–30.13	24.89	CM-2000 (K)	Punjab-2000 (D)
3	Total free amino acid (g/100 g)	1.62–3.34	2.54	Tamaman-13 (K)	Wild Hybrid-15 (D)
4	Albumins (mg/g s. wt.)	11.50–227.67	139.55	CM-72 (D)	Sheenghar-2000 (D)
5	Globulins (mg/g s. wt.)	243.33–720.00	474.76	Wild Hybrid-15 (D)	ICCV-96030 (D)
6	Salt-soluble proteins (mg/g s. wt.)	99.50–200.00	150.75	Wild Hybrid-1 (D)	ILWC-247 (D)
7	Hordein (mg/g s. wt.)	1.38–112.36	38.98	Noor-2013 (K)	NIAB-CH104 (D)
8	Glutelin (mg/g s. wt)	3.33–203.33	76.49	Wild Hybrid-9 (D)	CH16/06 (D)
9	Total soluble sugars (mg/g s. wt.)	77.97–102.63	93.99	Paidar-91 (D)	CM1051/11 (D)
10	Non-reducing sugars (mg/g s. wt.)	64.61–95.28	85.95	Paidar-91 (D)	NIAB-CH2016 (D)
11	Reducing sugars (mg/g s. wt.)	3.59–17.33	8.04	Wild Hybrid-1 (D)	Punjab-2000 (D)
12	Starch content (%)	14.13–83.69	46.71	Wild Hybrid-6 (D)	CH55/09 (K)
(II) Anti-nutritional components					
13	Tannins (uM /g s. wt.)	5,425–13,775	7382.22	Wild Hybrid-1 (D)	Wild Hybrid-3 (D)
14	Phytic acid (mg/g s. wt.)	0.18–6.42	3.28	Bhakhar-2011 (D)	Tamaman-13 (K)

*D, Desi; K, Kabuli.

Crude protein (CP)

A significant variation in seed CP content provided the basis for the classification of tested genotypes into low, medium, and high categories (Table 1). The low category consisted of four genotypes (3 kabuli and 1 desi), which accounted for 13% of the kabuli type and 2% of the desi-type genotypes used in the study. However, among these genotypes, the one with the least CP content was identified in a kabuli genotype, specifically CM-2000, with a value of 20.97 ± 0.031 g/100 g DW. The medium category consisted of 72 genotypes, with a CPCP value ranging from 22.50 to 26.97 g/100 g DW. Within this category, 15 (77%) of the genotypes belonged to the desi type, while 21 (87%) were of the kabuli type. In the high category, a total of 14 genotypes (21%) were grouped, all of which belonged to the desi type. These genotypes exhibited a CP value ranging from 27.13 to 30.13 g/100 g DW. Remarkably, the desi genotype Punjab-2000 had the highest CP content, with a value of 30.13 ± 0.063 g/100 g DW. On the whole, the average value of CP was 24.89 g/100 g DW (Table 2).

Total free amino acid (TFA)

Based on the observed differences in seed TFAs, desi and kabuli genotypes were assembled into three distinct groups, i.e., low, medium, and high (Table 1). In the high category, there were six genotypes grouped with values ranging from 3.00 to 3.34 g/100 g DW. In the high category, 4% of genotypes belong to the desi type and 12% were of the kabuli type. In general, the highest 'TFA' content (3.34 ± 0.043 g/100 g DW) was detected in a desi type, i.e., Wild Hybrid-15 (Supplementary Figure S3). In the medium category, 86 genotypes with 'TFA' values ranging from 2.00 to 2.97 g/100 g DW were grouped. Among these, 94% of genotypes belonged to the desi type and 75% were of the kabuli type. In the low category, four genotypes were placed, with values ranging from 1.62 to 1.87 g/100 g DW. The low category represented 13% of the kabuli type and 2% of desi-type genotypes, while the least 'TFA' content with a value of 1.62 ± 0.004 g/100 g DW was detected in a kabuli genotype, i.e., Tamaman-13, and the overall average of TFAs was 2.54 g/100 g DW (Table 2).

Differential protein estimation

Albumins

Based on the observed differences in hordein content, desi and kabuli genotypes were arranged into three classes, i.e., low, medium, and high (Table 1). In the low category, six genotypes were placed with albumin content ranging from 11.50 to 22.67 mg/g s. wt. Among these genotypes, 8% were of desi type and 4% were of kabuli type. The lowest value of albumin (11.50 ± 0.500 mg/g s. wt.) was found in desi-type CM-72. Out of all tested genotypes, 80 genotypes were grouped in the intermediate category with a value ranging from 83.33 to 198.167 mg/g s. wt. In this class, 92% of the genotypes were of the kabuli type and 88% were of the desi type. In the high category, four genotypes were grouped with values ranging from 201.66 to 227.66 mg/g s. wt. Among these genotypes, 4% were of kabuli type and 4% were of desi type (Supplementary Figure S4). However, among all the tested genotypes, sheenghar-2000 (desi type) showed the highest value (227.67 ± 1.333 mg/g s. wt.) for seed albumin content and the average value was 139.55 mg/g s. wt. (Table 2).

Globulins

A significant variation in seed globulins provided the base for the categorization of tested genotypes in low, medium, and high groups (Table 1). In the high category, there were two genotypes grouped with values ranging from 674 to 720 mg/g s. wt., and both were of desi type, accounting for 3% of total desi-type genotypes used in the study (Supplementary Figure S5). The highest seed globulins (720 ± 4.66 mg/g s. wt.) were observed in a desi type, i.e., ICCV-96030. In the intermediate category, 79 genotypes with globulins ranged from 400.33 to 596 mg/g s. wt. were categorized. Among these, 83% of genotypes belonged to the kabuli type and 89% were of the desi type. In the low category, nine genotypes were found, with values ranging from 243.33 to 399 mg/g s. wt. In the low category, 8% desi-type and 17% of kabuli-type genotypes were grouped. However, the lowest globulins with a value (243.33 ± 1.66 mg/g s. wt.) were detected in a desi-type genotype, i.e., wild hybrid-15, and the average value was 474.76 mg/g s. wt. (Table 2).

Salt-soluble proteins

Based on the observed differences in the studied parameters, desi and kabuli genotypes were placed into three sets, i.e., low, medium, and high (Table 1). In the low category, 18 genotypes were placed with salt-soluble proteins ranging from 99.50 to 120 mg/g s. wt. Among these genotypes, 21% were of desi type and 17% were of the kabuli type. The lowest value of salt-soluble protein (99.50 ± 3 mg/g s. wt.) was found in desi-type Wild Hybrid-1. Out of all tested genotypes, 61 genotypes were grouped in the intermediate category with a value ranging from 120.167 to 187.67 mg/g s. wt. In this class, 71% of the genotypes were of the kabuli type and 67% were of the desi type. In the high category, 11 genotypes were grouped with values ranging from 191.33 to 200 mg/g s. wt. Among these genotypes, 12% were of kabuli type and 12% were of desi type (Supplementary Figure S6). However, among all the tested genotypes, ILWC-247 (desi type) showed the highest value (200.00 ± 6.33 mg/g s. wt.) for seed salt-soluble proteins, and the overall average value was 150.75 mg/g s. wt. (Table 2).

Hordein

A significant variation in seed Hordein provided the basis for the categorization of tested genotypes in low, medium, and high groups (Table 1). In the high category, there were three genotypes grouped with values ranging from 132.33 to 236.33 mg/g s. wt. Among these two genotypes, one belongs to the kabuli type and the other belongs to the desi type, accounting for 2% of the desi type and 8% of the kabuli genotypes used in the study (Figure 3) 0.27. The highest seed hordein content (236.33 ± 9 mg/g s. wt.) was observed in a desi type, i.e., NIAB-CH104. In the intermediate category, 80 genotypes with hordein values ranging from 10 to 91.33 (mg/g s. wt.) were grouped. Among these, 84% of genotypes belonged to the kabuli type and 90% were of the desi type. In the low category, seven genotypes were found, with values ranging from 1.38 to 6.83 mg/g s. wt. (Supplementary Figure S7). In the low category, 8% of desi-type and 8% of kabuli-type genotypes were grouped. However, the lowest hordein protein content with a value of 1.38 ± 0.027 mg/g s. wt. was detected in a kabuli type genotype, i.e., Noor 2013, the overall average value was 38.98 mg/g s. wt. (Table 2).

Glutelin

Based on the observed differences in glutelin content, desi and kabuli genotypes were arranged into three categories, i.e., low, medium, and high (Table 1). In the low category, 16 genotypes were placed with glutelin content ranging from 3.33 to 29.33 mg/g s. wt. Among these genotypes, 17% were of desi type and 21% were of kabuli type. The lowest value of glutelin (3.33 ± 0.67 mg/g s. wt.) was found in desi-type Wild Hbrid-9. Out of all tested genotypes, 69 genotypes were grouped in the intermediate category with a value ranging from 30 to 148.67 mg/g s. wt. In this class, 67% of the genotypes were of the kabuli type and 79% were of the desi type. In the high category, six genotypes were grouped with values ranging from 154 to 203.33 mg/g s. wt. Among these genotypes, 12% were of kabuli type and 4% were of desi type (Supplementary Figure S8). However, among all the tested genotypes, CH16/06 (desi type) showed the highest value (203.33 ± 4 mg/g s. wt.) for seed glutelin content, and the overall average value was 76.49 mg/g s. wt. (Table 2).

Sugar contents

Total soluble sugars (TSS)

Based on the observed differences in the studied parameter, desi and kabuli genotypes were assembled into three groups, i.e., low, medium, and high (Table 1). In the low category, 13 genotypes were placed with TSSs ranging from 77.97 to 87.91 mg/g s. wt. Among these genotypes, 17% were of desi type and 8% were of kabuli type. The lowest value of TSS (77.97 ± 0.004 mg/g s. wt.) was found in desi-type Paidar-91. Out of all tested genotypes, 64 genotypes were grouped in the intermediate category with a value ranging from 88.034 to 99.72 mg/g s. wt. In this class, 79% of the genotypes were of the kabuli type and 68% were of the desi type. In the high category, 13 genotypes were grouped with values ranging from 100.41 to 102.63 mg/g s. wt. Among these genotypes, 13% were of kabuli type and 15% were of desi type (Supplementary Figure S9). However, among all the tested genotypes, CM1051/11 (desi type) depicted the highest value (102.63 ± 0.005 mg/g s. wt.) for seed TTS, while the overall observed average value was 93.99 mg/g s. wt. (Table 2).

Non-reducing sugars (NRS)

A significant variation in seed non-reducing sugars (NRS) provided the base for the categorization of tested genotypes in low, medium, and high groups (Table 1). In the high category, there were seven genotypes grouped with values ranging from 92.16 to 95.28 mg/g s. wt. Among these, one genotype belongs to the kabuli type and six were of the desi type, accounting for 9% of desi and 4% of kabuli genotypes used in the study (Supplementary Figure S10). The highest seed NRS (95.28 ± 0.013 mg/g s. wt.) was detected in a desi type, i.e., NIAB-CH2016. In the intermediate category, 79 genotypes with NRS values ranging from 77.11 to 91.95 mg/g s wt. were grouped. Among these, 96% of genotypes belonged to the kabuli type and 85% were of the desi type. In the low category, 13 genotypes

were placed, with values ranging from 64.61 to 76.73 mg/g s. wt. In the low category, 17% desi-type and 8% of kabuli-type genotypes were grouped. However, the lowest NRS with a value (64.61 ± 0.015 mg/g s. wt.) was detected in a desi-type genotype, i.e., Paidar-91, and the overall average value of NRS was 85.95 mg/g s. wt., illustrated in Table 2.

Reducing sugars (RS)

Based on the observed differences in the studied parameter, desi and kabuli genotypes were organized into three sections, i.e., low, medium, and high (Table 1). In the low category, 13 genotypes were placed with reducing sugars (RS) ranging from 3.59 to 4.58 mg/g s. wt. Among these genotypes, 15% were of desi type and 4% were of kabuli type. The lowest value of RS (3.59 ± 0.008 mg/g s. wt.) was found in desi-type Wild Hybrid-1. Out of all tested genotypes, 71 genotypes were grouped in the intermediate category with a value ranging from 5.09 to 11.93 mg/g s. wt. In this group, 92% of the genotypes were of kabuli type and 74% were of desi type. In the high category, eight genotypes were placed with values ranging from 12.38 to 17.33 mg/g s. wt. Among these genotypes, 4% were of kabuli type and 11% were of desi type (Supplementary Figure S11). However, among all the tested genotypes, Punjab-2000 (desi type) depicted the highest value (17.33 ± 0.100 mg/g s. wt.) for seed RS. On the whole, the average value of RS was 8.04 mg/g s. wt. (Table 2).

Starch content

A significant variation in seed starch content provided the basis for the categorization of tested genotypes in low, medium, and high groups (Table 1). In the high category, there were 16 genotypes grouped with values ranging from 70.53 to 83.69%. Among these, 25% were of kabuli type and desi type, accounting for 15% of the total desi-type genotypes used in the study (Supplementary Figure S12). The highest seed starch content (83.69 ± 0.50%) was observed in a kabuli-type genotype, i.e., CH55/09. In the intermediate category, 69 genotypes with starch values ranging from 19.25 to 69.40% were grouped. Among these, 75% of genotypes belonged to the kabuli type and 77% were of the desi type. In the low category, five genotypes were found, with values ranging from 14.13 to 18.15%, all were of desi type, accounting for 8% of desi genotypes used in the study. On the whole, the lowest starch content (14.13 ± 0.019%) was observed in desi type, i.e., Wild Hybrid-6, and the overall average value of starch was 46.71% (Table 2).

Anti-nutritional parameters

Tannins

Based on the observed differences in the studied parameter, desi and kabuli genotypes were placed into three sets, i.e., low, medium, and high (Table 1). In the low category, 12 genotypes were placed with Tannins ranging from 5,425 to 5,925 uM /g s. wt. Among these genotypes, 12% were of desi type and 17% were of kabuli type. The lowest value of Tannins (5,425 ± 25 uM /g s. wt.) was found in desi-type Wild Hybrid-1. Out of all tested genotypes, 68 genotypes were grouped in the intermediate category with a value ranging from 6,250 to 8,900 uM /g s. wt. In this group, 75% of the genotypes were of the kabuli type and 76% were of the desi type. In the high category, 10 genotypes were placed with values ranging from 9,050 to 13,775 uM /g s. wt. Among these genotypes, 8% were of kabuli type and 12% were of desi type (Supplementary Figure S13). However, among all the tested genotypes, Wild Hybrid-3 (desi type) depicted the highest value (13,775 ± 425 uM /g s. wt.) for seed Tannins. On the whole, 7382.22 uM/g s. wt., Tannins were found in genetic resources under investigation (Table 2).

Phytic acid (PA)

A significant variation in seed PA content provided the base for the categorization of tested genotypes in low, medium, and high groups (Table 1). In the high category, there were 21 genotypes grouped with values ranging from 4.06 to 6.42 mg/g s. wt. In the high category, 21% of desi-type and 29% of kabuli-type genotypes were grouped (Supplementary Figure S14). Overall, the highest seed PA content (6.42 ± 0.29 mg/g s. wt.) was detected in a Kabuli type, i.e., Tamaman-13. In the intermediate category, 64 genotypes with PA values ranging from 2.02 to 3.96 mg/g s. wt. were grouped. Among these, 71% of genotypes belonged to the kabuli type and 71% were of the desi type. In the low category, five genotypes were placed, with values ranging from 0.18 to 1.92 mg/g s. wt. In the low category, all the genotypes were of desi type, accounting for 8% of desi genotypes used in the present study. However, the lowest PA with value (0.18 ± 0.015 mg/g s. wt.) was detected in a desi-type genotype, i.e., Bhakhar-2011. The overall average value of PA was 3.28 mg/g s. wt. (Table 2).

Agglomerative hierarchical clustering analysis

Data for 14 nutritional and anti-nutritional traits along with experimental genotypes were subjected to agglomerative hierarchal cluster analysis, and a dendrogram was generated to visually inspect the clusters of genotypes. Cluster analysis cleaved 90 genotypes (desi, kabuli) into three distinct groups shown in Figure 1. Cluster I encompassed the genotypes with high mean values of CP contents, albumins, hordein, and glutelin. Cluster II contained the genotypes with high mean values of TSPs, TSSs, non-reducing sugars, globulins, salt-soluble proteins, starch, and TFAs. The genotypes with high mean values of tannins, reducing sugars, and PA were assembled in Cluster III (Table 3). The composition of clusters demonstrated that the largest cluster was II, which contained 38 genotypes, including 25 (38%) desi and 13 (54%) kabuli type, followed by Cluster I, which retained 28 genotypes consisting of 25 (38%) desi and 3 (13%) of kabuli type. Cluster III acquired 24 genotypes, including 16 (24%) desi and 8 (33%) kabuli type (Table 4).

Principal component analysis (PCA)

Seed nutritional and anti-nutritional properties

PCA is a non-parametric, simple method for mining imperative information related to confusing data sets. In the present investigation, PCA analysis was conducted for 14 seed nutritional and

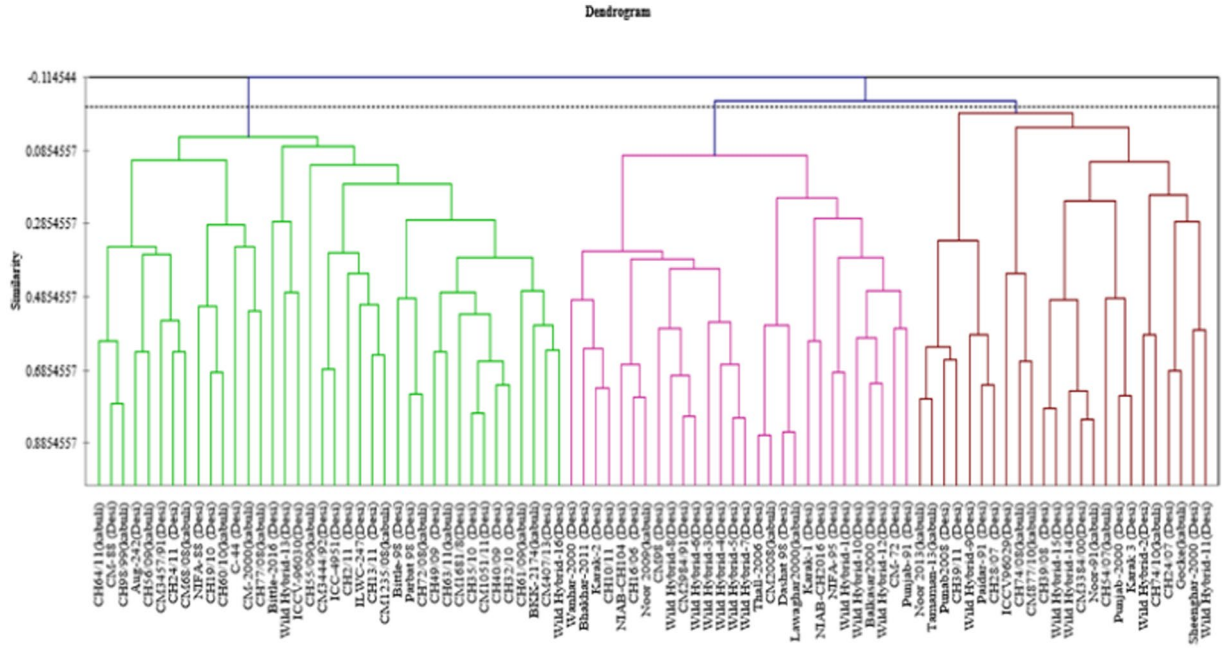

FIGURE 1
Tree diagram based on seed nutritional and anti-nutritional constituents for chickpea genotypes used in study.

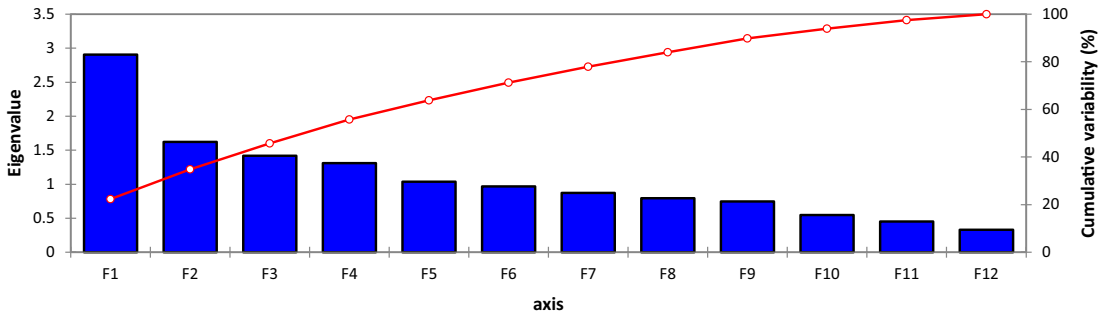

FIGURE 2
Scree plot of seed nutritional and anti-nutritional attributes representing variability.

anti-nutritional traits of chickpea seeds. The objective of PCA is to pinpoint the minimum possible number of principal components, which can elucidate the maximum variation based on the PC scores.

A scree plot was also created, which is a graphical approach to anticipate the extent of the variability accompanying each one of the components extracted in a PCA (Figure 2). Out of 13 Principal component (PCs), only 6 PCs presented more than 1.0 Eigenvalue; consequently, these 6 PCs were given due importance in the present study for further explanation because the remaining PCs were not contributing significant variations (Table 4). Individually, PC-I rendered 20.83% of the cumulative variability, while PC-II, PC-III, PC-IV, PC-V, and PC-VI elucidated 11.82, 10.24, 9.52, 8.22, and 7.35% of the variability, respectively. Cumulatively, these six PCs described 68.01% of the total variability among the traits. PC-I showed positive factor loading with 10 traits including tannins, TSPs, CPs, TSSs, non-reducing sugars, reducing sugars, globulins, PA, starch, and TFAs, while the maximum contribution was delivered by TSSs (0.859), followed by starch content (0.729). It was observed that in PC-I, positive factor loading (0.072) was given by kabuli-type genotypes, while desi types showed negative factor loading (−0.072). In the case of PC-II, eight parameters represented positive factor loading, which was TSSs, non-reducing sugars, albumins, globulins, salt-soluble proteins, hordein, glutelin, and TFAs, while maximum contribution was rendered by non-reducing sugars (0.733), followed by TSSs (0.299) and anti-nutritional traits such as tannins and PA negative factor loading. It was observed that in PC-II positive factor loading (0.067) was given by the kabuli type, while desi types showed negative factor loading (−0.065). PC-III revealed positive factor loading with nine traits, including tannins, TSPs, CPs, reducing sugars, globulins, salt-soluble proteins, hordein, glutelin, and starch; however, the highest positive contribution was given by salt-soluble proteins (0.693), followed by globulin (0.433). In the case of PC-IV 8 traits showed positive factor loading, which were tannins, TSPs, TSSs, non-reducing sugars, reducing sugars, albumins, globulins, and

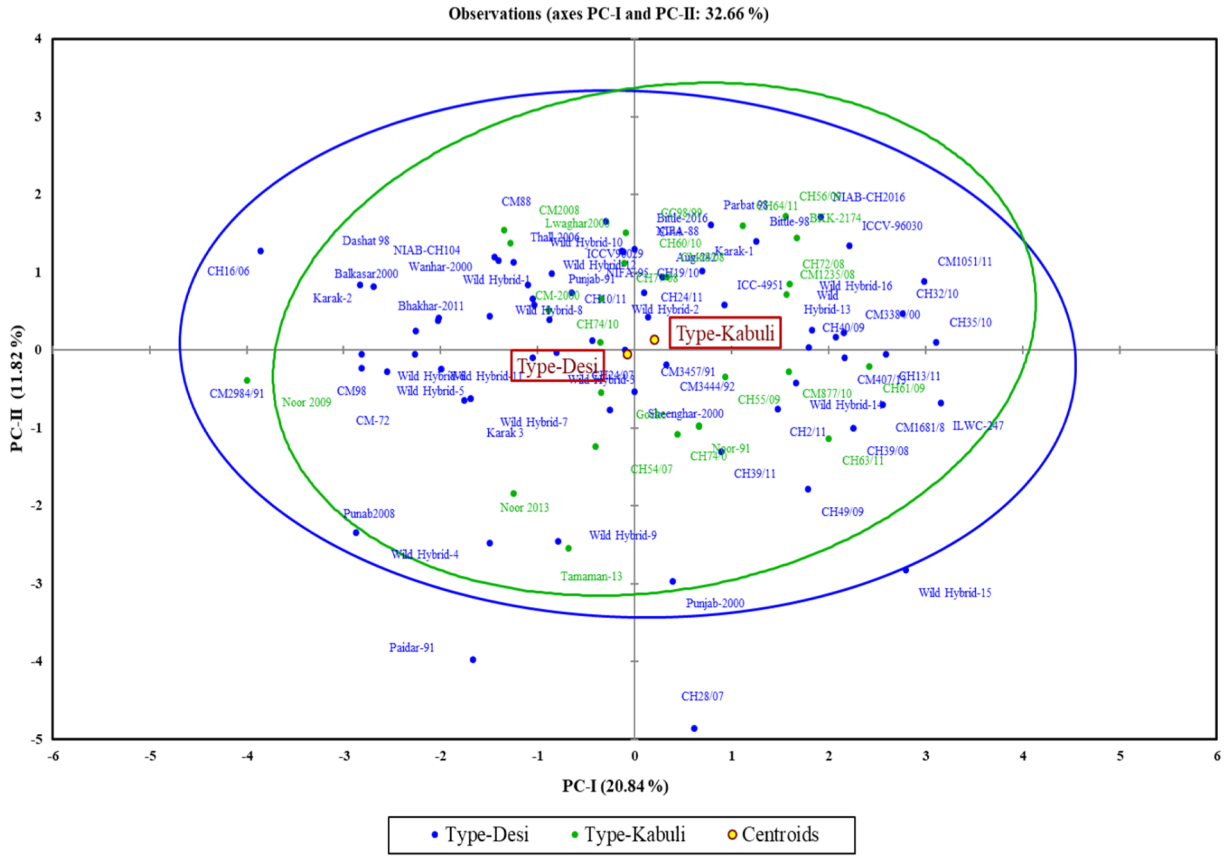

FIGURE 3
Distribution of desi and kabuli genotypes in biplot for first two principal components.

hordein; remaining traits denoted negative factor loading; however, maximum participation was given by albumins (0.626), followed by tannins (0.471). In PC-V, positive factor loading was shown by 10 traits, including TSPs, CPs, non-reducing sugars, TSSs, albumins, globulins, salt-soluble proteins, glutelin, starch, and PA; however, the highest positive factor loading was given by TSPs (0.636), followed by PA (0.322). In the case of Cluster VI, positive factor loading was given by eight traits, including CPs, TSSs, reducing sugars, albumins, globulins, hordein, glutelin, and TFAs; moreover, maximum participation was given by CPs (0.839), followed by albumins (0.301) (Supplementary Table S1). To study the interaction between genotypes and traits under investigation, a genotype-by-trait biplot was created.

The first two principal components (PC-I and PC-II), which accounted for 32.66% of the total variability, were used for the construction of a genotype by trait biplot. In the biplot, along the x-axis, the PC-I score was plotted, and along the *y*-axis, the PC-II score was plotted along with all experimental genotypes. To understand the interrelationship of studied traits, a vector line for all traits is drawn from the origin. The knowledge about the angles between the trait vectors is deployed for interpreting the relationship of traits. An angle of 180 degrees denotes a negative connection, an angle of 90 degrees indicates a weak correlation, and a smaller angle indicates a stronger positive correlation. Through this approach, we were able to group accessions according to their relationships and defining traits.

The polygon view of the biplot assisted in recognizing the genotypes with high positive or negative values for one or more traits (Figure 3). Additionally, it was observed that the desi and kabuli genotypes were widely dispersed across all four quadrants, indicating significant genetic divergence for the traits under investigation (Figure 4).

In the PCA biplot, desi and kabuli genotypes located at or near the vertices of the polygon demonstrate significant factor scores. For PC-I, genotypes such as CH35/10, ILWC-247, Wild Hybrid-15, CH1051/11, ICCV-96030, and CH56/09 exhibited high positive factor scores. Conversely, genotypes such as Noor 2009, CH16/06, Wild Hybrid-4, Paidar-91, and Lawaghar show negative factor scores. Similarly, for PC-II, genotypes such as CM-88, Parbat 98, C-44, CH16/06, NIAB-CH2016, ICCV-98030, and CC98/99 have high positive scores. In contrast, genotypes including CH28/07, Paidar-91, CH28/07, WH-4, WH-9, and Noor-91 display negative factor scores. Furthermore, genotypes far from the origin demonstrated more variability for traits under study. While those are near each other, the origin of the biplot can be considered as genotypes with little or no variations concerning traits under investigation.

Correlation matrix

The correlation coefficient was carried out to retrieve information about the relationship between the traits under

10.3389/fnut.2024.1407096

investigation (Figure 5). Tannins, TSPs, and CP content represented no significant correlation with all other traits. TSSs depicted a significant positive correlation with non-reducing sugars, reducing sugars, PA, starch content, and TFAs; however, it revealed a significant negative correlation with gluten. Non-reducing sugars showed a significant positive association with TSSs and TFAs, while they had a significant negative association with reducing sugars. Reducing sugars had a significant positive correlation with TSSs and starch content, though it negatively correlated with non-reducing sugars and gluten content. A significant negative correlation was observed between albumin and salt-soluble proteins; however, a significant positive correlation was found between globulins and starch content. Salt-soluble protein revealed a significant negative correlation with albumin content, while a significant negative correlation was found between hordein and PA. Gluten content exhibited a significant negative association with TSSs, reducing sugars, PA, starch content, and TFAs. PA revealed a significant positive correlation with TSSs, and it had a significant negative association with hordein and gluten content. A significant positive association was revealed by starch content with TSSs, reducing sugars, globulins, and TFAs, while it had a significant negative association with gluten content. TFAs exhibited a significant positive correlation with TSSs, non-reducing sugars, and starch, and they depicted a significant negative correlation with gluten content (Supplementary Table S2).

Discussion

Unhealthy diet and chronic diseases are the chief causes of two-thirds of global deaths. According to the WHO report, the four key metabolic changes, including obesity, high blood pressure, hyperglycemia, and hyperlipidemia, are linked with chronic disease, and they intensify the chance of death (44). To devitalize the aforementioned health risk factors, a proper and balanced plant-based nutritious diet including legumes, vegetables, and fruits could be the best option (45). For meeting the human nutritional prerequisite, the bioavailability and digestibility of plant protein are the key factors mainly when looking for substitutes for animal-based proteins (46). Legume seeds possess great nutritional value and are considered an incredible source of protein, carbohydrates, fiber, minerals, and other bioactive compounds and are poor in fats (47).

Chickpea seed-based diets are well known for their low hypersensitivity and rich nutritional package (protein, carbohydrates, minerals, vitamins, etc.), and their protein quality is considered superior to that of other legumes (25, 48). In order to address the issues of global food security and malnutrition, dedicated efforts are needed to amplify the nutritional potential of crops such as chickpeas (49).

To get in-depth biochemical insights into a diverse set (desi: kabuli) of chickpea genetic resources, seed-based nutritional, anti-nutritional, and mineral constituents were inspected in the current study. Protein represents an imperious component of chickpea seeds;

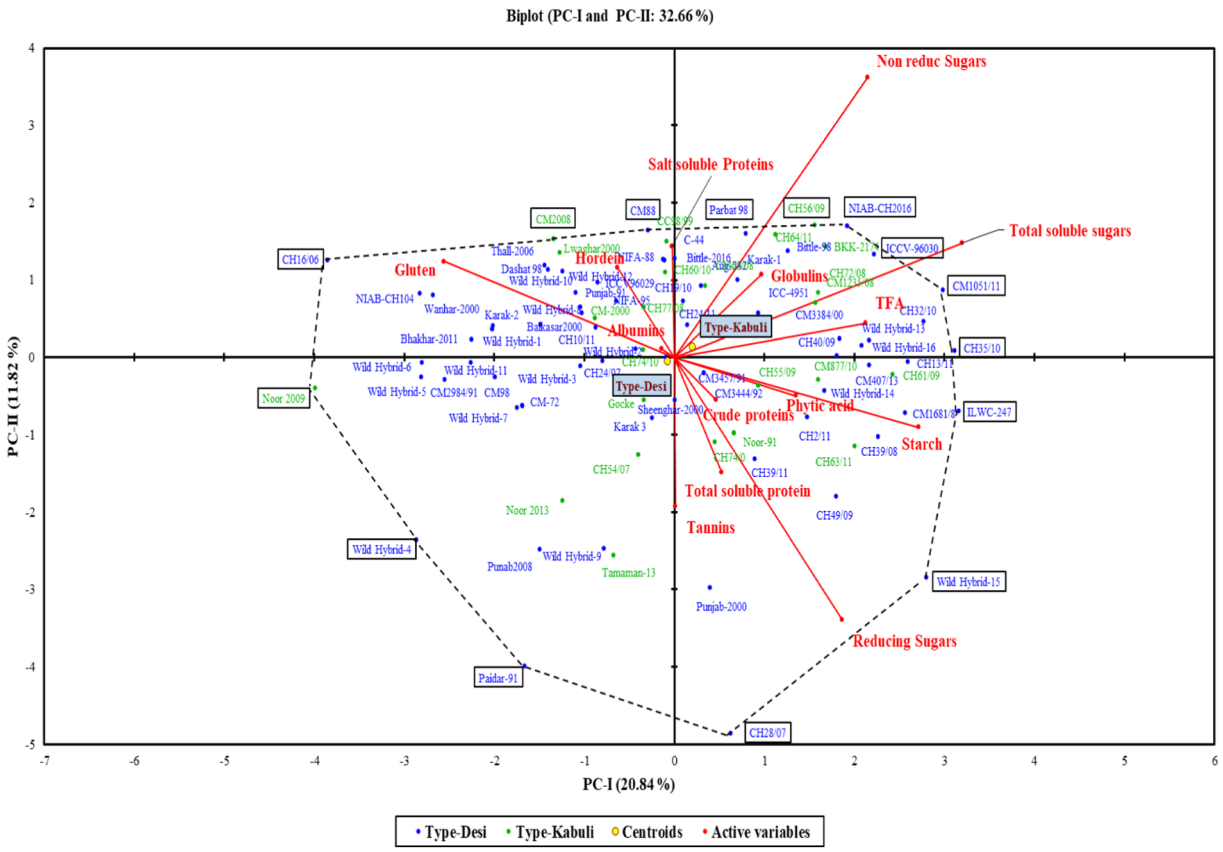

FIGURE 4
Biplot of chickpea genotypes for PC-I and PC-II.

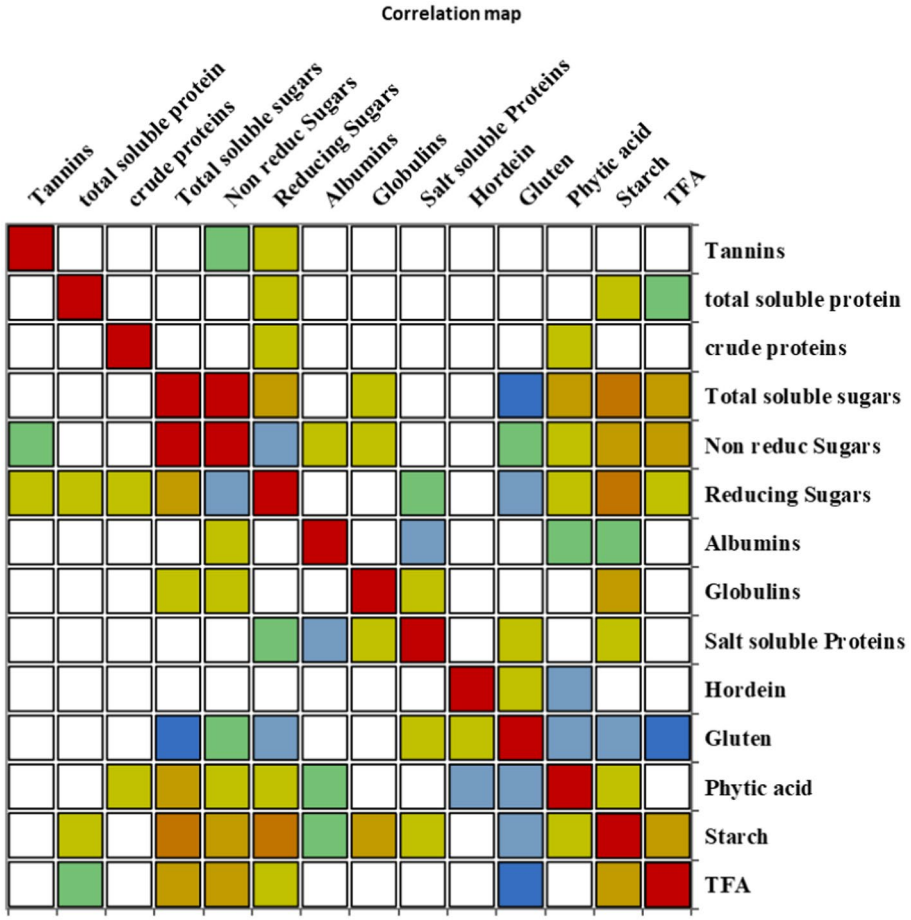

FIGURE 5
Correlation matrix showing Pearson's correlation among nutritional and anti-nutritional traits, in chickpea genotypes.

its composition describes their application in different food products (50). Findings showed that the highest TSPs (34.92%) and CPs (30.13%) were detected in Punjab-2000, which belongs to the desi type, followed by the kabuli genotype Gocke. A previous report suggested that sheenghar-2000 exhibited 34.06% and Thall-2006 exhibited 23% TSP. The present findings were in the previous range for these genotypes (32). It was noticed that chickpea protein depicts good functional properties, such as oil and water absorbing capacity, solubility, foaming, emulsifying, and gelling properties, which give excellent baking characteristics (51). The range of CPs observed in the present study was 20.97–30.13%. Other studies reported that, in chickpea seeds, the maximum CPs was 30.5 and 26% noticed in desi-type chickpeas, with similar results observed in the current study (52). Another report supports our findings in which the average CPs in kabuli and desi varied from 26.7 to18.2% (53).

In the central metabolism of the seeds, amino acids play an important role. They are principally used for the synthesis of seed storage proteins, but also act as a source of energy and assist as precursors for the biosynthesis of secondary metabolites. Free amino acids are the class of amino acids that are not bound in proteins (54). The highest TFAs with a value of 3.34% was detected in a desi-type genotype, Wild Hybrid-15. In earlier research, the maximum TFAs in chickpea rhizobium-inoculated seeds of Pusa-362 was 2.65% observed, which is 0.69% less than the present finding (55). Chickpea seed storage proteins are mainly composed of albumin, globulins, glutelin, residual protein, and prolamin, and they play an important role in human nutrition and plant reproduction as well (56, 57). Albumin is a most important transporter of amino acids and a storage reservoir of protein; because of their solubility in water, they are unique (58). Present findings illustrated that maximum albumin content (22.76%) was detected in sheenghar-2000 (desi type). Previously it was reported that albumin content was 8–12%, they play an indispensable role in chickpea nutrition and growth by supplying essential amino acids (59). Globulins are salt-soluble fractions of the protein, mainly composed of vicilin and legumin; in chickpeas major, globulin is legumin and hexameric proteins (60). A desi-type ICCV-96030 showed the highest globulin content (72%). In the previous report, it was noticed that chickpea seed protein was comprised of 56% globulin, which was 16% lower than the present findings (61). Maximum salt-soluble protein (20%) was noticed in ILWC-247 (desi type). In a previous study, it was observed that 16.24% salt-soluble protein was found in wheat (34); however, the present study revealed 4% higher salt-soluble protein in chickpeas than already reported in wheat grain. Hordein, a prolamin alcohol-soluble glycoprotein found in barley and other food crops, is a concern for some individuals with gluten intolerance or celiac disease. Because of gluten intolerance or celiac disease (CD), some people are

10.3389/fnut.2024.1407096

TABLE 3 Mean values of seed nutritional and anti-nutritional constituent of chickpea genotypes in cluster analysis.

Class	Tannins	total soluble protein	crude proteins	Total soluble sugars	Non-reducing sugars	Reducing sugars	Albumins	Globulins	Salt-soluble proteins	Hordein	Gluten	Phytic acid	Starch	TFA
1	7330.357	270.714	**25.147**	90.184	84.556	5.628	**158.190**	458.524	154.875	**49.857**	**117.095**	3.036	30.776	2.387
2	7081.579	**277.136**	24.607	**97.600**	**89.092**	8.507	120.601	**510.202**	**159.636**	39.199	62.039	3.322	**58.827**	**2.633**
3	**7918.750**	267.472	25.056	92.725	82.592	**10.132**	147.806	437.583	131.861	35.516	51.701	**3.488**	46.116	2.582

Values in bold font showed the highest mean value of respective traits.

sensitive to hordein intake, so foods with low hordein content are recommended (62). Minimum hordein (0.13%) was detected in kabuli type Noor-2013, followed by desi-type Wild Hybrid-16 with a value of 0.33%, while maximum hordein (11%) was found in NIAB-CH104 (Desi). In the previous study on chickpeas, a small fraction (3–7%) of prolamine was detected, but in chickpeas, they are not well characterized (63). Glutelins are a class of prolamine proteins present in the endosperm of certain seeds, mostly soluble in alkali detergent or dilute acids, and in the presence of reducing or chaotropic agents. They constitute the most important component of the protein composite collectively designated as gluten (64). Current results revealed that the fewest glutelins (0.33%) were found in Wild Hbrid-9 (desi), while CH16/06 (desi) depicted the highest (20.33%) glutelins. Earlier it was observed that chickpea seeds contained 19–25% glutelins; they are nutritional imperatives containing higher levels of cysteine and methionine than globulins (50). Consumption of gluten-containing foods such as cereals causes CD. CD is an immune-mediated disease that damages the villi that are responsible for nutrient absorption. There are only a few gluten-free food products available on the market that are more expensive (65). So the chickpea genotype Wild Hbrid-9, containing the lowest value of glutelin (3.33 ± 0.67 mg/g s. wt.), could be a promising cultivar for the food industry. The quantity of soluble sugar is an essential physiological trait that affects seed production and its cooking quality and plays an important function in abiotic stress tolerance in seeds and in storability (66). TSSs in chickpea seed was detected with the highest value (10.26%) in CM1051/11 (desi), and the least value (7.79%) was detected in the Paidar-91 desi type. Several studies reported different fractions of TSS in chickpea seeds. Goñi et al. (67) found 9.33% TSS, while Sánchez-Mata et al. (68) found 5.89 to 8.21% TSS in chickpeas. Present findings exhibited results within the previously studied range. Another study showed that the DBGV-165 genotype depicted 11.10 mg/100 g of total sugars (69). A higher concentration of approximately 17% was reported in a previous study (70). Reduced sugars are simple sugars that can oxidize other compounds. Reducing sugars are vital in central metabolic pathways, facilitating the production of secondary metabolites that boost the medicinal properties of plants (71). The highest reducing sugars were detected in Punjab-2000 (desi type) with a value of 1.733%, while the lowest value of 0.359% was found in Wild Hybrid-1. In the literature, the range of reducing sugars in chickpeas seeds was varied from 0.86 to 2.37%, and the present results are in accordance with the previous findings (72). Another finding exhibited a lower value of 0.158% reducing sugars in chickpea variety DIBG-201 (69). In the present study, the range for non-reducing sugars was given from 6.61 to 9.53%; however, the maximum value was detected in NIAB-CH2016, and the least content was observed in Paidar-91 both were of desi type. The literature indicates a lower range of non-reducing sugars in chickpea varieties, ranging from 1.3% to 3.3% (72). Another study on three Pakistani chickpea varieties reported a relatively low (3.30%) amount of non-reducing sugars than the present results (73). Starch, a major storage carbohydrate, is primarily composed of amylose and amylopectin, both of which have α-1,4- and α-1,6-linked glucose units (74). Legumes are not only an affordable source of protein but also starch, which has the advantage of being resistant to starch compared with cereal, root, and tuber starch (75). The present study depicted that chickpea seed

TABLE 4 Distribution of chickpea (desi and kabuli) genotypes in different clusters based on seed nutritional and anti-nutritional constituents.

Clusters	No of genotypes	Genotypes
I	28	**25 Desi** (CM-72, Karak-1, Punjab-91, NIFA-95, CM98, Balkasar-2000, Wanhar-2000, Dashat-98, Karak-2, Thall-2006, Bhakhar-2011, NIAB-CH2016, NIAB-CH104, CH10/11, CH16/06, CM2984/91, Wild Hybrid-1, Wild Hybrid-3, Wild Hybrid-4, Wild Hybrid-5, Wild Hybrid-6, Wild Hybrid-7, Wild Hybrid-8, Wild Hybrid-10, Wild Hybrid-12)**: 3 Kabuli** (Lawaghar-2000, CM-2008, Noor-2009)
II	38	**25 Desi** (C-44, NIFA-88, CM-88, Bittle-98, Parbat-98, Bittle-2016, CH40/09, CH49/09, CH32/10, CH35/10, CH2/11, CH13/1, CH24/11, CH19/10, CM1051/11, CM1681/8, CM407/13, CM3444/92, CM3457/91, Wild Hybrid-13, Wild Hybrid-16, Aug-242, ICCV-96030, ICC-4951, ILWC-247)**: 13 Kabuli** (CM-2000, CH77/08, CH55/09, CH56/09, CH61/09, BKK-2174, CH63/11, CH64/11, CM68/08, CH60/10, CH98/99, CH72/08, CM1235/08)
III	24	**16 Desi** (Paidar-91, Sheenghar-2000, Punjab-2000, Punjab-2008, Karak-3, CH28/07, CH39/08, CH39/11, CH24/07, CM3384/00, Wild Hybrid-2, Wild Hybrid-9, Wild Hybrid-11, Wild Hybrid-14, Wild Hybrid-15, ICCV-96029)**: 8 Kabuli** (Noor-91, Noor-2013, Tamaman-13, CH74/08, CH74/10, CH54/07, CM877/10, Gocke)

starch content ranged from 14.13 to 83.69%, and the highest starch was detected in the kabuli type (CH55/09) and the least starch was found in the desi type (Wild Hybrid-6). Earlier studies reported that starch content in chickpea seeds ranged from 37.5 to 50.8% (76). Chickpea seeds contain higher amounts of resistant starch and amylose. In the small intestine, chickpea starch is more resistant to digestion, resulting in a lower availability of glucose, which reduces the demand for insulin by slowing glucose entry into the bloodstream (77). Resistant starch-rich diets offer numerous health benefits, including colon cancer prevention, reduced coronary cases, weight management, healthy colon, and type 2 diabetes management (78).

Anti-nutritional factors, also known as secondary metabolites, are bioactive compounds that can lower the nutritional value of plants or plant derivatives that are often utilized in human diet or animal feed (79). Anti-nutritional factors are biologically deleterious substances present in the diet that behave antagonistically to one or multiple nutrients, reducing bioavailability (80). This is generally conducted via complex formation, which diminishes nutrient absorption, leading to impaired metabolic performance and gastrointestinal functions (81). PA, tannins, gossypol, raffinose, enzyme inhibitors, saponins, lectins, goitrogens, glucosinolates, oxalic acid, alkaloids, erucic acid, hydrogen cyanide (HCN), and β-N-oxalyl amino alanine (BOAA) are prominent anti-nutritional agents found in food (82). Phytate is found in all grain legumes, while tannins are primarily condensed in dark-seeded grains (83). Tannins are polyphenolic compounds present in food legumes. Tannins have the ability to interact with enzymes, proteins, non-enzymes, hampering protein solubility, digestibility, and amino acid accessibility (31, 84). This study revealed tannins in chickpea seeds ranged from 5,425 to 13,775 uM/g s. wt.; however, in the high category out of 10 genotypes, 8 were of desi type, and maximum tannins were detected in Wild Hybrid-3 (desi type), which showed that in the desi type more tannins are present as compared to the kabuli type. A previous report suggested that desi chickpeas have higher tannins compared to the kabuli type because most of the tannins are condensed in dark-colored seed coats (85). Tannins, which are concentrated in the dark-colored and rough seed coat of desi chickpeas, contribute to their astringent taste, which is why smooth surface kabuli chickpeas are preferred in some regions; similar results were observed in the present study, in which desi genotypes had higher tannins than kabuli genotypes (86, 87). Some domestic processing, such as pressure cooking and roasting, significantly reduced the tannin contents in chickpeas (88).

PA, also known as inositol hexaphosphate, is a bioactive sugar molecule featuring a simple ring structure with six phosphate groups attached to each carbon atom. Pulse, cereals, nuts, and oilseeds contain substantial amounts of PA (89). The presence of anti-nutrient PA in legumes hinders the bioavailability of proteins and absorption of trace elements and macro elements such as Ca, Zn, Mg, and Fe (90–92). PA is a proton contributor that generates "phytate" anion and hydrogen ions (H^+) that quickly form salts with available proteins and minerals (93). Furthermore, it has also been studied that the existence of PA restrains micronutrient fortification approaches because it can hamper the fortified micronutrients, leading to ineffectiveness (94).

The present study depicted PA in chickpeas ranging from 0.18 to 6.42 mg/g s. wt., and the maximum value was noticed in the kabuli genotype Tamaman-13; however, the least value was observed in the desi genotype Bhakhar-2011. It was noticed that in the low category, all the genotypes belong to the desi type, so the small seed contained a low PA concentration compared to the large-seeded. In a previous report, a considerably higher concentration of approximately 11.16 mg/g of PA was detected in chickpea seeds (95). Another study suggested that in comparison with other legumes, chickpeas contained relatively low PA and desi biotypes exhibited lower concentrations (96). Another study reported a relatively higher PA range (5.95 to 9.09 mg/g) in various chickpea cultivars (97).

Results of PCA revealed the diversity of genotypes for the traits under study. It was noticed that genotypes CH35/10, ILWC-247, Wild Hybrid-15, CH1051/11, ICCV-96030, CH56/09, etc. represented high positive factor scores, while Noor 2009, CH16/06, Wild Hybrid-4, Paidar-91, Lawaghar, etc. represented negative factor scores in PC-1. For PC-II, genotypes such as CM-88, Parbat 98, C-44, CH16/06, NIAB-CH2016, ICCV-98030, and CC98/99 have high positive scores. In contrast, genotypes including CH28/07, Paidar-91, CH28/07, WH-4, WH-9, and Noor-91 display negative factor scores. According to the results of PCA,

genotypes with high positive factor scores in PC-I can be identified as promising genotypes for nutritional traits with high positive scores such as TSPs, CPs, TSSs, non-reducing sugars, reducing sugars, globulins, starch, and TFAs. Conversely, genotypes with high negative factor scores in PC-I are considered less nutritionally rich. In the case of PC-II, genotypes with high positive scores for key nutritional traits such as non-reducing sugars, TSSs, globulins, and salt-soluble proteins are identified as promising. These genotypes also exhibit lower levels of anti-nutritional factors, as both tannins and PA have negative factor scores in PC-II. This analysis provides valuable insights for selecting and breeding chickpea varieties with optimal nutritional profiles, enabling the development of varieties that are both nutritionally rich and low in anti-nutritional factors. The cluster analysis divided the 90 genotypes (desi and kabuli) into three distinct groups. Cluster I comprised the genotypes with high average values for CPs, albumin, hordein, and glutelin. These genotypes are important for breeding programs focused on enhancing protein content and quality in chickpeas. In contrast, Cluster II is composed of the genotypes with high mean values of TSPs, TSSs, non-reducing sugars, globulins, salt-soluble proteins, starch, and TFAs. These traits are crucial for improving the overall nutritional profile of chickpeas, making them more beneficial for human consumption. However, Cluster III contains genotypes with high mean values of anti-nutritional factors such as tannins, reducing sugars, and PA. These anti-nutritional factors can interfere with the absorption of essential nutrients. Identifying these genotypes helps in breeding programs aimed at reducing anti-nutritional factors. Identified chickpea genotypes through different analyses will serve as essential stable donors in chickpea biofortification strategies. They will also facilitate the expansion of biofortified crop cultivation, contributing significantly to health and nutritional security in developing countries.

Conclusion

The present study revealed that both desi and kabuli genotypes represented vast genetic diversity for different seed nutritive and anti-nutritive traits. Genotypes with maximum TSPs, CPs, reducing sugars (Punjab-2000: D), TFAs (Wild Hybrid-15: D), albumins (Sheenghar-2000: D), globulins (ICCV-96030: D), salt-soluble proteins (ILWC-247: D), TSSs (CM1051/11: D), non-reducing sugars (NIAB-CH2016: D), starch content (CH55/09:K), and the genotypes with a minimum value of anti-nutritional constituents, i.e., glutelin (Wild Hybrid-9: D), hordein (Noor-2013: K), tannins (Wild Hybrid-1: D), and PA (Bhakhar-2011: D) are the promising cultivars for improving seed quality attributes. The findings of this study could also be helpful in addressing malnutrition-related life-threatening challenges. However, seed quality traits can be significantly influenced by environmental factors, so testing genotypes under diverse climatic conditions will ensure that the findings are robust and reliable, enhancing their practical utility in breeding programs, the food industry, and efforts to combat malnutrition. Additionally, exploring the genetic basis of these traits could uncover new genes and pathways that could be targeted in future breeding programs.

Data availability statement

The original contributions presented in the study are included in the article/Supplementary material, further inquiries can be directed to the corresponding author.

Author contributions

SJ: Data curation, Formal analysis, Investigation, Validation, Visualization, Writing – original draft. AH: Conceptualization, Project administration, Resources, Supervision, Writing – review & editing. TS: Funding acquisition, Resources, Supervision, Writing – review & editing. CC: Funding acquisition, Resources, Supervision, Writing – review & editing.

Funding

The author(s) declare that no financial support was received for the research, authorship, and/or publication of this article.

Acknowledgments

The paper is from PhD thesis research work of the first author (S. Jameel). Authors are thankful for the provision of IRSIP scholarship by the Higher Education Commission (HEC), Pakistan for conducting a part of PhD research work under the supervision of Clarice J. Coyne at USDA–ARS Plant Germplasm Introduction and Testing, Washington State University, Pullman, WA 99164, United States.

Conflict of interest

The authors declare that the research was conducted in the absence of any commercial or financial relationships that could be construed as a potential conflict of interest.

Publisher's note

Supplementary material

The Supplementary material for this article can be found online at: https://www.frontiersin.org/articles/10.3389/fnut.2024.1407096/full#supplementary-material

References

1. Merga B, Haji J. Economic importance of chickpea: production, value, and world trade. *Cogent Food Agricul*. (2019) 5:1615718. doi: 10.1080/23311932.2019.1615718

2. Zamrsky D, Oude Essink GH, Bierkens MF. Global impact of sea level rise on coastal fresh groundwater resources. *Earth's Future*. (2024) 12:3581. doi: 10.1029/2023EF003581

3. Imathiu S. Neglected and underutilized cultivated crops with respect to indigenous African leafy vegetables for food and nutrition security. *J Food Secur*. (2021) 9:115–25. doi: 10.12691/jfs-9-3-4

4. Richards C, Gauch H, Allwood J. International risk of food insecurity and mass mortality in a runaway global warming scenario. *Futures*. (2023) 150:103173. doi: 10.1016/j.futures.2023.103173

5. Vandemark GJ, Grusak MA, Mcgee RJ. Mineral concentrations of chickpea and lentil cultivars and breeding lines grown in the U.S. Pacific northwest. *Crop J*. (2018) 6:253–62. doi: 10.1016/j.cj.2017.12.003

6. Maitra C. (2018).A review of studies examining the link between food insecurity and malnutrition. Technical Paper. FAO, Rome. 70 pp. Licence: CC BY-NC-SA 3.0 IGO. Available at: http://www.fao.org/3/CA1447EN/ca1447en.pdf

7. Avery A. Food insecurity and malnutrition. *Kompass Nutr Diet*. (2021) 1:41–3. doi: 10.1159/000515968

8. Alaimo K, Chilton M, Jones SJ. Food insecurity, hunger, and malnutrition. *Present Knowl Nutr*. (2020):311–326. doi: 10.1016/B978-0-12-818460-8.00017-4

9. FAO, IFAD, UNICEF, WFP and WHO. (2020). The state of food security and nutrition in the world 2020. FAO, IFAD, UNICEF, WFP and WHO. Available at: https://openknowledge.fao.org/handle/20.500.14283/ca9692en

10. Jeje O, Oluwafemi G, Omowaye-Taiwo O. Mitigation of hidden hunger through biofortification: an appraisal. *Int J Food Sci Nutr*. (2023) 6:13–29.

11. Naveed M, Khalid H, Ayub MA, Rizwan M, Rasul A. Biofortification of cereals with zinc and iron: recent advances and future perspectives. *Res Use Efficiency Agricul*. (2020):615–46. doi: 10.1007/978-981-15-6953-1_17

12. Chacha JS, Laswai HS. Micronutrients potential of underutilized vegetables and their role in fighting hidden hunger. *Int J Food Sci*. (2020):1–5. doi: 10.1155/2020/9408315

13. Rosendaal FR. Venous thrombosis: a multicausal disease. *Lancet*. (1999) 353:1167–73. doi: 10.1016/S0140-6736(98)10266-0

14. Li C, Yao S, Song B, Zhao L, Hou B, Zhang Y, et al. Evaluation of cooked Rice for eating quality and its components in Geng Rice. *Food Secur*. (2023) 12:3267. doi: 10.3390/foods12173267

15. Maphosa Y, Jideani VA. The role of legumes in human nutrition. *Fun Food Improve Health Adequate Food*. (2017) 1:13.

16. Edwards RA, Ng XY, Tucker MR, Mortimer JC. Plant synthetic biology as a tool to help eliminate hidden hunger. *Curr Opin Biotechnol*. (2024) 88:103168. doi: 10.1016/j.copbio.2024.103168

17. Rehman HM, Cooper JW, Lam HM, Yang SH. Legume biofortification is an underexploited strategy for combatting hidden hunger. *Plant Cell Environ*. (2019) 42:52–70. doi: 10.1111/pce.13368

18. Kaur R, Prasad K. Technological, processing and nutritional aspects of chickpea (*Cicer arietinum*)-A review. *Trends Food Sci Technol*. (2021) 109:448–63. doi: 10.1016/j.tifs.2021.01.044

19. Irshad S, Matloob A, Iqbal S, Ibrar D, Hasnain Z, Khan S, et al. Foliar application of potassium and moringa leaf extract improves growth, physiology and productivity of kabuli chickpea grown under varying sowing regimes. *PLoS One*. (2022) 17:e0263323. doi: 10.1371/journal.pone.0263323

20. Tripathi S, Singh RK, Parida SK, Chaturvedi S, Gaur P. Biofortification of chickpea. *Biofortification Staple Crops*. (2022):335–44. doi: 10.1007/978-981-16-3280-8_13

21. Moreno M-T, Cubero J. Variation in *Cicer arietinum* L. *Euphytica*. (1978) 27:465–85. doi: 10.1007/BF00043173

22. FAOSTAT (2024). Available at: https://www.fao.org/faostat/en/#data/Qcl/visualize.

23. Fatima K, Habib A, Sahi S, Cheema H. Integrated management of Fusarium spp. associated with chickpea (*Cicer arietinum* L.) wilt disease in the Punjab, Pakistan. *Appl Ecol Environ Res*. (2022) 20:527–41. doi: 10.15666/aeer/2001_527541

24. Sofi SA, Muzaffar K, Ashraf S, Gupta I, Mir SA. Chickpea. *Pulses*. Springer International Publishing (2020):55–76. doi: 10.1007/978-3-030-41376-7_4

25. Wang J, Li Y, Li A, Liu RH, Gao X, Li D, et al. Nutritional constituent and health benefits of chickpea (*Cicer arietinum* L.): A review. *Food Res Int*. (2021) 150:110790. doi: 10.1016/j.foodres.2021.110790

26. Olika E, Abera S, Fikre A. Physicochemical properties and effect of processing methods on mineral composition and antinutritional factors of improved chickpea (*Cicer arietinum* L.) varieties grown in Ethiopia. *Int J Food Sci*. (2019):1–7. doi: 10.1155/2019/9614570

27. Patil ND, Bains A, Sridhar K, Rashid S, Kaur S, Ali N, et al. Effect of sustainable pretreatments on the nutritional and functionality of chickpea protein: implication for innovative food product development. *J Food Biochem*. (2024) 2024:5173736. doi: 10.1155/2024/5173736

28. Zhang J, Wang J, Zhu C, Singh RP, Chen W. Chickpea: its origin, distribution, nutrition, benefits, breeding, and symbiotic relationship with Mesorhizobium species. *Plan Theory*. (2024) 13:429. doi: 10.3390/plants13030429

29. Nespor B, Andrianova A, Pollack S, Pfau C, Arifuzzaman M, Islam N, et al. Metformin uptake and translocation in chickpeas: determination using liquid chromatography–mass spectrometry. *ACS Omega*. (2020) 5:1789–95. doi: 10.1021/acsomega.9b02783

30. Witten S, Böhm H, Aulrich K. Effect of variety and environment on the contents of crude nutrients and amino acids in organically produced cereal and legume grains. *Org Agric*. (2020) 10:199–219. doi: 10.1007/s13165-019-00261-7

31. Yegrem L. Nutritional composition, Antinutritional factors, and utilization trends of Ethiopian chickpea (*Cicer arietinum* L.). *Int J Food Sci*. (2021):5570753. doi: 10.1155/2021/5570753

32. Shah S, Ullah F, Munir I. Biochemical characterization for determination of genetic distances among different indigenous chickpea (*Cicer arietinum* L.) varieties of north-West Pakistan. *Braz J Biol*. (2020) 81:977–88. doi: 10.1590/1519-6984.232747

33. Jameel S, Hameed A, Shah TM. Biochemical profiling for antioxidant and therapeutic potential of Pakistani chickpea (*Cicer arietinum* L.) genetic resource. *Front Plant Sci*. (2021) 12:663623. doi: 10.3389/fpls.2021.663623

34. Khalid A, Hameed A. Seed biochemical analysis based profiling of diverse wheat genetic resource from Pakistan. *Front Plant Sci*. (2017) 8:1276. doi: 10.3389/fpls.2017.01276 (Accessed August 05, 2024).

35. Bradford N. A rapid and sensitive method for the quantitation microgram quantities of a protein isolated from red cell membranes. *Anal Biochem*. (1976) 72:e254. doi: 10.1016/0003-2697(76)90527-3

36. Singhai B, Shrivastava S. Nutritive value of new chickpea (*Cicer arietinum*) varieties. *J Food Agriculture Environ*. (2006) 4:48.

37. Bradford MM. A rapid and sensitive method for the quantitation of microgram quantities of protein utilizing the principle of protein-dye binding. *Anal Biochem*. (1976) 72:248–54. doi: 10.1016/0003-2697(76)90527-3

38. Dubois M, Gilles K, Hamilton J, Rebers P, Smith F. A colorimetric method for the determination of sugars. *Nature*. (1951) 168:167. doi: 10.1038/168167a0

39. Miller GL. Use of dinitrosalicylic acid reagent for determination of reducing sugar. *Anal Chem*. (1959) 31:426–8. doi: 10.1021/ac60147a030

40. Malik C. P., Srivastava A. K. (1979). Text book of plant physiology. Kalyani, New Delhi.

41. Hamilton PB, Van Slyke DD. The gasometric determination of free amino acids in blood filtrates by the ninhydrin-carbon dioxide method. *J Biol Chem*. (1943) 150:231–50. doi: 10.1016/S0021-9258(18)51268-0

42. Ainsworth EA, Gillespie KM. Estimation of total phenolic content and other oxidation substrates in plant tissues using Folin–Ciocalteu reagent. *Nat Protoc*. (2007) 2:875–7. doi: 10.1038/nprot.2007.102

43. Dhole VJ, Reddy KS. Genetic variation for phytic acid content in mungbean (*Vigna radiata* L. Wilczek). *Crop J*. (2015) 3:157–62. doi: 10.1016/j.cj.2014.12.002

44. Didinger C, Foster MT, Bunning M, Thompson HJ. Nutrition and human health benefits of dry beans and other pulses. *Dry Beans Pulses*. (2022):481–504. doi: 10.1002/9781119776802.ch19

45. Marette S, Roosen J. Just a little bit more legumes! Results of an online survey in Europe. *Int Food Agribusi Manag Rev*. (2022) 25:329–45.

46. Gu J, Bk A, Wu H, Lu P, Nawaz MA, Barrow CJ, et al. Impact of processing and storage on protein digestibility and bioavailability of legumes. *Food Rev Intl*. (2022) 39:1–28. doi: 10.1080/87559129.2022.2039690

47. Elamine Y, Alaiz M, Girón-Calle J, Guiné RP, Vioque J. Nutritional characteristics of the seed protein in 23 Mediterranean legumes. *Agronomy*. (2022) 12:400. doi: 10.3390/agronomy12020400

48. Amoah YS, Rajasekharan SK, Reifen R, Shemesh M. Chickpea-derived prebiotic substances trigger biofilm formation by *Bacillus subtilis*. *Nutrients*. (2021) 13:4228. doi: 10.3390/nu13124228

49. Jha UC, Nayyar H, Thudi M, Beena R, Vara Prasad P, Siddique KH. Unlocking the nutritional potential of chickpea: strategies for biofortification and enhanced multinutrient quality. *Front Plant Sci*. (2024) 15:1391496. doi: 10.3389/fpls.2024.1391496

50. Grasso N, Lynch NL, Arendt EK, O'mahony JA. Chickpea protein ingredients: A review of composition, functionality, and applications. *Compr Rev Food Sci Food Saf*. (2022) 21:435–52. doi: 10.1111/1541-4337.12878

51. Shaabani S, Yarmand MS, Kiani H, Emam-Djomeh Z. The effect of chickpea protein isolate in combination with transglutaminase and xanthan on the physical and rheological characteristics of gluten free muffins and batter based on millet flour. *LWT*. (2018) 90:362–72. doi: 10.1016/j.lwt.2017.12.023

52. Goswami D, Dineshkumar R, Bansal N, Prashat G, Bharadwaj C, Lekshmy S, et al. Profiling of total nitrogen content and soluble proteins in popular varieties of desi chickpea, Kabuli chickpea and pigeon pea. *Int J Chem Stud*. (2021) 9:2276–9. doi: 10.22271/chemi.2021.v9.i1af.11563

53. Sahu VK, Tiwari S, Gupta N, Tripathi M, Yasin M. Evaluation of physiological and biochemical contents in desi and Kabuli chickpea. *Legume Res Int J*. (2022) 45:1197–208.

54. Amir R, Galili G, Cohen H. The metabolic roles of free amino acids during seed development. *Plant Sci*. (2018) 275:11–8. doi: 10.1016/j.plantsci.2018.06.011

55. Harendra S, Mritunjay T, Pratibha S, Singh R. Biochemical and physiological studies on rhizobium inoculated chickpea (*Cicer arietinum* L.) cultivar grown in eastern up. *Legum Res*. (2018) 41:263–6. doi: 10.18805/lr.v0iOF.9103

56. Saharan K, Khetarpaul N. Protein quality traits of vegetable and field peas: varietal differences. *Plant Foods Hum Nutr*. (1994) 45:11–22. doi: 10.1007/BF01091225

57. Singh PK, Shrivastava N, Chaturvedi K, Sharma B, Bhagyawant SS. Characterization of seed storage proteins from chickpea using 2D electrophoresis coupled with mass spectrometry. *Biochem Res Int*. (2016):1049462. doi: 10.1155/2016/1049462

58. Singh N. (2017). *Pulses: An overview journal of food science and technology*. Berlin/Heidelberg, Germany: Springer, 853–857.

59. Clemente A, Vioque J, Sánchez-Vioque R, Pedroche J, Bautista J, Millán F. Factors affecting the in vitro protein digestibility of chickpea albumins. *J Sci Food Agric*. (2000) 80:79–84. doi: 10.1002/(SICI)1097-0010(20000101)80:1<79::AID-JSFA487>3.0.CO;2-4

60. Day L. Proteins from land plants–potential resources for human nutrition and food security. *Trends Food Sci Technol*. (2013) 32:25–42. doi: 10.1016/j.tifs.2013.05.005

61. Watson RR, Preedy VR. Bioactive food as dietary interventions for diabetes Amsterdam, Netherlands: Academic Press (2019).

62. Scherf KA, Catassi C, Chirdo F, Ciclitira PJ, Feighery C, Gianfrani C, et al. Recent progress and recommendations on celiac disease from the working group on prolamin analysis and toxicity. *Front Nutr*. (2020) 7:29. doi: 10.3389/fnut.2020.00029

63. Stone AK, Nosworthy MG, Chiremba C, House JD, Nickerson MT. A comparative study of the functionality and protein quality of a variety of legume and cereal flours. *Cereal Chem*. (2019) 96:1159–69. doi: 10.1002/cche.10226

64. Song J, Jiang L, Qi M, Han F, Li L, Xu M, et al. Influence of magnetic field on gluten aggregation behavior and quality characteristics of dough enriched with potato pulp. *Int J Biol Macromol*. (2024) 254:128082. doi: 10.1016/j.ijbiomac.2023.128082

65. Alshehry G, Algarni E, Aljumayi H, Algheshairy RM, Alharbi HF. Development and characterization of multigrain Pan bread prepared using quinoa, Lupin, and fenugreek seeds with yellow maize as a gluten-free diet. *J Food Qual*. (2022):4331353. doi: 10.1155/2022/4331353

66. Weng Y, Ravelombola WS, Yang W, Qin J, Zhou W, Wang Y-J, et al. Screening of seed soluble sugar content in cowpea (*Vigna unguiculata* (L.) Walp). *American. J Plant Sci*. (2018) 9:1455–66. doi: 10.4236/ajps.2018.97106

67. Goñi I, Garcia-Diz L, Mañas E, Saura-Calixto F. Analysis of resistant starch: a method for foods and food products. *Food Chem*. (1996) 56:445–9. doi: 10.1016/0308-8146(95)00222-7

68. Sánchez-Mata M, Hurtado MC, Dıez-Marqués C. Effect of domestic processes and water hardness on soluble sugars content of chickpeas (*Cicer arietinum* L.). *Food Chem*. (1999) 65:331–8. doi: 10.1016/S0308-8146(98)00219-2

69. Veenakumari V, Kasturiba B, Vijaykumar A. Mineral composition and sugars content in chickpea (*Cicer arietinum* L.) varieties. *Int J Curr Res*. (2017) 12:62144–7.

70. Fedeli R, Vannini A, Celletti S, Maresca V, Munzi S, Cruz C, et al. Foliar application of wood distillate boosts plant yield and nutritional parameters of chickpea. *Ann Appl Biol*. (2023) 182:57–64. doi: 10.1111/aab.12794

71. Khatri D, Chhetri SBB. Reducing sugar, total phenolic content, and antioxidant potential of nepalese plants. *Biomed Res Int*. (2020) 2020:7296859. doi: 10.1155/2020/7296859

72. Yadav RK, Tripathi MK, Tiwari S. Estimation of biochemical parameters in chickpea (*Cicer arietinum* L.) genotypes. *Legume Res Int J*. (2024) 1:9. doi: 10.18805/LR-5327

73. Shad MA, Pervez H, Zafar ZI, Zia-Ul-Haq M, Nawaz H. Evaluation of biochemical composition and physicochemical parameters of oil from seeds of desi chickpea varieties cultivated in arid zone of Pakistan. *Pak J Bot*. (2009) 41:655–62.

74. Apriyanto A, Compart J, Fettke J. A review of starch, a unique biopolymer–structure, metabolism and in planta modifications. *Plant Sci*. (2022) 318:111223. doi: 10.1016/j.plantsci.2022.111223

75. Tayade R, Kulkarni KP, Jo H, Song JT, Lee J-D. Insight into the prospects for the improvement of seed starch in legume—a review. *Front Plant Sci*. (2019) 10:1213. doi: 10.3389/fpls.2019.01213

76. Yniestra Marure LM, Núñez-Santiago MC, Agama-Acevedo E, Bello-Perez LA. Starch characterization of improved chickpea varieties grown in Mexico. *Starch Stärke*. (2019) 71:1800139. doi: 10.1002/star.201800139

77. Jukanti AK, Gaur PM, Gowda C, Chibbar RN. Nutritional quality and health benefits of chickpea (*Cicer arietinum* L.): a review. *Br J Nutr*. (2012) 108:S11–26. doi: 10.1017/S0007114512000797

78. Too BC, Van N, Thuy NM. Formulation and quality evaluation of noodles with starchy flours containing high levels of resistant starch. *Acta Sci Pol Technol Aliment*. (2022) 21:145–54. doi: 10.17306/J.AFS.2022.1011

79. Li M, Xia M, Imran A, De Souza TS, Barrow C, Dunshea F, et al. Nutritional value, phytochemical potential, and biological activities in lentils (*Lens culinaris* Medik.): A review. *Food Rev Intl*. (2023) 40:1–31. doi: 10.1080/87559129.2023.2245073

80. Small BC. Nutritional physiology. *Fish Nutr*. (2022):593–641. doi: 10.1016/B978-0-12-819587-1.00007-0

81. Samtiya M, Aluko RE, Dhewa T. Plant food anti-nutritional factors and their reduction strategies: an overview. *Food Prod Process Nutr*. (2020) 2:1–14.

82. Duraiswamy A, Sneha ANM, Jebakani KS, Selvaraj S, Pramitha JL, Selvaraj R, et al. Genetic manipulation of anti-nutritional factors in major crops for a sustainable diet in future. *Front Plant Sci*. (2023) 13:1070398. doi: 10.3389/fpls.2022.1070398

83. David LS, Nalle CL, Abdollahi MR, Ravindran V. Feeding value of Lupins, field peas, Faba beans and chickpeas for poultry: an overview. *Animals*. (2024) 14:619. doi: 10.3390/ani14040619

84. Roy A, Ghosh S, Kundagrami S. Food processing methods towards reduction of Antinutritional factors in chickpea. *Int J Curr Microbiol App Sci*. (2019) 8:424–32. doi: 10.20546/ijcmas.2019.801.044

85. Sharma S, Yadav N, Singh A, Kumar R. Nutritional and antinutritional profile of newly developed chickpea (*Cicer arietinum* L) varieties. *Int Food Res J*. (2013) 20:805–810.

86. Rajput S, Jain S, Tiwari S, Gupta N, Sikarwar R, Tripathi N, et al. Biochemical characterization of chickpea (*Cicer arietinum* L.) genotypes. *Plant Cell Biotechnol Mol Biol*. (2023) 24:1–9. doi: 10.56557/PCBMB/2023/v24i3-48239

87. Tiwari PN, Tiwari S, Sapre S, Tripathi N, Payasi DK, Singh M, et al. Prioritization of physio-biochemical selection indices and yield-attributing traits toward the acquisition of drought tolerance in chickpea (*Cicer arietinum* L.). *Plan Theory*. (2023) 12:3175. doi: 10.3390/plants12183175

88. Idate A., Shah R., Gaikwad V., Kumathekar S., Temgire S. (2021). A comprehensive review on antinutritional factors of chickpea (*Cicer arietinum* L.). *The Pharma Innovation Journal*, 10:816-823. doi: 10.22271/tpi.2021.v10.i5k.6306

89. Bose S, Maity M, Kar S. Antinutrient Phytic acid: can be proved to be a boon for colorectal Cancer. *J Adv Zool*. (2023) 44:1972–1979.

90. Rosalina L, Bernward B, Sumaryati S, Asmar Y. Role of Tempe from West Sumatra as A source of vitamin B12 and antioxidant capacity. *MSJ*. (2024) 2:312–9. doi: 10.61942/msj.v2i1.65

91. Thi H. H. P., Nguyen T. L. (2021). Nutraceutical properties of legume seeds: Phytochemical compounds. *IntechOpen*. doi: 10.5772/intechopen.100171

92. Zhang YY, Stockmann R, Ng K, Ajlouni S. Revisiting phytate-element interactions: implications for iron, zinc and calcium bioavailability, with emphasis on legumes. *Crit Rev Food Sci Nutr*. (2022) 62:1696–712. doi: 10.1080/10408398.2020.1846014

93. Sarkhel S, Roy A. Phytic acid and its reduction in pulse matrix: structure–function relationship owing to bioavailability enhancement of micronutrients. *J Food Process Eng*. (2022) 45:1–21. doi: 10.1111/jfpe.14030

94. Saha S, Roy A. Whole grain rice fortification as a solution to micronutrient deficiency: technologies and need for more viable alternatives. *Food Chem*. (2020) 326:127049. doi: 10.1016/j.foodchem.2020.127049

95. Sinkovič L, Pipan B, Šibul F, Nemeš I, Tepić Horecki A, Meglič V. Nutrients, Phytic acid and bioactive compounds in marketable pulses. *Plan Theory*. (2023) 12:170. doi: 10.3390/plants12010170

96. Dragičević V, Kratovalieva S, Dumanović Z, Dimov Z, Kravić N. Variations in level of oil, protein, and some antioxidants in chickpea and peanut seeds. *Chem Biol Technol Agric*. (2015) 2:1–6. doi: 10.1186/s40538-015-0031-7

97. Tripathi A, Varma A, Mishra S. Changes in phytic acid, polyphenol, free fatty acid content and calorific value in chickpea varieties during storage. *Int J Chem Stud*. (2020) 8:3496–501. doi: 10.22271/chemi.2020.v8.i4ar.10192

frontiers | Frontiers in Sustainable Food Systems

TYPE Original Research
PUBLISHED 09 December 2024
DOI 10.3389/fsufs.2024.1445993

OPEN ACCESS

EDITED BY
Reza Rastmanesh,
American Physical Society, United States

REVIEWED BY
Jing Si,
Beijing Forestry University, China
Antero Ramos-Fernández,
Instituto de Ecología (INECOL), Mexico

*CORRESPONDENCE
Di Liu
✉ liudi@ybu.edu.cn

RECEIVED 08 June 2024
ACCEPTED 20 November 2024
PUBLISHED 09 December 2024

CITATION
Lu Y and Liu D (2024) Metabolomics profiles of the liquid co-culture of *Sanghuangporus vaninii* and *Pleurotus sapidus*. *Front. Sustain. Food Syst.* 8:1445993. doi: 10.3389/fsufs.2024.1445993

Metabolomics profiles of the liquid co-culture of *Sanghuangporus vaninii* and *Pleurotus sapidus*

Yuantian Lu[1] and Di Liu[1,2]*

[1]Agricultural College, Yanbian University, Yanji, China, [2]Institute of Edible and Medicinal Fungi, Agricultural College, Yanbian University, Yanji, China

Introduction: Fungal secondary metabolites (SMs) have broad application prospects in the food and medicine industries. Co-culturing strategies that simulate natural symbiotic relationships among microorganisms are used to discover and enhance the production of new SMs. We aimed to use the abundant resources of large edible and medicinal fungi to enhance the yield of desired metabolites through co-culture and potentially produce metabolites that cannot be generated in pure cultures.

Methods: We assessed the biomass and intracellular polysaccharide (IPS) content of liquid co-cultures of *Sanghuangporus vaninii* and *Pleurotus sapidus*. Subsequently, the effect of the liquid co-culture on fungal intracellular metabolites was studied using UPLC-QTOF.

Results: Co-culturing of *S. vaninii* with *P. sapidus* resulted in significantly increased biomass and IPS content; however, *P. sapidus* had a significant inhibitory effect on the growth of *S. vaninii*. Metabolomic data further indicated that amino acid, nucleotide, and glycerophospholipid metabolisms were the primary metabolic pathways affected by symbiosis.

Discussion: This study provides insights into fungal interactions and cellular metabolic mechanisms, contributing to the understanding and enhancement of the fungal fermentation potential.

KEYWORDS

***Sanghuangporus vaninii*, *Pleurotus sapidus*, polysaccharide, co-culture, metabolomics profiles**

1 Introduction

Secondary metabolites (SMs) are a class of low-molecular-weight compounds produced by microorganisms with various biological activities (Wang Y. et al., 2023). In a continuous interaction state, microorganisms activate complex regulatory mechanisms, specifically for SM production, to induce the biosynthesis of highly symbiotic natural products or novel metabolic compounds (Liu et al., 2022). Rather than passively existing in natural or unnatural growth environments, microorganisms establish physiological and metabolic interactions and adapt to changes in their living environments by regulating their metabolism, particularly through SM production (Singh and Lee, 2018). However, the underlying mechanisms regulating microbial interactions, community composition, dynamics, and functions remain elusive (Bertrand et al., 2013a,b). Fungal SMs have broad application prospects in the food and medicine industries (Guo et al., 2024). Therefore, many studies have been conducted on the

co-cultures of microorganisms to increase SM yield (Li et al., 2023; Tan et al., 2024; Xu et al., 2024).

In 1925, Sack first proposed the concept of microbial co-culture (Sun, 2022). Microbial co-culture usually involves the culturing of two or more strains (including fungus–fungus, fungus–bacteria, and bacteria–bacteria) in one culture vessel (Mantravadi et al., 2019) and is considered an excellent strategy to enhance SM yield and variety (Caudal et al., 2022). As microorganisms continually interact, they compete for survival space and nutrients, which activates the expression of gene clusters encoding SMs, affecting the metabolic activities of the strains (Costa et al., 2019). Because microbial co-cultures involve interactions between different species or strains of the same species, effective detection methods for metabolites in co-cultures are particularly essential (Adnani et al., 2015).

Metabolomic analysis has been shown to effectively reveal the metabolic accumulation mechanisms of co-cultured microorganisms (Li et al., 2024) and enable the simultaneous measurement of changes in various cellular small-molecule metabolites to determine all metabolic changes in a biological system before and after stimulation, elucidating the metabolic network (Wang J. et al., 2024). Metabolomics represents a significant tool for studying fungus-induced changes in metabolites during fermentation and has broad applications in fields such as food science, agriculture, and microbiology, with metabolite levels revealing the functional state of the cell (Liu et al., 2022). For example, co-culturing *Eurotium amstelodami* GZ23 and *Bacillus licheniformis* GZ241 significantly enhanced the inhibitory effect on *Staphylococcus aureus* ATCC25923. Non-targeted metabolomics analysis revealed that, intracellularly, the differential metabolites primarily involved the metabolism of amino acids, nucleic acids, and glycerophospholipids (Wang Y. et al., 2023). When *Aspergillus oryzae* AS3.951 and *Zygosaccharomyces rouxii* HH18 were co-cultured, *A. oryzae* significantly inhibited the growth of *Z. rouxii*. Analysis of intracellular and extracellular metabolites using UPLC-QTOF-MS technology showed that the main pathways affected by co-culturing included histidine metabolism and Phenylalanine, tyrosine, and tryptophan biosynthesis (Liu et al., 2022).

Sanghuangporus spp., belonging to the genus *Sanghuangporus*, are large medicinal mushrooms with food and medicinal purposes (Gao et al., 2024). Their medicinal value was first recorded in the Chinese herbal classic "Shennong Bencao Jing," and they are internationally recognized among the best medicinal large fungi with anti-cancer effects (Luan et al., 2022; Wu et al., 2022; Hu et al., 2024). Polysaccharides are among the primary active components of Sanghuang that contribute to its pharmacological effects (Wang et al., 2022) and possess anti-tumor (Boateng et al., 2024), anti-inflammatory (Hou et al., 2020), hepato-protective (Chiu et al., 2023), and immune-modulating properties (Wang F. et al., 2024). The current studies on Sanghuang polysaccharides primarily focus on fruiting bodies and pure liquid cultures, whereas studies on its co-cultures are rare.

In a preliminary study (Lu and Liu, 2024), we screened seven species of large edible and medicinal fungi and found that a co-culture of *Sanghuangporus vaninii* and *Pleurotus sapidus* yielded the optimum results. Based on preliminary research findings, it is speculated that under co-culture conditions, *S. vaninii* and *P. sapidus* interact to alter the abundance of intracellular metabolites, affecting their functions. In this study, we compared and measured the biomass and intracellular polysaccharide (IPS) content of pure cultures and co-cultures of *S. vaninii* and *P. sapidus* through liquid cultures. Additionally, we conducted a differential analysis of the intracellular metabolites of pure cultures and co-cultures of *S. vaninii* and *P. sapidus* using non-targeted metabolomics to explore the impact of co-culture on intracellular metabolism. This study primarily aimed to (1) understand the interactions between co-cultures of *S. vaninii* and *P. sapidus*; (2) determine and analyze the biomass and IPS content of pure cultures and co-cultures of *S. vaninii* and *P. sapidus*; and (3) explore the changes in the abundance of intracellular metabolites after co-culturing *S. vaninii* and *P. sapidus*. We aimed to use the abundant resources of large edible and medicinal fungi to enhance the yield of desired metabolites through co-culture and potentially produce metabolites that cannot be generated in pure cultures. This study seeks to contribute theoretical reference materials for the diversification of *S. vaninii* or *P. sapidus* products and the sustainable development of the industry.

2 Materials and methods

2.1 Strains

Strains of *S. vaninii* ST (NMDC Accession: NMDCN0003GMT) and *P. sapidus* BLZ (NMDC Accession: NMDCN0002T9L) were obtained from the Institute of Edible and Medicinal Fungi, Agricultural College, Yanbian University, Yanji, China.

2.2 Culture medium

PDA medium: potato 200 g/L, glucose 20 g/L, agar 20 g/L, and natural pH.

Seed medium: yeast extract 5 g/L, glucose 20 g/L, KH_2PO_4 1.5 g/L, $MgSO_4{\cdot}7H_2O$ 0.5 g/L, and natural pH.

Co-culture medium: yeast extract 6 g/L, glucose 30 g/L, KH_2PO_4 1.5 g/L, $MgSO_4{\cdot}7H_2O$ 2 g/L, and pH 9.

2.3 Strain activation

Using an inoculating loop, 0.5*0.5 cm mycelial block was transferred from the seed tube into a fresh PDA medium plate and incubated invertedly in the dark at 28°C. The mycelium grew until it covered approximately 90% of the plate, indicating completion of strain activation.

2.4 Liquid co-culture of *Sanghuangporus vaninii* and *Pleurotus sapidus*

Cultivate according to the methods in the preliminary research findings (Lu and Liu, 2024).

Five blocks of *S. vaninii* and one block of *P. sapidus*, each 9 mm in diameter, were inoculated separately into 250-mL shake flasks

Abbreviations: SMs, Secondary metabolites; IPS, Intracellular polysaccharide; PCA, Principal component analysis; OPLS-DA, Orthogonal partial least squares discriminant analysis; VIP, Variable importance in projection; TCA, Tricarboxylic acid.

containing 100 mL of seed medium. The *S. vaninii* and *P. sapidus* were cultured for 7 and 5 days, respectively. After culturing, the seed culture solution was homogenized using an adjustable high-speed homogenizer. At an inoculation volume of 20% (v/v), the seed culture solution was transferred into 250-mL shake flasks containing 80 mL of seed medium. The *S. vaninii* and *P. sapidus* were cultured for 2 and 0 days, respectively, to obtain the seed pre-culture solution.

Pure culture of *S. vaninii* and *P. sapidus*: With an inoculation volume of 10% (v/v), the seed pre-culture solutions of *S. vaninii* and *P. sapidus*, which were cultured for 0 days, were transferred into 250-mL shake flasks containing 95 mL of a co-culture medium, where *S. vaninii* and *P. sapidus* were cultured for 7 and 5 days, respectively.

Co-culture of *S. vaninii* and *P. sapidus*: With inoculation volumes of 6.9 and 3.1% (v/v), the seed pre-culture solutions of *S. vaninii* and *P. sapidus* were transferred into 250-mL shake flasks containing 95 mL of a co-culture medium and cultured for 5 days. All culture conditions were at 28°C and 150 × *g*.

2.5 Biomass determination and sample preparation

After culturing, all fermentation liquids were centrifuged at 5,000 × *g* at 4°C for 5 min. The supernatant was discarded, and the mycelia were collected, which were washed with distilled water and divided into two parts. One part was dried in a 60°C constant temperature oven until a constant weight was achieved, cooled, and weighed for biomass measurement. The dried mycelia were crushed and sieved through a 60-mesh standard sieve, and the samples were collected for IPS concentration determination. For the other part, based on the different mycelium colors and morphologies of different strains, the mycelia were isolated from the co-culture to obtain a pure mycelial strain, which was treated with liquid nitrogen and stored at −80°C for metabolomics analysis.

2.6 IPS content determination

We adopted the method of Wang (2021) with slight modifications.

(1) IPS extraction: The tested sample (0.3 g) was placed in a centrifuge tube, followed by the addition of distilled water at a material-to-liquid ratio of 1:30 (g/mL) and extraction at 90°C in a constant temperature water bath for 2 h. Subsequently, centrifugation was performed at 6,000 × *g* for 10 min, and the supernatant was collected. The extraction was repeated twice, and the supernatants were combined. The supernatant was concentrated to one-fifth of the original volume in a 60°C electric constant temperature drying oven. Four times the volume of anhydrous ethanol was added, and the mixture was allowed to stand for 12 h at 4°C. Next, centrifugation was performed at 8,000 × *g* for 30 min, and the precipitate was collected, dried at 60°C, and dissolved in distilled water. The volume was made up to obtain the IPS solution for testing.

(2) Glucose standard curve preparation: Glucose standard solution (0.1 mg/mL): Glucose standard (0.1 g) was placed in a 100-mL beaker and dissolved in distilled water (to obtain a volume of 1,000 mL) and stored at 4°C. Pipettes (0, 0.2, 0.4, 0.6, 0.8, and 1.0 mL) of the glucose standard solution were placed into test tubes, followed by the addition of distilled water (to obtain a volume of 1.0 mL) and thorough mixing. Subsequently, 1 mL of 5% phenol and 5 mL of concentrated sulfuric acid were added, mixed thoroughly, placed in a boiling water bath for 15 min, and quickly cooled under running water. After 10 min at room temperature, the absorbance was measured at 490 nm using distilled water as the blank. The glucose standard curve was plotted with glucose content (mg) on the *x*-axis and absorbance on the *y*-axis. The linear regression equation for the glucose standard is $Y = 10.185X - 0.0453$ ($R^2 = 0.9927$).

(3) IPS content determination: We measured according to step (2) and calculated the IPS content thus:

$$\text{IPS content}\left(\text{mg}/\text{g}\right) = \frac{m_1 \times V_1}{m \times V} \times N$$

where m_1 is the glucose content calculated from the standard curve (mg), V_1 is the volume (mL), N is the dilution factor, m is the sample mass (g), and V is the volume of the sample solution used for the measurement (mL).

2.7 Metabolomic analysis

2.7.1 Intracellular metabolite extraction

Frozen samples were mixed into a fine powder in liquid nitrogen. A 50 mg sample and 1,000 μL of extraction liquid (methanol: acetonitrile: deionized water = 2:2:1, v/v) and 20 mg/L internal standard (L-2-chlorophenylalanine) were vortexed for 30 s. The mixture was thoroughly ground using a grinder (45 Hz, with steel balls), followed by ultrasonic extraction for 10 min in an ice-water bath. Subsequently, the samples were left to stand at −20°C for 1 h and centrifuged for 15 min (13,000 × *g*, 4°C), and 500 μL of the supernatant was collected into a PE tube, where they extracted a vacuum concentrator. To the extract, 160 μL of extraction liquid (acetonitrile: deionized water = 1:1, v/v) was added, followed by vortexing for 30 s, ultrasonication for 10 min (in an ice-water bath), and centrifugation for 15 min (12,000 × *g*, 4°C). Next, 120 μL of the supernatant was taken into a 2 mL sample vial, with 10 μL from each sample mixed into a QC sample for analysis (Dunn et al., 2011).

2.7.2 Metabolomics detection

The samples were analyzed using Waters Acquity I-Class PLUS ultra-performance liquid chromatography on a Waters Xevo G2-XS QTOF high-resolution mass spectrometer. The chromatographic column was Waters Acquity UPLC HSS T3 (1.8 um, 2.1 mm × 100 mm). The operational parameters were as follows: injection volume 1 μL; flow rate 400 μL/min; mobile phase, 0.1% (v/v) formic acid aqueous solution (A) and formic acid acetonitrile (B). The gradient program was as follows: 2% solvent B (0 min) increased to 98% (10 min) and maintained at 98% for 3 min, reduced to 2% at 13.00–13.10 min and maintained at 2% for 1.90 min; the total runtime was 15 min. Mass charge ratio (m/z) acquisition range 50–1,200, capillary voltage 2,500 V (positive ion mode) or − 2,000 V (negative ion mode), cone voltage 30 V, ion source temperature 100°C, desolvation gas temperature 500°C, cone gas flow rate 50 L/h, desolvation gas flow rate 800 L/h, a low collision energy of 2 V, a high

collision energy range of 10–40 V, and the scanning frequency was 0.2 s/spectrum (Wang et al., 2016).

2.8 Data processing and statistical analysis

The determination of biomass and IPS content in pure and co-cultured liquid cultures of *S. vaninii* and *P. sapidus* was performed thrice, and metabolomic analyses were performed six times. Data were presented as mean ± standard deviation. Microsoft Excel 2022 was used for the statistical analysis and plotting. Biomass and IPS contents were determined using a one-way ANOVA and Duncan's test ($p < 0.05$).

The raw data collected using MassLynx V4.2 were processed using Progenesis QI software for peak extraction, peak alignment, and other data processing operations, based on the Progenesis QI software online METLIN database and Biomark's self-built library for identification, as well as theoretical fragment identification and mass deviation, which were within 100 ppm (Wang et al., 2016). After normalizing the original peak area information to the total peak area, a follow-up analysis was performed. Principal component analysis (PCA) and Spearman's correlation analysis were used to assess the repeatability of the samples within the group and the quality control samples. The identified compounds were searched for classification and pathway information in the KEGG, HMDB, and lipid map databases. Based on the grouping information, we calculated and compared the difference multiples, and a *t*-test was used to calculate the significance *p*-value of each compound. The R language package ropls was used to perform orthogonal partial least squares discriminant analysis (OPLS-DA) modeling, and permutation tests were performed 200 times to verify the reliability of the model. The variable importance in the projection (VIP) value of the model was calculated using multiple cross-validations. The method of combining the difference multiple, *p* value, and VIP value of the OPLS-DA model was adopted to screen the differential metabolites. The screening criteria were (VIP) ≥ 1 and *p* value ($p < 0.05$). Differences in metabolites with significant KEGG pathway enrichment were calculated using the hypergeometric distribution test.

3 Results and discussion

3.1 Physical interactions in the co-culture of *Sanghuangporus vaninii* and *Pleurotus sapidus*

Extensive interactions between microbes of the same or different species regulate the activities (such as replication, transcription, translation, and metabolism) of this biological community at different levels (Wu and Liu, 2022). We conducted a liquid co-culture study to understand the interactions between *S. vaninii* and *P. sapidus* during liquid co-culturing. After the co-culturing, we assessed the mycelial growth rate by comparing the size of the mycelia of the strains with those of the pure cultures. The mycelium morphology (Figures 1A–C) showed that the growth rate of *P. sapidus* under co-culture conditions did not significantly decline compared with that under pure culture conditions, and the color of the mycelial pellets showed no significant changes. However, under co-culture conditions, *S. vaninii* was slowed down, the color of the mycelial pellets became lighter, the pellets were smaller, and the mycelia were fewer and shorter, indicating that *P. sapidus* inhibited *S. vaninii* growth. Therefore, further studies were conducted on the biomass and IPS content in the co-culture and pure cultures of *S. vaninii* and *P. sapidus* to assess the influence of the co-culture on the fungi. The biomass under co-culture conditions was 3.23 and 1.08 times those of *S. vaninii* and *P. Sapidus*, respectively, in pure cultures (Figure 1D); the IPS content under co-culture conditions was 5.08 and 1.23 times those of *S. vaninii* and *P. sapidus*, respectively, in pure cultures (Figure 1E), indicating that the co-culture of *S. vaninii* and *P. sapidus* enhanced the biomass and IPS content in the liquid co-culture system.

3.2 Metabolite qualitative and quantitative analysis and data quality assessment

Fungal SMs have several applications in the food and medicine industries. Therefore, the co-culture of multiple microorganisms has a common application in various studies to increase SM yield (Liu et al., 2022). However, studies on the differences in SMs between *S. vaninii* and *P. sapidus* under pure culture and co-culture conditions are rare. To determine the changes in related metabolomes after co-culturing *S. vaninii* and *P. sapidus*, we conducted an untargeted metabolomic analysis of the mycelia of both species under pure culture and co-culture conditions. The 17,589 peaks were detected in the positive and negative ion modes, annotating 3,188 metabolites. Multivariate statistical analysis was performed to determine changes in metabolite profiles between the different treatments. PCA score plots showed a significant separation trend of metabolites for the pure culture of *S. vaninii* (S), co-culture of *S. vaninii* (S_C), pure culture of *P. sapidus* (P), and co-culture of *P. sapidus* (P_C) (PC1: 35.11%, PC2: 14.34%) (Figure 2A), indicating significant differences between groups and good consistency within the groups. This trend was also illustrated in the sample correlation graph (Figure 2B), a possible "stress" response during co-culturing.

To show a smaller value, we plotted OPLS-DA score graphs for the pure cultures and co-cultures of *S. vaninii* and *P. sapidus*. The results showed that Component 1 accounted for 41 and 26% of the variation, whereas Component 2 accounted for 18 and 25% (Figures 2C,D). In the PCA score plot, the overlapping samples (P and P_C) were distinguished in the OPLS-DA score plot. The R2Y values were 0.99 and 0.967, and the Q2Y values were 0.942 and 0.854, respectively. R2Y explains the calibration of the model samples, and Q2Y describes the predictive capability. According to a study, when the R2Y and Q2Y are strikingly similar, the model in the OPLS-DA score plot shows meaningful results (Bevilacqua and Bro, 2020). Thus, this result implies that the model is stable, reliable, and suitable for further screening of differential metabolites and indicates significant reprogramming of the metabolome after co-culturing *S. vaninii* and *P. sapidus*.

3.3 Differential metabolite analysis

Based on the OPLS-DA, differential metabolites were determined using VIP ≥ 1 and $p < 0.05$ as criteria. A total of 1,591 significantly different metabolites were found between the pure cultures and

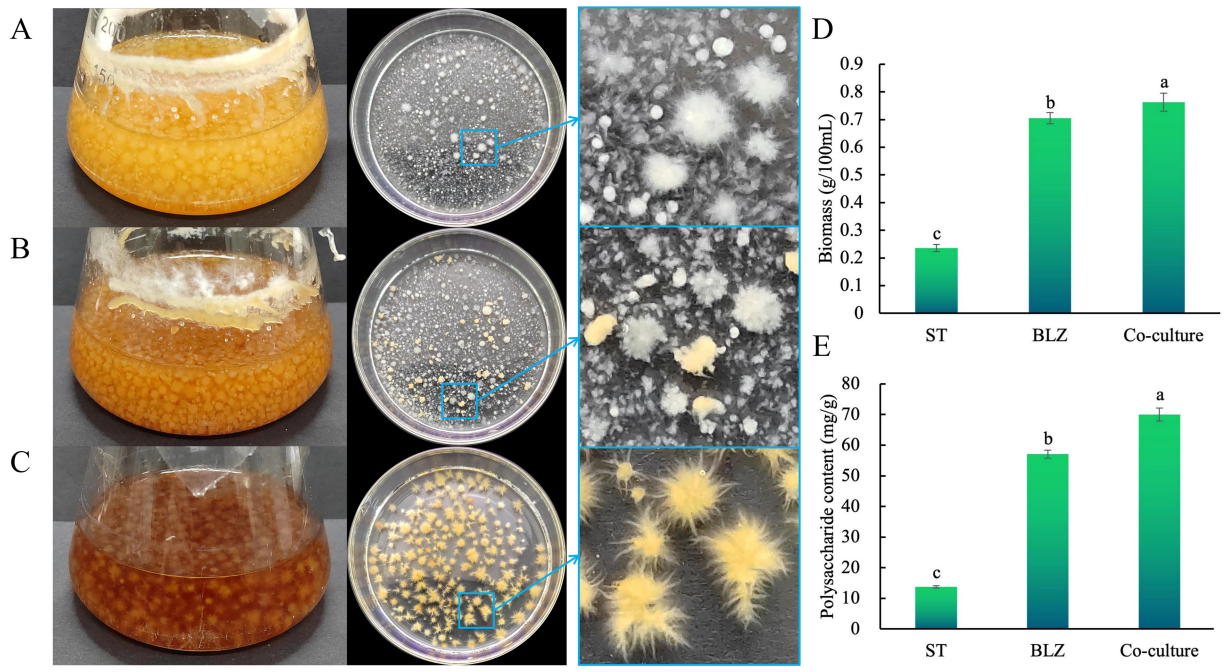

FIGURE 1
(A) Pure culture of *Pleurotus sapidus*; **(B)** co-culture of *Sanghuangporus vaninii* and *P. sapidus*; **(C)** pure culture of *S. vaninii*; **(D)** biomass; and **(E)** polysaccharide content. Lowercase letters indicate significant differences at a *p* value of <0.05 level.

co-cultures of *S. vaninii* (907 upregulated and 684 downregulated) (Figure 3A). Many upregulated metabolites were annotated as amino acids, peptides, and analogs (Supplementary Table S1), such as D-glutamine, D-proline, glutathione, L-threonine, L-histidine, L-isoleucine, and L-glutamate. Additionally, the contents of carbohydrates and carbohydrate conjugates (Supplementary Table S2) and fatty acids and conjugates, including D-fucose, D-ribulose, L-rhamnose, rutinose, isomaltose, undecylic acid, suberic acid, heptadecanoic acid, and nonadecanoic acid, were enhanced (Supplementary Table S3). However, during co-culturing, the content of certain amino acids, peptides, and analogs (Supplementary Table S4) and fatty acids and conjugates (Supplementary Table S5), such as L-aspartic acid, L-serine, L-asparagine, octanoic acid, azelaic acid, hexadecanedioate, and butanoic acid, were decreased, indicating that *S. vaninii* requires significant protein and fatty acid metabolism to cope with the competition for space and nutrients in the co-culture. The differentially expressed metabolites were used for functional pathway enrichment in the KEGG database. The results showed that the differential metabolites primarily participate in carotenoid biosynthesis, caffeine metabolism, indole diterpene alkaloid biosynthesis, lysine degradation, and carbon fixation in photosynthetic organisms (Figure 3C).

Between the pure cultures and co-cultures of *P. sapidus*, 855 significantly different metabolites were screened (401 upregulated and 454 downregulated) (Figure 3B). Compared with those in pure cultures, many upregulated metabolites, such as L-glutamine and tryptophyl-tryptophan, were annotated as amino acids, peptides, and analogs (Supplementary Table S6). Among the downregulated metabolites, L-serine and DL-O-tyrosine were annotated as amino acids, peptides, and analogs (Supplementary Table S7). Additionally, the contents of some fatty acids and conjugates (Supplementary Table S8), such as itaconate, suberic acid, azelaic acid, and hexadecanoic acid, were decreased. Itaconate is a small-molecule metabolite with significant anti-inflammatory activity discovered in macrophages in recent years (Chen et al., 2022), playing a crucial role in antibacterial defense and inflammation inhibition (McGettrick et al., 2024). It was not until 2011 that it was identified as a related metabolite produced by macrophages (Lang and Siddique, 2024). However, some studies have shown that itaconate can be obtained through microbial fermentation processes, including filamentous fungi, yeasts, and bacteria (Diankristanti and Ng, 2023; Blaga et al., 2024). Additionally, in the HMDB data, the route of exposure includes mushroom, such as *Chanterelle*, *Common mushroom*, and *Shiitake*.[1] Based on this, we hypothesize that *P. sapidus* can produce itaconate in co-cultures, and further research is needed to elucidate the molecular mechanisms by which it is produced through co-culture. The above indicates that *P. sapidus* requires significant protein and fatty acid metabolism to cope with the competition for space and nutrients in the co-culture. The primary KEGG functional pathways enriched with differential metabolites were vancomycin resistance, biosynthesis of various antibiotics, pentose phosphate pathway, furfural degradation, and one-carbon pool by folate (Figure 3D). Vancomycin is a clinically significant glycopeptide antibiotic, isolated in 1956 from *Amycolatopsis orientalis* (also known as *Streptomyces orientalis* and *Nocardia orientalis*) (Chen S. et al., 2024; Pisani et al., 2024). Moussa et al. (2022) summarized that 39 compounds and extracts from edible

1 https://hmdb.ca/metabolites/HMDB0002092

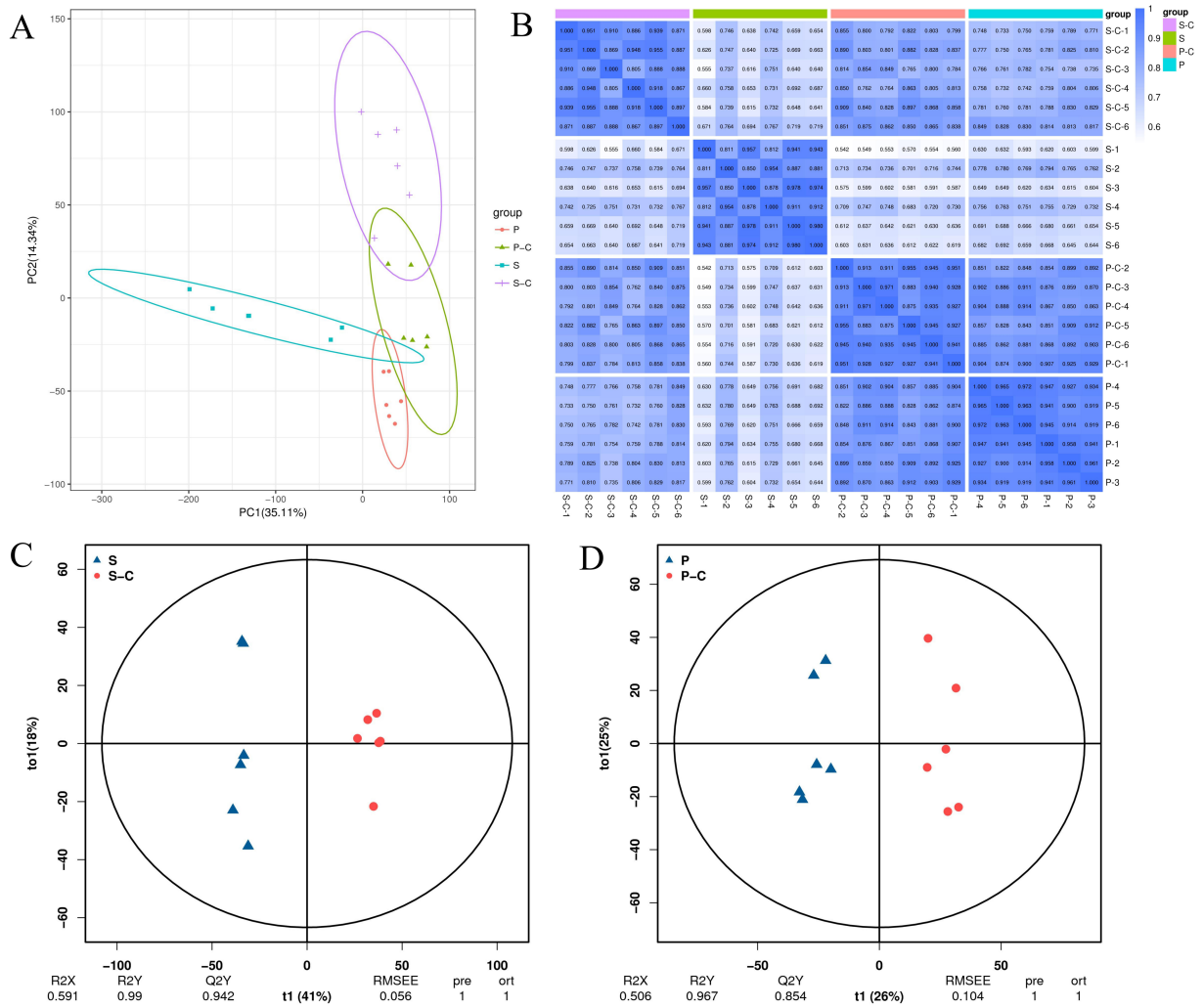

FIGURE 2
(A) PCA analysis of all samples; **(B)** correlation map between samples; **(C)** S-vs-S_C OPLS-DA score plot; **(D)** P-vs-P_C OPLS-DA score plot. S, Pure culture of *Sanghuangporus vaninii*; S_C, Co-culture of *S. vaninii*; P, Pure culture of *Pleurotus sapidus*; P_C, Co-culture of *P. sapidus*.

mushrooms exhibited activity against VRSA (vancomycin-resistant *Staphylococcus aureus*), with terpenoids showing the strongest antimicrobial effects. Li et al. (2021) summarized the isolation of a tricyclic diterpenoid antibiotic, pleuromutilin, from the species *Pleurotus mutilis* and *Pleurotus passeckeranius*, which demonstrated good inhibitory activity against vancomycin-intermediate *Staphylococcus aureus* (VISA), heterogeneous VISA (hVISA), and vancomycin-resistant *Staphylococcus aureus* (VRSA). *Pleurotus sapidus*, *Pleurotus mutilis*, and *Pleurotus passeckeranius* all belong to the *Pleurotus*. In our study, the vancomycin-resistance pathway showed the most significant differences, while reports on vancomycin resistance in large edible and medicinal fungi are rare.

3.4 Analysis of key metabolic pathways

3.4.1 Glycolysis pathway

Glycolysis is an essential metabolic pathway for most organisms to obtain energy through the oxidation of sugars, consisting of a total of 10 enzymatic reactions (Pyrihová et al., 2024). In the seventh and eighth enzymatic reactions, under the action of phosphoglycerate kinase, the high-energy phosphoryl group of 1,3-bisphosphoglycerate is transferred to ADP to form ATP and 3-phosphoglycerate. Subsequently, 3-phosphoglycerate is converted to 2-phosphoglycerate under the catalysis of phosphoglycerate mutase (Chandel, 2021a). Additionally, 3-phosphoglycerate is a key intermediate in several central metabolic pathways, including glycolysis and glucose generation (Jang et al., 2009). During co-culture, the expression of both 3-phosphoglycerate and 2-phosphoglycerate was significantly upregulated in *S. vaninii*, while both were significantly downregulated in *P. sapidus* (Supplementary Table S9). This indicates that in the co-culture system, the glycolytic activity of *S. vaninii* is stronger than that of *P. sapidus*, providing more energy and starting materials for synthesizing substances in other metabolic pathways.

3.4.2 Tricarboxylic acid cycle

The TCA cycle is the center of glucose, protein, lipid, and energy metabolisms within the cell (Kato et al., 2022). The expression of succinate and fumarate related to the TCA cycle was significantly upregulated in *S. vaninii*, whereas fumarate was significantly

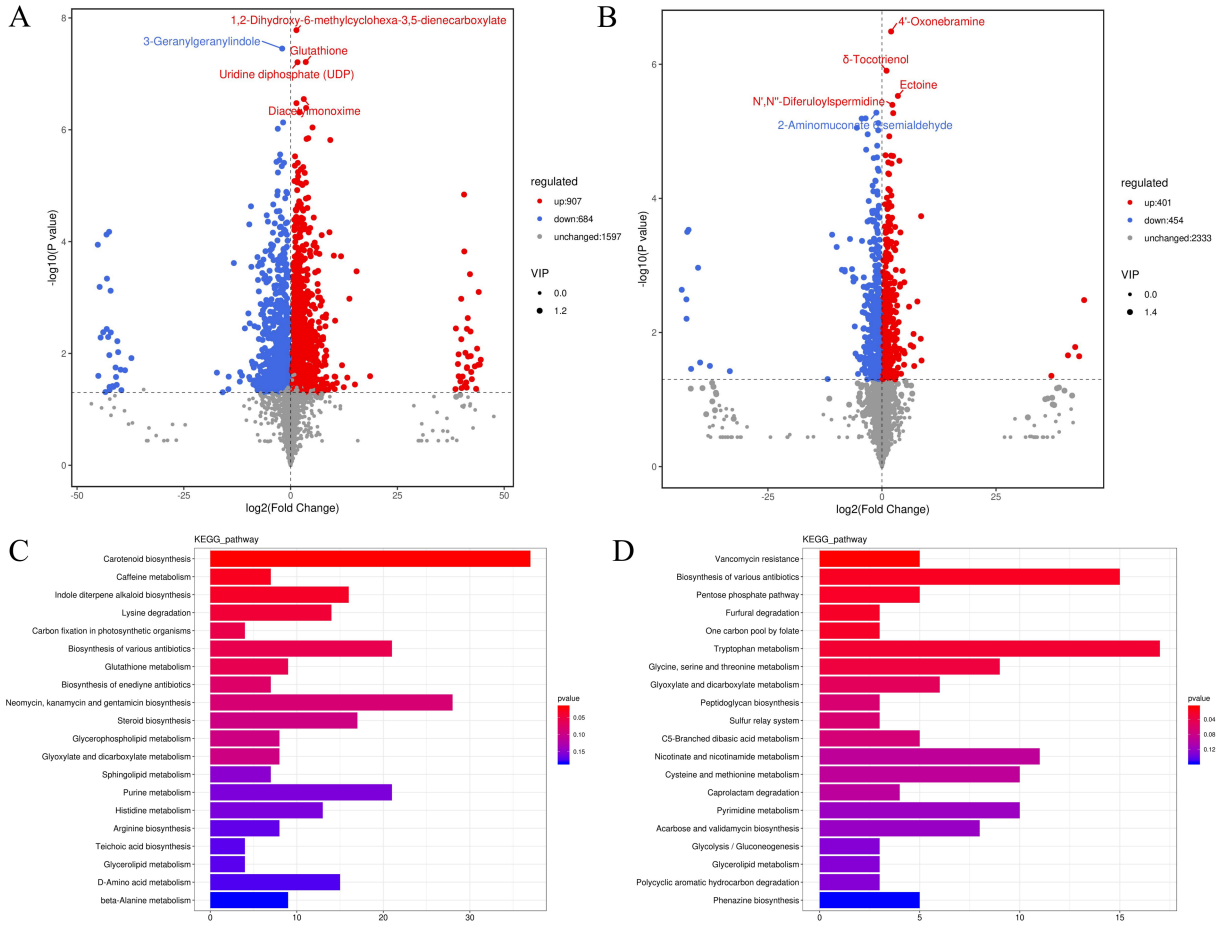

FIGURE 3
(A) Volcano plot of S-vs-S_C differential metabolites; **(B)** volcano plot of P-vs-P_C differential metabolites; **(C)** bar chart of S-vs-S_C differential metabolite pathways; **(D)** bar chart of P-vs-P_C differential metabolite pathways. S, Pure culture of *Sanghuangporus vaninii*; S_C, Co-culture of *S. vaninii*; P, Pure culture of *P. sapidus*; P_C, Co-culture of *P. sapidus*.

downregulated in *P. sapidus* (Supplementary Table S10). Succinate plays a crucial role in mitochondrial energy production and is also involved in signaling pathways, reactive oxygen species generation, and other processes (Chen H. et al., 2024). Mitochondrial respiratory complex II (CII) reversibly oxidizes succinate to fumarate, producing electrons that are transported via the Fe–S cluster chain to the ubiquinone membrane pool, thus providing ubiquinol QH2 for the respiratory chain during oxidative phosphorylation (Markevich et al., 2020). In summary, the *S. vaninii* TCA system in the co-culture system is in an active state, providing an effective energy and material exchange mechanism for its growth and metabolism. Co-culturing *S. vaninii* with *P. sapidus* accelerated the energy and material metabolism of *S. vaninii*, providing a material synthesis and energy foundation for maintaining the stability of *S. vaninii* in the external environment.

3.4.3 Nucleotide metabolism

Nucleotides are DNA and RNA components that provide energy, activate signaling pathways, and increase cellular biomass in living cells (Ariav et al., 2021; Chandel, 2021b). In the co-culture systems, the expression levels of cytidine and cytosine in cells were significantly downregulated, whereas those of uridine, uracil, guanine, xanthosine, xanthine, and adenine were significantly upregulated (Supplementary Table S11). These results indicate that the interactions in the co-culture play a role in regulating cell division. This further suggests a symbiotic, mutually beneficial stage during the co-culturing process between *S. vaninii* and *P. sapidus*.

3.4.4 Amino acid metabolism

As a glutamine precursor, glutamate regulates cellular nitrogen assimilation through the synergistic action of glutamine synthetase/glutamate synthase (GS/GOGAT) (Sanz-Luque et al., 2015). In the co-culture, glutamate expression in *S. vaninii* was significantly increased along with the constancy of glutamine, and glutamine expression in *P. sapidus* was also significantly increased, indicating that the symbiotic system effectively utilized the nitrogen source in the medium to survive by maintaining stable levels of these amino acids (León-Vaz et al., 2021). Threonine, which has strong antioxidant properties (Huang et al., 2021), showed significantly increased expression in *S. vaninii* during co-culturing (Supplementary Table S12), indicating that it participates in the balance of oxidative stress in the system, further enhancing its self-defense capabilities.

3.4.5 Polysaccharide synthesis

The most extensively studied monosaccharides in mushrooms are glucose, mannose, galactose, xylose, arabinose, rhamnose, and fucose (Wang et al., 2017). Previous results showed that the IPS in the co-culture was higher than that in pure cultures of *S. vaninii* and *P. sapidus*. The expression levels of mannose, galactose, and glucose were significantly increased in *S. vaninii* but not in *P. sapidus*. In the fructose and mannose metabolism pathways, L-rhamnose expression in *S. vaninii* was significantly increased, with a difference multiple of 16.38 (Supplementary Table S13). These results indicate that the co-culture primarily promoted an increase in monosaccharide expression in *S. vaninii* cells, while the impact on *P. sapidus* was relatively small. This significant increase in monosaccharide expression enhanced the stability and resistance of *S. vaninii* cells to the co-culture environment.

3.4.6 Antioxidant system

The activation of a robust and complex antioxidant system is the reaction mechanism of the symbiotic system to environmental stress, including non-enzymatic antioxidants (glutathione, betaine, proline, and ascorbic acid) and antioxidant enzymes (Wang J. et al., 2023). The expression levels of reduced glutathione, oxidized glutathione, and D-proline were significantly increased in *S. vaninii* but not in *P. sapidus* (Supplementary Table S12). Glutathione is the most abundant intracellular antioxidant (Wang et al., 2014) that primarily alleviates intracellular oxidative stress (Mochizuki et al., 2023). Glutathione expression was significantly increased in *S. vaninii*, indicating its participation in alleviating cellular stress. Proline is a multifunctional amino acid that is essential for protein biosynthesis. Proline plays a significant role in enhancing abiotic stress tolerance (Jurkonienė et al., 2023), acting as an osmoprotectant, stabilizing macromolecules, scavenging free radicals, and maintaining redox balance (Alvarez et al., 2022). This indicates that the co-culture environment imposed survival pressure on *S. vaninii*, prompting the overexpression of glutathione and proline under unfavorable conditions to maintain cellular homeostasis.

3.4.7 Transport proteins

ABC transport proteins are ubiquitous in prokaryotic (blue-green algae) and eukaryotic (fungi) cells and obtain energy through ATP hydrolysis to mediate active transmembrane transport (Nickerson et al., 2018). In the ATP hydrolysis process, ABC transport proteins transport natural metabolites and various xenobiotics, including antifungal compounds, making certain ABC transporters crucial players in antifungal resistance (Víglaš and Olejníková, 2021). The activation of the ABC transport protein system (Supplementary Table S14) in the co-culture system signifies that the environmental pressure exerted by co-culturing caused the rapid exchange and transport of substances inside and outside the cells to maintain the stability requirements of symbiosis between *S. vaninii* and *P. sapidus* in the co-culture system.

3.5 Metabolic molecular mechanism of the co-culture system of *Sanghuangporus vaninii* and *Pleurotus sapidus*

The cumulative effects on *S. vaninii* and *P. sapidus* owing to co-culturing are attributable to the fact that fungal interactions in the co-culture enhance IPS production within the system, making the production of commercially valuable products feasible. The synthesis of the intermediate product, UDP-Glc, was sufficient to support this conclusion. In *S. vaninii*, co-culturing leads to the upregulation of substances related to the glycolysis pathway, indicating that the stress produced by co-culturing benefits the cycle. The expression of substances involved in the TCA cycle was upregulated, leading to more SMs entering different pathways for amino acid, fatty acid, transport protein, and nucleotide synthesis (Figure 4). It provides a

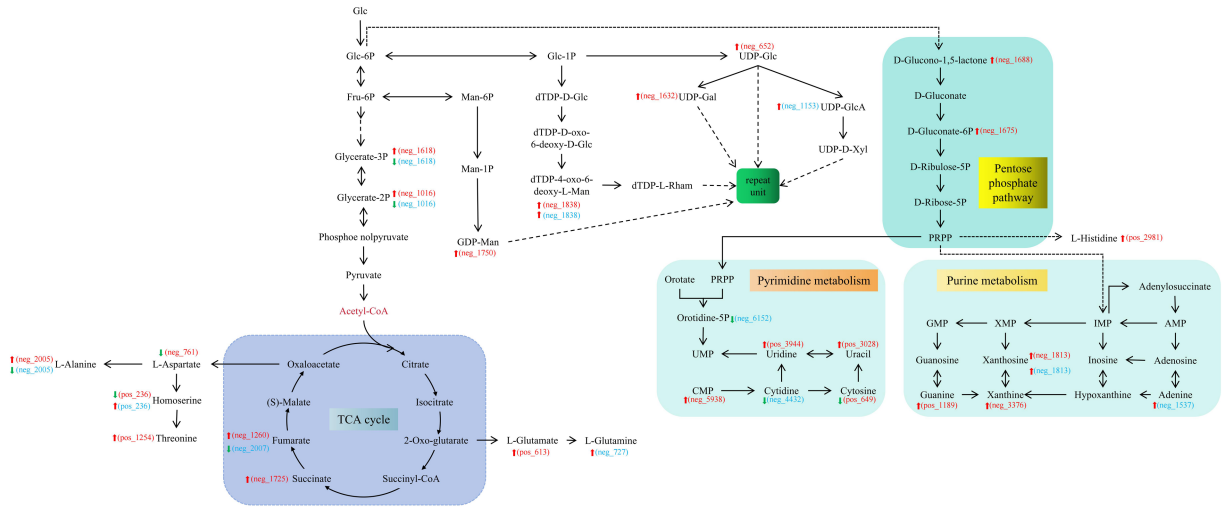

FIGURE 4
Key metabolic network diagram of the co-culture of *Sanghuangporus vaninii* and *Pleurotus sapidus*. The red font ID represents the differential metabolites in S_vs_S-C. The blue font ID represents the differential metabolites in P_vs_P-C. S, Pure culture of *S. vaninii*; S_C, co-culture of *S. vaninii*; P, Pure culture of *P. sapidus*; P_C, Co-culture of *P. sapidus*.

co-culture system with buffering and supplementation to cope with environmental pressures and nutritional competition.

4 Conclusion

The liquid co-culturing of *S. vaninii* and *P. sapidus* significantly enhanced the biomass and IPS content of the co-culture system. Similarly, *P. sapidus* exerted a noticeable inhibitory effect on *S. vaninii* growth. The detection of intracellular metabolites indicated that fungal co-culture affects SM production via multiple metabolic pathways. In addition, it elucidates the rapid adaptation to environmental changes in co-cultures, a process revealed to involve the regulation of several metabolic pathways (amino acid metabolism, TCA cycle, glycolysis pathway, polysaccharide metabolism, and nucleotide metabolism). These results provide new insights into the selection of good co-culture combinations and activation of silent gene clusters for microbial SM synthesis. In the future, we will investigate whether new metabolites are produced and explore the molecular mechanisms underlying these changes. This study will help enrich the product development of large edible and medicinal fungi by providing new ideas.

Data availability statement

The original contributions presented in the study are included in the article/Supplementary material, further inquiries can be directed to the corresponding author.

Author contributions

YL: Conceptualization, Data curation, Formal analysis, Investigation, Methodology, Writing – original draft, Writing – review & editing. DL: Funding acquisition, Project administration, Supervision, Writing – review & editing.

Funding

The author(s) declare that financial support was received for the research, authorship, and/or publication of this article. This study was supported by the National Key Research and Development Program of China (Grant No.2017YFD0300104).

Conflict of interest

The authors declare that the research was conducted in the absence of any commercial or financial relationships that could be construed as a potential conflict of interest.

Publisher's note

Supplementary material

The Supplementary material for this article can be found online at: https://www.frontiersin.org/articles/10.3389/fsufs.2024.1445993/full#supplementary-material

References

Adnani, N., Vazquez-Rivera, E., Adibhatla, S. N., Ellis, G. A., Braun, D. R., and Bugni, T. S. (2015). Investigation of interspecies interactions within marine micromonosporaceae using an improved co-culture approach. *Mar Drugs* 13, 6082–6098. doi: 10.3390/md13106082

Alvarez, M. E., Savouré, A., and Szabados, L. (2022). Proline metabolism as regulatory hub. *Trends Plant Sci* 27, 39–55. doi: 10.1016/j.tplants.2021.07.009

Ariav, Y., Chng, J. H., Christofk, H. R., Ron-Harel, N., and Erez, A. (2021). Targeting nucleotide metabolism as the nexus of viral infections, cancer, and the immune response. *Sci Adv* 7:eabg6165. doi: 10.1126/sciadv.abg6165

Bertrand, S., Schumpp, O., Bohni, N., Bujard, A., Azzollini, A., Monod, M., et al. (2013a). Detection of metabolite induction in fungal co-cultures on solid media by high-throughput differential ultra-high pressure liquid chromatography–time-of-flight mass spectrometry fingerprinting. *J Chromatogr A* 1292, 219–228. doi: 10.1016/j.chroma.2013.01.098

Bertrand, S., Schumpp, O., Bohni, N., Monod, M., Gindro, K., and Wolfender, J.-L. (2013b). De novo production of metabolites by fungal co-culture of *Trichophyton rubrum* and *Bionectria ochroleuca*. *J Nat Prod* 76, 1157–1165. doi: 10.1021/np400258f

Bevilacqua, M., and Bro, R. (2020). Can we trust score plots? *Meta* 10:278. doi: 10.3390/metabo10070278

Blaga, A. C., Kloetzer, L., Cascaval, D., Galaction, A.-I., and Tucaliuc, A. (2024). Studies on reactive extraction of itaconic acid from fermentation broths. *PRO* 12:725. doi: 10.3390/pr12040725

Boateng, I. D., Guo, Y.-Z., and Yang, X.-M. (2024). Extraction, purification, structural characterization, and antitumor effects of water-soluble intracellular polysaccharide (IPSW-1) from *Phellinus igniarius* mycelia. *J Agric Food Chem* 72, 19721–19732. doi: 10.1021/acs.jafc.4c01059

Caudal, F., Tapissier-Bontemps, N., and Edrada-Ebel, R. A. (2022). Impact of co-culture on the metabolism of marine microorganisms. *Mar Drugs* 20:153. doi: 10.3390/md20020153

Chandel, N. S. (2021a). Glycolysis. *Csh Perspect Biol* 13:a040535. doi: 10.1101/cshperspect.a040535

Chandel, N. S. (2021b). Nucleotide metabolism. *Cold Spring Harb Perspect Biol* 13:a040592. doi: 10.1101/cshperspect.a040592

Chen, H., Jin, C., Xie, L., and Wu, J. (2024). Succinate as a signaling molecule in the mediation of liver diseases. *Biochim Biophys Acta (BBA) Mol Basis Dis* 1870:166935. doi: 10.1016/j.bbadis.2023.166935

Chen, L.-L., Morcelle, C., Cheng, Z.-L., Chen, X., Xu, Y., Gao, Y., et al. (2022). Itaconate inhibits TET DNA dioxygenases to dampen inflammatory responses. *Nat Cell Biol* 24, 353–363. doi: 10.1038/s41556-022-00853-8

Chen, S., Rao, M., Jin, W., Hu, M., Chen, D., Ge, M., et al. (2024). Metabolomic analysis in *Amycolatopsis keratiniphila* disrupted the competing ECO0501 pathway for enhancing the accumulation of vancomycin. *World J Microbiol Biotechnol* 40:297. doi: 10.1007/s11274-024-04105-9

Chiu, C.-H., Chen, M.-Y., Lieu, J.-J., Chen, C.-C., Chang, C.-C., Chyau, C.-C., et al. (2023). Inhibitory effect of styrylpyrone extract of *Phellinus linteus* on hepatic steatosis in HepG2 cells. *Int J Mol Sci* 24:3672. doi: 10.3390/ijms24043672

Costa, J. H., Wassano, C. I., Angolini, C. F. F., Scherlach, K., Hertweck, C., and Pacheco Fill, T. (2019). Antifungal potential of secondary metabolites involved in the interaction between citrus pathogens. *Sci Rep* 9:18647. doi: 10.1038/s41598-019-55204-9

Diankristanti, P. A., and Ng, I.-S. (2023). Microbial itaconic acid bioproduction towards sustainable development: insights, challenges, and prospects. *Bioresour Technol* 384:129280. doi: 10.1016/j.biortech.2023.129280

Dunn, W. B., Broadhurst, D., Begley, P., Zelena, E., Francis-McIntyre, S., Anderson, N., et al. (2011). Procedures for large-scale metabolic profiling of serum and plasma using gas chromatography and liquid chromatography coupled to mass spectrometry. *Nat Protoc* 6, 1060–1083. doi: 10.1038/nprot.2011.335

Gao, Y., Li, X., Xu, H., Sun, H., Zhang, J., Wu, X., et al. (2024). The liquid-fermentation formulation of *Sanghuangporus sanghuang* optimized by response surface methodology and evaluation of biological activity of extracellular polysaccharides. *Food Secur* 13:1190. doi: 10.3390/foods13081190

Guo, L., Xi, B., and Lu, L. (2024). Strategies to enhance production of metabolites in microbial co-culture systems. *Bioresour Technol* 406:131049. doi: 10.1016/j.biortech.2024.131049

Hou, C., Chen, L., Yang, L., and Ji, X. (2020). An insight into anti-inflammatory effects of natural polysaccharides. *Int J Biol Macromol* 153, 248–255. doi: 10.1016/j.ijbiomac.2020.02.315

Hu, X., Ganesan, K., Khan, H., and Xu, B. (2024). Critical reviews on anti-cancer effects of edible and medicinal mushroom *Phellinus linteus* and its molecular mechanisms. *Food Rev Int* 40, 1118–1137. doi: 10.1080/87559129.2023.2212036

Huang, L., Fang, Z., Gao, J., Wang, J., Li, Y., Sun, L., et al. (2021). Protective role of l-threonine against cadmium toxicity in *Saccharomyces cerevisiae*. *J Basic Microbiol* 61, 339–350. doi: 10.1002/jobm.202100012

Jang, M., Kang, H. J., Lee, S. Y., Chung, S. J., Kang, S., Chi, S. W., et al. (2009). Glyceraldehyde-3-phosphate, a glycolytic intermediate, plays a key role in controlling cell fate via inhibition of caspase activity. *Mol Cell* 28, 559–564. doi: 10.1007/s10059-009-0151-7

Jurkonienė, S., Mockevičiūtė, R., Gavelienė, V., Šveikauskas, V., Zareyan, M., Jankovska-Bortkevič, E., et al. (2023). Proline enhances resistance and recovery of oilseed rape after a simulated prolonged drought. *Plan Theory* 12:2718. doi: 10.3390/plants12142718

Kato, Y., Inabe, K., Hidese, R., Kondo, A., and Hasunuma, T. (2022). Metabolomics-based engineering for biofuel and bio-based chemical production in microalgae and cyanobacteria: a review. *Bioresour Technol* 344:126196. doi: 10.1016/j.biortech.2021.126196

Lang, R., and Siddique, M. N. A. A. (2024). Control of immune cell signaling by the immuno-metabolite itaconate. *Front Immunol* 15:1352165. doi: 10.3389/fimmu.2024.1352165

León-Vaz, A., Romero, L. C., Gotor, C., León, R., and Vigara, J. (2021). Effect of cadmium in the microalga *Chlorella sorokiniana*: a proteomic study. *Ecotoxicol Environ Saf* 207:111301. doi: 10.1016/j.ecoenv.2020.111301

Li, W., Huang, X., Liu, H., Lian, H., Xu, B., Zhang, W., et al. (2023). Improvement in bacterial cellulose production by co-culturing *Bacillus cereus* and *Komagataeibacter xylinus*. *Carbohydr Polym* 313:120892. doi: 10.1016/j.carbpol.2023.120892

Li, X., Li, J., Zhu, Z., Li, T., Zhang, W., Xia, J., et al. (2021). Advances of Lefamulin: a new pleuromutilin antibiotic. *Acta Pharm Sin* 56, 1006–1015. doi: 10.16438/j.0513-4870.2020-1617

Li, Q., Lin, W., Zhang, X., Wang, M., Zheng, Y., Wang, X., et al. (2024). Transcriptomics integrated with metabolomics reveal the competitive relationship between co-cultured *Trichoderma asperellum* HG1 and *Bacillus subtilis* Tpb55. *Microbiol Res* 280:127598. doi: 10.1016/j.micres.2023.127598

Liu, Z., Kang, B., Duan, X., Hu, Y., Li, W., Wang, C., et al. (2022). Metabolomic profiles of the liquid state fermentation in co-culture of *A. oryzae* and *Z. rouxii*. *Food Microbiol* 103:103966. doi: 10.1016/j.fm.2021.103966

Lu, Y., and Liu, D. (2024). Optimization of polysaccharide conditions and analysis of antioxidant capacity in the co-culture of *Sanghuangporus vaninii* and *Pleurotus sapidus*. *PeerJ* 12:e17571. doi: 10.7717/peerj.17571

Luan, F., Peng, X., Zhao, G., Zeng, J., Zou, J., Rao, Z., et al. (2022). Structural diversity and bioactivity of polysaccharides from medicinal mushroom *Phellinus* spp.: a review. *Food Chem* 397:133731. doi: 10.1016/j.foodchem.2022.133731

Mantravadi, P. K., Kalesh, K. A., Dobson, R. C. J., Hudson, A. O., and Parthasarathy, A. (2019). The quest for novel antimicrobial compounds: emerging trends in research, development, and technologies. *Antibiotics* 8:8. doi: 10.3390/antibiotics8010008

Markevich, N. I., Galimova, M. H., and Markevich, L. N. (2020). Hysteresis and bistability in the succinate-CoQ reductase activity and reactive oxygen species production in the mitochondrial respiratory complex II. *Redox Biol* 37:101630. doi: 10.1016/j.redox.2020.101630

McGettrick, A. F., Bourner, L. A., Dorsey, F. C., and O'Neill, L. A. J. (2024). Metabolic messengers: itaconate. *Nat Metab* 6, 1661–1667. doi: 10.1038/s42255-024-01092-x

Mochizuki, R., Kobayashi, A., Takayama, H., Toida, T., and Ogra, Y. (2023). Simultaneous determination of intracellular reduced and oxidized glutathiones by the König reaction. *Anal Methods* 15, 3426–3431. doi: 10.1039/D3AY00860F

Moussa, A. Y., Fayez, S., Xiao, H., and Xu, B. (2022). New insights into antimicrobial and antibiofilm effects of edible mushrooms. *Food Res Int* 162:111982. doi: 10.1016/j.foodres.2022.111982

Nickerson, N. N., Jao, C. C., Xu, Y., Quinn, J., Skippington, E., Alexander, M. K., et al. (2018). A novel inhibitor of the LolCDE ABC transporter essential for lipoprotein trafficking in gram-negative bacteria. *Antimicrob Agents Chemother* 62:16. doi: 10.1128/AAC.02151-17

Pisani, S., Tufail, S., Rosalia, M., Dorati, R., Genta, I., Chiesa, E., et al. (2024). Antibiotic-loaded nano-sized delivery systems: an insight into gentamicin and vancomycin. *J Funct Biomater* 15:194. doi: 10.3390/jfb15070194

Pyrihová, E., King, M. S., King, A. C., Toleco, M. R., van der Giezen, M., and Kunji, E. R. (2024). A mitochondrial carrier transports glycolytic intermediates to link cytosolic and mitochondrial glycolysis in the human gut parasite *Blastocystis*. *eLife* 13:RP94187. doi: 10.7554/eLife.94187

Sanz-Luque, E., Chamizo-Ampudia, A., Llamas, A., Galvan, A., and Fernandez, E. (2015). Understanding nitrate assimilation and its regulation in microalgae. *Front Plant Sci* 6:899. doi: 10.3389/fpls.2015.00899

Singh, D., and Lee, C. H. (2018). Volatiles mediated interactions between aspergillus oryzae strains modulate morphological transition and exometabolomes. *Front Microbiol* 9:628. doi: 10.3389/fmicb.2018.00628

Sun, Y. (2022). Induction mechanism and secondary metabolites in co-culture of *Aspergillus sydowii*. Dalian, Liaoning, China: Dalian University of Technology.

Tan, X., Zhang, Q., Liu, J., Shang, Y., Min, Y., Sun, X., et al. (2024). Enhanced γ-aminobutyric acid production by co-culture fermentation with *Enterococcus faecium* AB157 and *Saccharomyces cerevisiae* SC125. *LWT* 208:116739. doi: 10.1016/j.lwt.2024.116739

Víglaš, J., and Olejníková, P. (2021). An update on ABC transporters of filamentous fungi – from physiological substrates to xenobiotics. *Microbiol Res* 246:126684. doi: 10.1016/j.micres.2020.126684

Wang, L. (2021). The effect of different light quality on the main active components of *Sanghuangporus vaninii* mycelium and transcriptomics study. Yanji, Jilin, China: Yanbian University.

Wang, Y., Chen, Y., Xin, J., Chen, X., Xu, T., He, J., et al. (2023). Metabolomic profiles of the liquid state fermentation in co-culture of *Eurotium amstelodami* and *Bacillus licheniformis*. *Front Microbiol* 14:1080743. doi: 10.3389/fmicb.2023.1080743

Wang, F., Li, N., Li, H., Di, Y., Li, F., Jiang, P., et al. (2024). An alkali-extracted neutral heteropolysaccharide from *Phellinus nigricans* used as an immunopotentiator in immunosuppressed mice by activating macrophages. *Carbohydr Polym* 335:122110. doi: 10.1016/j.carbpol.2024.122110

Wang, H., Ma, J.-X., Zhou, M., Si, J., and Cui, B.-K. (2022). Current advances and potential trends of the polysaccharides derived from medicinal mushrooms sanghuang. *Front Microbiol* 13:965934. doi: 10.3389/fmicb.2022.965934

Wang, W., Tang, L., Zhou, W., Yang, Y., Gao, B., Zhao, Y., et al. (2014). Progress in the biosynthesis and metabolism of *glutathione*. *China Biotechnol* 34, 89–95. doi: 10.13523/j.cb.20140714

Wang, J., Tian, Q., Kang, J., Zhou, H., Yu, X., Qiu, G., et al. (2024). Metabolomics-based analysis of the interaction effects and stress response mechanisms in the co-culture system of fungi and microalgae under cadmium stress. *J Clean Prod* 447:141473. doi: 10.1016/j.jclepro.2024.141473

Wang, J., Tian, Q., Zhou, H., Kang, J., Yu, X., and Shen, L. (2023). Key metabolites and regulatory network mechanisms in co-culture of fungi and microalgae based on metabolomics analysis. *Bioresour Technol* 388:129718. doi: 10.1016/j.biortech.2023.129718

Wang, Q., Wang, F., Xu, Z., and Ding, Z. (2017). Bioactive mushroom polysaccharides: a review on monosaccharide composition, biosynthesis and regulation. *Molecules* 22:955. doi: 10.3390/molecules22060955

Wang, J., Zhang, T., Shen, X., Liu, J., Zhao, D., Sun, Y., et al. (2016). Serum metabolomics for early diagnosis of esophageal squamous cell carcinoma by UHPLC-QTOF/MS. *Metabolomics* 12:116. doi: 10.1007/s11306-016-1050-5

Wu, M., and Liu, G. (2022). Co-culture strategy for activating the cryptic gene cluster in microorganisms. *Acta Microbiol Sin* 62, 4247–4261. doi: 10.13343/j.cnki.wsxb.20220320

Wu, F., Zhou, L.-W., Vlasak, J., and Dai, Y.-C. (2022). Global diversity and systematics of *Hymenochaetaceae* with poroid hymenophore. *Fungal Divers* 113, 1–192. doi: 10.1007/s13225-021-00496-4

Xu, Z., Theodoropoulos, C., and Pittman, J. K. (2024). Optimization of a *Chlorella–Saccharomyces* co–culture system for enhanced metabolite productivity. *Algal Res* 79:103455. doi: 10.1016/j.algal.2024.103455

frontiers | Frontiers in Nutrition

TYPE Original Research
PUBLISHED 18 December 2024
DOI 10.3389/fnut.2024.1487074

OPEN ACCESS

EDITED BY
Naseeb Singh,
RC NEH, Central Institute of Agricultural Engineering (ICAR), India

REVIEWED BY
Chaitanya Pareek,
CNRS UMR 1234, Indian Institute of Technology Kharagpur, India
Syed Imran,
Central Institute of Agricultural Engineering (ICAR), India
Ramesh Sahni,
Central Institute of Agricultural Engineering (ICAR), India

*CORRESPONDENCE
R. Kavitha
✉ kavitha@tnau.ac.in

RECEIVED 27 August 2024
ACCEPTED 21 November 2024
PUBLISHED 18 December 2024

CITATION
Yallappa D, Kavitha R, Surendrakumar A, Suthakar B, Mohan Kumar AP, Kannan B and Kalarani MK (2024) Improving agricultural spraying with multi-rotor drones: a technical study on operational parameter optimization. *Front. Nutr.* 11:1487074.
doi: 10.3389/fnut.2024.1487074

Improving agricultural spraying with multi-rotor drones: a technical study on operational parameter optimization

D. Yallappa[1], R. Kavitha[1]*, A. Surendrakumar[1], B. Suthakar[1], A. P. Mohan Kumar[1], Balaji Kannan[2] and M. K. Kalarani[3]

[1]Department of Farm Machinery and Power Engineering, Agricultural Engineering College and Research Institute, Tamil Nadu Agricultural University, Coimbatore, India, [2]Department of Soil and Water Conservation Engineering, Agricultural Engineering College and Research Institute, Tamil Nadu Agricultural University, Coimbatore, India, [3]Directorate of Crop Management, Tamil Nadu Agricultural University, Coimbatore, India

Drones play a key role in enhancing nutrient management efficiency under climate change scenarios by enabling precise and adaptable spray applications. Current aerial spray application research is primarily focused on examining the influence of drone spraying parameters *viz.,* flight height, travel speed, rotor configuration, droplet size, payload, spray pressure, spray discharge and wind velocity on spray droplet deposition characteristics. The present study aimed to study and optimize the effect of spray height, operating pressure, nozzle spacing and spray nozzle mounting configuration on spray discharge rate, spray width, spray distribution pattern, spray uniformity and spray liquid loss. A spray patternator of 5.0 m x 5.0 m was developed per Bureau of Indian Standards (BIS) standard to study the spray volume distribution pattern of boom and hex nozzle configuration. Initially, drone spray operational parameters *viz.,* spray discharge rate (Lm^{-1}), operating pressure (kg cm^{-2}) and spray angle (°) were measured using digital nozzle tester, digital pressure gauge and digital protractor, respectively, in the laboratory. Then optimized the nozzle spacing for boom configuration attachment to drone sprayer and recorded best spray uniformity at 0.6 m nozzle spacing. The drone sprayer hovered at three different heights, *viz.,* 1.0, 2.0 and 3.0 m from the top of the patternator and spray operating pressure was maintained at 4.0 kg cm^{-2} in outdoor condition. Single pass distribution pattern and one-direction application distribution pattern method used for optimizing height of spray, operating pressure and nozzle mounting confirmation from the results of discharge rate, spray angle, effective spray width, spray liquid loss and spray distribution uniformity. Results showed that, the better spray uniformity distribution was found when the drone sprayer hover height was increased from the top of the patternator (2.0 m). More round spray droplet vertex pattern was generated during the 1.0 m hover height compared to the 2.0 and 3.0 m hover heights due to the direct impact of downwash airflow generated by the rotors. Finally it was concluded that, the good spray volume distribution was found at 2.0 m height of spray with standard hexa nozzle configuration arrangement as compared to the boom spray nozzle arrangement.

KEYWORDS

boom spray, discharge rate, drone sprayer, distribution pattern, hover height, patternator

1 Introduction

Technological advancements in precision farming, especially through the integration of multi-rotor drones with sprayer devices have revolutionized agricultural practices. These drones enable precise and targeted nutrient management, enhancing crop efficiency and resilience in the face of climate change, thus have transformed pesticide, herbicide, and fertilizer applications (1, 2). These drones provide precise, targeted pesticide delivery, reducing waste, lowering environmental impact, and boosting overall crop health (3). The efficiency of these drone sprayers, however, is strongly reliant on the optimization of their operational parameters. Spray height, nozzle type, droplet size, flight speed, and application rate must all be precisely adjusted to guarantee even coverage and successful pest control. Optimizing these parameters is crucial not only for maximizing the efficacy of the chemicals used, but also for preserving and improving crop nutritional quality. Drones have greatly become benefited with advanced features in autonomous spraying systems, including autonomous path planning, break point continue to spray (4), terrain following radar module (auto altitude adjustment), high-precision obstacle avoidance radar, spray task list, spray solution empty indication, battery level warning, and high-accuracy Real Time Kinematics (RTK) location to significantly increase functional stability, efficiency, accuracy, and ease of use (5). Nutrient composition is directly influenced by the right executive management of nutrients and protective agents, which aids in crop development (6, 7). For example, uniform and optimal spraying can guarantee that crops receive the proper amount of nutrients, resulting in improved growth and nutrient buildup in edible sections of the plant. Furthermore, accurate spraying can reduce crop stress from pests, diseases, and environmental conditions, increasing their resistance. Stress resilience, another important element of crop health, can be strongly influenced by the efficacy of pesticide use. Crops that are less stressed grow faster, produce more, and have superior nutritional profiles. The drone machine operational parameters, *viz.*, flight height, travel speed, payload and configuration, have a great impact on the distribution and penetration of droplets (8). The most important benefit of using a drone (multi-rotor) for chemical spraying is that, due to its unique rotor structure and principle of motion, it generates powerful downwash airflow during flight operation, changing the crop disturbance and improving liquid penetration (9). The downwash airflow velocity of the rotors can create a strong velocity distribution of plants during spraying. This helps the spray droplets to atomize much further with enhanced deposition onto the crop surface. Spray droplet velocity has positive effects on spray swath, deposition, and drift, influencing the operation's consequences (10). Yallappa et al. (11) studied spray volume distribution pattern for boom nozzle configuration using drone sprayer under laboratory condition.

There is lack of detailed study regarding performance of spray operational parameters *viz.*, height of spray, spray pressure, travel speed, discharge rate, spray droplet distribution uniformity and spray nozzle spacing for efficient chemical spray application using drone sprayer. Commercial drone manufacturers are adopting drones without having basic information on the performance and efficacy of the drone spraying system in terms height of spray, nozzle flow rate, operating pressure, type of nozzle and nozzle configuration, spray uniformity and application rate. The present investigation was taken up to study and optimize spray operational parameters of drone sprayer under laboratory condition.

The overall goal of this research was to develop a suitable size patternator for measuring, analyzing and optimizing the spray operational parameters of drone sprayer with the specific objectives *viz.*, (1) development of a suitable customized spray patternator for measuring spray pattern distributions; (2) evaluation for optimizing the effect of height of spray, nozzle spacing and operating pressure on spray discharge rate, effective spray width, spray angle, spray uniformity and spray volume distribution pattern (3) investigation on the impact of drone sprayer machine parameter as downwash airflow on spray distribution systems at different hover heights in outdoor conditions. (4) Recommending the best spray nozzle configuration to drone sprayer based on the spray volume uniformity distribution before actual use in field condition. Optimizing the spray operational parameters of multi-rotor agricultural drones is crucial for accurately estimating and enhancing crop resilience. By delivering precise, timely, and efficient applications, these drones support the development of stronger, more resilient crops, ultimately contributing to sustainable agricultural practices and improved food and nutritional security.

2 Materials and methods

2.1 Drone

The drone sprayer used in the present investigation, was an E610P six-rotor electric (M/s. EFT Electronic Technology Co., Ltd., Hefei City, China) is shown in Figure 1 and specifications are presented in Table 1. The spraying system of the drone sprayer mainly consisted of Flight controller (1), Brushless direct current (BLDC) motors arm (2), Fluid hose pipe (3), BLDC motor (4), Support frame (5), Pesticide tank (6), Landing gear (7), Foldable propeller (8), Lithium polymer (LiPo) batteries (9). The UAV sprayer has two LiPo batteries of 6 cells each with a capacity of 16,000 mAh to supply the necessary current required for the propulsion system. A 24 V BLDC motor coupled with a pump was used to pressurize the spray liquid and then atomize it into fine spray droplets. This drone spray model has the functions of GPS route planning and breakpoint return, which could complete aerial spraying operations autonomously.

2.2 Study the machine and operational parameters of drone sprayer

The selected autonomous battery-operated drone sprayer (Make: EFT Electronic Technology, Model: E610P) was tested and calibrated in the laboratory condition Agricultural Machinery Research Centre (AMRC), Department of Farm Machinery and Power Engineering, Agricultural Engineering College and Research Institute Agricultural University, Coimbatore (11.0122° N, 76.9354° E) by taking different variables which mainly influence the functional performance. ASAE (S341.5) standard calibration procedure has been followed to assess the different spray operational parameters (19).

2.2.1 Measurement of nozzle discharge rate, spray operating pressure and spray angle

A handheld portable digital nozzle tester (AAMS, Maldegem, Belgium) and digital liquid pressure gauge instrument (Make:

FIGURE 1
Electric battery-operated drone sprayer.

TABLE 1 Specifications of drone sprayer.

Main parameter	Norms and numerical values
Type	Hexacopter
Item Model	E610P
Unfold fuselage size, (L × W × H), mm	2000 × 1800 × 670
Folding Size, (L × W × H), mm	950 × 850 × 670
Power source	12S 16,0000 mAh LiPo Battery
Payload capacity, L	10
Self-weight, kg	6.9
Take-off weight, kg	26
Flight height, m	1–20
Forward travel speed, ms^{-1}	0–8
Type of spray nozzle	Flat fan shape
Number of nozzles	4
Discharge rate, l m^{-1}	0–3.2
Swath width of spray, m	3–5
Liquid pressure, kg cm^{-2}	3.4
Remote controller distance, km	1.5
No-load flight time, min	25
Charging time, min	90

Shanghai XuYan Precision Technology Co., Ltd., Model: XY-PG560R) were used to measure spray liquid discharge rate and operating pressure at specific time interval while operating the drone sprayer under normal conditions. A24 V DC brushless direct current (BLDC) motor and diaphragm pump were used to pressurize the spray fluid. This BLDC motor is connected to power distribution board and signal wires were connected to motor port in flight controller (Make: JIYI, Model: K++ V2, Version: V1.5.1).

This autonomous drone sprayer has inbuilt intelligent/ precise spray discharge rate control system at different rotation of BLDC motor speed with PWM from Agri Assistant mobile app (Version: V1.5.1). The Agri Assistant App has a display showing the flow rate of diaphragm pump in terms of Pulse Width Modulation (PWM) ranging from 0 to 100% as shown in Figure 2.

2.2.2 Experimental setup

The diaphragm pump inlet is connected to the fluid tank and its outlet is connected to the main line of four nozzles (2020A-132 series, M/s Ningbo Licheng Agricultural Spray Technology Co., Ltd., Zhejiang, China). Digital liquid pressure gauge and spray flow sensor (Make: Sea, Model: T1A/K3A) were connected in between diaphragm pump outlet and nozzles main hose pipe and pressure was recorded in terms of kg cm^{-2}. An experiment was conducted to assess the effect of drone sprayer BLDC spray motor speed on pump operating pressure, nozzle discharge rate and spray angle. The experimental layout in Agricultural Machinery Research Centre (AMRC), Department of Farm Machinery and Power Engineering, Agricultural Engineering College and Research Institute, Agricultural University, Coimbatore (11.0122° N, 76.9354° E) and is shown in Figure 3.

Initially, transmitter sends the PWM percentage signals (1) to flight controller through receiver. Then spray water flows from fluid tank (2) to spray diaphragm pump (3). The rotational speed of BLDC motor was recorded as a PWM percentage and then converted it in to revolutions per minute using a contactless digital tachometer (Make: Kusam Meco, Model: Km-2234Bl) (4). The operating pressure of spray fluid was recorded using digital liquid pressure gauge instrument (5) and provides the live water flow rate feedback information from water flow sensor (6). Then, recorded the pump flow rate of nozzle (7) in terms of liter per min at 0, 10, 20, 30, 40, 50, 60, 70, 80, 90 and 100% of PWM using a handheld portable nozzle tester (8). Simultaneously, captured the images of each nozzle spray and calculated the actual spray angle using a digital protractor (Make: Yuzuki, Model: IP65). The experimental setup and arrangement for measurement of spray liquid discharge rate, spray motor speed and spray angle are shown in Figures 4–6, respectively.

2.3 Development of spray patternator

A spray patternator of 5.0 m x 5. 0 m was developed as per the BIS standard (IS: 10064–1982) to study and optimize the spray operational

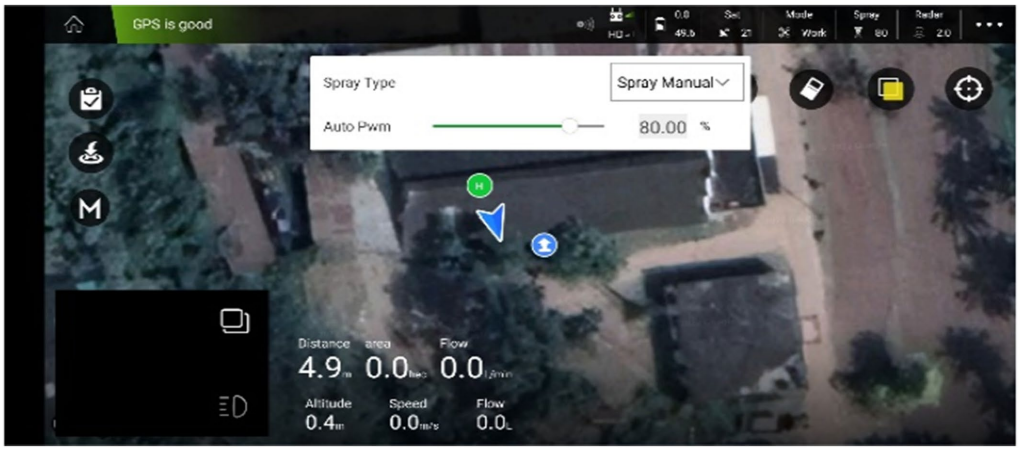

FIGURE 2
Screen display view of intelligent/precise spray liquid flow control system in terms of PWM (%).

parameters of the drone sprayer *viz.,* height of spray, operating pressure and nozzle mounting configuration under laboratory condition (21). The patternator was fabricated using M.S. channel for the frame and sheet (Figure 7). The spray patternator surface was composed of 0.2 cm thick M.S. sheet positioned horizontally over the frame. The patternator has 91 continuous V- type channels at equal spacing mounted on the rectangular frame. According to IS: 8548 and IS 10064 standards, channels should have 25 ± 0.25 mm width and 100 mm depth (20, 21). These constraints make patternator difficult and costly to develop. Bended M.S. sheet in V shape channels with 55 mm width is more than the recommended width to eliminate splash-back between the measurement grooves due to high downwash airflow produced by the rotor propellers of the drone sprayer. The rectangular frame on which sheets were placed, was made up of 5 mm × 5 mm L-shaped MS channel. Measuring cylinders of 190 mL capacity were placed below each channel to collect the spray liquid. The arrangement of measuring jars and funnel in spray patternator is shown in Figures 8, 9 respectively. Patternator has 25° slope for easy movement of water to the jar. The developed spray patternator is shown in Figure 10. The specifications are mentioned in Table 2.

2.4 Optimization the nozzle spacing and operating pressure for boom and hexa nozzle configuration attachment drone

The experiment was conducted for spray volumetric distribution patterns using a specially designed and fabricated spray patternator at the Agricultural Machinery Research Centre (AMRC), Department of Farm Machinery and Power Engineering, Agricultural Engineering College and Research Institute, Tamil Nadu Agricultural University, Coimbatore (11.0122° N, 76.9354° E). The Drone sprayer volume distribution test was conducted as per the IS: 8548 and IS: 10064 and ASAE (S386.2) standards (20–22).

2.4.1 Experimental setup

Two types of nozzles mounting configuration *viz.,* boom and hexa standard type were used in drone sprayer to understand the spray volume distribution system. In the hexa standard type nozzle configuration (Figure 11), four nozzles were mounted below the rotors of the drone sprayer as per the motor BLDC motor configuration and another set of four numbers of flat fan nozzles were placed on the boom type nozzle configuration at equal interval distance (Figure 12).

The nozzle spacing of boom type nozzle configuration was optimized at three operating pressures (3.0, 4.0 and 5.0 kg cm^{-2}) and three nozzles spacing (0.30, 0.45 and 0.60 m). The height of spray 0.545 m is the distance between the tip of the nozzle to the top of patternator V channel surface was selected as per the recommendation IS: 3652 for flat fan nozzle. A Light Detection and Ranging (LIDAR) distance meter instrument (M/s, DEKOPRO, LRE520 80 M) was used to adjust the height of spray. The spray liquid was horizontally directed and landed on the equidistance V shaped channels. When the fluid reaches the patternator surface, it will be collected in different channels. Each channel is provided with own graduated cylinder at the base of the patternator. The spray liquid in the graduated cylinder of the patternator was collected and the quantity of liquid from each channel was measured and noted. The layout of boom and standard hexa type nozzle configuration with patternator is shown in Figures 13, 14 respectively.

2.4.2 Analysis of spray distribution system

The coefficient of uniformity and spray width were the two main parameters for optimizing the nozzle spacing and operating pressure. These parameters directly influence work efficiency and spray quality.

2.4.3 Liquid distribution uniformity coefficient

The liquid distribution uniformity coefficient (CV) compiles all the patternator data points and summarizes them into a simple percentage, indicating the amount of variation within a given distribution. The uniformity coefficient (CV) (Equations 1–3) is commonly used to quantify the uniformity of spray systems; higher CV values indicate poor uniformity in the spray pattern and the uniformity coefficient is calculated according to the following equation (12, 13):

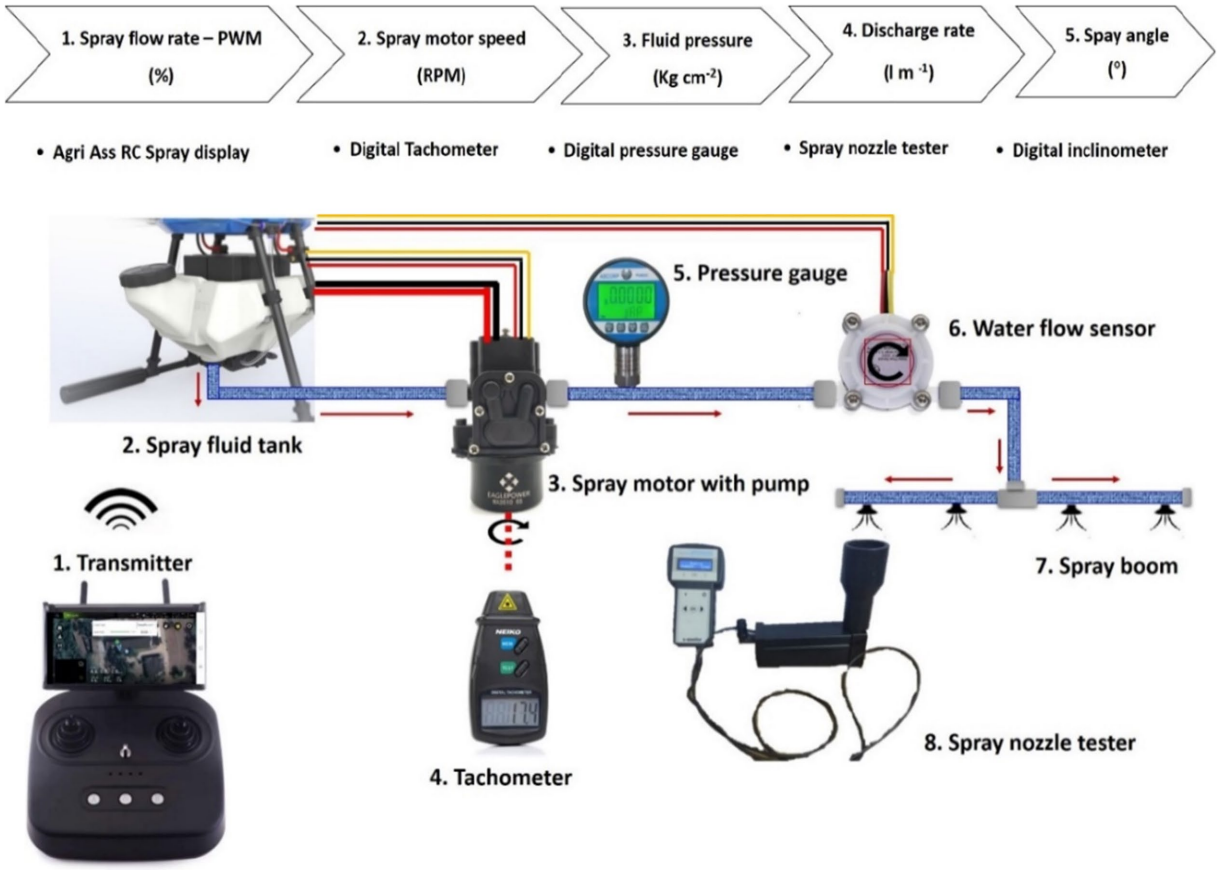

FIGURE 3
Experimental layout for measurement of spray motor speed, sprayer discharge rate, operating pressure and spray nozzle angle.

$$Coefficient of Variation\left(CV\right)=\frac{SD}{X}x100 \quad (1)$$

$$Mean\left(X\right)=\frac{\sum X_i}{N} \quad (2)$$

$$Standard deviation\left(SD\right)=\sqrt{\frac{\sum_1^N\left(X_i-X\right)^2}{N-1}} \quad (3)$$

Where,

CV – Liquid distribution uniformity coefficient.

X – Volume of liquid contained in specific container, ml.

X_i – Average volume of liquid, ml.

N – Number of analysed containers.

Spray distribution uniformity can be obtained with a low coefficient of variation. The above procedure was followed throughout this investigation to determine the coefficient of variation of spray uniformity distribution of the drone sprayer with boom arrangement.

2.4.4 Effective spray width

The effective spray width is the distance between the points on either side of a single swath where the deposit rate equals one-half of the effective application rate. The effective spray width was determined in a manner that will give the most uniform overall application rate.

2.5 Test of spray volume distribution pattern in hover outdoor condition

Uniformity coefficient was selected to study and optimized nozzle spacing and operating pressure of operational parameters boom and standard hexa nozzle configuration attachment to drone sprayer in outdoor condition.

2.5.1 Experimental setup

Four flat fan nozzles were mounted on the boom with optimized nozzle spacing (0.60 m) and attached below the drone sprayer fluid tank and landing gear structure. The arrangement of optimized nozzle spacing on the spray boom and attachment to drone sprayer is shown in Figures 15, 16. Another set of four nozzles were mounted below the BLDC rotors as a hexa standard nozzle configuration attachment and is shown in Figures 17, 18.

To record and analyse the spray volume distribution pattern for boom and hexa standard nozzle configuration, the drone sprayer hovered at three flight heights *viz.,* 1.0 m, 2.0 m, and 3.0 m. These are the independent variables that mainly influence the functional

FIGURE 4
Experimental layout for measurement of spray discharge rate using nozzle tester.

FIGURE 5
Experimental layout for measurement of spray motor speed.

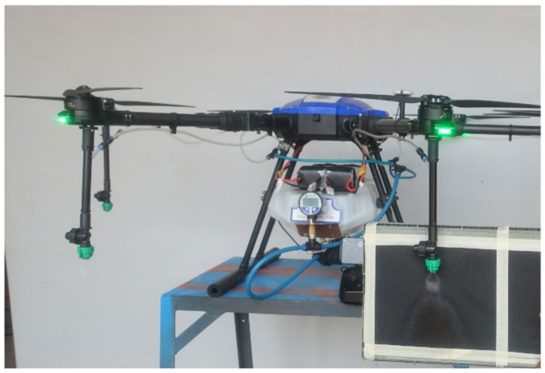

FIGURE 6
Experimental layout for measurement of spray angle.

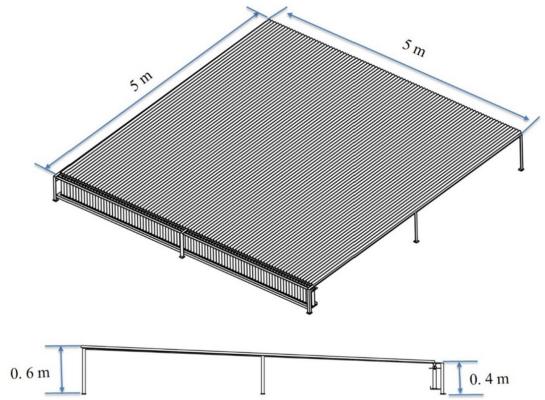

FIGURE 7
Isometric view of spray patternator.

FIGURE 8
Arrangement of measuring jar in spray patternator.

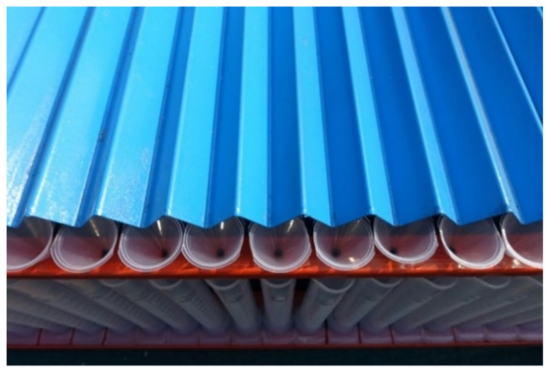

FIGURE 9
Arrangement of funnel in spray patternator.

performance of the drone spray volume distribution pattern in terms of quantity of spray volume collected (ml), coefficient of uniformity (%) and spray width (mm). For each treatment, a 10 litre water tank was filled and the spray volume was measured in each measuring jar. Each treatment was carried out three times. The coefficient of uniformity and spray width were calculated for three spray hover heights. This spray volume distribution pattern test procedure was followed as per IS: 8548 and ASAE (S386.2) standards (20, 22). Figure 19 and Supplementary Figures S1, S2 show the volumetric distribution of the drone sprayer with boom and hexa standard nozzle configuration in the patternator and the volume of liquid collected in the measuring jar.

FIGURE 10
Developed spray patternator for spray volume distribution measurement.

TABLE 2 Speciation of developed spray patternator.

Main parameter		Norms and numerical value
Overall Size, (L × W × H), mm		5,000 × 5,000 × 600
Support frame structure		L-shaped M.S. channel
Sheet material	Size (L x W), mm	2,500 × 1,250
	Material	M.S sheet
	Number of sheets	12
V channel	Numbers	91
	Width, mm	55
	Depth, mm	35
Patternator inclined slope, degree		25
Number of measuring cylinders		91

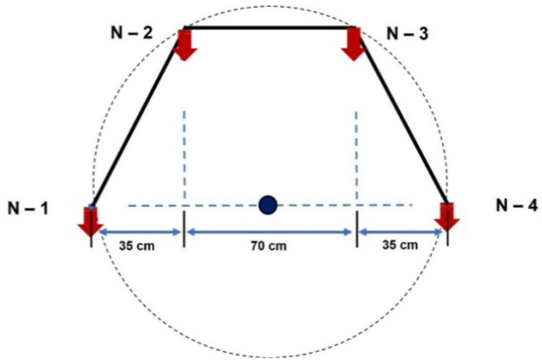

FIGURE 11
Hexa standard type spray nozzle arrangement.

2.6 Statistical analysis

A study included two independent variables: (1) nozzle spacing (i.e., 300, 450 and 600 mm), (2) operating pressure (i.e., 3, 4 and 5 kg cm^{-2}), and two dependent variables (i.e., uniformity distribution and spray width) with three replications. The factorial CRD design for the analysis of variance (Two-way ANOVA) tests to determine if there are significant differences between the spraying nozzle spacing and operating pressure. All tests were replicated thrice and the statistical analysis was carried out in OPSTAT Software (O. P. Sheoran, a computer programmer at CCS HAU, Hisar, India) to determine the level of significance.

2.7 Recording of meteorological parameters during outdoor condition test

During the drone spray volume distribution pattern test for optimizing the height of spray and nozzle configuration, the different meteorological parameters *viz.*, air temperature, wind velocity, humidity and rainfall were recorded during at outdoor condition. A portable anemometer was mounted on a square iron pipe (20 x 20 x 2 mm) at 2.0 m above the ground level to measure the wind velocity. Weather conditions, including wind speed, air temperature, and relative humidity during the study, are presented in Table 3.

3 Results and discussion

3.1 Results of drone spray operational parameters

The spray operational parameters such as operating pressure, nozzle discharge rate and spray angle were measured using standard procedure. The mean value of total spray discharge rate, spray angle and operating pressure of combined four nozzles at different motor speed mode of 0, 10, 20, 30, 40, 50, 60, 70, 80, 90, and 100% of PWM is furnished in Table 4.

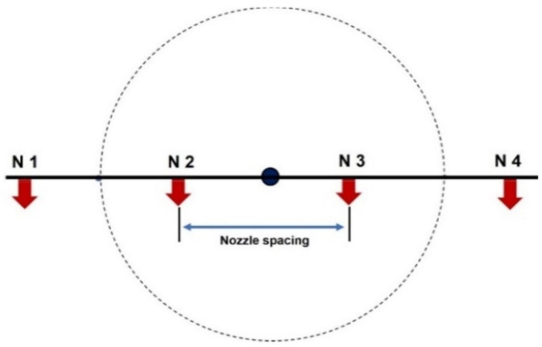

FIGURE 12
Boom type spray nozzle arrangement.

From Table 4, it was observed that the spray discharge rate and spray angle increased with the increase in spray operating pressure. Spray angle was measured using digital protractor and shown in Supplementary Figure S3. Among the 10 different modes of spray motor speed, 50, 70 and 100% modes were selected as it produced discharge rate 2.8 L m^{-1}, 3.1 L $m^{-1}$and 3.4 lm^{-1} at 3 kg cm^{-2}, 4 kg $cm^{-2}$and 5 kg cm^{-2}, respectively for the investigation on the spray volume distribution pattern of boom and hexa standard nozzles experiment in hover condition.

3.2 Results of spray volume distribution pattern for single nozzle

The volume discharge rate of single nozzle was tested at a different pressure level of 3.0, 4.0 and 5.0 kg cm^{-2} on the patternator in the

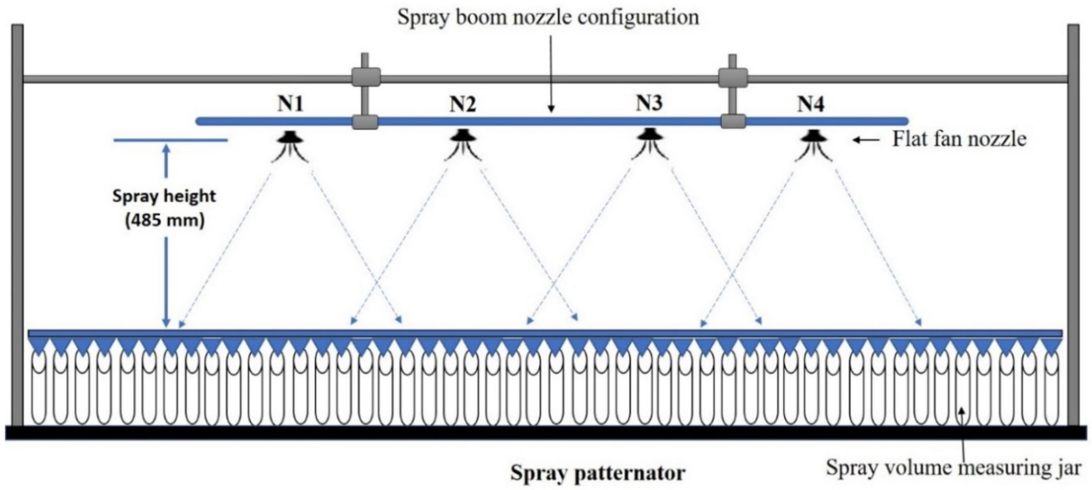

FIGURE 13
Experimental layout for mounting of spray boom type nozzles arrangement on spray patternator.

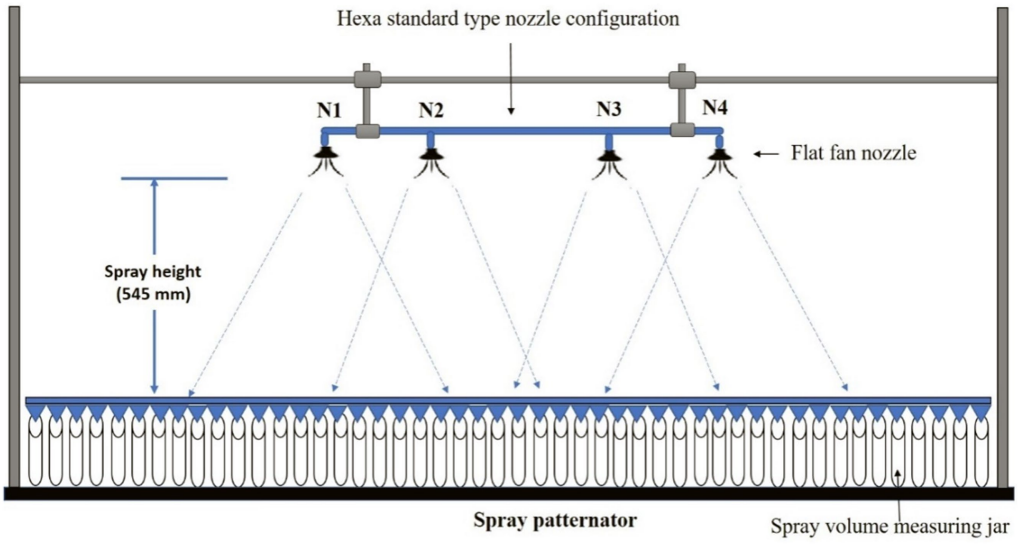

FIGURE 14
Mounting of nozzle in hexa standard arrangement on spray patternator.

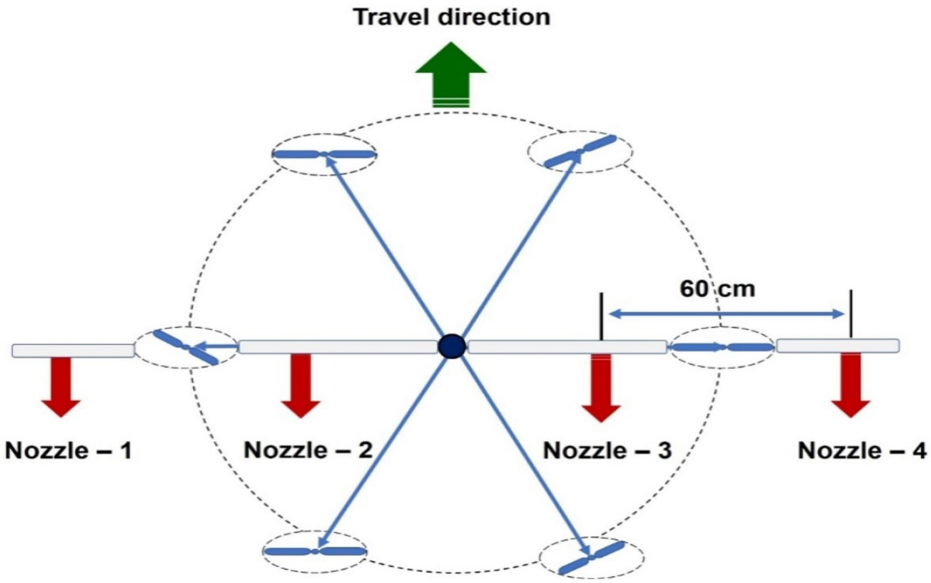

FIGURE 15
Top view of mounting of spray boom type nozzle arrangement to drone sprayer.

FIGURE 16
Arrangement of spray nozzles on boom configuration and attachment to Drone sprayer.

laboratory prior to the outdoor test trials. Spray pattern at 4.0 kg cm^{-2} pressure was found to have uniform distribution pattern based on the CV. The spray pattern of a single flat fan nozzle at different operating pressures are shown in Supplementary Figure S4.

The volume of liquid collected from each container in respect to the total volume of liquid collected from all the containers and the coefficient of variation was calculated for different pressures. The standard bell curve was observed at all the nozzle pressures. Based on coefficient of variation (53.0%), the spray volume distribution pattern was found to be high at 4.0 kg cm^{-2} nozzle pressure. From the laboratory test, an optimized nozzle pressure of 4.0 kg cm^{-2} was maintained to test the drone spray with different nozzle arrangements at outdoor condition.

3.3 Effect of nozzle spacing and operating pressure on spray uniformity

The effect of nozzle configuration, operating pressure and nozzle spacing on spray uniformity distribution and spray width was analyzed. The spray distribution pattern test for optimization of nozzle spacing and operating pressure for both boom type and hexa standard nozzle configuration based on coefficient of variation is presented in Table 5 and Supplementary Figure S5. The minimum coefficient of variation (CV) represents the better spray uniformity distribution Luck et al. (12) and Padhee et al. (13).

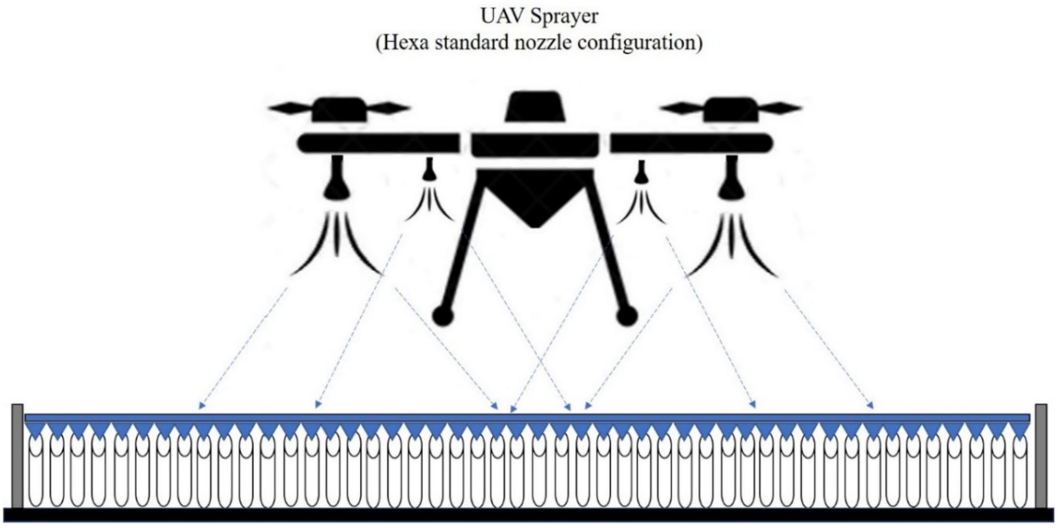

FIGURE 17
Schematic diagram of nozzles arrangement in hexa standard configuration attachment to drone sprayer for outdoor test.

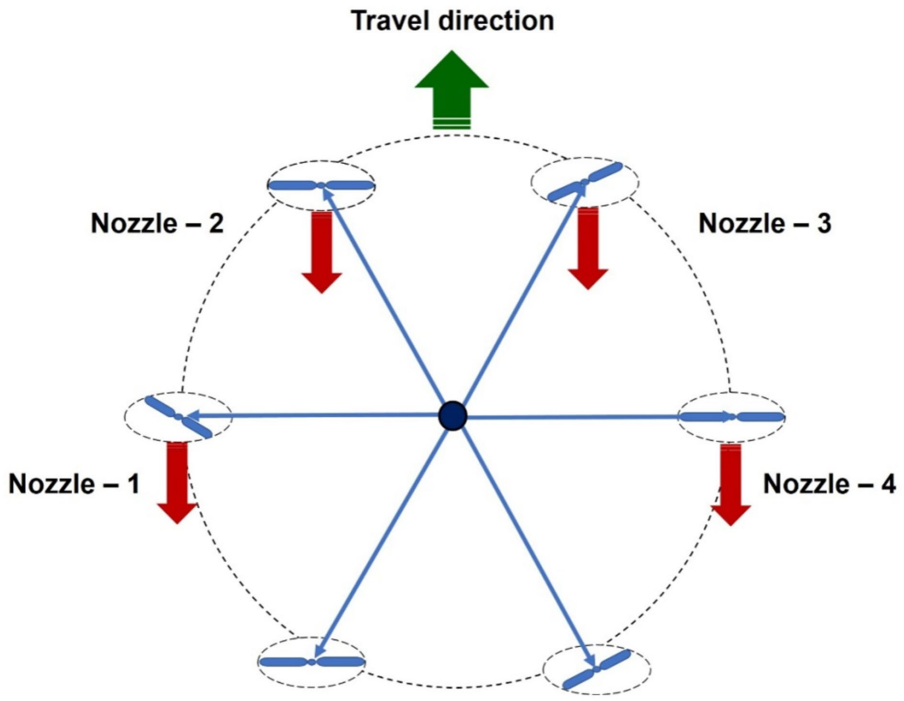

FIGURE 18
Top view of mounting of hexa standard arrangement type nozzle arrangement to drone sprayer.

From Table 5 and Supplementary Figure S5, for boom spray arrangement, the maximum coefficient variance (CV) value was found to be 52.08% at 3 kg cm^{-2} operating pressure and 300 mm nozzle spacing. The minimum CV value was found to be 36.99% at pressure of 4.0 kg cm^{-2} and 600 mm nozzle spacing. Luck et al. (12) and Padhee et al. (13) presented spray liquid uniformity distribution was better with lower CV value. Hence on the spray uniformity distribution results in Table 5, the optimized nozzle spacing of 600 mm and a 4.0 kg cm^{-2} operating pressure were selected with lower CV value 36.99% for boom spray arrangement on the drone sprayer for hover condition test. The maximum spray width value was found to be 3,235 mm at 4 kg cm^{-2} operating pressure and 600 mm nozzle spacing. The minimum spray width value was found to be 2,035 mm at pressure of 3.0 kg cm^{-2} and 300 mm nozzle spacing.

In the hexa standard type nozzle configuration, four nozzles were mounted below the rotors of the drone sprayer. The spray distribution pattern test for optimization of operating pressure for hexa standard nozzle configuration based on coefficient of variation is presented in

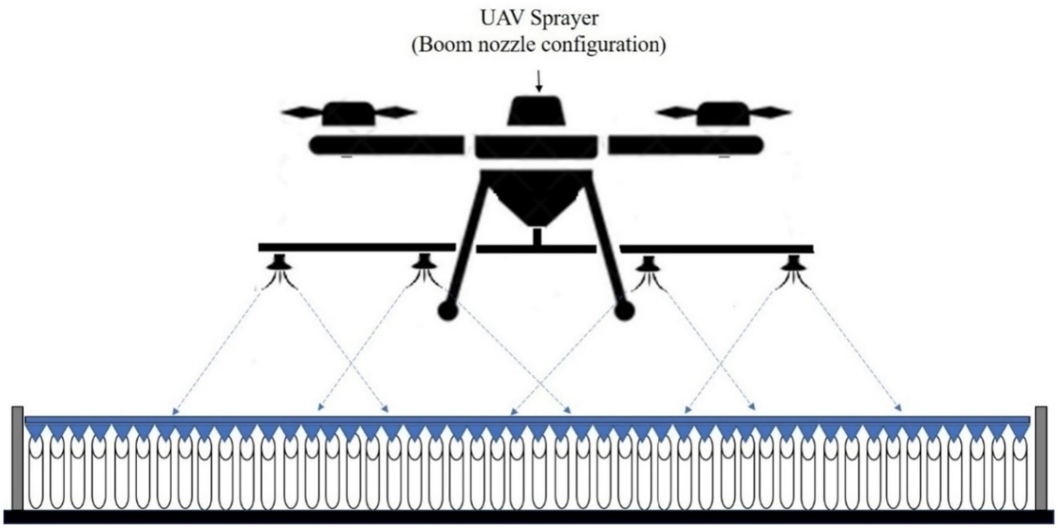

FIGURE 19
Schematic diagram of nozzles arrangement in boom configuration attachment to drone sprayer for outdoor test.

TABLE 3 Meteorological data during the spray volume distribution pattern test.

Environmental parameters	Values
Air temperature, °C	28.3 to 30.9
Relative humidity, %	54.5 to 60.2
Wind velocity, ms^{-1}	0.11 to 0.21
Rainfall, mm	0

TABLE 4 Results of spray motor speed, pressure, nozzle flow rate and nozzle spray angle.

Motor speed mode (%)	Motor speed (RPM)	Pressure (kg cm^{-2})	Discharge rate (lm^{-1})	Spray angle (degree)
10	247.0	0.2	1.0	66.52
20	606.0	0.3	1.5	71.25
30	1192.3	0.6	1.8	75.92
40	1730.3	1.5	2.1	86.87
50	2197.7	3.0	2.8	92.67
60	2781.0	3.7	3.0	97.07
70	3394.7	4.0	3.2	99.32
80	4017.3	4.3	3.3	101.25
90	4491.0	4.6	3.3	103.37
100	4514.0	5.0	3.4	105.17

Table 5. From Table 5 and Supplementary Figure S6, for hexa standard nozzle arrangement, the maximum CV value was found to be 50.57% at 5 kg cm^{-2} operating pressure. The minimum CV value was found to be 48.31% at pressure of 4.0 kg cm^{-2}. Based on the spray uniformity distribution value, the optimized 4.0 kg cm^{-2} operating pressure was selected for hexa standard spray arrangement on the drone sprayer for hover condition test.

Supplementary Table S1 presents the statistical analysis, i.e., analysis of variance showing the *p*-value for dependent variable at 5% significance level. A p-value above 0.05 was observed for uniformity of distribution and spray width. Therefore, the nozzle spacing had a significant effect on uniformity distribution and spray width. Operating pressure shows not significant in uniformity distribution and significant in spray width. There is significant interaction effect between nozzle spacing and operating pressure for spray width.

3.4 Spray volume distribution pattern of drone sprayer in hover at outdoor condition

The spray volume distribution pattern test was conducted and analyzed to optimize the height of spray based on coefficient of variation at outdoor condition. For boom type nozzle configuration, four numbers of flat fan nozzles were placed with 0.60 m spacing and in the hexa standard nozzle configuration, four nozzles were mounted below the rotors of the drone sprayer operated at 4.0 kg cm^{-2} operating pressure. The drone sprayer with boom spray nozzle configuration hovered at three heights of spray *viz.*, 1.0, 2.0 and 3.0 m and spray volume were collected from each jar during outdoor conditions (average wind speed, air temperature and relative humidity were measured as 0.19 m s^{-1}, 28.3°C and 57%, respectively). The effects of nozzle configuration and hover height on spray uniformity distribution, spray width and total quantity of liquid collected were analyzed in single pass distribution method and presented in Supplementary Table S2.

3.4.1 Effect of nozzle configuration and height of spray on spray uniformity

According to the coefficient of variation results presented in Supplementary Table S2, the spray height has a significant impact on spray uniformity distribution. Lower spray uniformity distribution

TABLE 5 Results on effect of type of nozzle configuration, nozzle spacing and operating pressure on uniformity of distribution and spray width.

Type of Nozzle configuration	Nozzle spacing (mm)	Operating pressure (kg cm^{-2})	Uniformity of distribution, CV (%)	Spray width (mm)
Boom	300	3	52.08	2034
		4	55.80	2,145
		5	54.29	2,145
	450	3	45.72	2,530
		4	44.61	2,640
		5	44.21	2,640
	600	3	37.63	3,025
		4	36.99	3,235
		5	38.35	3,235
Hexa	35/70	3	49.36	2,530
		4	48.31	2,695
		5	50.57	2,751

(57.21%) was found at 1.0 m height of spray for hexa standard nozzle configuration. Similarly, the maximum spray uniformity distribution was found as 47.26% at 2.0 m height of spray. It was also observed that when the drone sprayer hover height was increased from 1.0 m to 2.0 m from the top of the patternator, better spray uniformity distribution was recorded. When the height was increased from 2.0 m to 3.0 m from the top of the patternator, the volume of liquid collected and uniformity of distribution from the target area was reduced, which may be due to side drift. In boom nozzle configuration, lower spray uniformity distribution of 58.42% was found at 1.0 m hover height. Similarly, the maximum spray uniformity distribution of 54.80% was observed at 2.0 m hover height. It was also observed that when the drone sprayer hover height was increased from 1.0 m to 2.0 m from the top of the patternator, better spray uniformity distribution was found for both nozzle configuration.

3.4.2 Effect of nozzle configuration and height of spray on spray width

From Supplementary Table S2, the spray width of hexa standard nozzle arrangement was found to be minimum, (3,145 mm) for 1.0 m hover height, whereas it was found to be maximum, (3,865 mm) at 2.0 m hover height. In boom nozzle configuration, the minimum spray width was found as 4,450 mm for boom nozzle arrangement at 1.0 m height, which was higher (3,145 mm) than the hexa standard nozzle arrangement at the same hover height. The maximum spray width was found as 4,902 mm at 2.0 m height of boom spray. It was observed that the spray width increased by increasing the height of spray from 1.0 to 2.0 m from the patternator. The height of spray did not influence the discharge rate during the laboratory trials. Generally, it was observed that the spray width of boom nozzle arrangement is higher than the hexa standard nozzle arrangement.

3.4.3 Effect of hover height on quantity of liquid collected

In hexa standard nozzle configuration, four numbers flat fan nozzles *viz.*, N1, N2, N3 and N4 are mounted below the rotor propeller. The horizontal distance between the nozzles N1 to N2 and N3 to N4 were measured as 35 cm, whereas the distance between the nozzles N2 to N3 was measured as 70 cm. The spray volume was collected at three hover heights, *viz.*, 1,000, 2,000 and 3,000 mm from the top of the patternator surface and results are presented in Supplementary Table S1 and Supplementary Figure S7. When compared to the height of spray, the volume of water collected at the central portion of the drone sprayer was less (5,389 mL) when hovered at 1.0 m height compared to 2.0 m (5,949 mL) and 3.0 m (5,559 mL) heights.

From the Supplementary Table S2 and Supplementary Figure S8 for boom nozzle configuration, it was found that, due to downwash air flow and increase in horizontal distance between the nozzles N2 and N3, the volume of liquid collected below the drone was less, irrespective of the height of operation of the drone above the patternator, it was also observed that more round vertex patterns were generated at 1.0 m hover height compared to the hover height of 2.0 and 3.0 m due to the direct impact of downwash airflow generated by the rotor propellers on the droplets. At 1.0 m hover height, most of the spray droplets were distributed back to the upper side and did not move towards the downside V-channel surface of the patternator. The liquid collected at the center of drone sprayer was less (5,190 mL) at 1.0 m hover height, whereas it was 6,230 mL and 5,146 mL at 2.0 m and 3.0 m hover heights, respectively.

Supplementary Table S3 presents the statistical analysis, i.e., analysis of variance showing the p-value for dependent variable at 5% significance level. Therefore, the nozzle configuration, height of spray had a significant effect on uniformity distribution, spray width and quantity of liquid collected. There is significant interaction effect between nozzle configuration and height of spray for uniformity of distribution, spray width and quantity of liquid collected.

3.5 Spray volume distribution pattern test in one direction application method

In one direction application method, the overlaps between two passes were considered. The spray uniformity and effective spray

width were calculated and the results are presented in Supplementary Table S4.

According to the coefficient of variation results in Supplementary Table S4 and Supplementary Figures S9, S10, spray height has a significant impact on spray uniformity distribution. Lower spray uniformity distribution with maximum CV was found as 19.83 and 21.62% and at 1.0 m height of spray for boom and hexa standard nozzle configuration. Similarly, the maximum spray uniformity distribution with minimum CV was found as 18.90 and 17.95% at 2.0 m height of spray boom and hexa standard nozzle configuration. It was also observed that when the drone sprayer hover height was increased from 1.0 m to 2.0 m from the top of the patternator, better spray uniformity distribution was found.

Similarly, the minimum spray width was found to be 2,805 mm and 2,035 mm at 1.0 m height of spray for boom and hexa standard nozzle arrangement, respectively. The maximum spray width was found to be 3,190 mm and 2,310 mm at 2.0 m height of spray for boom and hexa standard nozzle arrangement, respectively. It was observed that the spray width was increased by increasing the height of spray from 1.0 m to 2.0 m from the patternator. The effective spray width in one direction spray distribution for boom nozzle configuration at 1.0, 2.0 and 3.0 m height of spray is shown in Supplementary Figure S10. Similarly, for hexa standard nozzle configuration, the spray distribution pattern is given in Supplementary Figure S9.

Supplementary Table S5 presents the statistical analysis, i.e., analysis of variance showing the *p*-value for dependent variable at 5% significance level. A *p*-value above 0.05 was observed for uniformity of distribution for nozzle configuration. Therefore, the height of spray had a significant effect on uniformity distribution and spray width. There is significant interaction effect between nozzle configuration and height of spray for uniformity of distribution and spray width.

In boom nozzle arrangement (Supplementary Figure S9), it was also observed that more round vertex patterns were generated during the 1.0 m and 3.0 m hover height compared to the 2.0 m hover height due to the direct impact of downwash airflow generated by the rotors. At 1.0 m hover height, most of the spray droplets were distributed back to the upper side and did not move towards the downside V-channel surface of the patternator. In hexa standard nozzle arrangement (Supplementary Figure S10), it was also observed that there was less round vertex pattern generated during hexa configuration nozzle spray compared to boom type nozzles due to the direct impact of downwash airflow generated by the rotor propeller. The downwash airflow produced by the rotor propellers reduced the liquid distribution uniformity coefficient and significantly influenced the change of the lateral distribution pattern of spray drops produced by the flat fan spray nozzles. Similarly, as in previous research works Berner and Chojnacki (14) and Qing et al. (15) there was a change in the shape of liquid deposition on the patternator due to the influence of downwash airflow produced by the drone rotor propellers.

Similarly, as in previous research works Yallappa et al. (11) and Pachuta et al. (16) the asymmetry of the airflow distribution generated by the drone rotors with respect to the nozzle axis is what causes the lateral spray liquid distribution of the settled liquid on the patternator to change shape. The volume of the liquid that was deposited in the patternator later grooves also varied significantly Chojnacki and Pachuta (17). A higher spray distribution amount of the liquid was sprayed from the twin flat nozzle than from the single flat nozzle (18). Earlier reported work was done at a constant spray height, where in the present investigation, the results were obtained at varying sprays heights (1.0, 2.0 and 3.0 m) and nozzle spacing (30, 45, 60 cm) at an optimized operating pressure (5.0 kg cm^{-2}). The results showed that there were obvious differences in the distribution of spray volume patterns for boom and hexa configuration nozzles.

4 Conclusion

Food and nutritional security is the situation where in public around the globe, in all conditions must maintain constant physical and financial, ensuring reliable global access to sufficient nutritious and safe food. Results of in this experiment are study and optimized the spray operational parameters *viz.*, height of spray, nozzle spacing and spray operating pressure. Nozzle spacing and operating pressure for boom and hexa standard nozzle configuration to drone sprayer was optimized by using developed spray patternator (5.0×5.0 meter). The optimized nozzle spacing of 0.6 m and a 4.0 kg cm^{-2} operating pressure was chosen for the drone sprayer distribution test at outdoor conditions based on the spray uniformity distribution value. The spray volume distribution for both boom and hexa standard nozzle arrangement in hover condition, observed that when the drone sprayer hover height was increased from 1.0 m to 2.0 m from the top of the patternator, better spray uniformity distribution, spray width and quantity of liquid collected was recorded. The central portion of the patternator collected less water (5,194 mL) when a drone sprayer hovered at 1.0 m height compared to 2.0 (5,416 mL) and 3.0 m (6,231 mL) hover heights. With the increase of hover height, the change of the downwash airflow led to a gradual decrease in spray volume distribution in the effective spray area. A better spray uniformity distribution was found when the drone sprayer hover height was increased from the top of the patternator. A more round spray droplet vertex pattern was generated during the 1.0 m hover height compared to the 2.0 and 3.0 m hover heights due to the direct impact of downwash airflow generated by the rotors. Downwash airflow produced by rotor propellers reduced the liquid distribution uniformity coefficient and significantly influenced the change of lateral distribution pattern of spray drops produced by the flat fan spray nozzles. Thus, the drone sprayer should be operated at an appropriate spray height of 2.0 m to attain the recommended application rate of pesticides. The good spray uniform distribution was found in hexa configuration nozzle arrangement as compared to the boom arrangement of nozzles. The study provides references for the height of spray and different nozzle configuration arrangement to drone sprayer for efficient operation. Lastly, the study demonstrates that optimizing drone sprayer parameters, such as spray height and nozzle configuration, ensures efficient pesticide application, leading to enhanced food and nutritional security by promoting sustainable agricultural practices under varying climate conditions.

Data availability statement

The datasets presented in this study can be found in online repositories. The names of the repository/repositories and accession number(s) can be found in the article/Supplementary material.

Author contributions

DY: Conceptualization, Methodology, Software, Writing – original draft, Writing – review & editing, Data curation, Formal analysis, Investigation, Supervision, Validation. RK: Funding acquisition, Project administration, Resources, Validation, Visualization, Writing – review & editing. AS: Conceptualization, Data curation, Formal analysis, Resources, Validation, Visualization, Writing – review & editing. BS: Formal analysis, Investigation, Methodology, Validation, Visualization, Writing – review & editing. AM: Conceptualization, Data curation, Formal analysis, Supervision, Writing – review & editing. BK: Writing – original draft, Writing – review & editing, Software, Formal analysis, Data curation, Investigation. MK: Writing – original draft, Writing – review & editing, Project administration, Supervision, Investigation, Resources.

Funding

The author(s) declare that no financial support was received for the research, authorship, and/or publication of this article.

Acknowledgments

The authors wish to acknowledge the financial assistance provided by the Indian Council of Agricultural Research (ICAR), All India Coordinated Research Project (AICRP) on Farm Implements and Machinery (FIM) and Tamil Nadu Agricultural University, Coimbatore, Tamil Nadu (India) for providing necessary research facilities for conducting the experiment.

Conflict of interest

The authors declare that the research was conducted in the absence of any commercial or financial relationships that could be construed as a potential conflict of interest.

Publisher's note

All claims expressed in this article are solely those of the authors and do not necessarily represent those of their affiliated organizations, or those of the publisher, the editors and the reviewers. Any product that may be evaluated in this article, or claim that may be made by its manufacturer, is not guaranteed or endorsed by the publisher.

Supplementary material

The Supplementary material for this article can be found online at: https://www.frontiersin.org/articles/10.3389/fnut.2024.1487074/full#supplementary-material

References

1. Choi Y.S., Lee W.S. Reconfigurable beam switching antenna with horizontal parasitic element reflector (HPER) for UAV applications. In 2020 IEEE international symposium on antennas and propagation and north American radio science meeting (2020) (pp. 433–434). IEEE.

2. Li S, Jin Z, Bai J, Xiang S, Xu C, Yu F. Research on fertilization decision method for rice tillering stage based on the coupling of UAV hyperspectral remote sensing and WOFOST. *Front Plant Sci*. (2024) 15:1405239. doi: 10.3389/fpls.2024.1405239

3. Positano F, Lizzi L, Staraj R. Design and on-field test of ESPAR antenna for UAVbased long-range IoT applications. *Front Antennas Propag*. (2024) 2:1429710. doi: 10.3389/fanpr.2024.1429710

4. Wang XD, Wang YL, Zhang YP, Xiang J, Zhang YK, Zhu DF, et al. The nitrogen topdressing mode of indica-japonica and indica hybrid rice are different after side-deep fertilization with machine transplanting. *Sci Rep*. (2021) 11:1494. doi: 10.1038/s41598-021-81295-4

5. Yang F, Xue X, Cai C, Sun Z, Zhou Q. Numerical simulation and analysis on spray drift movement of multirotor plant protection unmanned aerial vehicle. *Energies*. (2018) 11:2399. doi: 10.3390/en11092399

6. Elemike EE, Uzoh IM, Onwudiwe DC, Babalola OO. The role of nanotechnology in the fortification of plant nutrients and improvement of crop production. *Appl Sci*. (2019) 9:499. doi: 10.3390/app9030499

7. Sande TJ, Tindwa HJ, Alovisi AMT, Shitindi MJ, Semoka JM. Enhancing sustainable crop production through integrated nutrient management: a focus on vermicompost, bio-enriched rock phosphate, and inorganic fertilisers – a systematic review. *Front Agron*. (2024) 6:1422876. doi: 10.3389/fagro.2024.1422876

8. Yan Y, Lan Y, Wang G, Hussain M, Wang H, Yu X, et al. Evaluation of the deposition and distribution of spray droplets in citrus orchards by plant protection drones. *Front Plant Sci*. (2023) 14:1303669. doi: 10.3389/fpls.2023.1303669

9. Lan Y, Qian S, Chen S, Zhao Y, Deng X, Wang G, et al. Influence of the downwash wind field of plant protection UAV on droplet deposition distribution characteristics at different Flight Heights. *Agronomy*. (2021) 11:2399. doi: 10.3390/agronomy11122399

10. Li JY, Lan YB, Shi YY. Research progress on airflow characteristics and field pesticide application system of rotary-wing UAV. *Trans CSAE*. (2018) 34:104–18. doi: 10.11975/j.issn.1002-6819.2018.12.013

11. Yallappa D, Kavitha R, Surendrakumar A, Suthakar B, Kumar APM, Kannan B, et al. Influence of the downwash airflow in Hexacopter drone on the spray distribution pattern of boom sprayer. *J Appl Nat Sci*. (2023) 15:391–400. doi: 10.31018/jans.v15i1.4346

12. Luck JD, Schaardt WA, Sharda A, Forney SH. Development and evaluation of an automated spray patternator using digital liquid level sensors. *Appl Eng Agric*. (2016) 32:47–52. doi: 10.13031/aea.32.11381

13. Padhee D, Verma S, Rajwade SS, Ekka H, Chandniha SK, Tiwari SK. Evaluating the effect of nozzle type, nozzle height and operating pressure on spraying performance using a horizontal spray patternator. *J Pharm Phytochem*. (2019) 8:2137–41.

14. Berner B, Chojnacki J. Zastosowaniebezzałogowychstatkówpowietrznych do opryskiwaniauprawrolniczych. *TechnikaRolniczaOgrodniczaLeśna*. (2017) 2:23–25.

15. Qing T, Ruirui Z, Liping C, Min X, Tongchuan Y, Bin Z. Droplets movement and deposition of an eight-rotor agricultural UAV in downwash flow field. *Int J Agric Biol Eng*. (2017) 10:47–56. doi: 10.3965/j.ijabe.20171003.3075

16. Pachuta A., Berner B., &Chojnacki J. Evaluation of liquid transverse distribution under a twin spray jet installed on a drone. In Proceedings of the 25th International PhD Students Conference (MendelNet 2018), Brno, Czech Republic (2018). (pp. 7–8).

17. Chojnacki J, Pachuta A. Impact of the parameters of spraying with a small unmanned aerial vehicle on the distribution of liquid on young cherry trees. *Agriculture*. (2021) 11:1094. doi: 10.3390/agriculture11111094

18. Coombes M, Newton S, Knowles J, Garmory A. The influence of rotor downwash on spray distribution under a quadrotor unmanned aerial system. *Comput Electron Agric*. (2022) 196:106807. doi: 10.1016/j.compag.2022.106807

19. ASABE. Standards procedure for measuring distribution uniformity and calibrating granular broadcast spreaders. St. Joseph, MI: ASABE (2018).

20. Indian Standard Institution. Is: 8548–1977 Power-Operated Hydraulic Sprayer. (1977). Bureau of Indian Standards, Ministry of Consumer Affairs, Food & Public Distribution, Government of India, New Delhi.

21. Indian Standard Institution. Is: 10064–1982 Hydraulic spray nozzles for pest control equipment. (1982). Bureau of Indian Standards, Ministry of Consumer Affairs, Food & Public Distribution, Government of India, New Delhi.

22. ASABE Standards. Calibration and distribution pattern testing of agricultural aerial application equipment. St. Joseph, MI, USA: ASABE (2018).

23. Indian Standard Institution. IS 3652-1995 Crop protection equipment foot sprayer specification. (1995). Bureau of Indian Standards, Ministry of Consumer Affairs, Food & Public Distribution, Government of India, New Delhi.

frontiers | Frontiers in Nutrition

TYPE Review
PUBLISHED 15 January 2025
DOI 10.3389/fnut.2024.1504958

OPEN ACCESS

EDITED BY
Simardeep Kaur,
The ICAR Research Complex for North Eastern Hill Region (ICAR RC NEH), India

REVIEWED BY
Madhuresh Dwivedi,
National Institute of Technology Rourkela, India
Venkatachalapathy Natarajan,
National Institute of Food Technology, Entrepreneurship and Management, Thanjavur (NIFTEM-T), India

*CORRESPONDENCE
Sandeep Singh Rana
✉ sandeepsingh.rana@vit.ac.in

RECEIVED 01 October 2024
ACCEPTED 23 December 2024
PUBLISHED 15 January 2025

CITATION
Shanker MA and Rana SS (2025) Prospects of cold plasma in enhancing food phenolics: analyzing nutritional potential and process optimization through RSM and AI techniques. *Front. Nutr.* 11:1504958.
doi: 10.3389/fnut.2024.1504958

Prospects of cold plasma in enhancing food phenolics: analyzing nutritional potential and process optimization through RSM and AI techniques

M. Anjaly Shanker and Sandeep Singh Rana*

Department of BioSciences, School of Bio Science and Technology (SBST), Vellore Institute of Technology, Vellore, India

Consumption of plant-based food is steadily increasing and follows an augmented trend owing to their nutritive, functional, and energy potential. Different bioactive fractions, such as phenols, flavanols, and so on, contribute highly to the nutritive profile of food and are known to have a sensitivity toward higher temperatures. This limits the applicability of traditional thermal treatments for plant products, paving the way for the advancement of innovative and non-thermal techniques such as pulsed electric field, microwave, ultrasound, cold plasma, and high-pressure processing. Among these techniques, cold plasma would be an operative choice in plant-based applications due to their higher efficacy, greenness, chemical exclusivity, and quality retention. The efficiency of the plasma process in ensuring the bioactive potential depends on several factors, such as feeding gas, input voltage, exposure time, pressure, and current flow. This review explains in detail the optimization of process parameters of the cold plasma technique, ensuring greater extractability or retention of total phenols and antioxidant potential. Response surface methodology (RSM) is one of the common techniques involved in the optimization of these course factors. It also covers the convention of artificial intelligence-based methods, such as artificial neural networks (ANN) and genetic algorithms (GA), in evaluating the data on process parameters. The review critically examines the strengths of each optimization tool in determining the optimal process parameters for maximizing phenol retention and antioxidant activity. The ascendancy of these techniques was mentioned in the studies regarding fruit, vegetables, and their products, and they can also be applied to other food products.

KEYWORDS

total phenols, bioactive potential, cold plasma, artificial neural networks, efficacy

1 Introduction

Food is a well-recognized source of nutrients and bioactive components essential for sustaining life and promoting health. In recent years, food has emerged as a functional component with additional physiological benefits, including the prevention or delay of illnesses and health conditions. A new diet-health concept with a major emphasis on positive aspects of food beyond basic nutrition is followed by different groups of people irrespective of age, culture, and social domains (1). Current research is focused on exploring the health-promoting, disease-preventing, and protective capabilities of major food groups. Amid these stands, plant-based diets comprising fruits, vegetables, herbs,

seeds, and so on have immense health potential with basic nutritional value and incidence of other bioactive components. The bioactive potential of these food groups has sparked interest in their health-promoting roles, encouraging their incorporation into regular diets. The presence of bioactive compounds in food is considered essential, as they can influence the body holistically or target specific tissues, contributing to overall health and wellness. These compounds do not fit into the category of nutrients as they are not considered elemental, but their existence offers a constructive effect on the body in terms of their biological activity. The major classes of bioactive components in plant foods are phenols, flavonoids, carotenoids, plant sterols, tannins, and other sulfur-based compounds (2). They are present in multiple forms, such as esterified, glycosylated, hydroxylated, and so on, in plant-derived food items and have an influential role in overall systematic functioning (3). Fruits and vegetables are known for their functional and antioxidant bioactive profile, which contribute to antitumor, anti-cardiac, anti-inflammatory, anti-mutagenic, anti-cancer, and neuroprotective potential (4).

Polyphenols are one of the important classes of secondary metabolites, and they have a large range of structural and functional possibilities in fruits, vegetables, and other plants. Known as natural antioxidants, they are secondary metabolites of plants structured with an aromatic ring consisting of 2 or more hydroxyl moieties. They are water-soluble fractions having a molecular weight of around 500 to 4,000 Da and have more than 8,000 types of recognized orientations (5). They range from simple phenolics, such as hydrobenzoic acids, to large high-molecular polymers such as tannins. These compounds are considered to be important determinants of agricultural produce, as they are physiological, sensorial, morphological, and nutritional.

The phenol content of produce is dependent on environmental factors such as sun exposure and soil type and varies according to genetics, maturity, post-harvest operations, and other factors. Choosing the right methods for technological processing is crucial to maintaining the availability of high-quality agricultural produce throughout the supply chain (6).

1.1 Phenols & their classes

Phenolic compounds include not only an array of molecules with a basic polyphenol structure but also those with a single phenol ring-like phenolic acids. They are divided into different categories, conferring the number of phenol rings present and the structural elements that bind these rings to each other (Figure 1). The major classes of polyphenols are flavonoids, phenolic acids, lignans, tannins, and stilbenes (4). Flavonoids, the most abundant type of phenolic compounds, feature a basic C6-C3-C6 structure that includes 15 carbon atoms. The characteristic construction of flavonoids comprises two aromatic rings (A & B) combined by a 3-carbon bridge in the form of a heterocyclic ring (C) (7). Varying substitution arrangements of ring C result in the cataloging of flavonoids as flavones, flavonols, flavanols, flavanones, flavanonols, isoflavones, and anthocyanidins. Similarly, substitutions such as oxygenation, glycosylation, acylation, alkylation, and sulfonation to the aromatic rings (A & B) create variations within each category of flavonoids. Owing to their high redox potential, flavonoids are important antioxidants present widely in agricultural produce, and they have a positive role in reducing diseases such as cancer and heart-related issues (8). Among the different classes of flavonoids, the structurally diverse and commonly found class of compounds are flavonols and flavones. The structural configuration of these classes is a basic flavonoid structure with a double bond between the C2-C3 position and an oxygen atom at the C4 position with an addition of a hydroxyl group at the C3 position for flavonols. Flavanones are characterized by a saturated three-carbon chain and a C4 position substituted by an oxygen atom, whereas isoflavones constitute a diphenyl propane structure with the B ring positioned at C3 (9). Although flavanones are predominantly found in high concentrations in citrus fruit, they are also present in tomatoes, grapefruits, licorice, berries, and aromatic plants such as mint (10).

The basic structure of anthocyanins is anthocyanidins, which consist of aromatic ring A bonded to oxygen-substituted heterocyclic ring C, which in turn is linked with ring B by a carbon-carbon bond (11). They are water-soluble pigments characterized in agriculture and produced by red, purple, and blue color profiles. They are rich in red grapes, raspberries, cherries, strawberries, and berries. Six common anthocyanidins present in plants are petunidin, cyanidin, delphinidin, pelargonidin, peonidin, and malvidin (12). Phenolic acids represent one-third of dietary phenols and are categorized into two major subgroups: hydroxybenzoic and hydroxycinnamic acids. The former group, which has a characteristic C6-C1 structure, is commonly represented by gallic acid, vanillic, p-hydroxybenzoic acid, and so on. In contrast, the latter group with caffeic, ferulic, sinapic, and coumaric acids as cinnamic acid derivatives are represented by three carbon side chains (C6-C3) (13). While there is a very low distribution of hydroxybenzoic groups in plants, excluding certain red fruits and onions, the incidence of hydroxycinnamic acids is widespread in fruits and vegetables, with blueberry, cherry, plum, and kiwi having the highest content of this class (3).

Tannins are high molecular compounds that are further grouped as hydrolyzable and condensed tannins. The most widely recognized forms of condensed tannins are epicatechin and catechin, which are polymerized flavonoids in nature (14). Hydrolysable tannins are gallic acid derivatives that can be easily degraded by biological systems. Tannic acid is an example of this class, comprising eight to 10 molecules of gallic acid. Tannins have described competence of substantial structural variations and are considered potential metal chelators, biological antioxidants, and protein precipitating agents (15). Lignans are widely distributed compounds in the plant domain derived from oxidative dimerization of two phenylpropane units. Based on the positioned oxygen in their structural skeleton, oxidation levels of side chains, and cyclization pattern, the compounds are classified into eight different subgroups, including furan, furofuran, dibenzyl butane, and so on. Lariciresinol, pinoresinol, matairesinol, and secoisolariciresinol are commonly found in lignans in plants and are distributed in fruits, vegetables, seeds, and in beverages such as juices, coffee, and wine (16). Stilbenes appear in plants in cis and trans configurations with major dietary sources such as grapes, wine, juices, and peanuts. Resveratrol, one of the common forms of stilbenes, is known for its chemopreventive, anti-inflammatory, anti-proliferative, and antioxidant properties and includes grapes, berries, pines, and so on as their major sources (17).

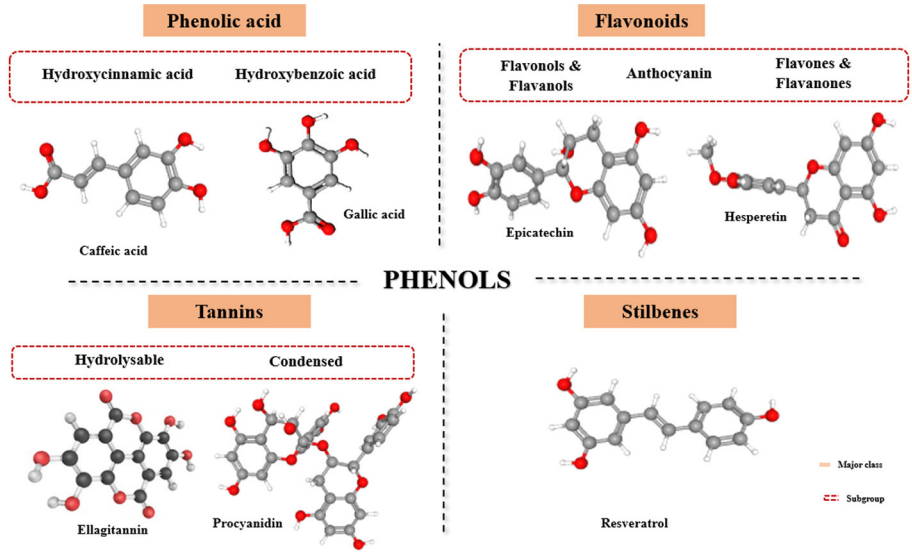

FIGURE 1
Summary of major phenols in agricultural produce.

1.2 Importance of the cold plasma technique

Thermal treatments are the primary traditional methods used in the post-harvest treatment of vegetables and fruits to extend the shelf life of the produce. Traditional techniques can reduce the nutritional and functional potential of produce by altering its component profile, which is a significant drawback. Research on innovative non-thermal technologies gained popularity and interest in this context, contemplating the demand for good, safe, functional, and nutritionally superior food products in the consumer markets (18). Cold plasma is a non-thermal technique that ensures the quality of food products with maximum retention of quality and safety. The reliability and versatility of this green technique have promoted the application of the plasma technique and have been reported to have a substantiated potential in food packaging modification, decontamination, toxin removal, enzyme inactivation, and even wastewater treatment (19). The efficiency of the process in ensuring the bioactive and functional profile of fruits and vegetables is dependent on several factors such as feeding gas, input voltage, exposure time, pressure, current flow, and so on. Optimization of process parameters and application of different optimization techniques ensure maximum quality and nutritive retention, along with a detailed understanding of the effect of each parameter on the efficiency of the process. This review aims to explore the possibilities of plasma technique in retaining the phenolic profile of vegetables and fruits along with the optimization of process parameters with different statistical methods such as response surface methodology and artificial intelligence-based techniques such as artificial neural networks (ANN) and genetic algorithms (GA).

Mentioned as the fourth state of matter, plasma denotes quasi-neutral ionized gas comprising ions, reactive species, photons, and free electrons in addition to their excited or fundamental states with a net neutral charge in the system (20). Similar to the phase change from solid to liquid to gas, increasing the energy input beyond a certain threshold in the gas phase leads to particle excitation, resulting in the formation of plasma. The general classification of a plasma system based on thermal equilibrium includes thermal and low-temperature (non-equilibrium) plasma (21). The former condition involves plasma generation by heating gases to higher temperatures, thereby attaining a thermal equilibrium within the species. The latter is further classified into quasi-equilibrium, where the constituents are in local thermal equilibrium (100°C−150°C), and non-equilibrium plasma, where they exist in thermal non-equilibrium (<60°C). The low-temperature, non-thermal, or non-equilibrium plasma with a lower temperature range is termed cold plasma (22). Any source of energy that can ionize gases can be employed in the generation of these increased energy levels of plasma in a system. It can be generated with the help of thermal, electrical, optical, radioactive, or electromagnetic energy sources applied through a gas system, resulting in the atoms' dissociation, excitation, and ionization. However, the widely accepted and applied generation mode involves electric and electromagnetic sources. In addition to the source and type, another important point of consideration in plasma generation is the selection of operational gas. Common gases involved in the generation process are oxygen, nitrogen, and carbon dioxide, and there is a possibility of encompassing noble gases such as argon and helium into the system as operational gases (23). The selection of gas involved in plasma generation, in turn, affects the efficiency and economic feasibility of the process, making it one of the important parameters of the process.

The different approaches actively involved in plasma generation are dielectric barrier discharge (DBD), corona discharge, microwave (MW), radio frequency plasma (RFP), atmospheric plasma jet (APPJ), glow discharge (GDP), gliding arc discharge (GAD), and resistive barrier discharge (RBD) plasma (24). Among

these, DBD and plasma jet are the common techniques involved in the treatment of food particulates. However, this commonality is not always applicable, as the selection of a system of operation should be dependent on the product characteristics. A dielectric plasma system involves the generation of plasma by applying a voltage between two known electrodes maintained at a small distance from each other. This economically feasible and viable option can be employed at a range of pressures, voltages, and frequencies under different gas sources (25). The versatility in application parameters of the DBD system presents it as a common generation type with a wide application range. The plasma jet system setup comprises a nozzle with two concentric electrodes through which the carrier gas passes and is subjected to a high voltage of 100–250V. Common carrier gases used in the system are oxygen, carbon dioxide, helium, or a mixture of gases treated at higher frequencies. Microwave discharge plasma system setup encompasses a power source, standing wave radiometer, circulator, quartz tube, and microwave-to-plasma applicator (26). Here, the generation of plasma and excitation of gas electrons is aided by the origination of microwaves at a general frequency of 2.45 GHz. This plasma system functioned at a pressure range of $1–10^5$ Pa and does not require an electrode to generate plasma. The application of different systems, in turn, results in the effective excitation and ionization of gases, leading to the interactions between reactive species and food components. These interactions act as the sole reason for the modification of the functional, chemical, nutritional, and microbiological profile of the food.

2 Mechanism of action on phenols

The relevance of cold plasma in food, including its interactions and its effect on food components, remains an exploratory field of study. A proper interpretation of the interactions of food and plasma components has a decisive role in integrating the system in the treatment of any food. In the case of phenolic compounds, this mechanism of action is related to the synergistic effect of generated plasma reactive species on the structural conformities of phenolic compounds in food (23). There are different explanatory approaches related to the variations in the phenolic profile owing to the cold plasma treatment. Oxidation caused by reactive oxygen species is a primary mechanism affecting phenol concentrations (27). Interaction results in the alteration of structural features of phenol fractions, resulting in the formation of new carbonyl and carboxylic groups. Alteration in chemical structure could be due to intense surface oxidation, which affects the antioxidative and functional properties of the fraction. Hydroxylation reactions that cause structural modification in benzene rings owing to the reactive species result in a gush of related interreactions, such as the formation of carbonyl radicals and generation of phenoxyl radicals altering the phenolic content and functional activity of the samples (28). For instance, superoxide radicals formed by the dissociation of oxygen molecules in the plasma environment exhibit oxidative degradation as well as double-bond structural disruption in different phenolic compounds owing to the formation of carboxylic and carbonyl compounds (29). Concurrently, the reactive plasma species also includes a reactive nascent oxygen species created by the dissociation of molecular oxygen by electron effect. This powerful oxidizing atomic form reacts with the benzene ring of phenol, forming primary diol products such as catechol and resorcinol, which, in turn, react with atomic oxygen, forming secondary products (30).

The presence of ozone is inevitable due to the high reactivity of the compounds, which leads to the hydroxylation of the benzene ring, forming hydroquinone. These dihydric phenols then undergo ring cleavage, producing major intermediates such as oxalic acids and glyoxalic acid, and are known to cause modifications in the cell wall that enhance phenolic compounds (31). Furthermore, hydroxyl radicals, which are reactive fragments generated by plasma, initiate the hydroxylation of the benzene ring to form hydroquinone (32). This is followed by an oxidation reaction that leads to the production of intermediate benzoquinone and, subsequently, the formation of fumaric, maleic, and oxalic acids as end products. Consequently, reactive species from cold plasma can affect cell viability by causing the rupture or disruption of the cell membrane, thereby affecting the availability of phenolics. Another significant approach resulting in phenol concentration variations is the nitration process, where the accumulation of nitrates or nitrites leads to the formation of nitrophenols, affecting the functional profile and polymerization reactions, forming larger polymeric structures of phenols modifying solubility and bioavailability of these compounds (31). Approaches on the effect of plasma on phenylalanine ammonia-lyase, an important enzyme in synthesizing phenol concentration, influence the phenol activity in samples. Inactivation or modification of enzymes encompassed in the synthesis pathway of phenols can directly alter the phenolic content of a product.

The effect of plasma on phenol and bioactive components exhibits a varying trend involving positive and negative inclinations. Compared to thermally treated and untreated samples, there is a rise in phenol concentration of plasma-treated samples with dependency on various parameters, including time, gas flow rate, and so on, which is explained in detail in the coming sections. There is a reported increase in phenolics by 64%−69% owing to the plasma treatment at 4–5s in cloudy apple juice (33). Parallel to these results, a more than 10% increase was induced by atmospheric plasma treatment in cashew apple juice (34). There are reported affirmations on the positive inclination of plasma in apple juice (35), acerola juice (36), sour cherry juice (37), and pomegranate juice (38).

Contrary to these samples, a decreasing trend in phenolic activity was noticed in the case of prebiotic orange juice (39), white grape juice (40), and strawberry fruit (41). These variations are highly dependent on the product and the process characteristics, and it is important to identify the significance of each parameter to maximize the process efficacy. The outcome of plasma on phenolic concentrations in various fruits and vegetables is given in Table 1.

3 Decisive parameters in cold plasma treatment

Laterally, with the generation systems, the levels of different parameters, such as input power, gas flow rates, treatment periods, and sample placement, influence the positive and negative variations observed in the food system (61). Power or voltage applied across the electrode has an unswerving influence on the reactive species generated. The dielectric breakdown of air is

TABLE 1 Details on the effect of plasma on phenol concentrations.

Sample	Treatment conditions	Observations	Advantages	References
Tomato juice	DBD plasma Voltage: 60 kV Frequency: 50 Hz Time: 10, 15 min	Rise in phenol content by 4% at 10-min treatment. A slight decreasing effect was reported in the case of 15-min treatment	• Higher retention of nutrients • Color improvement • Minimal impact on physicochemical properties	(42)
Apple juice	Jet plasma Frequency: 25 kHz Time: 30–120s	The increase in time was favorable, with treatment time at 120s resulting in a 14% increase in phenolic content	• Microbial resistance • Non-destructive in nature and shorter treatment times • Retention of sensory and nutritional properties	(35)
Banana slices	DBD plasma system Voltage: 4.8–6.9 kV Frequency: 12–22 kHz Time: 35–155 s	Total phenol & flavonoid content exhibited an increasing trend, mounting the treatment time and voltage. The optimum treatment condition was at 6.9 kV for 46s	• Enhanced bioactives and antioxidant activity • Retention of vitamin content • Effective in enzyme inactivation	(43)
Strawberry fruit	DBD plasma system Voltage: 60 kV Frequency: 50 Hz Time: 10–30 min	Treatment at 15 min was found to have a positive effect on the phenolic content	• Quality preservation • Enhanced bioactive potential • Synergistic effects	(41)
Cherry	DBD plasma system Voltage: 40, 60, 80 kV Time: 60, 80, 100, 140 s	Higher voltages have a detrimental effect on the overall phenolic content, with 60 kV treatment having no significant effect. Treatment time does not negatively affect the phenol content	• Enhanced shelf life • Retention of key quality attributes such as color, firmness • Enhanced bioactive potential	(44)
Fresh-cut pitaya fruit	DBD plasma Voltage: 60 kV Time: 5 min	The cumulative trend in the phenolic content was observed at the prescribed parameter range	• Promoted levels of antioxidants • Better product quality	(45)
Tomato pomace	DBD plasma Voltage: 120 V Frequency: 60 kHz Time: 15 min Working gas: air, argon, helium, and nitrogen	Higher phenolic content was observed in the nitrogen and helium plasma-treated samples compared to the control, whereas air and argon did not exhibit much difference.	• Enhanced phenolic content and antioxidant activity • Synergistic mechanisms • Retention of physicochemical quality	(46)
Orange juice	Jet plasma Frequency: 25 kHz Time: 30–120s	More than 9% increase in phenolic concentration owing to treatment time of 120s	• Microbial stability • Minimal processing and reduced treatment times • Effective retention of nutritional and sensorial parameters	(35)
Chokeberry juice	Jet plasma Power: 4 W Frequency: 25 kHz Time: 3, 5 min	No substantial change was noted in the treatment	• Polyphenol stability • Reduction in aerobic bacteria and yeast counts	(47)
Fresh cut apples	DBD plasma Frequency: 12.7 kHz Time: 15–120 min	No difference in phenolic content after 30 min of treatment. A decrease in phenolic content by 9%—33% was observed after the 30- and 120-min treatment period.	• Reduced enzyme activity and browning reactions • Increased shelf life	(48)
Apple juice	DBD plasma Power: 30–50 W Time: 0–40 s	Higher time periods and power had a detrimental effect on phenolic content value. Lower voltage values at 30 and 40 W did not have a substantial effect	• Faster treatment • Faster inactivation of microbial populations • Color retention • Enhanced phenol concentration	(49)
Blueberry	DBD plasma system Voltage: 12 kV Frequency: 5 kHz Time: 0–90 s	Increase in phenol content with an increase in treatment time	• Faster treatment • Reduction in decay rate • Retention of firmness value	(50)
Siriguela juice	Glow discharge plasma Time: 5–15 min Nitrogen flow rate: 10–30 mL/min	A gas flow rate of 30 mL/min showed a reduction in phenolic content by 30%. A 58% increase in phenolic content was exhibited at a 15 min and 20 mL/min gas flow rate.	• Color stability • Enhanced microbial stability • Enhanced bioactive components	(51)
Orange juice	DBD plasma system Voltage: 230 V Frequency: 50 Hz Time: 15–60 s	Phenolic content was affected only after 60s of treatment. Till 45s of treatment, the total phenolic content of the samples was retained	• Retention of physicochemical and sensorial factors of the sample • Smaller treatment times • Enhanced oligosaccharide content	(39)
Pomegranate juice	Plasma jet Frequency: 25 kHz Time: 3, 5, 7 min Gas flow rate: 0.75, 1, 1.25 dm^3min^{-1}	A moderate treatment time of 5 min resulted in an increase of phenolic content by 33%. There was a small decrease observed with augmented flow rate	• Fast, accurate, and non-invasive treatment • Better stability of the sample	(38)

(Continued)

TABLE 1 (Continued)

Sample	Treatment conditions	Observations	Advantages	References
Carrot juice	DBD plasma system Voltage: 60–80 kV Frequency: 50 Hz Time: 3, 4 min	No significant change between the different evaluation parameters. Maximum retention of phenolics was found with 70 kV treatment for 4 min	• A superior and viable alternative to thermal treatment • Maximum inactivation of enzymes and microbes • Enhanced stability of the juice	(52)
Okra pods	DBD plasma system Power: 750 W Frequency: 20 kHz Time: 5–30s	With an increase in time, there is a noted difference in total phenol content of 5%, 13%, and 20%.	• Increase in chlorophyll beta content • Faster treatment • Better flavonoid retention	(53)
Tomato juice	DBD plasma system Voltage: 220 V Frequency: 10 kHz Time: 0–5 min	Slight reduction in total phenol content by an increase in time of more than 15%	• Faster treatment times • Effective in fungicide degradation • Better quality product	(54)
Carrot juice	DBD plasma system Voltage: 8, 10, 12 kV Frequency: 18 kHz Time: 0–5 min	Total phenolics of the sample did not show much difference at 8 kV treatment, followed by a decrease at 10 kV and a further increase in total phenolic content	• Superior to traditional heat treatment • Extended shelf life • Better quality retention	(55)
Mango	Gliding arc plasma Power: 600 W Gas flow rate: 2 to 8 L/min Time: 5, 10 min	An increase in treatment time had a negative impact on total phenolics. The increase in gas flow rate resulted in an initial phenolic content increase of 5 L/min, followed by a reduction in parameters.	• Reduction in pesticide residues • Increase in carotenoid content	(56)
Avocado pulp	DBD plasma system Time: 10–30 min Gas flow rate: 10 to 30 mL/min	An increase in treatment time and lower gas flow rates positively influence the phenolic content of the sample. Treatment at 10 mL/min for 30 min was reported to have an increase of 18% in the phenol content of the sample.	• Increased carotenoid levels • Retention of quality attributes	(57)
Persian lime fruit juice	Gliding arc plasma Power: 300 W Flow rate: 10 mL Frequency: 50 Hz Time: 30–120s	Rising trend in the total phenolic content till the 60s of treatment, followed by fluctuations with an increase in time. The higher phenolic content was observed in the treatment at 60s.	• Enhanced post-harvest storage life • Retention of juice yield and other sensorial attributes • Better microbial stability	(58)
Yam slices	Glow discharge plasma Power: 500 W Time: 90–180s	CP treatment showed retention in the phenol content of the sample with the highest phenolic content at the 90s of treatment.	• Reduction in peroxidase activity • Enhanced antioxidant activity	(59)
Tomato juice	DBD plasma system Voltage: 40, 45 V Time: 3, 4, 5 min	Significant reductions in the phenolic content of the samples were observed with a rise in voltage and treatment time. Higher values were reported at 40 V for 3 min of the treatments, followed by 45 V for 3 min.	• Reduction in fungicide levels • Prolonged shelf life • Microbial stability	(60)

known to be achieved by the application of electric field power at 30 kV/cm (31). The power or voltage should be maintained in a plasma system so that it is sufficient for the generation of plasma, but it should not have a detrimental effect on the quality properties of food. The effective parameter range depends on the product characteristics, and it is known to have positive inclinations at a lower range of voltage applied. An increase and retention in the phenol concentration was reported in the case of cherry samples treated by cold plasma at a voltage of 40–60 kV (44). Elevated voltage levels resulted in a detrimental effect on the total phenol concentration of the sample, which emphasizes the viability of moderate treatment conditions. A similar trend was observed in the case of apple juice, which underwent jet plasma treatment, conveying an elevated power-dependent decrease in phenol concentrations (35). Polyphenol content increased from 30.57 to 43 mg/100 g of fresh weight in banana slices with an increasing voltage from 4.8 to 6.9 kV. The antioxidant activity and total flavonoid content also followed a similar increasing trend with a change in voltage (43). Plasma species and their reactivity play a vital role in the interactions that happen post-treatment in food products. Gas flow rates directly impact the reactivity of these generated plasma species, and a reported increase is shown in this with an increase in the discussed parameter. As in the case of power applied, moderate conditions of gas flow rates are favorable, with higher or elevated rates tending to shorten the residence time of active species and thereby reduce the system efficacy. On the contrary, very low flow rates may not be adequate for initiating the interaction of plasma species with a short half-life. In this case, higher flow rates will increase the likelihood of interactions in the plasma environment (5). Retention of phenolics was safeguarded in acerola juice samples when the flow rate was maintained at 10 mL/min, and a further increase in flow rate (up to 20 mL/min) induced a decreasing trend in phenolic concentration (36). Siriguela juice showed a varied result of positive correlation with a gas flow rate of up to 20mL/min followed by a reduction in the phenol concentration of 30% with a surge in the flow rate to 30 mL/min (51). Ten mL/min was considered to be ideal in plasma treatment of avocado pulp samples, with an increase in

phenolic content by 5%−18%. Lower gas flow rate values were found to safeguard a milder effect on the degradation reactions, upholding the level of phenolic content in the sample. Higher flow rates in the range of 20–30 mL/min were not favorable in the retention of phenolics in the sample, and there was a substantial decrease reported when the gas flow rate was increased to 30 mL/min (57). Observations exhibited highlight the fact that an ultimate elucidation on the feasible parameter range is not conceivable, as the inclinations vary according to the product and process characteristics.

Another important parameter under consideration is plasma generation frequency, as it is directly associated with the excitation behavior of ions from the plasma system. A maximum phenolic activity of 720 mg gallic acid equivalent/g was reported in apple cubes treated with a dielectric plasma system at a frequency of 60 0Hz (62). A higher excitation frequency (900 Hz) was reported to have a detrimental effect on the phenolic profile of the treated sample. Differing from the stated results, plasma-treated samples showed higher phenolic content at lower and higher (200 and 960 Hz) frequency ranges. An increase in frequency levels of plasma treatment has substantially affected the phenol content and antioxidant activity of camu-camu juices (63). The decrease in phenol concentration was observed at moderate frequency levels of 420–628 Hz in treated camu-camu juice. A similar trend is observed in the case of the antioxidant activity of the samples, as the phenolic content has a contributory effect on the mentioned parameter. Variations in results can be viewed regarding the difference in the synergistic profile of parameters such as power and frequency or time and frequency of the plasma system and the generated plasma species. Even the characteristics of the treated sample will act as a combinatorial factor in the efficacy of the plasma system. Feed gas is a significant parameter that alters the nature of the plasma reactive species and the food interactions employed in the system. For example, the change in oxygen concentration significantly affected phenolic content during the CP jet treatment of blueberry juice (64). The stable nature of argon gas does not affect the chemical composition of the food product, retaining the phenolic content and antioxidant capacity. A rise in O_2 concentration had directed a positive change in phenolics with maximum concentration at a higher percentage of O_2 in the system. The combination of inert gas and oxygen resulted in decreased oxidative degradation of functional compounds, maintaining their concentration and antioxidant properties. Higher phenolic content was observed in the nitrogen and helium plasma-treated samples compared to the control, while air plasma treatment did not differ much (46). Treatment time is one common and conducive parameter that ensures the effectiveness of any treatment in food particulates. In the case of plasma treatment, the time designed for treatment will endorse the extent of the interactive nature of the reactive plasma species. Reactive plasma species should have sufficient time to interact with food components, positively influencing the functional nature or engrossing in degradative inter-reactions that closely affect the food characteristics at elevated times. The prolonged processing time of CP treatment has displayed higher phenolic content in blueberry juice (60), and this was in accordance with studies on mandarin peel (65) and cashew apple juice (35) with maximum retention of phenolic content.

Meanwhile, reported results showed a decrease in phenolic content from 2.52 to 1.93 g/L in orange juice, owing to plasma exposure for more than 60s (39). Higher treatment time also showed a negative impact on the phenolic content of white grape juice (40), acerola juice (36), and sour cherry marasca juice (37). These contradictory findings emphasize the importance of a detailed understanding of the product and active species interaction to effectively comprehend the plasma process. Along with the product-reactive species interactions, it is important to understand how the plasma-treated samples behave during the shelf-life period. The phenolic content and antioxidant activity of the plasma-treated samples followed an increasing trend during the initial storage period, followed by a decreasing inclination compared to the control sample. However, the superiority of the plasma-treated samples in terms of phenolic content was sustained in whole blueberry samples for a period of 40 days (50). Similar tendencies over the storage periods were reported in the case of potato tubers treated with a plasma jet reactor for 0–40s time. The total phenolics of the samples decreased with longer storage hours after displaying an increasing trend during the initial days. After 8 days of storage, comparative analysis showed that the phenolic content of the potato slices treated for 20 were 18% higher than the control samples (66). The treatment at 20 and 30 maintained a phenol content value superior to the control samples throughout 16 days of storage, whereas treatment at 40s was found to be inferior. Time dependence on the efficiency of the process has already been discussed, and there is a visible influence of the parameter variation even in keeping the quality of the product. More investigations are necessary to understand the parameter fluctuation range affecting the process and the product.

In addition, external factors such as relative humidity, sample matrix, and pH have an effect on the properties of reactive species and the interactions happening in the system (67). When considering the case of sample properties, starting from the state of the food product, there will be changes in the interaction. Plasma species interactions with a solid matrix will differ entirely from a liquid matrix, with higher area or contact points. Within the solid matrix, there will be differences according to the surface microstructure & porosity, component profile, and even the moisture content (68). This difference exists in regard to the relative humidity and pH of the treatment environment, as the type and effectiveness of the reactive species are, in turn, added to the variations in these parameters. Supplementary to the discussed aspects, the source type, material of construction, and packaging variations, i.e., whether the process involves an open treatment or in-package treatment of plasma, influence the effectiveness of the interactions, thereby influencing the process variables.

4 Process optimization & modeling

Statistical methods can evaluate the extent of influence of intrinsic parameters involved in the process dependency representations are performed with the help of models. This study proposes the right experimental model by following different screening levels, aligning, and optimizing data values.

4.1 Response surface methodology

RSM is a set of statistical and mathematical models ascertained on the fit of the polynomial model to data, which should exhibit the conduct of the whole data set for making statistical predictions. This approach effectively evaluates, optimizes, conceives, and refines the processes where a response(s) is controlled by the variation of several other variables (69). In the evaluation process, the value of the response is envisaged based on the factors considered, and the intricate interplay between the presence of several independent variables is comprehended. The following result encompasses a mathematical model having an ideal combination of factors to deliver optimized results. Selecting an appropriate experimental design is crucial for RSM analysis, as the design of the experiment determines the points at which the response should be assessed. The most used experimental design models in the food industry are central composite design (CCD), central composite design (CCRD), Box-Behnken design (BBD), multilevel factorial design, and so on. The application of RSM techniques in food research follows a longer trail with applications around food drying, extraction, encapsulation, enzymatic hydrolysis, blanching, and certain food formulations (70).

4.1.1 Central composite design

CCD is an effective and most commonly applied form of design that provides equitable evidence for investigating the lack of fit of data without including larger experimental runs. Applied design has the competency to predict both linear and quadratic models with high quality, and they can also be employed to study factors at three or four levels. In the case of cold plasma treatment, CCD is believed to be the most common design form employed in optimizing the parameters related to the quality of the final product (71). A central composite design with 16 experimental trials, three independent variables including gas flow, sample volume, treatment time, and one output parameter was used to evaluate the efficacy of gas phase plasma treatment in sour cherry Marasca juice (35). Based on the analysis, the major factorial change was induced by variation in the treatment time of the plasma technique, while the other two factors remain minor contributory. Optimal treatment conditions for maximum phenolic retention were 3 min, 3 mL, and 0.75 L/min of treatment time, sample volume, and gas flow. Ideal values of plasma parameters in retaining the phenolic content of ginger samples were determined by the interaction between dependent and independent variables in CCD design (72). The independent factors involved in the study are power, time, pressure, and rotation, and each of them is assigned three coded levels with a total of 37 trials in the system. A linear effect of each parameter was visible in the retention of TPC in the plasma-treated samples. With increased treatment power and time, there is a negative inclination in TPC values, ranging from 35 mg to 14 GAE/g. The rotation of samples was found to be effective in retaining the phenolic content, having an observable difference from the non-rotated sample. The factors involved in the study have distinct and combined effects on the final phenol content of the sample. The optimized treatment conditions after 1 min at a power level of 50 W and pressure of 0.65 mbar retained higher concentrations of phenols in the sample.

Central composite face-centered design (FCCD) is one of the different designs within CCD that evaluate and optimize the parameters in cold plasma treatment of blended beverages (73). FCCD with two independent parameters, including treatment time and voltage, are involved in the evaluation process. The optimized treatment conditions recognized through RSM analysis reflected a delicate steadiness between the analyzed parameters. Both voltage and time had an influential role in the antioxidant activity of the sample, exhibiting a plummeting trend with an increase in the combined parameter values. Plasma treatment at a voltage of 18 kV for 1.75 min was optimized to balance the antioxidant profile and microbial safety. FCCD design with six center points, four cube points, and four axial points was used to assess the effect of DBD cold plasma on the phenol content and antioxidant activity of green tea leaves (74).

Three levels of treatment time and power were taken as independent variables to understand the effect these variables have on the final output. The influence of power and time on the TPC values of the samples was significant, but the independent effect of time on the phenolic profile was found to be marginal. A predominant effect on the phenolic profile emanates from the variation of power in the treatment and its combination with treatment time. The optimized treatment parameters were obtained as a power of 15 W for a treatment time of 15 min for achieving an increase in phenol content by 41% and antioxidant activity by 41.04%. Analogous to plasma treatments, CCD is also employed in assessing the effect of different independent parameters such as time, temperature, and solvent-to-solid ratio on three responses during the extraction of phenols from potato peels (75). Experimental design with 20 runs, eight factorial points, and six axial and central points each provided an optimum parameter value of 30 min of treatment time at a temperature of 75°C and 60 mLg^{-1} solvent-to-solid ratio.

4.1.2 Central composite rotary design

Central composite rotary design is considered an alternative to the factorial design and can quantify the relationship between controllable inputs and resultant responses. The key advantage of the process design over other models is its capacity to optimize multiple operational variables with a small experimental data set. These possibilities assisted in the application of this design format when the values of certain investigations were altered by experimental error (76). CCRD has been found to be efficient in predicting and formulating the interactions of input parameters with the possible responses of cold plasma treatment (77). CCRD, with five levels and two independent factors, including time and voltage, is studied against six other parameters, including phenolic content and antioxidant activity. Linear and square regression coefficients of two independent variables are found to impact the particular responses with optimized parameters at a range of 35 kV voltage for a treatment time of 510 seconds. The phenolic content value of the treated sample showed an initial increase up to a certain point, followed by a decreasing trend due to the rise in voltage and time. The linear coefficients of both voltage and time are positively correlated with phenolic content, whereas there

is a negative correlation of square coefficients of parameters. In the CCRD design of the experimental evaluation of cold plasma parameters in kiwifruit juice, the juice depth was utilized as an additional independent parameter (78). A set of 20 experiential runs with six output parameters was involved in the experiential pattern, and there was a linear dependency of TPC over-voltage and time. Voltage and depth show a positive dependency on the final phenolic content, and negative dependency was observed on treatment time. There is a positive correlation between the phenolic content of the sample and the voltage and time values up to a certain point. Beyond this point, the phenolic content decreases. In operations such as cold plasma, where each independent parameter can insinuate a certain degree of variation in totality, it is always preferred to choose these methods or designs where multivariate analysis is feasible on a larger scale.

4.1.3 Box-Behnken design

BBD was first designed by Box and Behnken with the ability to go with fewer experimental runs and has a definite set of factorial combinations from the 3 k factorial design. This three-level design has an economic ascendancy over other models, as the employed experimental runs can be a minimum (76). The Box–Behnken experimental design effectively predicted the independent parameters' possible interactive effects during the cold plasma treatment of kiwi turbid juice (79). Here, voltage and treatment time have an added authority over the phenolic responses of the product more than the third factor. The phenol content of the samples reported a decreasing trend with increasing treatment voltage and time. The optimum experimental conditions were reported to be at a treatment voltage of 12 kV and a volume of 18 ml for a treatment period of 1 min. Parallel to these findings, the optimization efficacy of the BBD design model in ultrasound-assisted extraction from cherry fruit was reported. With 29 experimental runs, four independent parameters, and two dependent parameters, the experimental data were placed in a second-order polynomial equation to understand the fit (80). Independent variables showed a significant quadratic effect in the phenolic content of the plasma-treated samples, whereas the effect of linear variables was insignificant. The optimal conditions with maximized response variables were found to be a 26 mLg^{-1} solvent-solid ratio, a solvent concentration of 58%, and 28% amplitude for a treatment time of 31 min. Even though economic feasibility is associated with the process, it comes under the category of the least explored design aspect regarding cold plasma treatment and needs more experimental data to conclude the degree of efficacy.

4.2 Model fitting

The application of different model systems is common in the scientific research field, and it is also invariable in the case of the food research segment. The feasibility and effectiveness of each model in a system are deeply correlated with the parameters and processes involved (Table 2). In the case of cold plasma treatment of agricultural produce, regression models are commonly involved in checking the feasibility of predicted responses. The validation and selection of the model are based on their fit and alignment with the experimentally obtained results. The model's fit is validated by ensuring a significant p-value of <0.05, no significant lack of fit, a high R^2 value, and a difference of <0.2 between the predicted and experimental values (69). This predictive evaluation involves the mathematical representation of response surfaces as regression equations. Depending on the correlation between the response surface and the input variables, the equations can be first or second order in description (71). Response surface plots of 3 min cold plasma treatment of sour cherry juice followed a 2^{nd} order polynomial equation, and there are linear, quadratic, and interaction coefficients predicting the desired final response value (37). All four variables exhibited a quadratic effect on the phenol concentration of the sour cherry juice and were reported to have significant interaction between the variables. The experimental values obtained after evaluation were found to be 98% of the predicted phenolic responses, emphasizing the model's success in envisaging the interactive correlations. From the discussed instances, we have gained an understanding that time has a significant impact on the efficiency of cold plasma. Therefore, optimizing the process study with a broader range of time values can enhance the model's efficacy. Similar is the case with the regression equation based on plasma treatment in tender coconut water (81). The parameter range is so limited that the interactive effects of the independent factors are difficult to recognize. The proposed model of this study was effective as there were adequate data points within the proposed smaller range of study. A good fit concerning the experimental and predicted data is denoted by a higher R^2 value and a p-value of lack of fit higher than 0.05. A higher value of R^2 can be considered the strength of the quadratic representative form of cold plasma treatment of sour cherry juice. RSM analysis of cold plasma treatment data showed an R^2 value higher than 0.95 and a p-value below 0.05, emphasizing the uniformity of predicted and experimental values (80). The model's fitness in defining the data set can be attributed to its characteristic aspect in judging the response structure over a range of input variables. The 2^{nd} order polynomial regression equation expressing the relationship between the input variable and phenolic response is given as:

$$Y = -14.15 + 3.13\,x_1 + 0.01x_2 + 5.12 \times 10^{-6}\,x_1x_2 - 0.043\,{x_1}^2 - 2.3 \times 10^{-5}{x_2}^2 \quad (1)$$

These coefficients, x_1 (voltage) and x_2 (time), represent the two independent variables, and y is the response, in this case, phenol content (77). Cross-product terms in the equation are responsible for model interactions between the explanatory variables. The single variable accounts for the linear effect, and the squared terms account for the quadratic effects and are responsible for response curvature. The positive values in the regression equation represent a synergistic effect, whereas a negative term denotes an antagonistic effect on the final parameter. Linear and squared regression coefficients of voltage and time display a considerable effect on the response of the samples, with marginal influence from the interaction coefficients. Linear coefficients exhibit a positive correlation in contrast with negatively correlated interaction

TABLE 2 Details on RSM analysis of cold plasma treatment variables.

Sample	Experimental variables	Optimized conditions	Equation	Pros & cons of the selected model	References
Kiwi turbid juice	Voltage Time Volume	Voltage: 12 kV Time: 1 min Volume: 18 ml	$Y_2 = 2.84 - 0.11A + 0.79B - 0.11C + 0.11AC + 0.19A^2 + 0.52B^2$	• Easy to interpret & consolidate • Works well with the linear relation of parameters with phenol content • Issues may arise when dealing with complex relations • Sensitive to outliner data	(79)
Tender coconut water	Voltage Time	Voltage: 18 kV Time: 2.85 min	$Y_1 = 26.59–0.85x_1 - 0.77x_2 - 0.23 x_1x_2 - 0.34 x_1^2 + 0.11 x_2^2$	• Simple in form • Have moderate flexibility • Assumes a linear relationship between independent and non-independent variables • Increased risk of overfitting • Need of more resources	(81)
Ginger	Power Time Pressure Rotation	Power: 50 W Time: 1 min Pressure: 0.65 mbar Rotation: On	$Y_4 = 8.49–0.4619A - 1.04B + 0.1556 C-0.1318D - 0.5973AB - 0.2191AC + 0.0714AD- 0.0282BC- 0.0234BD- 0.0203 CD + 0.4917A2 - 0.0564B2 - 0.8279 C2$	• Provides interaction effect analysis • Reduction in experimental runs • Provides perceptive visualization of connected variables • Does not provide mechanistic insights into the processes affecting the sample properties	(72)
Green tea leaves	Power Time	Power: 15 W Time: 15 min	$Y1 = 840.87 - 15.83A - 56.00B + 2.75AB + 2.52B^2$	• Reduction in number of experiments saves time, resources, and cost • Generates equivalences that envisage extraction efficiency and antioxidant activity under different experimental conditions • Sensitive to input data	(74)
Pineapple juice	Voltage Time	Time: 510 s Voltage: 35 kV	$Y_{TPC} = -14.15 + 3.13 x_1 + 0.01 x_2 + 5.12 \times 10^{-6} x_1 x_2 - 0.043x_1^2 - 2.3 \times 10^{-5} x_2^{\ 2}$	• Comprehensive optimization • Generated outcomes can aid in scaling up and process optimization functions • This might result in oversimplification of the non-linear effects of DBD plasma treatment • Accuracy depends on the provided data quality	(77)
Siriguela juice	Gas flow Time	Gas flow: 20 mL/min Time: 15 min	$Z = 820.69–102.76x + 6.0 x^2 + 25.23 - 0:55y^2 - 013xy$	• Systematic optimization of cold plasma parameters • Effective interpretation of the plotted data in understanding the underlying interactions • Effect the fit of the data if we consider more complex interactions • Limited to specific parameters involved in the study	(51)
Kiwifruit juice	Voltage Juice depth Time	Voltage: 27.6 kV Time: 6.8 min Juice depth: 5.2 mm	$Y_i = c_0 + c_1 x_1 + c_2 x_2 + c_3 x_3 + c_4 x_1 x_2 + c_5 x_2x_3 + c_6 x_3x_1 + c_7 x_1^2 + c_8 x_2^2 + c_9 x_3^2$	• Exploration of interactive effects on juice quality • Additional validation is required owing to parameter specificity • Limited scalability	(78)
Pear cactus fruit	Power Time	Power: 750 W Time: 40 min	$Y_i = 57.458 - 0.076X_1 + 1.028X_2 + 2.171X_1X_2 + 1.101X_1^2 + 2.171X_2^2$	• Involves fewer trial runs in predicting the outcomes of the conditions tested effectively • Customization potential • Identifies correlations but limits in apprehending the underlying mechanisms • Limited in managing data complexity	(82)
Red globe grapes	Gas flow rate Time Voltage	Gas flow rate: 2.87 SLPM Time: 1 min Voltage: 3.36 kV	$Y_i = +0.8440 + 0.0006 X_1 + 0.0094 X_2 + 0.0075 X_3 + 0.0010 X_1 X_2 - 0.0002 X_1 X_3 - 0.0077 X_2 X_3 - 0.0032 X_1^2 - 0.0053 X_2^2 0.0020 X_3^2$	• Effective in predicting responses related to the sample quality • Data complexity is affecting the efficacy of a selected representative model • Sensitive to the input data quality	(83)

coefficients. The coefficient of determination of treatment values was around 0.945, explaining the goodness of fit and the parallel nature of the target and predicted values.

Table 2 gives an explanation of the polynomial equation involved in cold plasma treatment of food products. With an R^2 value of 0.928, the quadratic regression model equation exhibited a good fit between the predicted and experimental values of cold plasma treatment of ginger samples (72). The model was developed with a broader range of parameter values, which has helped in understanding the interactions when it comes to higher ranges of values. However, the iterations, or the number of data points between the ranges, appear to be small and can be included to provide a more profound understanding of the interactions. Cold plasma treatment evaluations have already shown us how the dependency of the process changes with the alterations in process parameter values. Analogous to the results, the quadratic model representing the phenol retention efficacy in cold plasma treatment of green tea leaves (74) has made efforts to have a wider range of independent variables, contributing to the model efficacy. The proposed model is based on 3 data points in the case of both variables, which could have affected the efficiency of the optimization process.

Furthermore, including additional lower data points within a modified broader range would have positively impacted the proposed model. The model representing the DBD plasma modification of kiwifruit juice (78) presented an R^2 value of 0.95 with quadratic terms of voltage and time, showing a significant effect in the response variable. Representing a larger data point in two variables, the process evaluates several interactive parameter combinations, which positively affect the suitability of the proposed polynomial equation. In the case of the third variable (time), there is a scope for extending the lower range of the data set, thereby improving the proposed model.

4.3 Artificial intelligence based techniques

Artificial intelligence has now become prevalent across a different range of industries and sectors, such as healthcare, finance, manufacturing, transportation, and retail markets. It has also speckled down to applications in agriculture and food industries. The conceivable role of AI in the food industry is to leverage developmental opportunities to enhance product quality, safeguard consumer needs, manage supply chains, improve production, and drive a sustainable and successive industrial stature. The basic idea behind the AI technique revolves around the emulation of the human thinking process, learning ability, and storage of knowledge. It involves the development of algorithms and computational models that enable machines to process and analyze large amounts of data, identify patterns and relationships, and make predictions or decisions based on that analysis (84).

The system incorporates a diverse array of algorithms, such as artificial neural networks (ANNs), genetic algorithms (GAs), logic programming, cognitive science, expert systems, swarm intelligence, and fuzzy logic (FL). These algorithms facilitate process estimation based on the sample set and the final output. Notably, FL and ANN are specifically used for predicting and classifying parameters, which contributes to increased yield, reduced production costs, and enhanced safety and quality of the final product (85).

4.3.1 Artificial neural networks

ANN is a powerful and unique modeling system that outshines in capturing non-linear relationships and indicates superior predicting capabilities. The elementary structure of an ANN consists of an input layer, a few hidden layers, and a yield layer. Each structural layer consists of a set of neurons interconnected by a link, and communication between these neurons is achieved by a value assigned to each link called weight. It is one of the artificial intelligence-based elements fabricated to mimic the human brain and evaluate the data through learning and interneuron connections (85). The system's expediency and capability have accelerated feasibility studies on its application in areas such as quality analysis, food safety management, image analysis, classification, prediction of parameters, and modeling of various processing operations.

The ANN model benefitted from the prediction and modeling of the relation between input and output parameters in the non-thermal plasma treatment of pineapple juice (77). A feed-forward neural network with an input layer of two neurons (time and voltage), a single hidden layer, and an output layer of 6 neurons, including total phenol content and total antioxidant activity (Figure 2), was used in the analysis. The number of hidden layers is determined through an iterative trial-and-error method. During this process, the hidden layer of the training with the maximum R-value and minimum MSE value is selected. A total of 12 experiment data sets for the program were categorized as 70% for training, 15% for testing, and 15% for validation with transfer functions for output and hidden layers as linear transfer functions (purelin) and tangent transfer functions (tansig). The objective of data set categorization in the ANN system is to ensure the network's robustness and normalize the network error, which is considered to be a greater positive of the system than others. High correlation coefficient (R) and low mean square value (MSE) were used to confirm the feasibility of the number of hidden layers employed and the model's appropriateness. The final evaluating structure consisted of two neurons in the input layer, eight in the hidden layer, and six in the output. Training, testing, and validation correlation coefficients were found to be 0.9986, 0.9997, and 0.9983, with an R-value of 0.9996 for the overall developed ANN model, ensuring the system's credibility in evaluating and predicting data. An analogous R-value of 0.9997 was obtained for ultrasound-assisted extraction of polyphenols from Meghalayan cherry fruit via an artificial neural network (80). Here, the input layer consisting of four variables, eight neurons in one hidden layer, and the output layer with two neurons constituted a feasible design for forecasting this experimental data with a minimum MSE value of 0.61. Input, hidden, and output layer combinations, the transfer functions involved, data categorization, and the number of neurons in each layer depend on the characteristics of the data that's been handled and the way it is handled (Table 3). Parallel to these results, a categorization of the data set as 70% for training, 15% for validation, and

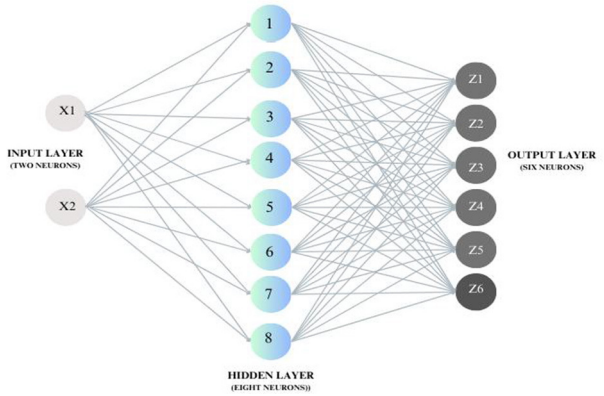

FIGURE 2
A schematic diagram of the ANN model used with two input layers, one hidden layer, and six output layers.

TABLE 3 Summary of the reported transfer functions involved in cold plasma data modeling.

Structural design	Transfer functions involved in the process
Input layer	• $f(p) = \frac{1}{1-e^{-p}}$
Hidden layer	• $f(p) = \frac{1}{1-e^{-p}}$ • $(n) = \frac{2}{1+e^{-2n}} - 1$ • $(n) = \frac{2}{(1+\exp(-2*n))-1}$ • $(n) = \frac{1}{1+\exp(-n)}$
Output layer	• $(n) = n$ • $f(p) = \frac{1}{1-e^{-p}}$

15% for testing was employed in the 3:10:10 ANN model for thermosonication of sohshang fruit juice. The obtained value of the coefficient of variation was around 0.97, which explains the acceptability of the predicted fit. There is an excellent agreement between the predicted and experiential values in the regression analysis plots, justifying the significant relationship between the data sets (86).

A good correlation of 0.99947 was obtained during ANN analysis of plasma treatment of tender coconut water (81). In this structured evaluation of parameters, it is important to fix the number of hidden layers chosen, as too many layers may cause overfitting of data. In contrast, too few may cause slower processing of data in the network (77). A structured 2-7-2 model was utilized for cold plasma treatment with one of the output neurons as antioxidant activity. This design showcases the significance of interneuron connections between the layers, weight, threshold values, and the matrix arrangement within the system's input, output, and hidden layers. The R^2 values for individual processes were 0.9993 for training, 0.9998 for validation, and 0.99976 for testing (81). The correlation coefficient value states the positive relationship between the actual and predicted values of the experiential learning procedure; the values showing closeness to 1 always emphasize a positive correlation in the study. A minimum R^2 value above 0.80 is considered a standard for all optimal models, and with these higher correlation coefficient values, the model's accuracy is ensured. Training, validation, and testing of microwave processing parameters on enzyme activity and phenolic content of tender coconut water also showed similar correlation coefficients of 0.99967, 0.99945, and 0.99987 for the tests, respectively (87). A neural network type of 3-9-1 topology efficiently evaluated the total phenolic content in strawberries. The result validates the effectiveness of threshold transfer functions of purelin in the output layer and transig in the hidden layer in achieving an R^2 value of 0.9806 and a low MSE value of 0.00470, respectively (88).

In the ANN modeling of CP-independent parameters, an experimental data distribution of 80%, 10%, and 10% was used for training, validation, and testing, respectively, utilizing a multilayer feed-forward neural network design (78). This network consists of an input layer with three neurons (time, voltage, and juice depth), two hidden layers, and an output layer with six neurons, including measures for total phenolic content and total antioxidant activity. The first and second hidden layers employed hyperbolic tangent and log sigmoid transfer functions, respectively. After several trials, the number of neurons in the hidden layers was increased to ten, achieving a maximum R-squared (R^2) value of 0.999. Correspondingly, the R^2 values for the training, validation, and testing phases each also reached 0.999.

The regression analysis data exhibited all regression lines closer to 1. The error histogram of the evaluated value showcases that the maximum data, in this case, exhibits a very low error of 0.00142, verifying the prediction performance of the process evaluation. With a low error value of 0.0527, the error histogram was divided between 20 vertical bins between −3.424 and 1.6 in predicting the quality attributes of pineapple juice after non-thermal plasma treatment (77). These error values predict the difference between the predicted and target values. Having a low error value for the maximum data among the analyzed values signifies the correctness of the data involved. Considerable data points amount to an analogous error value of 0.080006, indicating the accuracy in modeling the data related to the thermosonication of sohphie fruit juice (89). Regression analysis of the data also showed a greater correlation between the predicted and the actual values throughout overall data sets. The correlation between the actual and predicted data values always delivers a sense of reliability and accuracy in the system's application in evaluating the experimental array of data. Although the related data on ANN looks assuring and precise, added data evaluation, further experimental data sets, more permutations, and combinations are needed to ensure the process's applicability, dependability, and accuracy.

4.3.2 ANN-GA optimization

A genetic algorithm (GA) recognized as a global search engine in combination with ANN modeling will assist in plummeting the complexity of the problems and discovering optimum process conditions. The evaluation process helps obtain an optimum value with maximum accuracy and minimum error (90). The process commences with choosing a set of initial populations followed by their corresponding set of fitness functions evaluated based on Darwin's theory or principles of genetics involving selection, crossover, mutation, and reproduction. The best among the present chromosomes is selected for the upcoming generation

and combined during crossover to create progenies. Different food processing operations, such as extraction, drying, puffing, and roasting, have followed the application of a combination of ANN-GA in evaluating, modeling, and optimizing the available data set. The input parameters of cold plasma treatment in pineapple juice were evaluated by coupling ANN with this built-in optimization tool (77). The fitness function involved in the optimization process is based on your data set and the output parameters considered in the function. The fitness function of CP treatment in pineapple juice is given by Equation 1 with three input parameters and six output parameters, including the total phenol content of the treated juice after treatment.

$$F = Y(1) + \frac{1}{1 + Y(2)} + Y(3) + Y(4) + Y(5) + Y(6) \quad (2)$$

The optimization of the ANN model was completed after 68 generations amid voltage, juice depth, and treatment time values of 30 kV, 5 mm, and 6.7 min. The predicted and validated responses of the process remained comparable, with a small error value of 0.83%. This shows the accuracy of the optimized values, and in comparison with the control values, these results exhibited the retention of TPC content of the plasma-treated sample. Ultrasound-assisted extraction of total phenols and other phytocomponents from dragon fruit peel was modeled and optimized by the combined ANN-GA technique (91). The output parameters or responses were selected based on the highest fitness function, and the optimum value parameters of the process were found to be 59.96°C, 60%, 20 min, and 25:1 for ultrasonic temperature, solvent concentration, treatment time, and solvent-to-solid ratio, respectively. The optimization process was validated by conducting experiments at predicted ideal conditions, and these obtained values are equated with the predicted data set to identify the associated deviation. Relative deviations between the predicted and target values of optimized parameters in ultrasound treatment were 1.2–2.05, which emphasizes the accuracy of the optimization process. GA optimization has reported an ideal parameter combination of temperature at 40°C, the amplitude of 50% for a treatment time of 60 min for thermosonication of *Elaeagnus latifolia* fruit juice, and the results were found to closely match with real outcomes based on optimized results (86).

Optimal values for parameters of CP-treated kiwifruit juice were found to be 38 kV and 631 s after 176 generations of the ANN-GA optimization process. The optimal values of the process exhibit good retention of phenolic compounds and reveal comparable phenolic and antioxidant content on evaluation with thermally treated samples. The lower percentage errors (1.00%) between the predicted values and the targeted experimental values show the suitability of the fit in the cold plasma technique. ANN coupled with GA aided in predicting the optimum parameter values for the thermosonication process of sohphie fruit juice after 15 iterations in the study (89). The results obtained with optimized parameter values were in conjunction with the projected denominations produced by the ANN model with the least error values associated. The optimized parameters for the ultrasonic treatment were a 40°C temperature, 50% amplitude, and a treatment period of 60 min.

Precision in the GA optimization process is achieved by either minimizing or maximizing the GA output parameters to secure a high-fitness functional value. For the ANN-GA-optimized process of cold plasma (CP) treatment in tender coconut water, minimal error values were noted between the predicted and experimental values. Optimal results were achieved at a voltage of 18 kV and a treatment time of 2.85 min, with the predicted scavenging activity around 26.71%. Similarly, extraction process parameters of pectin from sunflower heads were determined using a coupled ANN-GA with a second-order polynomial equation serving as the fitness function. The maximum yield of pectin was comparable to the predicted results obtained from GA optimization, affirming the adequacy of these models. The reliability and accuracy of these predictions are evidenced by minimizing error values, underscoring the effectiveness of GA as a robust optimization tool for managing experimental CP data.

5 Conclusion and future prospects

Cold plasma has gained significant popularity and interest among stakeholders in recent years due to its innovative and substantial potential in processing and preserving agricultural produce. While most of the studies and findings revolve around the possibility and viability of plasma in rendering a safe product, the likelihood of the technique in functional and quality characteristics of food particulates is still nascent. Phenolic fractions are important bioactive compounds in agricultural produce that can be regarded as contributory aspects or determinants of antioxidant potential. The prospects for quality modifications of plasma in agricultural produce are directly correlated with the generated active plasma species, processing conditions, and induced food interactions. Reaction chemistry is crucial in understanding the intensity of functional and nutritional modification of food. Reported outcomes of oxidative degradation, hydroxylation of benzene rings, nitration of phenols, and so on are proposed as the conceivable explanations prompting the functional and structural modification of the phenolic profile. There is still a prerequisite need to understand and elucidate the intricate molecular-level interactions behind these food interactions to increase the efficiency of the whole process.

Cold plasma treatment, without a doubt, has been reported to have a positive impact and the upper hand in the retention of bioactive components compared with traditional thermal treatments. The degree and inclination of this plasma impact depend on different process parameters such as treatment time, power, voltage, and gas flow rate. The system's mode of action and efficiency can also vary according to the generation mechanism and food characteristics. Careful selection of treatment parameters is essential to achieving desired results and maintaining system efficacy. One aspect of accomplishing this is conducting extensive research encompassing parameter range variations and closely inspecting the effects these variations have on product characteristics. This is where the application of modeling, prediction, and control tools comes into the picture. Comprehension of a feasible set of parameters significant to the

study is made possible by the application of statistical-based experiment design in different processes involved. Statistical-based methods such as RSM could effectively help us understand the cross relationships between these regulating parameters and predict the possible permutations and combinations related to the plasma treatment of agricultural produce. The application of AI techniques such as ANN and GA optimization in cold plasma can also widen the prospects of application by disregarding the complexity of the selection of parameters, thereby contributing to the efficacy of functional improvement in agricultural produce. This possibility of statistical method lacks practice in investigating parameters related to the plasma treatment of agricultural produce. The studies related to the application of statistical methods such as ANN and RSM in cold plasma investigations were found to be imperative in concluding the influential parameters and their effects on product functional quality. Further research on plasma treatment using statistical and predictive tools will help in drawing conclusions about its efficiency and enhancing our understanding of the process.

Author contributions

MS: Writing – original draft, Writing – review & editing. SR: Supervision, Validation, Writing – review & editing.

Funding

The author(s) declare that no financial support was received for the research, authorship, and/or publication of this article.

Conflict of interest

The authors declare that the research was conducted in the absence of any commercial or financial relationships that could be construed as a potential conflict of interest.

Generative AI statement

The author(s) declare that no Gen AI was used in the creation of this manuscript.

Publisher's note

All claims expressed in this article are solely those of the authors and do not necessarily represent those of their affiliated organizations, or those of the publisher, the editors and the reviewers. Any product that may be evaluated in this article, or claim that may be made by its manufacturer, is not guaranteed or endorsed by the publisher.

References

1. Landry MJ, Ward CP. Health benefits of a plant-based dietary pattern and implementation in healthcare and clinical practice. *Am J Lifestyle Med.* (2024) 18:657–65. doi: 10.1177/15598276241237766

2. Rana A, Bajwa HK, Khan H. The biological role of bioactive compounds from plants, bacteria, and bee products in cancer prevention and therapy. *Indian J Biochem Biophys.* (2024) 61:455–71. doi: 10.5281/zenodo.545778

3. Yalcin H, Çapar TD. Bioactive compounds of fruits and vegetables. In: Yildiz F, Wiley R. editors. *Minimally processed refrigerated fruits and vegetables.* Boston, Springer (2017). p. 723–745. doi: 10.1007/978-1-4939-7018-6_21

4. Shashirekha MN, Mallikarjuna SE, Rajarathnam S. Status of bioactive compounds in foods, with focus on fruits and vegetables. *Crit Rev Food Sci Nutr.* (2015) 55:1324–39. doi: 10.1080/10408398.2012.692736

5. Bolat E, Saritaş S, Duman H, Eker F, Akdaşçi E, Karav S, et al. Polyphenols: secondary metabolites with a biological impression. *Nutrients.* (2024) 16:2550. doi: 10.3390/nu16152550

6. Delgado AM, Issaoui M, Chammem N. Analysis of main and healthy phenolic compounds in foods. *J AOAC Int.* (2019) 102:1356–64. doi: 10.5740/jaoacint.19-0128

7. Chagas MD, Behrens MD, Moragas-Tellis CJ, Penedo GX, Silva AR, Gonçalves-de-Albuquerque CF. Flavonols and flavones as potential anti-inflammatory, antioxidant, and antibacterial compounds. *Oxidat Med Cell Longev.* (2022) 2022:9966750. doi: 10.1155/2022/9966750

8. Brodowska KM. Natural flavonoids: classification, potential role, and application of flavonoid analogues. *Eur J Biol Res.* (2017) 7:108–23. doi: 10.56042/ijbb.v61i8.2093

9. Russo D. Flavonoids and the structure-antioxidant activity relationship. *J Pharmacogn Nat Prod.* (2018) 4:e109. doi: 10.4172/2472-0992.1000e109

10. Lima G, Lima GP, Vianello F, Corrêa CR, Campos RA, Borguini MG. Polyphenols in fruits and vegetables and its effect on human health. *Food Nutr Sci.* (2014) 5:1065–82. doi: 10.4236/fns.2014.511117

11. Zhang P, Zhu H. Anthocyanins in plant food: current status, genetic modification, and future perspectives. *Molecules.* (2023) 28:866. doi: 10.3390/molecules28020866

12. Qi Q, Chu M, Yu X, Xie Y, Li Y, Du Y, et al. Anthocyanins and proanthocyanidins: chemical structures, food sources, bioactivities, and product development. *Food Rev Int.* (2023) 39:4581–609. doi: 10.1080/87559129.2022.2029479

13. da Silva AP, Sganzerla WG, John OD, Marchiosi R. A comprehensive review of the classification, sources, biosynthesis, and biological properties of hydroxybenzoic and hydroxycinnamic acids. *Phytochem Rev.* (2023) 2023:1–30. doi: 10.1007/s11101-023-09891-y

14. Das AK, Islam MN, Faruk MO, Ashaduzzaman M, Dungani R. Review on tannins: extraction processes, applications and possibilities. *South African J Botany.* (2020) 135:58–70. doi: 10.1016/j.sajb.2020.08.008

15. Shirmohammadli Y, Efhamisisi D, Pizzi A. Tannins as a sustainable raw material for green chemistry: a review. *Ind Crops Prod.* (2018) 126:316–32. doi: 10.1016/j.indcrop.2018.10.034

16. Andrés-Lacueva C, Medina-Remon A, Llorach R, Urpi-Sarda M, Khan N, Chiva-Blanch G, et al. Phenolic compounds: chemistry and occurrence in fruits and vegetables. In: de la Rosa LA, Alvarez-Parrilla E, González-Aguilar GA. editors. *Fruit and vegetable phytochemicals: chemistry, nutritional value, and stability.* New York, USA: John Wiley & Sons (2009). p. 53–88. doi: 10.1002/9780813809397.ch2

17. Ignat I, Volf I, Popa VI. A critical review of methods for characterisation of polyphenolic compounds in fruits and vegetables. *Food Chem.* (2011) 126:1821–35. doi: 10.1016/j.foodchem.2010.12.026

18. Meneses-Espinosa E, Gálvez-López D, Rosas-Quijano R, Adriano-Anaya L, Vázquez-Ovando A. Advantages and disadvantages of using emerging technologies to increase postharvest life of fruits and vegetables. *Food Rev Int.* (2024) 40:1348–73. doi: 10.1080/87559129.2023.2212061

19. Zhang B, Tan C, Zou F, Sun Y, Shang N, Wu W. Impacts of cold plasma technology on sensory, nutritional and safety quality of food: a review. *Foods.* (2022) 11:2818. doi: 10.3390/foods11182818

20. Pankaj SK, Wan Z, Keener KM. Effects of cold plasma on food quality: a review. *Foods.* (2018) 7:4. doi: 10.3390/foods7010004

21. Misra NN, Schlüter O, Cullen PJ. *Cold Plasma in Food and Agriculture: Fundamentals and Applications.* London: Academic Press. (2016). doi: 10.1016/B978-0-12-801365-6.00001-9

22. Varilla C, Marcone M, Annor GA. Potential of cold plasma technology in ensuring the safety of foods and agricultural produce: a review. *Foods.* (2020) 9:1435. doi: 10.3390/foods9101435

23. Chen YQ, Cheng JH, Sun DW. Chemical, physical and physiological quality attributes of fruit and vegetables induced by cold plasma treatment: Mechanisms and application advances. *Crit Rev Food Sci Nutr.* (2020) 60:2676–90. doi: 10.1080/10408398.2019.1654429

24. Rao W, Li Y, Dhaliwal H, Feng M, Xiang Q, Roopesh MS, et al. The application of cold plasma technology in low-moisture foods. *Food Eng Rev.* (2023) 15:86–112. doi: 10.1007/s12393-022-09329-9

25. Ganesan AR, Tiwari U, Ezhilarasi PN, Rajauria G. Application of cold plasma on food matrices: a review on current and future prospects. *J Food Proc Preserv.* (2021) 45:15070. doi: 10.1111/jfpp.15070

26. Bußler S, Rawel HM, Schlüter OK. Impact of plasma processed air (PPA) on phenolic model systems: Suggested mechanisms and relevance for food applications. *Innov Food Sci Emer Technol.* (2020) 64:102432. doi: 10.1016/j.ifset.2020.102432

27. Muhammad AI, Liao X, Cullen PJ, Liu D, Xiang Q, Wang J, et al. Effects of nonthermal plasma technology on functional food components. *Compr Rev Food Sci Food Safety.* (2018) 17:1379–94. doi: 10.1111/1541-4337.12379

28. Pipliya S, Kumar S, Babar N, Srivastav PP. Recent trends in non-thermal plasma and plasma activated water: Effect on quality attributes, mechanism of interaction and potential application in food & agriculture. *Food Chem Adv.* (2023) 2:100249. doi: 10.1016/j.focha.2023.100249

29. Sgonina K, Bruno G, Wyprich S, Wende K, Benedikt J. Reactions of plasma-generated atomic oxygen at the surface of aqueous phenol solution: experimental and modeling study. *J Appl Phys.* (2021) 130:043303. doi: 10.1063/5.0049809

30. Alothman M, Kaur B, Fazilah A, Bhat R, Karim AA. Ozone-induced changes of antioxidant capacity of fresh-cut tropical fruits. *Innov Food Sci Emer Technol.* (2010) 11:666–71. doi: 10.1016/j.ifset.2010.08.008

31. Kumar S, Pipliya S, Srivastav PP. Effect of cold plasma on different polyphenol compounds: a review. *J Food Proc Eng.* (2023) 46:14203. doi: 10.1111/jfpe.14203

32. Tappi S, Ramazzina I, Rizzi F, Sacchetti G, Ragni L, Rocculi P. Effect of plasma exposure time on the polyphenolic profile and antioxidant activity of fresh-cut apples. *Appl Sci.* (2018) 8:1939. doi: 10.3390/app8101939

33. Illera AE, Chaple S, Sanz MT, Ng S, Lu P, Jones J, et al. Effect of cold plasma on polyphenol oxidase inactivation in cloudy apple juice and on the quality parameters of the juice during storage. *Food Chem X.* (2019) 30:100049. doi: 10.1016/j.fochx.2019.100049

34. Rodríguez Ó, Gomes WF, Rodrigues S, Fernandes FA. Effect of indirect cold plasma treatment on cashew apple juice (*Anacardium occidentale* L.). *LWT.* (2017) 84:457–63. doi: 10.1016/j.lwt.2017.06.010

35. Dasan BG, Boyaci IH. Effect of cold atmospheric plasma on inactivation of *Escherichia coli* and physicochemical properties of apple, orange, tomato juices, and sour cherry nectar. *Food Biopr Technol.* (2018) 11:334–43. doi: 10.1007/s11947-017-2014-0

36. Fernandes FA, Santos VO, Rodrigues S. Effects of glow plasma technology on some bioactive compounds of acerola juice. *Food Res Int.* (2019) 115:16–22. doi: 10.1016/j.foodres.2018.07.042

37. Garofulić IE, Jambrak AR, Milošević S, Dragović-Uzelac V, Zorić Z, Herceg Z. The effect of gas phase plasma treatment on the anthocyanin and phenolic acid content of sour cherry Marasca (*Prunus cerasus* var. Marasca) juice. *LWT-Food Sci Technol.* (2015) 62:894–900. doi: 10.1016/j.lwt.2014.08.036

38. Herceg Z, Kovačević DB, Kljusurić JG, Jambrak AR, Zorić Z, Dragović-Uzelac V. Gas phase plasma impact on phenolic compounds in pomegranate juice. *Food Chem.* (2016) 190:665–72. doi: 10.1016/j.foodchem.2015.05.135

39. Almeida FD, Cavalcante RS, Cullen PJ, Frias JM, Bourke P, Fernandes FA, et al. Effects of atmospheric cold plasma and ozone on prebiotic orange juice. *Innov Food Sci Emer Technol.* (2015) 32:127–35. doi: 10.1016/j.ifset.2015.09.001

40. Pankaj SK, Wan Z, Colonna W, Keener KM. Effect of high voltage atmospheric cold plasma on white grape juice quality. *J Sci Food Agric.* (2017) 97:4016–21. doi: 10.1002/jsfa.8268

41. Rana S, Mehta D, Bansal V, Shivhare US, Yadav SK. Atmospheric cold plasma (ACP) treatment improved in-package shelf-life of strawberry fruit. *J Food Sci Technol.* (2020) 57:102–12. doi: 10.1007/s13197-019-04035-7

42. Mehta D, Sharma N, Bansal V, Sangwan RS, Yadav SK. Impact of ultrasonication, ultraviolet and atmospheric cold plasma processing on quality parameters of tomato-based beverage in comparison with thermal processing. *Innov Food Sci Emer Technol.* (2019) 52:343–9. doi: 10.1016/j.ifset.2019.01.015

43. Pour AK, Khorram S, Ehsani A, Ostadrahimi A, Ghasempour Z. Atmospheric cold plasma effect on quality attributes of banana slices: its potential use in blanching process. *Innov Food Sci Emer Technol.* (2022) 76:102945. doi: 10.1016/j.ifset.2022.102945

44. Wu X, Zhao W, Zeng X, Zhang QA, Gao G, Song S. Effects of cold plasma treatment on cherry quality during storage. *Food Sci Technol Int.* (2021) 27:441–55. doi: 10.1177/1082013220957134

45. Li X, Li M, Ji N, Jin P, Zhang J, Zheng Y, et al. Cold plasma treatment induces phenolic accumulation and enhances antioxidant activity in fresh-cut pitaya (*Hylocereus undatus*) fruit. *Lwt.* (2019) 115:108447. doi: 10.1016/j.lwt.2019.108447

46. Bao Y, Reddivari L, Huang JY. Development of cold plasma pretreatment for improving phenolics extractability from tomato pomace. *Innov Food Sci Emer Technol.* (2020) 65:102445. doi: 10.1016/j.ifset.2020.102445

47. Kovačević DB, Kljusurić JG, Putnik P, Vukušić T, Herceg Z, Dragović-Uzelac V. Stability of polyphenols in chokeberry juice treated with gas phase plasma. *Food Chem.* (2016) 212:323–31. doi: 10.1016/j.foodchem.2016.05.192

48. Ramazzina I, Tappi S, Rocculi P, Sacchetti G, Berardinelli A, Marseglia A, et al. Effect of cold plasma treatment on the functional properties of fresh-cut apples. *J Agric Food Chem.* (2016) 64:8010–8. doi: 10.1021/acs.jafc.6b02730

49. Liao X, Li J, Muhammad AI, Suo Y, Chen S, Ye X, et al. Application of a dielectric barrier discharge atmospheric cold plasma (Dbd-Acp) for *Eshcerichia coli* inactivation in apple juice. *J Food Sci.* (2018) 83:401–8. doi: 10.1111/1750-3841.14045

50. Ji Y, Hu W, Liao J, Jiang A, Xiu Z, Gaowa S, et al. Effect of atmospheric cold plasma treatment on antioxidant activities and reactive oxygen species production in postharvest blueberries during storage. *J Sci Food Agric.* (2020) 100:5586–95. doi: 10.1002/jsfa.10611

51. Paixão LM, Fonteles TV, Oliveira VS, Fernandes FA, Rodrigues S. Cold plasma effects on functional compounds of siriguela juice. *Food Bioproc Technol.* (2019) 12:110–21. doi: 10.1007/s11947-018-2197-z

52. Umair M, Jabbar S, Nasiru MM, Sultana T, Senan AM, Awad FN, et al. Exploring the potential of high-voltage electric field cold plasma (HVCP) using a dielectric barrier discharge (DBD) as a plasma source on the quality parameters of carrot juice. *Antibiotics.* (2019) 8:235. doi: 10.3390/antibiotics8040235

53. Zielinska S, Staniszewska I, Cybulska J, Zdunek A, Szymanska-Chargot M, Zielinska D, et al. Modification of the cell wall polysaccharides and phytochemicals of okra pods by cold plasma treatment. *Food Hydrocoll.* (2022) 131:107763. doi: 10.1016/j.foodhyd.2022.107763

54. Ali M, Cheng JH, Sun DW. Effects of dielectric barrier discharge cold plasma treatments on degradation of anilazine fungicide and quality of tomato (*Lycopersicon esculentum* Mill) juice. *Int J Food Sci Technol.* (2021) 56:69–75. doi: 10.1111/ijfs.14600

55. Nasri AH, Kazemzadeh P, Khorram S, Moslemi M, Mahmoudzadeh M. A kinetic study on carrot juice treated by dielectric barrier discharge (DBD) cold plasma during storage. *LWT.* (2023) 190:115563. doi: 10.1016/j.lwt.2023.115563

56. Phan KT, Phan HT, Boonyawan D, Intipunya P, Brennan CS, Regenstein JM, et al. Non-thermal plasma for elimination of pesticide residues in mango. *Innov Food Sci Emer Technol.* (2018) 48:164–71. doi: 10.1016/j.ifset.2018.06.009

57. Batista JD, Dantas AM, dos Santos Fonseca JV, Madruga MS, Fernandes FA, Rodrigues S, et al. Effects of cold plasma on avocado pulp (*Persea americana* Mill): Chemical characteristics and bioactive compounds. *J Food Proc Preserv.* (2021) 45:e15179. doi: 10.1111/jfpp.15179

58. Akaber S, Ramezan Y, Khani MR. Effect of post-harvest cold plasma treatment on physicochemical properties and inactivation of *Penicillium digitatum* in Persian lime fruit. *Food Chem.* (2024) 437:137616. doi: 10.1016/j.foodchem.2023.137616

59. Shen C, Chen W, Li C, Cui H, Lin L. The effects of cold plasma (CP) treatment on the inactivation of yam peroxidase and characteristics of yam slices. *J Food Eng.* (2023) 359:111693. doi: 10.1016/j.jfoodeng.2023.111693

60. Ali M, Liao L, Zeng XA, Manzoor MF, Durrani Y, Moazzam M. Dielectric barrier discharge plasma processing: Impact on thiram fungicide degradation and quality of tomato juice. *J Agric Food Res.* (2024) 16:101061. doi: 10.1016/j.jafr.2024.101061

61. Kumar NS, Dar AH, Dash KK, Kaur B, Pandey VK, Singh A, et al. Recent advances in Cold Plasma Technology for modifications of proteins: a comprehensive review. *J Agric Food Res.* (2024) 16:101177. doi: 10.1016/j.jafr.2024.101177

62. Farias TR, Alves Filho EG, Silva LM, De Brito ES, Rodrigues S, Fernandes FA, et al. evaluation of apple cubes and apple juice composition subjected to two cold plasma technologies. *LWT.* (2021) 150:112062. doi: 10.1016/j.lwt.2021.112062

63. de Castro DR, Mar JM, da Silva LS, da Silva KA, Sanches EA, de Araújo Bezerra J, et al. Dielectric barrier atmospheric cold plasma applied on camu-camu juice processing: effect of the excitation frequency. *Food Res Int.* (2020) 131:109044. doi: 10.1016/j.foodres.2020.109044

64. Hou Y, Wang R, Gan Z, Shao T, Zhang X, He M, et al. Effect of cold plasma on blueberry juice quality. *Food Chem.* (2019) 290:79–86. doi: 10.1016/j.foodchem.2019.03.123

65. Won MY, Lee SJ, Min SC. Mandarin preservation by microwave-powered cold plasma treatment. *Innov Food Sci Emer Technol.* (2017) 39:25–32. doi: 10.1016/j.ifset.2016.10.021

66. Yang X, An J, Wang X, Wang L, Song P, Huang J. Ar plasma jet treatment delay sprouting and maintains quality of potato tubers (*Solanum tuberosum* L.) by enhancing antioxidant capacity. *Food Biosci.* (2023) 51:102145. doi: 10.1016/j.fbio.2022.102145

67. Ekezie FG, Sun DW, Cheng JH. A review on recent advances in cold plasma technology for the food industry: current applications and future trends. *Trends Food Sci Technol.* (2017) 69:46–58. doi: 10.1016/j.tifs.2017.08.007

68. Saremnezhad S, Soltani M, Faraji A, Hayaloglu AA. Chemical changes of food constituents during cold plasma processing: a review. *Food Res Int.* (2021) 147:110552. doi: 10.1016/j.foodres.2021.110552

69. Sim CH. Application of response surface methodology for the optimization of process in food technology. *Food Eng Progr.* (2011) 15:97–115. doi: 10.13050/foodengprog.2011.15.2.97

70. Yolmeh M, Jafari SM. Applications of response surface methodology in the food industry processes. *Food Bioproc Technol.* (2017) 10:413–33. doi: 10.1007/s11947-016-1855-2

71. Nwabueze TU. Basic steps in adapting response surface methodology as mathematical modelling for bioprocess optimisation in the food systems. *Int J Food Sci Technol.* (2010) 45:1768–76. doi: 10.1111/j.1365-2621.2010.02256.x

72. Zargarchi S, Esatbeyoglu T. Assessing the impact of cold plasma rotational dynamics on ginger's total phenolic content, antioxidant activity, surface structure and color using response surface methodology. *LWT.* (2024) 208:116682. doi: 10.1016/j.lwt.2024.116682

73. Chutia H, Mahanta CL, Ojah N, Choudhury AJ. Fuzzy logic approach for optimization of blended beverage of cold plasma treated TCW and orange juice. *J Food Measur Character.* (2020) 14:1926–38. doi: 10.1007/s11694-020-00440-1

74. Keshavarzi M, Najafi G, Ahmadi Gavlighi H, Seyfi P, Ghomi H. Enhancement of polyphenolic content extraction rate with maximal antioxidant activity from green tea leaves by cold plasma. *J Food Sci.* (2020) 85:3415–22. doi: 10.1111/1750-3841.15448

75. Anastácio A, Silva R, Carvalho IS. Phenolics extraction from sweet potato peels: modelling and optimization by response surface modelling and artificial neural network. *J Food Sci Technol.* (2016) 53:4117–25. doi: 10.1007/s13197-016-2354-1

76. Malekjani N, Jafari SM. Food process modeling and optimization by response surface methodology (RSM). In: Sevda S, Singh A, editors. *Mathematical and statistical applications in food engineering.* Boca Raton: CRC Press (2020). p. 181-203. doi: 10.1201/9780429436963-13

77. Pipliya S, Kumar S, Srivastav PP. Effect of dielectric barrier discharge nonthermal plasma treatment on physicochemical, nutritional, and phytochemical quality attributes of pineapple [*Ananas comosus* (L.)] juice. *J Food Sci.* (2023) 88:4403–23. doi: 10.1111/1750-3841.16767

78. Kumar S, Pipliya S, Srivastav PP. Effect of cold plasma processing on physicochemical and nutritional quality attributes of kiwifruit juice. *J Food Sci.* (2023) 88:1533–52. doi: 10.1111/1750-3841.16494

79. Liu Z, Zhao W, Zhang Q, Gao G, Meng Y. Effect of cold plasma treatment on sterilizing rate and quality of kiwi turbid juice. *J Food Process Eng.* (2021) 44:13711. doi: 10.1111/jfpe.13711

80. Kashyap P, Riar CS, Jindal N. Optimization of ultrasound assisted extraction of polyphenols from Meghalayan cherry fruit (*Prunus nepalensis*) using response surface methodology (RSM) and artificial neural network (ANN) approach. *J Food Measur Character.* (2021) 15:119–33. doi: 10.1007/s11694-020-00611-0

81. Chutia H, Mahanta CL. Influence of cold plasma voltage and time on quality attributes of tender coconut water (*Cocos nucifera* L.) and degradation kinetics of its blended beverage. *J Food Proc Preserv.* (2021) 45:15372. doi: 10.1111/jfpp.15372

82. Kim SY, Lee SY, Min SC. Improvement of the antioxidant activity, water solubility, and dispersion stability of prickly pear cactus fruit extracts using argon cold plasma treatment. *J Food Sci.* (2019) 84:2876–82. doi: 10.1111/1750-3841.14791

83. Mishra R, Mishra A, Jangra S, Pandey S, Chhabra M, Prakash R. Process parameters optimization for red globe grapes to enhance shelf-life using non-equilibrium cold plasma jet. *Postharvest Biol Technol.* (2024) 210:112778. doi: 10.1016/j.postharvbio.2024.112778

84. Taneja A, Nair G, Joshi M, Sharma S, Sharma S, Jambrak AR, et al. Artificial intelligence: Implications for the agri-food sector. *Agronomy.* (2023) 13:1397. doi: 10.3390/agronomy13051397

85. Mavani NR, Ali JM, Othman S, Hussain MA, Hashim H, Rahman NA. Application of artificial intelligence in food industry—a guideline. *Food Eng Rev.* (2022) 14:134–75. doi: 10.1007/s12393-021-09290-z

86. Das P, Nayak PK, Sharma M, Raghavendra VB, Kesavan RK, Sridhar K. Computational modelling for optimization of thermosonicated sohshang (*Elaeagnus latifolia*) fruit juice using artificial neural networks. *J Food Proc Preserv.* (2024) 2024:5559422. doi: 10.1155/2024/5559422

87. Pandiselvam R, Prithviraj V, Manikantan MR, Beegum PS, Ramesh SV, Padmanabhan S, et al. Central composite design, Pareto analysis, and artificial neural network for modeling of microwave processing parameters for tender coconut water. *Measurement Food.* (2022) 5:100015. doi: 10.1016/j.meafoo.2021.100015

88. Golpour I, Ferrão AC, Gonçalves F, Correia PM, Blanco-Marigorta AM, Guiné RP. Extraction of phenolic compounds with antioxidant activity from strawberries: modelling with artificial neural networks (ANNs). *Foods.* (2021) 10:2228. doi: 10.3390/foods10092228

89. Das P, Nayak PK, Krishnan Kesavan R. Computational modeling for the enhancement of thermosonicated Sohphie (Myrica esculenta) fruit juice quality using artificial neural networks (ANN) coupled with a genetic algorithm. *Sustain Food Technol.* (2024) 2:790–805. doi: 10.1039/D4FB00004H

90. Tumuluru JS, McCulloch R. Application of hybrid genetic algorithm routine in optimizing food and bioengineering processes. *Foods.* (2016) 5:76. doi: 10.3390/foods5040076

91. Raj GB, Dash KK. Ultrasound-assisted extraction of phytocompounds from dragon fruit peel: optimization, kinetics and thermodynamic studies. *Ultrason Sonochem.* (2020) 68:105180. doi: 10.1016/j.ultsonch.2020.105180

frontiers | Frontiers in Plant Science

TYPE Original Research
PUBLISHED 16 January 2025
DOI 10.3389/fpls.2024.1521758

OPEN ACCESS

EDITED BY
Gurjeet Singh,
Texas A and M University, United States

REVIEWED BY
Viswanathan Satheesh,
Iowa State University, United States
Abhishek Singh,
Yerevan State University, Armenia
Pawan Saini,
Central Silk Board, India

*CORRESPONDENCE
Debasis Pattanayak
debasispattanayak@yahoo.co.in

RECEIVED 05 November 2024
ACCEPTED 18 December 2024
PUBLISHED 16 January 2025

CITATION
Kumari P, Bhattacharjee S, Venkat Raman K, Tilgam J, Paul K, Senthil K, Baaniya M, Rama Prashat G, Sreevathsa R and Pattanayak D (2025) Identification of *methyltransferase* and *demethylase* genes and their expression profiling under biotic and abiotic stress in pigeon pea (*Cajanus cajan* [L.] Millspaugh). *Front. Plant Sci.* 15:1521758. doi: 10.3389/fpls.2024.1521758

Identification of *methyltransferase* and *demethylase* genes and their expression profiling under biotic and abiotic stress in pigeon pea (*Cajanus cajan* [L.] Millspaugh)

Priyanka Kumari[1,2], Sougata Bhattacharjee[1,2], K. Venkat Raman[1], Jyotsana Tilgam[1,2], Krishnayan Paul[1,2], Kameshwaran Senthil[1], Mahi Baaniya[1,2], G. Rama Prashat[3], Rohini Sreevathsa[1] and Debasis Pattanayak[1*]

[1]National Institute of Plant Biotechnology, Indian Council of Agricultural Research (ICAR), New Delhi, India, [2]Division of Molecular Biology and Biotechnology, Indian Agricultural Research Institute, New Delhi, India, [3]Division of Genetics and Plant Breeding, Indian Agricultural Research Institute, New Delhi, India

The methylation- demethylation dynamics of RNA plays major roles in different biological functions, including stress responses, in plants. m^6A methylation in RNA is orchestrated by a coordinated function of methyl transferases (writers) and demethylases (Erasers). Genome-wide analysis of genes involved in methylation and demethylation was performed in pigeon pea. Blast search, using Arabidopsis gene sequences, resulted in the identification of two methylation genes (*CcMTA70*, *CcMTB70*), two genes encoding adaptor proteins for methylation (*CcFIPA* and *CcFIPB*) and 10 demethylase (ALKBH) genes (*CcALKBH1A*, *CcALKBH1B*, *CcALKBH1C*, *CcALKBH2*, *CcALKBH8*, *CcALKBH8A*, *CcALKBH8B*, *CcALKBH9*, *CcALKBH10A* and *CcALKBH10B*) in the pigeon pea genome. The identified genes were analyzed through phylogenetic relationship, chromosomal position, gene structure, conserved motif, domain and subcellular location prediction etc. These structural analyses resulted in categorization of MTs and FIPs into one group, i.e., *CcMTA/B* and *CcFIPA/B*, respectively; and ALKBHs into four groups, viz. *CcALKBH1/2*, *CcALKBH8*, *CcALKBH9* and *CcALKBH10*. Relative expression analysis of the identified genes in various tissues at different developmental stages revealed the highest level of expression in leaf and the least in root. *CcMT*s and *CcFIP*s had similar patterns of expression, and *CcALKBH10B* demonstrated the highest and *CcALKBH2* the lowest level of expression in all the tissues analyzed. *CcALKBH8* showed the highest induction in expression upon exposure to heat stress, and *CcALKBH10B* demonstrated the highest level of induction in expression during drought, salt and biotic (*Helicoverpa armigera* infestation) stresses. The present study would pave the way for detailed molecular characterization of m^6A methylation in pigeon pea and its involvement in stress regulation.

KEYWORDS

methylation, demethylation, pigeon pea, m^6A modification, ALKBHs

Introduction

Epigenetic modifications on both the DNA and RNAs, without any change of sequence, have emerged as an important player of gene regulation in living organisms (Meyer and Jaffrey, 2014). More than 160 RNA modifications have been identified in mRNA, tRNAs, rRNAs and long non-coding RNA until now (Cantara et al., 2010). Methylation is one of the dominant epigenetic modifications, and modification of adenine through methylation exists as an essential epigenetic mark in both DNAs and RNAs of eukaryotes (Liang et al., 2020). N^6-methyladenosine (m^6A), N^1-methyladenosine (m^1A), 5-methylcytidine (m^5C) and 7-methylguanosine (m^7G) are frequently identified in mRNA (Zhang et al., 2020). m^6A is the most frequent and reversible modification of RNA (Yue et al., 2019; Duan et al., 2017). It plays a major role in the metabolism of RNA which includes mRNA splicing (Haussmann et al., 2016), control of translation (Luo et al., 2020), stability of RNA (Wang et al., 2014), processing of primary microRNA (Bhat et al., 2020) etc. m^6A modification occurs mostly at the consensus sequence, RRACH (R = purine and H = A, C, or U), and this is conserved in animals and plants (Bhat et al., 2020). Also, a second consensus sequence, UGUAY (Y = pyrimidine), is found to be conserved only in plants for m^6A modification. Modulation of RNA methylation takes place with the help of two enzymes, viz. RNA methyl transferases ("writers") and demethylases ("erasers"). Writers help in installing and eraser in removing the methylation marks (Hu et al., 2019).

There are three broad groups for N^6A-methyltranferases (Iyer et al., 2016). MT-A70 clade constitutes group 1, consisting of MTA and MTB genes. It is further divided into six different eukaryotic subclades (Iyer et al., 2016). Clades 1–3 are known as METTL3, METTL4 and METTL14, respectively and these three clades are conserved in higher eukaryotes. Clades 4–6 of group 1 occur in unicellular photosynthetic eukaryotes, basal fungi, and haptophyte algae (Iyer et al., 2016). The other two groups, group 2 and group 3, show independent transfer from bacteria and have restricted distribution (Iyer et al., 2016). Group 2 has been found in archaeal dsDNA viruses and mycobacterium, which are often seen, fused to RNA-binding PPR domains. Group 3 has been observed only in case of the heterolobosean Naegleria (Iyer et al., 2016). m^6A modification is carried out by a core heterodimer formed by METTL3 and METTL14, whereas METTL4 is a DNA methylase (Greer et al., 2015). N^6A methylation is facilitated by an adaptor protein, WTAP (Wilm's tumor-associated protein), which stabilizes the heterodimer (formed by METTL3 and METTL14) in the nuclear speckle (Ping et al., 2014) and several co-factors like KIAA1429 and an RNA binding motif protein, RBM15/RBM15B. WTAP is found in the animal system, and its ortholog, FIP [FK506-binding protein 12 (FKBP12) interacting protein (FIP), FIP37 in case of Arabidopsis], is present in plants (Shen et al., 2016).

Demethylase (eraser) has been studied extensively in animals, but it is yet to be characterized in detail in plants. Nine demethylases have been reported in humans. Eight demethylases belong to ALKBH family (ALKBH 1-8) and the other one is FTO (Fat mass and obesity associated). Due to selectivity towards the substrate, functional diversity arises among the demethylases (Marcinkowski et al., 2020). Phylogenetic analysis could not detect presence of any FTO ortholog in plant system, but many orthologs of *ALKBH5* are identified in Arabidopsis (Liang et al., 2020).

AlkB homologs (ALKBH) are specific demethylases, which are members of the dioxygenase superfamily and require $Fe^{2+}$and α-ketoglutarate for demethylation catalysis of various substrates, viz. proteins, mRNA, tRNA, snRNA, ds/ss DNA, etc (Trewick et al., 2002). AlkB protein was initially found in *Escherichia. coli* (*Ec*AlkB) (Kataoka et al., 1983). This protein has de-alkylation activity that repairs the damage caused by alkylating agents. Repairing of 3-methylcytosine (3-meC) and 1-methyladenine (1-meA) base modifications is more efficient compared to that of 1-methylguanine (1-meG) and 3-methylthymine (3-meT), which undergo less efficient repairing process. A single gene encoding ALKB is present in *E. coli*, but many *ALKBH* gene families are present in animals and plants (Marcinkowski et al., 2020). Also, ALKBH has repairing as well as regulatory roles in eukaryotes indicating a broader range of functions.

Fourteen ALKBH families have been identified in Arabidopsis using bioinformatic tools (Mielecki et al., 2012; Ougland et al., 2015; Marcinkowski et al., 2020). These Arabidopsis ALKBH proteins have functional diversity and act on different substrates. ALKBH1D is present in chloroplast. ALKBH2 does the repairing of 1-meA and 3-meC, ALKBH8 takes part in modification of tRNA by hydroxylating mcm5U to (S)-mchm5U, ALKBH9A and ALKBH10A are related to abiotic stresses and ALKBH9B and ALKBH10B have N^6 demethylation activity (Eraser).

Methylase –demethylase system in Arabidopsis is involved in regulation of stem cell fate determination (Shen et al., 2016); embryo development (Zhong et al., 2008); and trichomes and leaf morphology (Wei et al., 2018). m^6A modification is found to affect sporogenesis in rice (Zhang et al., 2019). However, the function of the methylase-demethylase system is yet to be studied in many agriculturally important crops.

Pigeonpea (*Cajanus cajan*) is a climate resilient orphan crop with rich source of proteins, essential amino acids and vital minerals. It is an important pulse crop grown in tropical and subtropical areas. India is the largest producer of pigeon pea in the world and presently it is grown on over 5.65 m ha in India (FAOSTAT, 2022). Despite the development of high yielding varieties through breeding efforts the productivity is stagnant at around 825kg/ha (FAOSTAT, 2022) which is not sufficient to meet the demand of ever increasing human population. The methylase-demethylase system has not been studied in pigeon pea. It has been reported that m^6A modification has a role in abiotic and biotic stresses (Miao et al., 2020). Even though, pigeon pea considered as resilience to abiotic stresses, many factors like moisture and water logging stress affects the crop physiology and productivity. In North Western part of India, pigeon pea crop suffers from salinity stress (Choudhary et al., 2011). Extreme drought and heat conditions particularly at semi-arid areas, during the seedling and reproductive stages in pigeon pea plants often leads to yield loss (Bakala et al., 2024). Among Biotic stresses, infestation of pod borer (*H armigera* Hubner) poses major challenge to the pigeon pea productivity. With the availability of genomic sequence and annotations, there is a potential way to explore the genes to enhance the tolerance using

advanced genomic, genome editing and speed breeding tools. So, considering the diverse role of methylase-demethylase system we made an attempt to identify the methyl transferase and demethylase in pigeon pea and a bioinformatics analysis was conducted for identification and analysis of methylase and demethylase genes in pigeon pea. The expression pattern of the identified genes was analyzed in different tissues and upon exposure to biotic and abiotic stress conditions.

Materials and methods

Identification of *CcMTs*, *CcFIPs* and *CcALKBHs* and retrieving sequence from database

Arabidopsis MT, FIP and ALKBH cDNA and protein sequences were downloaded from the ensemble (https://plants.ensembl.org/index.html) using the gene ID provided in the literature (Ougland et al., 2015). The protein sequence was then used for blast search in the Legume Information Database (https://www.legumeinfo.org/) to see the orthologous proteins in pigeon pea. E-value threshold was kept at zero for blast search with 98-100% coverage.

Determination of protein weight and other parameters using Expasy

The different Expasy (https://www.expasy.org/) tools like ProtParam, compute pI/Mw etc was used to have a basic understanding of the identified genes in terms amino acid length, molecular weight, iso-electric point, GRAVY (Kyte and Doolittle, 1982), instability index and aliphatic index.

Determination of chromosomal location

The chromosomal position was identified from the LIS database (https://www.legumeinfo.org/) and subsequently, the locus ID was also identified from the NCBI database (https://www.ncbi.nlm.nih.gov/). Chromosome map was constructed using MapGene2Chrom web v2 (http://mg2c.iask.in/mg2c%5Fv2.1/).

Construction of phylogenetic tree for MTs, FIPs and ALKBHs of pigeon pea

A phylogenetic tree of the identified proteins was constructed to see their relative closeness. MEGA11 software was used for the phylogenetic tree construction (Tamura et al., 2021). First of all, after identification and retrieval of all the sequences Clustal omega (https://www.ebi.ac.uk/Tools/msa/clustalo/) was used to check for similarity among sequences. Further of full-length amino acid sequences of *Arabidopsis thaliana, Oryza sativa, Glycine max and C. cajan* were fed to MEGA and there again multiple sequence alignment was performed with ClustalW tool. The IDs for Oryza sativa and glycine max is provided in Table 1.While aligning the sequences of four species of crops in MEGA, alignments were made selecting "with gap option" and during construction of the phylogenetic tree, gap parameters were selected as 'Use all site'. Phylogenetic tree was constructed using the Maximum Likelihood method and JTT matrix-based model taking bootstrap value 1000 (Tamura et al., 2021). For visualization of the phylogenetic tree an 'Interactive Tree Of Life' (iTOL) v6 (https://itol.embl.de/) was used.

Identifying gene structure and conserved motif

For identification of gene structure GSDS 2.0 was used (http://gsds.gao-lab.org/). This gave the idea of exon-intron structure in *MTs*, *FIPs* and *ALKBHs* genes. The conserved motifs of the protein were examined using the MEME online software tool (https://meme-suite.org/meme/). The motif number was kept as 20. The motif width range was kept as minimum 6 and maximum of 50 (6-50) and in site distribution zero or one occurrence per sequence was selected.

TABLE 1 List of gene ID of methyltransferase and demethylase genes for rice and soybean.

Gene Type	Name	*Oryza sativa* gene ID	*Glycine max* gene ID
WRITER	*MTA*	LOC_Os02g45110	Glyma.16G033100
Methyltransferase	*MTB*	LOC_Os01g16180	Glyma.20G161800
	FIP37	LOC_Os06g27970	Glyma.17G086600
ERASER	*ALKBH1A*	LOC_Os03g60190	Glyma.18G006200
Demethylase	*ALKBH1B*	LOC_Os11g29690	Glyma.19G263000
	ALKBH1C		
	ALKBH1D		Glyma.01G129600
	ALKBH2	LOC_Os06g17830	Glyma.09G014800
	ALKBH6	LOC_Os10g28410	Glyma.09G156400
	ALKBH8	LOC_Os04g51360	Glyma.04G107300
	ALKBH8A	LOC_Os11g43610	Glyma.09G217100
	ALKBH8B		Glyma.14G026500
	ALKBH9A	LOC_ Os06g04660	Glyma.17G220300
	ALKBH9B		
	ALKBH9C		Glyma.14G106000
	ALKBH10A	LOC_Os05g33310	Glyma.02G149900
	ALKBH10B	LOC_Os10g02760	

Prediction of conserved domain and sub-cellular localization of MTs, FIPs and ALKBHs of pigeon pea

The conserved domain of the genes was predicted using an online 'CD Search tool' (https://www.ncbi.nlm.nih.gov/Structure/bwrpsb/bwrpsb.cgi). The sub-cellular localization of pigeon pea MTs, FIPs, and ALKBHs was predicted using the WoLF PSORT web tool (https://wolfpsort.hgc.jp/).

Identification of cis-elements in the promoter region of *MT*s, *FIP*s and *ALKBH*s and prediction of their methylation position

Upstream genomic sequences of 2 kb from transcription start site (including 5' UTR) were retrieved from the LIS database for *MT*s, *FPI*s and *ALKBH*s. Cis-regulatory elements were identified using the Plant Pan v3.0 (http://PlantPAN.itps.ncku.edu.tw/). Data obtained from the web tool was analyzed in MS Excel V.2013 and visualized in the TB tool (https://bio.tools/tbtools). Upstream sequences for *MT*s, *FPI*s and *ALKBH*s were analyzed to predict the m^6A- methylation using the EpiSemble R-package v.0.1.1 (http://cabgrid.res.in:5799/). MethSemble 6mA tool was used in EpiSemble R-package to predict the methylation site. This package uses three models viz gradient boosting, random forest and Support vector machine.

Biotic and abiotic stress conditions

Pigeon pea genotype, Pusa 992, was grown in the net house in a 4-inch pot (loamy soil) under natural day length (14hr light and 10 hr. dark) and temperature(30-32 °C) in July 2023 at ICAR-NIPB, New Delhi. Initially watering was done on every alternate day up to three leaved stage. After that when soil used to dry based on that watering was done. Plants were grown in triplicates. For heat stress, 20 days old seedlings are kept in a heat chamber at 42 °C and 60% relative humidity. Plants were kept for 6 hrs. (from 11:00 am to 5:00 pm) for two days (Supplementary Figure 1). After the second day leaf samples were taken. For drought stress, 20% PEG 6000 was prepared by adding 200gm of PEG 6000 in 1000ml of autoclaved water and 100ml of PEG was given per pot which contained a single plant. (Supplementary Figure 1). For salt stress 150 mM of NaCl was prepared by adding 8.766 gm in 1000 ml autoclaved water. and 100 ml of the solution was given to 20 days old seedlings (single plant in one pot) (Mi et al., 2024; Dokka et al., 2024) (Supplementary Figure 1). *Helicoverpa armigera* was used for biotic stress. Larvae were obtained from an in-house culture facility The larvae of *H. armigera* larvae were raised on an artificial diet with a 16 h light and 8 h dark photoperiod, at a temperature of 26± 1°C and 70-80% relative humidity was maintained. The second instar larvae of the polyphagous insect pest, *Helicoverpa armigera*, was reared on leaves of 20 days old seedlings of pigeon pea. Larvae were given 7 hrs. starvation and then two larvae were released per pot (1 Plant in each pot). Plants were covered with the perforated polythene which was secured with rubber band on the pots to prevent escape of larvae. After four days of infestation leaf samples were collected.

Plant material and qPCR analysis of identified genes in tissue-specific manner and under biotic and abiotic stress conditions

For tissue-specific expression studies different tissues were collected at different stages, but for stress related studies leaf tissues were collected from 20 days old seedlings. For abiotic stress-induced plants leaf samples were collected after 48 hours of treatment. Leaf samples were collected after 4 days of *H. armigera* infestation for gene expression study under biotic stress. Total RNA was isolated from different tissues (leaf, roots, internode, shoot apical meristem, flower apical meristem and immature pod) for tissue-specific qPCR and from leaf samples for stress-specific qPCR using RNA isolation kit (Genes2Me; India) according to the 'manufacturer's instruction. Isolated RNA was treated with DNaseI (RNase free) to remove any genomic DNA contamination. The quality of total RNA was checked using a Nanodrop spectrophotometer (Thermo Scientific). Total RNA was then immediately stored at -80°C. cDNA was prepared using a PrimesScript cDNA synthesis kit (TaKaRa) and stored at -20 °C for further use. *MT*s, *FIP*s and *ALKBH*s-specific primers (Supplementary Table 2) were designed using the IDT web tool (https://www.idtdna.com/). qPCR assay was performed in Light Cycler 96 PCR detection system (Roche, Basel, Switzerland) using TB green master mix (TaKaRa) using the following conditions: initial denaturation at 95 °C for 5 min, 40 cycles of amplification, each cycle of 95 °C for 30 sec, 60 °C for 30 sec and 72 °C for 20 sec. Also, three biological and three technical (cDNA replicates) replicates were taken for each sample. The *CcIF4* was used as a reference gene (Bhattacharjee et al., 2023). The Sequence of the internal primer pair for the reference gene is included in the Supplementary File (Supplementary Table 2). The relative abundance of *CcMTs, CcFIPs* and *CcALKBHs* was calculated using the $2^{-\Delta\Delta Ct}$ method (Livak and Schmittgen, 2001).

Statistical analysis

For the gene expression study, three biological (separate plants grown in separate pots under different abiotic and biotic stress) and three technical replicates were taken. Wherein, an equal amount of each biological replicate was pooled for RNA isolation. Mean values were given with an error bar (standard error of means) for all the parameters. At 5%, the least significant difference (LSD) was calculated to see the significance of different treatment effects. After that, the significance level between and among the treatments in each experiment was checked by performing a range test.

Results

Identification of Arabidopsis MT, FIP and ALKBH orthologs of pigeon pea

The sequence information of methyl transferase and demethylase was retrieved from the LIS database and cross-checked through blast at NCBI database, which gave the Locus ID of respective genes. Arabidopsis has 2 *MT*, 1 *FIP* and 14 *ALKBH* genes, whereas in pigeon pea, 2 *MT*, 2 *FIP* and 10 *ALKBH* genes were identified (Table 2).

Determination of protein weight and other parameters using the Expasy database

This exercise provided a complete framework of basic information on iso-electric point (pI), molecular weight (MW), instability index (II), aliphatic index (AI) and grand average of hydropathicity (GRAVY) of the proteins identified in pigeon pea (Table 3). When the protein sequence of identified MTs, FIPs and ALKBHs of pigeon pea was analyzed it was found that there was variation in the genes. For instance, in case of predicted protein length, the amino acid sequence varies from 761 aa to 1089 aa for MTs, 337 aa to 338 for FIPs and 205 aa to 515 aa for ALKBHs family of pigeon pea. The iso-electric point for MTs ranged from 6 to 7, and for FIPs, it was between 5 and 6. The iso-electric point ranged from 5.57 to 8.7 for ALKBHs with CcALKBH1C having the highest PI and *Cc*ALKBH8B the lowest. All proteins of MTA, FIPs and ALKBH were hydrophilic as confirmed by GRAVY. Also, instability index analysis showed that MTA was more stable than MTB, and FIPA was more stable than FIPB. Among ALKBH proteins *CcALKBH8* was the most stable, and *CcALKBH8B* was the least stable protein. Aliphatic index analysis indicated that MTA and FIPA had more aliphatic amino acids compared to MTB and FIPB, respectively. *CcALKBH8* had the highest aliphatic index and *CcALKBH9* had the lowest aliphatic index. The higher aliphatic index, the better the thermo-stability of protein.

Determination of chromosomal location using LIS database and construction of chromosomal map using MapGene2Chrom web v2.1

From the analysis of the chromosomal position of the genes encoding pigeon pea MTs, FIPs and ALKBHs it was found that all the genes were localized within six chromosomes, viz. chr.01, chr.02, chr.03, chr.05, chr.06 and chr. 11. However, the majority of the genes were localized on the chr.03 (Table 4).

A chromosomal map had been constructed showing the distribution of genes on chromosomes. Cc*MTA* and Cc*MTB* were located on chromosomes 01 and 02, respectively. Cc*FIPA* and Cc*FIPB* were located on chr.03 and 11, respectively. Two ALKBH genes, *CcALKBH1A* and *CcALKBH1B*, were located on chr.01, one ALKBH gene, *CcALKBH10A*, was on chr.02, and four genes, viz, *CcALKBH1C, CcALKBH2, CcALKBH8* and *CcALKBH10B*, were onchr.03. *CcALKBH8B, and CcALKBH9* were present on chr.05 and *CcALKBH8A* was found on chr. 06 (Figure 1).

Phylogenetic analysis of identified genes in pigeon pea

Deduced protein sequences of MTs, FIPs and ALKBHs from Arabidopsis (*A. thaliana*), rice (*O. sativa*), soybean *(G. max*) and pigeon pea (*C. cajan*) were taken and a phylogenetic tree was constructed using MEGA11 to find out the relationships between the identified genes and to see the evolutionary relics (Tamura et al., 2021) (Figure 2**).** The tree sub-clades were clubbed into groups to understand their evolutionary relations. One group for MTs and FIPs, viz. MTA/B and FIPA/B, respectively, and four groups for ALKBHs were made, viz,

TABLE 2 List of methyl transferase and demethylase genes involved in RNA methylation in pigeon pea.

Gene Type	Name	Arabidopsis gene ID	Target RNA	Function	Pigeonpea ortholog	Animal homolog
WRITER Methyltransferase	*MTA*	At4g10760			Cc_02310	*METTL3*
	MTB	At4g09980			Cc_04693	*METTL14*
	FIP37	At3g54170			Cc_26978	*WTAP*
ERASER Demethylase	*ALKBH1A*	At1g11780			Cc_00082	*ALKBH1*
	ALKBH1B	At3g14140			Cc_01989	*ALKBH2*
	ALKBH1C	At3g14160			Cc_08628	
	ALKBH1D	At5g01780				
	ALKBH2	At2g22260			Cc_06617	
	ALKBH6	At4g20350				*ALKBH6*
	ALKBH8	At1g36310			Cc_06586	*ALKBH8*
	ALKBH8A	At1g31600	tRNA mcm5U		Cc_13896	
	ALKBH8B	At4g02485	tRNA mcm5U		Cc_12521	
	ALKBH9A	At1g48980	m6A			*ALKBH5*
	ALKBH9B	At2g17970		Viral	Cc_11071	
	ALKBH9C	At4g36090		infection		
	ALKBH10A	At2g48080			Cc_03631	
	ALKBH10B	At4g02940	m6A	Flowering	CC_07468	

TABLE 3 Details of identified proteins involved in methylation-demethylation in pigeon pea.

Gene name	Protein length	Molecular Weight (Kd)	PI	GRAVY	II	AI
CcMTA	761	84.24	6.08	-0.458	49.48	76.49
CcMTB	1089	120.9	6.87	-1.185	53.52	42.65
CcFIPA	337	38.37	5.64	-0.878	52.01	71.31
CcFIPB	338	38.38	5.17	-0.891	60.75	69.02
CcALKHB1A	345	38.93	8.48	-0.448	50.16	81.68
CcALKHB1B	481	53.42	8.24	-0.587	53.26	69.46
CcALKHB1C	276	30.51	8.64	-0.550	59.11	73.44
CcALKHB2	205	22.28	5.80	-0.640	58.79	71.37
CcALKHB8	386	42.6	6.18	-0.165	31.87	88.65
CcALKHB8A	342	38.28	6.92	-0.314	54.79	84.39
CcALKHB8B	219	25.11	5.50	-0.376	70.84	85.53
CcALKHB9	480	53.5	6.18	-0.673	45.13	68.02
CcALKHB10A	511	56.32	6.09	-0.370	52.72	75.42
CcALKHB10B	515	56.71	5.71	-0.348	51.44	76.95

(ALKBH1/2, ALKBH8, ALKBH9, ALKBH10) following earlier nomenclature (Marcinkowski et al., 2020). The number of genes of MTs and FIPs was almost the same in above mentioned species. However, the number of *ALKBH* genes varied among species. The highest number of *ALKBH* genes (14) was found in Arabidopsis, while the least number of ALKBHs (10) was found in pigeon peas. The ALKBH6 group was found absent in pigeon pea. The ALKBH1 group had the highest number of genes (4), while ALKBH2 and AlKBH9 had the lowest number of genes (1). ALKBH10 was similar and related to m^6A RNA demethylation in Arabidopsis.

Identification of gene structure and conserved motifs for *MTs*, *FIPs* and *ALKBHs*

Gene structure plays a major role in the evolution of gene families. A phylogenetic tree was constructed using the neighbor joining method grouped *CcALKBs* into 4 paralogous clades. The members of *Cc*ALKBH1, *Cc*ALKBH2 and *Cc*ALKBH8 were 3 distinct clades whereas, the members of *Cc*ALKBH9 and *Cc*ALKBH10 together grouped as a separate clade (Figure 3A).

TABLE 4 Specific chromosomal location of the identified methylase and demethylase genes in pigeon pea.

Gene name	Locus ID	Start position	End position	Location
CcMTA	LOC109796915	17132963	17136525	Chr1
CcMTB	LOC109806648	29180464	29187590	Chr2
CcFIPA	LOC109807646	722001	728778	Chr3
CcFIPB	LOC109796750	12049020	12058710	Chr11
Cc ALKBH 1A	LOC109795359	1402570	1404882	Chr1
Cc ALKBH 1B	LOC109816189	73711	75566	Chr1
Cc ALKBH 1C	LOC109798028	29340539	29341174	Chr3
Cc ALKBH 2	LOC109800658	1113721	1116509	Chr3
Cc ALKBH 8	LOC109796724	1470740	1472313	Chr3
Cc ALKBH 8A	LOC109815811	95041	98599	Chr6
Cc ALKBH 8B	LOC109795028	14318278	14318937	Chr5
Cc ALKBH 9A	LOC109818090	212627	216263	Chr5
Cc ALKBH 10A	LOC109795864	24839450	24844871	Chr2
Cc ALKBH 10B	LOC109795704	16277867	16284890	Chr3

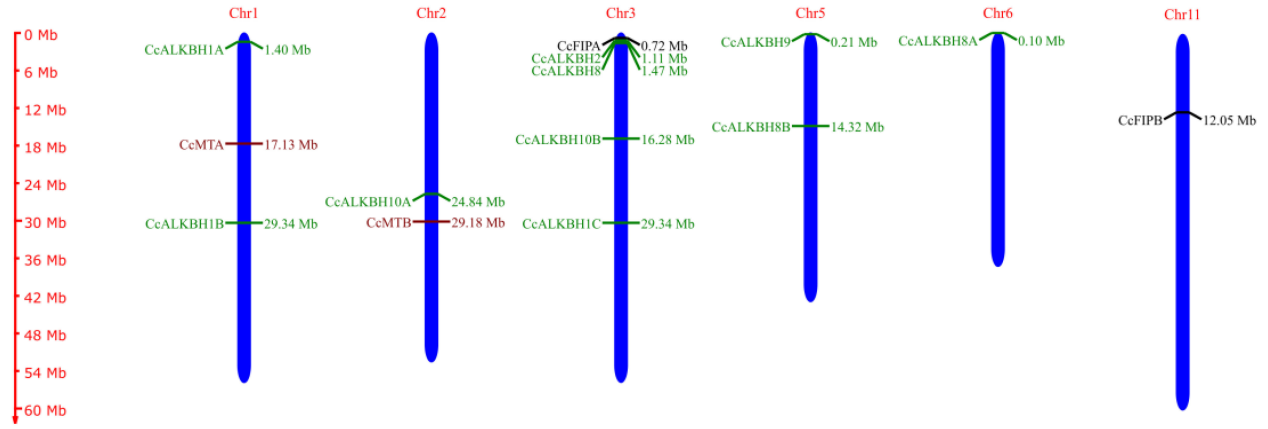

FIGURE 1
Chromosomal map (made using Map Gene 2 chromosome software) depicting chromosomal locations of the identified genes involved in methylation-demethylation in pigeon pea. The maroon colour indicates *CcMTs*, green indicates *CcALKBHs* and black indicates *CcFIPs*.

Analysis of the exon-intron structure of *MT*s revealed that seven and six exons were present in *MTA* and *MTB*, respectively, but intronic portion was more in *MTB* (Figure 3B). In case of *FIPA* and *FIPB* there were eight and thirteen exons, respectively, and for *FIPA*, UTR was found only at the 3' end (Figure 3B). Intronic portion was found to be more in *FIPB*. Further, for ten *ALKBH*s, it has been found that variations were present among the genes. Seven exons were present in five of the *ALKBH*s, viz. *CcALKBH1A*, *CcALKBH8A*, *CcALKBH9*, *CcALKBH10A* and *CcALKBH10B*; and the rest five *ALKBH*s, viz. *CcALKBH2*, *CcALKBH1B*, *CcALKBH1C*, *CcALKBH8* and *CcALKBH8B*, had varying numbers of exons (five to one, respectively). *CcALKBH10A* and *CcALKBH10B* contained the largest intronic regions. It was noticed that the *CcALKBH2* gene was devoid of any UTR region (Figure 3B).

The MEME suite was used for conserved motif analysis, and 20 motifs were identified. According to the phylogenetic analysis (Figure 4A), motif distribution was found conserved for closely related genes as shown in Figure 4B. All 20 motifs were found to be present in both the *MT*s, but their distance varied. *FIP*s had all the motifs conserved and at the same distance. For *ALKBH*s, *CcALKBH10A* and *CcALKBH10B* had the greatest number of genes conserved at the same distance (Figure 4B). Motif 1 was

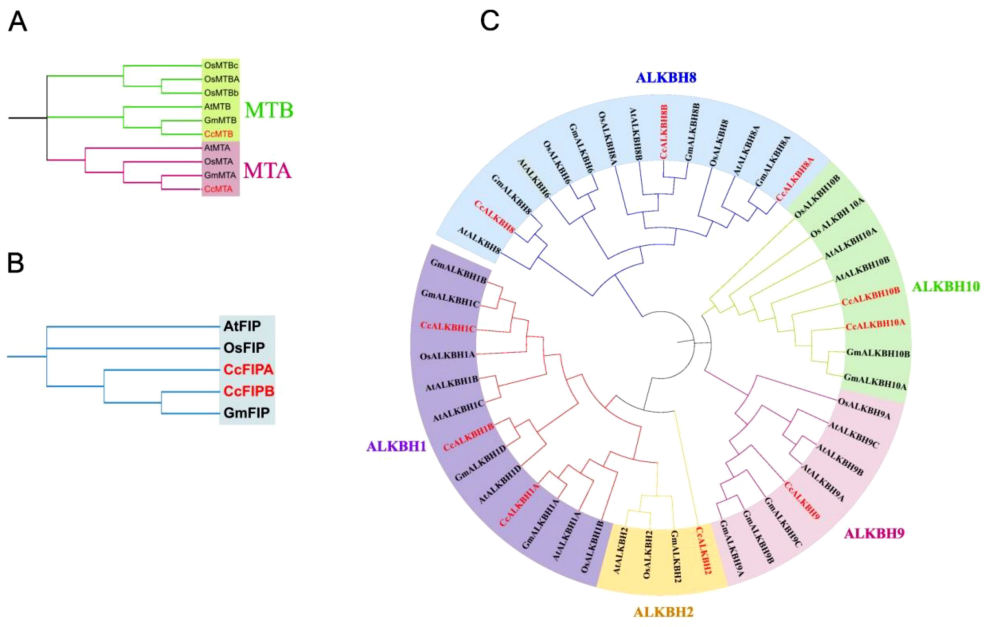

FIGURE 2
Phylogenetic tree showing the relationship and closeness among the identified methylation-demethylation genes of *Arabiopsis thaliana*, rice (*Oryza sativa*), soybean (*Glycine max*) and pigeon pea (*Cajanus cajan*). **(A)** *MT*s, **(B)** *FIP*s, **(C)** *ALKBH*s. Phylogenetic tree was constructed using MEGA11.0 software by selecting the Maximum likelihood and keeping the bootstrap value at 1000.

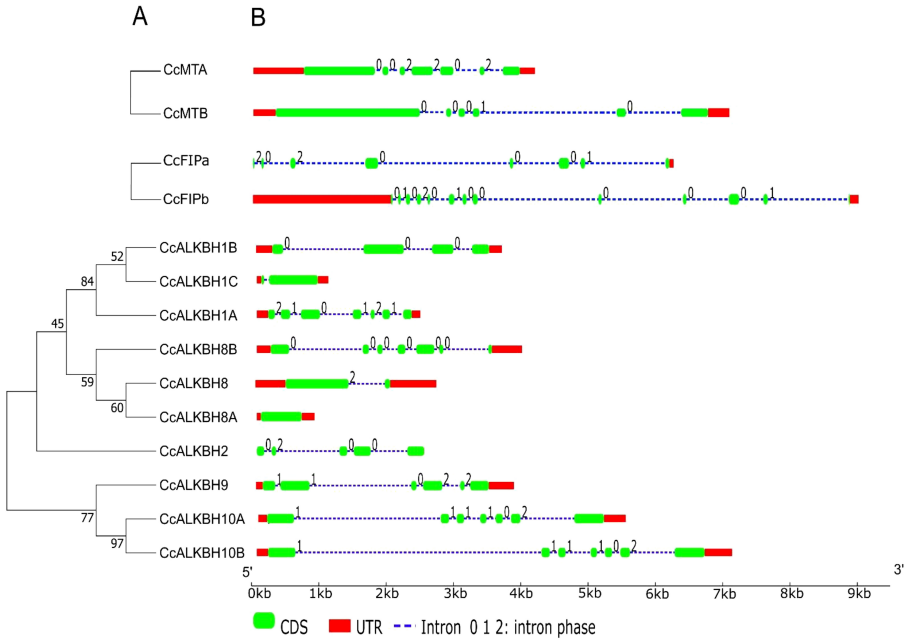

FIGURE 3
Phylogenetic tree showing gene structure of the identified genes of pigeon pea involved in methylation-demethylation. **(A)** Phylogenetic tree of identified pigeon pea MTs, FIPs and ALKBHs proteins. **(B)** Gene structures of *CcMTs, CcFIPs and CcALKBHs*. The exons, introns and UTRs were represented by red rectangles, black lines and green rectangles respectively. 0, 1 and 2 represent the intron phase of the respective genes.

found to be conserved in all the genes except for *CcALKBH2* and *CcALKBH8*. Motif 20 was specific to *CcALKBH8A* and *CcALKBH8B*. Similarly, motif 18 was specific to *CcALKBH1B* and *CcALKBH1C*, and motif 19 was specific to *CcALKBH2* and *CcALKBH8* (Figure 4B). *CcALKBH2* and *CcALKBH8* had shown the least conservation of motifs which might be an indication of performing different functions.

Domain and subcellular localization prediction

Domains are the self-stabilizing polypeptide chain that works independently. It was observed that MTs (*CcMTA* and *CcMTB*) contained domain MTA-70 which is a major domain involved in methylation (Figure 5). Microbial surface components recognizing

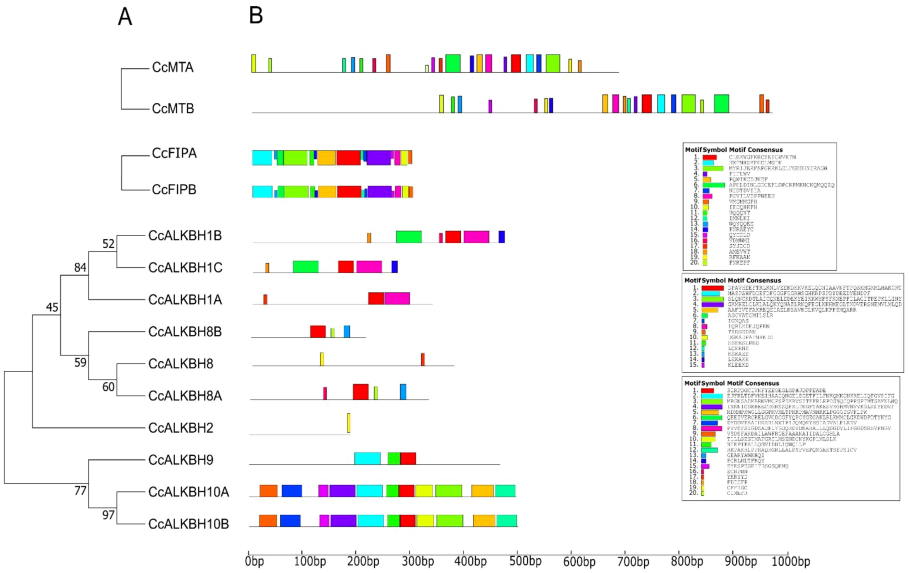

FIGURE 4
Phylogenetic tree showing conserved motifs. **(A)** Conserved motifs are present in the identified MTs, FIPs and ALKBHs proteins of pigeon pea. **(B)** Distribution of identified conserved motifs of *CcMTs, CcFIPs, and CcALKBHs* genes of pigeon pea. Different motifs are shown in different colors.

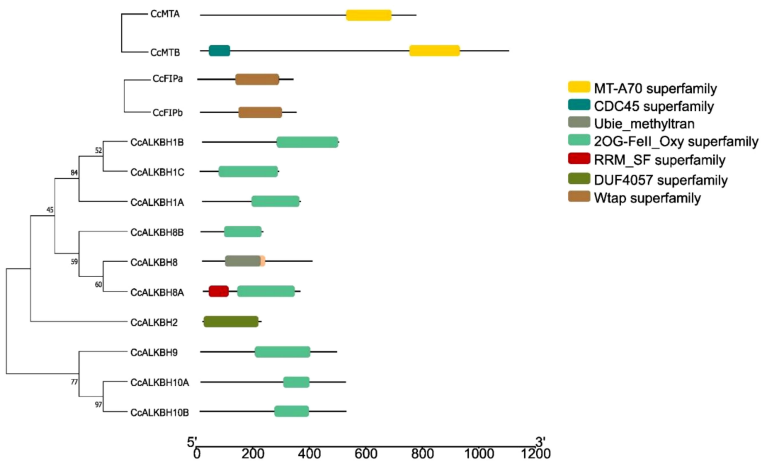

FIGURE 5
Phylogenetic tree constructed based on conserved domains of identified *CcMTs, CcFIPs* and *CcALKBHs* genes of pigeon pea. Different domains are shown in different colors.

adhesive matrix molecules domain was found in FIPs, *viz. CcFIPA* and *CcFIPB* (Figure 5). Most of the ALKBHs contained 2OG-FeII_Oxy_2 domain which is a characteristic feature of the *ALKBH* gene family. Although the 2OG-FeII_Oxy_2 domain was absent in *CcALKBH2*, it had a completely different domain of DUF4057 superfamily, which is yet to be characterized (Figure 5). Apart from this, *CcALKBH8A* was found to have an RRM (RNA recognition motif) domain, which is an essential domain involved in tRNA modification. In addition, *CcALKBH8* also had a methyl transferase domain. So, it might have a role in both demethylation and methylation.

Regarding subcellular location, it was found that MTs, FIPs and a majority of ALKBHs had nuclear localization signal. However, a few ALKBHs, viz. *CcALKBH1B, and CcALKBH10B*, had chloroplast targeting signals, *CcALKBH8* had signal peptide sequence targeting the plasma membrane (Supplementary Table 1), and *CcALKBH9* had both nuclear and cytoplasm localization signals.

Identification of cis-regulatory elements and m6A-methylation sites in the promoter region of *MT*s, *FIP*s and *ALKBH*s

The cis-regulatory elements in the promoter region of Pigeonpea *MT*s, *FIP*s and *ALKBH*s genes were predicted using the 2kb upstream sequence retrieved from the available database for pigeon pea (LIS database). The identified cis-elements were then selected based on their role in growth and development, hormone response and stress. Growth and development regulatory elements like ARID, AT-Hook, Dof, NAC, LOB, SBP, HD-ZIP, PLATZ and FAR1 were selected. AT-Hook, B3, BBR-BPC, BES1 were selected for hormone response and AP2, bHLH, MADS Box, GATA, WOX, WRKY, C3H-Zinc finger, Dehydrin and VOZ were selected for stress response. Cis-elements varied between genes based on the presence and absence and also on the frequency by which they appear. For instance, both the *MT*s, viz. *MTA* and *MTB*, had almost equal number of cis-elements (Figure 6). *MT*s had the highest number of AP2 binding sequences followed by Dof (Figure 7). Between the two *FIP*s, *FIPA* had a greater number of elements as compared to *FIPB*. CG, FAR1 and HD-ZIP binding sequences were absent in *FIPB* but present in *FIPA* (Figure 6). In case of *ALKBH*s, *CcALKBH9* had the highest number of cis-regulatory elements followed by *CcALKBH8* and *CcALKBH1B* (Figure 6). MYB cis-regulatory binding elements were found to be the highest among *ALKBH*s followed by cis-regulatory binding elements for GATA, bZIP and Dof. (Figure 7). A table of cis-elements with their numbers for all three genes, viz, *MT*s, *FIP*s and *ALKBH*s, were provided in the Supplementary Files (Supplementary Table 3).

EpiSemble R-package was used to predict the m^6A methylation pattern in *MT*s, *FIP*s and *ALKBH*s. This exercise was carried out to understand the epigenetic regulation of the genes. In case of *MT*s five and four methylation sites were found in the upstream 2 kb region (Figure 8). For *FIP*s, three and two sites were found for *FIPA* and *FIPB*, respectively (Figure 8). Further in case of *ALKBH*s, *CcALKBH9* and *CcALKBH10A* had the highest number of methylation site (six), but the lowest methylation site was found for *CcALKBH1B* and *CcALKBH10B* (two) (Figure 8).

Tissue-specific gene expression analysis

Quantitative polymerase chain reaction (q-PCR) was performed to understand the expression pattern of the identified *MT*s, *FIP*s and *ALKBH*s in pigeon pea. Different tissues (leaf, root, internode, shoot apical meristem, flower apical meristem and immature pod) were checked for the relative abundance of the transcripts (Figure 9). In case of *MT*s, it was found that overall expression of *CcMTA* was higher in the six selected tissues compared to that of *CcMTB*. The highest expression for *MTA* was observed in leaf tissues (~4.3 fold), while the highest expression for *MTB* was detected in FAM tissues (~3.7 fold). A similar kind of expression pattern was observed for these two genes in other tissues (root,

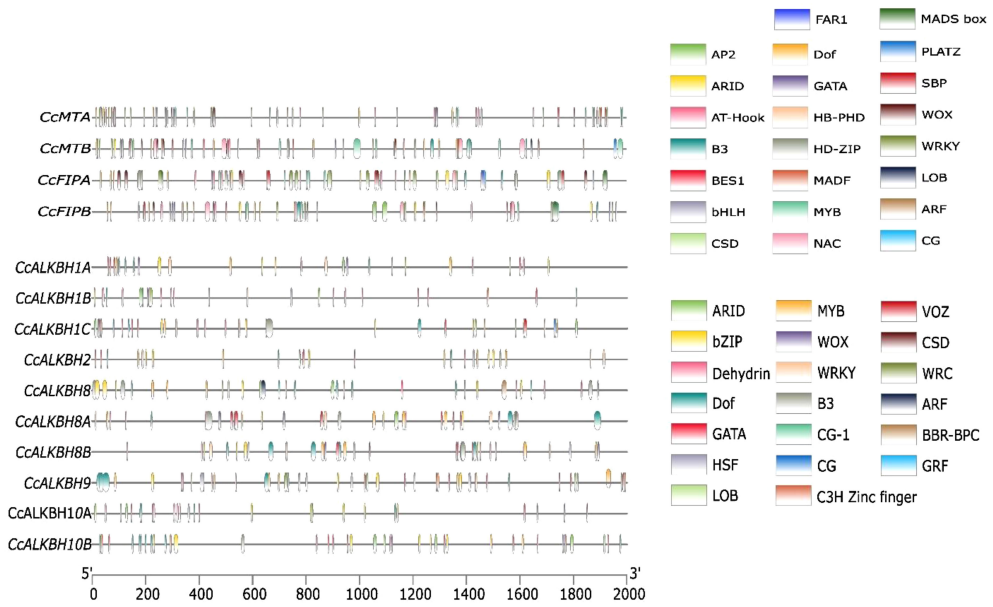

FIGURE 6
Cis-regulatory elements present in the promoter region of *CcMTs*, *CcFIPs* and *CcALKBHs* genes. Different colour lines represent different cis-regulatory elements.

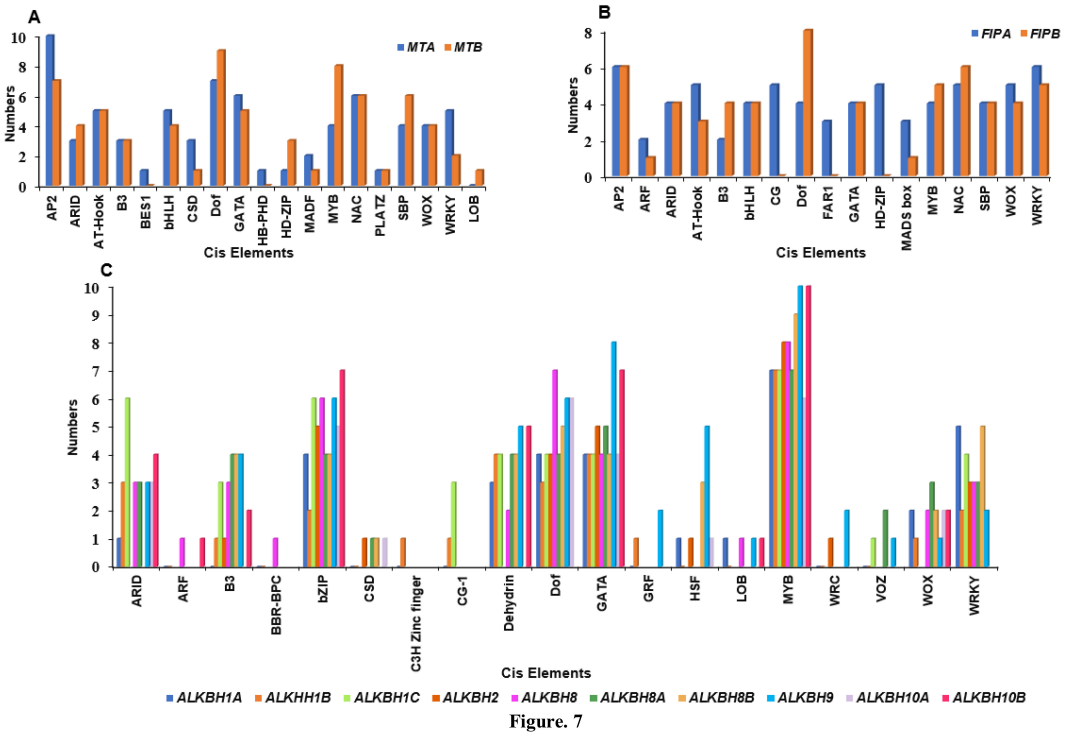

Figure. 7

FIGURE 7
Graph showing enrichment of cis-regulatory elements in identified *MTs*, *FIPs* and *ALKBHs*. **(A)** Enrichment graph for *MTA* (blue bar) and *MTB* (Maroon bar). **(B)** enrichment bar for *FIPA* (blue bar) and *FIPB* (Maroon bar). **(C)** Graph representing *ALKBHs* identifies *cis* elements analysis. Ten different colour bars represent the ten *ALKBHs* genes in pigeon pea.

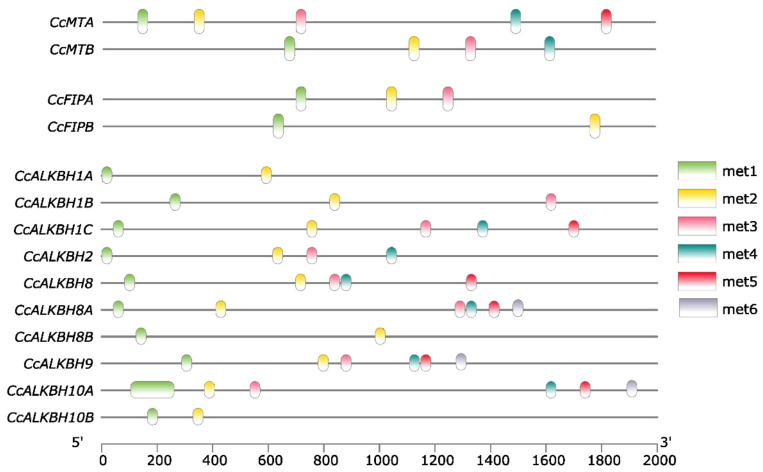

FIGURE 8
Predicted m6A-methylation position at identified *cis-regulatory* elements in the promoter region of *CcMTs*, *CcFIPs* and *CcALKBHs* genes. Different colour lines indicate the position of methylation.

internode, SAM and immature pod), but with varied expression levels i.e., *CcMTA* (~2.5 fold) had significantly higher expression compared to that of *CcMTB* (~1.0 fold) in root tissues. But, *CcMTB* (~3.7 fold) had more expression in SAM tissues compared to that of *CcMTA* (~3.1 fold) (Figure 9**).** In case of FIPs, both the genes, viz. *CcFIPA* and *CcFIPB*, showed the highest expression in leaf and internode. However, higher expression of *CcFIPB* was detected in the leaf (~6.0 fold) and root (~4.0 fold), and relatively more expression of *CcFIPA* was detected in FAM (~4.4 fold) tissues (Figure 9).

Majority of the genes encoding ALKBHs displayed similar kind of expression patterns with the highest level of expression in leaf

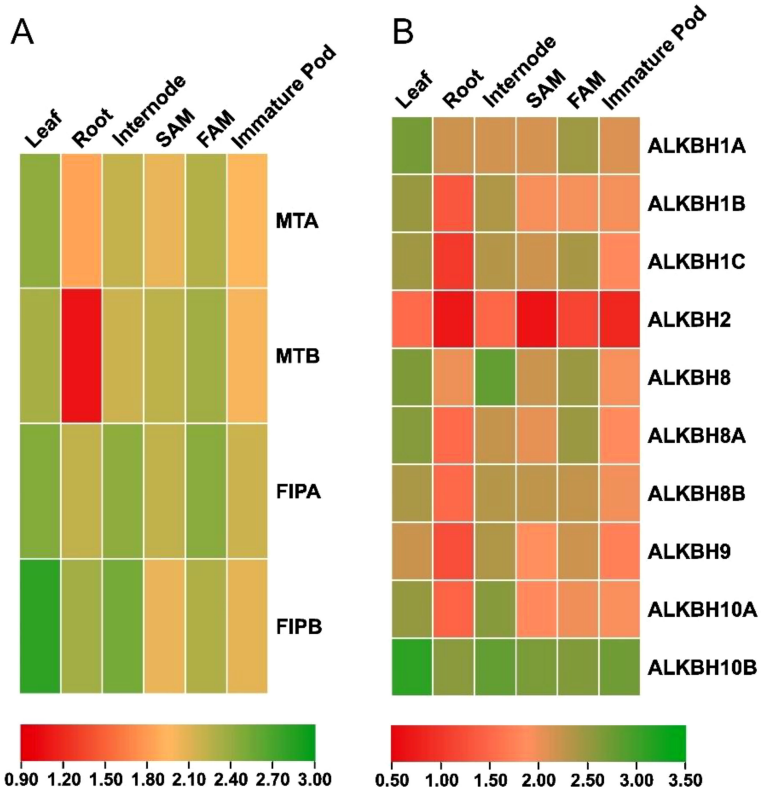

FIGURE 9
Expression analysis of the identified pigeon pea genes involved in methylation-demethylation. **(A)** Heat map analysis of pigeon pea *MTs* and *FIPs* genes. **(B)** Heat map analysis of pigeon pea *ALKBHs* genes. Column represents different plant tissues and rows represent the identified genes. Significant up-regulationin expression is shown in green, while significant down regulation in expression is shown in red.

tissues, except for *CcALKBH8* (~5.9 fold), *CcALKBH9* (~4.1 fold) and *CcALKBH10A* (~4.9 fold), which showed the highest expression in internode tissue. The second highest expression of seven *ALKBH* genes was also detected in internode tissue, but three genes, viz. *CcALKBH1A* (~4.5 fold), *CcALKBH1C* (~4.3 fold) and *CcALKBH8A* (~4.5 fold) showed the second highest expression in FAM tissue. Among the ten *ALKBH* genes, *CcALKBH10B* had the highest expression in all the six tissues analyzed and *CcALKBH2* had the lowest expression (Figure 9). Overall, the highest level of expression of genes encoding MTs, FIPs and ALKBHs was detected in leaf and the lowest expression in root tissues (Figure 9).

Expression profiling of identified genes in biotic and abiotic stress conditions

We wanted to see the expression level changes in the identified genes under various abiotic and biotic stresses. So, we subjected pigeon pea seedlings under various stresses and the morphological changes which was found is provided in Supplementary Figure 1 Further relative expression of *MT*s, *FIP*s and *ALKBH*s genes of pigeon pea during biotic and abiotic stresses was studied by qPCR analysis. During heat stress the highest induction in expression was observed in *CcALKBH8* (~9.5 fold) followed by *CcALKBH10B* (~8.0 fold), but no induction in expression was found in *CcALKBH2* (~1 fold) compared to that of control (Figure 10**).** Among the methyl transferase genes induction in expression was not so prominent, and about two-fold induction in expression was detected for *CcMTA* (~2.1fold) and *CcMTB* (~1.9 fold), whereas very low induction was observed for *CcFIPB* (~1.2 fold) and *CcFIPA* (~1.0 fold) during heat stress (Figure 10). Under drought stress, *CcALKBH10B* showed nine-fold more expression, followed by *CcALKBH9* (~7.5 fold) and *CcALKBH10A* (~7.3 fold). *CcALKBH2* (~1.0 fold) showed negligible induction (Figure 10). In case of methyl transferase genes, about four-fold induction in expression was observed in *CcMTA* (~4.3 fold) and *CcMTB* (~4.0 fold), but induction was not so prominent in *CcFIPB* (~1.1 fold) and *CcFIPA* (~1.0 fold) (Figure 10**).** The highest level of induction in gene expression of 13-fold was detected in *CcALKBH10B* (~13.3 fold) during salt stress. Two other genes, *CcALKBH10A* (~7.6 fold) and *CcALKBH9* (~5.7 fold) showed 8- and 6-fold induction, respectively, during salt stress. Whereas, *CcALKBH2* (~1) showed negligible induction (Figure 10**).** Two methyl transferase genes, *CcMTB* (~5.5 fold) and *CcMTA* (~5.3 fold), showed about five-fold more expression during salt stress. Again, *CcFIPB* (~1.6 fold) and *CcFIPA* (~1.0 fold) showed very little induction in expression during salt stress (Figure 10**).**

A higher level of induction in gene expression, ranging from 13 to 9-fold, was detected in *ALKBH* genes in pigeon pea upon *H. armigera* infestation. The highest induction was observed in *CcALKBH10B* (~13.5 fold), followed by *CcALKBH10A* (~12.2 fold), *CcALKBH9* (~9.4 fold) and *CcALKBH1C* (~8.6 fold). Again, *CcALKBH2* (~1.0 fold) showed negligible induction during biotic stress (Figure 10**).** Less pronounced induction was observed for *MT*s genes with about four-fold induction in *CcMTB* (~4.0 fold) and *CcMTA* (~3.8 fold) followed by 2-fold induction in *CcFIPB* (~1.9 fold). However, induction in *CcFIPA* (~1.0 fold) was not significant (Figure 10).

Discussion

Methylation and demethylation dynamics have a major role in epigenetic regulation of plants growth and development (Huong et al., 2020; Liang et al., 2020) and stress responses (Shoaib et al., 2021). The methylation of adenine (6-methyladenosine, m^6A) in plants was initially seen in maize, oats, and wheat (Nichols, 1980). mRNAs move to various body parts where they act as potential signaling molecules. The translational state in maize is correlated with m^6A methylation (Luo et al., 2020). Global m^6A RNA methylation in seagrass has a significant role in circadian regulation and may have an impact on their photo-biological behavior (Ruocco et al., 2020). Furthermore, m^6A methylation is required to maintain levels of mature miRNAs and their precursors, as evidenced by a report on its effects on microRNA (miRNA) production in *Arabidopsis* (Bhat et al., 2020). RNA methylation has a role in the mobility and transport of RNA in plants (Yang et al., 2018). Further m^6A demethylation plays an important role in abiotic stress (heat, drought and salt stress) response (Huong et al., 2020). The methyl transferase (*MT* gene family) and demethylase genes (*ALKBH* gene family) have been identified in the model plant Arabidopsis (Wan et al., 2015) and a major crop plant, rice (Liang et al., 2020). However, the *MTs* and *ALKBHs* gene families are yet to be studied in pigeon pea, an important legume crop. In the present study, we have carried out a genome-wide analysis by comparing the alignments of homologous ALKBH protein sequences from Arabidopsis and pigeon pea to find out methylation and demethylation-related genes. A total of four methylation-related (two methyl transferases, *MT*s and two adaptors proteins for methylation; *FIPA* and *FIPB*) and 10 *ALKBH* (*CcALKBH1A, CcALKBH1B, CcALKBH1C, CcALKBH2, CcALKBH18, CcALKBH8A, CcALKBH8B, CcALKBH9, CcALKBH10, and CcALKBH10B*) family genes had been identified. The identified *MT*s and *ALKBH*s were similar in number as that of tomato and sugar beet genomes, but gene numbers were less than that of Arabidopsis, rice, wheat and Populus. This could be possible because of the evolutionary time gap.

Phylogenetic analysis is used for the identification of orthologous proteins (Bauwens et al., 2018). In the present study, MT and FIP genes were divided into two groups each (*CcMTA*, *CcMTB* and *FIPA*, *FIPB)* and the ALKBH genes were divided into four groups, viz. *CcALKBH1A/1B/1C/2* like, *CcALKBH8/8A/8B* like, *CcALKBH9* like and *CcALKBH10A/10B* like. Whereas in Arabidopsis, one more group was found, i.e., *AtALKBH6* (Mielecki et al., 2012**),** which was absent in pigeon pea. Among the identified groups, *CcALKBH9* and *CcALKBH10A/10B* are homologs of *AtALKBH9A/9B/9C* and *AtALKBH10A/10B/10C*, respectively, which were reported to carry out m^6A demethylation (Duan et al., 2017; Martínez-Pérez et al., 2017). Therefore, it is perceived that *CcALKBH9* and *CcALKBH10A/10B* could be putative m^6A demethylases. However, this needs further validation. The gene structures of *CcMTs, CcFIP and CcALKBHs* were analyzed

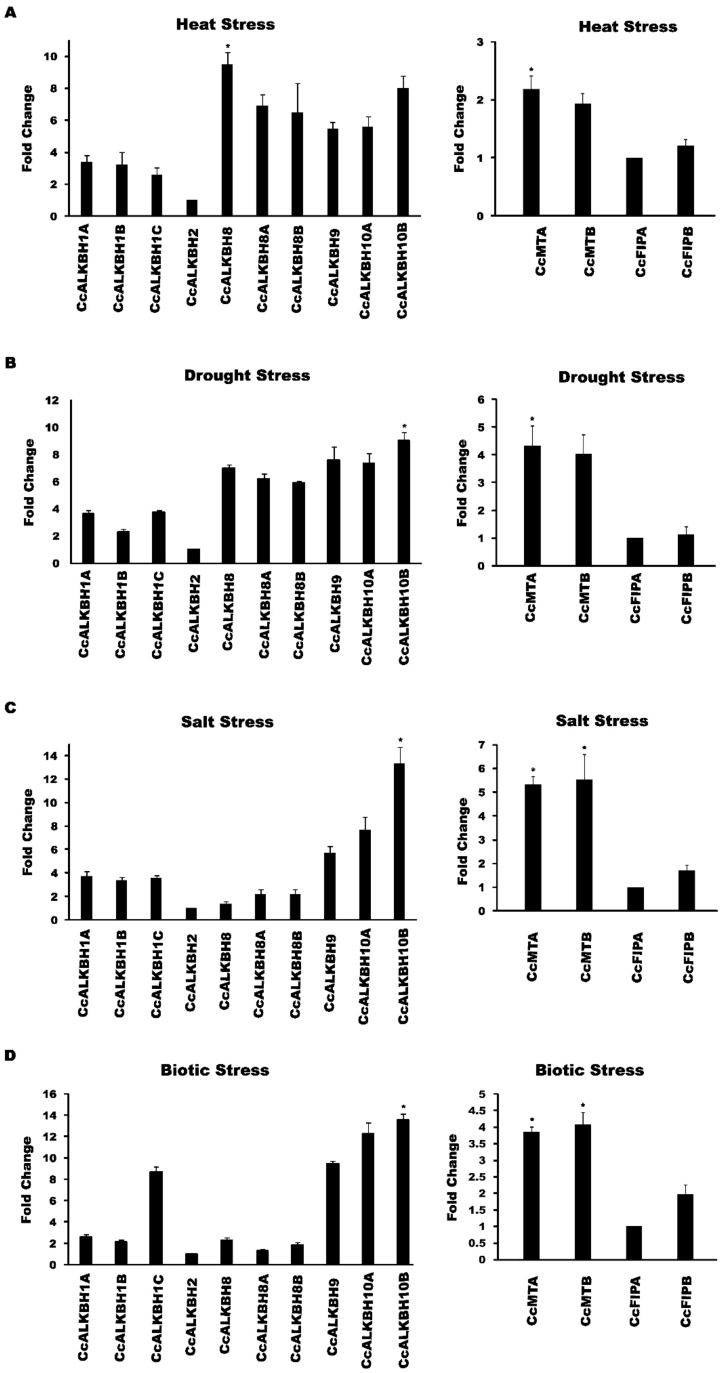

FIGURE 10
Graphical representations of fold change in expression of *CcMTs, CcFIPs, CcALKBHs* genes of pigeon pea under different stress conditions as revealed by qPCR analysis. **(A)** Heat stress induced change in expression of *CcALKBHs* (demethylase) and *CcMTs* & *CcFIPs* (methyl transferase). **(B)** Expression induction of *CcALKBHs* (demethylases) and *CcMTs* & *CcFIPs* (methyl transferases) during drought stress. **(C)** Salt stress-induced change in expression of *CcALKBHs* (demethylases) and *CcMTs* & *CcFIPs* (methyl transferases). **(D)** Fold change in expression of *CcALKBHs* (demethylases) and *CcMTs* & *CcFIPs* (methyl transferases) upon *H. armigera* infestation. Three biological and three technical replicates were taken for expression studies. Star mark indicates the significant difference between the different treatment. For the study of gene expression in abiotic and biotic stress condition three biological and three technical replicates were taken. And mean values were calculated and given error bar (standard error of means). So, Values are the mean ± SE obtained from three independent replicates. At 5% Least significant difference (LSD) was calculated to see the significance of different treatment effect and after that level of significance between and among the treatments in each experiment was checked by performing range test WASP package (AKMU ICAR-CCRI, GOA.).

(Figure 3B). It has been found that gene structure for methyl transferase genes is more or less conserved. This conservation of gene architecture for MTs could be to ensure gene stability and integrity and to limit random changes. However, genes encoding FIPs (adaptor protein for methylase transferase) and ALKBHs have shown variation in gene structure. These changes might have occurred during evolution, and this could be the basis for different functions of the identified demethylase genes.

*Cc*MTs had methyl transferase domain, which might be responsible for methylation. For the demethylation activity of ALKBH, one important factor is the presence of the Fe^{2+} binding domain required for its catalytic activity (Fedeles et al., 2015), and all the identified *CcALKBHs* contain the Fe^{2+} binding domain (Figure 4). This Fe^{2+} binding domain might mediate the oxidative demethylation of nucleic acids. Additionally, *CcALKBH8* contains a methyl transferase domain, which might be responsible for both methylation and demethylation activity.

Further, *CcALKBH8A* contains an RRM (RNA recognition motif), which is required for tRNA binding and its modification (Pastore et al., 2012). ALKBH of the same sub-group has been found to exhibit a similar pattern in gene structure and conserved motifs, but variation was present among the sub-groups. The conserved motifs analysis of the identified *MT*s, *FIP*s and *ALKBH*s of pigeon pea revealed that a few motifs were conserved across genes but some motifs were unique to some particular genes. The variation in sequence structure and motifs might be responsible for changes in function over a period of time.

Upstream promoter sequences analysis of *MT*s, *FIP*s and *ALKBH*s revealed presence of many regulatory elements related to abiotic stress, hormones and light responses. The promoter sequence of *MT*s harbors more recognition elements for AP2 which has an important role in transcription stimulation in low temperature and water deficit (Sharoni et al., 2011). *MTA* and *MTB* promoter sequences also have presence of GATA and Dof recognition sequence. These elements have role in development and growth of plant (Cai et al., 2020). *FIP* promoter has a high number of recognition elements for Dof which has a role in phytohormone production, seed development and cold stress. Further, *ALKBH* upstream sequence has elements for MYB, which has recently been reported to have a role in m^6A methylation modification (Xing et al., 2023).

The role of various *MTs* and *ALKBHs* has been characterized in a few plant species. *MTA* and *MTB* are reported to function in embryo development in Arabidopsis (Zhong et al., 2008). *MTA* has also been reported to impart drought tolerance in poplar by regulating the development of trichomes and roots through m^6A methylation (Lu et al., 2020). FIP37 has been reported to play a role in endosperm and embryo development (Zhong et al., 2008). It was first identified in Arabidopsis as an interacting partner of MTA. Similarly, ALKBHs of Arabidopsis act on different substrates, i.e., *ALKBH2* does repairing of 1-meA and 3-meC, *ALKBH8* takes part in modification of tRNA by hydroxylating mcm^5U to (S)-$mchm^5U$. *AtALKBH6* has been reported to have a role in abiotic stress response where it acts as negative regulator in cold and salt stress but a positive regulator in dehydration stress, viz, heat and drought (Huong et al., 2020). *AtALKBH9B* has been reported to modulate systemic viral infection by demethylating the alfalfa mosaic virus genome (Martínez-Pérez et al., 2017). *AtALKBH10B* has a role in floral transition by affecting the stability of key floral regulators, including FLOWERING LOCUS *T* (*FT*), SQUAMOSA PROMOTER BINDING PROTEIN-LIKE 3 (SPL3) and SPL9 which results in early flowering (Duan et al., 2017). *AtALKBH10B* is also involved in drought tolerance, where it affects m-RNA stability through demethylation of m^6A (Han et al., 2023). It also modulates ABA response during seed germination (Tang et al., 2021) and was found to impart tolerance to salt stress in Arabidopsis (Shoaib et al., 2021). A recent study showed that in case of cotton, *GhALKBH10B* affects the mRNA stability of genes linked to photosynthesis and GhSnRK2;3, which leads to a negative response to drought stress (Zhang et al., 2024). In case of tomato, *SlALKBH2* has been reported to have RNA demethylase activity, which delays fruit ripening (Zhou et al., 2019).

The qPCR analysis of the identified *MT*s, *FIP*s and *ALKBH*s revealed the changes in the expression level of genes in six different tissues (Leaf, Root, Internode, SAM, FAM and Immature pod). In case of *MT*s, *CcMTA* has a slightly higher expression as compared to *CcMTB*. Similarly, *CcFIPB* showed comparatively higher expression than that of *CcFIPA*. So, *CcMTA* and *CcMTB* could be the probable methyl transferase genes in pigeon pea, and *CcFIPB* might be the adaptor protein that stabilizes the methyl transferase components during methylation process. However, further validation is needed to confirm their function.

AtALKBH9B and *AtALKBH10B* have been reported as the major demethylases in Arabidopsis (Duan et al., 2017; Martínez-Pérez et al., 2017). The highest expression of *CcALKBH10B* was detected in different tissues of pigeon pea compared to that of *CcALKBH8*, *CcALKBH10A* and *CcALKBHB9*. Hence, it could be possible that *CcALKBH10B* could be primarily involved in demethylation in pigeon pea as perceived from the expression analysis.

Expression profiling of the *CcMTs*, *CcFIPs* and *CcALKBHs* under abiotic (Heat, Drought and salt) and biotic stress (*H. armigera*) revealed a similar trend of induction in expression. *CcMTA* and *CcMTB* showed similar patterns of induction under both the biotic and abiotic stresses. Similarly, a high level of induction in expression was observed in *CcALKBH8*, CcALKBH*10A* and *CcALKBH10B* under both the biotic and abiotic stress conditions. This indicated that both *CcMTA* and *CcMTB* could be the major methyl transferase genes, and *CcALKBH8*, *CcALKBH10A* and *CcALKBH10B* could be the major demethylase genes in pigeon pea. Arabidopsis demethylase gene, *AtALKBH10B*, was reported to be involved in drought and salt stress tolerance by affecting mRNA stability through demethylation of m^6A (Shoaib et al., 2021; Han et al., 2023).

Conclusion

Methylation demethylation dynamics plays an important role in imparting abiotic (like heat, drought and salt stress) and biotic (like against viral infection) tolerance. However, these genes and their function yet to be explored in pigeon pea. Hence, we conducted initial study to find out the different methyltrasferase and demethylase genes present in the pigeon pea genome and their expression pattern in different tissues and stress conditions. Now, from this study the genes which are expressing in response to stress will be selected for functional analysis. Hence this study has its

importance by providing the basic knowledge of different methyltransferase and demethylase gene present in pigeon pea and their expression level which will finally help in selection and manipulation of genes for imparting abiotic and biotic stress tolerance.

Data availability statement

The original contributions presented in the study are included in the article/Supplementary Material. Further inquiries can be directed to the corresponding author/s.

Author contributions

PK: Data curation, Formal analysis, Methodology, Validation, Visualization, Writing – original draft. SB: Methodology, Writing – review & editing. KV: Writing – review & editing, Investigation, Project administration. JT: Writing – review & editing. KP: Writing – review & editing, Methodology. KS: Writing – review & editing, Visualization. MB: Visualization, Writing – review & editing. GR: Writing – review & editing, Resources. RS: Resources, Writing – review & editing. DP: Resources, Writing – review & editing, Conceptualization, Supervision.

Funding

The author(s) declare financial support was received for the research, authorship, and/or publication of this article. The work was supported by in-house funding by ICAR-NIPB, New Delhi.

Acknowledgments

PK acknowledges the IARI Post Graduate School for providing fellowship for her Ph. D. study. We would like to acknowledge ICAR- National Institute for Plant Biotechnology, New Delhi, and ICAR- Indian Agricultural Research Institute, New Delhi for providing Research facilities and funds and other supports for this work.

Conflict of interest

The authors declare that the research was conducted in the absence of any commercial or financial relationships that could be construed as a potential conflict of interest.

Publisher's note

Supplementary material

The Supplementary Material for this article can be found online at: https://www.frontiersin.org/articles/10.3389/fpls.2024.1521758/full#supplementary-material

References

Bakala, H. S., Devi, J., Singh, G., and Singh, I. (2024). Drought and heat stress: insights into tolerance mechanisms and breeding strategies for pigeon pea improvement. *Planta.* 259, 123. doi: 10.1007/s00425-024-04401-6

22Bauwens, E., Joosten, M., Taganna, J., Rossi, M., Debraekeleer, A., Tay, A., et al. (2018). In silico proteomic and phylogenetic analysis of the outer membrane protein repertoire of gastric Helicobacter species. *Scientific Reports* 8(1), 15453.

Bhat, S. S., Bielewicz, D., Gulanicz, T., Bodi, Z., Yu, X., and Anderson, S. J. (2020). mRNA adenosine methylase (MTA) deposits m6A on pri-miRNAs to modulate miRNA biogenesis in *Arabidopsis thaliana*. *Proc. Natl. Acad. Sci. U.S.A.* 117, 21785–21795. doi: 10.1073/pnas.2003733117

Bhattacharjee, S., Bhowmick, R., Paul, K., Venkat Raman, K., Jaiswal, S., Tilgam, J., et al. (2023). Identification, characterization, and comprehensive expression profiling of floral master regulators in pigeon pea (*Cajanus cajan* [L.] Millspaugh). *Funct. Integr. Genomics* 23, 311. doi: 10.1007/s10142-023-01236-4

Cai, M., Lin, J., Li, Z., Lin, Z., Ma, Y., Wang, Y., et al. (2020). Allele specific expression of Dof genes responding to hormones and abiotic stresses in sugarcane. *PloS One* 15, e0227716. doi: 10.1093/pcp/pcq196

Cantara, W. A., Crain, P. F., Rozenski, J., McCloskey, J. A., Harris, K. A., Zhang, X., et al. (2010). The RNA modification database, RNAMDB. *Nucleic Acids Res.* 10, D195–D201. doi: 10.1093/nar/gkq1028

Choudhary, A. K., Sultana, R., Pratap, A., Nadarajan, N., and Jha, U. C. (2011). Breeding for abiotic stresses in pigeon pea. *J. Food Legumes.* 24, 165–174.

Dokka, N., Tyagi, S., Ramkumar, M. K., Rathinam, M., Senthil, K., and Sreevathsa, R. (2024). Genome-wide identification and characterization of DIRIGENT gene family (CcDIR) in pigeon pea (*Cajanus cajan* L.) provide insights on their spatial expression pattern and relevance to stress response. *Gene* 914, 148417. doi: 10.1016/j.gene.2024.148417

Duan, H. C., Wei, L. H., Zhang, C., Wang, Y., Chen, L., Lu, Z., et al. (2017). ALKBH10B is an RNA N 6-methyladenosine demethylase affecting Arabidopsis floral transition. *Plant Cell* 29, 2995–3011. doi: 10.1105/tpc.16.00912

FAOSTAT. (2022). https://www.fao.org/faostat/en/#home.

Fedeles, B. I., Singh, V., Delaney, J. C., Li, D., and Essigmann, J. M. (2015). The AlkB family of Fe (II)/α-ketoglutarate-dependent dioxygenases: repairing nucleic acid alkylation damage and beyond. *J. Biol. Chem.* 290, 20734–20742. doi: 10.1074/jbcR115.656462

Greer, E. L., Blanco, M. A., Gu, L., Sendinc, E., Liu, J., Aristizábal-Corrales, D., et al. (2015). DNA methylation on N6-adenine in C. *elegans*. *Cell* 161, 868–878. doi: 10.1016/j.cell.2015.04.005

Han, R., Shoaib, Y., Cai, J., and Kang, H. (2023). ALKBH10B-mediated m6A demethylation is crucial for drought tolerance by affecting mRNA stability in Arabidopsis. *Environ. Exp. Bot.* 209, 105–306. doi: 10.1016/j.envexpbot.2023.105306

Haussmann, I. U., Bodi, Z., Sanchez-Moran, E., Mongan, N. P., Archer, N., and Fray, R. G. (2016). m6A potentiates Sxl alternative pre-mRNA splicing for robust Drosophila sex determination. *Nature* 540, 301–304. doi: 10.1038/nature20577

Hu, J., Manduzio, S., and Kang, H. (2019). Epitranscriptomic RNA methylation in plant development and abiotic stress responses. *Front. Plant Sci.* 10. doi: 10.3389/fpls.2019.00500

Huong, T. T., Ngoc, L. N., and Kang, H. (2020). Functional characterization of a putative RNA demethylase ALKBH6 in Arabidopsis growth and abiotic stress responses. *Int. J. Mol. Sci.* 21, 6707. doi: 10.3390/ijms21186707

Iyer, L. M., Zhang, D., and Aravind, L. (2016). Adenine methylation in eukaryotes: Apprehending the complex evolutionary history and functional potential of an epigenetic modification. *Bioessays* 38, 27–40. doi: 10.1002/bies.201500104

Kataoka, H. I., Yamamoto, Y. O., and Sekiguchi, M. U. (1983). A new gene (alkB) of *Escherichia coli* that controls sensitivity to methyl methane sulfonate. *J. Bacteriol* 153, 1301–1307. doi: 10.1128/jb.153.3.1301-1307.1983

Kyte, J., and Doolittle, R. F. (1982). A simple method for displaying the hydropathic character of a protein. *J. Mol. Biol.* 157, 105–132. doi: 10.1016/0022-2836(82)90515-0

Liang, Z., Riaz, A., Chachar, S., Ding, Y., Du, H., and Gu, X. (2020). Epigenetic modifications of mRNA and DNA in plants. *Mol. Plant* 3, 14–30. doi: 10.1016/j.molp.2019.12.007

Livak, K. J., and Schmittgen, T. D. (2001). Analysis of relative gene expression data using real-time quantitative PCR and the 2– ΔΔCT method. *Methods* 25, 402–408. doi: 10.1006/meth.2001.126

Lu, L., Zhang, Y., He, Q., Qi, Z., Zhang, G., Xu, W., et al. (2020). MTA, an RNA m6A methyltransferase, enhances drought tolerance by regulating the development of trichomes and roots in poplar. *Int. J. Mol. Sci.* 21, 2462. doi: 10.3390/ijms21072462

Luo, J. H., Wang, Y., Wang, M., Zhang, L. Y., Peng, H. R., and Zhou, Y. Y. (2020). Natural variation in RNA m6A methylation and its relationship with translational status. *Plant Physiol.* 182, 332–344. doi: 10.1104/pp.19.00987

Marcinkowski, M., Pilžys, T., Garbicz, D., Steciuk, J., Zugaj, D., Mielecki, D., et al. (2020). Human and Arabidopsis alpha-ketoglutarate-dependent dioxygenase homolog proteins—New players in important regulatory processes. *IUBMB Life* 72, 1126–1144. doi: 10.1002/iub.2276

Martínez-Pérez, M., Aparicio, F., López-Gresa, M. P., Bellés, J. M., Sánchez-Navarro, J. A., and Pallás, V. (2017). Arabidopsis m6A demethylase activity modulates viral infection of a plant virus and the m6A abundance in its genomic RNAs. *Proc. Natl. Acad. Sci.* 114, 10755–10760. doi: 10.1073/pnas.1703139114

Meyer, K. D., and Jaffrey, S. R. (2014). The dynamic epitranscriptome: N6-methyladenosine and gene expression control. *Nat. Rev. Mol. Cel Bio* 15, 313–326. doi: 10.1038/nrm3785

Mi, J., Ren, X., Shi, J., Wang, F., Wang, Q., Pang, H., et al. (2024). An insight into the different responses to salt stress in growth characteristics of two legume species during seedling growth. *Front. Plant Sci.* 14. doi: 10.3389/fpls.2023.1342219

Miao, Z., Zhang, T., Qi, Y., Song, J., Han, Z., and Ma, C. (2020). Evolution of the RNA N 6-methyladenosine methylome mediated by genomic duplication. *Plant Physiol.* 182, 345–360. doi: 10.1104/pp.19.00323

Mielecki, D., Zugaj, DŁ., Muszewska, A., Piwowarski, J., Chojnacka, A., Mielecki, M., et al. (2012). Novel AlkB dioxygenases—alternative models for in *silico* and *in vivo* studies. *PloS One* 7, e30588. doi: 10.1371/journal.pone.0030588

Nichols, J. L. (1980). N6-methyladenosine in maize poly(A)-containing RNA. *Plant Sci. Lett.* 15, 357–361. doi: 10.1016/0304-4211(79)90141

Ougland, R., Rognes, T., Klungland, A., and Larsen, E. (2015). Non-homologous functions of the AlkB homologs. *J. Mol. Cell Biol.* 7, 494–504. doi: 10.1093/jmcb/mjv029

Pastore, C., Topalidou, I., Forouhar, F., Yan, A. C., Levy, M., and Hunt, J. F. (2012). Crystal structure and RNA binding properties of the RNA recognition motif (RRM) and AlkB domains in human AlkB homolog 8 (ABH8), an enzyme catalyzing tRNA hyper modification. *J. Biol. Chem.* 287, 2130–2143. doi: 10.1074/jbc.M111.286187

Ping, X. L., Sun, B. F., Wang, L. U., Xiao, W., Yang, X., Wang, W. J., et al. (2014). Mammalian WTAP is a regulatory subunit of the RNA N6-methyladenosine methyltransferase. *Cell Res.* 24, 177–189. doi: 10.1038/cr.2014.3

Ruocco, M., Ambrosino, L., Jahnke, M., Chiusano, M. L., Barrote, I., and Procaccini, G. (2020). m^6A RNA methylation in marine plants: First insights and relevance for biological rhythms. *Int. J. Mol. Sci.* 21, 1–21. doi: 10.3390/ijms21207508

Sharoni, A. M., Nuruzzaman, M., Satoh, K., Shimizu, T., Kondoh, H., Sasaya, T., et al. (2011). Gene structures, classification and expression models of the AP2/EREBP transcription factor family in rice. *Plant Cell Physiol.* 52, 344–360. doi: 10.1093/pcp/pcq196

Shen, L., Liang, Z., Gu, X., Chen, Y., Teo, Z. W., Hou, X., et al. (2016). N6-methyladenosine RNA modification regulates shoot stem cell fate in Arabidopsis. *Dev. Cell* 38, 186–200. doi: 10.1016/j.devcel.2016.06.008

Shoaib, Y., Hu, J., Manduzio, S., and Kang, H. (2021). Alpha-ketoglutarate-dependent dioxygenase homolog 10B, an N6-methyladenosine mRNA demethylase, plays a role in salt stress and abscisic acid responses in Arabidopsis thaliana. *Physiol. Plant* 173, 1078–1089. doi: 10.1111/ppl.13505

Tamura, K., Stecher, G., and Kumar, S. (2021). MEGA 11: molecular evolutionary genetics analysis version 11. *Mol. Biol. Evol.* 38 (7), 3022–3027. doi: 10.1093/molbev/msab120

Tang, J., Yang, J., Duan, H., and Jia, G. (2021). ALKBH10B, an mRNA m6A demethylase, modulates ABA response during seed germination in Arabidopsis. *Front. Plant Sci.* 12. doi: 10.3389/fpls.2021.712713

Trewick, S. C., Henshaw, T. F., Hausinger, R. P., Lindahl, T., and Sedgwick, B. (2002). Oxidative demethylation by *Escherichia coli* AlkB directly reverts DNA base damage. *Nature* 419, 174–178. doi: 10.1038/nature00908

Wan, Y., Tang, K., Zhang, D., Xie, S., Zhu, X., Wang, Z., et al. (2015). Transcriptome-wide high-throughput deep m6A-seq reveals unique differential m6A methylation patterns between three organs in *Arabidopsis thaliana*. *Genome Biol.* 16, 1–26. doi: 10.1186/s13059-015-0839-2

Wang, X., Lu, Z., Gomez, A., Hon, G. C., Yue, Y., and Han, D. (2014). N6-methyladenosine-dependent regulation of messenger RNA stability. *Nature* 505, 117–120. doi: 10.1038/nature12730

Wei, L. H., Song, P., Wang, Y., Lu, Z., Tang, Q., Yu, Q., et al. (2018). The m6A reader ECT2 controls trichome morphology by affecting mRNA stability in Arabidopsis. *Plant Cell* 30, 968–985. doi: 10.1105/tpc.17.00934

Xing, K., Liu, Z., Liu, L., Zhang, J., Qanmber, G., Wang, Y., et al. (2023). N6-methyladenosine mRNA modification regulates transcripts stability associated with cotton fiber elongation. *Plant J.* 115 (4), 967–985. doi: 10.1111/tpj.16274

Yang, Y., Hsu, P. J., Chen, Y. S., and Yang, Y. G. (2018). Dynamic transcriptomic m6A decoration: Writers, erasers, readers and functions in RNA metabolism. *Cell Res.* 28, 616–624. doi: 10.1038/s41422-018-0040-8

Yue, H., Nie, X., Yan, Z., and Weining, S. (2019). N6-methyladenosine regulatory machinery in plants: composition, function and evolution. *Plant Biotechnol. J.* 17, 1194–1208. doi: 10.1111/pbi.13149

Zhang, D., Li, M., Chen, C., Wang, Y., Cheng, Z., Li, W., et al. (2024). Downregulation of GhALKBH10B improves drought tolerance through increasing the stability of photosynthesis related-and ABA signalling pathway genes in cotton. *Environ. Exp. Bot.* 7, 105687. doi: 10.1016/j.envexpbot.2024.105687

Zhang, M., Yang, S., Nelakanti, R., Zhao, W., Liu, G., Li, Z., et al. (2020). Mammalian ALKBH1 serves as an N^6-mA demethylase of unpairing DNA. *Cell Res.* 30, 197–210. doi: 10.1038/s41422-019-0237-5

Zhang, F., Zhang, Y. C., Liao, J. Y., Yu, Y., Zhou, Y. F., Feng, Y. Z., et al. (2019). The subunit of RNA N6-methyladenosine methyltransferase OsFIP regulates early degeneration of microspores in rice. *PloS Genet.* 15, e1008120. doi: 10.1371/journal.pgen.1008120

Zhong, S., Li, H., Bodi, Z., Button, J., Vespa, L., Herzog, M., et al. (2008). MTA is an Arabidopsis messenger RNA adenosine methylase and interacts with a homolog of a sex-specific splicing factor. *Plant Cell* 20, 1278–1288. doi: 10.1105/tpc.108.058883

Zhou, L., Tian, S., and Qin, G. (2019). RNA methylomes reveal the m^6A-mediated regulation of DNA demethylase gene *SlDML2* in tomato fruit ripening. *Genome Biol.* 20, 1–23. doi: 10.1186/s13059-019-1771-7

frontiers | Frontiers in Sustainable Food Systems

TYPE Review
PUBLISHED 26 February 2025
DOI 10.3389/fsufs.2025.1551460

OPEN ACCESS

EDITED BY
Naseeb Singh,
The ICAR Research Complex for North Eastern Hill Region, India

REVIEWED BY
Karansher Singh Sandhu,
Bayer Crop Science, United States
Shashank Shekhar,
Banda University of Agriculture and Technology, India
Swati Mehra,
Chaudhary Charan Singh Haryana Agricultural University, India

*CORRESPONDENCE
Pawan Saini
✉ pawansaini-coapbg@pau.edu
Mercy Nabila Iliya
✉ lliyam@fuwukari.edu.ng

RECEIVED 25 December 2024
ACCEPTED 13 February 2025
PUBLISHED 26 February 2025

CITATION
Aziz D, Rafiq S, Saini P, Ahad I, Gonal B, Rehman SA, Rashid S, Saini P, Rohela GK, Aalum K, Singh G, Gnanesh BN and Nabila Iliya M (2025) Remote sensing and artificial intelligence: revolutionizing pest management in agriculture.
Front. Sustain. Food Syst. 9:1551460.
doi: 10.3389/fsufs.2025.1551460

Remote sensing and artificial intelligence: revolutionizing pest management in agriculture

Danishta Aziz[1], Summira Rafiq[1], Pawan Saini[2]*, Ishtiyaq Ahad[1], Basanagouda Gonal[2], Sheikh Aafreen Rehman[1], Shafiya Rashid[3], Pooja Saini[4], Gulab Khan Rohela[2], Khursheed Aalum[5], Gurjeet Singh[6], Belaghihalli N. Gnanesh[7] and Mercy Nabila Iliya[8]*

[1]Division of Entomology, Faculty of Agriculture, SKUAST-K, Wadura, Sopore, India, [2]Central Sericultural Research & Training Institute (CSR&TI), Central Silk Board, Pampore, India, [3]Division of Entomology, SKUAST-J, Chatha, Jammu, India, [4]Department of Plant Breeding, Genetics and Biotechnology, Dr. Khem Singh Gill College of Agriculture, Eternal University, Baru Sahib, Rajgarh, India, [5]Department of Botany, University of Kashmir, Srinagar, India, [6]Texas A&M Agrilife Research Center at Beaumont, Beaumont, TX, United States, [7]ICAR JSS-KVK Suttur, Mysore, India, [8]Department of Crop Production and Protection, Federal University Wukari, Wukari, Nigeria

The agriculture sector is currently facing several challenges, including the growing global human population, depletion of natural resources, reduction of arable land, rapidly changing climate, and the frequent occurrence of human diseases such as Ebola, Lassa, Zika, Nipah, and most recently, the COVID-19 pandemic. These challenges pose a threat to global food and nutritional security and place pressure on the scientific community to achieve Sustainable Development Goal 2 (SDG2), which aims to eradicate hunger and malnutrition. Technological advancement plays a significant role in enhancing our understanding of the agricultural system and its interactions from the cellular level to the green field level for the benefit of humanity. The use of remote sensing (RS), artificial intelligence (AI), and machine learning (ML) approaches is highly advantageous for producing precise and accurate datasets to develop management tools and models. These technologies are beneficial for understanding soil types, efficiently managing water, optimizing nutrient application, designing forecasting and early warning models, protecting crops from plant diseases and insect pests, and detecting threats such as locusts. The application of RS, AI, and ML algorithms is a promising and transformative approach to improve the resilience of agriculture against biotic and abiotic stresses and achieve sustainability to meet the needs of the ever-growing human population. In this article covered the leveraging AI algorithms and RS data, and how these technologies enable real time monitoring, early detection, and accurate forecasting of pest outbreaks. Furthermore, discussed how these approaches allows for more precise, targeted pest control interventions, reducing the reliance on broad spectrum pesticides and minimizing environmental impact. Despite challenges in data quality and technology accessibility, the integration of AI and RS holds significant potential in revolutionizing pest management.

KEYWORDS

agriculture, remote sensing, artificial intelligence, pest monitoring, management, economic loss

1 Introduction

In every field, whether rocket science or agriculture, there is a constant search for more convenient and intelligent tools to automate various processes and this can only be achieved through machines' ability to easily understand human intelligence. Agriculture, which involves the cultivation of food crops, is a labor-intensive yet essential occupation that sustains life on planet Earth. Furthermore, the world is facing an alarming situation due to the increasing population, climate change, depletion of natural resources, a reduction in farm workers, and the emergence of novel human diseases such as the COVID-19 pandemic. There are challenges in managing agricultural field to meet the necessary food demand and achieve the second sustainable development goal (SDG-2), which aims for zero hunger (Martos et al., 2021). During the last decade, there has been significant technological advancement in many industries worldwide and the European Commission has designated the year 2021 as the beginning of industrial innovation, referred to as Industry 5.0 (Martos et al., 2021). The use of wooden and metal farming tools was categorized under the first two phases of agricultural revolutions. During the third and fourth phases, significant technological advancements such as robotics, machinery, telecommunication systems, and decoding of genetic codes were the major achievements. The fifth agricultural industrial revolution involves current technological interventions, such as artificial intelligence (AI), machine learning (ML), and remote sensing (RS) (Martos et al., 2021). AI and RS tools now make it easier to manage agricultural fields, by improving methods for monitoring crop yield and health. This involves the timely management of insect pests, pathogens, and weeds, as well as efficient irrigation, nutrient supply, and soil fertility management (Kim et al., 2008).

Agriculture-linked robots are designed to facilitate the effective integration of AI in the agricultural sector, providing potential solutions to various challenges. With the help of AI, farmers can use chatbots as their virtual guides to receive timely advice and recommendations on various aspects of crop management. The use of unmanned aerial vehicles (UAVs) or drones, assisted by global positioning system (GPS), can be remotely controlled, replacing manual labor in various agricultural tasks such as crop health assessment, irrigation scheduling, herbicide application, weed and pest identification, and forecasting (Mogili and Deepak, 2018; Ahirwar et al., 2019). AI is constantly evolving in new directions as a result of advancements in computational techniques and along with many other sectors of the economy, agriculture has also begun to benefit from AI. It has made significant advancements in agriculture, such as in weeding, irrigation management, disease, and insect pest monitoring and management. It also suggests suitable sowing and harvest dates for specific crops and facilitates the sale of crops in the appropriate marketplace at the optimal time (Javaid et al., 2023).

AI has significantly assisted farmers in implementing various technologies, and the prior analysis of farm activities ensure a guaranteed crop quantity and quality (Vijayakumar and Balakrishnan, 2021; Subeesh and Mehta, 2021). AI can address numerous challenges in agriculture, such as labor shortages, by offering solutions like auto-driven tractors, smart irrigation systems, fertilization and pesticide applicators, and AI-based harvesting robots (Wongchai et al., 2022; Bu and Wang, 2019). Numerous datasets on temperature, soil moisture, and other resources required for optimal crop growth are utilized by AI and ML models to gain real-time insights into, when to plant, what to plant, when to fertilize, and when to harvest(Singh et al., 2022; Sabrina et al., 2022). AI algorithms can be useful in detecting insects of various sizes and feeding habits and promptly notify farmers about the invasion of insect pests in their fields through smartphones, enabling them to take timely actions to prevent crop losses. In this review, we explore the application AI and RS in managing insect pests. We analyze the success and challenges associated with utilizing these technologies in pest management. Additionally, we provide a comprehensive overview of AI and RS as potent tools for achieving sustainable and effective pest control in agricultural and ecological contexts.

2 Remote sensing (RS)

Currently, there has been a shift in the strategy, for identifying, detecting, classifying, and managing various insect pests and disease-causing pathogens from traditional methods to the use of innovative information-gathering tools and techniques such as remote sensors, geographic information systems (GIS), and GPS. RS is the art and science of gathering information about an object, area, or phenomenon through the analysis of data obtained by a device that does not make physical contact with the object under investigation (Lillesand et al., 2015). According to De Jong and Van der Meer (2007), the remote sensing process (Figure 1) consists of several stages, each of which plays a crucial role in acquiring and utilizing remotely sensed data. RS is a broad term used to encompass various technologies such as satellites, GIS, Internet of Things (IoT), cloud computing, sensors, Decision Support System (DSS), and autonomous robots. The process of RS is mainly influenced by the characteristics of electromagnetic radiation (EMR), which is used to collect data and interpret it. Based on the source of EMR; RS is categorized into two types: passive remote sensing and active remote sensing. Active remote sensors have their source of radiation, such as RADAR (Radio Detection and Ranging) and operates day and night as it does not depend on light. However, passive remote sensors do not have their radiation source, but rather depend on external sources to illuminate the object, therefore, work only during daytime.

The atmosphere plays a crucial role in the process of RS, as EMR passes through it before reaching the target object on the Earth's surface. When radiation interacts with gas molecules or small particles, such as aerosols, it can scatter in various directions, including backwards to the sensor. When EMR such as visible light, infrared, or microwave, from a remote sensing platform, such as a satellite or a drone, reaches the target object, several interactions may occur. These interactions are mainly determined by the inherent properties of the object and the characteristics of the incoming radiation. The three most common interactions are absorption, emission, and reflection. RS instruments are designed to detect and measure the reflected radiation and by analyzing the reflected radiation at different wavelengths, researchers can extract valuable information about the target's characteristics and make informed decisions for a wide range of applications (Pellikka and Rees, 2009). After the interaction between incoming radiation and the target object, a sensor (such as digital cameras, electromagnetic scanners, radar systems, multispectral scanners, and hyperspectral scanners) collects and records the data in the form of reflected or emitted electromagnetic radiation (Yang and Everitt, 2011). Radiation can be stored in either analog form (like aerial photographs) or digital formats (like signal values) stored on a magnetic CD or DVD. After recording the EMR

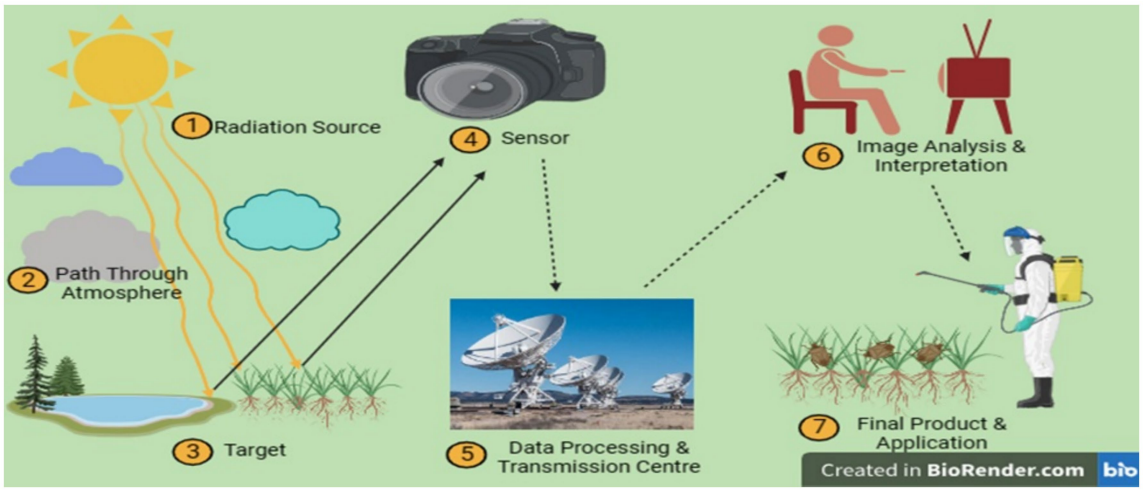

FIGURE 1
Schematic representation of different stages of the remote sensing process.

from the target objects using a remote sensor, the data is transmitted in electronic form to a receiving station for further processing. For image analysis, various software options are available, such as Imagga, Hive, and Anyline. These programs automatically apply advanced algorithms to input images to extract information from them. Three basic groups of information interpreted while observing the image, include the assignment of different class labels to separate pixels in an image, estimation of properties of the target object, and monitoring the changes in target properties over time (Jensen, 2007). The final output of a remote sensing process can sometimes be used as input for further examination, such as in GIS. At the same time; this information can be used in conjunction with other types of data for various research purposes.

Integrated pest management (IPM) is a comprehensive approach to controlling pests to reduce the use of pesticides on crops and soil and promote an eco-friendly environment. However, implementing IPM requires ongoing monitoring and surveillance of crops, which can be a challenging task. Therefore, AI can be utilized to address this issue (Murmu et al., 2022). AI can analyze large sets of data and draw inferences based on previous reports, enabling farmers to implement timely pest management practices (Katiyar, 2022). Numerous studies have been conducted which highlights the effectiveness of RS and AI in insect pest management. Prabhakar et al. (2012) demonstrated the use of satellite-based RS to monitor and predict the spread of a major insect pest, the fall armyworm (*Spodoptera frugiperda*), in maize fields. In another study, Smith et al. (2020) demonstrated how drones equipped with multispectral sensors were used to assess pest damage in vineyards, by analyzing the spectral signatures of the vines. The advancements in the RS process help to provide synoptic data of high precision at a very fast pace, even from inaccessible areas (Malinowski et al., 2015). The timeline illustrates the brief history (Figure 2) of advancements in RS technology.

2.1 Remote sensing platforms

The platform on which remote sensors are mounted, i.e., RS platforms, are categorized into three types, based on the elevation at which the sensors are placed from the earth's surface: ground-based, airborne, and spaceborne (Johnson et al., 2001). Ground-based platforms are positioned near or on the Earth's surface to examine specific characteristics of the environment, plants, or objects of interest and are particularly useful for conducting detailed and localized studies, focusing on individual plants or small patches of vegetation. Airborne platforms refer to aircraft used to carry RS instruments for aerial surveys. These platforms offer the advantage of operating at lower altitudes compared to satellites, which allows for higher spatial resolution and targeted data acquisition. Different types of tools used for aerial survey missions include airplanes, helicopters, and UAVs. Spaceborne platforms refer to sensors and instruments placed on satellites (geostationary satellites and sun-synchronous satellites) orbiting the Earth and capturing data from space, providing global and repetitive coverage of the Earth's surface. The data collected by these satellites is instrumental in various applications, including weather forecasting, climate monitoring, land cover mapping, agriculture, and disaster response (Roy et al., 2022). The most recent example of spaceborne RS is India's Chandrayaan-3 lander, Vikram, which softly landed on the South Pole of the moon on August 23, 2023. The rover, Pragyan, has conducted studies on the moon's atmosphere and confirmed the presence of oxygen and other mineral elements (Kanu et al., 2024).

3 Applications of remote sensing and artificial intelligence in agriculture

Modern agriculture and food production, aimed at supporting the ever-growing global population, are constantly challenged by the impact of global climate change, which in turn increases the pressure of abiotic and biotic stresses on crop production, leading to an imbalance in economic and environmental sustainability (Bakala et al., 2020). For this, AI and RS seem to be a ray of hope, as can quantify phenotypic data of crops using various tools (Jung et al., 2021). In addition to their applications in other fields, RS and AI play a vital role in agricultural and horticultural fields (Figure 3). The use of AI in the form of Unmanned Aircraft Systems (UAS) has provided

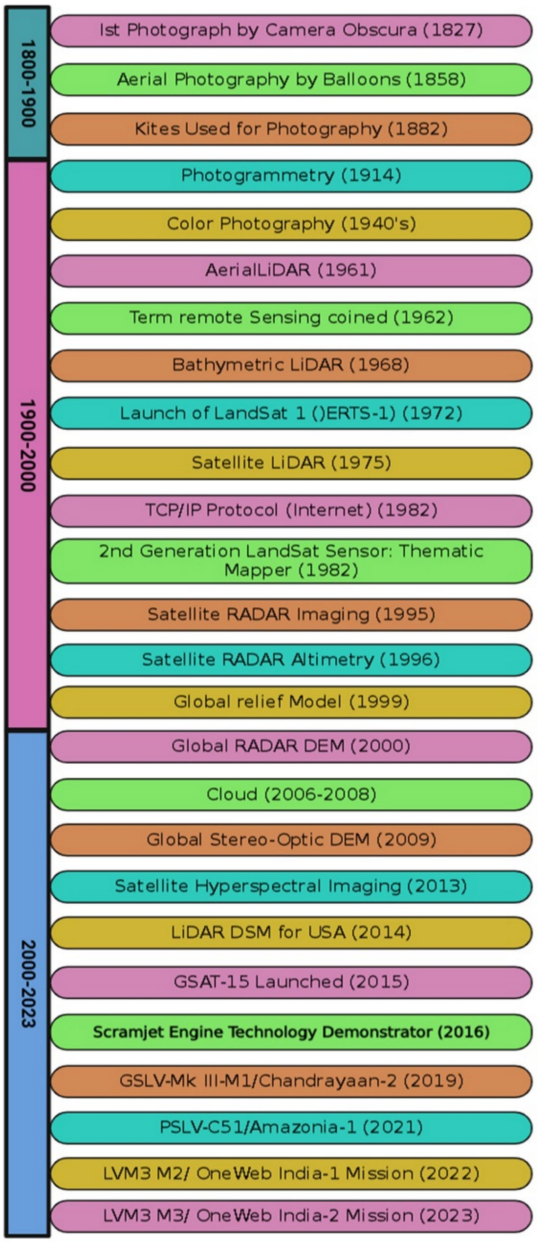

FIGURE 2
Timeline showing the history of remote sensing.

an unparalleled advantage in conducting advanced data analysis for the management of agricultural fields, thereby increasing the overall resilience and efficiency of the system (Coble et al., 2018). Various companies, such as AGEYE Technologies, aWhere, Blue Reiver Technology, FarmShots, Fasal, Harvest CROO Robotics, HelioPas AI, Hortau Inc., Ibex Automation, PEAT, Root AI, Trace Genomics, and VineView, have developed different AI-based tools for agriculture, performing various functions like predicting weather and its correlation with pest population dynamics, managing weed systems, picking and packaging fruits and vegetables, and monitoring irrigation and fertilization (Dutta et al., 2014). Remote sensing as a highly useful technology, allows continuous gathering of information about a crop without causing damage and at a very low cost (Barbedo, 2019). Images are captured by remote sensors, and with the assistance of deep learning machine models (DLMM), these images are classified. Based on the input image data, an interpretation is made to determine whether the plant is healthy or diseased. Convolutional neural networks (CNNs), a subset of AI was used to identify the disease-causing pathogen in plants by analyzing input data of lesions and spots on leaf images (Barbedo, 2019).

3.1 Crop identification

The RS and AI play an important role in identifying and classifying crops, by understanding the spectral characteristics of different vegetation cover, especially when the crops being studied have similar characteristics and are difficult to distinguish. As compared to traditional crop identification methods, AI offers a significant advantage by promoting greater accuracy and efficiency through the ability to analyze large datapools in less time, detect subtle variations in plant features and monitoring crops in real time leading to better decision making and optimized resource allocation to different crops. With the assistance of optical RS, Low and Duveiller (2014) defined the spatial resolution requirements for identifying a specific crop and reported no common pixel size (one-size-fits-all) for identifying every crop. However, the pixel size and purity required for crop identification vary from crop to crop and from one landscape to another. Also, not every type of sensor is suitable for identifying the majority of crops. For example, MODIS (250 meters) can identify the majority of crops in a particular field, while Landsat (30 meters) provides object-based classification. Zhang et al. (2016) used two consumer-grade cameras, namely the Red, Green, and Blue (RGB) camera, and a modified Near-Infrared (NIR) camera, mounted on an airborne RS platform for crop identification in Texas. The images captured by NIR cameras provide more effective classification results than those captured by RGB cameras and other non-spectral features.

AI-based crop identification is now readily available for identifying different field crops by analyzing images with the help of CNNs, which can identify, classify, and detect different objects based on image features (Ranjithkumar et al., 2021). Ibatullin et al. (2022) utilized RS and AI to monitor various crops, achieving an accuracy of 85–95% in crop identification using satellites such as Sentinel-1 and Sentinel-2. The genus *Ficus* comprises nearly 1,000 plant species worldwide, making it challenging for a common man to identify them manually with 100% accuracy. In this context, Kho et al. (2017) developed a baseline automated system using an artificial neural network (ANN) and support vector machine (SVM) to identify and classify crop images of three *Ficus* species: *F. benjamina*, *F. pellucidopunctata*, and *F. sumatrana* with an accuracy level of approximately 83%.

3.2 Crop acreage estimation

The demand for various agricultural and horticultural crops fluctuates over time due to unreliable prices or market values. Therefore, it is important to accurately determine the area needed for growing specific crops by market planning and export opportunities. Estimating crop area to achieve a desirable yield for feeding a large population is one of the most challenging tasks faced by policymakers. In the current scenario, satellite-based RS, GIS, and ML have estimated

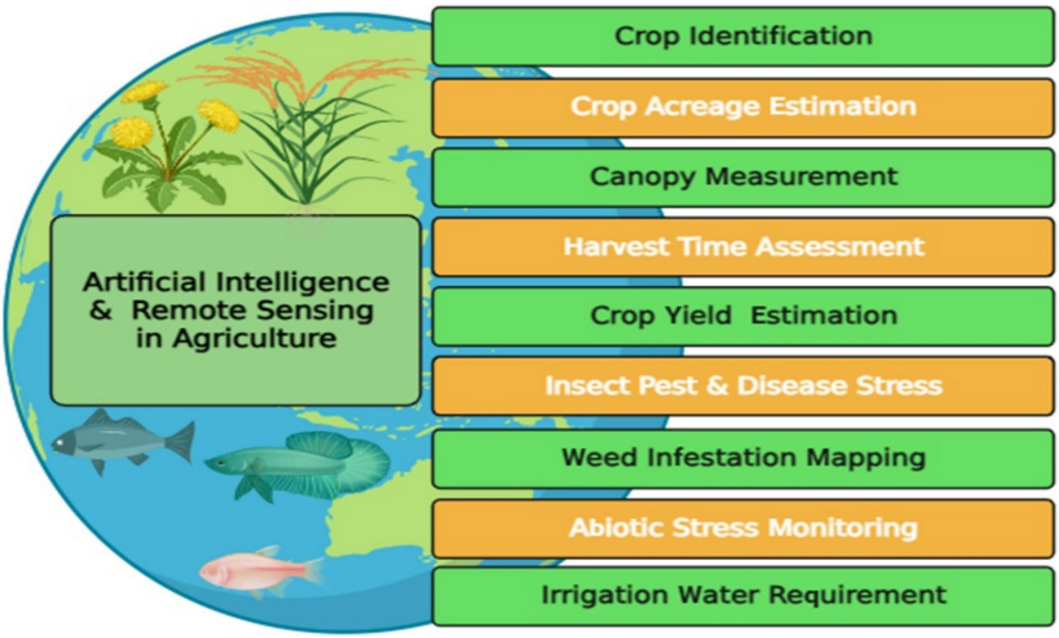

FIGURE 3
Role of artificial intelligence and remote sensing in agriculture.

crop acreage over vast geographic areas. Meraj et al. (2022) estimated the wheat crop acreage and its yield in Uttar Pradesh,India using satellite-acquired data and the Carnegie-Ames-Stanford Approach (CASA) model. Another satellite, SPOT-5 multispectral imagery data is used to identify the crop type and estimate the crop area simultaneously (Yang et al., 2006). Kshetrimayum et al. (2024) used integration of ML algorithms and Sentinel-1A satellite SAR data to know the pearl millet crop acreage in India, to predict the yield of pearl millet in Agra and Firozabad.

3.3 Canopy measurement

Canopy structure and volume are important factors in crops, particularly for the precise application of fertilizers, pesticides, and irrigation in horticultural crops (Sharma et al., 2022). According to Trout et al. (2008), remote sensors could be used to assess the canopy characteristics in horticultural crops by quantifying the photosynthetically active radiation (PAR) absorbed by the plant canopy. Ayyalasomayajula et al. (2009) measured the tree canopy volume and height of an automated citrus tree with 85% accuracy using oblique or orthoimages. The measurement of temperature at the canopy level is a crucial indicator for detecting water deficit in crop plants. One of the methods used to assess crop water deficit is thermography, which involves remotely measuring the temperature at the crop canopy. Giménez-Gallego et al. (2021)developed an automatic sensor for measuring crop canopy temperature in almonds using a low-cost thermal camera and AI-based image segmentation models. To analyze the data acquired by UAVs, a user-friendly application called Agroview was developed. This cloud and AI-based application can count and locate the position of plants in the field, differentiate between dead and live plants, measure various characteristics of the canopy, and create disease and pest stress maps. The Agroview app was used by Ampatzidis et al. (2020) to assess the phenotypic characteristics of citrus fields, including tree height, canopy size, and pest detection in both normal and high-density plantations.

3.4 Harvest time assessment

Due to the universal shift in market economies, the need for accurate and precise information has become crucial for strategic decision-making at all levels, including producers, resource management, market levels, and financing. Due to the predictive nature of RS, farmers can now depend on it to obtain information about the factors that affect the planting and harvesting seasons of a crop. The combination of conventional imaging techniques, spectroscopy, and hyperspectral imaging systems can be used to obtain spatial and spectral data from fruits, vegetables, and other crops to determine crucial quality parameters (Singh et al., 2009). According to Hahn (2004), tomatoes can be classified based on their firmness with 90%precision as hard, soft, and very soft using remote sensors. Temporal RIS-AWiFS data was utilized to determine the optimal harvesting dates in apple orchards. Previously, the prediction of harvest time relied on common statistical procedures, which often resulted in errors. To address this issue, a novel harvest time prediction model based on LSTM (Long Short-Term Memory) AI has been developed using real-time production and weather data (Liu et al., 2022). There has been integration of AI with UAVs to make a conceptual design of olive harvesting drones, in order to replace the traditional time consuming methods of olive harvesting and gathering, which was more labor intensive and a hectic job (Khan et al., 2024). As date fruit (*Phoenix dactylifera* L.) is having a diverse group of genotypes, varying in external features as well as biochemical

composition, this makes it difficult to assess proper harvesting time and post harvest handling of all genotypes separately in order to make it more market consuming. To deal with this problem, nowadays AI and computer vision technology is being put into use and considered to be accurate, non destructive, fast and efficient budding technology (Noutfia and Ropelewska, 2024). Nowadays, potato harvesting time is predicted by aome improved AI models like ResNet-59, which gives more precision and can rationalize the distribution of important resources, minimize waste and improve food security (Abdelhamid et al., 2024). AI- driven harvest time assessment of a crop is more impactful than traditional manual judging, because it gives more precision in ensuring the crop is harvested at peak period by keeping in view all the factors like even ripening of crop, market information, shelf life and waste reduction. By identifying the precise harvest window, AI minimizes the risk of uneven ripening (overripe/underripe), which leads to better quality produce and less post harvest losses, thus maintaining economic stability of people associated with farming. In contrast, traditional methods only rely on visual observations by farmers, which are often inaccurate due to factors like inconsist and uneven monitoring of large areas and weather variability.

3.5 Crop yield estimation

RS approach can be used by growers to assess the final yield of a particular crop and calculate the variations among different fields growing the same crop. Vegetation indices (VI's) based on spectral bands of multispectral imagery can be used, with the most widely used VIs being the NIR/Red ratio (Jordan, 1969) and NDVI (Normalized Difference Vegetation Index) (Rouse et al., 1973). Zaman et al. (2006) utilized an automatic ultrasonic system and a remote sensing-based yield monitoring system and reported a linear correlation between tree size and fruit yield. One more aspect of remote sensing, namely thermal imaging, has been utilized to estimate the number of fruits in orchards and groves. This is based on the principle that there is a temperature difference between the fruit and the surrounding environment. Crop yield depends on the interaction of various plant and environmental factors, such as temperature, rainfall, plant type, germination percentage, flowering percentage, and pesticide application. Therefore, it is crucial to estimate the impact of each factor on crop yield. Al-Adhaileh and Aldhyani (2022) employed the ANN model in Saudi Arabia to accurately predict crop yields using available data sets for various factors influencing potato, rice, sorghum, and wheat yields. Similarly, Babaee et al. (2021) used ANN to estimate the yield of rice crops. In a similar context, Hara et al. (2021) emphasized the importance of selecting independent variables to predict yield using artificial neural networks in conjunction with remotely sensed data. There has been a major integration between AI and data of Sentinel-2 satellite in precision agriculture, particularly for yield assessment in different crops like maize, wheat, rice (Aslan et al., 2024). Vegetation indices are derived from the images collected by satellite and then put to use for predicting yield with high accuracy by the integration of AI algorithms including ML and deep learning models. For validation of AI-based yield prediction models, common metrics used are mean absolute error (MAE), mean squared error (MSE), root mean squared error (RMSE), R-squared (R^2), and these validation metrics assess the accuracy and precision of data acquire by different models.

3.6 Stress due to pests and diseases

Identification of various insect pests and diseases on farmland and the collection of data on effective pest and disease control mechanisms are now being carried out using RS and AI. RS and AI/ML techniques are highly effective in measuring changes in plant biomass, pigments, coloration, and plant vigour during abiotic stress in crop plants (Pinter et al., 2003). Small et al. (2015)revealed that utilizing historical weather data could be beneficial in predicting potential disease outbreaks of late blight in tomatoes and potatoes. They proposed the development of a web-based DSS. RS can sense physical and physiological changes such as chlorosis, cell death, stunted growth, wilting, and rolling of leaves in plants. Fluorescence spectroscopy (Lins et al., 2009),fluorescence imaging (Moshou et al., 2005) and NIR Spectroscopy were used to detect fire blight disease in pear plants that showed no symptoms (Spinelli et al., 2006). A relatively new technique, electronic nose systems, is used for identifying plant diseases. The E-nose and fluorescence imaging has been innovatively used for assessing stress in plants caused due to insect pests and diseases, by detecting subtle changes in volatile organic compounds (VOCs) released by the plant through release of odour and changes in plant tissue fluorescence pattern. This leads to early detection of insect pests and diseases before any visible symptoms. E- noses were used for early identification and differentiation between fire blight and blossom blight disease in apple trees under laboratory conditions (Fuentes et al., 2018). A field experiment conducted by Lins et al. (2009) aimed to distinguish leaves into citrus canker-attacked leaves and chlorosis-infected healthy leaves. The SVM outperforms other ML techniques in predicting the occurrence and abundance of plant diseases and pests. Bhatia et al. (2020) utilized a hybrid approach, combining SVM and logistic regression algorithms, to detect powdery mildew disease in tomatoes. Similarly, Xiao et al. (2019) discussed the use of LSTM networks to correlate weather data with population dynamics and pest attacks of insects. An interesting smartphone application has been devised for on time detection and identification of pests and diseases in order to decrease substantial economic losses. This application is using python based REST API, PostgreSQL and Keycloak and is tested in field against various pests like *Tuta absoluta* in tomato (Christakakis et al., 2024).

3.7 Weed infestation mapping

RS techniques prove to be a more economical and quicker method for mapping weeds than traditional ground survey procedures, especially in large geographical areas. Weeds were categorized as broad-leaved and grass-weeds, according to their texture to develop targeted selective herbicides, using Gabour wavelets and neural networks. Digital color photographs were used to identify bare spots in blueberry fields (Zhang et al., 2010). Similarly, Backes and Jacobi (2006) detected weeds in sugarbeet fields using high-resolution satellite images from the QuickBird satellite. They were able to identify an extensive and dense infestation of Canadian thistle as a weed. Costello et al. (2022)developed a new method for detecting and mapping Parthenium-infested areas using RGB and hyperspectral imagery, supplemented by artificial intelligence.

The indiscriminate use of herbicides worldwide has led to herbicide resistance in various weeds and to manage this, advanced

strategies based on AI are required. Several AI-based tools are commercially available for weed management, including RS, robotics, and spectral analysis. However, despite the high potential of AI-based tools in managing herbicidal resistance in weeds, they are not used on a large scale (Ghatrehsamani et al., 2023). The accurate detection and identification of weed categories are necessary for targeted management. Nowadays, AI and UAVs are commonly used to manage weeds in rice fields (Ahmad et al., 2023). Su (2020) used drones equipped with hyperspectral cameras to identify weed species by capturing numerous images of different spectral bands. Machleb et al. (2020) demonstrated the use of autonomous mobile robots for monitoring, detecting various weeds, mapping weeds, and efficiently managing them. Similarly, various ML algorithms such as Random Forest Classifier (RFC), SVM, and CNN help classify different types of digital images to detect weeds in various crops like rice (Kamath et al., 2020).

3.8 Abiotic stress monitoring

Crop plants are generally affected by several environmental factors, such as light, temperature, and water, which result in abiotic stresses like drought, salinity, acidity, and heat. Monitoring abiotic stress in plants is crucial for effective agricultural management and assessment of crop health. RS techniques provide valuable tools for detecting and diagnosing various types of abiotic stresses. One common indicator of abiotic stress in plants is the reduction in chlorophyll content. When plants experience stress, such as water scarcity or mineral toxicity, their chlorophyll content degrades, leading to changes in their spectral reflectance properties.

A new approach has been developed to sense the stress level, particularly in the case of tree and row crops in which a shaded portion of tree canopy is taken into consideration (Jones et al., 2002). However, it has a limitation where stomata usually remain closed in the shade areas and there is less temperature variation. In the same way, the availability of surface water can be measured with the help of reflectance patterns in plant canopies with or without the presence of surface water (Pinter et al., 2003).

By combining spectral reflectance data with advanced data analysis techniques, such as vegetation indices (VIs) and ML algorithms, researchers can quantitatively assess stress levels and monitor the health of crops and vegetation over time, helping inthe early detection of abiotic stress, enabling timely interventions and better crop management practices. In addition, AI and ML-based algorithms can be used to enhance crop yield under different stress conditions. Further, the use of ML in QTL (quantitative trait loci) mining will help in identifying various genetic factors of stress tolerance in legumes (Singh et al., 2021). Different VIs used for analysing stress level particularly water stress in plants include NDVI (Karnieli et al., 2010), PRI (Photochemical Reflectance Index) (Ryu et al., 2021) and MSI (Mositure Stress Index) (Hunt et al., 1987). NDVI can be used to optimize irrigation scheduling by identifying the drought prone areas of field, thereby helpful in precise water scheduling of crops. PRI measures how efficiently a crop utilizes incoming radiations and assesses water stress in plant and how CO_2 is absorbed by plants. MSI works on the principle of measuring the amount of water present in leaves of plants and is used to analyze canopy stress, fire hazard conditions, ecosystem physiology and predict productivity. Navarro et al. (2022) utilized the leaf image hyperspectral data along with an AI model to reveal the etiological cause of different stresses. An ANN was used to read the reflectance pattern of visible and near-infrared region wavelengths which were the main cause of stress. Advancement in field of AI has led to development of high-throughput gadgets, which help to overcome the biotic and abiotic stresses, and provide big data sets like transportable array for remotely sensed agriculture and phenotyping reference platform (TERRA-REF) forecasts stress at an early as possible (Gou et al., 2024).

3.9 Irrigation water requirement

RS can detect changes in the water level of a field, whether it is experiencing water-logged or drought conditions, with the help of variable rate irrigation technology such as the centre pivot system (McDowell, 2017). A higher-resolution land data assimilation system was utilized as a computational tool to develop soil moisture and temperature maps. The system aimed to provide information about the amount of soil moisture present at a specific depth of land and soil temperature at various depths, including the rhizosphere (Das et al., 2017). There is a dire need to utilize AI and ML models to estimate the water requirement for crop irrigation. Mohammed et al. (2023) researched implementing AI-based models to predict the optimal water requirements for sensor-based micro-irrigation systems run by solar photovoltaic systems. FourML algorithms — LR, SVR, SLTM neural network, and extreme gradient boosting (XGBoost) were utilized and validated for predicting water requirements, and among all, LSTM and XGBoost were more accurate than SVR and LR in predicting irrigation requirements. Under limited water availability, the automatic irrigation decision support system can be helpful in intelligently scheduling irrigation to improve water use efficiency and enhance crop productivity. Katimbo et al. (2023) evaluated the performance of various AI-based algorithms and models for predicting crop evapotranspiration and crop water stress index. They achieved this by measuring soil moisture, canopy temperature, and NDVI from irrigated maize plants. Based on overall performance and scores, CatBoost and Stacked Regression were identified as the best models for calculating crop water stress index and crop evapotranspiration, respectively. To cope up with the problem of water scarcity in legume farming, in Uttar Pradesh, India AI integration was done with precision farming to raise pea crop and AI-based precision irrigation offered a significant edge in allocating water, enhancing crop production, decreasing greenhouse gas emmission and reducing cultivation cost (Kim and AlZubi, 2024).

4 Applications of remote sensing and artificial intelligence in insect pest management

The wavelength of electromagnetic radiation (EMR) changes based on its interaction with the plant surface. Therefore, the condition of plant vigour and health may significantly affect the reflectance pattern of leaves (Luo et al., 2013). The use of RS to assess plant defoliation caused by insect pests, chlorosis, and necrosis has been conducted by comparing spectral responses (Franklin, 2001). Several studies have been conducted on the use of RS, AI, and ML

TABLE 1 Application of remote sensing techniques in insect pest research.

Insect	Crop	Research parameter	Remote sensing technology used	Reference
Fruitfly	-	Species identification	RGB camera	Faria et al. (2014)
Stored grain pests	Wheat	Species identification	Proximal RS and hyperspectral reflectance profile	Singh et al. (2010)
Fruitfly	-	Species identification	Proximal RS	Dowell and Ballard (2012)
Tobacco bud worm and corn ear worm	Cotton	Species identification	Proximal RS	Jia et al. (2007)
Ants	-	Cryptic Species identification	Imaging Spectroscopy	Klarica et al. (2011)
Evacanthine Leafhopper	Jujubes	Species classification	Hyperspectral Imaging	Wang et al. (2016)
Vespa vellutina	-	Flight monitoring	Harmonic RADAR	Maggiora et al. (2019)
Leafhopper	Cotton	Infestation	Hyperspectral RS	Prabhakar et al. (2012)
Leaf miner	Tomato	Damage and incidence	Leaf reflectance spectroscopy	Xu et al. (2007)
Cyst nematode	Beet root	Mapping of symptoms	Combined use of remote sensing and GIS technique	Hillnhütter et al. (2011)
Cotton leaf worm	Cotton	Management timing	Satellite RS	Yones et al. (2012)
Mite	Cotton	Early infestation detection	Multispectral RS	Fitzgerald (2000)
Desert locust	-	Habitat detection and breeding zones	Remote sensing and GIS technique	Latchininsky and Sivanpillai (2010)
Brown plant hopper (BPH)	Rice	Changes in spectral characteristics due to brown plant hopper	Hyperspectral RS	Yang et al. (2007)
Mountain pine beetle	Pine	Infestation dynamics	NDMI Multispectral (Landsat) RS	Goodwin et al. (2008)
Aphid (*Diuraphisnoxia*)	Wheat	Quantification of stress level	Multispectral RS	Backoulou et al. (2011)

TABLE 2 Applications of remote sensing techniques in plant disease research.

Disease	Crop	Research parameter	Remote sensing technology used	Reference
Scald	Apple	Detection of scald induced browning in stored apples	Hyperspectral RS	Chivkunova et al. (2001)
Yellow rust	Wheat	Early disease detection	Hyperspectral RS	Bravo et al. (2003)
Orange rust	Sugarcane	Detection of disease	DWSI Hyperspectral (Hyperion) RS	Apan et al. (2004)
Powdery mildew and take all disease	Wheat	Identification of diseases caused by *Erysiphe graminis* and *Gaeumannomyces graminis*	Hyperspectral RS	Graeff et al. (2006)
Soft rot	Broccoli	Early detection of disease	Hyperspectral RS	Datt (2006)
Late leaf spot	Peanut	Change in spectral characteristics	Multispectral RS	Prabhakar et al. (2006)
Leaf rust	Wheat	Disease detection and identification	Hyperspectral (HyMap) RS	Franke and Menz (2007)
Bacterial leaf blight	Rice	Disease severity	MLR Hyperspectral RS	Yang (2010)
Wheat streak mosaic	Wheat	Disease severity	Multispectral (Landsat TM) RS	Meraj et al. (2022)
Stem rot	Oil Palm	Mapping and identification	Multispectral (QuickBird) RS	Santoso et al. (2011)

techniques for insect species identification, assessment of incidence and severity, mapping of new insect habitats and breeding areas, and identification of disease symptoms (Tables 1–3 and Figure 4).

AI algorithms have played a crucial role in identifying diseases and pests that affect cotton, by automatically detecting crop symptoms, environmental conditions, and physical characteristics associated with pests or diseases. In a study, Gopinath et al. (2022) introduced an automated big data framework specifically designed for classifying plant leaf diseases by employing a Convolutional Recurrent Neural Network Classifier (CRNN) algorithm to successfully differentiate

TABLE 3 Examples of application of artificial intelligence and machine learning in insect research.

Insect	Crop	Research parameter	Reference
Major pests	Coffee	Detection and identification	Lee and Tardaguila (2023)
Diamond back moth	Cabbage	Abundance forecasting	Kaur et al. (2022)
Major pests	Tomato	Prediction of pest outbreak	Holzinger et al. (2023)
Thrips	Tomato	Management	González et al. (2022)
Whitefly	Tomato	Life stages assessment and identification	Lutz and Coradi (2022)
Fruit fly	_	Species detection and identification	Murmu et al. (2022)
Aphid	Soybean	Population dynamics	Murmu et al. (2022)
Insect pests	-	Pest classification	Xia et al. (2023)
Insect pests	-	Insect activity	Rydhmer et al. (2022)
Whitefly	Cotton	detect crop symptoms, environmental conditions, and physical characteristics	Toscano-Miranda et al. (2022)
Aphid		Pest forecasting	Bourhis et al. (2021)
Brinjal shoot and fruit borer, Epilachna beetle	Brinjal	Detection, identification, and classification	Saikumar et al. (2023)
Aphid	-	Monitoring and forecasting	Batz et al. (2023)
Riptortuspedestris	Soyabean	Detection and forecasting	Park et al. (2023)
Locust	-	Monitoring and management	Klein et al. (2021)
Stored grain pest	Wheat	Grain damage	Sabanci (2020)

between healthy and diseased leaves across diverse plant species, including bananas, peppers, potatoes, and tomatoes. Sujithra and Ukrit (2022) employed a range of deep neural networks, such as CNN, Radial Basis Neural Network (RBNN), and Feed-Forward Neural Network (FFNN), to diagnose leaf diseases in banana and sugarcane. The workflow process of various AI models, along with deep learning algorithms, for making effective decisions in insect pest management is illustrated in Figure 5. UAV-based pest detection approach utilizes Unmanned Aerial Vehicles aided with various sensors and imaging technologies (RGB cameras, multispectral cameras, infrared thermal cameras, hyperspectral cameras) for identification of insect pests in crops. This approach leads to early detection of pests and judicious application of pesticides for their management keeping intact the ecological balance. The IoT based UAVs (Yadav et al., 2024) focuses on AI mechanism and python programming paradigm for sending the images of different rice pests to Imagga Cloud and provides valuable and timely information for necessary action (Bhoi et al., 2021).

4.1 Insect taxonomy and systematics

The concern about the invasion of non-native pest species is growing day by day, creating a biosecurity threat. This occurs due to activities such as tourism, inter-border trade, and global climate change (Hulme, 2009). Therefore, there is a need for strict quarantine and inspection approaches to prevent the spread of non-native invasive pests. To reduce inspection costs and processing time, automatic inspection and detection of invasive pest species in commodities, proximal RS is an effective approach. With the help of reflectance data gathered by an RGB camera, the wings and aculeus of three closely resembling fruit fly species were analyzed and three different fruit fly species—*Anastrepha fraterculus*, *A. oblique*, and *A. sororcula* were identified (Faria et al., 2014). Using a NIR and hyperspectral imaging system, researchers were able to differentiate healthy wheat kernels from insect-damaged ones in storage, by employing proximal RS and hyperspectral reflectance profiles (Singh et al., 2010). Using the same technique, two fruit fly species (Dowell and Ballard, 2012), tobacco budworm, and corn earworm (Jia et al., 2007) were also identified. Similarly, Klarica et al. (2011) used imaging spectroscopy to identify two cryptic ant species (*Tetramorium caespitum* and *T. impurum*). Wang et al. (2016) utilized a hyperspectral imaging of 37 spectral bands between 41.1 to 87 nm for insect classification, incorporating mitochondrial DNA analysis and morphometry and identified seven species of the Evacanthine leafhopper genus Bundera.

Despite species acting as core units for all research, morphologically identified species can be serving as ill found entities in organisms where intricate evolutionary processes like hybridization, polyploidy and mutation occur. So, integration of taxonomy with AI under a unified concept of species can enable data integration and automatic feature identification that reduce subjectivity of species delimitation (Karbstein et al., 2024). A ML algorithm was developed to identify the most common insect pests infesting coffee fields by analyzing images and was found to be more effective than traditional methods for detecting and identifying pests (Lee and Tardaguila, 2023). Deep learning, a branch of ML, was used to identify and detect the abundance of whiteflies in tomatoes by recognizing whiteflies at various stages (Lutz and Coradi, 2022). Saikumar et al. (2023)conducted experiments on the detection and classification of insect pests in brinjal using artificial intelligence. They utilized Python software with the Keras and Tensorflow frameworks, and the model employed was CNN-VGG-16. A total of 204 images of insect pests captured throughout the study were used as input data for the automatic identification and classification of insect pests like Brinjal shoot and fruit borers and Epilachna beetle (Saikumar et al., 2023).

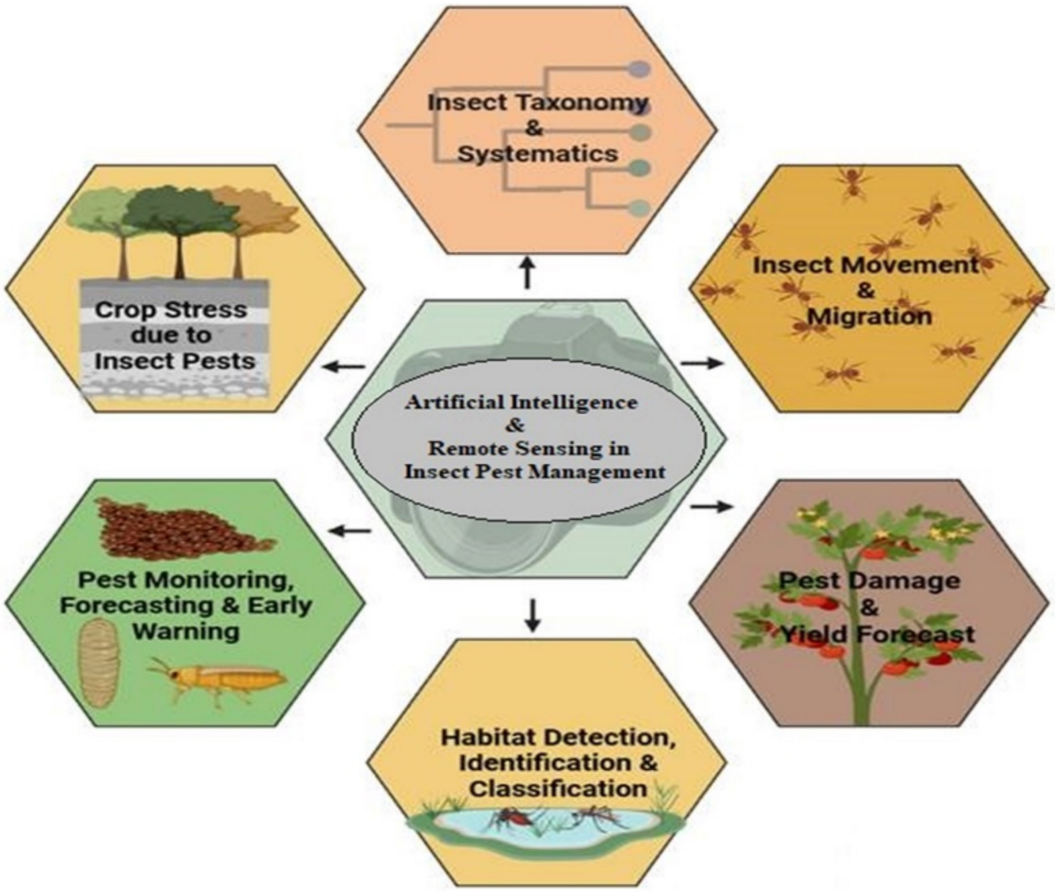

FIGURE 4
Application of artificial intelligence and remote sensing in insect pest management.

4.2 Insect movement and migration

The monitoring of migrant insect species can be conducted using entomological RADAR. RS technology can automatically monitor the height, horizontal speed, direction, orientation, body mass, and shape of insects. Recent advancements in RS technology have resulted in the development of innovative harmonic RADAR systems that are effective in tracking specific insect species, such as *Vespa vellutina*, flying at high altitudes of 500 meters (Maggiora et al., 2019). AI-based pest surveillance and monitoring systems use cameras and sensors for data collection and can accurately predict the infestation of a particular pest in an area. Scientists at California University have developed an AI-based pest monitoring system that helps to identify the cause and track the movement of pests (Sharma et al., 2022). The computer vision system and information and communication technology (ICT) algorithm proposed show promise as an automated solution for insect observations, serving as a valuable addition to existing systems for monitoring nocturnal insects (Bjerge et al., 2021). AMMODs (Automated Multisensor Stations for Monitoring Species Diversity) share similarities with weather stations and are operated as autonomous samplers designed to monitor a range of species, including plants, birds, mammals, and insects (Wägele et al., 2022).

4.3 Detection of biotic stress

Biotic stresses, diseases and insect pests, can severely affect crop productivity. Crop stress caused by pests and diseases can be detected using remote sensing, based on the principle that biotic stress causes changes in pigmentation, physical appearance of plants, and photosynthesis, which directly alter the absorption rate of incident energy and the reflectance pattern of plants (Prabhakar et al., 2012). Prabhakar et al. (2012) detected the level of stress and severity caused by leafhopper attacks in cotton plants by assessing chlorophyll content and relative water content (RWC) using ground-based hyperspectral RS and categorized plants into five infestation grades from 0 to 4, representing healthy to severe damage. The leaf minor damage in a tomato field was assessed using leaf reflectance spectra (Xu et al., 2007) and the symptoms of cyst nematode in beet were mapped using a combination of RS and GIS techniques (Hillnhütter et al., 2011). The abundance of diamondback moth in cabbage crop was predicted using a subset of deep learning within ML (Kaur et al., 2022). Similarly, to detect and identify different pests in tea plantation in Yunnan for preventing the quality deterioration of tea leaves, transfer learning CNN were used (Li et al., 2024).

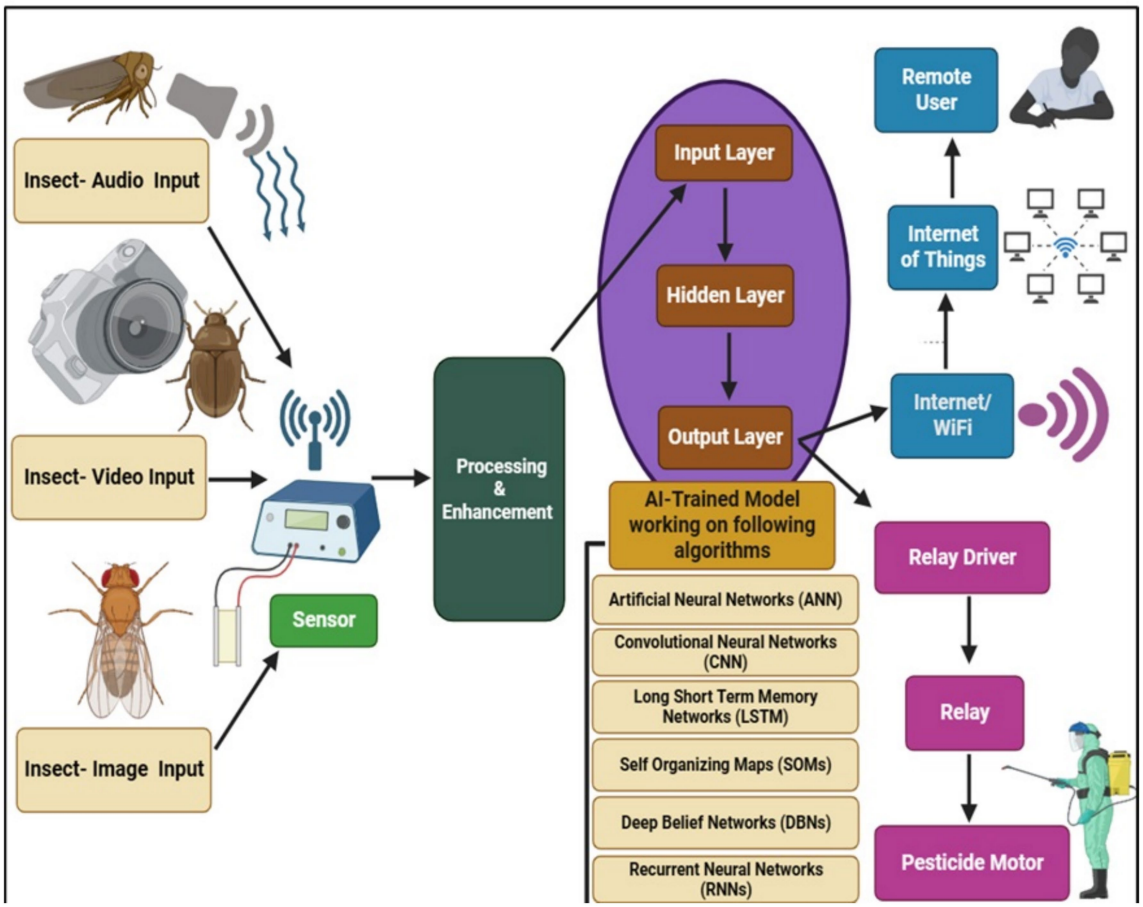

FIGURE 5
Workflow of AI-trained model for insect pest management.

4.4 Pest monitoring, forecasting, and early warning

Understanding the distribution of larval age in the field is an important factor in predicting primary and secondary pest outbreaks, as well as in determining the timing for effective insecticide application for pest management. RS plays a crucial role in providing information about the stage of insect pests present in the field based on accumulated degree days (Yones et al., 2012). The optimal timing for effective management of the cotton leafworm (*Spodoptera littoralis*) was determined based on degree days calculated from air temperature ranging between 174.85 and 197.59, using satellite RS (Yones et al., 2012). A study conducted by Nansen et al. (2015) on two species of insects, maize weevil (*Sitophilus zeamais*) and large flour black beetle (*Cynaus angustus*), revealed that temporal changes in body reflectance patterns were correlated with the response to two killing agents: entomopathogenic nematodes (EPNs) and insecticidal plant extract. Colour infrared photography was used to analyze infestations of black fly and brown spot scale in citrus orchards, as well as white fly infestation in cotton. Similarly, the infestation of mites in cotton fields was investigated at an early stage by observing changes in appearance, colour, and canopy over time using multispectral RS (Fitzgerald, 2000).

ML models can help predict pest outbreaks, for example, the major pests in tomato crops were predicted with significantly higher accuracy compared to traditional statistical models (Holzinger et al., 2023). ML can be used to develop DSS that correlate pest population dynamics with the environment, aiding in effective management. A DSS was developed using ML to manage thrips in tomatoes, resulting in a direct reduction in the use of insecticides (González et al., 2022). AI-based algorithms, such as ML, assist in early warning and forecasting of pests. In the case of fruit flies, different species were classified and detected based on their wing patterns (Murmu et al., 2022). The population dynamics of pests to environmental factors such as temperature and rainfall can be forecasted by ML algorithms. Deep learning algorithms can aid in predicting the occurrence and abundance of aphids in soybean (Murmu et al., 2022). AI has the potential to enhance aphid pest forecasting through various means, including optimizing monitoring infrastructure to improve predictive models (Bourhis et al., 2021).

The time required for analyzing a large number of samples collected by traditional insect collection techniques, such as suction traps, is extensive. Additionally, a skilled taxonomic expert is needed for precise sample processing, creating bottlenecks in monitoring insect populations. For this, AI-based image recognition and ML algorithms have emerged as a more promising approach. Aphids are capable of causing heavy losses in crop yield through direct feeding or by serving as vectors for plant viral diseases. Batz et al. (2023) investigated the potential of AI, ML, and image recognition in

systematically monitoring and forecasting insect pests. Detection of an important pest, *Riptortus pedestris*, which causes heavy damage to soybean pods and leaves, was conducted using a surveillance platform based on an unmanned ground vehicle equipped with a GoPro camera. The ML-based models used to study this pest were under the subset of deep learning algorithms, namely MRCNN, YOLOv3, and Detectron2 (Park et al., 2023). In the global population growing era, it becomes more important to early warn about invasion of new pests like locusts in areas where these are not present. Halubanza (2024) developed an advanced AI-based CNN model, specifically the MobileNet version 2 for automatic identification of different locust species which achieved a precision of 91% for *Locusta migratoria* and 85% for *Nomadacris septemfasciata*.

4.5 Detection, identification, and classification of insect habitats

With the assistance of multispectral scanners mounted on Earth-orbiting satellites such as Landsat, RS imagery can be obtained to aid in the detection of a particular insect's habitat. In the states of Nebraska and South Dakota, USA, mosquito larval habitats were detected in Lewis and Clarke Lake using a multispectral scanner. This lake was found to be the home of seven mosquito species: *Aedes dorsalis*, *A. vexans*, *Culex tarsalis*, *C. restruans*, *C. silinarius*, *Culiseta annulate,* and *Anopheles walker* (Hayes et al., 1985). Similarly, the use of RS and GIS techniques has helped to detect locust habitat monitoring and breeding zones in Africa, South Europe, and Southwest Asia (Latchininsky and Sivanpillai, 2010).

Infrared sensors can detect flying insect activity by using near-infrared LED lights and high-speed photodetectors (Rydhmer et al., 2022). Various parameters, such as wing beat frequency, melanisation, and wing-to-body ratio, can be measured in the field, automatically uploaded to a cloud database, and analyzed using ML and AI. Xia et al. (2023) evaluated the effectiveness of Vision Transformer (ViT) models in pest classification. The researchers utilized ResNet50, MMAINet, DNVT, and an ensemble learner to aggregate the predictions of these three models through a final classification vote. MMAINet incorporated an attention mechanism to identify discriminative image regions. The identified regions were then used to train fine-grained CNN-based classification models at different resolutions. Every year, the outbreak of locusts in different parts of world is common. This is due to the difficulty in mapping and monitoring locust habitats, which are mainly, located in inaccessible conflict zones of different countries. However, since the 1980s, RS applications have been utilized for monitoring and managing locust swarms. Nowadays, UAVs have brought new potential for more efficient and rapid management of locusts. The studies have utilized AVHRR, SPOT-VGT, and MODIS as well as Landsat for monitoring locust outbreaks (Klein et al., 2021).

4.6 Pest damage and yield forecast

One can analyze crop damage due to pests by knowing the reflectance pattern with the help of unmanned aircraft systems and the percentage of crops to be harvested under specific conditions like pest damage (Hunt and Rondon, 2017). The crop yield forecast has been done based on the relationship between VIs and yield with the help of remote sensors (Casa and Jones, 2005). The dependence of crop yield on various factors particularly pest and disease infestation, makes it a tough parameter to know properly but the detection of different growth profiles with the help of field sensors has made it possible to forecast the yield. Sharma et al. (2020) applied a fusion of CNN with LSTM models to raw imagery data for estimating the yield of wheat crops. The proposed model demonstrated a remarkable accuracy improvement of 74%over conventional methods for crop yield prediction and outperformed other deep learning models by 50%. Dharani et al. (2021) conducted a comparative analysis of three techniques namely ANN, CNN, and RNN with LSTM to assess their effectiveness in crop yield prediction. The results revealed that CNN exhibited superior accuracy compared to ANN, while RNN with LSTM outperformed all other techniques, achieving an accuracy of 89%. A CNN-RNN model was proposed for predicting soybean and corn yields in the United States (Khaki et al., 2020). Sabanci (2020) used AI techniques, including artificial bee colony optimization, ANN, and extreme learning machine algorithms, to detect sunn pest damage in wheat grains in Turkey. Toscano-Miranda et al. (2022) conducted a study on cotton crops using artificial intelligence techniques such as classification, image segmentation, and feature extraction. They employed algorithms including support vector machines, fuzzy inference, back-propagation neural networks, and CNN. The study focused on the most prevalent pests, whiteflies, and diseases such as root rot.

5 Challenges and future trends

The potential of AI and RS in insect pest management rests on creating precise and real time monitoring systems capable of forecasting pest outbreaks and facilitating more focused pest control approaches. However, significant challenges like data quality and availability, technological accessibility, computational cost, species identification complexity, regulatory frameworks for use of AI-driven pest management technologies and adaptation to environmental shifts, especially those caused by global climate change must be addressed, for ensuring responsible and sustainable pest management. The promising future directions in this aspect would be advanced image analysis, multi-sensor integration, predictive modeling, precision pest control, drone based monitoring, use of smart traps and lures and creating accessible platforms for stakeholders to share data, enabling better pest management.

6 Conclusion

Agriculture heavily relies on timely and accurate information, and RS and AI play a crucial role in providing such information. The ability of RS and AI to rapidly capture data and cover large agricultural areas enables farmers and decision-makers to make informed and timely decisions about crop management, irrigation, and pest control. One specific area where RS and AI have shown great potential is insect pest management. These techniques enable pest monitoring and detection, identification of pest outbreaks, early warning issuance, and determination of the optimal timing for pest control application. This

proactive approach could help farmers to prevent crop damage and minimize economic losses caused by pests. Furthermore, recent advancements in spectroscopy and other RS techniques have opened new opportunities for developing alternative and innovative approaches to crop management. The integration of RS data with traditional agricultural practices can lead to more precise and efficient resource utilization, optimizing inputs such as water, fertilizers, and pesticides. Efforts should be made to improve the speed of data acquisition and processing, allowing for a prompt response to changing conditions on the ground. This would make the information even more pertinent and practical for agricultural decision-makers and can lead to increased productivity and resilience in response to constantly changing environmental conditions.

Author contributions

DA: Conceptualization, Software, Writing – original draft. SMR: Conceptualization, Software, Writing – original draft. PaS: Resources, Supervision, Writing – review & editing. IA: Supervision, Writing – review & editing. BaG: Resources, Writing – review & editing. SAR: Resources, Writing – review & editing. SFR: Resources, Writing – review & editing. PoS: Resources, Writing – review & editing. GR: Resources, Writing – review & editing. KA: Resources, Writing – review & editing. GS: Resources, Writing – review & editing. BeG: Resources, Writing – review & editing. MN: Resources, Writing – review & editing.

Funding

The author(s) declare that no financial support was received for the research, authorship, and/or publication of this article.

Conflict of interest

The authors declare that the research was conducted in the absence of any commercial or financial relationships that could be construed as a potential conflict of interest.

Generative AI statement

The author(s) declare that no Generative AI was used in the creation of this manuscript.

Publisher's note

References

Abdelhamid, A. A., Alhussan, A. A., Qenawy, A. S. T., Osman, A. M., Elshewey, A. M., and Eed, M. (2024). Potato harvesting prediction using an improved ResNet-59 model. *Potato Res.*, 67, 1–20. doi: 10.1007/s11540-024-09773-6

Ahirwar, S., Swarnkar, R., Bhukya, S., and Namwade, G. (2019). Application of drone in agriculture. *Int. J. Curr. Microbiol. Appl. Sci.* 8, 2500–2505. doi: 10.20546/ijcmas.2019.801.264

Ahmad, S. N. I. S. S., Juraimi, A. S., Sulaiman, N., Che'Ya, N. N., Su, A. S. M., Nor, N. M., et al. (2023). Weeds detection and control in Rice crop using UAVs and artificial intelligence: a review. *Adv. Agric. Food Res. J.* 4:1–25. doi: 10.36877/aafrj.a0000371

Al-Adhaileh, M. H., and Aldhyani, T. H. (2022). Artificial intelligence framework for modeling and predicting crop yield to enhance food security in Saudi Arabia. *Peer J. Comput. Sci.* 8:e1104. doi: 10.7717/peerj-cs.1104

Ampatzidis, Y., Partel, V., and Costa, L. (2020). Agroview: cloud-based application to process, analyze and visualize UAV-collected data for precision agriculture applications utilizing artificial intelligence. *Comput. Electron. Agric.* 174:105457. doi: 10.1016/j.compag.2020.105457

Apan, A., Held, A., Phinn, S., and Markley, J. (2004). Detecting sugarcane 'orange rust'disease using EO-1 Hyperion hyperspectral imagery. *Int. J. Remote Sens.* 25, 489–498. doi: 10.1080/01431160310001618031

Aslan, M. F., Sabanci, K., and Aslan, B. (2024). Artificial intelligence techniques in crop yield estimation based on Sentinel-2 data: a comprehensive survey. *Sustain. For.* 16:8277. doi: 10.3390/su16188277

Ayyalasomayajula, B., Ehsani, R., and Albrigo, G. (2009). Automated citrus tree counting from oblique images and tree height estimation from oblique images. Proceedings of the symposium on the applications of precision agriculture for fruits and vegetables international conference. *Acta Hortic.* 824, 91–98. doi: 10.17660/ActaHortic.2009.824.10

Babaee, M., Maroufpoor, S., Jalali, M., Zarei, M., and Elbeltagi, A. (2021). Artificial intelligence approach to estimating rice yield. *Irrig. Drain.* 70, 732–742. doi: 10.1002/ird.2566

Backes, M., and Jacobi, J. (2006). Classification of weed patches in Quickbird images: verification by ground truth data. *EARSeL eProceedings* 5, 173–179.

Backoulou, G. F., Elliott, N. C., Giles, K., Phoofolo, M., and Catana, V. (2011). Development of a method using multispectral imagery and spatial pattern metrics to quantify stress to wheat fields caused by Diuraphisnoxia. *Comput. Electron. Agric.* 75, 64–70. doi: 10.1016/j.compag.2010.09.011

Bakala, H. S., Singh, G., and Srivastava, P. (2020). Smart breeding for climate resilient agriculture. *Plant Breeding-Curr. Future Views*, 4847:77–102. doi: 10.5772/intechopen.94847

Barbedo, J. G. A. (2019). Plant disease identification from individual lesions and spots using deep learning. *Biosyst. Eng.* 180, 96–107. doi: 10.1016/j.biosystemseng.2019.02.002

Batz, P., Will, T., Thiel, S., Ziesche, T. M., and Joachim, C. (2023). From identification to forecasting: the potential of image recognition and artificial intelligence for aphid pest monitoring. *Front. Plant Sci.* 14:1150748. doi: 10.3389/fpls.2023.1150748

Bhatia, A., Chug, A., and Singh, A. P. (2020). "Hybrid SVM-LR classifier for powdery mildew disease prediction in tomato plant", in Proceedings of the 2020 7th International Conference on Signal Processing and Integrated Networks (SPIN), (Noida, India), 218–223.

Bhoi, S. K., Jena, K. K., Panda, S. K., Long, H. V., Kumar, R., Subbulakshmi, P., et al. (2021). An internet of things assisted unmanned aerial vehicle based artificial intelligence model for rice pest detection. *Microprocess. Microsyst.* 80:103607. doi: 10.1016/j.micpro.2020.103607

Bjerge, K., Nielsen, J. B., Sepstrup, M. V., Helsing-Nielsen, F., and Høye, T. T. (2021). An automated light trap to monitor moths (Lepidoptera) using computer vision-based tracking and deep learning. *Sensors* 21:343. doi: 10.3390/s21020343

Bourhis, Y., Bell, J. R., van den Bosch, F., and Milne, A. E. (2021). Artificial neural networks for monitoring network optimisation—a practical example using a national insect survey. *Environ. Model. Softw.* 135:104925. doi: 10.1016/j.envsoft.2020.104925

Bravo, C., Moshou, D., West, J., McCartney, A., and Ramon, H. (2003). Early disease detection in wheat fields using spectral reflectance. *Biosyst. Eng.* 84, 137–145. doi: 10.1016/S1537-5110(02)00269-6

Bu, F., and Wang, X. (2019). A smart agriculture IoT system based on deep reinforcement learning. *Future Gen. Comput. Syst.* 99, 500–507. doi: 10.1016/j.future.2019.04.041

Casa, R., and Jones, H. G. (2005). LAI retrieval from multiangular image classification and inversion of a ray tracing model. *Remote Sens. Environ.* 98, 414–428. doi: 10.1016/j.rse.2005.08.005

Chivkunova, O. B., Solovchenko, A. E., Sokolova, S. G., Merzlyak, M. N., Reshetnikova, I. V., and Gitelson, A. A. (2001). Reflectance spectral features and detection of superficial scald–induced browning in storing apple fruit. *J. Russ. Phytopathol. Soc.* 2, 73–77.

Christakakis, P., Papadopoulou, G., Mikos, G., Kalogiannidis, N., Ioannidis, D., Tzovaras, D., et al. (2024). Smartphone-based citizen science tool for plant disease and

insect Pest detection using artificial intelligence. *Technologies* 12:101. doi: 10.3390/technologies12070101

Coble, K. H., Mishra, A. K., Ferrell, S., and Griffin, T. (2018). Big data in agriculture: a challenge for the future. *Appl. Econ. Persp. Pol.* 40, 79–96. doi: 10.1093/aepp/ppx056

Costello, B., Osunkoya, O. O., Sandino, J., Marinic, W., Trotter, P., Shi, B., et al. (2022). Detection of Parthenium weed (*Parthenium hysterophorus* L.) and its growth stages using artificial intelligence. *Agriculture* 12:1838. doi: 10.3390/agriculture12111838

Das, N. N., Entekhabi, D., Kim, S., Jagdhuber, T., Dunbar, S., Yueh, S., et al. (2017). "High-resolution enhanced product based on SMAP active-passive approach using sentinel 1A and 1B SAR data", in 2017 IEEE international geoscience and remote sensing symposium (Fort Worth, TX, USA, IGARSS), 2543–2545.

Datt, B. (2006). Early detection of exotic pests and diseases in Asian vegetables by imaging spectroscopy: a report for the Rural Industries Research and Development Corporation. *Rural Ind. Res. Dev. Corp.*:31.

De Jong, S. M., and Van der Meer, F. D. (2007). Remote sensing image analysis: Including the spatial domain. AA Dordrecht, The Netherlands: Springer Science & Business Media.

Dharani, M. K., Thamilselvan, R., Natesan, P., Kalaivaani, P. C. D., and Santhoshkumar, S. (2021). Review on crop prediction using deep learning techniques. *J. Physics* 1767:012026. doi: 10.1088/1742-6596/1767/1/012026

Dowell, F. E., and Ballard, J. W. O. (2012). Using near-infrared spectroscopy to resolve the species, gender, age, and the presence of Wolbachia infection in laboratory-reared Drosophila. *G3* 2, 1057–1065. doi: 10.1534/g3.112.003103

Dutta, S., Singh, S. K., and Panigrahy, S. (2014). Assessment of late blight induced diseased potato crops: a case study for West Bengal district using temporal AWiFS and MODIS data. *J. Ind. Soc. Remote Sens.* 42, 353–361. doi: 10.1007/s12524-013-0325-9

Faria, F. A., Perre, P., Zucchi, R. A., Jorge, L. R., Lewinsohn, T. M., and Rocha, A. (2014). Automatic identification of fruit flies (Diptera: Tephritidae). *J. Vis. Commun. Image Represent.* 25, 1516–1527. doi: 10.1016/j.jvcir.2014.06.014

Fitzgerald, G. (2000). Bug checking for mites – from the sky. *Austral. Cotton Grow.* 21, 29–31.

Franke, J., and Menz, G. (2007). Multi-temporal wheat disease detection by multi-spectral remote sensing. *Precis. Agric.* 8, 161–172. doi: 10.1007/s11119-007-9036-y

Franklin, S. (2001). Remote sensing for sustainable forest management. Boca Raton, Florida: Lewis publisher.

Fuentes, M. T., Lenardis, A., and De la Fuente, E. B. (2018). Insect assemblies related to volatile signals emitted by different soybean–weeds–herbivory combinations. *Agr. Ecosyst. Environ.* 255, 20–26. doi: 10.1016/j.agee.2017.12.007

Ghatrehsamani, S., Jha, G., Dutta, W., Molaei, F., Nazrul, F., Fortin, M., et al. (2023). Artificial intelligence tools and techniques to combat herbicide resistant weeds—a review. *Sustain. For.* 15:1843. doi: 10.3390/su15031843

Giménez-Gallego, J., González-Teruel, J. D., Soto-Valles, F., Jiménez-Buendía, M., Navarro-Hellín, H., and Torres-Sánchez, R. (2021). Intelligent thermal image-based sensor for affordable measurement of crop canopy temperature. *Comput. Electron. Agric.* 188:106319. doi: 10.1016/j.compag.2021.106319

González, M. I., Encarnação, J., Aranda, C., Osório, H., Montalvo, T., and Talavera, S. (2022). "The use of artificial intelligence and automatic remote monitoring for mosquito surveillance" in Ecology and control of vector-borne diseases (PA, Leiden, The Netherlands: Wageningen Academic Publishers), 1116–1121.

Goodwin, N. R., Coops, N. C., Wulder, M. A., Gillanders, S., Schroeder, T. A., and Nelson, T. (2008). Estimation of insect infestation dynamics using a temporal sequence of Landsat data. *Remote Sens. Environ.* 112, 3680–3689. doi: 10.1016/j.rse.2008.05.005

Gopinath, S., Sakthivel, K., and Lalith, S. (2022). A plant disease image using convolutional recurrent neural network procedure intended for big data plant classification. *J. Intell. Fuzzy Syst.* 43, 4173–4186. doi: 10.3233/JIFS-220747

Gou, C., Zafar, S., Fatima, N., Hasnain, Z., Aslam, N., Iqbal, N., et al. (2024). Machine and deep learning: artificial intelligence application in biotic and abiotic stress management in plants. *Front. Biosci. Landmark* 29:20–34. doi: 10.31083/j.fbl2901020

Graeff, S., Link, J., and Claupein, W. (2006). Identification of powdery mildew (*Erysiphe graminis* sp. *tritici*) and take-all disease (*Gaeumannomyces graminis* sp. *tritici*) in wheat (*Triticum aestivum* L.) by means of leaf reflectance measurements. *Open Life Sci.* 1, 275–288. doi: 10.2478/s11535-006-0020-8

Hahn, F. (2004). Spectral bandwidth effect on a Rhizopus stolonifer spore detector and its on-line behavior using red tomato fruits. *Can. Biosyst. Eng.* 46, 49–54.

Halubanza, B. (2024). A framework for an early warning system for the management of the spread of locust invasion based on artificial intelligence technologies (Doctoral dissertation,: The University of Zambia.

Hara, P., Piekutowska, M., and Niedbała, G. (2021). Selection of independent variables for crop yield prediction using artificial neural network models with remote sensing data. *Land* 10:609. doi: 10.3390/land10060609

Hayes, R. O., Maxwell, E. L., Mitchell, C. J., and Woodzick, T. L. (1985). Detection, identification, and classification of mosquito larval habitats using remote sensing scanners in earth-orbiting satellites. *Bull. World Health Organ.* 63, 361–374

Hillnhütter, C., Mahlein, A. K., Sikora, R. A., and Oerke, E. C. (2011). Remote sensing to detect plant stress induced by *Heterodera schachtii* and *Rhizoctonia solani* in sugar beet fields. *Field Crop Res.* 122, 70–77. doi: 10.1016/j.fcr.2011.02.007

Holzinger, A., Keiblinger, K., Holub, P., Zatloukal, K., and Müller, H. (2023). AI for life: trends in artificial intelligence for biotechnology. *New Biotechnol.* 74, 16–24. doi: 10.1016/j.nbt.2023.02.001

Hulme, P. E. (2009). Trade, transport and trouble: managing invasive species pathways in an era of globalization. *J. Appl. Ecol.* 46, 10–18. doi: 10.1111/j.1365-2664.2008.01600.x

Hunt, E. R. Jr., Rock, B. N., and Nobel, P. S. (1987). Measurement of leaf relative water content by infrared reflectance. *Remote Sens. Environ.* 22, 429–435. doi: 10.1016/0034-4257(87)90094-0

Hunt, E. R. Jr., and Rondon, S. I. (2017). Detection of potato beetle damage using remote sensing from small unmanned aircraft systems. *J. Appli. Remote Sens.* 11:026013. doi: 10.1117/1.JRS.11.026013

Ibatullin, S., Dorosh, Y., Sakal, O., Dorosh, O., and Dorosh, A. (2022). "Crop identification using remote sensing methods and artificial intelligence" in International conference of young professionals (European Association of Geoscientists & Engineers), 1–5.

Javaid, M., Haleem, A., Khan, I. H., and Suman, R. (2023). Understanding the potential applications of artificial intelligence in agriculture sector. *Adv. Agrochem.* 2, 15–30. doi: 10.1016/j.aac.2022.10.001

Jensen, J. R. (2007). Remote sensing of the environment: An earth resource perspective: Pearson Prentice Hall.

Jia, F., Maghirang, E., Dowell, F., Abel, C., and Ramaswamy, S. (2007). Differentiating tobacco budworm and corn earworm using near-infrared spectroscopy. *J. Econ. Entomol.* 100, 759–764. doi: 10.1093/jee/100.3.759

Johnson, L. F., Bosch, D. F., Williams, D. C., and Lobitz, B. M. (2001). Remote sensing of vineyard management zones: implications for wine quality. *Appl. Eng. Agric.* 17, 557–560. doi: 10.13031/2013.6454

Jones, H. G., Stoll, M., Santos, T., Sousa, C. D., Chaves, M. M., and Grant, O. M. (2002). Use of infrared thermography for monitoring stomatal closure in the field: application to grapevine. *J. Exp. Bot.* 53, 2249–2260. doi: 10.1093/jxb/erf083

Jordan, C. F. (1969). Derivation of leaf area index from quality of light on the forest floor. *Ecology* 50, 663–666. doi: 10.2307/1936256

Jung, J., Maeda, M., Chang, A., Bhandari, M., Ashapure, A., and Landivar-Bowles, J. (2021). The potential of remote sensing and artificial intelligence as tools to improve the resilience of agriculture production systems. *Curr. Opin. Biotechnol.* 70, 15–22. doi: 10.1016/j.copbio.2020.09.003

Kamath, R., Balachandra, M., and Prabhu, S. (2020). Paddy crop and weed discrimination: a multiple classifier system approach. *Int. J. Agron.* 2020, 1–14. doi: 10.1155/2020/6474536

Kanu, N. J., Gupta, E., and Verma, G. C. (2024). An insight into India's moon mission–Chandrayan-3: the first nation to land on the southernmost polar region of the moon. *Planetary Space Sci.* 242:105864. doi: 10.1016/j.pss.2024.105864

Karbstein, K., Kösters, L., Hodač, L., Hofmann, M., Hörandl, E., Tomasello, S., et al. (2024). Species delimitation 4.0: integrative taxonomy meets artificial intelligence. *Trends Ecol. Evol.* 39, 771–784. doi: 10.1016/j.tree.2023.11.002

Karnieli, A., Agam, N., Pinker, R. T., Anderson, M., Imhoff, M. L., Gutman, G. G., et al. (2010). Use of NDVI and land surface temperature for drought assessment: merits and limitations. *J. Clim.* 23, 618–633. doi: 10.1175/2009JCLI2900.1

Katimbo, A., Rudnick, D. R., Zhang, J., Ge, Y., DeJonge, K. C., Franz, T. E., et al. (2023). Evaluation of artificial intelligence algorithms with sensor data assimilation in estimating crop evapotranspiration and crop water stress index for irrigation water management. *Smart Agric. Technol.* 4:100176. doi: 10.1016/j.atech.2023.100176

Katiyar, S. (2022). "The use of pesticide management using artificial intelligence" in Artificial intelligence applications in agriculture and food quality improvement (IGI Global), 74–94.

Kaur, J., Sahu, K. P., and Singh, S. (2022). Optimization of pest management using artificial intelligence: fundamentals and applications, vol. *11*: Souvenir & Abstracts.

Khaki, S., Wang, L., and Archontoulis, S. V. (2020). A CNN-RNN framework for crop yield prediction. *Front. Plant Sci.* 10:1750. doi: 10.3389/fpls.2019.01750

Khan, H. A., Rao, S. A., and Farooq, U. (2024). Optimizing olive harvesting efficiency through UAVs and AI integration. *J. Agric. Sci.* 16:45. doi: 10.5539/jas.v16n11p45

Kho, S. J., Manickam, S., Malek, S., Mosleh, M., and Dhillon, S. K. (2017). Automated plant identification using artificial neural network and support vector machine. *Front. Life Sci.* 10, 98–107. doi: 10.1080/21553769.2017.1412361

Kim, T. H., and AlZubi, A. A. (2024). AI-enhanced precision irrigation in legume farming: optimizing water use efficiency. *Legum. Res.* 47, 1382–1389. doi: 10.18805/LRF-791

Kim, Y., Evans, R. G., and Iversen, W. M. (2008). Remote sensing and control of an irrigation system using a distributed wireless sensor network. *IEEE Trans. Instrum. Meas.* 57, 1379–1387. doi: 10.1109/TIM.2008.917198

Klarica, J., Bittner, L., Pallua, J., Pezzei, C., Huck-Pezzei, V., Dowell, F., et al. (2011). Near-infrared imaging spectroscopy as a tool to discriminate two cryptic Tetramorium ant species. *J. Chem. Ecol.* 37, 549–552. doi: 10.1007/s10886-011-9956-x

Klein, I., Oppelt, N., and Kuenzer, C. (2021). Application of remote sensing data for locust research and management—a review. *Insects* 12:233. doi: 10.3390/insects12030233

Kshetrimayum, A., Goyal, A., and Bhadra, B. K. (2024). Semi physical and machine learning approach for yield estimation of pearl millet crop using SAR and optical data products. *J. Spat. Sci.* 69, 573–592. doi: 10.1080/14498596.2023.2259857

Latchininsky, A. V., and Sivanpillai, R. (2010). Locust habitat monitoring and risk assessment using remote sensing and GIS technologies, in integrated Management of Arthropod Pests and Insect Borne Diseases. Dordrecht: Springer Netherlands, 163–188.

Lee, W. S., and Tardaguila, J. (2023). Pest and disease management, in advanced automation for tree fruit orchards and vineyards. Cham: Springer International Publishing, 93–118.

Li, Z., Sun, J., Shen, Y., Yang, Y., Wang, X., Wang, X., et al. (2024). Deep migration learning-based recognition of diseases and insect pests in Yunnan tea under complex environments. *Plant Methods* 20:101. doi: 10.1186/s13007-024-01219-x

Lillesand, T., Kiefer, R. W., and Chipman, J. (2015). Remote sensing and image interpretation: John Wiley & Sons.

Lins, E. C., Belasque, J., and Marcassa, L. G. (2009). Detection of citrus canker in citrus plants using laser induced fluorescence spectroscopy. *Precis. Agric.* 10, 319–330. doi: 10.1007/s11119-009-9124-2

Liu, S. C., Jian, Q. Y., Wen, H. Y., and Chung, C. H. (2022). A crop harvest time prediction model for better sustainability, integrating feature selection and artificial intelligence methods. *Sustain. For.* 14:14101. doi: 10.3390/su142114101

Low, F., and Duveiller, G. (2014). Defining the spatial resolution requirements for crop identification using optical remote sensing. *Remote Sens.* 6, 9034–9063. doi: 10.3390/rs6099034

Luo, J., Huang, W., Yuan, L., Zhao, C., Du, S., Zhang, J., et al. (2013). Evaluation of spectral indices and continuous wavelet analysis to quantify aphid infestation in wheat. *Precis. Agric.* 14, 151–161. doi: 10.1007/s11119-012-9283-4

Lutz, É., and Coradi, P. C. (2022). Applications of new technologies for monitoring and predicting grains quality stored: sensors, internet of things, and artificial intelligence. *Measurement* 188:110609. doi: 10.1016/j.measurement.2021.110609

Machleb, J., Peteinatos, G. G., Kollenda, B. L., Andújar, D., and Gerhards, R. (2020). Sensor-based mechanical weed control: present state and prospects. *Comput. Electron. Agric.* 176:105638. doi: 10.1016/j.compag.2020.105638

Maggiora, R., Saccani, M., Milanesio, D., and Porporato, M. (2019). An innovative harmonic radar to track flying insects: the case of Vespa velutina. *Sci. Rep.* 9:11964. doi: 10.1038/s41598-019-48511-8

Malinowski, R., Groom, G., Schwanghart, W., and Heckrath, G. (2015). Detection and delineation of localized flooding from WorldView-2 multispectral data. *Remote Sens.* 7, 14853–14875. doi: 10.3390/rs71114853

Martos, V., Ahmad, A., Cartujo, P., and Ordoñez, J. (2021). Ensuring agricultural sustainability through remote sensing in the era of agriculture 5.0. *Appl. Sci.* 11:5911. doi: 10.3390/app11135911

McDowell, R. W. (2017). Does variable rate irrigation decrease nutrient leaching losses from grazed dairy farming? *Soil Use Manag.* 33, 530–537. doi: 10.1111/sum.12363

Meraj, G., Kanga, S., Ambadkar, A., Kumar, P., Singh, S. K., Farooq, M., et al. (2022). Assessing the yield of wheat using satellite remote sensing-based machine learning algorithms and simulation modeling. *Remote Sens.* 14:3005. doi: 10.3390/rs14133005

Mogili, U. R., and Deepak, B. B. V. L. (2018). Review on application of drone systems in precision agriculture. *Proc. Comput. Sci.* 133, 502–509. doi: 10.1016/j.procs.2018.07.063

Mohammed, M., Hamdoun, H., and Sagheer, A. (2023). Toward sustainable farming: implementing artificial intelligence to predict optimum water and energy requirements for sensor-based micro irrigation systems powered by solar PV. *Agronomy* 13:1081. doi: 10.3390/agronomy13041081

Moshou, D., Bravo, C., Oberti, R., West, J., Bodria, L., McCartney, A., et al. (2005). Plant disease detection based on data fusion of hyper-spectral and multi-spectral fluorescence imaging using Kohonen maps. *Real Time Imaging* 11, 75–83. doi: 10.1016/j.rti.2005.03.003

Murmu, S., Pradhan, A. K., Chaurasia, H., Kumar, D., and Samal, I. (2022). Impact of bioinformatics advances in agricultural sciences. *AgroSci. Today* 3, 480–485.

Nansen, C., Ribeiro, L. P., Dadour, I., and Roberts, J. D. (2015). Detection of temporal changes in insect body reflectance in response to killing agents. *PLoS One* 10:e0124866. doi: 10.1371/journal.pone.0124866

Navarro, A., Nicastro, N., Costa, C., Pentangelo, A., Cardarelli, M., Ortenzi, L., et al. (2022). Sorting biotic and abiotic stresses on wild rocket by leaf-image hyperspectral data mining with an artificial intelligence model. *Plant Methods* 18:45. doi: 10.1186/s13007-022-00880-4

Noutfia, Y., and Ropelewska, E. (2024). What can artificial intelligence approaches bring to an improved and efficient harvesting and postharvest handling of date fruit (*Phoenix dactylifera* L.)? A review. *Postharvest Biol. Technol.* 213:112926. doi: 10.1016/j.postharvbio.2024.112926

Park, Y. H., Choi, S. H., Kwon, Y. J., Kwon, S. W., Kang, Y. J., and Jun, T. H. (2023). Detection of soybean insect pest and a forecasting platform using deep learning with unmanned ground vehicles. *Agronomy* 13:477. doi: 10.3390/agronomy13020477

Pinter, P. J. Jr., Hatfield, J. L., Schepers, J. S., Barnes, E. M., Moran, M. S., Daughtry, C. S., et al. (2003). Remote sensing for crop management. *Photogramm. Eng. Remote. Sens.* 69, 647–664. doi: 10.14358/PERS.69.6.647

Prabhakar, M., Prasad, Y. G., Mandal, U. K., Ramakrishna, Y. S., Ramalakshmaiaha, C., Venkateswarlu, N. C., et al. (2006). Spectral characteristics of Peanut crop infected by late leafspot disease under Rainfed conditions. *Agriculture and Hydrology Applications of Remote Sensing (SPIE)*, 109–115

Prabhakar, M., Prasad, Y. G., and Rao, M. N. (2012). "Remote sensing of biotic stress in crop plants and its applications for pest management" in Crop stress and its management: Perspectives and strategies (New York: Springer), 517–549.

Pellikka, P., and Rees, W. G. (2009). Remote sensing of glaciers: techniques for topographic, spatial and thematic mapping of glaciers. CRC Press. 1–315. doi: 10.1201/b10155

Ranjithkumar, C., Saveetha, S., Kumar, V. D., Prathyangiradevi, S., and Kanagasabapathy, T. (2021). AI based crop identification application. *Int. J. Res. Eng. Sci. Manag.* 4, 17–21.

Rouse, J. W., Haas, R. H., Shell, J. A., and Deering, D. W. (1973). "Monitoring vegetation systems in the Great Plains with ERTS-1" in Proceedings of third earth resources technology satellite symposium (Washington, DC: Goddard Space Flight Center), 309–317.

Roy, L., Ganchaudhuri, S., Pathak, K., Dutta, A., and Gogoi Khanikar, P. (2022). Application of remote sensing and GIS in agriculture. *Int. J. Res. Anal. Rev.* 9:460.

Rydhmer, K., Bick, E., Still, L., Strand, A., Luciano, R., Helmreich, S., et al. (2022). Automating insect monitoring using unsupervised near-infrared sensors. *Sci. Rep.* 12:2603. doi: 10.1038/s41598-022-06439-6

Ryu, J., Dohyeok, O. H., and Jaeil, C. H. O. (2021). Simple method for extracting the seasonal signals of photochemical reflectance index and normalized difference vegetation index measured using a spectral reflectance sensor. *J. Integr. Agric.* 20, 1969–1986. doi: 10.1016/S2095-3119(20)63410-4

Sabanci, K. (2020). Detection of sunn pest-damaged wheat grains using artificial bee colony optimization-based artificial intelligence techniques. *J. Sci. Food Agric.* 20, 1969–1986. doi: 10.1016/S2095-3119(20)63410-4

Sabrina, F., Sohail, S., Farid, F., Jahan, S., Ahamed, F., and Gordon, S. (2022). An interpretable artificial intelligence based smart agriculture system. *Comput. Mater. Contin.* 72, 3777–3797. doi: 10.32604/cmc.2022.026363

Saikumar, N., Emmanuel, N., Krishna, K. S. P., Chinnabbai, C., and Krishna, K. U. (2023). Artificial intelligence for classification and detection of major insect pests of Brinjal. *Ind. J. Entomol.*, 563–566. doi: 10.55446/IJE.2023.1388

Santoso, H., Gunawan, T., Jatmiko, R. H., Darmosarkoro, W., and Minasny, B. (2011). Mapping and identifying basal stem rot disease in oil palms in North Sumatra with QuickBird imagery. *Prec. Agric.* 12, 233–248. doi: 10.1007/s11119-010-9172-7

Sharma, R., Kumar, N., and Sharma, B. B. (2022). Applications of artificial intelligence in smart agriculture: a review. *Recent Innov. Comput.* 832, 135–142. doi: 10.1007/978-981-16-8248-3_11

Sharma, S., Rai, S., and Krishnan, N. C. (2020). Wheat crop yield prediction using deep LSTM model. *arXiv preprint arXiv, 01498*. doi: 10.48550/arXiv.2011.01498

Singh, D., Chaudhary, P., Taunk, J., Singh, C. K., Singh, D., Tomar, R. S. S., et al. (2021). Fab advances in fabaceae for abiotic stress resilience: from omics to artificial intelligence. *Int. J. Mol. Sci.* 22:10535. doi: 10.3390/ijms221910535

Singh, C. B., Jayas, D. S., Paliwal, J. N. D. G., and White, N. D. G. (2009). Detection of insect-damaged wheat kernels using near-infrared hyperspectral imaging. *J. Stored Prod. Res.* 45, 151–158. doi: 10.1016/j.jspr.2008.12.002

Singh, C. B., Jayas, D. S., Paliwal, J., and White, N. D. (2010). Identification of insect-damaged wheat kernels using short-wave near-infrared hyperspectral and digital colour imaging. *Comput. Electron. Agric.* 73, 118–125. doi: 10.1016/j.compag.2010.06.001

Singh, A., Mehrotra, R., Rajput, V. D., Dmitriev, P., Singh, A. K., Kumar, P., et al. (2022). Geoinformatics, artificial intelligence, sensor technology, big data: emerging modern tools for sustainable agriculture. *Sustain. Agric. Syst. Technol.*, 295–313. doi: 10.1002/9781119808565.ch14

Small, I. M., Joseph, L., and Fry, W. E. (2015). Development and implementation of the BlightPro decision support system for potato and tomato late blight management. *Comput. Electron. Agric.* 115, 57–65. doi: 10.1016/j.compag.2015.05.010

Smith, L., McElrone, A. J., and Hartin, J. (2020). Remote sensing assessment of insect damage in vineyards. *Remote Sens.* 12:2395.

Spinelli, F., Noferini, M., and Costa, G. (2006). Near infrared spectroscopy (NIRs): perspective of fire blight detection in asymptomatic plant material. Proceeding of 10th international workshop on fire blight. *Acta Hortic.* 704, 87–90. doi: 10.17660/ActaHortic.2006.704.9

Su, W. H. (2020). Crop plant signaling for real-time plant identification in smart farm: a systematic review and new concept in artificial intelligence for automated weed control. *Artif. Intel. Agric.* 4, 262–271. doi: 10.1016/j.aiia.2020.11.001

Subeesh, A., and Mehta, C. R. (2021). Automation and digitization of agriculture using artificial intelligence and internet of things. *Artif. Intel. Agric.* 5, 278–291. doi: 10.1016/j.aiia.2021.11.004

Sujithra, J., and Ukrit, M. F. (2022). Performance analysis of D-neural networks for leaf disease classification-banana and sugarcane. *Int. J. Syst. Assur. Eng. Manag.*, Eds. Pandey, K., Kushwaha, N.L., Pande, C.B., Singh, K.G. 13, 1–9. doi: 10.1007/s13198-022-01756-5

Toscano-Miranda, R., Toro, M., Aguilar, J., Caro, M., Marulanda, A., and Trebilcok, A. (2022). Artificial-intelligence and sensing techniques for the management of insect pests and diseases in cotton: a systematic literature review. *J. Agric. Sci.* 160, 16–31. doi: 10.1017/S002185962200017X

Trout, T. J., Johnson, L. F., and Gartung, J. (2008). Remote sensing of canopy covers in horticultural crops. *Hortic. Sci.* 43, 333–337. doi: 10.21273/HORTSCI.43.2.333

Vijayakumar, V., and Balakrishnan, N. (2021). Artificial intelligence-based agriculture automated monitoring systems using WSN. *J. Ambient Intell. Humani. Comput.* 12, 8009–8016. doi: 10.1007/s12652-020-02530-w

Wägele, J. W., Bodesheim, P., Bourlat, S. J., Denzler, J., Diepenbroek, M., Fonseca, V., et al. (2022). Towards a multisensor station for automated biodiversity monitoring. *Basic Appl. Ecol.* 59, 105–138. doi: 10.1016/j.baae.2022.01.003

Wang, Y., Nansen, C., and Zhang, Y. (2016). Integrative insect taxonomy based on morphology, mitochondrial DNA, and hyperspectral reflectance profiling. *Zool. J. Linnean Soc.* 177, 378–394. doi: 10.1111/zoj.12367

Wongchai, A., Shukla, S. K., Ahmed, M. A., Sakthi, U., and Jagdish, M. (2022). Artificial intelligence-enabled soft sensor and internet of things for sustainable agriculture using ensemble deep learning architecture. *Comput. Electric. Eng.* 102:108128. doi: 10.1016/j.compeleceng.2022.108128

Xia, W., Han, D., Li, D., Wu, Z., Han, B., and Wang, J. (2023). An ensemble learning integration of multiple CNN with improved vision transformer models for pest classification. *Ann. Appl. Biol.* 182, 144–158. doi: 10.1111/aab.12804

Xiao, Q., Li, W., Kai, Y., Chen, P., Zhang, J., and Wang, B. (2019). Occurrence prediction of pests and diseases in cotton on the basis of weather factors by long short term memory network. *BMC Bioinform.* 20, 1–15. doi: 10.1186/s12859-019-3262-y

Xu, H. R., Ying, Y. B., Fu, X. P., and Zhu, S. P. (2007). Near-infrared spectroscopy in detecting leaf miner damage on tomato leaf. *Biosyst. Eng.* 96, 447–454. doi: 10.1016/j.biosystemseng.2007.01.008

Yadav, M., Vashisht, B. B., Vullaganti, N., Jalota, S. K., Yadav, S. L., Singh, G., et al. (2024). "IoT-enabled unmanned aerial vehicle: an emerging trend in precision farming" in Artificial intelligence and smart agriculture: Technology and applications, 271–292.

Yang, C. M. (2010). Assessment of the severity of bacterial leaf blight in rice using canopy hyperspectral reflectance. *Precis. Agric.* 11, 61–81. doi: 10.1007/s11119-009-9122-4

Yang, C. M., Cheng, C. H., and Chen, R. K. (2007). Changes in spectral characteristics of rice canopy infested with brown planthopper and leaffolder. *Crop Sci.* 47, 329–335. doi: 10.2135/cropsci2006.05.0335

Yang, C., and Everitt, J. H. (2011). "Remote sensing for detecting and mapping whitefly (*Bemisia tabaci*) infestations" in The whitefly, *Bemisia tabaci* (Homoptera: Aleyrodidae) interaction with Geminivirus-infected host plants: *Bemisia tabaci*, Host plants and Geminiviruses (Dordrecht: Springer Netherlands), 357–381.

Yang, W., Huang, D., Tan, B., Stroeve, J. C., Shabanov, N. V., Knyazikhin, Y., et al. (2006). Analysis of leaf area index and fraction of PAR absorbed by vegetation products from the terra MODIS sensor: 2000-2005. *IEEE Transac. Geosci. Remote Sens.* 44, 1829–1842. doi: 10.1109/TGRS.2006.871214

Yones, M. S., Arafat, S., Abou Hadid, A. F., Abd Elrahman, H. A., and Dahi, H. F. (2012). Determination of the best timing for control application against cotton leaf worm using remote sensing and geographical information techniques. *Egypt. J. Remote Sens. Space Sci.* 15, 151–160. doi: 10.1016/j.ejrs.2012.05.004

Zaman, Q., Schumann, A. W., and Hostler, K. H. (2006). Estimation of citrus fruit yield using ultrasonically-sensed tree size. *Appl. Eng. Agric.* 22, 39–44. doi: 10.13031/2013.20186

Zhang, J., Yang, C., Song, H., Hoffmann, W. C., Zhang, D., and Zhang, G. (2016). Evaluation of an airborne remote sensing platform consisting of two consumer-grade cameras for crop identification. *Remote Sens.* 8:257. doi: 10.3390/rs8030257

Zhang, F., Zaman, Q. U., Percival, D. C., and Schumann, A. W. (2010). Detecting bare spots in wild blueberry fields using digital color photography. *Appl. Eng. Agric.* 26, 723–728. doi: 10.13031/2013.34938

frontiers | Frontiers in Nutrition

TYPE Original Research
PUBLISHED 27 February 2025
DOI 10.3389/fnut.2025.1542211

OPEN ACCESS

EDITED BY
Gurjeet Singh,
Texas A and M University, United States

REVIEWED BY
Anuj Kumar,
Independent researcher, Houston, TX, United States
ICAR-National Institute of Abiotic Stress Management, Indian Agricultural Research Institute (ICAR), India

*CORRESPONDENCE
Ravindra Singh
✉ Ravindra.Singh@icar.gov.in
Sharda Choudhary
✉ sharda.choudhary@icar.gov.in

RECEIVED 09 December 2024
ACCEPTED 17 February 2025
PUBLISHED 27 February 2025

CITATION
Singh R, Meena RS, Choudhary S, Meena NK, Meena RD, Verma AK, Mahatma MK, Yathendranaik R, Lal S, Shekhawat PK and Bhardwaj V (2025) Deciphering agronomic traits, biochemical components, and color in unique green-seeded fenugreek (*Trigonella foenum-graecum* L.) genotypes. *Front. Nutr.* 12:1542211. doi: 10.3389/fnut.2025.1542211

Deciphering agronomic traits, biochemical components, and color in unique green-seeded fenugreek (*Trigonella foenum-graecum* L.) genotypes

Ravindra Singh*, Ram Swaroop Meena, Sharda Choudhary*, Narottam Kumar Meena, Ram Dayal Meena, Arvind Kumar Verma, Mahesh Kumar Mahatma, Ravi Yathendranaik, Shiv Lal, Pooja Kanwar Shekhawat and Vinay Bhardwaj

ICAR-National Research Centre on Seed Spices, Ajmer, India

Fenugreek is a high-value legume known for its potential to enhance human health and combat a variety of diseases and metabolic disorders. This versatile crop has demonstrated promising therapeutic effects in managing obesity, diabetes, cancer, and poor metabolism conditions that have become major global health concerns. Despite the availability of multiple pharmaceutical remedies for these ailments in the market, often times the heavy chemical doses are accompanied by side effects on human body. To investigate the agronomic traits, medicinal potential, and color of fenugreek seeds, this study was conducted and identified fenugreek genotypes with green seed color (GSF1 to GSF10), which can prevent the progression of aforementioned diseases without the hassle of side effects. Ten unique green-seeded fenugreek (GSF) genotypes were compared with five released varieties (yellow-seeded fenugreek; YSF1 to YSF5) as check. The genotypes were assessed during rabi season for 3 consecutive years (2021–22 to 2023–24) in semi-arid Eastern Plain Zone of Rajasthan, India. The findings exhibited that agronomically GSF performed well, almost at par with the YSF. Harvest index (23.21 $\pm$ 0.37%) is higher in GSF with very marginal differences in other agronomic traits. The medicinal potential of the GSF showed that GSF6 has nearly 1.5 to 2 times higher insulinotropic 4-hydroxyisoleucine (0.90%) levels compared to the YSF genotypes. This unique non-protein branched amino acid is found in fenugreek seeds. GSF1 has a high concentration of chlorophyll (0.45 mg/100 g), GSF10 has low diosgenin and high 4-OHIle (261.80 mg/100 g and 0.85%, respectively), and GSF9 has low total soluble sugars (TSS; 3.50%). Oil content, phenols, and proteins were found to be higher in GSF making it preferable over YSF. The study further revealed that darkness of green color in the seed is directly related to its chlorophyll content and is directly associated with higher content of 4-OHIle and lower TSS. Among the studied genotypes, harvest index is higher in green-seeded genotypes with maximum seed yield (2473.74 Kg/ha) in genotype GSF8. The superior genotypes GSF1, GSF6, GSF8, GSF9, and GSF10 developed in the study hold potential for future breeding initiatives, aimed at boosting medicinal value, nutritional quality, and productivity.

KEYWORDS

obesity, insulin-resistance, cancer, seed color, medicinal, harvest index, PCA

Introduction

Fenugreek (*Trigonella foenum-graecum* L.), from the Leguminosae family, is an economically and medicinally important crop with a chromosome number of 2n = 16 (1). Fenugreek is a well-known seed spices crop, cultivated all over the world (2), commercially grown in India, Pakistan, Iran, Egypt, Turkey, Middle East, and North Africa (3). Its commercial and medicinal benefits have made it a popular crop which is grown in almost all parts of the country since ages. Its leaves and seeds have been found to be effective in medicinal preparations. They are used as food for humans and as fodder for animals and improve soil health by augmenting the availability of nitrogen (4). Leaves of this plant are pinnate and long stalked compound toothed (5). Seeds are small, hard, and yellow to brownish yellow in color with smooth texture (3). Leaves and seeds are commonly used in ancient medicinal herbs containing minerals such as potassium, magnesium, calcium, zinc, manganese, copper and iron (6), vitamins (7), and β-carotene (5). The seed is typically yellow-colored endosperm with a bitter taste. It is rich in lipid lowering agent 4-hydroxyisoleucine (8, 9), diosgenin (2), chlorophyll (10), protein, flavonoids, carbohydrates, free amino acids, essential oil, seed oil (11–13), and other medicinally important compounds.

The WHO reports revealed that 422 million adults were suffering from diabetes worldwide in 2014 and accounted for 6.7 million deaths in 2021. It is predicted to rise further, reaching as much as 366 million by 2030 and 783 million by 2045 (14, 15). Diabetes mellitus is now approaching epidemic proportions (16). The same report revealed that cancer is the second disease causing an estimated 10 million deaths globally (17). Cancer is predicted to become the leading cause of diabetes-related deaths in older people with type 2 diabetes overtaking cardiovascular diseases (18). Both these diseases may further stimulate other conditions such as neuropathy, nephropathy, retinopathy, chronic kidney disease, skin complications (19), heart attack, stroke (20) obesity, PCOD, infertility, hair loss, and many more. Natural dietary sources and balanced lifestyle might play a key role in the treatment and even prevent these diseases. There are many natural dietary sources such as green vegetables, fresh fruits, dry fruits, nuts, and cereals for a healthy mind and body. Some key components such as 4-hydroxyisoleucine and diosgenin have potential to manage diabetes and tumor formation (21–23). Insulin secretagogue properties of 4-OHIle and anti-cancerous properties of diosgenin support its consumption for treatment of insulin resistance, cancer, diabetes, and obesity (24, 25).

Both 4-OHIle and diosgenin are naturally found in fenugreek seeds. Multiple reports are available claiming the medicinal potential of fenugreek seeds for antidiabetic, anti-cancer, gastric stimulation, and antibacterial (26–28) properties. Bakhtiar et al. (29) reported light brown, brown, and olive colored seeds in Iranian fenugreek genotypes and studied their phytochemical traits and antioxidant properties. Fenugreek seeds are rich in nutraceutical properties, have positive effects on digestive system (30), and act as an anti-cancer agent (31, 32) and an antioxidant (26, 33, 34) and good for heart health (35).

Fenugreek is very hardy and farmer loving crop. Farming this crop is considered less risky as opposed to other seed spice crops. The presence of antioxidants and medicinal values increases its importance and enhances the marketing of the crop which leads to monetary benefit to the cultivators. Variability in seed color might enhance quality and visual attractiveness for consumers. Despite decent potential of yellow-seeded fenugreek as medicinal crop, new genotypes/varieties with more 4-OHILe and diosgenin content find greater allure due to their distinguished green color. The objective of the present study is to investigate the variation in morphological characteristics and identify the superior high 4-OHILe and balanced diosgenin content by biochemical characterization as well as color categorization based on L*a*b* and chlorophyll content. The study also takes into account yield potential and capability for healthy and functional sustenance.

Materials and methods

Plant material, experimental site, and experimental design

Green-seeded fenugreek plants were collected from the Agro climatic Zone-IIA (Transitional Plain of Inland Drainage) of Rajasthan, India. Collected genotypes were maintained and multiplied at Indian Council of Agricultural Research - National Research Centre on Seed Spices (ICAR-NRCSS) field. After 3 years of field experiments, the pure green-seeded fenugreek germplasm lines with stable color character were selected. All the ten germplasm lines, identified for green seed color, were registered at Indian Council of Agricultural Research-National Bureau of Plant Genetic Resources (ICAR-NBPGR), New Delhi, India, for unique Indian Collection (IC) number *viz*: IC-0633362 (GSF1), IC-0633363 (GSF2), IC-0633364 (GSF3), IC-0633365 (GSF4), IC-0633366 (GSF5), IC-0633367 (GSF6), IC-0633368 (GSF7), IC-0633369 (GSF8), IC-0633370 (GSF9), and IC-0633371 (GSF10) (Supplementary Table S1). All the ten genotypes were evaluated for agro-morphological and medicinally important compounds. Total fifteen genotypes including five varieties *viz:* AFg-1 (YSF1), AFg-2 (YSF2), AFg-3 (YSF3), AFg-4 (YSF4), and AFg-5 (YSF5) as checks were planted in the field in Randomized Block Design (RBD), three replications with plot size 3×3 m^2 with crop geometry 30×10 cm, during *rabi* season of 2021–22, 2022–23, and 2023–24. The experiment was conducted at research farm of ICAR-National Research Centre on Seed Spices (ICAR-NRCSS), Tabiji, Ajmer, situated at longitude 74° 35′ 31′ E and latitude 26° 21′ 59" N, at an altitude of 460.17 m above mean sea level. The region falls under agro climatic zone III a, "Semi-Arid Eastern Plain Zone" of Rajasthan (Figure 1). The field had a leveled topography and sandy loam soil texture. Mild winters and moderate summers with relatively high humidity from July to September are characteristics of this semi-arid and sub-tropical climatic zone. The mean annual rainfall is 550 mm, mostly received from southwest monsoon during the last week of June to September and the total rainfall during 2021–22, 2022–23 and 2023–24, i.e., the growing period of fenugreek was 24, 75, and 21 mm, respectively. The mean weekly meteorological observations recorded during the crop periods at the meteorological observatory of Research Farm, ICAR-NRCSS, Ajmer, are presented in Supplementary Table S2 and depicted in Figure 2. Data revealed that during growing crop cycle, maximum temperature ranged between 18.1°C to 39.8°C, 20.4°C to 34.6°C, and 18.1°C to 37.1°C, while minimum temperature ranged between 2.1°C to 20.5°C, 2.7°C to 20.9°C, and 4.7°C to 25.4°C during *rabi* 2021–22, 2022–23, and 2023–24, respectively. The mean daily maximum and minimum relative humidity varied between 43.1 and 90.7% during morning and 32.5 and 77.3% during afternoon across the years. Total annual rainfall during the years 2021–22, 2022–23, and 2023–24 was 624.7 mm, 915.3 mm, and

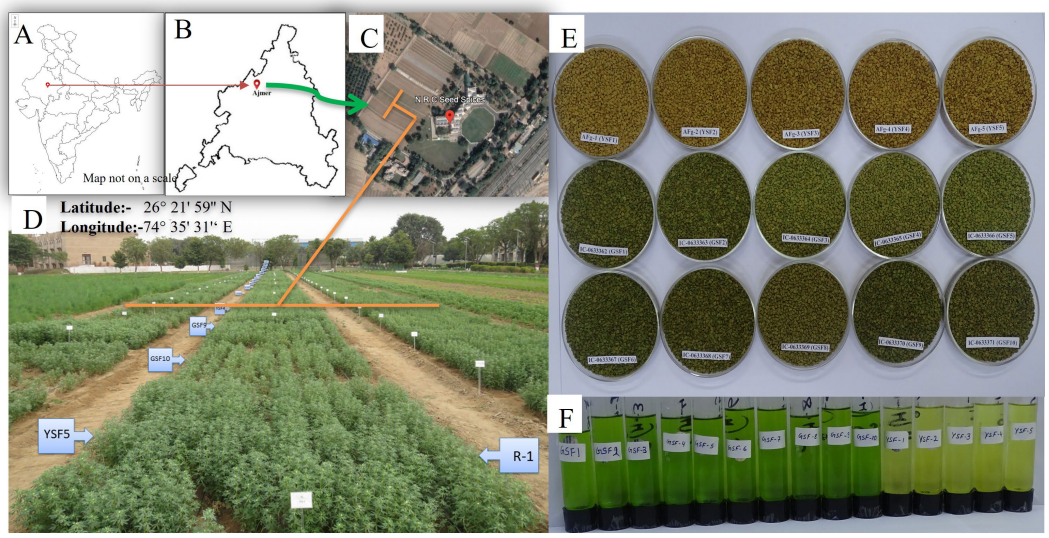

FIGURE 1
(A–C) Geo location of experimental site (India, Ajmer, ICAR-NRCSS), **(D)** Field view of experiment, **(E)** Seeds after harvesting and **(F)** Extract of seeds.

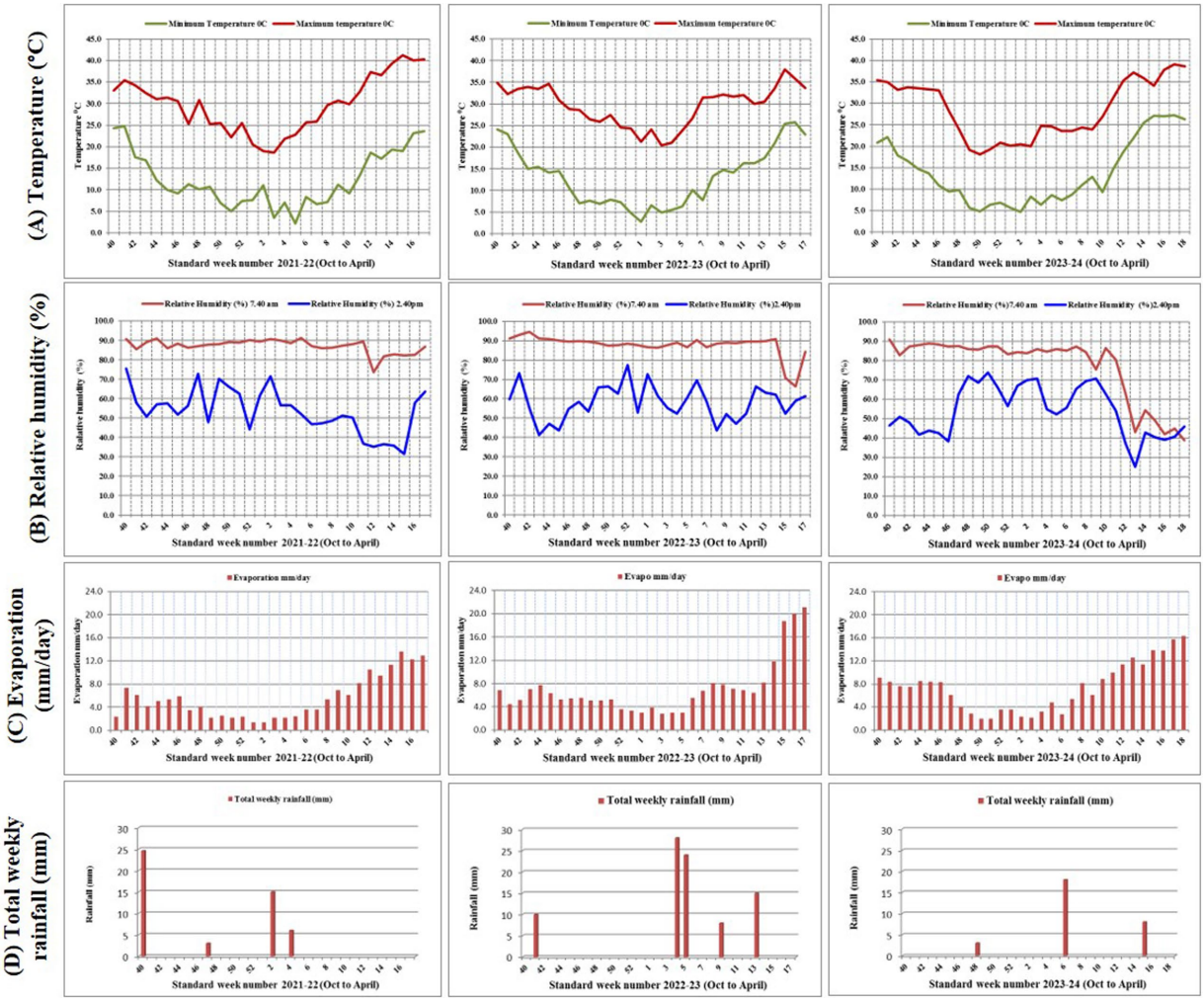

FIGURE 2
Meterological graph of 2021–22, 2022–23 and 2023–24 depicting **(A)** Temperature (°C) **(B)** Relative humidity (%) **(C)** Evaporation (mm/day) **(D)** Total weekly rainfall (mm).

996.0 mm, respectively, in the last 2 years; it was extremely high over average annual rainfall. The soil of experimental field had a salinity of 0.83 ds/m, pH of 8.2, organic matter of 0.28%, and lime of 5.6%, with available nitrogen, phosphorus, and potassium as 155.7 kg/ha, 12.7 kg/ha, and 240 kg/ha, respectively.

Observations of agronomic traits

The agronomic data recorded in the study included plant height (PH), primary branches (PB), secondary branches (SB), number of pods per plant (PPP), pod length (PL), secondary branches per plant (SPP), days to flowering (DF), maturity duration (MD), seed yield (SY), straw yield (StY), biological yield (BY), harvest index (HI), and test weight (TW). The plant height, primary branches, number of pods per plant, pod length, and number of secondary branches were recorded from randomly selected five plant from each plot, and other yield and yield attributes, *viz,* seed yield, straw yield, biological yield, harvest index, and test weight, were recorded after harvesting on plot basis. All the figures and tables generated are based on the pooled data analysis of three years.

Biochemical compounds

Fully matured harvest of green-seeded genotypes and yellow-seeded genotypes from the year 2023–24 were used for analysis of biochemical components such as (4-OHIle 4-hydroxyisoleucine), diosgenin, chlorophyll, free amino acid (FAA), total soluble sugar (TSS), protein, and oil.

Chlorophyll contents of green- and yellow-seeded fenugreek were determined following the spectrophotometric assay described by Mazza and Oomah (36). Dry seed samples (1 g) were grinded and extracted in a 50 mL centrifuge tube and homogenized with 18 mL acetone: 1 mL NH_4OH (0.1 N) solution for 30 min. Homogenates were stored in dark at 4°C for 2 min and then centrifuged at 5000 rpm. The supernatant was transferred to another test tube and read on a spectrophotometer (LAB INDIA Brand, Model no.3000+) at 700, 663, 645, and 626 nm. The reading taken at 700 nm was subtracted from each of the readings taken at 663, 645, and 626 nm. Total chlorophyll was calculated by summing the value of chlorophyll a and b after calculating them separately using the following formula:

$$\text{mg / g Chlorophyll a} = 14.18\ \text{X OD}\ 663 \times 2.91\ \text{X OD}\ 645 - 0.22\ \text{X OD}\ 626$$

and

$$\text{m / g Chlorophyll b} = 26.01\ \text{X OD}\ 645 - 4.66\ \text{X OD}\ 663 - 0.36\ \text{X OD}\ 626$$

A non-proteinogenic amino acid, 4-hydroxyisoleucine, from fenugreek seeds was extracted in 80% ethanol followed by 100% ethyl acetate. One gram of ground fenugreek seeds were taken, and 10 mL of 80.0% ethanol was added and filtrated. Extraction was repeated twice and pooled. Volume of the extract was reduced by evaporation in drybath (LABQUEST, model LBH010). Free amino acids were estimated by ninhydrin reagent. A standard curve was prepared with the use of leucine (0, 10, 20, 30, and 40 µg). For the estimation of 4-hydroxyisoleucine, amount of free amino acid was multiplied by 0.80 (37).

Saponins were extracted from fenugreek seed powder using 100% absolute ethanol (97) with continuous shaking in a shaker for 48 h. After extraction, solution was centrifuged for 20 min at 1000 rpm, and the supernatant was evaporated in drybath (LABQUEST, model LBH010) at 50°C. Dry residue was weighed and expressed as saponin content. Dry saponins were dissolved in 2 mL of 100% ethyl acetate in capped test tubes. To this, 1 mL of color-developing reagents consisted 0.5 mL of 0.5% (v/v) p-anisaldehyde and 0.5 mL of 50% H_2SO_4 was added. Both p-anisaldehyde and H_2SO_4 were prepared in ethyl acetate. The tubes were placed in a 60°C water bath for 10 min for color development; after that, 0.5 mL of distilled water was added to each tube.

A blank reagent was prepared similar way by taking 2 mL of ethyl acetate instead of samples. Ethyl acetate (100%) alone served as the control. Absorbance was measured at 430 nm on a LAB INDIA make spectrophotometer (Model no.3000+). A diosgenin calibration curve was prepared using standard solutions of diosgenin (10–80 µg/mL) prepared in 100% ethyl acetate. TSS were extracted in 80% ethanol and estimated by anthrone reagents. The intensity of color was read at 600 nm on spectrophotometer. A standard curve was prepared using 10 mg glucose per 100 ml distilled water (98).

Total amino acids were extracted in 80% ethanol and estimated by using ninhydrin reagent as described by Lee and Takahanshi (38). Total nitrogen content of the seeds was estimated by the method of Kjeldahl. Nitrogen content was multiplied by 6.25 factor and expressed as protein percent. Total oil from seeds of fenugreek was estimated by Soxhlet extraction method using n-hexane as solvent following the method of AOAC (39).

Color analysis

The colorimetric analysis of the samples was conducted using a handheld digital colorimeter (CR-400 Chroma Meter, Konica Minolta Sensing Americas, Inc.). The instrument was calibrated using black and white tiles to assess the variations in their color properties, focusing on lightness (L*), chromaticity coordinates (a* and b*), hue angle (h*), chroma (C*), color differences (ΔE), greenness index (GI), and yellowness index (YI). The results revealed significant differences among the samples. 'colordesigner.io' (40) tools were used to identify the color name and shade.

Statistical analysis

Statistical analysis was performed for all the traits observed, wherein mean values from three crop seasons *rabi* 2021–22, *rabi* 2022–23, and *rabi* 2023–24 with three replications were used. The descriptive statistics was performed for all observed traits using data analysis tool in MS Office Excel program. All the data were subjected to analysis of variance followed by mean comparison by *post-hoc* test. The means of green- and yellow-seeded fenugreek genotypes are presented as "Mean ± SE" and were compared using "Duncan's multiple range test" (DMRT) in R studio statistical software with package "Agricolae." Different lowercase letters indicate a significant difference, whereas mean values with the same lowercase letters are not significantly different ($p < 0.05$). Violin plots integrating boxplots for agronomical traits and two-way clustering heatmap were

performed in SRplot (41). Line graph as well as radar for biochemical traits and seed color representation was performed in MS Office Excel. By utilizing mean of all the traits, correlation analysis, scree plot, variable principal component analysis, PCA biplot, and two-way clustering heat map were constructed. Pearson's correlation analysis was performed by using *R* studio statistical software package "metan" to determine the relationship among traits. Principal component analysis and linear regression analysis were performed in General R based Analysis Platform Empowered by Statistics (*GRAPES 1.1.0*) (42).

Results

Agronomic traits

Field experiment was carried out in a randomized block design for three winter seasons (*Rabi* 2021–22, *Rabi* 2022–23, and *Rabi* 2023–24). Significant differences were observed among the genotypes for all measured traits ($p < 0.01$, Table 1) suggesting great variations among fenugreek genotypes. Violin plots for agronomic traits are represented in Figure 3.

Plant height

The plant height of the fenugreek genotypes was significantly affected over the growing years. Similarly, the GSF and YSF genotypes showed statistical differences when grown under the same field conditions in *rabi* 2021–22, 2022–23, and 2023–24. Plant height ranges from 69.60 cm to 81.53 cm in GSF genotypes and from 73.60 cm to 84.93 cm in YSF genotypes in 2021–22. In 2022–23, plant height ranges from 61.93 cm to 78.07 cm in GSF and 71.47 cm to 86.80 cm in YSF genotypes. Similarly in 2023–24, plant height ranged from 44.60 cm to 66.53 cm in GSF and 75.33 cm to 82.67 cm in YSF genotypes. Pooled data for all the three experimental years revealed that plant height ranged from 62.04 cm (GSF1) to 71.01 cm (GSF6) for green-seeded genotypes and for yellow-seeded genotypes it was from 74.84 cm (YSF1) to 82.84 cm (YSF2) (Table 1).

Primary and secondary branches per plant

The primary branches varied from 3.73 to 4.93 in GSF and from 4.00 to 5.20 in YSF in 2021–22, from 4.68 to 5.93 in GSF and from 5.47 to 5.73 in YSF in 2022–23, whereas it varied from 5.13 to 5.93 in GSF and from 5.47 to 5.87 in YSF in 2023–24 with pooled value over 3 years ranging from 4.82 (GSF9) to 5.24 (GSF5) in GSF and 5.02 (YSF5) to 5.51 (YSF3) in YSF genotypes. Both primary and secondary branches were comparable in GSF and YSF genotypes. Secondary branches varied from 6.87 to 7.87 in GSF and 7.20 to 8.07 in YSF during 2021–22, from 5.53 to 7.20 in GSF and 6.73 to 8.13 in YSF during 2022–23, and from 5.40 to 6.47 in GSF and 5.73 to 6.40 in YSF during 2023–24 with pooled value ranging from 6.22 (GSF3) to 7.09 (GSF7) in GSF and 6.73 (YSF5) to 7.29 (YSF1) in YSF genotypes (Table 1).

Pod-related traits

Number of pods/plant ranged from 35.80 to 43.40 in GSF and 37 to 45.53 in YSF in 2021–22, from 52.13 to 72.47 in GSF and 71.53 to 85.40 in YSF in 2022–23, and from 40.73 to 55.13 in GSF and 40.87 to 58.73 in YSF in 2023–24 with pooled value of all the 3 years ranging from 44.11 (GSF10) to 52.31 (GSF7) in GSF and 52.69 (YSF3) to 57.78 (YSF4) in YSF (Table 1).

Pod length ranged from 12.93 cm to 14.40 cm for GSF genotypes and 13.27 cm to 13.87 cm for YSF genotypes in 2021–22, 11.00 cm to 12.55 cm for GSF and 11.79 cm to 13.16 cm for YSF in 2022–23, and 11.59 to 12.47 cm for GSF and 11.75 to 12.53 cm for YSF in 2023–24 with pooled value ranging from 12.1 6 cm (GSF8) to 12.90 cm (GSF7) for GSF and from 12.42 cm (YSF4) to 13.08 cm (YSF3) for YSF (Table 1).

Seeds per pod were comparable for both GSF and YSF genotypes over all three *rabi* seasons 2021–22, 2022–23, and 2023–24. Generally, it ranged from 17.53 (GSF5) to 18.49 (GSF9) in GSF and 18.07 (YSF1) to 18.91 (YSF5) in YSF (Table 1).

Days to flowering

Flowering days ranged from 43 to 48 days for GSF (45.54 days) and 41 to 44 days for YSF (42.05 days) in 2021–22, from 47 to 48 days for GSF and up to 45 days for YSF in 2022–23, and from 45 to 46 days for GSF and 42 days for YSF in 2023–24 (Table 1).

Maturity days

Maturity days ranged from 141 to 142.67 days for GSF (141.85 days) and from 141 to 142.33 days for YSF (141.42 days) in 2021–22, 138.67 to 140.33 days for GSF (140 days) and from 142 to 143 days for YSF (142.25 days) in 2022–23, and 126 days for GSF and from 126 to 127.67 days for YSF (126.83 days) in 2023–24, with pooled value ranging from 135.67 to 136.22 days for GSF (135.81 days) and 136.33 to 137.33 days for YSF (136.83 days) (Table 1).

Seed yield

Seed yield showed significant differences in the *rabi* periods of (2021–22, 2022–23, and 2023–24) among the fenugreek genotypes grown under normal condition. Pooled data revealed that the highest seed yield was obtained from the genotypes GSF8 (2473.74 Kg/ha), followed by YSF1 (2349.88 kg ha^{-1}), YSF4 (2328.38 kg ha^{-1}), and GSF4 (2316.91 kg/ha) among all genotypes studied (Table 1).

Straw yield

Straw yield ranged from 6296.30 kg ha^{-1} to 8463.67 kg ha^{-1} for GSF genotypes and 3481.04 kg ha^{-1} to 8592.59 kg ha^{-1} for YSF genotypes in 2021–22, 6407.80 kg ha^{-1} to 11461.50 kg ha^{-1} for GSF genotypes and from 8479.30 kg ha^{-1} to 14681.57 kg ha^{-1} for YSF in 2022–23, and 3585.56 kg ha^{-1}to 4978.15 kg ha^{-1}for GSF and 5352.25 kg ha^{-1}to 6385.59 kg ha^{-1}for YSF in 2023–24 with pooled value of 5967.22 kg ha^{-1}(GSF10) to 8096.67 kg ha^{-1}(GSF2) for GSF

TABLE 1 Range, mean, standard error (SE), and coefficient of variation for different morphological traits in fenugreek.

			2021–22			2022–23			2023–24			Pooled		
SN	Traits	Type	Mean ± SE	Range	CV	Mean ± SE	Range	CV	Mean ± SE	Range	CV	Mean ± SE	Range	CV
1	PH (cm)	GSF	74.39 ± 1.09	69.60–81.53	4.63	68.96 ± 1.60	61.93–78.07	7.32	55.34 ± 1.95	44.60–66.53	11.13	66.23 ± 0.81[b]	62.04–71.01	3.85
		YSF	77.79 ± 1.99	73.60–84.93	5.73	80.89 ± 2.62	71.47–86.80	7.24	78.32 ± 1.36	75.33–82.67	3.88	79 ± 1.41[a]	74.84–82.84	4
2	PB	GSF	4.38 ± 0.15	3.73–4.93	10.6	5.173 ± 0.12	4.68–5.93	7.14	5.59 ± 0.08	5.13–5.93	4.73	5.05 ± 0.05[b]	4.82–5.24	2.88
		YSF	4.47 ± 0.20	4.00–5.20	9.9	5.61 ± 0.04	5.47–5.73	1.76	5.65 ± 0.08	5.47–5.87	3.16	5.24 ± 0.08[a]	5.02–5.51	3.6
3	SB	GSF	7.42 ± 0.10	6.87–7.87	4.3	6.44 ± 0.15	5.53–7.20	7.56	5.74 ± 0.11	5.40–6.47	6.18	6.53 ± 0.08[b]	6.22–7.09	3.95
		YSF	7.68 ± 0.17	7.20–8.07	5.08	7.47 ± 0.23	6.73–8.13	6.8	5.97 ± 0.12	5.73–6.40	4.37	7.04 ± 0.1[a]	6.73–7.29	3.07
4	DF	GSF	45.54 ± 0.6	43–48	4.16	47.8 ± 0.13	47–48	0.88	45.4 ± 0.15	45–46	1.07	46.14 ± 0.27[a]	44.94–47.25	1.73
		YSF	42.05 ± 0.58	41–44	3.09	45.00	-	-	42.00	-	-	43.12 ± 0.24[b]	42.57–43.64	1.12
5	MD	GSF	141.85 ± 0.25	141–142.67	0.53	140.00 ± 0.29	138.67–140.33	0.63	126.00 ± 0.10	126	-	135.81 ± 0.06[b]	135.67–136.22	0.12
		YSF	141.42 ± 0.32	141–142.33	0.45	142.25 ± 0.25	142–143	0.35	126.83 ± 0.48	126–127.67	0.76	136.83 ± 0.21[a]	136.33–137.33	0.30
6	PPP	GSF	39.59 ± 0.72	35.80–43.40	5.74	58.37 ± 1.92	52.13–72.47	10.39	46.01 ± 1.56	40.73–55.13	10.71	47.99 ± 0.85[b]	44.11–52.31	5.59
		YSF	40.45 ± 1.50	37.00–45.53	8.28	78.65 ± 3.07	71.53–85.40	8.73	48.39 ± 3.01	40.87–58.73	13.89	55.83 ± 0.96[a]	52.69–57.78	3.85
7	PL (cm)	GSF	13.67 ± 0.16	12.93–14.40	3.63	12.02 ± 0.18	11.00–12.55	4.71	11.89 ± 0.01	11.59–12.47	2.35	12.52 ± 0.09[a]	12.16–12.9	2.15
		YSF	13.52 ± 0.12	13.27–13.87	1.92	12.50 ± 0.24	11.79–13.16	4.23	12.10 ± 0.14	11.75–12.53	2.67	12.71 ± 0.12[a]	12.42–13.08	2.09
8	SPP	GSF	17.34 ± 0.19	16.53–18.07	3.54	17.96 ± 0.12	17.20–18.47	2.07	18.49 ± 0.12	18.07–19.13	1.98	17.93 ± 0.1[b]	17.53–18.49	1.78
		YSF	17.85 ± 0.14	17.47–18.20	1.72	18.83 ± 0.39	17.87–20.27	4.66	18.52 ± 0.21	17.80–18.93	2.49	18.4 ± 0.15[a]	18.07–18.91	1.84
9	SY (Kg/ha)	GSF	2536.99 ± 70.36	2073.33–2870.85	8.77	2472.07 ± 121.37	1978.52–2967.41	15.53	1311.82 ± 51.50	962.59–1582.96	12.42	2106.96 ± 59.27[a]	1897.9–2473.74	8.9
		YSF	2253.62 ± 279.63	1152.22–2617.41	27.75	2896.59 ± 79.39	2676.67–3094.44	6.13	1443.33 ± 31.57	1337.78–1508.15	4.89	2197.85 ± 110.89[a]	1759.01–2349.88	11.28
10	StY (Kg/ha)	GSF	7840.66 ± 224.65	6296.30–8463.67	9.06	9091.38 ± 471.74	6407.80–11461.50	16.41	4382.26 ± 125.65	3585.56–4978.15	9.07	7104.77 ± 223.16[a]	5967.22–8096.67	9.93
		YSF	7172.41 ± 937.15	3481.04–8592.59	29.22	10678.52 ± 1052.04	8479.30–14681.57	22.03	5931.07 ± 216.40	5352.25–6385.59	8.16	7927.33 ± 570.79[a]	6012.89–9587.29	16.1
11	BY (Kg/ha)	GSF	10377.65 ± 288.43	8369.63–11334.52	8.79	11563.46 ± 534.81	8458.17–13757.80	14.63	5694.07 ± 163.65	4548.15–6296.30	9.09	9211.73 ± 260.67[a]	7865.13–10166.8	8.95
		YSF	9426.03 ± 1214.24	4633.26–11174.41	28.8	13575.11 ± 1068.63	11155.96–17576.75	17.6	7374.40 ± 189.18	6857.80–7802.63	5.74	10125.18 ± 668.19[a]	7771.91–11915.67	14.76
12	HI (%)	GSF	24.50 ± 0.26	23.32–25.91	3.32	22.02 ± 0.72	18.35–24.24	10.29	23.09 ± 0.51	20.59–25.22	6.92	23.21 ± 0.37[a]	21.32–24.65	5.03
		YSF	24.04 ± 0.39	23.14–24.98	3.64	22.23 ± 1.06	18.32–24.06	10.65	19.75 ± 0.94	17.50–22.20	10.67	22.01 ± 0.32[a]	21.06–22.78	3.29
13	TW (gm)	GSF	14.43 ± 0.34	11.97–15.83	7.47	12.53 ± 0.33	10.90–14.03	8.28	11.83 ± 0.05	11.53–12.03	1.33	12.93 ± 0.16[b]	12.18–13.7	3.92
		YSF	14.29 ± 0.51	13.37–16.07	8.02	15.55 ± 0.68	13.50–16.83	9.74	13.14 ± 0.53	11.70–14.80	8.96	14.33 ± 0.38[a]	13.27–15.18	5.95

Data are presented as the mean ± SE. Different lowercase letters indicate a significant difference ($p < 0.05$); mean values with the same lowercase letters are not significantly different according to Duncan's multiple range test (DMRT; $p < 0.05$).

10.3389/fnut.2025.1542211

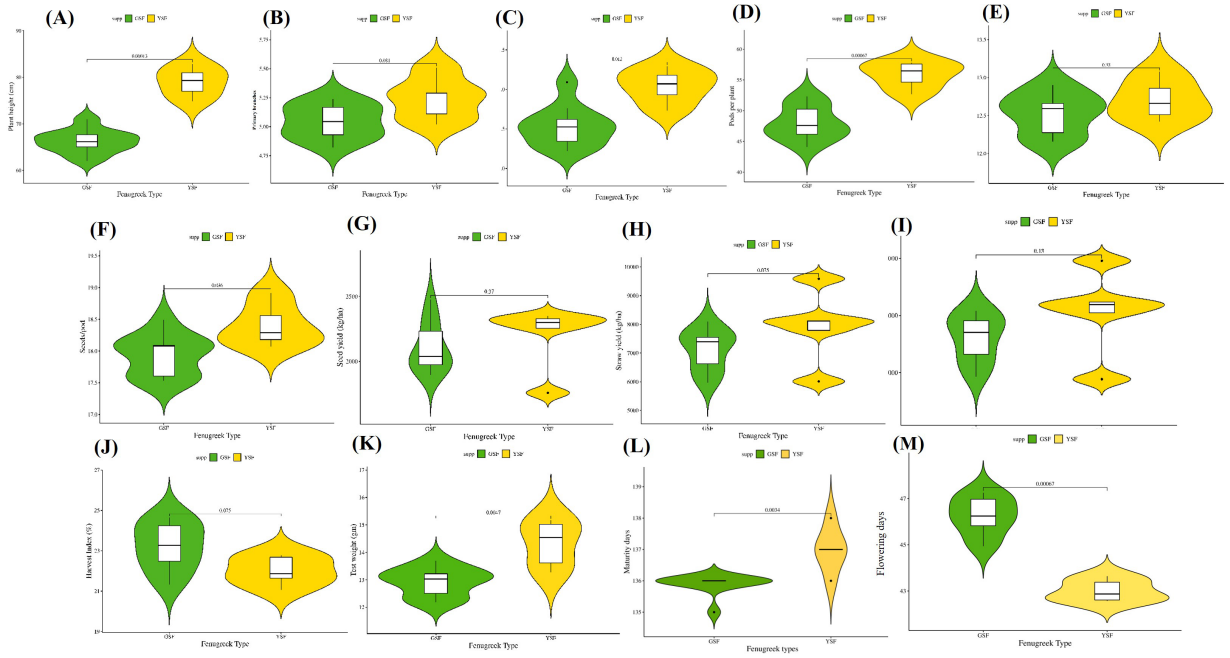

FIGURE 3
Comparative violin and boxplots of different morphological traits in green and yellow seeded fenugreek genotypes **(A)**. Plant height **(CM)**, **(B)**. Primary branches, **(C)**. Secondary branches, **(D)** Pods per plant, **(E)** Pod length (cm), **(F)** Seeds per pod, **(G)** Seed yield (Kg/ha), **(H)** Straw yield (Kg/ha), **(I)** Biological yield (Kg/ha), **(J)** Harvest Index (%), **(K)** Test weight (gm), **(L)** Maturity days, **(M)** Days to flowering.

and 6012.89 kg ha-^{1}(YSF3) to 9587.29 kg ha-^{1}(YSF4) for YSF. Yellow-seeded fenugreek genotypes are the better performing genotype for straw yield (Table 1).

Biological yield

Biological yield of fenugreek genotypes can vary significantly, depending on the genotypes and the environmental conditions. Biological yield ranged from 8369.63 kg ha-^{1} to 11334.52 kg ha-^{1}a for GSF genotypes and 4633.26 kg ha-^{1} to 11174.41 kg ha-^{1} for YSF genotypes in 2021–22, 8458.17 kg ha-^{1} to 13757.80 kg ha-^{1} for GSF and 11155.96 kg ha-^{1} to 17576.75 kg ha-^{1} for YSF in 2022–23, and 4548.15 kg ha-^{1} to 6296.30 kg ha-^{1} for GSF and 6857.80 kg ha-^{1} to 7802.63 kg ha-^{1} for YSF in 2023–24 with pooled value ranging from 7865.13 kg ha-^{1} to 10166.80 kg ha-^{1} in GSF and from 7771.91 kg ha-^{1} to 11915.67 kg ha-^{1} in YSF. The genotypes with highest biological yield are YSF4 (11915.67 kg ha-^{1}), YSF1 (10473.54 kg ha-^{1}), and YSF2 (10376.29 kg ha-^{1}) followed by green-seeded genotypes GSF2 (10166.80 kg ha-^{1}) and GSF8 (10145.83 kg ha-^{1}) (Table 1).

Harvest index

Harvesting index was comparable for both GSF and YSF genotypes over all three seasons 2021–22, 2022–23, and 2023–24. In our study, it ranged from 23.32 to 25.91% for GSF genotypes and from 23.14 to 24.98 for YSF in 2021–22, from 18.35 to 24.24% for GSF and 18.32 to 24.06% for YSF in 2022–23, and from 20.59 to 25.22% for GSF and 17.50 to 22.20% for YSF with pooled value of 21.32% (GSF1) to 24.65% (GSF8) for GSF and 21.06% (YSF4) to 22.78% (YSF5) for YSF (22.01%) (Table 1).

Test weight

Test weight (1,000 seed weight) depends on the genotype and other environmental factors. The test weight ranged from 11.97 g to 15.83 g for GSF and from 13.37 g to 16.07 g for YSF in 2021–22, from 10.90 g to 14.03 g for GSF and from 13.50 g to 16.83 g for YSF in 2022–23, and from 11.53 g to 12.03 g for GSF and 11.70 g to 14.80 g for YSF in the third year of experiment with pooled value ranging from 12.18 g (GSF5) to 13.70 g (GSF3) for GSF (12.93 g) and 13.27 g to 15.18 g for YSF (14.33 g) (Table 1).

Biochemical analysis

Total chlorophyll content

In our study, chlorophyll content ranged from 0.31 mg/100 g (GSF9) to 0.45 mg/100 g (GSF1) with mean value of 0.36 mg/100 g in GSF genotypes and 0.02 to 0.04 mg/100 g with mean value of 0.03 mg/100 g in YSF genotypes (Table 2).

4-hydroxyisoleucine (%)

The most abundant free amino acid in fenugreek, 4-hydroxyisoleucine (branched-chain amino acid), is found in the seed endosperm (43). Among the fenugreek genotypes studied, GSF1, GSF3, GSF6, GSF7, GSF9, and GSF10 exhibited the highest concentrations, measuring 0.81, 0.84, 0.90, 0.88, 0.81, and 0.85%, respectively, with mean value of 0.81% in green-seeded subgroup of fenugreek genotypes that is almost 1.5 times higher than yellow-seeded fenugreek genotypes with 0.44 to 0.73% (Table 2 and Figure 4).

TABLE 2 Biochemical characterization of GSF and YSF fenugreek genotypes.

SN	Fenugreek type	Genotypes	Total Chl (mg/100 g)	4-OHIle (%)	Diosgenin (mg/100 g)	FAA (mg/100 g)	TSS (%)	Total phenol (mg/100 g)	Oil (%)	Protein (%)
1	Green-seeded fenugreek	GSF1	0.45	0.81	382.28	1016.79	5.52	21.22	3.74	21.67
		GSF2	0.36	0.75	412.55	931.02	5.15	41.55	3.53	15.69
		GSF3	0.33	0.84	338.88	1048.95	4.05	42.59	3.45	19.28
		GSF4	0.38	0.70	326.79	861.57	3.9	26.37	3.13	18.22
		GSF5	0.35	0.75	366.72	937.04	4.05	31.36	3.39	18.03
		GSF6	0.35	0.90	295.05	1124.76	5.6	55.94	3.51	20.55
		GSF7	0.33	0.88	370.51	1094.87	4.3	35.12	3.37	19.89
		GSF8	0.35	0.77	413.09	962.24	3.8	21.58	3.66	17.96
		GSF9	0.31	0.81	388.35	1016.73	3.5	38.98	3.71	18.57
		GSF10	0.40	0.85	261.84	1057.14	4.55	18.17	3.53	18.44
		Mean	0.36 ± 0.01^{a}	0.81 ± 0.02^{a}	355.61 ± 15.72^{a}	1005.11 ± 25.79^{a}	4.44 ± 0.23^{b}	33.29 ± 3.75^{b}	3.5 ± 0.06^{b}	18.83 ± 0.52^{b}
		Range	0.31–0.45	0.7–0.9	261.84–413.09	861.57–1124.76	3.5–5.6	18.17–55.94	3.13–3.74	15.69–21.67
2	Yellow-seeded fenugreek	YSF1	0.02	0.44	261.44	554.02	6.39	113.33	4.3	20.58
		YSF2	0.04	0.48	508.1	606.39	6.23	116.21	4.24	20.42
		YSF3	0.02	0.58	289.9	722.1	5.79	116.31	4.1	24.26
		YSF4	0.04	0.73	319.55	911.99	5.77	96.78	3.97	20.83
		YSF5	0.02	0.5	452.74	633.49	6.04	8.84	4.48	21.15
		Mean	0.03 ± 0.01^{b}	0.55 ± 0.05^{b}	366.34 ± 48.27^{a}	685.6 ± 62.8^{b}	6.04 ± 0.12^{a}	90.29 ± 20.68^{a}	4.22 ± 0.09^{a}	21.45 ± 0.71^{a}
		Range	0.02–0.04	0.44–0.73	261.44–508.1	554.02–911.99	5.77–6.39	8.84–116.31	3.97–4.48	20.42–24.26

Data are presented as the mean ± SE. Different lowercase letters indicate a significant difference ($P < 0.05$); mean values with the same lowercase letters are not significantly different according to Duncan's multiple range test (DMRT; $p < 0.05$).

10.3389/fnut.2025.1542211

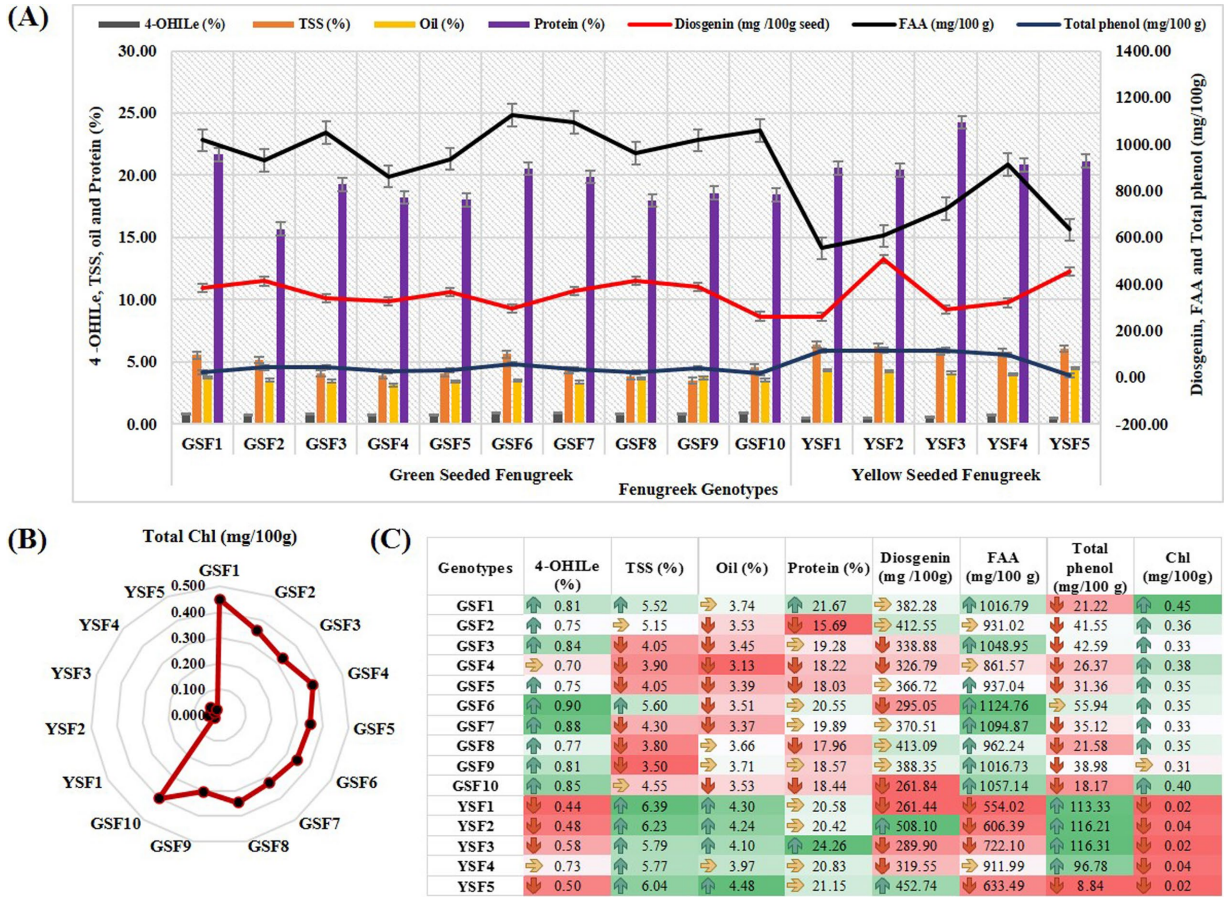

Genotypes	4-OHILe (%)	TSS (%)	Oil (%)	Protein (%)	Diosgenin (mg /100g)	FAA (mg/100 g)	Total phenol (mg/100 g)	Chl (mg/100g)
GSF1	0.81	5.52	3.74	21.67	382.28	1016.79	21.22	0.45
GSF2	0.75	5.15	3.53	15.69	412.55	931.02	41.55	0.36
GSF3	0.84	4.05	3.45	19.28	338.88	1048.95	42.59	0.33
GSF4	0.70	3.90	3.13	18.22	326.79	861.57	26.37	0.38
GSF5	0.75	4.05	3.39	18.03	366.72	937.04	31.36	0.35
GSF6	0.90	5.60	3.51	20.55	295.05	1124.76	55.94	0.35
GSF7	0.88	4.30	3.37	19.89	370.51	1094.87	35.12	0.33
GSF8	0.77	3.80	3.66	17.96	413.09	962.24	21.58	0.35
GSF9	0.81	3.50	3.71	18.57	388.35	1016.73	38.98	0.31
GSF10	0.85	4.55	3.53	18.44	261.84	1057.14	18.17	0.40
YSF1	0.44	6.39	4.30	20.58	261.44	554.02	113.33	0.02
YSF2	0.48	6.23	4.24	20.42	508.10	606.39	116.21	0.04
YSF3	0.58	5.79	4.10	24.26	289.90	722.10	116.31	0.02
YSF4	0.73	5.77	3.97	20.83	319.55	911.99	96.78	0.04
YSF5	0.50	6.04	4.48	21.15	452.74	633.49	8.84	0.02

FIGURE 4
(A) Comparison of medicinal compounds, **(B)** Total Chl (mg/100 g) contents and **(C)** Comparative value representation for medicinal compound and chlorophyll content. [4-OHIle (4-Hydroxyisoleucine), TSS (Total soluble sugar), FAA (Free fatty acid), Chl (Chlorophyll content)].

Total soluble sugar (%)

The present study revealed that total soluble sugar content in green-seeded fenugreek genotypes varied from 3.5% (GSF9) to 5.6% (GSF6) with mean value of 4.44%, i.e., much lower than (almost half) yellow-seeded fenugreek genotypes that contained 5.77% (YSF4) to 6.39% (YSF1) with mean value of 6.04% total soluble sugar (Table 2).

Diosgenin (mg/100gm)

Diosgenin ranged from 261.84 mg/100 g (GSF10) to 413.09 mg/100 g (GSF8) with mean value of 355.61 mg/100 g in green-seeded fenugreek genotypes and 261.44 mg/100 g (YSF1) to 508.10 mg/100 g (YSF2) with mean value of 366.34 mg/100 g in yellow-seeded fenugreek genotypes (Table 2).

Free amino acid (mg/100gm)

In our investigation study, FAA ranged from 861.57 mg/100 g to 1124.76 mg/100 g with average value of 1005.11 mg/100 g with higher content of 1124.76 mg/100 g in GSF6, 1057.14 mg/100 g in GSF10, and 1094.87 mg/100 g in GSF7. In case of yellow-seeded fenugreek, it ranged from 554.02 to 911.99 mg/100 g with mean value of 685.60 mg/100 g having higher content in YSF4 (911 mg/100 g) and 722.10 mg/100 g in YSF3 (Table 2).

Protein content (%)

Protein content ranged from 15.69% (GSF2) to 21.67% (GSF1) with mean value of 18.83% in green-seeded fenugreek genotypes, whereas it ranged from 20.42% (YSF2) to 24.26% (YSF3) with mean value of 21.45% in yellow-seeded fenugreek genotypes (Table 2).

Total phenol content (mg/100 g)

Total phenol content in this investigation study ranged from 18.17 (GSF10) to 55.94 (GSF6) mg/100 g with mean value of 33.29 mg/100 g in green-seeded fenugreek genotypes and from 8.84 (YSF5) to 116.31 (YSF3) with mean value of 90.29 mg/100 g (Table 2).

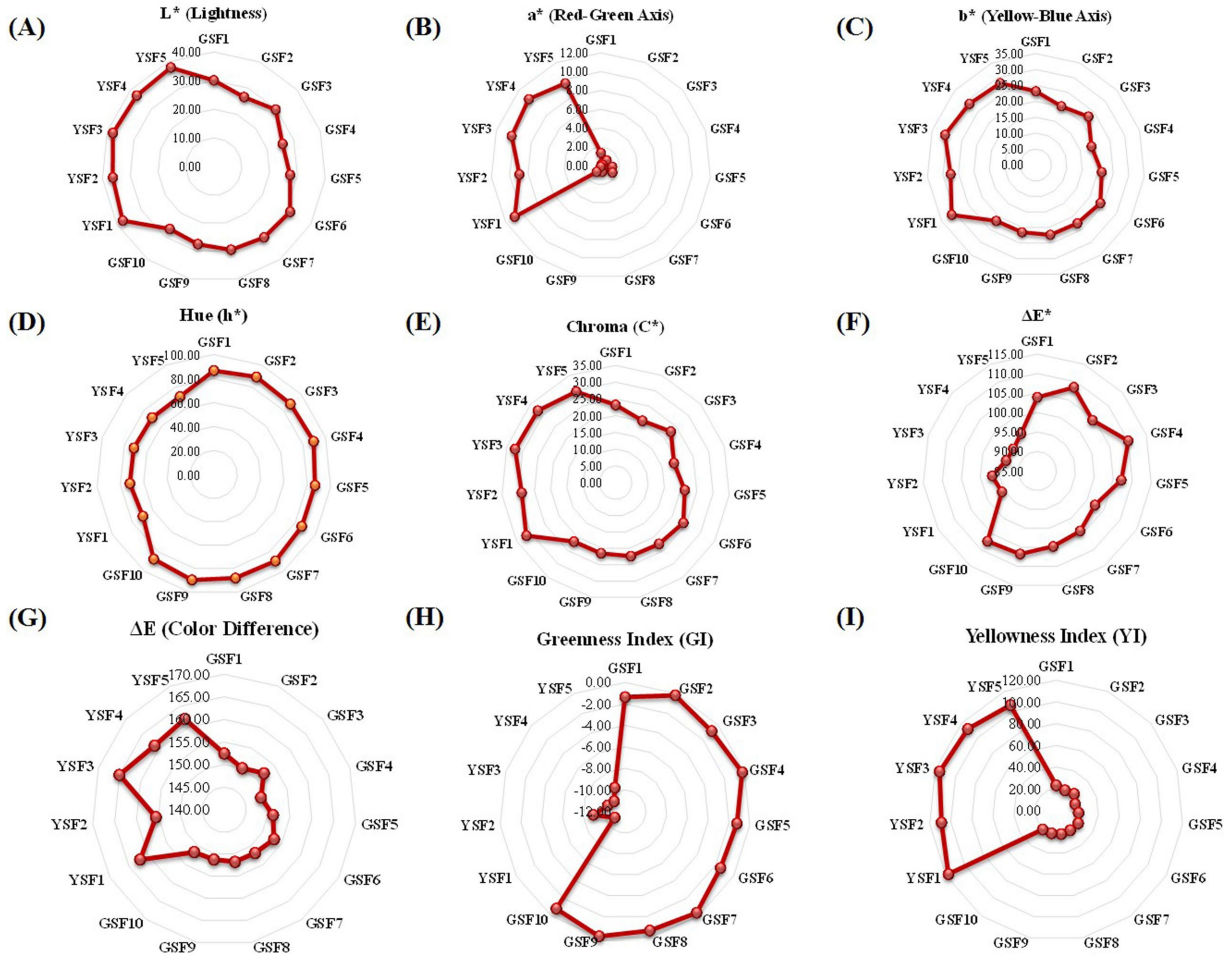

FIGURE 5
Radar graph representing the mean score of green and yellow seeded fenugreek genotypes **(A)** L* (Lightness) **(B)** a* (Red-Green Axis) **(C)** b* (Yellow-Blue Axis) **(D)** h* (Hue) **(E)** C* (Chroma) **(F)** ΔE True green **(G)** ΔE True yellow **(H)** (Greeness Index) **(I)** YI (Yellowness Index).

Oil content (%)

Oil content in green-seeded fenugreek genotypes varied from 3.13% (GSF4) to 3.74% (GSF1) with mean value of 3.50% results consistent with yellow-seeded fenugreek genotypes (Table 2).

Colorimetric characterization

Lightness (L*)

Lightness (L*), i.e., color brightness, ranged from 25.78 to 31.45 with mean value of 28.55 in GSF genotypes and from 36.31 to 37.93 with mean value of 37.34 in YSF genotypes. Colorimetric characterization values and respective graphs are represented in Figure 5 and Table 3.

Red green Axis (a*)

Red green axis (a*) component of colorimetric analysis represented positive values for all genotypes that ranges from 0.11 to 1.45 in green-seeded fenugreek and 8.94 to 10.86 in yellow-seeded fenugreek genotypes (Table 3).

Yellow blue Axis (b*)

Color coordinate study of yellow blue axis indicated that all genotypes had positive value that ranged from 18.78 to 23.91 with mean value of 21.82 in GSF and 27.52 to 31.23 with mean value of 29.26 in YSF indicating their shift toward yellowness (Table 3).

Hue (h*)

Hue in the present investigation ranged from 86.54° to 89.90° with mean value of 88.08° in GSF and 69.72° to 71.91° with mean value of 71.03° in YSF fenugreek genotypes (Table 3).

Chroma (C*)

Chroma ranged from 18.80 to 23.95 with 21.85 in GSF and 28.95 to 32.40 with mean value of 30.95 in YSF genotypes. YSF3 (32.40), YSF4 (32.09), YSF1 (31.60), and YSF5 (29.73) exhibited more saturated vividness compared to the GSF genotypes (Table 3).

Color difference (ΔE*)

ΔE* value ranged from 148.77 to 153.05 with average value of 151.40 in GSF and 155.60 to 165.01 with average value of 161.18 in

TABLE 3 Colorimetric characterization of green- and yellow-seeded fenugreek genotypes.

SN	Type	sample	L*	a*	b*	h*	Chroma (C*)	ΔE from True green	Greenness Index (GI)	ΔE* (True yellow)	Yellowness Index (YI)	Color shade code	Color shade name
1	Green-seeded fenugreek	GSF1	30.08	1.36	23.13	86.66	23.18	152.45	−1.36	103.92	23.13	#564724	Dark olive green
		GSF2	26.56	0.18	20.18	89.07	20.21	150.07	−0.18	108.48	20.18	#493e20	Dark olive green
		GSF3	29.74	0.85	22.74	87.84	22.77	152.10	−0.85	104.43	22.74	#524522	Dark olive green
		GSF4	25.78	0.21	18.78	89.45	18.80	148.77	−0.21	110.03	18.78	#473c20	Dark slate gray
		GSF5	27.38	1.23	21.27	86.69	21.31	151.12	−1.23	107.13	21.27	#4d3f20	Dim gray
		GSF6	31.45	1.45	23.91	86.54	23.95	153.05	−1.45	102.43	23.91	#584824	Dark olive green
		GSF7	30.48	0.34	22.59	89.18	22.61	151.85	−0.34	104.05	22.59	#584724	Dark olive green
		GSF8	29.62	0.66	22.39	88.30	22.40	151.77	−0.66	104.78	22.39	#524423	Dark olive green
		GSF9	27.59	0.11	21.54	89.90	21.56	151.25	−0.11	106.78	21.54	#4c4020	Dark olive green
		GSF10	26.81	0.82	21.65	87.15	21.73	151.60	−0.82	107.25	21.65	#463e1e	Dark olive green
		Mean	28.55 ± 0.61^{b}	0.72 ± 0.16^{b}	21.82 ± 0.47^{b}	88.08 ± 0.4^{a}	21.85 ± 0.48^{b}	151.4 ± 0.39^{b}	-0.72 ± 0.16^{a}	105.93 ± 0.75^{a}	21.82 ± 0.47^{b}		
		Range	25.78–31.45	0.11–1.45	18.78–23.91	86.54–89.9	18.8–23.95	148.77–153.05	−1.45 – −0.11	102.43–110.03	18.78–23.91		
2	Yellow-seeded fenugreek	YSF1	37.59	10.86	31.23	69.72	31.60	162.05	−10.86	95.72	117.51	#765125	Saddle brown
		YSF2	36.31	8.94	27.52	71.91	28.95	155.60	−8.94	96.92	108.88	#6f4f29	Saddle brown
		YSF3	37.93	10.24	30.70	71.67	32.40	165.01	−10.24	93.63	115.79	#765227	Saddle brown
		YSF4	37.04	10.59	28.72	70.76	32.09	161.24	−10.59	93.49	112.26	#745029	Saddle brown
		YSF5	37.84	9.58	28.14	71.09	29.73	161.99	−9.58	95.51	106.21	#74522b	Saddle brown
		Mean	37.34 ± 0.3^{a}	10.04 ± 0.35^{a}	29.26 ± 0.72^{a}	71.03 ± 0.39^{b}	30.95 ± 0.68^{a}	161.18 ± 1.54^{a}	-10.04 ± 0.35^{b}	95.05 ± 0.66^{b}	112.13 ± 2.1^{a}		
		Range	36.31–37.93	8.94–10.86	27.52–31.23	69.72–71.91	28.95–32.4	155.6–165.01	−10.86 – −8.94	93.49–96.92	106.21–117.51		

Data are presented as the mean ± SE. Different lowercase letters indicate a significant difference ($P < 0.05$); mean values with the same lowercase letters are not significantly different according to Duncan's multiple range test (DMRT; $P < 0.05$).

10.3389/fnut.2025.1542211

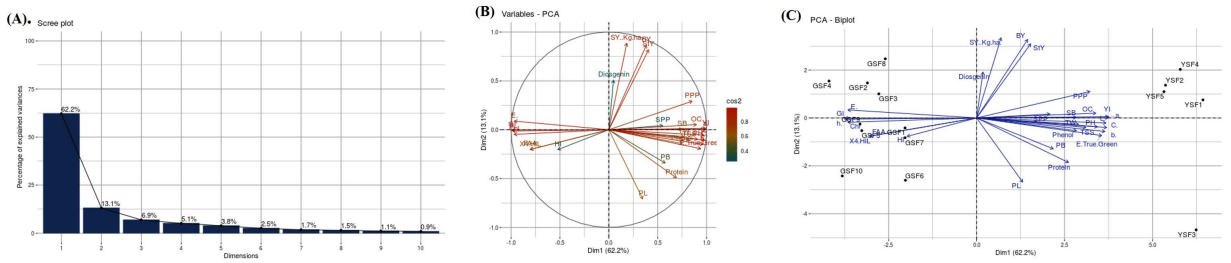

FIGURE 6
(A) Scree plot, **(B)** Variable PCA and **(C)** PCA biplot of Agronomic, Biochemical and color attributes representing variability Plant height (PH), primary branches (PB), secondary branches (SB), number of pods per plant (PPP), pod length (PL), secondary branches per plant (SPP), days to flowering (DF), maturity duration (MD), seed yield (SY), straw yield (StY), biological yield (BY), harvest index (HI) and test weight (TW), 4-hydroxyisoleucine (4-OHIle), Chlorophyll (Chl), Free amino acids (FAA), Total soluble sugars (TSS), Green Seeded Fenugreek (GSF) and Yellow Seeded Fenugreek (YSF).

YSF genotypes indicating varying degrees of deviation from a green reference, with all samples showing significant differences (Table 3).

Greenness index (GI)

Greenness index ranged from −1.45 to −0.11 with average value of −0.72 in GSF subgroup and − 10.86 to −8.94 with mean value of −10.04 in YSF subgroup of fenugreek genotypes. All GSF genotypes represented higher GI index indicating more greenness as compared to YSF subgroup of fenugreek genotypes (Table 3).

Yellowness index (YI)

Yellowness index ranged from 18.78 to 23.91 with mean value of 21.82 in GSF and from 106.21 to 117.51 with mean value of 112.13 in YSF subgroup of fenugreek genotypes. YSF subgroup had maximum value indicating more yellowness of their genotypes among all fenugreek genotypes (Table 3).

Color shade name and shade cade

Two types of genotypes were used in study: ten with green seed color (GSF) and five with yellow seed color (YSF). Green-seeded fenugreek genotypes are having three different shades, GSF1, GSF2, GSF3, GSF6, GSF7, GSF8, GSF9, and GSF10 are dark olive green, GSF4 is dark slate gray, and GSF5 is dim gray with different shade codes, whereas all the five YSF genotypes are saddle brown in color with different shade codes (Table 3).

Principal component analysis

PCA was conducted to dissect the variation patterns in fenugreek genotypes for all the studied traits. A scree plot, i.e., graphical approach (Figure 6A) was also created to represent the variability of each component. The PCA results for the GSF and YSF revealed that the total variation was dissected into 15 principal components (PCs). Out of 15 PCs, only 5 PCs presented more than 1.0 eigenvalue, whereas remaining PCs did not showcase significant variations. Individually, PC-1 had 62.18% of variance, whereas PC-2 and PC-3 illuminated 13.10 and 6.86% of the variability, respectively. Cumulatively, these three PCs described 82.14% of total variability among the attributes. PC-1 exhibited positive loading with 21 traits with maximum contribution delivered by yellowness index (0.228), red green axis (0.227), chroma (0.223), lightness (0.221), yellow blue axis (0.22), color difference (0.216), plant height (0.209), oil content (0.204), and pods per plant (0.195). In the case of PC-2, positive factor loadings were observed for 16 traits with maximum contribution delivered by pod length (0.37), protein content (0.25), primary branches per plant (0.162), harvest index (0.12), and 4-OHIle (0.103). To investigate the interaction between genotypes and traits, a genotype by trait biplot was created. The first two PC-1 and PC-2 accounted for 75.27% of the total variability and were used for the construction of a genotype by trait biplot. In the biplot, along the x-axis, the PC-1 score was plotted, and along the y-axis, the PC-2 score was plotted along with all fenugreek genotypes.

To understand the interrelationship of all investigated traits, a vector line for all traits was drawn from the origin. Through this approach, we were able to group genotypes according to their relationships and defining traits. It was noticed that the GSF and YSF genotypes were dispersed oppositely, indicating their significant genetic divergence for the traits under investigation. For PC-1, YSF genotypes exhibited high positive factor scores. Conversely, GSF genotypes exhibited negative factor scores. Furthermore, genotypes far from the origin demonstrated more variability for traits under study. It was observed that GSF genotypes were more inclined toward vectors of traits such as greenness index, color difference, chlorophyll content, 4-hydroxy isoleucine, free amino acid, days to 50% flowering, and harvest index as compared to remaining traits. Furthermore, it was interpreted that color contributing and biochemical traits such as 4-hydroxyisoleucine, chlorophyll, diosgenin, and total soluble sugar were major variability contributing traits (Figures 6B,C) (Supplementary Tables S3–S5).

Trait correlation analysis

The worth of independent secondary traits in the selection process can be determined by their significant correlation with a dependent trait of interest. The correlation coefficient analysis was estimated to assess the relationship between the traits under investigation

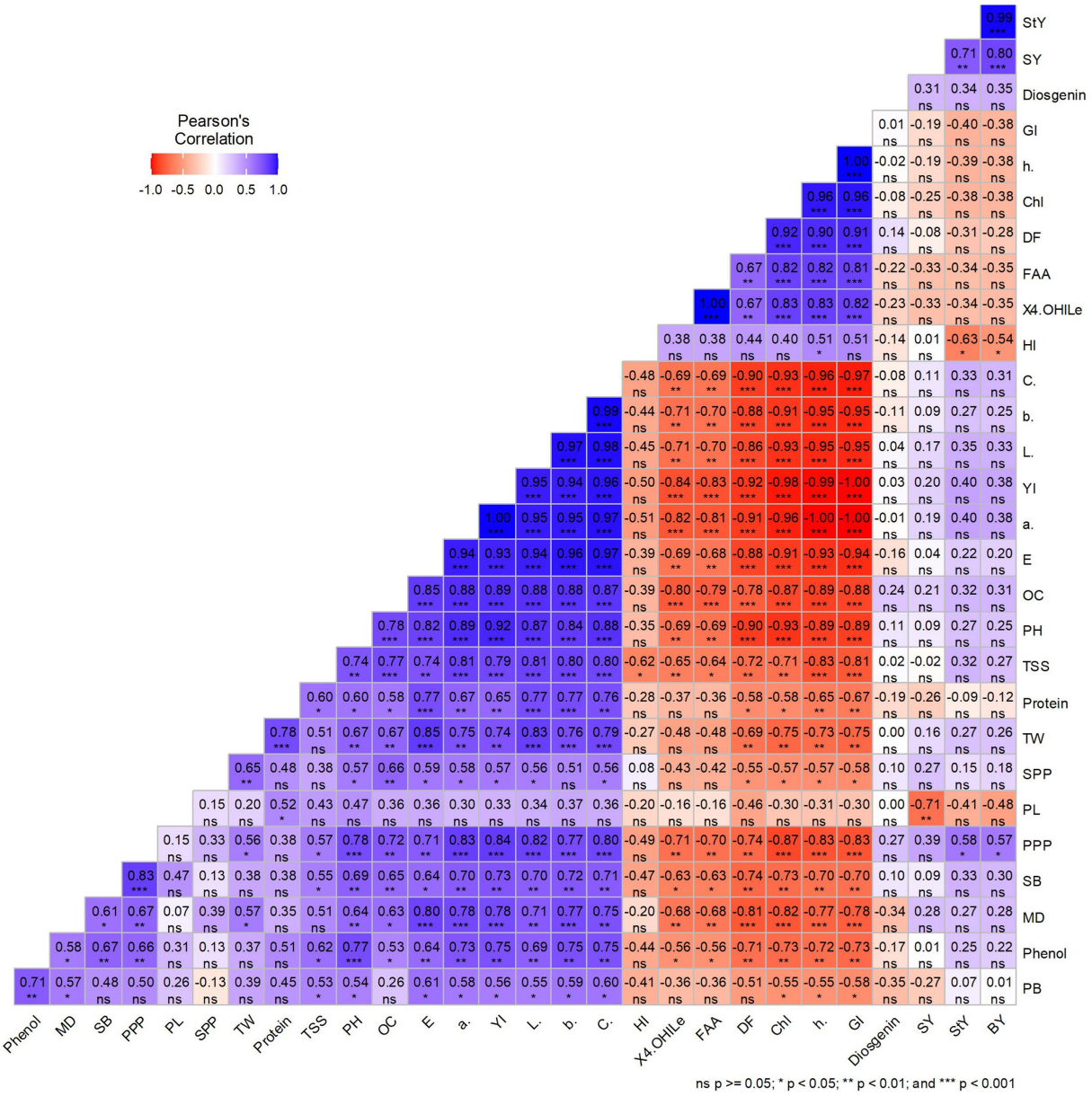

FIGURE 7
Correlation heat map for all studied traits among fenugreek genotypes PH (Plant height), PB (Primary branches per plant), SB (Secondary branches per plant), DF (Days to flowering), MD (Days to Maturity), PPP (Pods per plant), PL (Pod length), SPP (Seeds per pod), SY (Seed yield), BY (Biological yield), HI (Harvest index), TW (Test weight), 4-OHIle (4-Hydroxyisoleucine), TSS (Total soluble sugar), OC (Oil content), FAA (Free fatty acid), Chl (Chlorophyll content), L* (Lightness), a* (Red green axis), b* (Yellow blue axis), h (Hue), C (Chroma), E (Color difference), GI (Greeness index) YI (Yellowness index).

(Figure 7). 4-hydroxy isoleucine, chlorophyll content, free amino acid, hue, and greenness index were significantly positively correlated with each other. It appears that these traits are major contributors for enhancing the medicinal and nutritional status of fenugreek genotypes. An increase in chlorophyll content and greenness index is associated with higher level of 4-hydroxy isoleucine. Therefore, visually selecting fenugreek genotypes with green seeds may provide a promising option for addressing diabetes and obesity issues. Furthermore, it was observed that chroma, yellow blue axis, lightness, red green axis, color difference, oil content, plant height, total soluble sugar, pods per plant, secondary branches per plant, maturity days, and phenol content were significantly negatively correlated with 4-hydroxy isoleucine, free amino acid, days to flowering, chlorophyll content, hue, and greenness index. A significant negative correlation between 4-hydroxyisoleucine and total soluble sugar revealed their opposing behavior. This indicates that green-seeded fenugreek genotypes, with higher 4-OHIle will have lower TSS content, possess greater potential for human health benefits.

Yellow blue axis, chroma, lightness, yellowness index, red green axis, color difference, oil content, plant height, total soluble sugar, protein content, and test weight had significant positive correlation with each other. Number of seeds per pod depicted significant positive correlation with test weight, plant height, oil content, color difference, red green axis, yellowness index, lightness, and chroma, while it

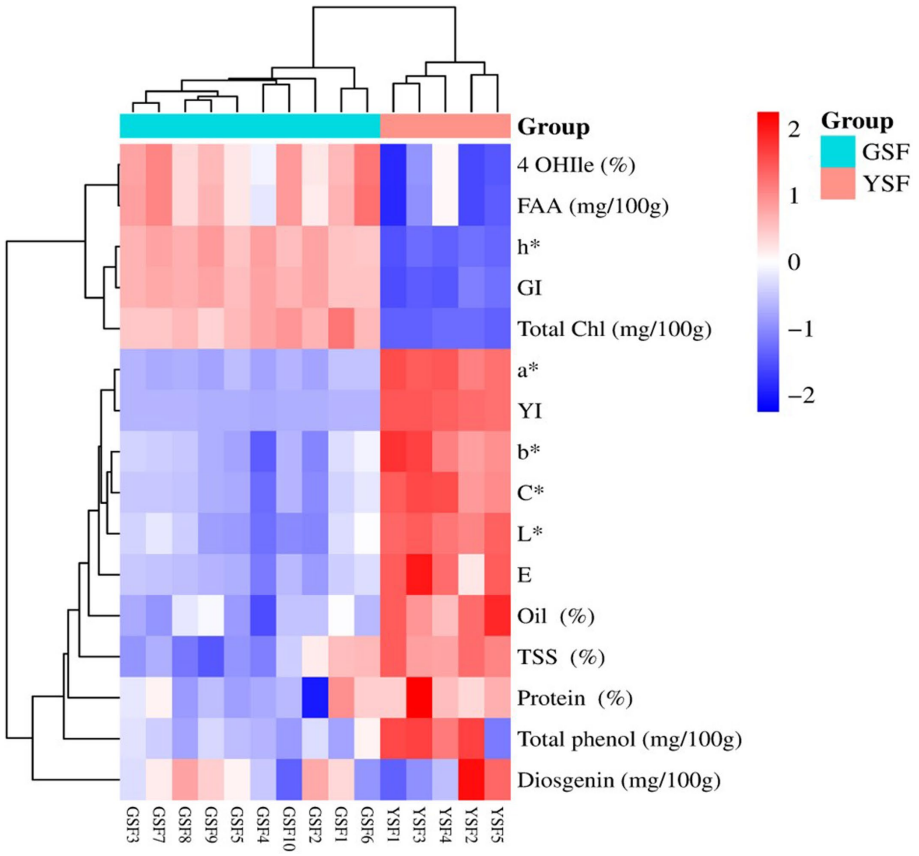

FIGURE 8
Two-way clustering heatmap for fenugreek genotype based on biochemical and seed color traits 4-OHIle (4-Hydroxyisoleucine), FAA (Free fatty acid), h* (Hue), GI (Greeness index), Total Chl (Total chlorophyll content), a*(Red green axis), YI (Yellowness index), b* (Yellow blue axis), C* (Chroma), L* (Lightness), E (Color difference), TSS (Total soluble sugar).

showed significant negative correlation with chlorophyll content, hue, and greenness index. Yellow-seeded fenugreek genotypes found to be agronomically better than green-seeded fenugreek genotypes; however, comparative performance difference for yield was not found to be so effective. The harvest index was higher in green-seeded genotypes due to differences in straw yield, highlighting their potential for commercial utilization too. In addition, there is scope to enhance the economic yield of green-seeded genotypes through the optimization of agronomical package of practices.

Two-way clustering heat map and regression analysis

Data for biochemical and color traits along with experimental genotypes were subjected to two-way clustering heat map analysis, and a dendrogram was generated to visually inspect the clusters of genotypes. Two-way clustering heat map illustrating relationships between different traits (biochemical and color traits) (y-axis) regarding fenugreek genotypes estimated (x-axis) is shown in Figure 8. Colors within the heat map range from light blue (least prevalent) to dark red (most prevalent), illustrating the prevalence of a particular trait within a particular group. Clustering analysis was performed based upon the colors generated using complete cluster method and Euclidean distance. Cluster analysis cleaved 15 genotypes into two clear-cut distinct groups, i.e., GSF (green-seeded fenugreek) and YSF (yellow-seeded fenugreek) genotypes.

The simple linear regression analysis was conducted to assess the relationship between yield-attributing traits (X-axis) and seed yield (Y-axis) and between biochemical traits (X-axis) and chlorophyll (Chl) content (Y-axis). The scatter plots, along with the fitted regression lines, are shown in Figure 9. The regression coefficients, with p-values <0.05 (alpha = 0.05), were found to be statistically significant for both the yield-contributing and biochemical traits. Among the agronomic traits, the biological yield (R^2 = 63.39%) explained the greatest variation in seed yield. The graph indicates a positive linear relationship between biological yield and seed yield, with the regression line suggesting that as biological yield increases, seed yield also increases. The regression equation for this relationship is "Y = 759.27 + 0.1448X." For the biochemical traits, 4-OHIle (R^2 = 68.08%) and TSS (R^2 = 49.75%) accounted for the highest proportions of variation in chlorophyll content. Both 4-OHIle and TSS showed linear relationships with chlorophyll content. Specifically, 4-OHIle exhibited a positive correlation, whereas TSS demonstrated a negative correlation with chlorophyll content. The regression equations for these relationships are "Y = −0.3978 + 0.8995X" for 4-OHIle and Y = 0.8269–0.1161X for TSS. These findings suggest that the biological yield and 4-OHIle

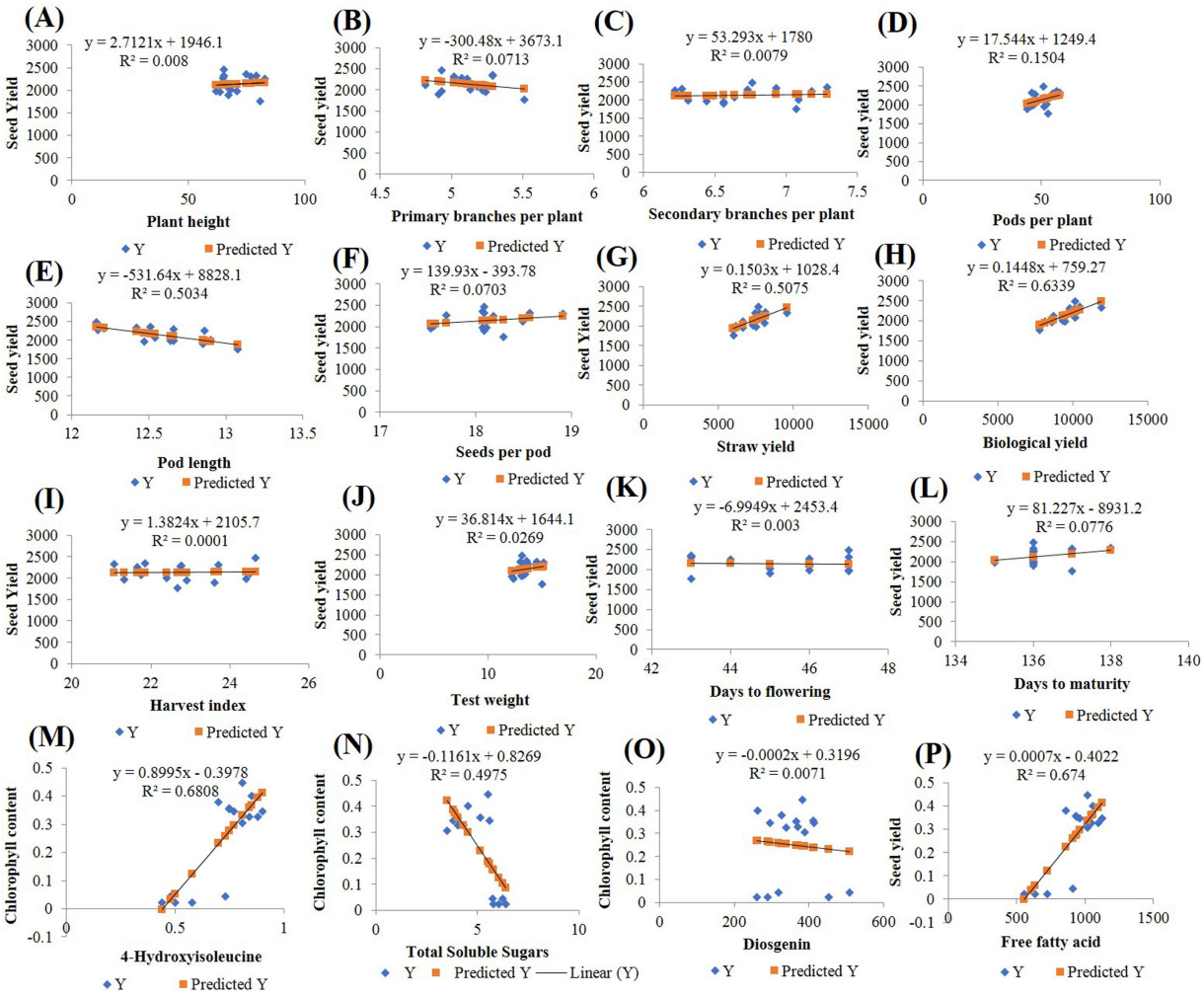

FIGURE 9
Regression analysis **(A)** Plant height **(B)** Primary branches per plant **(C)** Secondary branches per plant **(D)** Pods per plant **(E)** Pod length **(F)** Seeds per pod **(G)** Straw yield **(H)** Biological yield **(I)** Harvest index **(J)** Test weight **(K)** Days to flowering **(L)** Days to maturity **(M)** 4-Hydroxyisoleucine **(N)** Total soluble sugars **(O)** Disogenin **(P)** Free fatty acid.

significantly contribute to variations in seed yield and chlorophyll content, respectively.

Discussion

Fenugreek is a potential source of medicinal compounds, but very limited variability is available in this crop. Hence, an experiment was conducted to develop a variety/genotype of the crop having higher concentrations of beneficial compounds. Fenugreek varieties, cultivars, and wild species are typically available with yellow color seeds, whereas green seeds are unusual. It has been proven that these green-seeded fenugreek genotypes show better performance in terms of medicinal properties as compared to their yellow counterparts (10) thereby making them an important natural dietary source for the individuals suffering from diabetes, obesity, insulin resistance, and tumor formation tendency in the body.

Obesity, diabetes, insulin resistance, and tumor formation are some of the common diseases affecting a large percentage of population. Few decades back, these diseases were thought to be correlated with aging but today we find small kids, teenagers, and youngsters also facing these issues. The major reason behind this may be an unhealthy lifestyle and unhealthy/poor diet. Other than regular diet, some natural supplements may offer additional nutrients necessary for the body. While synthetic medicines and supplements are available in the market as secure to the mentioned diseases, they come with their own share of ill side effects. Such is not the case with fenugreek, being a legume crop fenugreek is considered as an incredible source of protein, fiber, and minerals (4). The major component, which is very crucial to manage the insulin in body, is 4-hydroxyisoleucine (4-OHIle), and Fenugreek seeds are a rich source of 4-OHIle (44). Its consumption as medicine has been approved safe by United States Food and Drug Administration (FDA). This crop is rich not only in 4-OHIle but also in diosgenin, protein, free amino acids, total soluble sugar, and natural oil content (24).

To gain a deeper understanding of the agronomic and medicinal significance, an experiment was conducted in which both green- and yellow-seeded fenugreek genotypes were sown in the field during the rabi season across 3 consecutive years: 2021–22, 2022–23, and

2023–24. Sowing was done in 44th week for all the 3 years when the lowest temperature was 12 to 15°C and highest was 31 to 34°C with relative humidity (RH) 85–92% in morning. Germination took place within 4–5 days in all the genotypes. Data were recorded timely for all the agronomic traits, and significant differences were observed among the genotypes for all measured traits ($p < 0.01$, Table 2) suggesting variations among fenugreek genotypes. These results are consistent with the previous published reports by different researchers (45–47).

During different stages of crop growth, data were recorded for days to flowering (DF) and days to maturity (MD). After harvesting of fully matured crop, the data were recorded for PH, PB, SB, PPP, PL, SPP, SY, StY, BY, HI, and TW. Boxplot (Figure 3) analysis revealed consistent variation for the mentioned traits. The plant height of the fenugreek genotypes was significantly different among the cropping years which may be because of different weather conditions and rain patterns. Green-seeded fenugreek (GSF) genotypes showed statistical difference in comparison with yellow-seeded fenugreek (YSF) genotypes. The results are also consistent with the previous study by Sharma and Sastry (48) and Singh et al. (49) who reported average plant height in fenugreek genotypes as 49.8 cm and 65.91 cm, respectively. Similarly in the present experiment, average plant height ranges from 62 to 71 cm in GSF genotypes and 75 to 83 cm in YSF. In pooled data, the average plant height values were more in YSF genotypes as compared to GSF genotypes. When plants have increased number of vegetative parts and decreased row spacing, they achieve more height when compared to others. This situation can be explained by the increasing light competition (50). In addition, it has been stated that the height of plants decreases with the restriction of irrigation (51, 52). Similarly, in a previous research study, plant height was reported to be 24.95–85.15 cm (53) and 26.8 ± 14.9 cm in Omani fenugreek accessions (54). The findings showed that the number of primary branches is almost similar in most of the GSF and YSF genotypes barring a few. The branch number values were higher in 2022–23 than other growing years. This situation supports the opinion that precipitation and other environmental factors play important role in increasing the number of branches in fenugreek genotypes. These findings were partly similar to the results of Sharma and Sastry (48), who reported that branch numbers varied between 2.3 and 7.5 in 245 fenugreek genotypes. Similarly, the branch number of different fenugreek genotypes was found to be 2.18–7.98 (55), 2.40–4.90 (56), and 1.00–4.33 (57). Seeds per pod were comparable for both GSF and YSF genotypes over all three *rabi* seasons 2021–22, 2022–23, and 2023–24. Generally, it ranged from 17 to 19 in both fenugreek types. Singh et al. (58) reported number of pods/plant, pod length, and number of seeds/pod as 41.2, 9.47, and 16.67, respectively. In previous study by Desai et al. (59), highest number of pods/plant, pod length, and seeds/pod were reported to be 57.07, 12.57 cm, and 15.89 in *Pusa* Early Bunching. These results are consistent with our results. Similarly, Al-Maamari et al. (54) reported number of pods (32.1 ± 21.4), pod length (9.1 ± 1.2 cm), and number of seeds (134.2 ± 101.7) in fenugreek accessions. Camlica Mahmut and Gulsum (53) also observed the seeds/pod from 3.56 to 14.30 and pod length from 7.01 to 36.10 cm.

Maturity days were recorded, and it was reported that all fenugreek genotypes studied had a maturation duration time of 135–40 days. Pusa Early Bunching variety of fenugreek matured in 125–130 days. Singh et al. (60) claimed an extra early maturing accession *IC 0624520* that matured in 120 to 140 days. It was observed in our study that green-seeded genotypes took 3–4 more days in 50% flowering when compared to YSF. Bhutia et al. (61) reported that flowering took place in approximately 49.25 days in fenugreek, whereas Sultana et al. (62) reported that 50% flowering took place in 44.60 days.

Seed yield showed significant differences in the *rabi* periods of 2021–22, 2022–23, and 2023–24 among the fenugreek genotypes grown under normal condition. Some of the main reasons for the difference in seed yield between years and genotypes is the difference in environmental and genetic factors during the vegetation period (63). It was reported that morphological properties such as plant height and branch number can be closely related to seed yield in fenugreek (64). It has been reported that the seed yield is higher in fenugreek genotypes with higher plant height, maturation time, and biological yield (65), but our GSF genotypes showed better seed yield in comparison with YSF genotypes although the plant height of GSF genotypes is less than the YSF genotypes. This may be because of the bold size of the seeds of GSF. In addition, it was also reported that seed yield varies depending on years, sowing date, harvest date, climatic conditions, and irrigation (66). In a study for standardization of organic module for sustainable production of fenugreek, the observed number of branches, number of pods, number of seeds, and highest grain yield were 6.76 per plant, 42 pods/plant, 16.01 seed/pod, and 1515.21 kg/ha, respectively (67).

Straw yield reported to be higher for YSF genotypes as compared to GSF genotypes indicating more photosynthates accumulation. Singh et al. (58) reported straw yield (4,954 kg/ha), which is almost half of our reported straw yield. This may be because of environment, genotype, and date of sowing variability. Biological yield of fenugreek genotypes can vary significantly, depending on the genotypes and the environmental conditions. Seed yield, biological yield, and harvest index of the green-seeded fenugreek genotypes are more in comparison with the yellow-seeded fenugreek genotypes, favoring the GSF genotypes in terms of the agronomic traits. The data showed that GSF genotypes performed better over YSF for PL, SY, StYBY, HI, and TW when lesser rains (624.7 mm in 2021–22) were received in comparison with 2022 to 2024 (915.3 mm and 996.0 mm). Further studies can reveal its adaptability to moisture stress. Given the medicinal potential of the green-seeded genotypes compared to the yellow-seeded ones, their slight yield loss is not a major concern. This can be offset by the higher commercial value of the GSF genotypes, making them a favorable choice for farmers in monetary terms while providing greater benefits from the same resources.

Yield is one of the important characters for any genotype/variety, but spices and medicinal crops are better judged based on the medicinal potential rather than the yield. In our experiment, all the tested GSF genotypes are superior to YSF genotypes in medicinal properties. The most abundant free amino acid in fenugreek, 4-hydroxyisoleucine, belongs to the category of amino acid derivatives or bioactive compounds but not secondary metabolites. It is primarily known for its role in modulating insulin secretion and influencing glucose metabolism and acts as a precursor for insulin secretion, which has made it a subject of study in diabetes management. This amino acid is primarily found in the seed endosperm of fenugreek (43), and its abundance in the seeds

contributes to the nutritional and medicinal value of the plant. Previous literature reports a wide range of 4-OHIle concentrations in fenugreek seeds, ranging from 0.015 to 0.4% (44, 68, 69). Haeri et al. (70) reported that germinated fenugreek seeds contain roughly double 4-OHIle as compared to dry fenugreek seeds. Rajabihashjin et al. (71) had suggested that temperature and solar irradiation play significant roles in the accumulation of 4-OHIle. 4-OHIle may be a potential treatment for insulin resistance by regulating blood glucose, lipotoxic reducer, liver function enhancer, and obesity inhibitor. GSF6, GSF7, GSF10, and GSF3 can be rich source for antidiabetic and anti-obesity effects having almost 1.5 to double amount of 4-OHIle in comparison with YSF and other reported genotypes by different researchers. 4-OHIle exerts its effect by enhancing Akt phosphorylation and reducing the stimulation of Jun N-terminal kinase (JNK) 1/2, extracellular signal regulated kinase (ERK) 1/2, p38 mitogen activated protein kinase (MAPK), and nuclear factor (NF)-κB (24).

Chlorophyll-rich food is associated with brain health, anti-cancer properties, neuroprotective, endocrine disruptor effects, and anti-obesity effects with ample of antioxidant properties (26). Its unique structure assists it to scavenge harmful free radicles, DNA damage repairment, and cellular process regulation (72–74). In a study, it was found that *in vivo* absorption of chlorophyll derivative using SCC tablets (300 mg/day) resulted in absorption of Cu-chlorin e4 ethyl ester in human gastrointestinal tract (75). Matured seeds of fenugreek contain the raffinose family oligosaccharides (RFOs) as the major storage sugars, i.e., 65.37 mg g^{-1} DW (76). Total soluble sugar plays a negative role for the diabetic persons. GSF genotypes are reported to be lower in TSS in comparison with YSF genotypes, favoring the consumption of GSF for sugar patients or health-conscious persons. The amount and type of carbohydrates in the diet impact blood glucose levels, which in turn affect insulin release and the rate of gastric emptying (77).

Diosgenin (*25R-spirost-en-3β-ol*), a steroidal compound, plays an important role in diabetes cure by cellular pathway modulation. It works by reducing intestinal glucose uptake, decreasing metabolism in organ and tissues, increasing insulin secretion, and improving insulin resistance. Diabetes alters pathways such as *serine/threonine protein kinase* and *protein kinase C /glucose transporter 4*, and peroxisome proliferator-activated receptor glucose absorption, and inhibits *α-amylase* and *α-glucosidase*, *sodium/glucose cotransporter 1,* and Na^+ K^+ *ATPase* activity. Diabetes may also be caused by a decrease in the expression of *sterol regulatory element binding protein 1* and its target genes, *fatty acid synthase*, *stearoyl-CoA desaturase-1,* and *acetyl-CoA carboxylase α* as well as a decrease in the levels of *C/EBP homologous protein*, *Caspase12,* and *Caspase3* proteins (78). Moreover, diosgenin possesses anticarcinogenic properties which reduce tumor cell proliferation and triggering apoptosis (79). But as studies by Khosravi et al. (80) show, overdose of diosgenin may cause male infertility. Diosgenin ranges from 0.1 to 0.90% in seeds (81). Diosgenin content is low in GSF10, supporting its consumption for males who are consuming fenugreek seeds for other health benefits.

FAAs, water-soluble compounds, are key quality signs of processing and storage conditions. In addition, some free amino acids contribute to taste and aroma by participating in Maillard reactions through the generation of volatile compounds (82). Higher amount of free amino acids in GSF is an additional feature of green-seeded fenugreek genotypes further enhancing its benefits.

Total phenol has antioxidant properties, i.e., preventive in chronic illnesses such as cancer, diabetes, cardiovascular disease, and neurodegenerative diseases (83, 84). Reactive oxygen species (ROS) includes superoxide, peroxide, singlet oxygen, nitric oxide, hydroxyl radical, and peroxynitrite that are produced during impaired antioxidant system leading to cellular damage (85). Researchers have indicated that fenugreek contains 6–8% (86), 6.7% (87), 8.94% (88), 3.25–6.88% (89), and 8% (90) oil content. Our study showed that the oil content is almost in similar range (3.0 to 4.5%) in both the GSF and YSF genotypes. Many researchers have reported fenugreek seed protein content ranging from 20–26% (86, 91, 92). In our study, YSF genotypes showed protein levels of 21–25%, higher than the 15.7–21.7% found in GSF genotypes.

Seed color is vital in breeding due to its role in germination, dormancy, and stress resistance (93, 94), serving as marker for genetic purity and seed quality (95). It significantly also impacts or influences marketability as uniform and desired appealing color meet consumer preferences and fetch premium prices. Integrating seed color traits ensures better performance, quality, and acceptance. The current seed chromatic analysis distinctly categorized different fenugreek genotypes into two distinct groups, i.e., yellow- and green-seeded. The GSF1 has greenest/darkest green color seeds with highest amount of chlorophyll among studied genotypes. YSF1 and YSF3 had maximum yellow pigment. Based on the values for L*a*b*, seed color code and color shade name were identified which revealed that the green-seeded fenugreek genotypes had three different shades of green color (dark olive green, dark slate gray, and dim gray), whereas all the five YSF genotypes had saddle brown shade of yellow color (Table 3). The findings showed wider diversity in terms of degree of greenness and yellowness among the GSF and YSF genotypes. Hence, these genotypes could be used as donor parents for incorporating and introgression of green, yellow, or intermediate color types of fenugreek seeds. In addition, seed color also symbolizes quality, and traits such as nutritional content as pigments like carotenoids and tannins contributed to both color and health benefits (96). The information generated in this study could also be utilized for identifying genotypes having higher levels of medicinal compounds, antioxidants, and phenolic and essential nutrients offering enhanced protection against oxidative stress. Understanding relationship between seed color and nutrition further allows breeders to develop varieties that combine aesthetic appeal with improved nutritional profiles meeting out both consumer demand and health objectives.

Conclusion

In the present study, significant variability was observed for agro-morphological traits, biochemical components, and color content in both types of the fenugreek genotypes. The findings showed that the green-seeded genotypes are the potential source for medicinal values with good amount of biological yield and harvest index. The yield of green-seeded fenugreek genotypes can be improved with more rigorous agronomic practices. GSF genotypes are rich source of 4-hydroxyisoleucine (4-OHIle%), which may play a very important role in insulin resistance and obesity. The green fenugreek seeds contain 1.5 to double amount of 4-OHIle and can be potential natural source as medicine for

diabetes and obesity. Genotype GSF6 (IC-0633367) is rich in 4-OHIle (0.90%), and genotype GSF9 (IC-0633370) has lowest amount of TSS with good amount of 4-OHIle (0.81%). Genotype GSF1 (IC-0633362) is rich in Chl content with darkest green color, good amount of 4-OHIle, oil, and protein. Genotype GSF8 (IC-0633369) showed better seed yield (2473.74 kg ha^{1}) and harvest index (24.65%). Green-seeded genotypes have been reported to be particularly valuable in future breeding projects for better fenugreek varieties, as well as in the medical, pharmaceutical, and ayurvedic industries. It is essential to study the agronomic and yield characteristics of fenugreek genotypes under various agro-ecological conditions to fully understand and further strengthen their potential and variability. In addition, exploring the genetic basis of these traits could uncover novel genes and pathways that can be targeted to enhance future breeding efforts and optimize the crop's therapeutic and agricultural value.

Data availability statement

The original contributions presented in the study are included in the article/Supplementary material, further inquiries can be directed to the corresponding authors.

Author contributions

RS: Conceptualization, Data curation, Investigation, Methodology, Project administration, Resources, Supervision, Writing – original draft, Writing – review & editing. RSM: Conceptualization, Investigation, Validation, Writing – review & editing. SC: Conceptualization, Data curation, Formal analysis, Investigation, Methodology, Validation, Visualization, Writing – original draft, Writing – review & editing. NM: Investigation, Writing – review & editing. RDM: Writing – review & editing. AV: Investigation, Writing – review & editing. MM: Formal analysis, Writing – review & editing. RY: Formal analysis, Writing – review & editing. SL: Formal analysis, Writing – review & editing. PS: Formal analysis, Software, Writing – review & editing. VB: Project administration, Supervision, Writing – review & editing.

Funding

The author(s) declare that no financial support was received for the research, authorship, and/or publication of this article.

Acknowledgments

The authors gratefully acknowledge the Director, ICAR-NRCSS, Ajmer, for providing research facility and support to conduct the study. Authors are thankful to employees (Mangilal and Rajesh Gena) who contributed to this study.

Conflict of interest

The authors declare that the research was conducted in the absence of any commercial or financial relationships that could be construed as a potential conflict of interest.

Generative AI statement

The authors declare that no Generative AI was used in the creation of this manuscript.

Publisher's note

All claims expressed in this article are solely those of the authors and do not necessarily represent those of their affiliated organizations, or those of the publisher, the editors and the reviewers. Any product that may be evaluated in this article, or claim that may be made by its manufacturer, is not guaranteed or endorsed by the publisher.

Supplementary material

The Supplementary material for this article can be found online at: https://www.frontiersin.org/articles/10.3389/fnut.2025.1542211/full#supplementary-material

References

1. Najafi S, Anakhatoon EZ, Avci BM. Karyotype characterisation of reputed variety of fenugreek (*Trigonella foenum-graecum*) in West Azerbaijan-Iran. *J Appl Biol Sci*. (2013) 7:31–4.

2. Paramesha M, Priyanka N, Crassina K, Shetty NP. Evaluation of diosgenin content from eleven different Indian varieties of fenugreek and fenugreek leaf powder fortified bread. *J Food Sci Technol*. (2021) 58:4746–54. doi: 10.1007/s13197-021-04967-z

3. Altuntaş E, Özgöz E, Taşer ÖF. Some physical properties of fenugreek (Trigonella foenum-graceum L.) seeds. *J Food Eng*. (2005) 71:37–43. doi: 10.1016/j.jfoodeng.2004.10.015

4. Choudhary S, Singh R, Ravi Y, Gena CB, Singh D, Harisha CB, et al. Phytotherapeutic, Nutraceutical, Medicinal, and forage properties of fenugreek (*Trigonella foenumgraecum* L.): a comprehensive review. *J Adv Biol Biotechnol*. (2024) 27:719–33. doi: 10.9734/jabb/2024/v27i101494

5. Srinivasan K. Fenugreek (*Trigonella foenum-graecum*): a review of health beneficial physiological effects. *Food Rev Int*. (2006) 22:203–24. doi: 10.1080/87559120600586315

6. Al-Jasass FM, Al-Jasser MS. Chemical composition and fatty acid content of some spices and herbs under Saudi Arabia conditions. *Sci World J*. (2012) 2012:1–5. doi: 10.1100/2012/859892

7. Leela N, Shafeekh K. Fenugreek. In: Parthasarathy, V.A., Chempakam, B. and Zachariah, T.J., Eds., Chemistry of Spices, CAB International . (2008). Pondicherry. 242–259.

8. Sauvaire Y, Girardon P, Baccou JC, Ristérucci AM. Changes in growth, proteins and free amino acids of developing seed and pod of fenugreek. *Phytochemistry*. (1984) 23:479–86. doi: 10.1016/S0031-9422(00)80363-5

9. Singh SP, Sashidhara KV. Lipid lowering agents of natural origin: an account of some promising chemotypes. *Eur J Med Chem*. (2017) 140:331–48. doi: 10.1016/j.ejmech.2017.09.020

10. Singh R, Meena RS, Sharda C, Meena NK, Meena RD, Verma AK, et al. Unique green seed fenugreek genotypes for higher insulinotropic 4-Hydroxyisoleucine (4-OHIle), chlorophyll and steroidal saponin diosgenin. *Natl Acad Sci Lett*. (2025)

11. Moneim A, Sulieman E, Ahmed HE, Abdelrahim AM. The chemical composition of fenugreek (*Trigonella foenum graceum* L) and the antimicrobial properties of its seed oil. *Gezira J Eng Appl Sci*. (2008) 3:52–71.

12. Niknam R, Kiani H, Mousavi ZE, Mousavi M. Extraction, detection, and characterization of various chemical components of *Trigonella foenum-graecum* L.

(fenugreek) known as a valuable seed in agriculture. *Fenugreek Biol Appl*. (2021):189–217. doi: 10.1007/978-981-16-1197-1_9

13. Singh N, Yadav SS, Kumar S, Narashiman B. Ethnopharmacological, phytochemical and clinical studies on fenugreek (*Trigonella foenum-graecum* L.). *Food Biosci*. (2022) 2022:101546. doi: 10.1016/j.fbio.2022.101546

14. Rafiullah M, Benabdelkamel H, Masood A, Ekhzaimy AA, Musambil M, Joy SS, et al. Urinary proteome differences in patients with type 2 diabetes pre and post Liraglutide treatment. *Curr Issues Mol Biol*. (2023) 45:1407–21. doi: 10.3390/cimb45020092

15. Campbell RK. Type 2 diabetes: where we are today: an overview of disease burden, current treatments, and treatment strategies. *J Am Pharm Assoc*. (2009) 49:S3–9. doi: 10.1331/JAPhA.2009.09077

16. Paul Zimmet K, Alberti JS. Global and societal implications of the diabetes epidemic. *Nature*. (2001) 414:782–7. doi: 10.1038/414782a

17. Ferlay J, Ervik M, Lam F, Colombet M, Mery L, Piñeros M, et al. Global cancer observatory: cancer today. Lyon: International agency for research on cancer (2020). 20182020 p.

18. Daviesa MJ, Ahmada E, Limb S, Lampteyc R, Webb DR. Cancer is becoming the leading cause of death in diabetes – Authors' reply. *Lancet J*. (2023) 401:1849–50.

19. American Diabetes Association. Diagnosis and classification of diabetes mellitus. Diabetes Care. (2012) 35:S64–71. doi: 10.2337/dc12-s064

20. Geiss LS, Herman WH, Smith PJ. Mortality in non-insulin-dependent diabetes. Diabetes in America. (1995) 2:233–55.

21. Acharya SN, Thomas JE, Basu SK. Fenugreek, an alternative crop for semiarid regions of North America. *Crop Sci*. (2008) 48:841–53. doi: 10.2135/cropsci2007.09.0519

22. Broca C, Breil V, Cruciani-Guglielmacci C, Manteghetti M, Rouault C, Derouet M, et al. Insulinotropic agent ID-1101 (4-hydroxyisoleucine) activates insulin signaling in rat. *Am J Physiol Endocrinol Metab*. (2000) 287:E463–71. doi: 10.1152/ajpendo.00163.2003

23. Kannan MR, Gayathri R, Priya VV. Cytotoxic potential of fenugreek extract on oral cancer cell lines – an in vitro study. *Drug Invent Today*. (2019) 11:1630–2.

24. Avalos-Soriano A, De La Cruz-Cordero R, Rosado JL, Garcia-Gasca T. 4-Hydroxyisoleucine from fenugreek (*Trigonella foenum-graecum*): effects on insulin resistance associated with obesity. *Molecules*. (2016) 21:1596. doi: 10.3390/molecules21111596

25. Laila U, Albina T, Zuha SS, Tamang H, Author C, Zuha S. Fenugreek seeds: nutritional composition and therapeutic properties. *Pharma Innov J*. (2022) 11:2417–25.

26. Madhava NM, Shyamala BN, Pura Naik J, Sulochanamma G, Srinivas P. Chemical composition and antioxidant activity of the husk and endosperm of fenugreek seeds. *LWT*. (2011) 44:451–6. doi: 10.1016/j.lwt.2010.08.013

27. Syed QA, Rashid Z, Ahmad MH, Shukat R, Ishaq A, Muhammad N, et al. Nutritional and therapeutic properties of fenugreek (*Trigonella foenum-graecum*): a review. *Int J Food Prop*. (2020) 23:1777–91. doi: 10.1080/10942912.2020.1825482

28. Salman MT, Qadeer F. Pharmacological actions and therapeutic potential of *Trigonella foenum-graecum* L. *Fenugreek Biol Appl*. (2021):523–37. doi: 10.1007/978-981-16-1197-1_22

29. Bakhtiar Z, Hassandokht M, Naghavi MR, Mirjalili MH. Variability in proximate composition, phytochemical traits and antioxidant properties of Iranian agro-ecotypic populations of fenugreek (*Trigonella foenum-graecum* L.). *Sci Rep*. (2024) 14:87. doi: 10.1038/s41598-023-50699-9

30. Platel K, Srinivasan K. Influence of dietary spices and their active principles on pancreatic digestive enzymes in albino rats. *Nahrung – Food*. (2000) 44:42–6. doi: 10.1002/(SICI)1521-3803(20000101)44:1<42::AID-FOOD42>3.0.CO;2-D

31. Sowmya P, Rajyalakshmi P. Hypocholesterolemic effect of germinated fenugreek seeds in human subjects. *Plant Foods Hum Nutr*. (1999) 53:359–65. doi: 10.1023/A:1008021618733

32. Mathern JR, Raatz SK, Thomas W, Slavin JL. Effect of fenugreek fiber on satiety, blood glucose and insulin response and energy intake in obese subjects. *Phyther Res*. (2009) 23:1543–8. doi: 10.1002/ptr.2795

33. Syeda BB, Muhammad IB, Shahabuddin M. Antioxidant activity from the extract of fenugreek seeds. *Pak J Anal Environ Chem*. (2008) 9:78–83.

34. Bhatia K, Kaur M, Atif F, Ali M, Rehman H, Rahman S, et al. Aqueous extract of *Trigonella foenum-graecum* L. ameliorates additive urotoxicity of buthionine sulfoximine and cyclophosphamide in mice. *Food Chem Toxicol*. (2006) 44:1744–50. doi: 10.1016/j.fct.2006.05.013

35. Blank I, Lin J, Devaud S, Fumeaux R, Fay LB. The principal flavor components of fenugreek (*Trigonella foenum-graecum* L.). In ACS symposium series *660*: 12–28. Washington, DC: American Chemical Society (1974).

36. Mazza G, Oomah B. Color evaluation and chlorophyll content in dry green peas. *J Food Qual*. (1994) 17:381–92. doi: 10.1111/j.1745-4557.1994.tb00159.x

37. Rathore SS, Saxena SN, Kakani RK, Sharma LK, Singh B. Rapid and mass screening methods for 4-hydroxyisoleucine compounds in fenugreek seeds. *Int J Seed Spices*. (2014) 4:93–4.

38. Lee YP, Takahanshi J. An improved determination of amino acid with use of ninhydrin. *Anal Biochem*. (1996) 14:71–7. doi: 10.1016/0003-2697(66)90057-1

39. AOAC. Official Methods of Analysis of AOAC International. *Off Methods Anal AOAC Int*. (2000). doi: 10.1093/9780197610145.001.0001

40. Wojciech Banaś. Available online at: https://colordesigner.io/tools.

41. Tang D, Chen M, Huang X, Zhang G, Zeng L, Zhang G, et al. SRplot: a free online platform for data visualization and graphing. *PLoS One*. (2023) 18:e0234236:e0294236. doi: 10.1371/journal.pone.0294236

42. Gopinath PP, Parsad R, Joseph B, Adarsh VS. GRAPES: General Rshiny Based Analysis Platform Empowered by Statistics. (2020). doi: 10.5281/zenodo.4923220

43. Srinivasa UM, Naidu MM. Fenugreek (*Trigonella foenum-graecum* L.) seed: promising source of nutraceutical. *Stud Nat Prod Chem*. (2021) 71:141–184. doi: 10.1016/B978-0-323-91095-8.00014-3

44. Hajimehdipoor H, Sadat-Ebrahimi S, Izaddoost M, Amin G, Givi E. Identification and quantitative determination of blood lowering sugar amino acid in fenugreek. *Planta Med*. (2008) 74. doi: 10.1055/s-0028-1084857

45. Gangopadhyay KK, Yadav SK, GunjeetKumar MBL, Mahajan RK, Mishra SK, Sharma SK. Correlation, path-coefficient and genetic diversity pattern in fenugreek (*Trigonella foenum-graecum*). *Indian J Agric Sci*. (2009) 79:521–6.

46. Riasat M, Heidari B, Pakniyat H, Jafari AA. Assessment of variability in secondary metabolites and expected response to genotype selection in fenugreek (Trigonella spp.). *Ind Crop Prod*. (2018) 123:221–31. doi: 10.1016/j.indcrop.2018.06.068

47. Kumar P, Kumar R, Chouhan S, Tutlani A. Exploring genetic variability, correlation and path analysis in fenugreek (*Trigonella foenum-graecum* L.) for crop improvement. *Int J Stress Manag*. (2023) 14:1523–1529. doi: 10.23910/1.2023.4922

48. Sharma KC, Sastry EVD. *Path analysis for seed yield and its component characters in fenugreek (Trigonella foenum-graecum L)*. (2008) 17:69–74.

49. Singh PP, Gujar M, Naruka IS. Association and path analysis in fenugreek (Trigonella foenum graecum). *Indian J Agric Sci*. (2016) 86:951–5. doi: 10.56093/ijas.v86i7.59854

50. Geçit HH, Çiftçi CY, Emeklier Y, İkincikarakaya SÜ, Adak MS, Kolsarıcı Ö, et al. Ankara Üniversitesi, Ziraat Fakültesi Yayınları (2009) 1569, Ders Kitabı:521.

51. Hussein F, Janat M, Yakoub A. Assessment of yield and water use efficiency of drip-irrigated cotton (*Gossypium hirsutum* L.) as affected by deficit irrigation. *Turkish J Agric For*. (2011) 35:611–21. doi: 10.3906/tar-1008-1138

52. İsotçu Ç. Determination of full and deficit irrigation effects on yield components and Fiber quality traits of cotton (*Gossypium hirsutum* L.) at f3:5 generation. Aydın, Türkiye: Adnan Menderes University (2016).

53. Çamlıca M, Yaldız G. Characterization of morphological and yield variation of fenugreek (*Trigonella foenum-graecum* L.) genotypes. *Legum Res*. (2019) 42:500–4. doi: 10.18805/LR-444

54. Al-Maamari IT, Khan MM, Al-Sadi AM, Iqbal Q, Al-Saady N. Morphological characterization and genetic diversity of fenugreek (*Trigonella foenum-graecum* L.) accessions in oman. *Bulg J Agric Sci*. (2020) 26:375–83.

55. Aşkın H. Determination of agricultural and some quality characteristics of different fenugreek (*Trigonella foenum-graecum* L.) genotypes. Master's thesis, graduate School of Bolu Abant Izzet Baysal University, Department of Field Crops, Bolu, Türkiye. (2021).

56. Al-Maamari IT, Khan MM, Ali A, Al-Sadi AM, Waly MI, Al-Saady NA. Diversity in phytochemical composition of omani fenugreek (Trigonella foenum - graecum L.) accessions. *Pakistan J Agric Sci*. (2016) 53:851–62. doi: 10.21162/PAKJAS/16.5559

57. Yaldiz G, Camlica M. Yield, yield components and some quality properties of fenugreek cultivar and lines. *Banat J Biotechnol*. (2020) XI:40–7. doi: 10.7904/2068-4738-xi(22)-40

58. Singh R, Choudhary S, Mehta RS, Aishwath OP, Lal G. Yield losses due to weeds, critical period for weed-crop competition in fenugreek (*Trigonella foenum-graecum* L.). *Legum Res*. (2022) 45:1317–24. doi: 10.18805/LR-4369

59. Desai R. (2012). E-course on farm power and machinery.

60. Singh OV, Singh K, Meena VS, Shekhawat N, Gupta V. Identification of an extra early maturing accession IC 0624520 of fenugreek (*Trigonella foenum-graecum* L.). *Int J Seed Spices*. (2021) 11:50–2.

61. Bhutia KC, Bhutia SO, Chatterjee R, Chattopadhyay N. Growth, phenology and yield of fenugreek (*Trigonella foenum-graecum* L.) as influenced by date of sowing. *Int J Curr Microbiol Appl Sci*. (2017) 6:1810–7. doi: 10.20546/ijcmas.2017.610.218

62. Sultana S, Das G, Das B, Sarkar S. Influence of dates of sowing on growth and yield dynamics of fenugreek (*Trigonella foenum-graecum* L.). *Int J Green Pharm*. (2016) 10:S233–6.

63. Camlica M, Yaldiz G. Comparison of twenty selected fenugreek genotypes grown under irrigated and dryland conditions: morphology, yield, quality properties and antioxidant activities. *Agronomy*. (2024) 14:713. doi: 10.3390/agronomy14040713

64. McCormick KM, Norton RM, Eagles HA. Phenotypic variation within a fenugreek (*Trigonella foenum-graecum* L.) germplasm collection. II. Cultivar selection based on traits associated with seed yield. *Genet Resour Crop Evol*. (2009) 56:651–61. doi: 10.1007/s10722-008-9391-1

65. Sadeghzadeh-ahari D, Hassandokht MR, Kashi AK, Amri A, Alizadeh KH. Genetic variability of some agronomic traits in the Iranian fenugreek landraces under drought

stress and non-stress conditions. *Plant Sci*. (2010) 4:012–20. http://www.academicjournals.org/AJPS

66. Pavlista AD, Santra DK. Planting and harvest dates, and irrigation on fenugreek in the semi-arid high plains of the USA. *Ind Crop Prod*. (2016) 94:65–71. doi: 10.1016/j.indcrop.2016.07.052

67. Lal G, Singh R, Mehta RS, Sharma YK, Kant K, Maheria SP. Standardization of organic module for sustainable production of fenugreek (Trigonella foenum graecum L.). *Legum Res*. (2017) 40:144–9. doi: 10.18805/lr.v0iOF.11314

68. Narender T, Puri A, Shweta S, Khaliq T, Saxena R, Bhatia G, et al. 4-Hydroxyisoleucine: an unusual amino acid as Antidyslipidemic and Antihyperglycemic agent. *Chem Inform*. (2006) 16:293–6. doi: 10.1016/j.bmcl.2005.10.003

69. Mehrafarin A, Qaderi A, Rezazadeh S, Naghdi Badi H, Noormohammadi G, Zand E. Bioengineering of important secondary metabolites and metabolic pathways in fenugreek (*Trigonella foenum-graecum* L.). *J Med Plants*. (2010) 9:1–18.

70. Haeri MR, Shams-Ardakani MR, Rahbani M, Izaddust M, Khanavi M. Quantification of 4-hydroxyisoleucine content in treated and untreated fenugreek seeds using GC. *J Med Plants*. (2010) 9:90–4.

71. Rajabihashjin M, Zeinalabedini M, Asghari A, Ghaffari MR, Salekdeh GH. Impact of environmental variables on yield related traits and bioactive compounds of the Persian fenugreek (*Trigonella foenum-graecum* L.) populations. *Sci Rep*. (2022) 12:7359. doi: 10.1038/s41598-022-10940-3

72. Martins T, Barros AN, Rosa E, Antunes L. Enhancing health benefits through chlorophylls and chlorophyll-rich agro-food: a comprehensive review. *Molecules*. (2023) 28. doi: 10.3390/molecules28145344

73. Queiroz Zepka L, Jacob-Lopes E, Roca M. Catabolism and bioactive properties of chlorophylls. *Curr Opin Food Sci*. (2019) 26:94–100. doi: 10.1016/j.cofs.2019.04.004

74. Perez-Galvez A, Viera I, Roca M. Chemistry in the bioactivity of chlorophylls: an overview. *Curr Med Chem*. (2018) 24:4515–36. doi: 10.2174/0929867324666170714102619

75. Egner PA, Stansbury KH, Snyder EP, Rogers ME, Hintz PA, Kensler TW. Identification and characterization of chlorin e4 ethyl ester in sera of individuals participating in the chlorophyllin chemoprevention trial. *Chem Res Toxicol*. (2000) 13:900–9006. doi: 10.1021/tx000069k

76. Lahuta LB, Szablińska J, Ciak M, Górecki RJ. The occurrence and accumulation of d-pinitol in fenugreek (Trigonella foenum graecum L.). *Acta Physiol Plant*. (2018) 40. doi: 10.1007/s11738-018-2734-4

77. Franz MJ, Bantle JP, Beebe CA, Brunzell JD, Chiasson JLGA. Evidence-based nutrition principles and recommendations for the treatment and prevention of diabetes and related complications. *Diabetes Care*. (2002) 25:202–12. doi: 10.2337/diacare.25.1.202

78. Tak Y, Kaur M, Chitranashi A, Samota MK, Verma P, Bali M, et al. Fenugreek derived diosgenin as an emerging source for diabetic therapy. *Front Nutr*. (2024) 11. doi: 10.3389/fnut.2024.1280100

79. Chen PS, Shih YW, Huang HC, Cheng HW. Diosgenin, a steroidal saponin, inhibits migration and invasion of human prostate cancer PC-3 cells by reducing matrix metalloproteinases expression. *PLoS One*. (2011) 6:e20164. doi: 10.1371/journal.pone.0020164

80. Zeinab K, Sedaghat R, Baluchnejadmojarad T, Roghani M. Diosgenin ameliorates testicular damage in streptozotocin-diabetic rats through attenuation of apoptosis, oxidative stress, and inflammation. *Int Immunopharmacol*. (2019) 70:37–46. doi: 10.1016/j.intimp.2019.01.047

81. Snehlata HS, Payal DR. Fenugreek (*Trigonella foenum-graecum* L.): an overview. *Int J Curr. Pharm Res*. (2012):169–187.

82. Pęksa A, Miedzianka J, Nemś A, Rytel E. The free-amino-acid content in six potatoes cultivars through storage. *Molecules*. (2021) 26. doi: 10.3390/molecules26051322

83. Johari MA, Khong HY. Total phenolic content and antioxidant and antibacterial activities of *Pereskia bleo*. *Adv Pharmacol Sci*. (2019) 2019:1–4. doi: 10.1155/2019/7428593

84. Rahman MM, Rahaman MS, Islam MR, Rahman F, Mithi FM, Alqahtani T, et al. Role of phenolic compounds in human disease: current knowledge and future prospects. *Molecules*. (2021) 27:233. doi: 10.3390/molecules27010233

85. Lin D, Xiao M, Zhao J, Li Z, Xing B, Li X, et al. An overview of plant phenolic compounds and their importance in human nutrition and management of type 2 diabetes. *Molecules*. (2016) 21:1374. doi: 10.3390/molecules21101374

86. El-Bahy GMS. FTIR and Raman spectroscopic study of fenugreek (Trigonella foenum graecum L.) seeds. *J Appl Spectrosc*. (2005) 72:111–6. doi: 10.1007/s10812-005-0040-6

87. Schuette HA, Cowley MA, Vogel HA, Muller MM. Fenugreek Seed Oil. *J Am Oil Chem Soc*. (2020). doi: 10.32388/yxv0yh

88. Ren XF, Zhu WJ. Optimal conditions for extraction of oil from fenugreek (Trigonella foenum - graecum L.) by supercritical CO2 fluids (SFE-CO2). *Adv Mater Res*. (2011) 236-238:2980–2983. doi: 10.4028/www.scientific.net/AMR.236-238.2980

89. Arivalagan M, Gangopadhyay KK, Kumar G. Determination of steroidal saponins and fixed oil content in fenugreek (*Trigonella foenum-graecum*) genotypes. *Indian J Pharm Sci*. (2013) 75:110–3. doi: 10.4103/0250-474X.113542

90. Savitha HG, Manohar B. Studies on grinding and extraction of oil from fenugreek (*Trigonella foenum-graecum*) seed. *Int J Food Eng*. (2015) 11:275–283. doi: 10.1515/ijfe-2014-0262

91. Munshi M, Arya P, Kumar P. Physico-chemical analysis and fatty acid profiling of fenugreek (*Trigonella foenum-graecum*) seed oil using different solvents. *J Oleo Sci*. (2020) 69:1349–58. doi: 10.5650/jos.ess20137

92. Bienkowski T, Zuk-Golaszewska K, Kaliniewicz J, Golaszewski J. Content of biogenic elements and fatty acid composition of fenugreek seeds cultivated under different conditions. *Chil J Agric Res*. (2017) 77:134–41. doi: 10.4067/S0718-58392017000200134

93. Liu H, Zhang J, Wang Y. The influence of seed coat color on germination and seedling growth of *Cyamopsis tetragonoloba* (L.) Taub. *Seed Sci Technol*. (2007) 70:29–38. doi: 10.1016/j.jaridenv.2006.12.011

94. Powell AM. The role of seed color in the germination ecology of annual plants. *Oikos*. (1989) 56:321–6.

95. Sujatha K, Sindhu S, Keerthana D, Arun KP, Elamparithi R. Seed coat colour variation and its impact on seed quality parameters of Horsegram var. Paiyur 2. *Agric Sci Dig A Res J*. (2022) 5451:1–3. doi: 10.18805/ag.d-5451

96. Lal S, Singh SK, Singh AK, Srivastav M, Singh A, Singh NK. Character association and path analysis for fruit chromatic, physicochemical and yield attributes in mango (*Mangifera indica*). *Indian J Agric Sci*. (2017) 87:122–31. doi: 10.56093/ijas.v87i1.67132

97. Le AV, Parks SE, Nguyen MH, Roach PD. Optimisation of the Microwave-Assisted Ethanol Extraction of Saponins from Gac (Momordica cochinchinensis Spreng.) Seeds. *Seeds. Medicines (Basel)*. (2018) 5:70. doi: 10.3390/medicines5030070

98. Franscistt W, David FB, Robert MD. The estimation of the total soluble carbohydrate in cauliflower tissue. Experiment in plant phyisiology. *Exp Plant Phyisiol Van Nostrand New York*. (1971) 16

frontiers | Frontiers in Nutrition

TYPE Original Research
PUBLISHED 09 April 2025
DOI 10.3389/fnut.2025.1567829

OPEN ACCESS

EDITED BY
Rakesh Bhardwaj,
National Bureau of Plant Genetic Resources, Indian Council of Agricultural Research (ICAR), India

REVIEWED BY
Amit Kumar,
Chandra Shekhar Azad University of Agriculture and Technology, India
Amandeep Kaur,
Panjab University, India

*CORRESPONDENCE
Hammylliende Talang
✉ hammylliende@gmail.com
M. Bilashini Devi
✉ bilashini1712@gmail.com
Nongmaithem Uttam Singh
✉ uttam.singh@icar.gov.in
Sandip Patra
✉ sandippatra47@gmail.com

†These authors have contributed equally to this work

RECEIVED 28 January 2025
ACCEPTED 24 March 2025
PUBLISHED 09 April 2025

CITATION
Talang H, Mawlong GT, Kjam L, Devi MB, Gurung B, Biswakarma N, Singh NU, Verma VK, Rymbai H, Raviteja P, Das B, Angami T, Yanthan AW, Patra S, Makdoh B, Ch Sangma RH, Assumi SR, Sangma CBK, Chanu LJ and Hazarika S (2025) Assessment of nutritional quality of *taro* (*Colocasia esculenta* L. Schott.) genotypes of the Eastern Himalaya, India.
Front. Nutr. 12:1567829.
doi: 10.3389/fnut.2025.1567829

Assessment of nutritional quality of *taro* (*Colocasia esculenta* L. Schott.) genotypes of the Eastern Himalaya, India

Hammylliende Talang[1*†], Gabriella T. Mawlong[1†], Lanamika Kjam[1], M. Bilashini Devi[1*], Bishal Gurung[2], Niraj Biswakarma[1], Nongmaithem Uttam Singh[1*], Veerendra Kumar Verma[1], Heiplanmi Rymbai[1], Palavalasa Raviteja[1], Bapi Das[3], Thejangulie Angami[4], Aabon W. Yanthan[5], Sandip Patra[1*], Badapamain Makdoh[1], Rumki H. Ch Sangma[1], Shiwot Ruth Assumi[5], Christy B. K. Sangma[1], L. Joymati Chanu[1] and Samarendra Hazarika[1]

[1]ICAR Research Complex for NEH Region, Umiam, Meghalaya, India, [2]North Eastern Hill University, Umshing Mawkynroh, Shillong, Meghalaya, India, [3]ICAR Research Complex for NEH Region, Tripura Centre, Lembucherra, Tripura, India, [4]ICAR Research Complex for NEH Region, Arunachal Pradesh Centre, Basar, Arunachal Pradesh, India, [5]ICAR Research Complex for NEH Region, Nagaland Centre, Medziphema, Nagaland, India

Introduction: The eastern Himalayan region of India with diverse agro-climatic conditions is one of the important hotspots of the world's biodiversity. A wide range of genetic variability of plant species like Colocasia is available in the region which is consumed by the local tribes.

Materials and methods: A field study was conducted during 2022–23 to evaluate the yield, biochemical, mineral, and an-tioxidant parameters of 30 *Colocasia esculenta* L. Schott. genotypes under a split-plot design with three replications.

Results and discussion: Significant ($p < 0.05$) variations were observed among genotypes for all traits. Tamachongkham exhibited the highest corm weight and yield, while Tamitin recorded the maximum cormel weight and total yield. Megha Taro-2 and Megha Taro-1 had the highest cormel numbers and cormel yield, respectively. In mineral composition, Tamitin had the highest N, K, Zn, Cu, and Mn, Tagitung White recorded the highest P, and BCC-2 had the highest Fe and Ca + Mg. Biochemically, Tamachongkham had the highest dry matter content; Khweng-2 had the highest starch, total sugar, and reducing sugar; Rengama had the highest crude protein, and crude fiber; and Mairang Local had the highest ash content. A significant positive correlation was observed between total yield and corm, cormel yield, cormel weight, and corm weight, while correlations with starch and other parameters were non-significant. Total phenolic content and anthocyanin were significantly correlated with Ferric Reducing Antioxidant Power (FRAP). Genotype-by-trait biplot analysis using the first two principal components (PC1: 19.4%, PC2: 14%) high-lighted total sugar, reducing sugar, cormel numbers, crude fiber, anthocyanin, and FRAP as major contributors to phenotypic diversity. The observed variations indicate the potential of these genotypes for future breeding programs aimed at improving taro production in the Eastern Himalayas.

KEYWORDS

taro, genotypes, bio-chemical, antioxidant, principal component analysis

1 Introduction

The Eastern Himalayan region of India with diverse agro-climatic conditions is one of the important hotspots of the world's biodiversity. A wide range of genetic variability of plant species like Colocasia is available in the region which is consumed by the local tribes. Taro (*Colocasia esculenta* L. Schott.) also referred to as arvi or taro, belongs to the family Araceae comprising of 110 genera and more than 2000 species (1). It is cultivated in an area of around 1.9 million hectares around the world with an annual production of 12.39 MT (2). This crop is an integral part of dietary system of tribals and is grown abundantly in their jhum land or kitchen garden as mixed cropping. The most significant traits of taro are its adaptability, and capacity to give rise to high yields under a variety of conditions, particularly in tropical regions (3).

The underground corms and cormels, the primary edible components of taro, are highly nutritious and contain various bioactive compounds with potential health benefits (4). Taro is predominantly cultivated for its underground corms, which consist of 70–80% starch (5). It has been suggested that taro was traditionally grown to bridge seasonal food gaps, as it can yield well even under conditions where other crops may struggle due to various production constraints (5, 6). Morphologically, taro is an erect, monocotyledonous, and herbaceous perennial root crop. The plants possess a variety of chemical compounds that add to their therapeutic value, including alkaloids, glycosides, resins, volatile oils, gums, and tannins. Its tuber contains low fat with high protein and carbohydrate content, similar to other root crops. It is also a good source of potassium and has a moderate quantity of phosphorus. Besides, the tuber is also a richer source of vitamin B-complex than whole milk (7). In addition to being a very rich source of vitamin C, niacin, potassium, copper, and manganese, it is also a good source of iron, zinc, thiamine, riboflavin, and other minerals (8). The tuber has excellent digestibility. Its efficiency of effective simultaneous release of nutrients during digestion and absorption is attributed to the small granule size of its starch constituting the tuber (9). Despite the rich genetic diversity of taro (*Colocasia esculenta* L. Schott.) in the Eastern Himalayan region and its significance as a staple food for tribal communities, limited systematic studies have been conducted to assess the nutritional composition and agronomic potential of its diverse genotypes. While previous research has primarily focused on agronomic performance or isolated biochemical traits, comprehensive evaluations integrating yield attributes, biochemical composition, mineral content, and antioxidant properties across multiple genotypes remain scarce. Additionally, most studies have not employed multivariate analyses to identify superior genotypes for targeted breeding and genetic improvement. Given the increasing demand for nutrient-rich, climate-resilient crops, a deeper understanding of genotype-specific variations in taro is essential for its effective utilization in breeding programs. This study addresses this gap by evaluating 30 genotypes for key nutritional and antioxidant parameters, providing valuable insights for future genetic improvement and conservation efforts in the Eastern Himalaya region.

2 Materials and methods

2.1 Materials and experimental site

The study on the 30 genotypes of *Colocasia esculenta* L. cultivated at the Horticulture Experimental Farm of ICAR-Research Complex for North-Eastern Hill Region, Umiam, Meghalaya was performed during 2022–23. These 30 genotypes of *Colocasia esculenta* L. were selected based on their genetic diversity and wide representation from different geographical locations across the Eastern Himalayan region. This ensured a comprehensive evaluation of yield attributes, biochemical composition, and antioxidant properties for potential breeding and conservation efforts. The selected genotypes were treated as individual treatments. Each treatment was replicated thrice in split plot design. Throughout the trial, all the recommended cultivation techniques were adhered to in order to ensure optimal growth and yield. The genotypes were assigned to the blocks in the field experiment which was set up using split plot design. The split-plot design was chosen to efficiently evaluate the effects of multiple factors on the yield, biochemical, and antioxidant parameters of *Colocasia esculenta* L. genotypes. This design allowed for better control of variation by assigning genotypes to main plots and subplots, thus improving the precision of comparisons while accommodating field heterogeneity.

2.2 Quantitative analysis

Twenty-five matured corms and cormels of each genotype were used for carrying out all the analysis. The harvested samples were washed with distilled water and kept at room temperature for 10 min to remove the adhering water before analysis. The parameters, viz., corm and cormels weights (gm) were determined using an electronic balance (Adair Dutt-1620C). Corm yield (t ha^{-1}), cormel yield (t ha^{-1}) and total yield (t ha^{-1}) of the genotypes were determined following standard methods (10, 11).

2.3 Determination of tissue nutrient

The leaf samples were collected and carefully washed to remove any surface contamination according to the method of Chapman (12). The samples were then oven dried and ground using a Wiley grinding machine to obtain a homogenous sample, which was subsequently digested in a tri-acid mixture of $HClO_4$:HNO_3:H_2SO_4 in a 2:5:1 ratio as described by Chapman and Pratt (13). The tri-acid extracts were used for the determination of total P as per the vanadomolybdate method given by Hesse (14), total K using the flame photometry method (13), micronutrients viz., copper, iron, manganese and zinc content using an atomic absorption spectrophotometer as described by Zasoski and Burau (15), and calcium and magnesium using the versenate (EDTA) method as described by Cheng and Bray (16). Total N was estimated following the Microkjeldahl method by Jackson (17).

2.4 Determination of biochemical attributes

Starch was estimated as per the procedure described by Hedge and Hofreiter (18), total sugar (Dubois et al. 1956) (19), Reducing Sugar (Miller 1959) (20), Oxalate (AOAC 1984) (21), crude protein (AOAC 1990) (22), crude fiber content (Maynard 1970) (23), ash content (James 1995) (24) with slight modification where two grams of the powdered sample was weighed (W_1) into a pre-weighed empty crucible (W_0) and placed into a muffle furnace until the sample was completely ashed at temperature 600°C. Dry-matter content of the

samples was determined by oven-drying 100 g of freshly sliced tubers at 60°C, till a constant weight was attained and calculated as:

$$\text{Dry Matter}\,(\%) = (\text{Dry weight} / \text{Fresh weight}) \times 100$$

2.5 Determination of antioxidant activity and anthocyanin

2.5.1 Total phenolic content

The total phenolic content (TPC) was determined spectrophotometrically using the Folin–Ciocalteu method, as described by Keskin-Sasic et al. (25). The assay utilized Folin–Ciocalteu reagent, sodium carbonate (7.5% w/v), and gallic acid as the standard. For the analysis, 1 mL of the diluted sample extract was added to 2 mL of a 1:10 diluted Folin–Ciocalteu reagent and allowed to react for 10 min. Following this, 1.6 mL of sodium carbonate solution was added, and the mixture was incubated at room temperature for 30 min. The absorbance was then measured at 743 nm and TPC was expressed as gallic acid equivalents (GAE) in mg/100 g. The concentration of polyphenols in the samples was calculated using a standard calibration curve of gallic acid ($y = 0.0232x–0.0602$, $R^2 = 0.9885$).

$$\text{TPC}\ (\text{mg GAE}/100\,\text{g dw}) = \frac{\text{Conc. of GA from standard curve} \times \text{volume of extract} \times 100}{\text{Weight of the sample}}$$

2.5.2 Ferric reducing antioxidant power assay

The reducing power of the extracts was assessed as per the method described by Benzie and Strain (26). 0.1 mL of extracts/standard were taken in the labeled test tubes and 3 mL of FRAP Reagent was added to all the test tubes and the samples were allowed to react with the FRAP solution in the dark for 30 min followed by absorbance measurement. The FRAP values are expressed as millimoles of $FeSO_4$ equivalents ($FeSO_4E$) per 100 g of the sample using the standard curve constructed for different concentrations of Ferrous sulfate.

$$\text{FRAP value}\ (\text{mM } FeSO_4E/100\,\text{g dw}) = \frac{\text{Conc.of } FeSO_4 \text{ from standard curve} \times \text{volume of extract}}{\text{Weight of the sample}}$$

2.5.3 DPPH (2,2-Diphenyl-1-picrylhydrazyl) radical scavenging assay

Free radical scavenging ability of the extracts was tested by DPPH radical scavenging assay as described by Shen et al. (27). For each sample/standard, 0.2, 0.4, 0.6, 0.8 and 1.0 mL were taken and the volume was made up to 1 mL with methanol followed by the addition of 3 mL DPPH solution. The samples were incubated for 30 min in the dark. Control solution was prepared by mixing methanol with DPPH solution. The absorbance was measured spectrophotometrically at 517 nm using methanol as blank. Percentage DPPH radical scavenging activity was calculated by the following equation:

$$\text{DPPH Scavenging activity}(\%) = \frac{\text{Ac} - \text{At}}{\text{Ac}} \times 100$$

Where, Ac is the absorbance of the control reaction and At is the absorbance of the sample of the extracts. The antioxidant activity of the extract was expressed as IC50 (the concentration of sample required to decrease the absorption at 517 nm by 50%). The IC50 value was expressed as the concentration in milligram of extract per ml that inhibited the formation of DPPH radicals by 50%.

2.5.4 Anthocyanin estimation

This estimation was carried out according to the procedure given by Srivastava and Kumar (28). A 10 g dried sample was mixed with 10 mL of ethanolic HCl and transferred to a 100 mL volumetric flask and the volume was made up to the mark with ethanolic HCl. The sample was kept overnight in the refrigerator at 4°C, filtered through Whatman no.1 filter paper and the OD was recorded at 535 nm.

Calculations:

$$\text{Total OD}/100\,\text{g} = (\text{OD} \times \text{Volume made up} \times 100) / \text{weight of sample taken}$$

$$\text{Anthocyanin}\,(\text{mg}/100\,\text{g dw}) = (\text{Total OD}/100\,\text{g}) / 98.2$$

2.6 Statistical analysis

All tests were conducted in triplicates and the replicated data were statistically analyzed using IBM SPSS version 22.0. The results were expressed as mean ± standard deviation (SD) and subjected to one-way ANOVA followed by Tukey's HSD (honestly significant difference) test at $p < 0.05$ for multiple comparisons. The relationships between yield, biochemical parameters, and antioxidant properties were evaluated using Pearson's correlation coefficient. Pearson's correlation analysis was conducted to evaluate the strength and direction of relationships among the examined traits, with Pearson's correlation analysis was performed to assess the strength and direction of associations among the studied parameters, with statistical significance assessed at a 95% confidence level ($p < 0.05$). Furthermore, Principal Component Analysis (PCA) was employed to identify key variables contributing to the total variation and to reduce the dimensionality of the dataset. Eigenvalues greater than 1 were retained for interpretation, and factor loadings were analyzed to determine the contribution of each parameter to the principal components. A scree plot was used to visualize the variance explained by each component, providing insights into the underlying structure of the data.

Additionally, biplots were generated to illustrate the relationships between variables and principal components, aiding in the interpretation of trait clustering. The correlation matrix was examined to identify strong associations between parameters, which could further support PCA findings. Kaiser-Meyer-Olkin (KMO) and Bartlett's test were performed to assess the suitability of the dataset for PCA. Higher KMO values indicated data adequacy, while Bartlett's test ensured that correlations were sufficiently large for meaningful PCA. The cumulative variance explained by retained principal components was considered to determine the proportion of total

10.3389/fnut.2025.1567829

variability captured. Finally, variables with high loadings in the same principal component were grouped, allowing for an integrated understanding of trait interactions and their overall contribution to data variability.

3 Results and discussion

3.1 Yield parameters

There was significant ($p < 0.05$) variation observed in yield and related parameters under study (Table 1). Among all the genotypes studied, the corm weight was recorded to be in the range of 80 ± 16.09 g to 641.67 ± 18.77 g where genotype Tamachongkham showed maximum value and the minimum in ML-3. Cormel weight was recorded highest in genotype Tamitin (151.67 ± 12.58 g) while Muktakeshi genotype recorded lowest cormel weight (19.53 ± 4.32 g). Cormel numbers was in the range of 2.67 ± 0.16 to 6.93 ± 0.71 with Megha Taro-2 exhibiting highest cormel numbers and Tamitim recorded the lowest. Corm yield was recorded to be in the range of 5.86 ± 1.79 t/ha to 21.02 ± 4.23 t ha^{-1} with the highest corm yield shown by genotype Tamachongkham and lowest in RC Taro-6. Cormel yield was recorded between the range 6.50 ± 3.57 and 20.19 ± 2.91 t ha^{-1} where genotype Megha Taro-1 displayed maximum cormel yield and Muktakeshi minimum. The total yield was observed maximum in genotype Tamitin (35.77 ± 0.90 t ha^{-1}) and lowest (18.97 ± 7.45 t ha^{-1}) in Rengama. This finding is similar to the findings of Khatemenla et al. (29) Kay (30) and Bekele and Boru (31). Thirugnanavel et al. 2015 (32) observed wide range of variations among the Colocasia

TABLE 1 Yield parameters of 30 genotypes of *Colocasia esculenta*.

Genotypes	Acc.	Corm weight (g)	Cormel weight (g)	Cormel nos./plants	Corm yield (t/ha)	Cormel yield (t/ha)	Total yield (t/ha)
BCC-2	1	208.33 ± 17.56^{k-m}	63 ± 7.55^{d-h}	5 ± 0.8^{ab}	11.5 ± 3.77^{ab}	13.66 ± 4.58^{ab}	25.16 ± 7.03^{a}
Kandha local	2	246.67 ± 12.58^{h-l}	55 ± 9^{e-m}	6.04 ± 0.94^{ab}	14.8 ± 4.53^{ab}	13.09 ± 5.26^{ab}	27.89 ± 5.9^{a}
Wahiajer local	3	344 ± 21.28^{cd}	45.20 ± 6.75^{f-n}	5.44 ± 0.76^{ab}	16.22 ± 4.08^{ab}	12.24 ± 3.79^{ab}	28.46 ± 0.39^{a}
Mairang local	4	310 ± 26.91^{c-g}	85 ± 10^{b-d}	4.12 ± 0.08^{ab}	14.02 ± 4^{ab}	19.37 ± 4.12^{ab}	33.39 ± 6.99^{a}
Thangitang	5	106.67 ± 15.28^{o}	63.93 ± 8.67^{d-g}	6 ± 1.73^{ab}	10.06 ± 3.93^{ab}	19.89 ± 4.98^{ab}	29.95 ± 7.74^{a}
RC Taro-6	6	100 ± 12^{o}	56.67 ± 7.51^{e-l}	5 ± 0^{ab}	5.86 ± 1.79^{b}	14.54 ± 4.06^{ab}	20.4 ± 3.54^{a}
AR3	7	128.33 ± 13.50^{no}	44.67 ± 9.29^{f-n}	5.2 ± 0.83^{ab}	6.34 ± 2.49^{b}	13.15 ± 4.31^{ab}	19.49 ± 3.82^{a}
ML2	8	316.67 ± 23.86^{c-f}	51.73 ± 9.6^{e-m}	4.78 ± 0.8^{ab}	15.64 ± 3.11^{ab}	14.5 ± 3.83^{ab}	30.14 ± 6.12^{a}
ML3	9	80 ± 16.09^{o}	25.67 ± 8.74^{no}	5 ± 0^{ab}	9.32 ± 3.89^{b}	10.3 ± 3.73^{ab}	19.62 ± 0.29^{a}
Naga local	10	283.33 ± 12.58^{e-i}	61.67 ± 9.50^{d-i}	4.07 ± 0.42^{ab}	12.79 ± 2.82^{ab}	12.78 ± 4.61^{ab}	25.57 ± 4.02^{a}
AR2	11	632 ± 14^{a}	40.67 ± 6.03^{g-o}	5.04 ± 1.88^{ab}	14.33 ± 3.81^{ab}	12.14 ± 4.78^{ab}	26.47 ± 8.59^{a}
C3	12	363.67 ± 12.58^{c}	58 ± 6^{e-k}	5 ± 0^{ab}	17.24 ± 3.85^{ab}	15.24 ± 4.66^{ab}	32.48 ± 8.48^{a}
C-14-9	13	170 ± 20^{mn}	65.67 ± 6.03^{d-f}	5 ± 0^{ab}	8.84 ± 3.35^{b}	16.07 ± 4.94^{ab}	24.91 ± 1.63^{a}
Tagitung white	14	287.33 ± 14.19^{d-h}	38.67 ± 6.11^{i-o}	5.05 ± 1.13^{ab}	14.89 ± 3.31^{ab}	13.82 ± 4.3^{ab}	28.71 ± 6.92^{a}
ML9	15	525 ± 15^{b}	104 ± 9.54^{b}	3.01 ± 0.06^{b}	14.93 ± 3.74^{ab}	17.37 ± 4^{ab}	32.3 ± 10^{a}
Tamakhan	16	104 ± 13.86^{o}	37.33 ± 5.03^{j-o}	5.76 ± 0.35^{ab}	10.53 ± 3.92^{ab}	14.81 ± 4.31^{ab}	25.34 ± 0.42^{a}
Naya bungalow	17	118.67 ± 22.03^{no}	20.33 ± 4.51^{o}	5.58 ± 2.73^{ab}	9.5 ± 3.79^{ab}	18.53 ± 3.62^{ab}	28.02 ± 3.86^{a}
Khweng-3	18	201.67 ± 17.56^{lm}	35 ± 5^{k-o}	5.29 ± 1.92^{ab}	10.3 ± 2.55^{ab}	14.47 ± 4.14^{ab}	24.77 ± 5.22^{a}
Tagitung purple	19	100 ± 15.10^{o}	33.33 ± 5.03^{l-o}	4.07 ± 0.16^{ab}	13.98 ± 3.14^{ab}	14.5 ± 3.76^{ab}	28.48 ± 6.2^{a}
Tamachongkham	20	641.67 ± 18.77^{a}	71.67 ± 7.$^{64c-e}$	3.72 ± 0.31^{ab}	21.02 ± 4.23^{a}	13.73 ± 3.29^{ab}	34.75 ± 0.94^{a}
Tamitin	21	625 ± 25^{a}	151.67 ± 12.58^{a}	2.67 ± 0.16^{b}	16.47 ± 4.32^{ab}	19.3 ± 3.9^{ab}	35.77 ± 0.90^{a}
Rengama	22	215 ± 20^{j-m}	31 ± 5^{m-o}	5 ± 0^{ab}	9.75 ± 3.45^{ab}	9.22 ± 4^{ab}	18.97 ± 7.45^{a}
Khweng-2	23	225 ± 23.90^{i-m}	63 ± 8.19^{d-h}	4.95 ± 2.37^{ab}	9.93 ± 3.85^{ab}	13.21 ± 4.15^{ab}	23.14 ± 0.7^{a}
White Gaurya	24	261 ± 23.26^{f-k}	39 ± 6.56^{h-o}	5 ± 0^{ab}	15.13 ± 4.62^{ab}	12.5 ± 3.79^{ab}	27.62 ± 7.34^{a}
Muktakeshi	25	251.67 ± 16.56^{g-l}	19.53 ± 4.32^{o}	5 ± 0^{ab}	14.98 ± 4.56^{ab}	6.5 ± 3.57^{b}	21.48 ± 7.11^{a}
IGB-5	26	241.67 ± 20.55^{h-l}	45 ± 6^{f-n}	4.89 ± 1.05^{ab}	10.94 ± 1.27^{ab}	11.62 ± 5.13^{ab}	22.56 ± 4.22^{a}
Megha Taro-1	27	270 ± 20^{e-j}	59.67 ± 6.51^{e-j}	5.08 ± 2.34^{ab}	14.22 ± 1.95^{ab}	20.19 ± 2.91^{a}	34.41 ± 4.86^{a}
Megha Taro-2	28	276 ± 17.09^{e-i}	90.33 ± 10.02^{bc}	6.93 ± 0.71^{a}	14.47 ± 4.07^{ab}	16.52 ± 4.17^{ab}	30.99 ± 3.77^{a}
Megha col	29	124 ± 10.15^{no}	55.33 ± 6.11^{e-l}	5.05 ± 0.93^{ab}	8.47 ± 3.43^{b}	14.38 ± 4.09^{ab}	22.85 ± 7.5^{a}
TBd 17–9	30	323.33 ± 22.48^{c-e}	56.17 ± 5.34^{e-l}	3.58 ± 0.08^{ab}	10.66 ± 3.79^{ab}	12.21 ± 4.15^{ab}	22.87 ± 6.7^{a}

Values given are mean ($n = 3$) with SD. Superscript lower case letters on each column designated statistical significance ($p < 0.05$).

germplasm for plant growth, no. of leaves, no. of suckers, leaf morphology, floral morphology, corm characters, yield characters, quality and Phytophthora leaf blight incidence. The differences in the corm weight and yield of taro may be attributed to the differences in accumulation of dry matter which been translocated to the corm, combined with a higher rate of yield-attributing characters, viz., plant height, leaf area etc., throughout growth, environmental conditions and the genetic makeup of the different genotype, which might have impacted the plant growth habit and number and size of corms and cormels (33, 34).

3.2 Mineral composition

The mineral composition of the Colocasia genotypes is presented in Table 2. There were significant ($p < 0.05$) differences in mineral composition among the genotypes studied. The nitrogen (N) content ranged between 0.62 to1.79% with Tamitin genotype recording the highest N and least in Khweng-2. The phosphorus (P) content was registered highest in Tagitung white (0.49 ± 0.04%) and lowest (0.10 ± 0.02) in Megha Col. Further, the potassium (K) content ranges from (0.71 ± 0.02%) in Tagitung purple to (3.80 ± 0.03%) in Tamitin. The range in value of the minerals is probably due to the potential of each genotype to obtain nutrients from the soil (35). Buragohain et al. (36) reported similar findings.

A diet rich in minerals such as potassium plays a crucial role in preventing hypertension, heart disease, stroke, renal damage, kidney stones, hypercalciuria, and osteoporosis (37). Additionally, potassium influences sugar metabolism, polymerization, and starch synthesis (38). In this study, calcium (Ca) and magnesium (Mg) content among the genotypes ranged from 1.03 ± 0.03% to 2.37 ± 0.04%, with BCC-2 recording the highest value and Wahiajer Local the lowest. Similarly, iron (Fe) content varied from 65.40 ± 4.88 ppm in Megha Col to 118 ± 5.00 ppm in BCC-2,

TABLE 2 Mineral composition of the 30 genotypes of *Colocasia esculenta*.

Genotypes	N (%)	P (%)	K (%)	Ca + Mg%	Fe (ppm)	Zn (ppm)	Cu (ppm)	Mn (ppm)
BCC-2	1.58 ± 0.05^{bc}	0.39 ± 0.04^{a-d}	1.83 ± 0.03^{d}	2.37 ± 0.04^{a}	118 ± 5^{a}	10.21 ± 1.95^{kl}	3.24 ± 0.04^{q}	22.56 ± 2.16^{fg}
Kandha local	1.69 ± 0.05^{ab}	0.36 ± 0.05^{b-f}	1.54 ± 0.04^{fg}	1.5 ± 0.03^{g-i}	69.26 ± 4.95^{mn}	23.68 ± 3.41^{c-h}	4.23 ± 0.03^{n}	44.62 ± 2.69^{b}
Wahiajer local	1.41 ± 0.05^{de}	0.35 ± 0.04^{b-g}	1.26 ± 0.02^{kl}	1.03 ± 0.03^{q}	70.79 ± 3.84^{l-n}	28.27 ± 2.11^{b-f}	3.79 ± 0.04^{o}	18.8 ± 3.33^{f-i}
Mairang local	0.85 ± 0.04^{i-k}	0.3 ± 0.04^{c-h}	1.31 ± 0.01^{jk}	1.66 ± 0.04^{d}	89.55 ± 3.75^{e-i}	28.92 ± 2.32^{b-e}	2.67 ± 0.04^{r}	19.74 ± 3.73^{f-h}
Thangitang	1.55 ± 0.06^{b-d}	0.35 ± 0.05^{b-g}	1.11 ± 0.02^{op}	1.3 ± 0.04^{k-o}	90.74 ± 5.61^{e-h}	31.72 ± 2.83^{a-d}	5.78 ± 0.04^{i}	10.58 ± 1.98^{i}
RC Taro-6	1.25 ± 0.06^{ef}	0.43 ± 0.05^{ab}	3.62 ± 0.02^{b}	1.6 ± 0.04^{d-g}	78.64 ± 3.63^{h-n}	20.54 ± 3.85^{e-j}	3.81 ± 0.04^{o}	15.34 ± 1.95^{g-i}
AR3	0.64 ± 0.05^{m}	0.28 ± 0.02^{e-i}	1.37 ± 0.03^{ij}	1.85 ± 0.03^{c}	69.64 ± 4.39^{mn}	18.33 ± 3.08^{g-k}	6.16 ± 0.04^{g}	12.36 ± 1.81^{hi}
ML2	1.51 ± 0.06^{cd}	0.29 ± 0.02^{d-i}	1.58 ± 0.03^{fg}	1.45 ± 0.03^{h-j}	87.36 ± 4.57^{e-j}	10.19 ± 1.96^{kl}	7.51 ± 0.02^{c}	18.62 ± 2.63^{f-i}
ML3	1.24 ± 0.05^{f}	0.25 ± 0.03^{f-j}	1.13 ± 0.03^{nop}	1.25 ± 0.05^{m-o}	72.82 ± 3.5^{j-n}	12.31 ± 1.9^{j-l}	3.5 ± 0.04^{p}	24.38 ± 2.9^{e-g}
Naga local	1.22 ± 0.06^{f}	0.43 ± 0.02^{ab}	1.56 ± 0.03^{fg}	1.12 ± 0.05^{pq}	84.68 ± 4.48^{f-l}	17.73 ± 3.65^{g-l}	7.31 ± 0.04^{d}	20.95 ± 3.44^{f-h}
AR2	0.69 ± 0.06^{lm}	0.43 ± 0.05^{ab}	1.39 ± 0.02^{i}	1.82 ± 0.03^{c}	85.63 ± 4.5^{f-k}	24.35 ± 1.95^{b-g}	4.67 ± 0.03^{k}	19.31 ± 3.3^{f-i}
C3	1.26 ± 0.06^{ef}	0.23 ± 0.03^{h-j}	1.7 ± 0.03^{e}	1.34 ± 0.05^{j-n}	68.91 ± 4.6^{mn}	19.23 ± 3.22^{f-k}	2.54 ± 0.04^{s}	20.57 ± 1.64^{f-h}
C-14-9	0.63 ± 0.04^{m}	0.19 ± 0.04^{h-k}	1.59 ± 0.02^{f}	1.2 ± 0.03^{op}	76.04 ± 3.39^{i-n}	12.87 ± 2.46^{i-l}	3.15 ± 0.04^{q}	24.68 ± 2.56^{d-f}
Tagitung white	1.28 ± 0.05^{ef}	0.49 ± 0.04^{a}	1.9 ± 0.03^{cd}	1.54 ± 0.03^{f-h}	107.8 ± 4.33^{a-c}	31.61 ± 3.55^{a-d}	7.89 ± 0.04^{b}	19.33 ± 2.11^{f-i}
ML9	0.65 ± 0.05^{m}	0.21 ± 0.04^{h-j}	1.56 ± 0.02^{fg}	1.61 ± 0.04^{d-f}	84.75 ± 4.25^{f-l}	27.94 ± 2.68^{b-f}	5.16 ± 0.03^{j}	33.24 ± 3.87^{c-e}
Tamakhan	1.57 ± 0.06^{bc}	0.40 ± 0.03^{a-d}	1.23 ± 0.03^{k-m}	1.8 ± 0.03^{c}	76.04 ± 4.07^{i-n}	30.5 ± 4.47^{b-d}	4.38 ± 0.04^{m}	33.47 ± 2.82^{cd}
Naya bungalow	0.70 ± 0.05^{klm}	0.38 ± 0.05^{a-e}	1.51 ± 0.03^{gh}	1.55 ± 0.03^{e-h}	80.93 ± 4.46^{g-m}	25.74 ± 3.66^{b-g}	2.52 ± 0.04^{s}	50.39 ± 2.85^{ab}
Khweng-3	0.82 ± 0.05^{i-l}	0.20 ± 0.05^{h-k}	0.98 ± 0.02^{r}	1.36 ± 0.04^{j-l}	77.47 ± 4.31^{h-n}	18.12 ± 3.05^{g-k}	5.22 ± 0.05^{j}	22.26 ± 2.84^{fg}
Tagitung purple	0.9 ± 0.06^{h-j}	0.15 ± 0.03^{jk}	0.71 ± 0.02^{s}	2.1 ± 0.03^{b}	94.03 ± 4.75^{c-g}	16.44 ± 1.69^{g-l}	7.16 ± 0.04^{e}	12.09 ± 2.01^{hi}
Tamachongkham	1.19 ± 0.05^{fg}	0.41 ± 0.03^{a-c}	1.89 ± 0.03^{cd}	1.35 ± 0.04^{j-n}	112.78 ± 4.51^{ab}	22.47 ± 3.46^{d-h}	3.78 ± 0.04^{o}	33.24 ± 3.94^{c-e}
Tamitin	1.79 ± 0.05^{a}	0.40 ± 0.02^{a-d}	3.8 ± 0.03^{a}	1.35 ± 0.02^{j-m}	82.79 ± 4.65^{f-m}	40.54 ± 4.70^{a}	8.12 ± 0.04^{a}	59 ± 4.07^{a}
Rengama	0.75 ± 0.05^{j-m}	0.25 ± 0.03^{f-j}	1.07 ± 0.02^{pq}	2.28 ± 0.03^{a}	105.89 ± 4.49^{a-d}	10.66 ± 3.46^{kl}	4.22 ± 0.03^{n}	25.61 ± 2.85^{d-f}
Khweng-2	0.62 ± 0.06^{m}	0.18 ± 0.03^{i-k}	1.03 ± 0.02^{qr}	1.26 ± 0.04^{l-o}	72.38 ± 5.16^{k-n}	17.68 ± 2.71^{g-l}	6.48 ± 0.04^{f}	22.09 ± 3.1^{fg}
White Gaurya	0.97 ± 0.06^{hi}	0.23 ± 0.03^{h-j}	1.44 ± 0.03^{hi}	1.4 ± 0.03^{i-k}	84.53 ± 3.79^{f-l}	22.27 ± 3.1^{d-i}	5.93 ± 0.03^{h}	22.49 ± 2^{fg}
Muktakeshi	1.51 ± 0.06^{cd}	0.30 ± 0.04^{c-h}	1.95 ± 0.03^{c}	1.07 ± 0.03^{q}	95.19 ± 4.94^{c-g}	14.25 ± 1.92^{h-l}	2.3 ± 0.04^{t}	12.38 ± 1.9^{hi}
IGB-5	0.93 ± 0.06^{hi}	0.24 ± 0.04^{g-j}	1.31 ± 0.02^{jk}	1.21 ± 0.04^{op}	96.73 ± 4.22^{c-f}	33.32 ± 3.1^{ab}	4.55 ± 0.03^{l}	22.38 ± 1.65^{fg}
Megha Taro-1	1.4 ± 0.05^{de}	0.45 ± 0.03^{ab}	1.19 ± 0.03^{l-n}	1.65 ± 0.04^{de}	91.3 ± 5.06^{d-h}	32.19 ± 2.03^{a-c}	4.44 ± 0.04^{lm}	35.56 ± 3.59^{c}
Megha Taro-2	1.15 ± 0.06^{fg}	0.25 ± 0.02^{f-j}	1.17 ± 0.03^{m-o}	1.4 ± 0.04^{i-k}	101.06 ± 6.16^{b-e}	29.71 ± 3.34^{b-e}	6.17 ± 0.04^{g}	26.24 ± 3.14^{d-f}
Megha col	0.85 ± 0.05^{i-k}	0.10 ± 0.02^{k}	1.27 ± 0.02^{kl}	1.24 ± 0.02^{no}	65.4 ± 4.88^{n}	8.33 ± 0.60^{l}	2.09 ± 0.04^{u}	12.17 ± 2.01^{hi}
TBd 17–9	1.05 ± 0.05^{gh}	0.48 ± 0.03^{a}	1.71 ± 0.03^{e}	1.8 ± 0.03^{c}	105.72 ± 5.07^{a-d}	33.44 ± 3.16^{ab}	7.84 ± 0.04^{b}	57.2 ± 2.97^{a}

Values given are mean ($n = 3$) with SD. Superscript lower case letters on each column designated statistical significance ($p < 0.05$).

aligning with findings reported by Khatemenla et al. (29). Iron is essential for photosynthesis and various metabolic processes in plants. In humans, iron deficiency is a leading cause of anemia, a widespread nutritional disorder globally. Additionally, inadequate iron intake has been linked to impaired brain function in infants, highlighting its critical role in human health (38).

Zinc (Zn) content was recorded highest in the genotype Tamitin (40.54 ± 4.70 ppm) and lowest in Megha Col. Similar findings were reported in a study by Brandao et al. (39). Zn is important for human growth and development because it synthesizes hormones and enzymes that promote mental and physical growth, helps in tissue repair, wound healing and other functions (40). Copper (Cu) is another essential mineral which is associated with the formation and growth of bones and absorption of iron during hemoglobin synthesis (41). From the present study it is found that the Cu content of the assessed genotypes ranges from (2.09 ± 0.04 ppm) in Megha Col to (8.12 ± 0.04 ppm) in Tamitin. Similarly, the study also revealed a wide range of variation in manganese (Mn) content of the genotypes evaluated where Tamitin recorded the highest value (59 ± 4.07 ppm). Lebot et al. (42) have also documented a high level of variability for the mineral contents as well as other nutrients in the South East Asian and Pacific taro germplasm. Furthermore, Boampong et al. (35) while highlighting the competitiveness of taro with other root and tuber crops reported significant genetic variations in mineral nutrients among the taro test genotypes in Ghana. The high content of essential elements such as K, Ca, Mg and Zn in the present accessions of taro can be an asset for alleviating hidden hunger especially in the rural and poor communities where access to a balanced diet is limited. Genetic differences may be attributed to the variations in mineral concentrations among the studied genotypes because the growing conditions (i.e., the same plot, the same planting distance, and the same planting date) were identical. Furthermore, Wills et al. (43) argued that variation in value for the minerals is probably due to the potential of each genotype to obtain nutrients from the soil.

3.3 Biochemical parameters

The maximum dry matter content was documented in Tamachongkham and least in Khweng-2 (Table 3). There were also a significant ($p < 0.05$) differences in starch content among different genotypes. Further, the highest starch content (35.49 ± 4.20%) was recorded in Khweng-2 while ML-9 recorded the lowest (15.16 ± 3%). This result is in line with the finding of 33. Varietal variation in starch and dry matter content in taro was also reported (43). Khweng-2 recorded the highest total sugar (5.60 ± 0.08%) and reducing sugar (3.74 ± 0.08%) while lowest total sugar (2.70 ± 0.07%) was recorded in Tamitin and reducing sugar in Naya Bungalow (1.68 ± 0.06%). Similar findings were reported by Sangeeta et al. 2023 (34) who stated that variation in sugar content could be due to the accumulation and translocation of photosynthates from leaves to fruits as carbohydrates are manufactured in the leaves. The degradation of insoluble polysaccharides and genetic makeup that result in the variable synthesis of total sugars, as well as variations in soil, environmental factors, and crop genetic makeup, could be the cause of the elevated level of total sugar. Total oxalate was found to be minimum (70.82 ± 5.99 mg/100 g dw) in C-3 and maximum (208.54 ± 5.21 mg/100 g dw) in Rengama. Soluble oxalate was also recorded in the range 18.52 ± 5.45 mg/100 g dw to 104 ± 3.40 mg/100 g dw where Rengama exhibited the maximum value. Insoluble oxalate ranged between 20 ± 4.84 mg/100 g dw and 160.32 ± 4.10 mg/100 g dw with genotype Muktakeshi showing the highest value. Similar findings were reported (44). Oxalate content is of interest because of its negative impact on nutrient bioavailability (45). The genotypes with lower oxalate content are desirable. The calcium oxalate content varies among different taro genotypes (33, 40). Since all genotypes were cultivated under similar climatic conditions, soil type, and cultivation practices, the observed variations in biochemical composition can be attributed primarily to genotypic differences. These inherent varietal differences ultimately influence the nutritional value of the crop (46).

3.4 Crude protein, crude fiber and ash content

Data in Table 3 indicated significant variation in crude protein, crude fiber, and ash content among taro genotypes. Crude protein content ranged 3.25 ± 0.04% to 7.10 ± 0.04% with BCC-2 recorded the lowest and Rengama the highest, showcasing variability across different genotypes. Notably, the observation in our study align closely with those reported for other taro variety (47). Fagbemi and Olaofe (48) reported that taro can be an excellent source of protein to children who are sensitive to milk. Crude fiber ranged between 2.20 ± 0.02% to 3.23 ± 0.04% with maximum value shown by Rengama and minimum in Mairang local. This findings corresponds to the report (35, 49). The findings are important as crude fiber provides roughages that aid digestion (50). Ash content varied considerably from 3.90 ± 0.08% in Khweng-2 to 7.40 ± 0.05% in Mairang Local. These results are in agreement with the work done (49, 51, 52). This ash content may indicate that these samples could contain substantial amounts of dietary minerals, as confirmed in an earlier report (47).

3.5 Antioxidant activity

3.5.1 FRAP assay

FRAP antioxidants capacity is a simple and inexpensive assay that offers a putative index of the potential antioxidant activity of plant materials. Principally, the FRAP assay treats the antioxidants in the sample as reductants in a redox-linked colourimetric reaction. The reducing power assay, i.e., the transformation of Fe3C to Fe2C in the presence of either the extract or the standard (ascorbic acid), is a measure of reducing capability (53). Our study as presented in Table 4 indicated that among all the genotypes studied, the FRAP values recorded highest in Rengama (52 ± 4.55 mM $FeSO_4$E/100 g dw), while the lowest value was recorded in Tamakhan (35 ± 4.13 mM $FeSO_4$E/100 g dw). Similar FRAP value was recorded in a study (54). The variation may be related to genotypic differences, environmental factors, and methods used for determination (55).

3.5.2 DPPH radical scavenging activity assay

The free radical chain reaction is widely accepted as the most important mechanism of lipid peroxidation. Radical scavengers terminate the peroxidation chain reaction by directly counteracting and quenching peroxide radicals. The capacity of polyphenols to transport labile H atoms to radicals is a probable mechanism of antioxidant

TABLE 3 Biochemical parameters of the 30 genotypes of *Colocasia esculenta*.

Genotypes	Dry matter %	Starch %	Total Sugar %	Reducing Sugar %	Total Oxalate (mg/100 g) dw	Soluble Oxalate (mg/100 g) dw	Insoluble Oxalate (mg/100 g) dw	Crude Protein%	Crude Fiber %	Ash %
BCC-2	31.88 ± 4.36^{ab}	19.23 ± 3.81^{b-d}	3.05 ± 0.05^{o}	1.75 ± 0.05^{o}	85.78 ± 5.28^{h-k}	34.42 ± 3.82^{d-f}	51.36 ± 8.12^{j-l}	3.25 ± 0.04^{q}	3.06 ± 0.04^{bcd}	4.65 ± 0.04^{mn}
Kandha local	24.49 ± 4.48^{ab}	27.19 ± 3.01^{a-d}	4.95 ± 0.06^{b}	3.29 ± 0.08^{cd}	74.27 ± 4.05^{kl}	28.6 ± 4.18^{e-g}	45.68 ± 0.38^{k-m}	5.7 ± 0.03^{f}	2.91 ± 0.04^{e-h}	7.4 ± 0.05^{a}
Wahiajer local	28.44 ± 4.17^{ab}	31.49 ± 3.74^{a-c}	3.42 ± 0.07^{lm}	3.25 ± 0.07^{cd}	80.58 ± 4.5^{i-l}	25.29 ± 5.13^{f-g}	55.3 ± 4.92^{i-l}	6.53 ± 0.05^{d}	2.96 ± 0.04^{d-g}	4.53 ± 0.04^{n}
Mairang local	27.14 ± 4.95^{ab}	28.93 ± 3.3^{a-d}	3.42 ± 0.07^{lm}	2.91 ± 0.06^{fg}	94.42 ± 4.06^{g-i}	35.72 ± 4.37^{c-f}	58.69 ± 8.41^{i-k}	5.65 ± 0.04^{fg}	2.20 ± 0.02^{p}	7.40 ± 0.05^{a}
Thangitang	25.4 ± 4.16^{ab}	20.39 ± 3.86^{b-d}	3.97 ± 0.08^{ef}	2.86 ± 0.06^{f-h}	90 ± 5^{h-j}	18.81 ± 4.46^{g}	71.19 ± 8.08^{hi}	5.77 ± 0.05^{f}	2.96 ± 0.04^{d-g}	6.49 ± 0.03^{e}
RC Taro-6	35.25 ± 5.11^{ab}	19.58 ± 4.36^{b-d}	3.63 ± 0.07^{h-k}	3.17 ± 0.08^{de}	79.97 ± 4.35^{i-l}	49.2 ± 4.4^{c}	30.77 ± 4.16^{mn}	5.69 ± 0.04^{fg}	2.3 ± 0.04^{op}	4.66 ± 0.05^{mn}
AR3	28.12 ± 4.6^{ab}	25.5 ± 4.92^{a-d}	3.64 ± 0.09^{h-k}	2.8 ± 0.08^{f-i}	80.05 ± 4.81^{i-l}	29.4 ± 5.18^{d-g}	50.65 ± 0.39^{j-l}	3.31 ± 0.04^{q}	3.17 ± 0.04^{ab}	6.41 ± 0.04^{e}
ML2	29.35 ± 3.87^{ab}	33.44 ± 4.9^{ab}	3.52 ± 0.08^{j-l}	2.66 ± 0.06^{h-j}	92.58 ± 4.44^{g-i}	34.5 ± 4.88^{c-f}	58.08 ± 0.63^{i-k}	5.76 ± 0.05^{f}	2.97 ± 0.04^{d-f}	7.22 ± 0.04^{b}
ML3	26.18 ± 5.04^{ab}	18.49 ± 4.75^{cd}	3.71 ± 0.07^{g-j}	3.01 ± 0.04^{ef}	97.27 ± 3.81^{gh}	28.32 ± 3.96^{e-g}	68.96 ± 7.77^{h-j}	5.57 ± 0.05^{g}	3.19 ± 0.05^{a}	4.8 ± 0.04^{l}
Naga local	28.49 ± 5.02^{ab}	25.32 ± 3.96^{a-d}	3.46 ± 0.06^{k-m}	3.25 ± 0.08^{cd}	106.1 ± 4.9^{g}	25.37 ± 4.8^{fg}	80.73 ± 8.52^{gh}	3.37 ± 0.05^{pq}	2.92 ± 0.04^{e-h}	6.98 ± 0.04^{c}
AR2	32.41 ± 4.21^{ab}	23.55 ± 5.21^{a-d}	3.27 ± 0.08^{mn}	2.03 ± 0.08^{n}	136.76 ± 4.24^{ef}	31.32 ± 5^{d-g}	105.44 ± 4.43^{d-f}	5.24 ± 0.05^{h}	2.47 ± 0.05^{mn}	4.7 ± 0.05^{lm}
C3	25.11 ± 4.76^{ab}	17.68 ± 5.67^{cd}	4.79 ± 0.06^{bc}	3.45 ± 0.07^{bc}	70.82 ± 5.99^{l}	23.89 ± 4.3^{fg}	46.93 ± 1.74^{k-m}	5.33 ± 0.04^{h}	2.3 ± 0.04^{op}	4.39 ± 0.04^{o}
C-14-9	28.32 ± 5.02^{ab}	24.91 ± 4.86^{a-d}	3.5 ± 0.06^{j-l}	1.8 ± 0.07^{o}	76.43 ± 3.99^{j-l}	36.18 ± 4.01^{c-f}	40.25 ± 4.02^{k-m}	3.44 ± 0.04^{p}	2.87 ± 0.05^{f-i}	5.04 ± 0.04^{k}
Tagitung white	27.58 ± 4.53^{ab}	27.7 ± 4.47^{a-d}	3.74 ± 0.06^{g-i}	2.15 ± 0.06^{mn}	128.15 ± 4.56^{f}	35.32 ± 4.76^{c-f}	92.83 ± 4.98^{fg}	6.31 ± 0.04^{e}	2.81 ± 0.04^{h-j}	4.18 ± 0.02^{p}
ML9	28.54 ± 4.92^{ab}	15.16 ± 3^{d}	3.84 ± 0.06^{e-h}	2.69 ± 0.06^{g-j}	74.51 ± 3.9^{kl}	32.26 ± 4.16^{d-g}	42.25 ± 4.15^{k-m}	5.28 ± 0.04^{h}	3.14 ± 0.04^{a-c}	5.2 ± 0.04^{j}
Tamakhan	35.29 ± 5.04^{ab}	25.52 ± 4.49^{a-d}	3.46 ± 0.04^{k-m}	2.63 ± 0.07^{ij}	85.28 ± 4.61^{h-l}	65.27 ± 5.77^{b}	20 ± 4.84^{n}	3.44 ± 0.04^{p}	2.84 ± 0.03^{g-i}	4.19 ± 0.04^{p}
Naya bungalow	34.05 ± 7.01^{ab}	31.27 ± 5.16^{a-c}	3.15 ± 0.07^{no}	1.68 ± 0.06^{o}	196.87 ± 4.5^{ab}	36.97 ± 4.3^{c-f}	159.9 ± 7.78^{a}	6.48 ± 0.05^{d}	2.37 ± 0.04^{no}	5.43 ± 0.04^{i}
Khweng-3	34.64 ± 6.05^{ab}	26.04 ± 4.55^{a-d}	4 ± 0.07^{de}	3.17 ± 0.08^{de}	73.93 ± 4.61^{kl}	34.68 ± 4.55^{c-f}	39.25 ± 4.94^{lm}	4.66 ± 0.03^{ij}	2.76 ± 0.04^{ij}	4.06 ± 0.04^{p}
Tagitung purple	30.77 ± 4.76^{ab}	20.73 ± 4.52^{b-d}	3.78 ± 0.06^{f-h}	2.63 ± 0.06^{ij}	134.47 ± 4.17^{ef}	29.26 ± 4.78^{d-g}	105.2 ± 4.32^{d-f}	3.6 ± 0.03^{o}	2.23 ± 0.03^{p}	5.64 ± 0.04^{gh}
Tamachongkham	36.93 ± 3.83^{a}	20.43 ± 3.98^{b-d}	3.51 ± 0.07^{j-l}	2.89 ± 0.06^{fg}	193.14 ± 3.88^{b}	41.76 ± 4.37^{c-e}	151.38 ± 0.65^{ab}	6.49 ± 0.04^{d}	2.7 ± 0.04^{jk}	6.18 ± 0.05^{f}
Tamitin	23.29 ± 5.21^{ab}	19.24 ± 5.53^{b-d}	2.7 ± 0.07^{p}	1.79 ± 0.07^{o}	187.29 ± 4.54^{bc}	102.46 ± 4.34^{a}	84.82 ± 7.3^{gh}	4.76 ± 0.05^{i}	2.62 ± 0.04^{kl}	6.68 ± 0.04^{d}
Rengama	21.12 ± 4.6^{b}	20.56 ± 4.74^{b-d}	4.63 ± 0.06^{c}	3.34 ± 0.07^{cd}	208.54 ± 5.21^{a}	104 ± 3.40^{a}	104.54 ± 7.79^{d-f}	7.10 ± 0.04^{a}	3.23 ± 0.04^{a}	7.26 ± 0.04^{b}
Khweng-2	20 ± 3.39^{b}	35.49 ± 4.20^{a}	5.6 ± 0.08^{a}	3.74 ± 0.08^{a}	165.96 ± 5.34^{d}	30.79 ± 4.45^{d-g}	135.16 ± 8.82^{bc}	3.79 ± 0.04^{n}	3.04 ± 0.04^{c-e}	3.90 ± 0.08^{q}
White Gaurya	26.74 ± 4.37^{ab}	30.46 ± 4.17^{a-c}	3.85 ± 0.07^{e-g}	3.23 ± 0.08^{d}	174.18 ± 3.78^{cd}	24.25 ± 4.72^{fg}	149.93 ± 7.39^{ab}	4.58 ± 0.05^{jk}	2.41 ± 0.03^{no}	5.61 ± 0.04^{h}
Muktakeshi	23.26 ± 4.62^{ab}	24.44 ± 5.11^{a-d}	3.16 ± 0.09^{no}	2.37 ± 0.07^{kl}	186.52 ± 3.99^{bc}	26.21 ± 4.81^{fg}	160.32 ± 4.10^{a}	4.26 ± 0.04^{m}	3.12 ± 0.04^{a-c}	6.19 ± 0.05^{f}
IGB-5	28.54 ± 4.85^{ab}	17.35 ± 5.06^{cd}	3.76 ± 0.07^{g-i}	2.65 ± 0.08^{h-j}	141.16 ± 4.54^{ef}	18.52 ± 5.45^{g}	122.64 ± 0.94^{cd}	6.74 ± 0.04^{c}	2.62 ± 0.04^{kl}	7.35 ± 0.04^{ab}
Megha Taro-1	31.37 ± 4.79^{ab}	31.28 ± 3.85^{a-c}	2.74 ± 0.06^{p}	2.25 ± 0.05^{lm}	142.75 ± 4.72^{e}	32.95 ± 4.25^{d-g}	109.8 ± 7.74^{def}	4.52 ± 0.05^{kl}	2.57 ± 0.08^{lm}	5.65 ± 0.04^{gh}
Megha Taro-2	27.69 ± 4.12^{ab}	30.41 ± 4.95^{a-c}	3.2 ± 0.06^{no}	1.81 ± 0.06^{o}	148.54 ± 4.58^{e}	35.22 ± 5.05^{c-f}	113.32 ± 4.69^{de}	6.94 ± 0.05^{b}	2.58 ± 0.04^{k-m}	6.39 ± 0.05^{e}
Megha col	31.08 ± 5.57^{ab}	18.3 ± 5.41^{cd}	4.2 ± 0.06^{d}	3.64 ± 0.07^{ab}	165.37 ± 4^{d}	43.82 ± 4.28^{cd}	121.55 ± 7.23^{cd}	7.09 ± 0.04^{a}	2.95 ± 0.04^{d-g}	6.88 ± 0.05^{c}
TBd 17–9	27.48 ± 4.06^{ab}	21.41 ± 4.97^{a-d}	3.56 ± 0.06^{i-l}	2.58 ± 0.08^{jk}	134.62 ± 4.56^{ef}	35.36 ± 4.69^{c-f}	99.27 ± 4.8^{e-g}	4.43 ± 0.04^{l}	2.6 ± 0.04^{kl}	5.77 ± 0.05^{g}

N, Nitrogen; P, Phosphorus; K, Potassium; Ca, calcium; Mg, Magnesium; Fe, Iron; Zn, Zinc; Cu, Copper; Mn, Manganese. Values given are mean (n = 3) with SD. One way analysis of variance (ANOVA) plus post-hoc Tukey test was done to compare means. Superscript lower case letters on each column designated statistical significance ($p < 0.05$).

10.3389/fnut.2025.1567829

10.3389/fnut.2025.1567829

TABLE 4 Antioxidant activity of 30 genotypes of *Colocasia esculenta*.

Genotypes	FRAP (mM $FeSO_4$E/100 g) dw	DPPH (IC_{50}) sample (mg/ml) dw	Total phenolic content (mgGAE/100 g) dw	Total anthocyanin content (mg/100 g) dw
BCC-2	$38.09 \pm 3.28^{b\text{-}d}$	1.13 ± 0.07^{a}	$91.78 \pm 3.4^{a\text{-}e}$	0.50 ± 0.04^{k}
Kandha local	36.91 ± 3.28^{cd}	1.12 ± 0.05^{a}	$86.19 \pm 3.95^{b\text{-}f}$	$0.73 \pm 0.04^{a\text{-}i}$
Wahiajer local	$48.13 \pm 3.99^{a\text{-}d}$	$1.01 \pm 0.05^{a\text{-}f}$	$84.02 \pm 3.55^{c\text{-}f}$	$0.66 \pm 0.05^{e\text{-}j}$
Mairang local	$40.74 \pm 4.1^{a\text{-}d}$	$0.83 \pm 0.05^{g\text{-}i}$	$94.17 \pm 4^{a\text{-}d}$	0.55 ± 0.05^{jk}
Thangitang	$47.75 \pm 4.64^{a\text{-}d}$	$1 \pm 0.05^{a\text{-}f}$	$81.93 \pm 3.35^{d\text{-}f}$	$0.74 \pm 0.04^{a\text{-}i}$
RC Taro-6	$48.01 \pm 4.45^{a\text{-}d}$	1.09 ± 0.05^{ab}	$84.37 \pm 4^{c\text{-}f}$	$0.62 \pm 0.05^{h\text{-}k}$
AR3	$45.2 \pm 4.63^{a\text{-}d}$	$0.82 \pm 0.04^{g\text{-}i}$	$91.64 \pm 3.44^{a\text{-}e}$	$0.72 \pm 0.05^{a\text{-}i}$
ML2	50.92 ± 3.59^{ab}	0.72 ± 0.05^{i}	$97.01 \pm 4.18^{a\text{-}c}$	$0.67 \pm 0.04^{d\text{-}j}$
ML3	36.27 ± 4.18^{cd}	1.07 ± 0.06^{ab}	$88.79 \pm 3.46^{a\text{-}f}$	$0.81 \pm 0.05^{a\text{-}d}$
Naga local	$47.87 \pm 4.51^{a\text{-}d}$	$0.83 \pm 0.05^{g\text{-}i}$	$95.1 \pm 4.62^{a\text{-}d}$	$0.73 \pm 0.05^{a\text{-}i}$
AR2	$49.96 \pm 4.22^{a\text{-}c}$	$0.89 \pm 0.05^{d\text{-}h}$	$84.55 \pm 4.45^{c\text{-}f}$	0.84 ± 0.05^{ab}
C3	$40.85 \pm 4.22^{a\text{-}d}$	$0.95 \pm 0.05^{b\text{-}g}$	$94.91 \pm 4.4^{a\text{-}d}$	$0.75 \pm 0.06^{a\text{-}h}$
C-14-9	36.9 ± 4.14^{cd}	1.09 ± 0.06^{ab}	80.22 ± 3.32^{ef}	$0.64 \pm 0.05^{f\text{-}j}$
Tagitung white	$45.76 \pm 4.52^{a\text{-}d}$	0.72 ± 0.06^{i}	$95.09 \pm 3.3^{a\text{-}d}$	$0.76 \pm 0.05^{a\text{-}g}$
ML9	$37.72 \pm 4.93^{b\text{-}d}$	$1.05 \pm 0.06^{a\text{-}c}$	$83.71 \pm 4.26^{d\text{-}f}$	$0.68 \pm 0.04^{c\text{-}j}$
Tamakhan	35 ± 4.13^{d}	1.13 ± 0.05^{a}	$82.67 \pm 4.47^{d\text{-}f}$	$0.64 \pm 0.04^{g\text{-}k}$
Naya bungalow	$43.24 \pm 3.41^{a\text{-}d}$	$0.86 \pm 0.06^{e\text{-}i}$	$90.63 \pm 3.69^{a\text{-}f}$	$0.7 \pm 0.05^{b\text{-}i}$
Khweng-3	$49.64 \pm 4.39^{a\text{-}c}$	0.73 ± 0.04^{i}	$94.52 \pm 4.45^{a\text{-}d}$	$0.82 \pm 0.04^{a\text{-}c}$
Tagitung purple	$44.1 \pm 4.06^{a\text{-}d}$	$0.95 \pm 0.05^{b\text{-}g}$	$94.86 \pm 4.55^{a\text{-}d}$	$0.71 \pm 0.05^{a\text{-}i}$
Tamachongkham	$49.61 \pm 4.53^{a\text{-}c}$	$1.02 \pm 0.05^{a\text{-}e}$	98.98 ± 4.33^{ab}	$0.78 \pm 0.05^{a\text{-}f}$
Tamitin	$40.68 \pm 4.02^{a\text{-}d}$	$0.86 \pm 0.05^{f\text{-}i}$	$92.92 \pm 3.97^{a\text{-}e}$	$0.8 \pm 0.05^{a\text{-}e}$
Rengama	52 ± 4.55^{a}	0.71 ± 0.06^{i}	100 ± 4.88^{a}	0.86 ± 0.05^{a}
Khweng-2	$46.14 \pm 5.18a^{\text{-}d}$	0.72 ± 0.06^{i}	$94.3 \pm 5.01^{a\text{-}d}$	0.84 ± 0.05^{ab}
White Gaurya	$40.7 \pm 3.89^{a\text{-}d}$	1.11 ± 0.05^{a}	$86.14 \pm 4.74^{b\text{-}f}$	$0.82 \pm 0.04^{a\text{-}c}$
Muktakeshi	$46.11 \pm 4.85^{a\text{-}d}$	$1.03 \pm 0.04^{a\text{-}d}$	78 ± 4.08^{f}	$0.74 \pm 0.05^{a\text{-}i}$
IGB-5	$45.04 \pm 4.54^{a\text{-}d}$	0.76 ± 0.05^{hi}	$90.57 \pm 4.24^{a\text{-}f}$	$0.79 \pm 0.06^{a\text{-}f}$
Megha Taro-1	36.43 ± 4.61^{cd}	1.08 ± 0.05^{ab}	$83.68 \pm 3.14^{d\text{-}f}$	$0.6 \pm 0.05^{i\text{-}k}$
Megha Taro-2	$42.81 \pm 4.47^{a\text{-}d}$	$0.94 \pm 0.05^{b\text{-}g}$	80.21 ± 4.58^{ef}	$0.66 \pm 0.05^{e\text{-}j}$
Megha col	$42.66 \pm 3.91^{a\text{-}d}$	$1.07 \pm 0.05^{a\text{-}c}$	$93.09 \pm 4.34^{a\text{-}e}$	$0.77 \pm 0.05^{a\text{-}g}$
TBd 17–9	$41.38 \pm 4.23^{a\text{-}d}$	$0.91 \pm 0.04^{c\text{-}h}$	$93.69 \pm 4.49^{a\text{-}d}$	$0.63 \pm 0.05^{g\text{-}k}$

Values given are mean ($n = 3$) with SD. Superscript lower case letters on each column designated statistical significance ($p < 0.05$).

protection, which can be assessed universally and rapidly using DPPH. Furthermore, DPPH is the most common and cost-effective way to determine the free radical scavenging capacity of natural products, which are major factors in biological damage caused by oxidative stress (56). In the present study we was observed that IC_{50} values ranged from 0.71 ± 0.06 mg/mL dw in Rengama to 1.13 ± 0.07 mg/mL dw in BCC-2 which indicatesthat all the taro genotypes exhibited antioxidant activity, although there were differences in the extent of this property between the genotypes ($p < 0.05$). This observation was in line with the results reported in previous studies by Gonçalves et al. (57). Ali et al. (58) reported that lower IC_{50} value reflects better DPPH radical scavenging activity. Therefore,Rengama with least IC_{50} may be considered to have higher antioxidant activity or better radical scavenging activity than BCC-2 with highest IC_{50} value as argued by Mariod et al. (59).

3.5.3 Total phenolic content

Phenolic compounds may act as antioxidants, attractants, structural polymers, and signal compounds. They prevent oxidative damage to biomolecules due to the chelating of metal ions that cause the production of free radicals (60). Our results indicated the presence of significant variation in total phenol content among the *Colocasia* genotypes. Total phenolic content varied significantly from 78 ± 4.08 mgGAE/100 g dw in Muktakeshi to 100 ± 4.88 mgGAE/100 g dw in Rengama. Notably, Ouédraogo et al. (61) reported similar observation with respect to total phenolic content of taro. This variation in phenolic content could be attributed to environmental factors, extraction conditions, genetic factors, existence of distinct phenolic compounds and analytical method (61–64).

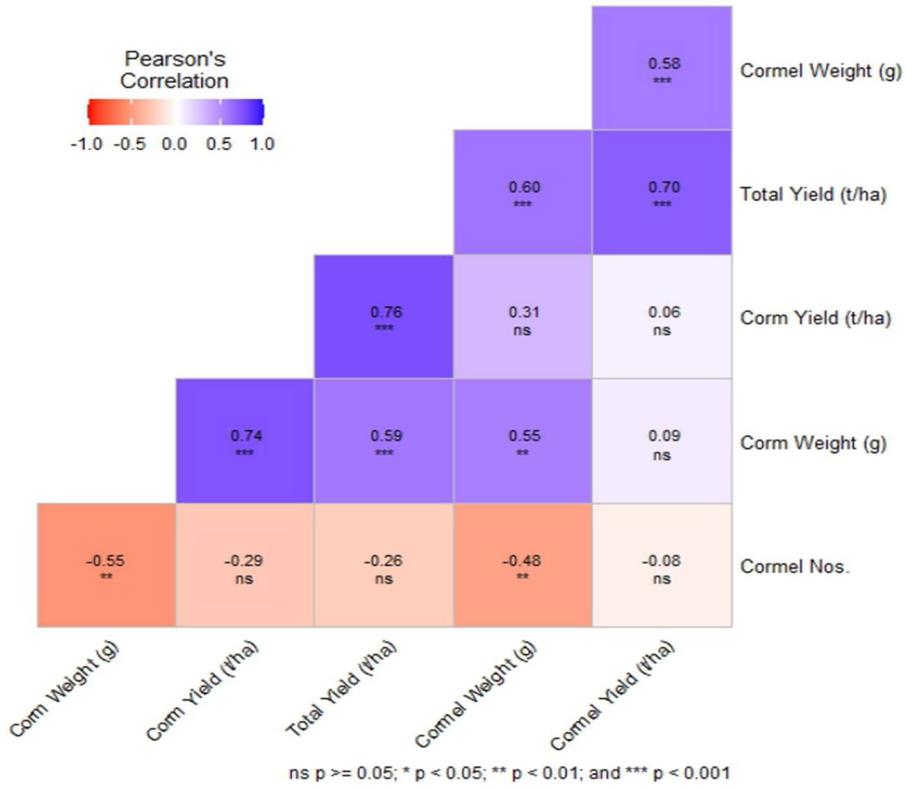

FIGURE 1
A Pearson's correlation heatmap illustrating the correlation among the yield parameters of *Colocasia esculenta* L. genotypes. Different colors represent negative (red) to positive (blue) correlation.

3.5.4 Anthocyanin content

Anthocyanins are water-soluble and vacuolar pigments found in most species in the plant kingdom. It plays a role in preventing, ameliorating, and scrubbing oxidative stress, thus retarding several diseases and physiological malfunctions (65). A significant variation in anthocyanin content was observed among the genotypes. The anthocyanin content ranged 0.50 ± 0.04 mg/100 g dw to 0.86 ± 0.05 mg/100 g dw with Rengama recorded maximum and BCC-2 the minimum. Our finding is in line with Das et al. (66) who reported similar anthocyanin content in raw taro powder. This difference in anthocyanin content might be due to the effects of genetics, agro-ecological conditions such as pH, light, temperature, and horticultural practices (67).

3.6 Correlation among yield and quality traits

Correlation analysis is a crucial statistical approach used to understand the interrelationships among multiple traits in plant breeding and agronomic research. In this study, Pearson's correlation coefficient was employed to quantify the strength and direction of associations between yield related traits, biochemical parameters, and antioxidant properties in Colocasia. The rationale for implementing correlation analysis lies in its ability to identify key traits that influence overall crop performance, allowing breeders and researchers to make informed decisions in trait selection and genetic improvement programs. By analyzing correlation patterns, we can determine whether improvements in a particular trait, such as yield, have a direct or indirect effect on other parameters, including nutritional and antioxidant properties. A strong positive correlation suggests that traits can be co-selected for genetic enhancement, whereas a negative correlation indicates potential trade-offs that must be considered in breeding strategies. Additionally, correlation analysis provides insights into the physiological and biochemical linkages among traits, revealing how metabolic pathways influence yield and quality attributes. For instance, the accumulation of starch and sugars in corms may affect other biochemical properties such as phenolic content and antioxidant activity, which are crucial for both nutritional value and storage quality.

The total yield exhibited a significant positive correlation with corm yield, cormel yield, cormel weight, and corm weight, suggesting that these yield-related traits are interdependent and can be used as selection criteria for improving overall productivity (Figure 1). This is in accordance with the study (68). Likewise, the correlation coefficient of all the other yield related traits is presented in the heatmap below (Figure 1) further illustrates the strength and direction of these relationships.

Among quality traits, dry matter content showed a significant positive correlation with DPPH but a significant negative correlation with anthocyanin and total sugar (Figure 2). This indicates that higher dry matter content may enhance antioxidant activity (DPPH), while possibly reducing anthocyanin and sugar accumulation. However, starch content which is the most desirable quality trait in Colocasia

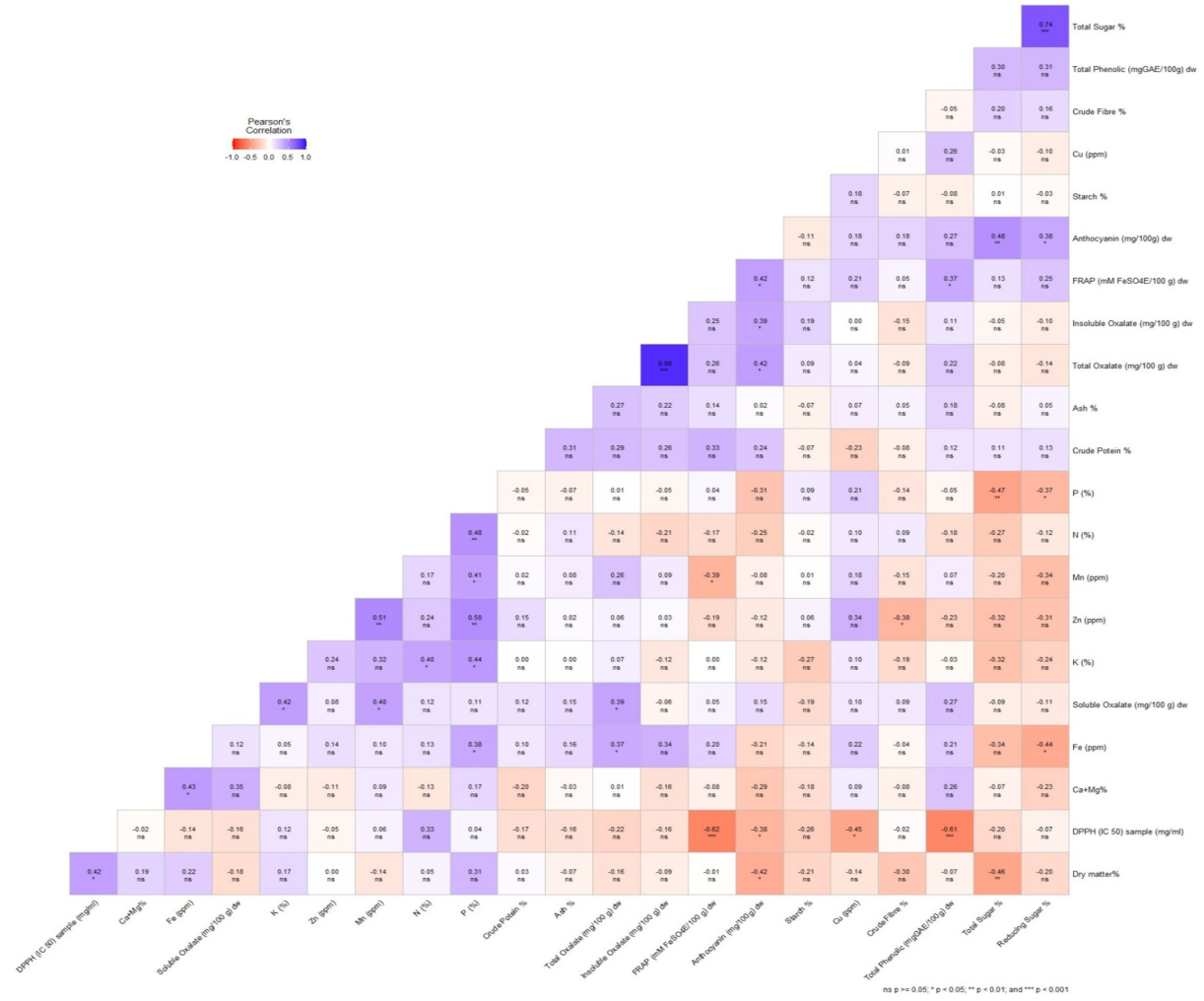

FIGURE 2
A Pearson's correlation heatmap illustrating the correlation among the biochemical and antioxidant parameters of *Colocasia esculenta* L. genotypes. Different colors represent negative (red) to positive (blue) correlation.

showed positive but non-significant correlation with insoluble oxalate, Cu, FRAP, total oxalate, P, Zn, Mn and total sugar and negative non-significant correlation with the other quality parameters (Figure 2). This suggests that while starch accumulation is largely independent of these traits, external factors such as genetic variation and environmental conditions may play a crucial role in starch biosynthesis. A study (61) reported no significant correlation between starch and antioxidant properties (DPPH, FRAP) or sugar content. Additionally, there was no significant positive correlation between crude protein and mineral content (Figure 2), suggesting that selecting for high protein does not necessarily result in increased mineral levels. This finding aligns with a study by Boampong et al. (35), which also reported that most minerals did not show a significant correlation with protein content.

With respect to antioxidants parameters, total phenolic content exhibited the highest positive significant correlation with FRAP ($r = 0.37$, $p < 0.05$) and highly significant negative correlation with DPPH ($r = -0.61$, $p < 0.001$). FRAP had significant positive correlation with anthocyanin ($r = 0.42$, $p < 0.05$) and a highly significant negative correlation with DPPH ($r = -0.62$, $p < 0.001$). A significant negative correlation was observed between DPPH and anthocyanin ($r = -0.38$, $p < 0.05$; Figure 2). Makori et al. (69) also reported a similar positive correlation between total phenolic content and FRAP ($r^2 = 0.535$, $p < 0.001$). Previous studies have also reported a positive correlation between antioxidant activity and both phenolic and anthocyanin content (70, 71), highlighting the crucial role of polyphenols in plant extracts in determining their antioxidant potential (72). This correlation serves as a reliable indicator of the antioxidant properties of plant-based compounds (73). By understanding these correlations, breeding programs can prioritize traits that contribute to both yield and quality, ensuring the development of high-yielding Colocasia cultivars with enhanced nutritional and functional properties.

3.7 Principal component analysis

The principal component analysis (PCA), a multivariate statistical technique, was used in the current study for: (i) dimension reduction or selection of a minimum data set (MDS) and (ii) computation of weights (Wi). The system attributes are best represented by the principal components with high eigenvalues and variables with high factor loadings. Therefore, we examined only the PCs with eigenvalues

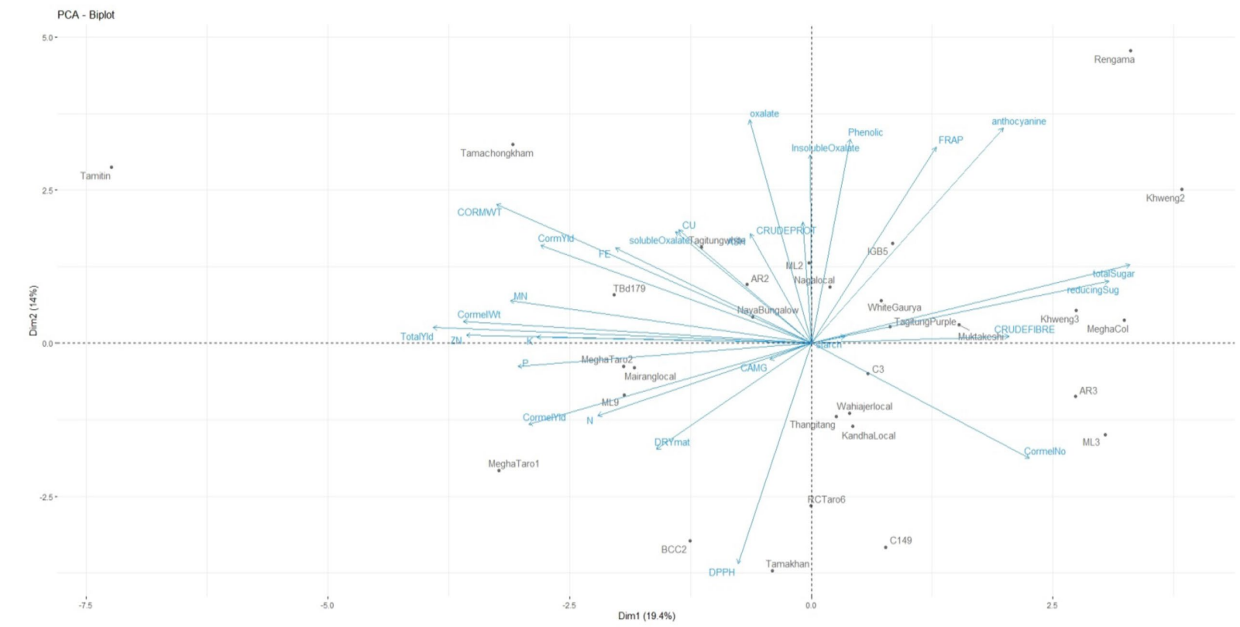

FIGURE 3
Genotype-by-trait biplot analysis for two principal components of *Colocasia esculenta* L. genotypes.

≥1.0. PCA helps in understanding the underlying structure of a complex dataset by transforming correlated variables into a set of uncorrelated components ranked by their contribution to overall variance. This transformation allows for better interpretation of the relationships among yield-related and biochemical parameters, enabling the identification of key traits that significantly influence Colocasia productivity and quality.

Phenotypic data of 30 *Colocasia esculenta* L. genotypes for yield and related traits were utilized for generating genotype-by-trait biplot graphs (Figure 3) and analyzed using the first two principal components. PC1 explained 19.4% of the total variation, while PC2 accounted for 14%. Among the 28 yield-contributing and biochemical traits, total sugar, reducing sugar, cormel numbers, crude fiber, anthocyanin, and FRAP contributed maximally to the diversity in PC1 (Table 5). PC1 primarily explains the trade-off between yield and biochemical properties such as sugar content and fiber accumulation. The selection of genotypes with high yield traits should consider their sugar accumulation, as higher sugar content may indicate enhanced palatability but could inversely impact dry matter content and storage quality. The significant contribution of FRAP suggests that yield improvements must be balanced with maintaining antioxidant potential for enhanced nutritional quality. Similarly, total oxalate, anthocyanin, total phenolics, FRAP, insoluble oxalate, corm weight, crude protein, soluble oxalate, Cu, ash, corm yield, Fe, total sugar, and reducing sugar exhibited maximum diversity in PC2. PC2 represents biochemical and anti-nutritional components, indicating that genotypes with higher antioxidant activity tend to accumulate phenolic compounds and oxalates. While high phenolic content is beneficial for human health, excessive oxalate levels can hinder mineral bioavailability. Thus, breeders should focus on achieving an optimal balance between antioxidant properties and oxalate content for developing nutritionally superior Colocasia varieties.

The positioning of genotypes in different quadrants of the biplot graph suggests distinct trait associations. For instance, genotypes such as Tamitin, Tamachongkham, Tagitung, and AR2 in the first (top left) quadrant exhibited high loadings for yield-contributing and mineral traits like corm weight, corm yield, Mn, Zn, and K, suggesting potential for high productivity. Meanwhile, Rengama, Khweng-2, and IGB-5 in the second (top right) quadrant contains seven variables such as anthocyanin, FRAP, phenolic, total sugar, reducing sugar, crude fiber and starch. The genotypes positioned in these quadrants suggest potential breeding lines for different end uses. High-yielding genotypes are suitable for commercial production, while those rich in antioxidants are valuable for nutraceutical applications. This classification aids in targeted breeding strategies to meet diverse consumer and industrial demands. Genotypes in the third (bottom right) quadrant, such as C3, AR3, Wahiajer Local, Thangitang, Kandha Local, and ML3, primarily influenced cormel numbers, which could impact propagation efficiency. Higher cormel numbers indicate superior propagation ability, which is beneficial for mass multiplication and commercial production. However, trade-offs with yield and biochemical traits should be carefully evaluated to ensure that productivity is not compromised. The fourth (bottom left) quadrant, containing Megha Taro-2, Mairang Local, and ML9, was associated with P, cormel yield, N, Ca + Mg, dry matter, and DPPH, highlighting genotypes with higher nutrient density and stress resilience. These genotypes exhibit superior nutrient profiles and stress tolerance, making them ideal candidates for improving soil nutrient efficiency and resilience under variable environmental conditions. Selection of such genotypes can contribute to sustainable agricultural practices and improved food security. The identified traits within the axes of the first five PCs with maximum variance exhibited significant influence on the phenotypes of the Colocasia genotypes evaluated and could efficiently be utilized for future selection among these genotypes. The study revealed distribution of variance over multiple PCs, which may be attributed to the poor correlation among yield and related traits (74). The results indicate that multiple independent factors contribute to yield and biochemical variation in Colocasia. This insight helps in

TABLE 5 Principal component analysis of *Colocasia esculenta* L. genotypes.

PCs	PC1	PC2	PC3	PC4	PC5	PC6
% variance expected	19.4	14	8.6	8.3	6.8	6.3
Corm weight (g)	−0.26	0.22	−0.09	0.07	−0.18	0.18
Cormel weight (g)	−0.29	0.03	−0.13	**0.33**	−0.03	−0.001
Cormel nos.	0.19	−0.18	−0.16	−0.30	0.12	−0.18
Corm yield (t/ha)	−0.23	0.15	−0.24	−0.09	−0.18	0.24
Cormel yield (t/ha)	−0.24	−0.13	−0.23	0.06	0.25	0.03
Total yield (t/ha)	−0.32	0.02	−0.33	−0.03	0.04	0.19
Dry matter %	−0.13	−0.17	0.18	−0.19	−0.20	**0.41**
Starch %	0.03	0.01	−0.25	−0.25	**0.42**	−0.10
Total sugar %	**0.27**	0.12	−0.18	0.25	0.02	0.02
Reducing sugar %	0.25	0.10	−0.18	0.24	−0.14	0.16
Total oxalate (mg/100 g) dw	−0.05	**0.35**	0.07	−0.26	−0.13	−0.30
Soluble oxalate (mg/100 g) dw	−0.12	0.18	0.25	0.24	−0.03	−0.31
Insoluble oxalate (mg/100 g) dw	−0.001	0.30	−0.05	−0.40	−0.12	−0.17
FRAP (mM $FeSO_4$E/100 g) dw	0.11	0.31	0.05	−0.13	0.05	0.25
DPPH (IC 50) sample (mg/ml dw)	−0.06	−0.35	−0.01	−0.05	−0.40	−0.09
Total phenolic (mgGAE/100 g) dw	0.03	0.32	0.16	0.17	0.13	0.27
Anthocyanin (mg/100 g) dw	0.16	0.34	−0.13	0.09	−0.12	−0.13
N %	−0.18	−0.11	−0.02	0.02	−0.15	−0.12
P %	−0.25	−0.04	0.20	−0.13	0.09	−0.04
K %	−0.23	0.01	0.15	0.20	−0.21	−0.12
Ca + Mg %	−0.04	−0.03	**0.45**	0.002	0.21	0.11
Fe (ppm)	−0.17	0.15	0.32	−0.27	0.03	0.13
Zn (ppm)	−0.29	0.01	−0.18	−0.02	0.17	−0.15
Cu (ppm)	−0.11	0.18	0.03	0.15	0.41	0.05
Mn (ppm)	−0.26	0.07	0.03	0.12	0.06	−0.37
Crude protein %	−0.01	0.19	−0.18	−0.17	−0.23	−0.02
Crude fiber %	0.17	0.01	0.12	0.15	−0.10	−0.19
Ash %	−0.05	0.17	−0.02	−0.02	−0.11	−0.06

Bold values indicates traits contributing maximum towards respective PCs.

designing a multi-trait selection strategy that can enhance both productivity and quality traits, ensuring superior cultivar development. This statistical approach provides a robust framework for the selection of Colocasia genotypes with optimal agronomic performance, nutritional quality, and biochemical properties, facilitating targeted breeding for improved cultivar development.

4 Conclusion

The results of this study indicate significant ($p < 0.05$) variations among the 30 *Colocasia esculenta* genotypes in terms of yield, biochemical composition, mineral content, and antioxidant parameters. Correlation analysis revealed that corm weight and cormel weight can serve as effective selection indices for yield improvement. Notably, Tamachongkham exhibited the highest corm yield, Tamitin had the highest total yield and key minerals (N, K, Zn, Cu, Mn), while Khweng-2 was rich in starch and sugars. Furthermore, Rengama recorded high crude protein and crude fiber, and BCC-2 had superior Fe and Ca + Mg content. The genotypes also demonstrated a diverse nutritional profile, including significant antioxidant properties. Based on these findings, Tamachongkham and Tamitin emerge as the most promising genotypes for future breeding programs aimed at enhancing yield and nutritional quality. These genotypes, along with others exhibiting superior biochemical and mineral traits, should be conserved as a genetic resource for future improvement programs to support food security and sustainability, particularly for the tribal communities of the North-Eastern Hill Region, India. These findings have practical applications in breeding programs for selecting high-yielding and nutrient-rich taro varieties, contributing to food security and crop diversification efforts. Future research should focus on assessing genotype performance under different environmental conditions, exploring anti-nutritional factors and utilizing genomic tools to accelerate the breeding of superior taro cultivars.

Data availability statement

The original contributions presented in the study are included in the article/supplementary material, further inquiries can be directed to the corresponding author.

Author contributions

HT: Conceptualization, Data curation, Formal analysis, Investigation, Methodology, Resources, Supervision, Validation, Writing – original draft, Writing – review & editing. GM: Data curation, Formal analysis, Investigation, Methodology, Writing – original draft, Writing – review & editing. LK: Formal analysis, Investigation, Methodology, Writing – review & editing. MD: Funding acquisition, Investigation, Writing – original draft, Writing – review & editing. BG: Data curation, Formal analysis, Methodology, Software, Writing – review & editing. NB: Formal analysis, Writing – original draft, Writing – review & editing. NS: Funding acquisition, Writing – review & editing. VV: Resources, Supervision, Writing – review & editing. HR: Formal analysis, Writing – review & editing. PR: Investigation, Methodology, Writing – review & editing. BD: Investigation, Writing – review & editing. TA: Resources, Writing – review & editing. AY: Methodology, Writing – review & editing. SP: Formal analysis, Funding acquisition, Writing – review & editing. BM: Methodology, Resources, Writing – review & editing. RC: Data curation, Investigation, Writing – review & editing. SA: Investigation, Writing – review & editing. CS: Formal analysis, Methodology, Writing – review & editing. LC: Investigation, Resources, Writing – review & editing. SH: Funding acquisition, Supervision, Writing – review & editing.

Funding

The author(s) declare that financial support was received for the research and/or publication of this article. The authors gratefully acknowledge the support received from the Director, ICAR Research Complex for NEH Region, Umiam, Meghalaya and All India Coordinated Research Project on Tuber Crops during the course of the study. The authors are also thankful to the farmers for the support during study.

Conflict of interest

The authors declare that the research was conducted in the absence of any commercial or financial relationships that could be construed as a potential conflict of interest.

Generative AI statement

The author(s) declare that no Gen AI was used in the creation of this manuscript.

Publisher's note

All claims expressed in this article are solely those of the authors and do not necessarily represent those of their affiliated organizations, or those of the publisher, the editors and the reviewers. Any product that may be evaluated in this article, or claim that may be made by its manufacturer, is not guaranteed or endorsed by the publisher.

References

1. Vinutha YN, Lohakare AS, Wankhede SR. Evaluation of taro (*Colocasia esculenta* L.) genotypes for quantitative traits under Marathwada conditions. *Int J Adv Biochem Res*. (2024) 8:386–9. doi: 10.33545/26174693.2024.v8.i2e.572

2. FAOSTAT. FAO Statistical Database; (2023). Available online at: https://www.fao.org/faostat/en/#ata/QCL (Accessed March 3, 2025).

3. Legesse T, Bekele T. Evaluation of improved taro (*Colocasia esculenta* (L.) Schott) genotypes on growth and yield performance in north-bench woreda of bench-Shekozone, South-Western Ethiopia. *Heliyon*. (2021) 7:e08630. doi: 10.1016/j.heliyon.2021.e08630

4. Wang Z, Sun Y, Huang X, Li F, Liu Y, Zhu H, et al. Genetic diversity and population structure of eddoe taro in China using genome-wide SNP markers. *Peer J*. (2020) 8:e10485. doi: 10.7717/peerj.10485

5. Rashmi DR, Anitha B, Anjum SR, Raghu N, Gopenath TS, Chandrashekrappa GK, et al. An overview of Taro (*Colocasia esculenta*): a review. *Acad J Agricul Res*. (2018) 6:346–53. doi: 10.15413/ajar.2018.0144

6. Tewodros M, Getachew W, Kifle B. Genetic diversity of Taro (*Colocasia esculenta* (L.) Schott) genotypes in Ethiopia based on agronomic traits. *Time J Agri and Veterin Sci*. (2013) 1:23–30.

7. Soudy ID, Delatour P, Grancher D. Effects of traditional soaking on the nutritional profile of taro flour (*Colocasia esculenta* L. Schott) produced in Chad. *Revue De Med Vet*. (2010) 161:37–42.

8. Quach ML, Melton LD, Harris PJ, Burdon JN, Smith BG. Cell wall compositions of raw and cooked corms of taro (*Colocasia esculenta*). *J Sci Fd and Agri*. (2001) 81:311–8. doi: 10.1002/1097-0010(200102)81:3<311::aid-jsfa816>3.0.co;2-b

9. Krishnapriya TV, Suganthi A. Biochemical and phytochemical analysis of *Colocasia esculenta* (L.) Schott tubers. *Int J Res in Pharmacy and Pharma Sci*. (2017) 2:21–5.

10. Bremner JM. Total nitrogen In: CA Black, DD Evans, JL White and FE Clark, editors. Methods of analysis. Madison (WI): Academic Press (1965). 1149–78.

11. Gupta PK. Soil, plant, water and fertilizer analysis. *Agrobios, New Delhi, India*. (2000):438.

12. Chapman HD. Suggested foliar sampling and handling techniques for determining the nutrient status of some field, horticultural and plantation crops. *Ind J Hort*. (1964) 21:97–119.

13. Chapman HD, Pratt PF. Methods of analysis for soils, plants and water. Riverside: Division of Agricultural Sciences, University of Florida (1961).

14. Hesse PR. A textbook of soil chemical analysis. *2nd* ed. London: John Muray Company Ltd. (1971).

15. Zasoski RJ, Burau RG. A rapid nitric-perchloric acid digestion method for multi-element tissue analysis. *Commun Soil Sci Plant Anal*. (1977) 8:425–36. doi: 10.1080/00103627709366735

16. Cheng KL, Bray RH. Determination of calcium and magnesium in soil and plant material. *Soil Sci*. (1951) 72:449–58. doi: 10.1097/00010694-195112000-00005

17. Jackson ML. Soil chemical analysis. New Delhi: Prentice Hall of India Pvt. Ltd. (1973).

18. Hedge JE, Hofreiter BT In: RL Whistler and JN Be Miller, editors. Carbohydrate chemistry. New York: Academic Press (1962). 4: 17.

19. DuBois M, Gilles KA, Hamilton JK, Rebers PA, Smith F. Colorimetric method for determination of sugars and related substances. *Anal Chem*. (1956) 28:350–6. doi: 10.1021/ac60111a017

20. Miller GL. Use of Dinitrosalicylic acid reagent for determination of reducing sugar. *Anal Chem*. (1959) 31:426–8. doi: 10.1021/ac60147a030

21. AOAC. Official methods of analysis. *14th edn*., Association of Analytical Chemists, Washington DC (1984) p. 249–252.

22. AOAC (Association of Official Analytical Chemists). Officials method of analysis. Washington DC: Helriok Publisher (1990). 1230 p.

23. Maynard AJ. Methods in food analysis. New York: Academic Press (1970).176 p.

24. James CS. Analytical chemistry of food. Chapmen and Hall: London (1995) p. 64–65.

25. Keskin-Sasic I, Tahirovic I, Topcagic A, Klepo L, Salihovic M, Ibragic S, et al. Total phenolic content and antioxidant capacity of fruit juices. *Bullet Chem Technol Bos Herzeg*. (2012) 39:25–8.

26. Benzie IF, Strain JJ. Ferric reducing/antioxidant power assay: direct measure of total antioxidant activity of biological fluids and modified version for simultaneous

measurement of total antioxidant power and ascorbic acid concentration. *Methods Enzymol*. (1999) 299:15–27. doi: 10.1016/s0076-6879(99)99005-5

27. Shen Q, Zhang B, Xu R, Wang Y, Ding X, Li P. Antioxidant activity in vitro of the selenium-contained protein from the se-enriched *Bifidobacterium animalis* 01. *Anaerobe*. (2010) 16:380–6. doi: 10.1016/j.anaerobe.2010.06.006

28. Srivastava RP, Kumar S. Fruit and vegetable preservation: Principle and practice. *3rd Edn*. (Lucknow: Inter Book distribution company, India). (2002) 360–361.

29. Khatemenla SA, Phookan DB, Kalita P, Barooah M, Talukdar MC. Morphological characterization of some upland Taro (*Colocasia esculenta* L. Schott) genotypes of north-East India. *Int J Curr Microbiol App Sci*. (2019) 8:1944–64. doi: 10.20546/ijcmas.2019.806.232

30. Kay DE. Crop and Product Digest, No. 2 – Root Crops. *Second* ed. London: Tropical Development and Research Institute (1987). 380 p.

31. Bekele D, Boru M. Evaluation of released Taro (*Colocasia esculenta* L.) varieties at Assosa District, Western Ethiopia. *Ecol and Evol Biol*. (2020) 5:43–6. doi: 10.11648/j.eeb.20200503.12

32. Thirugnanavel A, Deka BC, Rangnamei L, Meyase M, Patel JK. Colocasia and its genetic diversity in Northeast India. Umiam, Meghalaya: ICAR Research Complex for NEH Region (2015). 793103 p.

33. Angami T, Jha AK, Buragohain J, Deka BC, Verma VK, Nath A. Evaluation of taro (*Colocasia esculenta* L.) cultivars for growth, yield and quality attributes. *J Hortl Sci*. (2015) 10:183–9. doi: 10.24154/jhs.v10i2.127

34. Sangeeta D, Latha GK, Arunkumar B, Ravi CS, Kantharaj Y, HSY K. Evaluation of Taro (*Colocasia esculenta* L.) genotypes for growth, yield and quality attributes under the hill zone of Karnataka. *Biolog Forum – An Inter J*. (2023) 15:36–41.

35. Boampong R, Aboagye LM, Nyadanu D, Essilfie ME, Amoah RA. Biochemical characterization of some Taro (*Colocasia esculenta* L. Schott) germplasm in Ghana. *Adv Agri*. (2019) 7:1965761. doi: 10.1155/2019/1965761

36. Buragohain J, Angami T, Choudhary BU, Singh P, Bhatt BP, Thirugnanavel A, et al. Quality evaluation of indigenous Taro (*Colocasia esculenta* L.) cultivars of Nagaland. *Indian J Hill Farm*. (2013) 26:16–20.

37. Lewu MN, Adebola PO, Afolayan AJ. Effect of cooking on the mineral contents and anti-nutritional factors in seven accessions of *Colocasia esculenta* (L.) Schott growing in South Africa. *J Food Compos Anal*. (2010) 23:389–93. doi: 10.1016/j.jfca.2010.02.006

38. Mergedus A, Kristl J, Ivancic A, Sober A, Sustar V, Krizan T, et al. Variation of mineral composition in different parts of taro (*Colocasia esculenta*) corms. *Food Chem*. (2015) 170:37–46. doi: 10.1016/j.foodchem.2014.08.025

39. Brandao NA, Tagliapietra BL, MTPS C. Taro [*Colocasia esculenta* (L.) Schott]: a critical review of its nutritional value and potential for food application. *Food Sci Technol*. (2023) 43:e00118. doi: 10.5327/fst.00118

40. Chien-Chun H, Woan-Chin C, Chiun-CR W. Comparison of Taiwan paddy and upland cultivated taro (*Colocasia esculenta* L.) genotypes for nutritive values. *Fd Chem*. (2007) 102:250–6. doi: 10.1016/j.foodchem.2006.04.044

41. Gerrano AS, Mathew I, Shayanowako AIT, Amoo S, Mellem JJ, Rensburg WJV, et al. Variation in mineral element composition of landrace taro (*Colocasia esculenta*) corms grown under dryland farming system in South Africa. *Heliyon*. (2021) 7:e06727. doi: 10.1016/j.heliyon.2021.e06727

42. Lebot V, Gunua T, Pardales JR, Prana MS, Thongjiem M, Viet NV. Characterisation of taro (*Colocasia esculenta* (L.) Schott) genetic resources in Southeast Asia and Oceania. *Genetic Res Crop Evol*. (2004) 51:381–92. doi: 10.1023/B:GRES.0000023453.30948.4d

43. Wills RBH, Lim JSK, Greenfield H, Bayliss-Smith T. Nutrient composition of taro (*Colocasia esculenta*) genotypes from the Papua New Guinea highlands. *J Sci of Fd and Agri*. (1983) 34:1137–42. doi: 10.1002/jsfa.2740341015

44. Zulkhairi AM, Razali M, Umikalsum MB, Norfaizal GM, Athirah AA, Aisyah MNS. Determination of oxalates in corms of selected Taro (*Colocasia esculenta*) varieties in Malaysia using ultra high-performance liquid chromatography. *Asian J Chemical Sci*. (2020) 7:28–37. doi: 10.9734/AJOCS/2020/v7i319023

45. Libert B, Franceschi VR. Oxalate in crop plants. *J Agri Fd Chem*. (1987) 35:926–38. doi: 10.1021/jf00078a019

46. Barooah H. Collection, screening and evaluation of some local *Colocasia* (*Colocasia esculenta* L. Schott) and Xanthosoma (*Xanthosoma sagittifolium* L. Schott.) genotypes of Assam. (1982) m.Sc. (Agri.) thesis, AAU, Jorhat

47. Adane T, Shimelis A, Negussie R, Tilahun B, Haki GD. Effect of processing method on the proximate composition, mineral content and antinutritional factors of Taro (*Colocasia esculenta*, L.) growth in Ethiopia. *Afr J Food Nutr Sci*. (2013) 13:7383–98. doi: 10.18697/ajfand.57.10345

48. Fagbemi TN, Olaofe O. The chemical composition and functional properties of raw and precooked taro (*Cococasia esculenta*) flour. *J Biol Phys Sci*. (2000) 1:98–103.

49. Bradbury JH, Holloway WD. Chemistry of tropical root crops: significance for nutrition and agriculture in the Pacific. No. 6 Canberra: ACIAR Monograph (1988).

50. Ricketts E. Food, health and you; a book on nutrition with special reference to East Africa, *Australian Centre for International Agricultural Research, Government of Australia*. (1966).

51. Amon AS, Soro RY, Koffi PKB, Dué EA, Kouamé LP. Biochemical characteristics of fours from ivorian taro (*Colocasia esculenta*, cv Yatan) corm as affected by boiling time. *Adv J Food Sci Technol*. (2011) 3:424–35.

52. Kaur M, Kaushal P, Singh KS. Studies on physicochemical and pasting properties of Taro (*Colocasia esculenta* L.) flour in comparison with a cereal, tuber and legume flour. *J Food Sci Technol*. (2013) 50:94–100. doi: 10.1007/s13197-010-0227-6

53. Singh S, Singh DR, Salim KM, Srivastava A, Singh LB, Srivastava RC. Estimation of proximate composition, micronutrients and phytochemical compounds in traditional vegetables from Andaman & Nicobar Islands. *Int J Food Sci Nutr*. (2012) 62:765–73. doi: 10.3109/09637486.2011.585961

54. Kasote DM, Bhalerao BM, Jagtap SD, Khyade MS, Deshmukh KK. Antioxidant and alpha-amylase inhibitory activity of methanol extract of *Colocasia esculenta* corm. *Pharmacologist*. (2011) 2:715–21.

55. Banti M, Atlaw T, Urugo MK, Agza B, Hailu D, Teka TA. Characterization of taro (*Colocasia esculenta*) genotypes for nutrients, anti-nutrients, phytochemicals composition, and antioxidant potentials in Southwest Ethiopia. *J Agri Food Res*. (2025) 19:101591. doi: 10.1016/j.jafr.2024.101591

56. Prior RL, Wu X, Schaich K. Standardized methods for the determination of antioxidant capacity and phenolics in food and dietary supplements. *J Agric Food Chem*. (2005) 53:4290–302. doi: 10.1021/jf0502698

57. Gonçalves RF, Silva AMS, Silva AM, Valentão P, Ferreres F, Gil-Izquierdo A, et al. Influence of taro (*Colocasia esculenta* L. Schott) growth conditions on the phenolic composition and biological properties. *Food Chem*. (2013) 141:3480–5. doi: 10.1016/j.foodchem.2013.06.009

58. Ali SS, Kasoju N, Luthra A, Singh A, Sharanabasava H, Sahu A, et al. Indian medicinal herbs as sources of antioxidants. *Fd Res Intl*. (2008) 41:1–15. doi: 10.1016/j.foodres.2007.10.001

59. Mariod AA, Abdelwahab SI, Elkheir S, Ahmed YM, Fauzi PNM, Chuen CS. Antioxidant activity of different parts from *Annona squamosa* and *Catunaregam nilotica* methanolic extract. *Acta Sci Pol Technol Aliment*. (2012) 11:249–58.

60. Kaur A, Sangha MK, Devi V, Pathak M, Singla D. Nutritional, antinutritional and antioxidant assessment of immature Abelmoschus pods: implications for crop improvement from cultivated and wild varieties. *South Afri J Bot*. (2024) 174:485–94. doi: 10.1016/j.sajb.2024.09.022

61. Ouédraogo N, Sombié PAED, Traoré RE, Sama H, Bationo Kando P, Sawadogo M, et al. Nutritional and phytochemical characterization of taro [*Colocasia esculenta* (L.) Schott] germplasm from Burkina Faso. *J Plant Breed Crop Sci*. (2023) 15:32–41. doi: 10.5897/JPBCS2022.0999

62. Shan B, Cai YZ, Sun M, Corke H. Antioxidant capacity of 26 spice extracts and characterization of their phenolic constituents. *J Agric Food Chem*. (2005) 53:7749–59. doi: 10.1021/jf051513

63. Rajurkar NS, Hande SM. Estimation of phytochemical content and antioxidant activity of some selected traditional Indian medicinal plants. *Indian J Pharm Sci*. (2011) 73:146–51. doi: 10.4103/0250-474x.91574

64. Zheng W, Wang SY. Antioxidant activity and phenolic compounds in selected herbs. *J Agril and Fd Chem*. (2001) 49:5165–70. doi: 10.1021/jf010697n

65. Andersen ØM, Jordheim M. Basic anthocyanin chemistry and dietary sources In: TC Wallace and MM Giusti, editors. Anthocyanins in health and disease. Boca Raton, FL: CRC Press (2013)

66. Das S, Kandali R, Baishya S. Development and nutritional analysis of Taro powder [*Colocasia esculenta* (L.) Schott.] enriched with natural colorants. *Intern J Environ Climate Change*. (2023) 13:2883–95. doi: 10.9734/IJECC/2023/v13i92523

67. Ma Y, Zhao M, Wu H, Yuan C, Li H, Zhang Y. Effects of fruit bagging on anthocyanin accumulation and related gene expression in peach. *J Am Soc Hortic Sci*. (2021) 146:217–23. doi: 10.21273/JASHS05019-20

68. Sangeeta D, Srinivasa V, Lakshmana D, Kantharaj Y, Arunkumar B. Studies on genetic variability, correlation coefficient and path coefficient analysis for growth and yield attributes in taro (*Colocasia esculenta* L.). *Pharma Innov J*. (2021) 10:1508–13.

69. Makori SI, Mu TH, Sun HN. Total polyphenol content, antioxidant activity, and individual phenolic composition of different edible parts of 4 sweet potato cultivars. *Nat Prod Commun*. (2020) 15:1–12. doi: 10.1177/1934578X20936931

70. Cui L, Liu C, Li D, Song J. Effect of processing on taste quality and health-relevant functionality of sweet potato tips. *Agric Sci China*. (2011) 10:456–62. doi: 10.1016/S1671-2927(11)60025-4

71. Gan LJ, Yang D, Shin JA, Kim SJ, Hong ST, Lee JH, et al. Oxidative comparison of emulsion systems from fish oil-based structured lipid versus physically blended lipid with purple-fleshed sweet potato (*Ipomoea batatas* L.) extracts. *J Agric Food Chem*. (2012) 60:467–75. doi: 10.1021/jf203708y

72. Kiselova Y, Ivanova D, Chervenkov T, Gerova D, Galunska B, Yankova T. Correlation between the in vitro antioxidant activity and polyphenol content of aqueous extracts from bulgarian herbs. *Phytother Res*. (2006) 20:961–5. doi: 10.1002/ptr.1985

73. Khurnpoon L, Rungnoi O. The correlation between Total phenol and antioxidant capacity of sweet potato (*Ipomoea batatas* L.) with varying flesh color. *Acta Hortic*. (2012) 945:413–9. doi: 10.17660/ActaHortic.2012.945.56

74. Verma VK, Kumar A, Rymbai H, Talang H, Devi MB, Baiswar P, et al. Genetic diversity and stability analysis of sweet potato accessions of North-Eastern India grown under the mid-hill conditions of Meghalaya. *Plant Genetic Resources: Characterization and Utilization*. (2023) 21:537–47. doi: 10.1017/S1479262123001041

frontiers | Frontiers in Nutrition

TYPE Original Research
PUBLISHED 17 April 2025
DOI 10.3389/fnut.2025.1559537

OPEN ACCESS

EDITED BY
Muthukumar Serva Peddha,
Central Food Technological Research Institute (CSIR), India

REVIEWED BY
Lalita Rana,
Dr. Rajendra Prasad Central Agricultural University, India
R. Arivuchudar,
Periyar University, India

*CORRESPONDENCE
Xibao Gao
✉ chem@sdu.edu.cn
Yumin Liu
✉ liuyumin666@126.com

†These authors have contributed equally to this work

RECEIVED 13 January 2025
ACCEPTED 03 April 2025
PUBLISHED 17 April 2025

CITATION
Wang Y, Ma R, Wei J, Fu X, Zhang S, Zhao Z, Lin H, Xu Y, Tan D, Gao X and Liu Y (2025) Enhancing micronutrient bioavailability in wheat grain through organic fertilizer substitution.
Front. Nutr. 12:1559537.
doi: 10.3389/fnut.2025.1559537

Enhancing micronutrient bioavailability in wheat grain through organic fertilizer substitution

Yafei Wang[1,2†], Ronghui Ma[3†], Jianlin Wei[2], Xiaoyan Fu[3], Shanshan Zhang[3], Zichao Zhao[2], Haitao Lin[2], Yu Xu[2], Deshui Tan[2], Xibao Gao[1*] and Yumin Liu[2*]

[1]Department of Physical and Chemical Inspection, School of Public Health, Cheeloo College of Medicine, Shandong University, Jinan, China, [2]State Key Laboratory of Nutrient Use and Management, Key Laboratory of Agro-Environment of Huang-Huai-Hai Plain, Ministry of Agriculture and Rural Affairs, Institute of Agricultural Resources and Environment, Shandong Academy of Agricultural Sciences, Jinan, China, [3]Shandong Agricultural Technology Extension Center, Jinan, China

The effect of organic fertilizer substitution (OFS) on crop micronutrients often varies due to differences in environmental conditions, soil types, and nutrient status. This study aims to evaluate the effects of OFS on wheat grain micronutrients and bioavailability across five sites in Shandong Province from 2021 to 2022. All experimental sites included five common treatments: control, traditional farming, optimized practices, and 15 and 30% OFS for chemical nitrogen. The results revealed regional variation in wheat yield; the average wheat yield was 9.06 Mg ha^{-1}, and the highest yield was 9.58 Mg ha^{-1} in the 15%OF treatment. No significant differences in soil micronutrient availability were observed. Compared to the control, the OFS treatments exhibited significant increases in grain Fe (24.69%) and Zn (19.19%) contents. The OFS treatments significantly increased Fe and Zn bioavailability by reducing the PA/Fe and PA/Zn molar ratios. Organic fertilizer substitution also increased micronutrient nutritional yields and reduced the current health burden of Fe and Zn. Under the pessimistic scenario, the OFS treatment reduced health burdens of Zn and Fe deficiencies by 2.38 and 1.31%, respectively, whereas these mitigation efficiencies substantially increased to 7.15 and 3.94% under the optimistic scenario. In conclusion, OFS improved the content and bioavailability of Fe and Zn without affecting yield, which enhanced the nutritional quality of these nutrients, and alleviate the health burden of Fe and Zn deficiency. The findings demonstrate that a 15% organic fertilizer substitution (OFS) optimally enhances wheat grain Fe and Zn bioavailability and nutritional quality while maintaining crop yield, offering region-specific evidence for sustainable agricultural practices to mitigate micronutrient deficiencies and improve human health outcomes.

KEYWORDS

organic fertilizer substitution, micronutrients, wheat, bioavailability, nutritional yield, DALYs

Introduction

Micronutrients are vital for the growth and development of plants, animals, and humans (1). Micronutrient deficiencies (MD) may lead to health problems such as underdevelopment, intellectual disability, decreased or even loss of labor capacity, and decreased immunity (2). Inadequate dietary micronutrient intake is a major cause of MD in humans (3). Wheat, one

of the world's three major food crops, plays an important role in ensuring human nutritional health and food security (4). However, the low content of micronutrients in wheat grains has become a limiting factor for human micronutrient supplementation in China (5). The average Fe and Zn content of wheat grain in the North China Plain is 41.7 and 23.7 mg kg^{-1}, respectively (5), which are below the WHO's proposed fortification targets for Fe and Zn in wheat grains (57 and 45 mg kg^{-1}, respectively) (6). Therefore, increasing the content of micronutrients in wheat grains to improve human nutritional health is important for ensuring the high-quality green production of wheat and enhancing the health of the human population.

Organic fertilizer substitution (OFS) is an effective measure for improving soil fertility and quality while maintaining crop yields (7, 8). In addition, micronutrients contained in organic fertilizers can affect the micronutrient profiles of crops (9). A long-term experiment conducted in the North China Plain by Li et al. (10) demonstrated that OFS at 70% significantly increased the soil's available Fe, manganese (Mn), copper (Cu), and Zn content. Zhang et al. (11) also showed that 25 and 50% OFS increased the Zn content in wheat grains by 57–67% compared with chemical fertilizer treatment. However, many studies have shown that organic substitution has no effect on the content of soil or crop micronutrients (12, 13). In fact, the micronutrient nutritional benefits of OFS are often limited by the environment, and the effect varies with soil type, climate, and soil fertility conditions. However, since previous studies have predominantly focused on enhancing crop grain micronutrient content through micronutrient fertilizer application (14, 15), research investigating the effects of OFS on crop micronutrient profiles remains limited and inconclusive. Consequently, multiple trials in diverse settings are needed to clarify the effect of OFS on the micronutrient nutrition of crops.

Phytic acid (myo-inositol 1,2,3,4,5,6-hexakisphosphate, $InsP_6$, PA) in wheat grains limits the bioavailability of micronutrients (16). The molar ratios of PA to micronutrients are widely used as a simplified measure of micronutrient bioavailability in the human diet (17, 18). However, the unresolved interaction between OFS-driven micronutrient enrichment and PA-mediated chelation remains inconclusive. Therefore, it is particularly important to study the effect of OFS on micronutrient bioavailability under different soil conditions. Recently, scientists and policymakers have recognized that traditional food production indicators often overlook human nutritional needs, which are crucial for assessing the sustainability of intensive agricultural systems (19). Consequently, new quality parameters such as nutritional yield have been widely used to assess crop productivity based on their nutritional value (20). Disability-adjusted life years (DALYs) are commonly used to quantify the burden of disease and injury in human populations (21). Estimating the health burden of Zn and Fe deficiency using the DALYs equation and evaluating the health impact of OFS grains. This has practical significance for improving the nutritional intake of the population, especially the rural population in general, and for improving overall health.

Here, the effect of OFS on the content and bioavailability of micronutrients was assessed across five experimental sites varying in fertility levels in Shandong Province to ensure the representativeness of the findings. We hypothesized that a suitable ratio of OFS can enhance grain micronutrients bioavailability while maintaining crop yield. The main objectives of this study were to (1) investigate the effect of OFS on the content of micronutrients (Fe, Mn, Cu, and Zn) in soil and wheat grains; (2) assess the effect of OFS on micronutrient bioavailability in wheat grains; and (3) assess the nutritional yield, health impact (the DALYs saved) and economic benefit of micronutrients in wheat grains.

Materials and methods

Site description and experimental design

The field trials were conducted in five counties (Cao County, Shen County, Yangxin County, Liangshan County and Yuncheng County) in the major wheat-producing region of Shandong Province during 2021–2022. All experimental sites have a cool-to-warm temperate monsoon climate. The mean temperature and annual precipitation of the wheat growing season in all experiment sites are shown in Supplementary Table S1. The soil types and initial properties of all experimental sites are shown in Supplementary Table S2.

All experiments consisted of five treatments with three replications: (1) no fertilization (CK); (2) farmers' conventional cultivation pattern (FP), in which the nitrogen, phosphorus, and potassium application rates were determined based on preliminary investigations in each region; (3) modified farmers' conventional cultivation pattern (OPT), in which fertilization rates were optimized based on wheat nutrient requirements and the local soil nutrient supply capacity; (4) 15%OF, in which organic fertilizer substituted 15% of chemical nitrogen fertilizer; and (5) 30%OF, in which organic fertilizer substituted 30% of chemical nitrogen fertilizer. Individual plots are 4 × 10 m (40 m^2) in size, with a randomized complete block design. The amounts of inorganic fertilizers used at each experimental site are presented in Supplementary Table S3. The types and nutrient contents of organic fertilizers used at each experimental site are presented in Supplementary Table S4. At each experimental site, 50% N fertilizer (including organic N and urea N) and phosphate and potassium fertilizers were applied basally. Additionally, 50% N fertilizer as urea was applied at the jointing stage of wheat production. The wheat varieties, planting density, and irrigation were in accordance with the recommended local high-yield cultivation techniques. All plots were irrigated before winter and during the wheat stem elongation period. General pesticides were applied in wheat-growing seasons to control disease, weeds, and insects.

Sampling and analysis

At the harvest stage of wheat in June 2022, soil samples were collected at each site using a stainless-steel auger along an "X" pattern with five borings (20 cm deep) per plot, which were subsequently merged into single samples. Soil samples were air-dried and sieved through an 8-mesh screen for subsequent determination of the pH and the available phosphorus (P), available potassium (K), DTPA-Fe, DTPA-Mn, DTPA-Cu, and DTPA-Zn content. Total nitrogen (N) and organic matter (OM) content of the soil was then measured for soil samples ground and passed through a 100-mesh sieve. A soil pH meter (SevenExcellence, Mettler-Toledo, China) was used to measure soil pH with a soil-to-water ratio of 1:2.5. Available P and available K were determined according to the methods of Murphy and Riley (22) and Walker and Barber (23), respectively. Total N and organic matter in the soil were analyzed using the wet oxidation method with a Vario

Max CN instrument (VarioMax CN; Elementar, Langenselbold, Germany). Soil available Fe, Mn, Cu, and Zn (DTPA-extractable fractions) were extracted using diethylenetriamine pentaacetic triethanolamine (DTPA-TEA) buffer (pH 7.3) and quantified by inductively coupled plasma optical emission spectrometry (ICP-OES, ICAP RQ, Thermo, Waltham, MA, United States), with instrument detection limits of 0.003, 0.002, 0.001, and 0.001 mg L^{-1} for DTPA-Fe, DTPA-Mn, DTPA-Cu, and DTPA-Zn, respectively (24). Soil standard samples (ASA-15) were used for quality control.

At wheat maturity, a central 4 m^2 (2.0 m × 2.0 m) area of wheat and a randomly selected sample of adjacent wheat plants (0.5 m in length) were harvested in each plot to determine the wheat yield and grain micronutrient content of each plot, respectively. Samples were taken from areas with uniform density, growth height, and growth stage to reduce sampling variation. Deionized water was used to wash the grain samples and dried at 60–65°C until a constant weight was achieved; they were then ground into powder for micronutrient analysis using a stainless steel mill. The samples were subjected to microwave-assisted digestion using a HNO_3-H_2O_2 mixture in closed digestion vessels (CEM, Matthews, NC, United States). The contents of Fe, Mn, Cu, and Zn in the resulting digestates were quantified by ICP-OES (ICAP RQ, Thermo, Waltham, MA, United States), with instrument detection limits of 0.003, 0.002, 0.001, and 0.001 mg L^{-1}, respectively. Standard samples (IPE684) (Wageningen University, Netherlands) were used to monitor the quality of the results. The phytic acid content was determined calorimetrically (at 519 nm) as described by Reichwald and Hatzack (25).

Calculation

Nutritional yield

The nutritional yield (NY) denotes the number of adults per hectare per year that can be fully satisfied with their recommended dietary reference intake (DRI) of a specific nutrient from a given crop (20). The NY (adults ha^{-1}) is calculated as shown in the following equation:

$$NY = C^{*}GY / DRI / 365$$

where C is the content of micronutrients in grains, GY is the dry weight of harvested grains per hectare, and DRI is the daily recommended dietary intake. The calories per 100 g of wheat are 339 kcal (26). The DRI of energy, Fe, Mn, Cu, and Zn are 8.47 MJ day^{-1}, 13.00, 2.05, 0.90 and 9.50 mg day^{-1}, respectively (27, 28).

Health and economic impact

$$\text{Health impact} = \text{Health burden saved by OFS} / \text{Health burden without OFS} \times 100.$$

In this equation, health burden is equivalent to DALYs. The current health burden (the DALYs lost) was calculated based on De Steur et al. (29). Zn and Fe are predominantly stored in the wheat bran, which gets removed during the wheat processing stage. Merely 31.0% of Zn and 21.7% of Fe are recovered into the grain (30). Consequently, the daily Zn and Fe intake obtained from OFS grains is equivalent to the sum of the status quo daily Zn and Fe intake and the additional total daily Zn and Fe intake, with the latter being calculated by taking into account the recovery rate. Details regarding the daily consumption of wheat (31), the status quo of the daily intake of Zn and Fe (32), as well as the recommended nutrient intake (RNI) (6, 33) are presented in the Supplementary Table S5. In this study, two coverage rates were defined: 20% in the pessimistic scenario and 60% in the optimistic scenario. To evaluate the potential health impacts of OFS wheat grains, the health benefits, represented by the DALYs saved, were calculated. This calculation was based on the increased Zn and Fe contents and was carried out through the methodologies proposed by De Steur et al. (29) and Liu et al. (31).

The following equation was utilized to calculate the economic benefit of OFS wheat grains:

$$\text{Economic benefit} = \text{Total DALYs saved} \times \text{PCNI} - \text{Organic fertilizer cost.}$$

where PCNI refers to the per capita net income of China, which is based on a previous study (34). Since the labor required for the application of organic and chemical fertilizers is comparable, in the current study, only the cost of organic fertilizer (900 RMB ha^{-1}) was taken into account, in accordance with the survey results.

Statistical analysis

Data were organized and calculated using Excel 2016. Statistical analyses were conducted using SAS 9.4 software. A one-way analysis of variance (ANOVA) was employed to assess intergroup variability, followed by Fisher's least significant difference (LSD) *post hoc* test for pairwise comparisons of treatment means. Statistical significance was determined at a predefined level of 0.05, with all hypothesis tests adhering to a two-tailed probability framework. Pearson correlation analysis was conducted using SPSS 27.0 software, with significance levels determined through two-tailed testing. Graphs were made using SigmaPlot 14.0. In order to explore the significant effects of yield and different soil physico-chemical properties on the variation of Fe-Zn content in wheat grains, the Random Forest (RF) method was used to rank the importance of the variables. This step is implemented by R 4.3.1 using the "importance" function in the "randomForest" R package (35). To assess the significance of the variables, we calculated the percentage increase in the mean square error (MSE) (36). The significance of the model and R-squared and the significance of the factors are indicated by R 4.3.1 in the R packages "A3" and "rfPermute," respectively (37, 38).

Results

Spatial distribution of the yield and content of micronutrients

Across all experimental sites, the wheat yields ranged from 5.12 to 11.09 Mg ha^{-1}, and the average yield was 9.06 Mg ha^{-1} (Table 1). The regional variation among sites was 7.07–9.85 Mg ha^{-1}, with the lowest and highest yields occurring in Yangxin County and Cao

TABLE 1 Descriptive statistics of the grain yield and Fe, Mn, Cu, and Zn content of wheat.

Parameters	Mean	SD	Median	Range	Regional variation	CV (%)
Yield (Mg ha^{-1})	9.06	1.37	9.47	5.12–11.09	7.07–9.85	15.08%
Fe (mg kg^{-1})	37.13	10.24	34.93	19.60–61.94	26.48–52.86	27.56%
Mn (mg kg^{-1})	31.26	6.10	29.48	21.75–50.96	27.05–41.06	17.64%
Cu (mg kg^{-1})	4.42	1.06	4.23	2.23–6.39	3.06–5.73	23.60%
Zn (mg kg^{-1})	24.61	3.73	23.98	18.40–33.66	22.21–28.51	10.16%

County, respectively. The content of micronutrients in wheat grains was variable, with ranges of 19.60–61.94 mg kg^{-1} for Fe, 21.75–50.96 mg kg^{-1} for Mn, 2.23–6.39 mg kg^{-1} for Cu, and 18.40–33.66 mg kg^{-1} for Zn. The mean values of Fe, Mn, Cu, and Zn were 37.13, 31.26, 4.42, and 24.61 mg kg^{-1}, respectively. The highest grain Fe, Mn, Cu, and Zn content was observed in Yangxin County, with mean values of 52.86, 41.06, 5.73, and 28.51 mg kg^{-1}, respectively. The mean values of the grain Fe, Mn, and Cu content in Shen County and the grain Zn content in Cao County were the lowest (26.48, 27.05, 3.06, and 22.21 mg kg^{-1}, respectively). The coefficients of variation (CV) were all greater than 10%; the Fe content was the most variable across all plots, and the Zn content was the least variable.

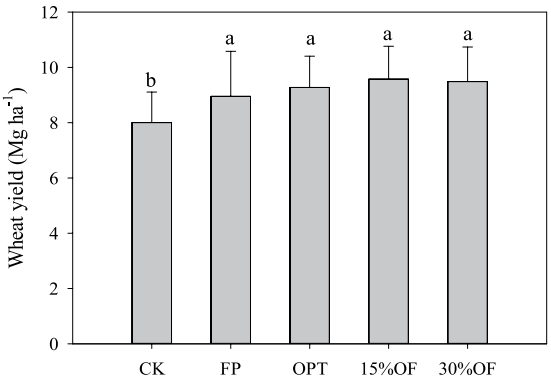

FIGURE 1
Effect of OFS on wheat grain yield. Columns with the same lowercase letters are not significantly different at $p < 0.05$.

Effects of OFS on wheat yield and nutritional yield

The lowest yield was observed in the CK (8.00 Mg ha^{-1}), and the yield was significantly lower in the CK compared with the other treatments ($p < 0.05$, Figure 1). The highest yield was observed in the 15%OF treatment, with an average of 9.58 Mg ha^{-1}; the yield was 19.75 and 7.04% higher in the 15%OF treatment than in the CK and FP treatment (8.95 Mg ha^{-1}), respectively. There were no significant differences in wheat yield among the other treatments.

Organic fertilizer substitution had similar effects on the nutritional yields of Fe, Zn, and energy in wheat grain. The lowest nutritional yields were observed in the CK, with 53.41, 51.22 and 36.72 adults ha^{-1} for Fe, Zn, and energy, respectively, which was significantly lower than that in other treatments ($p < 0.05$). The highest nutritional yields were observed in the 15%OF treatment, with 78.35, 72.71, and 43.94 adults ha^{-1} for Fe, Zn, and energy, respectively. However, the highest nutritional yield of Mn was observed in the OPT treatment and the lowest nutritional yield of Cu was observed in the FP treatment. This represents significant increases of 19.15, 19.13, and 21.71% for Fe, Cu, and Zn, respectively, in the 15%OF treatment compared with the FP treatment ($p < 0.05$). In all treatments, the nutritional yields of Fe and Zn were 64.87 and 54.09% higher than energy nutritional yield, respectively (Table 2).

Effects of OFS on soil physicochemical properties and micronutrients in soils and wheat grains

Organic fertilizer substitution had no significant effects on soil OM, pH, total N, available P, available K and DTPA-Fe, Mn, Cu, and Zn contents after wheat harvest (Supplementary Table S6).

The Zn content in wheat grain from the organic substitution treatments was significantly higher than that observed in the other treatments ($p < 0.05$, Figure 2). However, no significant difference in the Zn content was observed between the 15%OF and the 30%OF treatments. The wheat grain Fe content of 15%OF and 30%OF treatments were significantly higher than CK treatment ($p < 0.05$), and there was no significant difference between other treatments. The average grain Mn and Cu content among all treatments was 29.24–33.21 and 4.17–4.58 mg kg^{-1}, respectively. The organic substitution treatments in this experiment did not significantly affect the Mn, and Cu content in the grain.

Factors affecting the Fe and Zn content of wheat grain

Random forest analysis showed that yield, pH, soil available P, and soil total N had significant effects on grain Fe content ($p < 0.05$), except for DTPA-Fe (Figure 3A). Whereas, for grain Zn content, soil available P, DTPA-Zn, and yield had a significant effect ($p < 0.05$), pH and soil total N had a non-significant effect (Figure 3B).

Effects of OFS on the bioavailability of micronutrients in wheat grains

The average PA content of each treatment ranged from 8.20 to 8.92 g kg^{-1}, and no significant differences in the PA content were observed among all treatments (Figure 4). Organic fertilizer substitution significantly decreased the molar ratios of PA/Fe and PA/Zn in wheat

TABLE 2 Effects of OFS on Fe, Mn, Cu, Zn, and energy nutritional yields in wheat grains.

Treatments	Nutritional yield (adults ha^{-1})[a]				
	Fe	Mn	Cu	Zn	Energy
CK	53.41 ± 13.04d	328.45 ± 60.50c	110.48 ± 27.60b	51.22 ± 8.33c	36.72 ± 5.06b
FP	65.76 ± 8.23c	374.32 ± 34.07ab	110.45 ± 19.98b	59.74 ± 11.18b	41.08 ± 7.47a
OPT	70.10 ± 12.46bc	401.23 ± 56.25a	118.50 ± 19.87ab	63.80 ± 9.93b	42.55 ± 5.19a
15%OF	80.37 ± 11.53a	397.59 ± 40.98ab	131.58 ± 23.96a	72.71 ± 8.73a	43.94 ± 5.45a
30%OF	77.65 ± 12.95ab	366.18 ± 25.04b	126.54 ± 30.99ab	72.71 ± 11.25a	43.53 ± 5.74a

The values are the means ± SD of five experimental sites.
[a]The same lowercase letters in the same column indicated that there was no statistically significant difference between different treatments at $p < 0.05$.

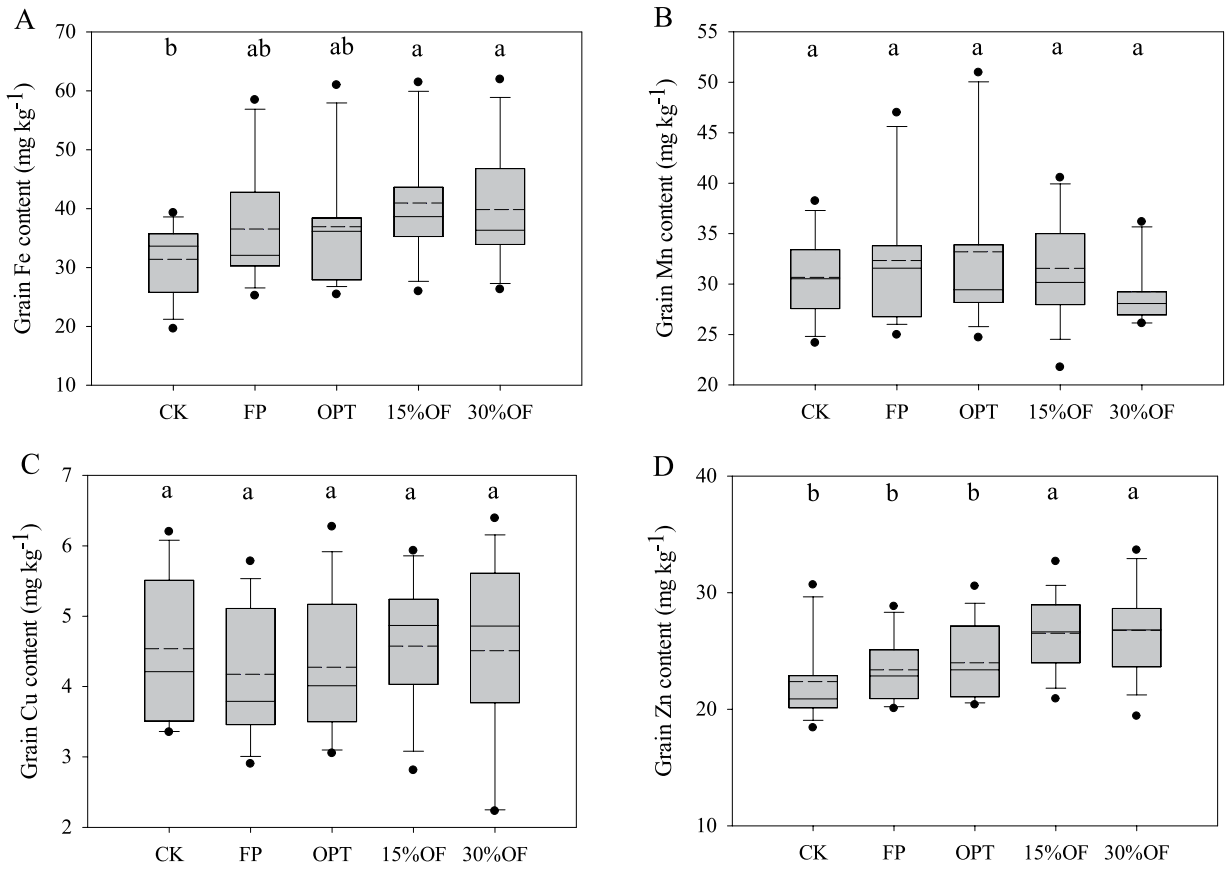

FIGURE 2
Effect of OFS on the content of micronutrients in wheat grains **(A–D)**. The solid and dashed lines indicate the median and mean values, respectively. Columns with the same lowercase letters are not significantly different at $p < 0.05$.

grains in this study ($p < 0.05$). The molar ratios of PA/Fe and PA/Zn were significantly lower in the 15%OF and 30%OF treatments than in the CK, respectively ($p < 0.05$, Figure 5). However, there were no significant differences in the molar ratios of PA/Fe and PA/Zn between the 15%OF and 30%OF treatments. Differences in the molar ratios of PA/Mn and PA/Cu among all treatments were not significant.

Health impacts of wheat grain with OFS in Shandong Province

Compared to the OPT wheat grain, 15%OF and 30%OF grain increased the daily Zn and Fe intake, the percentage of the RNI, the DALYs saved in the studied population and the potential economic income (Table 3). In the pessimistic scenario, when compared with the OPT grains, the 15%OF and 30%OF grains reduced the current Zn-related health burden in Shandong Province by 2.28 and 2.48% respectively, and the Fe-related health burden by 1.50 and 1.12%, respectively. In the optimistic scenario, the grains in 15%OF and 30%OF treatments also reduced the current Zn-related health burden in Shandong Province by 6.84 and 7.45% respectively, and the Fe-related health burden by 4.50 and 3.37% respectively, compared with the OPT grains. Moreover, in the pessimistic scenario, the economic income generated by the OFS grains could range from 460 to 800 million RMB, while in the optimistic scenario, it could range from 1.4 to 2.4 billion RMB.

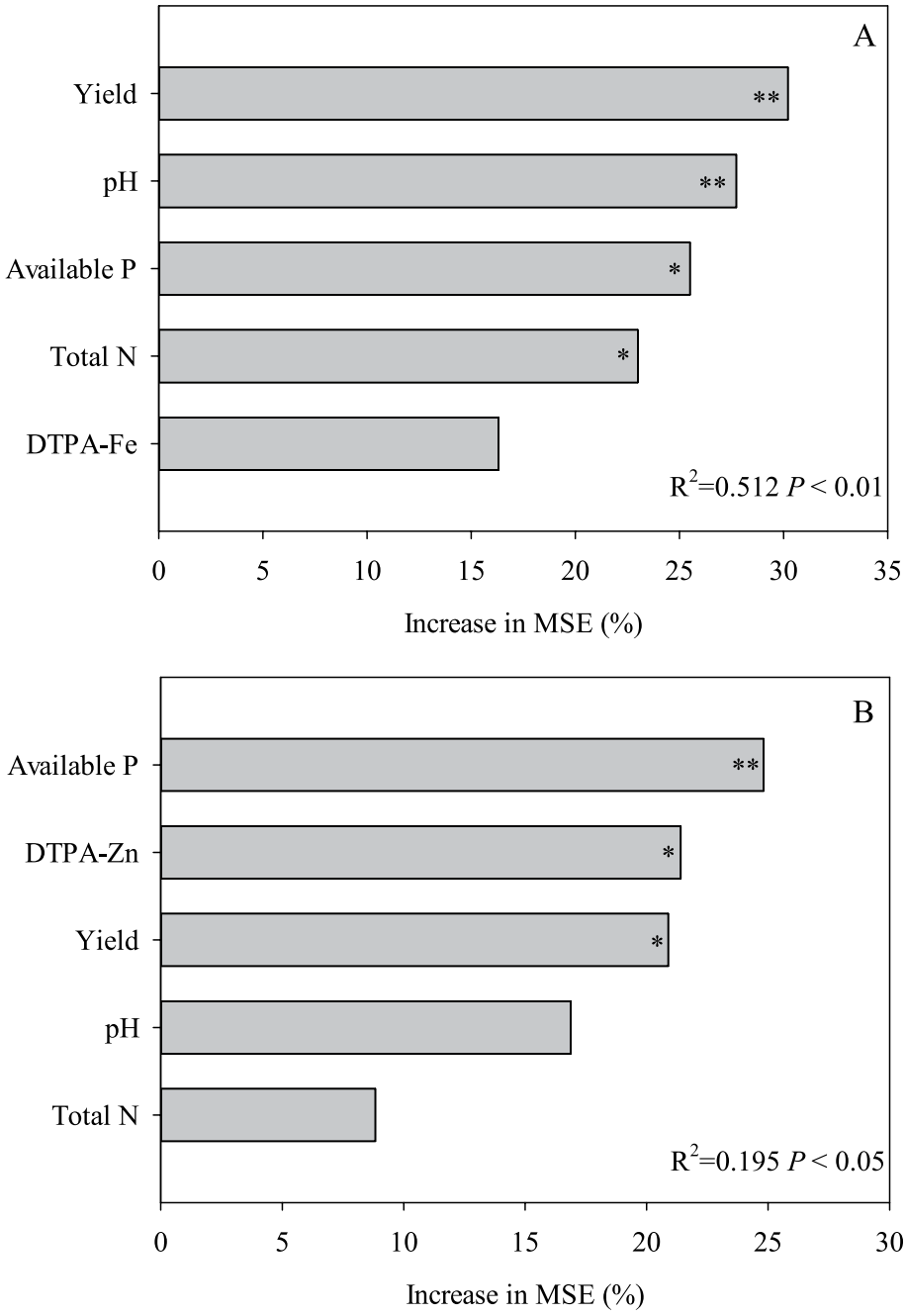

FIGURE 3
Random forest analysis for grain Fe **(A)** and Zn **(B)** content variations. Increases in MSE (mean squared error) indicate the importance of those variables in the random forest analysis. *$p < 0.05$ and **$p < 0.01$.

Discussion

Effects of OFS on wheat yield and nutritional yield

The overall average wheat yield observed in this study aligns with the established yield benchmarks reported in prior agronomic research conducted across the North China Plain (39, 40). And the variation in yield among regions can be attributed to differences in climatic and soil conditions of the experimental sites. Organic fertilizer substitution is an effective fertilization measure for promoting crop growth and increasing yield because of its high richness in nutrients and organic matter content (41). Many previous studies have demonstrated that moderate OFS conditions can maintain or increase crop yields (42, 43). However, a high ratio of OFS can lead to a reduction in wheat yields (40). This can be attributed to the slow release of nutrients from high proportions of organic fertilizers, which results in a lack of available nutrients that are unable to meet crop needs (44). A meta-analysis of studies revealed a significant reduction in wheat yield when OFS was 43% or more (45).

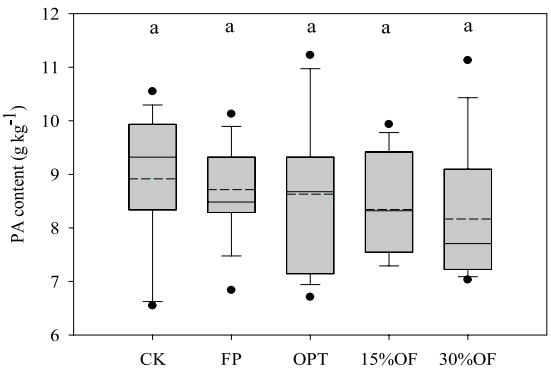

FIGURE 4
Effect of OFS on the content of phytic acid in wheat grains. The solid and dashed lines indicate the median and mean values, respectively. Columns with the same lowercase letters are not significantly different at $p < 0.05$.

In the current study, OFS at 15 and 30% did not reduce wheat yield, which was consistent with the results of Moreira-Ascarrunz et al. (46). This phenomenon may be attributed to the short-term nature of the experiment (first-year implementation), where crop productivity remained strongly influenced by baseline soil fertility conditions. Further multi-season trials are needed to assess long-term effects of OFS on agroecosystem dynamics.

Enhancing land use efficiency in food production is essential for providing sufficient calories and micronutrients for the global population given increasing pressure on land resources (20). Nutritional yield serves as a standardized metric to assess the agronomic efficacy of cultivation methodologies across field-and farm-scale agricultural systems, through the quantification of bioavailable micronutrient output per unit land area (46). In this study, the nutritional yields of Fe, Mn, Cu, and Zn in wheat grains exceeded energy needs, indicating that wheat grain consumption can meet both energy and nutritional needs. The nutritional yields of Fe and Zn were significantly higher in the OFS treatments than in the FP treatment, this suggests that OFS can improve the micronutrient output of current food production systems. The widespread adoption of organic substitution techniques can provide valuable insights for integrating diverse agricultural practices to enhance crop quality and human health in the future.

Effect of OFS on micronutrient content of grains

The bioavailable soil micronutrient pool constitutes a critical agroecosystem functionality indicator, enabling systematic assessment of wheat grain micronutrient density and thereby serving as a predictor for population-level nutritional security indices within spatially heterogeneous regions (47). In this study, the content of DTPA-Fe, Mn, Cu, and Zn in soil was similar to the background content of these nutrients in Shandong Province (48). According to the classification standard of soil available micronutrients in China, the content of DTPA-Fe, Mn, Cu, and Zn in this study was near values indicative of deficiency (48). Organic fertilizer substitution did not affect the soil DTPA-Fe, Mn, Cu, and Zn content in this study, which contrasts with the results of Li et al. (10) showing that organic fertilizer application for 19 years significantly increased the content of soil DTPA-Fe, Mn, Cu, and Zn. This likely stemmed from the fact that short-term organic application did not provide adequate micronutrients for enhancing soil availability.

The grain contents of Fe, Mn, Cu, and Zn in this study were lower than those observed in the North China wheat region (5). This dilution effect is attributed to the significantly higher grain yields in this study compared with the average wheat yield in North China (49). Organic fertilizer substitution significantly affected the wheat grain Fe and Zn content but had no effect on Mn, and Cu levels, which is consistent with the results of Li et al. (12). In this study, OFS did not affect the soil DTPA-Zn content, suggesting that the increase in grain Zn was not due to enhanced soil Zn availability for crop uptake. Organic fertilization may enhance grain Zn accumulation by releasing endogenous Zn and increasing organic acids, with organic acids improving Zn bioavailability through rhizospheric pH reduction (50, 51). Zinc complexes with low-molecular-weight organic acids comprise more bioavailable forms for crop uptake, which facilitates Zn absorption by plant roots and enhances the Zn content in wheat grains (52). Furthermore, specific growth-promoting bacteria and fungi in soil are critically involved in Zn cycling or possess Zn-solubilizing capacity, which is closely associated with soil Zn availability (53). In this study, the highest Fe and Zn content was 67.63 and 70.47% of the biofortification targets established by HarvestPlus, respectively. This indicates that OFS alone is insufficient for addressing crop micronutrient deficiencies. Nonetheless, these findings provide valuable insights for enhancing crop nutritional quality through agronomic practices.

Pearson correlation analysis revealed strong negative correlations between grain Fe content and both yield and soil available P, whereas no significant correlations were observed with Zn content (Supplementary Table S7). However, random forest analysis identified yield and soil available P as key determinants of grain Fe and Zn content. This discrepancy may arise from nonlinear pathways through which yield and soil available P influence Zn uptake, such as threshold effects or interactions with OM. Previous experimental studies have also documented inverse relationships between grain yield and micronutrient contents (54). Meanwhile, the results of Zhao et al. (55) also showed highly significant correlation between Fe and Zn and P content of wheat grains ($R^2 = 0.55$). Wheat grain Fe and Zn content decreases with increasing soil available P, which may be attributed to a decrease in mycorrhizal infestation of wheat roots due to increasing soil available P (56). Moreover, DTPA-Fe did not affect grain Fe content and DTPA-Zn significantly affected grain Zn content which is similar to the findings of Nikolic et al. (57). This suggests that increasing exogenous Fe inputs will not increase grain Fe levels in fields with low DTPA-Fe levels (58), whereas combined exogenous Zn supplementation can be used as an important way to increase wheat grain Zn levels in fields with low DTPA-Zn levels (59). In fact, grain micronutrient contents are influenced by a synergistic interplay of edaphic properties, fertilization regimes, and climatic variables. Crucially, soil Zn bioavailability and grain Zn accumulation exhibit significant heterogeneity across soil types (60), with such variations being consistently observed under both irrigated and rainfed management systems (61). In future research, the impacts of these factors on micronutrients bioavailability should be comprehensively considered and evaluated.

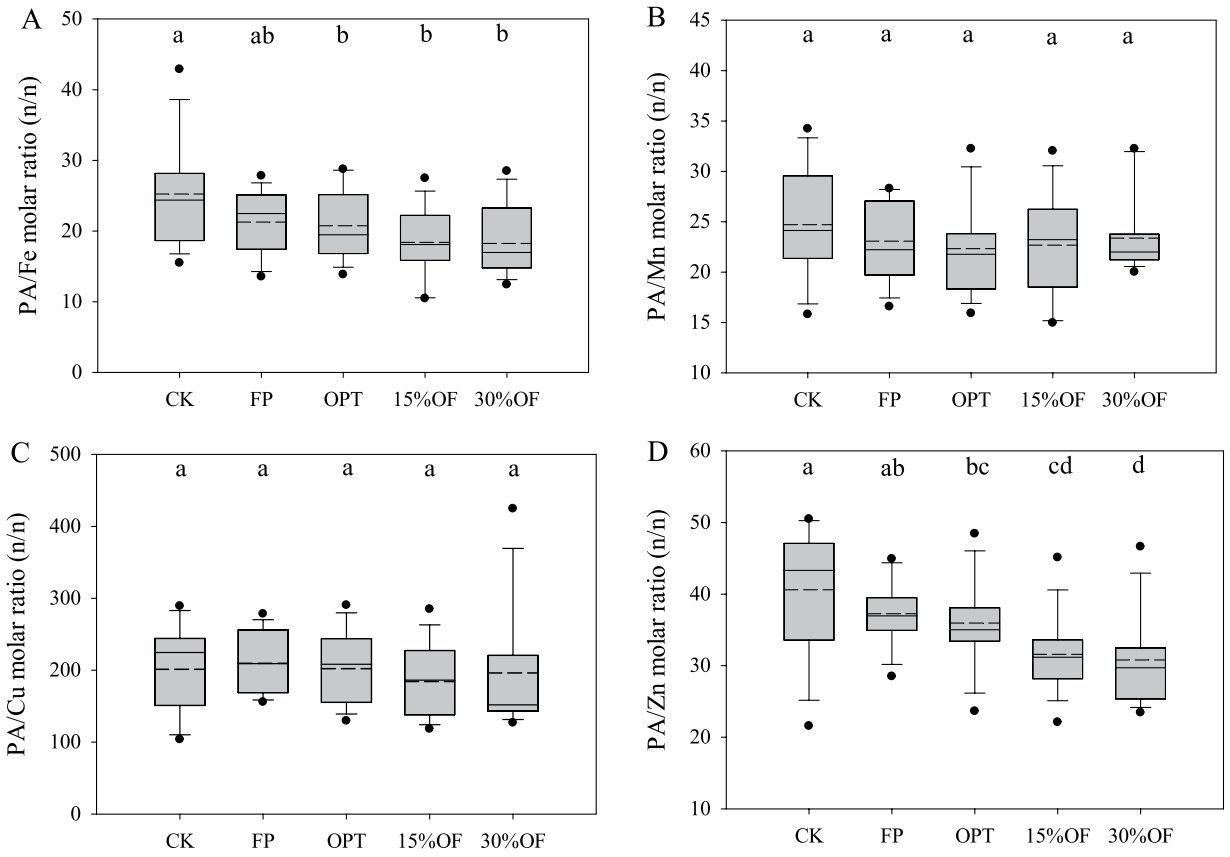

FIGURE 5
Effects of OFS on the bioavailability of micronutrients in wheat grains **(A–D)**. The solid and dashed lines indicate the median and mean values, respectively. Columns with the same lowercase letters are not significantly different at $p < 0.05$.

Effects of organic substitution on the bioavailability of grain micronutrients

Micronutrient bioavailability more accurately reflects the extent of micronutrient absorption from grains by the human body compared with the content of micronutrients (31). The results of our study showed that OFS significantly reduced the PA/Fe and PA/Zn molar ratios of wheat grain, which was consistent with the findings of Manzeke et al. (62) showing that organic fertilizer reduced the molar ratio of PA/Zn in maize grains. Tura et al. (63) suggested that the micronutrients are better absorbed by the human body when the molar ratios of PA to Zn and Fe are reduced to less than 15 and 1, respectively. In this study, the lowest molar ratios of PA to Zn and Fe were 31.19, and 18.89, respectively. This indicates that while organic substitution can enhance the bioavailability of Zn and Fe in wheat grains, it remains relatively low and is significantly limited. Therefore, reducing the grain PA content while increasing micronutrient concentrations is essential for further improving micronutrient bioavailability.

Health impacts of OFS wheat grain in Shandong Province

Given the significance of wheat in the dietary structure of North China and the fact that the bioavailability of Zn and Fe OFS grains is markedly higher than that in OPT grains, substituting conventional wheat grains with OFS grains could significantly mitigate Zn and Fe malnutrition. Our findings indicate that, in terms of the human health impact (the DALYs saved), the 15%OF grains have a greater effect on improving Zn-related health, while the 30%OF grains have a greater impact on Fe-related health. Notably, even under the optimistic scenario with a 60% coverage rate, the health impacts are less than those reported in previous studies (64), but may be more realistic because the amount of Zn and Fe carried over from organic fertilizers is limited. Furthermore, considering the large-scale wheat cultivation area in Shandong Province, which amounts to 4.0 million hectares, implementing the OFS strategy can yield relatively high economic benefits. The economic benefits are more pronounced in rural areas of Shandong Province with relatively lower income levels. Overall, these results suggest that, similar to with Zn and Fe biofortification and genetic biofortification in wheat (65, 66), agronomic biofortification with OFS can reduce the health burden attributable to Zn and Fe deficiency in the studied population. Moreover, it has the potential to boost the economic income of rural households in Shandong Province. These findings have alleviated population-wide micronutrient deficiencies through dietary approaches, particularly benefiting populations in impoverished regions where grain-based diets predominate. This study conducted regional-scale validation of organic fertilization strategies in enhancing grain micronutrient enrichment and bioavailability, providing robust scientific evidence to inform integrated agricultural and public health policies, addressing dietary micronutrient deficiencies in specific regions.

10.3389/fnut.2025.1559537

TABLE 3 Health impacts of 15%OF and 30%OF wheat grain in Shandong Province.

Parameters	15%OF		30%OF	
	Pessimistic scenario	Optimistic scenario	Pessimistic scenario	Optimistic scenario
Zinc				
Daily Zn intake (mg day^{-1}, status quo)				
Infants	4.90	4.90	4.90	4.90
Children	6.00	6.00	6.00	6.00
Daily Zn intake with OFS (mg day^{-1})				
Infants	4.96	4.96	4.97	4.97
Children	6.12	6.12	6.13	6.13
% of recommended nutrition intake with OFS (RNI)				
Infants	71.88	71.88	72.03	72.03
Children	76.50	76.50	76.63	76.63
Health impact (DALYs saved)				
Infants	771	2,313	896	2,689
Children	5,254	15,763	5,673	17,018
% reduction in the current health burden	2.28	6.84	2.48	7.45
Iron				
Daily Fe intake (mg day^{-1}, status quo)				
Children <5 years	11.90	11.90	11.90	11.90
Children 6–14 years	18.70	18.70	18.70	18.70
Men 15+	24.40	24.40	24.40	24.40
Women 15+	21.20	21.20	21.20	21.20
Pregnant women	21.20	21.20	21.20	21.20
Daily Fe intake with OFS (mg day^{-1})				
Children <5 years	12.03	12.03	12.00	12.00
Children 6–14 years	18.83	18.83	18.80	18.80
Men 15+	24.66	24.66	24.59	24.59
Women 15+	21.46	21.46	21.39	21.39
Pregnant women	21.46	21.46	21.39	21.39
% of recommended nutrition intake with OFS (RNI)				
Children <5 years	84.13	84.13	83.92	83.92
Children 6–14 years	80.13	80.13	80.00	80.00
Men 15+	90.00	90.00	89.74	89.74
Women 15+	36.50	36.50	36.38	36.38
Pregnant women	36.50	36.50	36.38	36.38
Health impact (DALYs saved)				
Children <5 years	10,211	30,632	7,915	23,744
Children 6–14 years	15,975	47,924	12,337	37,011
Men 15+	49,304	147,912	36,519	109,558
Women 15+	9,781	29,342	7,166	21,497
Pregnant women	44	132	32	96
% reduction in the current health burden	1.50	4.50	1.12	3.37
Economic impact (RMB)	8.0×10^8	2.4×10^9	4.6×10^8	1.4×10^9

Organic substitution is commonly adopted in intensive crop farming systems in China for its synergistic enhancement of crop yields, sustainability, and soil fertility (8, 39). In this study, no significant difference was observed between chemical and organic fertilizer application treatments, suggesting that OFS even at 30% could maintain high wheat yields. And OFS significantly increased the nutritional yield of Fe, Mn, Cu, Zn, and energy. In addition, OFS treatments increased the soil OM content by 6%, which increased soil fertility. Our findings also indicated that OFS increased the grain Fe and Zn content by 10.59 and 13.99%, respectively, compared with the FP treatment. The grain bioavailability of Fe and Zn also significantly increased by decreasing the PA/Fe and PA/Zn ratio by 18.23 and 17.81%, respectively. More importantly, OFS can alleviate Zn and Fe deficiency in the studied population. Our findings demonstrated that 15%OF is more effective than 30%OF. Overall, organic substitution stabilizes yields, enhances soil quality, and improves the nutritional quality of grains. Under China's Dual Carbon Strategy (Carbon Peak and Carbon Neutrality), the agricultural practice of substituting chemical fertilizers with organic fertilizers has been increasingly adopted as a prevailing approach. This strategy demonstrates significant potential to synergistically enhance the nutritional quality of grain products and safeguard residents' health through improved micronutrient bioavailability in the region, thereby aligning with sustainable agricultural transitions and public nutrition security objectives.

Conclusion

We investigated the effects of OFS on the content and bioavailability of grain micronutrients across diverse sites. Organic fertilizer substitution did not increase wheat yield, but it increased the content and bioavailability of Fe and Zn in grains. Additionally, OFS significantly increased the nutritional yields of Fe, Mn, Cu, Zn, and energy. Organic fertilizer substitution also reduces the current health burden and makes an important contribution to human nutrition and health. An OFS ratio of 15% was optimal for balancing crop yield and nutrient quality. Consequently, the 15%OF protocol can be scaled up for broader implementation. Meanwhile, organic fertilizer varieties should be strategically selected based on regional livestock and poultry breeding patterns to minimize input costs while optimizing local sourcing feasibility for farmers. These findings provide valuable insights into OFS from agricultural, nutritional, and health perspectives, which has implications for improving the safety, sustainability, and economics of future crop production. Moreover, future studies should expand trials across diverse soil types and climatic conditions, coupled with mechanistic investigations into how soil physicochemical properties govern grain micronutrient accumulation. Such efforts will clarify environmental modulation of organic fertilizer substitution effects, optimize fertilizer use efficiency, and ultimately enhance the micronutrient density of grains.

Data availability statement

The original contributions presented in the study are included in the article/supplementary material, further inquiries can be directed to the corresponding authors.

Author contributions

YW: Writing – original draft, Data curation, Investigation, Formal analysis. RM: Investigation, Resources, Writing – original draft. JW: Formal analysis, Investigation, Writing – original draft. XF: Investigation, Formal analysis, Writing – original draft. SZ: Formal analysis, Investigation, Writing – original draft. ZZ: Investigation, Formal analysis, Writing – original draft. HL: Investigation, Formal analysis, Writing – original draft. YX: Formal analysis, Investigation, Writing – review & editing. DT: Investigation, Writing – review & editing, Formal analysis. XG: Methodology, Writing – review & editing. YL: Conceptualization, Methodology, Supervision, Writing – review & editing.

Funding

The author(s) declare that financial support was received for the research and/or publication of this article. This research was funded by National Key Research and Development Projects (2021YFD1900903), National Agricultural Science and Technology Project: Smart Fertilization Project (20221805), National Natural Science Foundation of China (32102486), the Earmarked Fund (CARS-03), Shandong Province Key Research and Development Program (2024CXPT075), and Shandong-Chongqing Science and Technology Cooperation Project: Integrated Application of Collaborative Ecological Technologies for Quality Improvement of Low-to-Medium Yield Sloped Cultivated Land and Soil Carbon Sequestration Enhancement.

Conflict of interest

The authors declare that the research was conducted in the absence of any commercial or financial relationships that could be construed as a potential conflict of interest.

Generative AI statement

The authors declare that no Gen AI was used in the creation of this manuscript.

Publisher's note

Supplementary material

The Supplementary material for this article can be found online at: https://www.frontiersin.org/articles/10.3389/fnut.2025.1559537/full#supplementary-material

References

1. Ding G. Promoting balanced dietary structure and preventing micronutrient deficiencies. *Chin J Environ Occup Med*. (2019) 36:407–9. doi: 10.13213/j.cnki.jeom.2019.19194

2. Bouis HE. Enrichment of food staples through plant breeding: a new strategy for fighting micronutrient malnutrition. *Nutrition*. (2000) 16:701–4. doi: 10.1016/S0899-9007(00)00266-5

3. Rehman A, Farooq M, Ullah A, Nadeem F, Im SY, Park SK, et al. Agronomic biofortification of zinc in Pakistan: status, benefits, and constraints. *Front Sustain Food Syst*. (2020) 4:591722. doi: 10.3389/fsufs.2020.591722

4. Li F, Zhou M, Shao J, Chen Z, Wei X, Yang J. Maize, wheat and rice production potential changes in China under the background of climate change. *Agric Syst*. (2020) 182:102853. doi: 10.1016/j.agsy.2020.102853

5. Chu H, Mu W, Dang H, Wang T, Sun R, Hou S, et al. Evaluation on concentration and nutrition of micro-elements in wheat grains in major wheat production regions of China. *Acta Agron Sin*. (2022) 48:2853–65. doi: 10.3724/SP.J.1006.2022.11099

6. Allen L, de Benoist B, Dary O, Hurrell R. Guidelines on food fortification with micronutrients. Geneva: WHO (2006).

7. Li X, Li B, Chen L, Liang J, Huang R, Tang X, et al. Partial substitution of chemical fertilizer with organic fertilizer over seven years increases yields and restores soil bacterial community diversity in wheat-rice rotation. *Eur J Agron*. (2022) 133:126445. doi: 10.1016/j.eja.2021.126445

8. Qaswar M, Jing H, Ahmed W, Li D, Liu S, Lu Z, et al. Yield sustainability, soil organic carbon sequestration and nutrients balance under long-term combined application of manure and inorganic fertilizers in acidic Paddy soil. *Soil Tillage Res*. (2020) 198:104569. doi: 10.1016/j.still.2019.104569

9. Provolo G, Manuli G, Finzi A, Lucchini G, Riva E, Sacchi GA. Effect of pig and cattle slurry application on heavy metal composition of maize grown on different soils. *Sustainability*. (2018) 10:2684. doi: 10.3390/su10082684

10. Li BY, Huang SM, Wei MB, Zhang HL, Shen AL, Xu JM, et al. Dynamics of soil and grain micronutrients as affected by long-term fertilization in an aquic inceptisol. *Pedosphere*. (2010) 20:725–35. doi: 10.1016/s1002-0160(10)60063-x

11. Zhang G, Song K, Miao X, Huang Q, Ma J, Gong H, et al. Nitrous oxide emissions, ammonia volatilization, and grain-heavy metal levels during the wheat season: effect of partial organic substitution for chemical fertilizer. *Agric Ecosyst Environ*. (2021) 311:107340. doi: 10.1016/j.agee.2021.107340

12. Li BY, Zhou DM, Cang L, Zhang HL, Fan XH, Qin SW. Soil micronutrient availability to crops as affected by long-term inorganic and organic fertilizer applications. *Soil Tillage Res*. (2007) 96:166–73. doi: 10.1016/j.still.2007.05.005

13. Mohanty S, Saha S, Saha B, Asif SM, Poddar R, Ray M, et al. Substitution of fertilizer-N with biogas slurry in diversified rice-based cropping systems: effect on productivity, carbon footprints, nutrients and energy balance. *Field Crop Res*. (2024):307. doi: 10.1016/j.fcr.2023.109242

14. Dimkpa CO, Singh U, Bindraban PS, Elmer WH, Gardea-Torresdey JL, White JC. Zinc oxide nanoparticles alleviate drought-induced alterations in sorghum performance, nutrient acquisition, and grain fortification. *Sci Total Environ*. (2019) 688:926–34. doi: 10.1016/j.scitotenv.2019.06.392

15. Rana L, Kumar N, Rajput J, Sow S, Ranjan S, Kumari S, et al. Unlocking potential: the role of zinc fortification combating hidden hunger and enhancing nutritional security. *J Exp Agric Int*. (2024) 46:625–42. doi: 10.9734/jeai/2024/v46i102986

16. Gupta PK, Balyan HS, Sharma S, Kumar R. Biofortification and bioavailability of Zn, Fe and Se in wheat: present status and future prospects. *Theor Appl Genet*. (2021) 134:1–35. doi: 10.1007/s00122-020-03709-7

17. Kumari A, Roy A. Enhancing micronutrient absorption through simultaneous fortification and phytic acid degradation. *Food Sci Biotechnol*. (2023) 32:1235–56. doi: 10.1007/s10068-023-01255-8

18. Sheethal HV, Baruah C, Subhash K, Ananthan R, Longvah T. Insights of nutritional and anti-nutritional retention in traditionally processed millets. *Front Sustain Food Syst*. (2022) 5:735356. doi: 10.3389/fsufs.2021.735356

19. Zhao QY. Approaches and influencing factors of synergistic improvement of productivity and grain nutritional quality of wheat and maize In: Dissertation/doctor's thesis. Beijing: China Agricultural University (2023)

20. DeFries R, Fanzo J, Remans R, Palm C, Wood S, Anderman TL. Global nutrition metrics for land scarce agriculture. *Science*. (2015) 349:238–40. doi: 10.1126/science.aaa5766

21. Chen H, Lu J, Li Y. Secular trends in the prevalence of and disability-adjusted life years due to common micronutrient deficiencies in China from 1990 to 2019: an age-period-cohort study and joinpoint analysis. *Front Nutr*. (2022) 9:754351. doi: 10.3389/fnut.2022.754351

22. Murphy J, Riley JP. A modified single solution method for the determination of phosphate in natural Waters. *Anal Chim Acta*. (1962) 27:31–6. doi: 10.1016/s0003-2670(00)88444-5

23. Walker JM, Barber SA. Absorption of potassium and rubidium from the soil by corn roots. *Plant Soil*. (1962) 17:243–59. doi: 10.1007/bf01376227

24. Lindsay WL, Norvell WA. Development of a DTPA soil test for zinc, iron, manganese, and copper. *Soil Sci Soc Am J*. (1978) 42:421–8. doi: 10.2136/sssaj1978.03615995004200030009x

25. Reichwald K, Hatzack F. Application of a modified Haug and Lantzsch method for the rapid and accurate photometrical phytate determination in soybean, wheat, and maize meals. *J Agric Food Chem*. (2008) 56:2888–91. doi: 10.1021/jf0730690

26. State Food and Nutrition Consultant Committee (2004). Nutrient composition of major foods. Available online at: https://sfncc.caas.cn/yyjk/37012.htm. (Accessed January 6, 2025)

27. Institute of Medicine. Dietary reference intakes for vitamin A, vitamin K, arsenic, boron, chromium, copper, iodine, iron, manganese, molybdenum, nickel, silicon, vanadium, and zinc. Washington, DC: National Academies Press (2002).

28. Institute of Medicine. Dietary reference intakes for energy, carbohydrate, fiber, fat, fatty acids, cholesterol, protein, and amino acids. Washington, DC: National Academies Press (2005).

29. De Steur H, Gellynck X, Blancquaert D, Lambert W, Van Der Straeten D, Qaim M. Potential impact and cost-effectiveness of multi-biofortified rice in China. *New Biotechnol*. (2012) 29:432–42. doi: 10.1016/j.nbt.2011.11.012

30. Guttieri MJ, Seabourn BW, Liu C, Baenziger PS, Waters BM. Distribution of cadmium, iron, and zinc in millstreams of hard winter wheat (*Triticum aestivum* L.). *J Agric Food Chem*. (2015) 63:10681–8. doi: 10.1021/acs.jafc.5b04337

31. Liu D, Liu Y, Zhang W, Chen X, Zou C. Agronomic approach of zinc biofortification can increase zinc bioavailability in wheat flour and thereby reduce zinc deficiency in humans. *Nutrients*. (2017) 9:465. doi: 10.3390/nu9050465

32. Chai W (2009) Chinese dietary vitamin intake and deficiency in recent ten years based on systematic analysis. Proceedings of the 2nd International Meeting of the Micronutrient Forum Micronutrients.

33. FAO/WHO. Vitamin and mineral requirements in human nutrition: report of a joint FAO/WHO expert consultation. *2nd* ed. Bangkok: FAO/WHO (2004).

34. Liang L, Wang Y, Ridoutt BG, Lal R, Wang D, Wu W, et al. Agricultural subsidies assessment of cropping system from environmental and economic perspectives in North China based on LCA. *Ecol Indic*. (2019) 96:351–60. doi: 10.1016/j.ecolind.2018.09.017

35. Liaw A, Wiener M. Classification and regression by randomforest. *R News*. (2002) 2:18–22.

36. Genuer R, Poggi J-M, Genuer R, Poggi J-M. Random Forests with R. Cham: Springer (2020).

37. Fortmann-Roe S. Consistent and clear reporting of results from diverse modeling techniques: the A3 method. *J Stat Softw*. (2015) 66:1–23. doi: 10.18637/jss.v066.i07

38. Archer E (2016) Rfpermute: estimate permutation *p*-values for random forest importance metrics. Available online at: https://cran.r-project.org/web/packages/rfPermute/rfPermute.pdf. (Accessed March 25, 2025)

39. Cui Y, Yao H, Li Q, Yao Y, Lu L, Wu L, et al. Effects of partial substitution of chemical fertilizer by organic fertilizer on growth, quality and nitrogen efficiency of quality wheat. *Acta Agric Bor Sin*. (2023) 38:158–66. doi: 10.7668/hbnxb.20194150

40. Lu L, Yao H, Cao Z, Zhang J, Yao Y, Jia X. Effects of organic fertilizer instead of chemical fertilizer on yield, quality and nitrogen efficiency of wheat. *Acta Agric Bor Sin*. (2022) 37:166–72. doi: 10.7668/hbnxb.20193206

41. Adekiya AO, Ejue WS, Olayanju A, Dunsin O, Aboyeji CM, Aremu C, et al. Different organic manure sources and Npk fertilizer on soil chemical properties, growth, yield and quality of okra. *Sci Rep*. (2020) 10:16083. doi: 10.1038/s41598-020-73291-x

42. Li Y, Wei J, Ma L, Wu X, Zheng F, Cui R, et al. Enhancing wheat yield through microbial organic fertilizer substitution for partial chemical fertilization: regulation of nitrogen conversion and utilization. *J Soil Sci Plant Nutr*. (2024) 24:935–43. doi: 10.1007/s42729-023-01597-6

43. Shen C, Yuan J, Li X, Zhang S, Ren X, Wang F, et al. Improving winter wheat N utilization efficiency and soil fertility through replacement of chemical N by 20% organic manure. *J Plant Nutr Fertil*. (2020) 26:1395–406. doi: 10.11674/zwyf.19504

44. Liu Y, Ma R, Yang Y, Wang J, Guan X, Wang M, et al. Effect of partial organic fertilizer substitution on heavy metal accumulation in wheat grains and associated health risks. *Agronomy*. (2023) 13:2930. doi: 10.3390/agronomy13122930

45. Li Y, Wu X, He G, Wang Z. Benefits of yield, environment and economy from substituting fertilizer by manure for wheat production of China. *Sci Agric Sin*. (2020) 53:4879–90. doi: 10.3864/j.issn.0578-1752.2020.23.013

46. Moreira-Ascarrunz S, Larsson H, Prieto-Linde M, Johansson E. Mineral nutritional yield and nutrient density of locally adapted wheat genotypes under organic production. *Foods*. (2016) 5:89. doi: 10.3390/foods5040089

47. Chu H, Dang H, Wang T, Sun R, Hou S, Huang Q, et al. Evaluations and influencing factors of soil available Fe, Mn, Cu and Zn concentrations in major wheat production regions of China. *Acta Pedol Sin*. (2024) 61:129–39. doi: 10.11766/trxb202205070236

48. Wang C, Li B, Gong B, Yang J, Zhang X, Cai Y. Study on the bioavailability and impact factors of Fe, Mn, Cu and Zn in the soils of Xichang City. *J Soil Sci*. (2010) 41:447–51. doi: 10.19336/j.cnki.trtb.2010.02.039

49. Xia H, Wang L, Qiao Y, Kong W, Xue Y, Wang Z, et al. Elucidating the source-sink relationships of zinc biofortification in wheat grains: a review. *Food Energy Secur*. (2020) 9:e243. doi: 10.1002/fes3.243

50. Laurent C, Bravin MN, Crouzet O, Pelosi C, Tillard E, Lecomte P, et al. Increased soil Ph and dissolved organic matter after a decade of organic fertilizer application mitigates copper and zinc availability despite contamination. *Sci Total Environ*. (2020) 709:709. doi: 10.1016/j.scitotenv.2019.135927

51. Zhao QY, Xu SJ, Zhang WS, Zhang Z, Yao Z, Chen XP, et al. Identifying key drivers for geospatial variation of grain micronutrient concentrations in major maize production regions of China. *Environ Pollut*. (2020) 266:266. doi: 10.1016/j.envpol.2020.115114

52. Habiby H, Afyuni M, Khoshgoftarmanesh AH, Schulin R. Effect of preceding crops and their residues on availability of zinc in a calcareous Zn-deficient soil. *Biol Fertil Soils*. (2014) 50:1061–7. doi: 10.1007/s00374-014-0926-7

53. Wu D, Ma Y, Yang T, Gao G, Wang D, Guo X, et al. Phosphorus and zinc are strongly associated with belowground fungal communities in wheat field under long-term fertilization. *Microbiol Spectr*. (2022) 10:e0011022. doi: 10.1128/spectrum.00110-22

54. Kaur H, Tyagi V, Kumar J, Roy JK, Chugh V, Ahmed N, et al. Identification and pyramiding of iron and zinc homeostasis genes introgressed from non-progenitor *Aegilops* species to bread wheat. *Euphytica*. (2024) 167:220. doi: 10.1007/s10681-024-03418-y

55. Zhao FJ, Su YH, Dunham SJ, Rakszegi M, Bedo Z, McGrath SP, et al. Variation in mineral micronutrient concentrations in grain of wheat lines of diverse origin. *J Cereal Sci*. (2009) 49:290–5. doi: 10.1016/j.jcs.2008.11.007

56. Huang T, Huang Q, She X, Ma X, Huang M, Cao H, et al. Grain zinc concentration and its relation to soil nutrient availability in different wheat cropping regions of China. *Soil Tillage Res*. (2019) 191:57–65. doi: 10.1016/j.still.2019.03.019

57. Nikolic M, Nikolic N, Kostic L, Pavlovic J, Bosnic P, Stevic N, et al. The assessment of soil availability and wheat grain status of zinc and iron in Serbia: implications for human nutrition. *Sci Total Environ*. (2016) 553:141–8. doi: 10.1016/j.scitotenv.2016.02.102

58. Han Y, Yang M, Liu L, Lei X, Wang Z, Liu J, et al. Grain mineral concentration of Chinese winter wheat varieties released between 1970 and 2005 under diverse nutrient inputs. *Field Crop Res*. (2022) 284:108576. doi: 10.1016/j.fcr.2022.108576

59. Liu C, Wang H, Ma Y, Guan P, Sun Q, Wang Z, et al. Key factors influencing wheat grain zinc and manganese concentration in areas with different soil available phosphorus. *Field Crop Res*. (2024) 317:109558. doi: 10.1016/j.fcr.2024.109558

60. Carmo Luis I, Lidon FC, Campos Pessoa C, Coelho Marques A, Coelho ARF, Simoes M, et al. Zinc enrichment in two contrasting genotypes of *Triticum aestivum* L. grains: interactions between edaphic conditions and foliar fertilizers. *Plants*. (2021) 10:204. doi: 10.3390/plants10020204

61. Ali M, Sharif M, Ahmed I. Enhancement of wheat productivity and zinc accumulation through integrated use of zinc and beneficial microbes under irrigated and rainfed conditions. *Commun Soil Sci Plant Anal*. (2024) 55:517–28. doi: 10.1080/00103624.2023.2274034

62. Manzeke GM, Mapfumo P, Mtambanengwe F, Chikowo R, Tendayi T, Cakmak I. Soil fertility management effects on maize productivity and grain zinc content in smallholder farming Systems of Zimbabwe. *Plant Soil*. (2012) 361:57–69. doi: 10.1007/s11104-012-1332-2

63. Tura DC, Belachew T, Tamiru D, Abate KH. Optimization of a formula to develop iron-dense novel composite complementary flour with a reduced phytate/minerals molar ratio from Dabi Teff-field pea-based blends using a D-optimal mixture design. *Front Nutr*. (2023) 10:1244571. doi: 10.3389/fnut.2023.1244571

64. Yu BG, Liu YM, Chen XX, Cao WQ, Ding TB, Zou CQ. Foliar zinc application to wheat may lessen the zinc deficiency burden in rural Quzhou, China. *Front Nutr*. (2021) 8:697817. doi: 10.3389/fnut.2021.697817

65. Xu M, Liu M, Si L, Ma Q, Sun T, Wang J, et al. Spraying high concentrations of chelated zinc enhances zinc biofortification in wheat grain. *J Sci Food Agric*. (2022) 102:3590–8. doi: 10.1002/jsfa.11705

66. Kamaral C, Neate SM, Gunasinghe N, Milham PJ, Paterson DJ, Kopittke PM, et al. Genetic biofortification of wheat with zinc: opportunities to fine-tune zinc uptake, transport and grain loading. *Physiol Plant*. (2022) 174:e13612. doi: 10.1111/ppl.13612

Frontiers in Nutrition

Explores what and how we eat in the context of health, sustainability and 21st century food science

A multidisciplinary journal that integrates research on dietary behavior, agronomy and 21st century food science with a focus on human health.

Discover the latest Research Topics

See more →

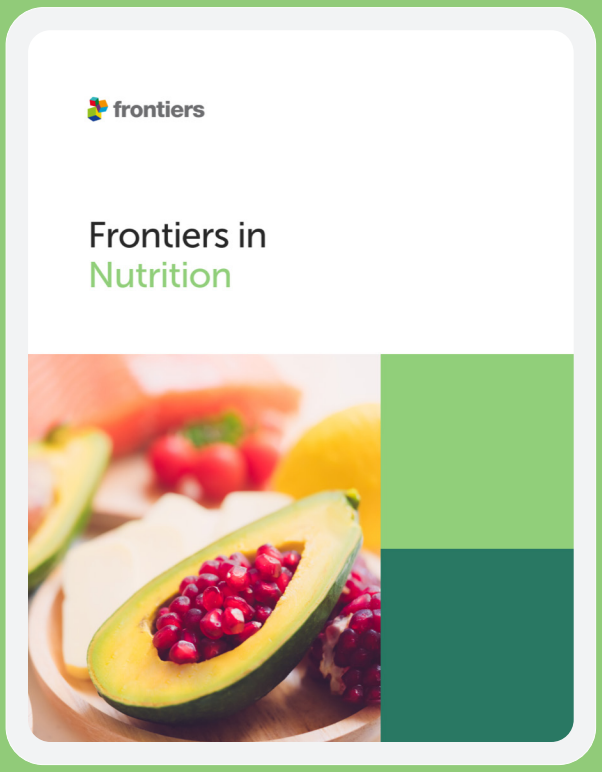

Frontiers

Avenue du Tribunal-Fédéral 34
1005 Lausanne, Switzerland
frontiersin.org

Contact us

+41 (0)21 510 17 00
frontiersin.org/about/contact